



SEDIMENTARY INFLUENCE ON THE
DEFORMATION OF DEEP WATER DEPOSITS
OFFSHORE NIGERIA

Stephen Joseph King

A thesis submitted in partial fulfilment of the requirements for the degree
of Doctor of Philosophy at Cardiff University

December 2016

DECLARATION

This work has not been submitted in substance for any other degree or award at this or any other university or place of learning, nor is being submitted concurrently in candidature for any degree or other award.

Signed (candidate) Date
.....

STATEMENT 1

This thesis is being submitted in partial fulfilment of the requirements for the degree of PhD

Signed (candidate) Date

STATEMENT 2

This thesis is the result of my own independent work/investigation, except where otherwise stated.

Other sources are acknowledged by explicit references. The views expressed are my own.

Signed (candidate) Date

STATEMENT 3

I hereby give consent for my thesis, if accepted, to be available online in the University's Open Access repository and for inter-library loan, and for the title and summary to be made available to outside organisations.

Signed (candidate) Date

STATEMENT 4: PREVIOUSLY APPROVED BAR ON ACCESS

I hereby give consent for my thesis, if accepted, to be available online in the University's Open Access repository and for inter-library loans **after expiry of a bar on access previously approved by the Academic Standards & Quality Committee.**

Signed (candidate) Date

Summary

A volume of 3D seismic data has been used to study the interplay of Cenozoic structural deformation and its relationship to sediment deposition offshore South-West Nigeria. The 3D survey encompasses an area that includes sediments derived from both the Niger Delta in the east and the Benin Embayment to the north. Sediments derived from the Niger Delta are comprised of deep water sands and shales deposited in channel levee turbidites and hemipelagic sheets, whilst those from the Benin Embayment are primarily fine grained and encompass large scale levees.

The study area can be divided into two vertically separated tectonic domains, which are divided by a detachment interval. The vertical separation occurs at a level which is coincident with an apron of mass transport deposits which extends beyond the limits of the data, this complex is interpreted to have been deposited at the end of the Cretaceous.

The Cenozoic interval has been modified by gravity driven tectonic activity which has resulted in two structurally dissimilar regions, which are separated by a strike slip fault zone. To the west of this strike slip fault zone is a region of primarily compressional deformation, to the east the majority of the deformation is extensional. The structural styles recognised, extension, compression and strike slip motion have been analysed to establish the timing and the causes of the deformation.

The influence of the sediment dispersal upon the location and timing of the tectonic deformation has been inferred indicating that structural deformation in this region pre dates the onset of deposition from the Niger Delta. The deformation which occurred prior to the Niger Delta outbuilding was controlled by the sediment dispersal from the Benin Embayment and this earlier, sediment controlled deformation, has subsequently played a role in the modified gravity tectonics which has been observed.

Authors Notes

During the course of this study, the author presented a poster at the AAPG annual convention in 2010:

KING, S. J. & CARTWRIGHT, J. A. 2010. Mass Transport Deposits and Their Role in Thin Skinned Tectonics - An Example from the NW Niger Delta *AAPG Annual Conference*. New Orleans.

In addition the author contributed to the writing of the following papers in collaboration with his supervision of a PhD student, Dominic Maloney, at Durham University

MALONEY, D., DAVIES, R., IMBER, J. & KING, S. 2012. Structure of the footwall of a listric fault system revealed by 3D seismic data from the Niger Delta. *Basin Research*, 24, 107-123.

MALONEY, D., DAVIES, R. J., IMBER, J., HIGGINS, S. & KING, S. 2009. The Implications of Detachment Unit Deformation on Fold and Thrust Belt Evolution: Examples from the Deepwater Niger Delta *AAPG Hedberg Conference, Deep Water Fold and Thrust Belts*. Tirrenia, Italy.

MALONEY, D., DAVIES, R. J., IMBER, J., HIGGINS, S. & KING, S. 2010. New insights into deformation mechanisms in the gravitationally driven Niger Delta deep-water fold and thrust belt. *AAPG Bulletin*, 94, 1401-1424.

Acknowledgements

This study would not have been possible were it not for the support and advice which was received from a number of people listed below:

Ann King, CEO of Mont D`Or Petroleum, for providing access to an SMT Kingdom licence without which this study could not have been completed.

Lawrence Sams of PGS for persuading PGS to allow the use of the 3D seismic data and Dan Whaling for granting the permission.

Professor Joe Cartwright for his advice and support, if it were not for his support and encouragement his thesis would have never been started.

Professor Tiago Alves for his valuable insights and suggestions concerning deep water processes.

Dr Emanuel Enu, who offered insights into Nigerian geology gained from his extensive knowledge of the Niger Delta.

A number of ex-colleagues at BG group with whom I was able to exchange ideas and who offered insights into deep water depositional systems, in particular Dr Phil Thompson, Dr Jonathan Turner, Dr Stephanie Kape and Gianluca Badalini

Dr Stephen Hubbard for providing insights into deep water slope deposition in the field, allowing me to see in outcrop the processes identified within the 3D.

Dr Dominic Maloney with whom I discussed a number of ideas about shelf collapse whilst he was studying for his PhD and who was kind enough to consider me as co- author on his published material.

Dr Carina King for providing encouragement and advice on the processes involved in compiling a thesis.

Table of Contents

| | | |
|---------|---|----|
| 1. | Introduction..... | 1 |
| 1.1 | Rationale | 1 |
| 1.2 | Hypothesis..... | 2 |
| 1.3 | Structure of the thesis..... | 3 |
| 1.4 | Overview | 4 |
| 1.5 | What are the key focus areas? | 9 |
| 1.5.1 | Mass-transport deposits as the base of Cenozoic deformation | 9 |
| 1.5.2 | Strike-slip faulting | 9 |
| 1.5.3 | Levee construction | 10 |
| 1.5.4 | Intra levee deformation | 10 |
| 2 | Deltaic deformation..... | 12 |
| 2.1 | Introduction..... | 12 |
| 2.2 | Extensional zone | 13 |
| 2.3 | Transition zone | 15 |
| 2.4 | Compressional zone (outer thrust belt) | 15 |
| 2.5 | Diapir zone | 16 |
| 2.6 | Inner thrust belt..... | 18 |
| 2.7 | Detachment surface..... | 18 |
| 3 | Outline | 20 |
| 3.1 | Introduction..... | 20 |
| 3.2 | Plate tectonic aspects..... | 21 |
| 3.2.1 | Rifting | 21 |
| 3.2.2 | Drifting..... | 23 |
| 3.2.3 | Senonian Unconformity | 28 |
| 3.2.4 | Thermal Subsidence..... | 28 |
| 3.3 | Regional Stratigraphy | 30 |
| 3.3.1 | Lithostratigraphy..... | 32 |
| 3.3.1.1 | Niger Delta | 32 |
| 3.3.2 | Chronostratigraphy | 34 |
| 3.3.2.1 | Syn-rift (Barremian to Aptian)..... | 35 |
| 3.3.2.2 | Pre-Senonian Interval (Albian to Turonian) | 40 |
| 3.3.2.3 | Post-Senonian (Campanian to Maastrichtian)..... | 40 |
| 3.3.2.4 | Cenozoic..... | 40 |
| 3.3.3 | Sequence Stratigraphy | 41 |
| 3.4 | Regional Sedimentology..... | 41 |
| 3.4.1 | Niger Delta | 42 |

| | | |
|---------|--|----|
| 3.4.2 | Benin Basin | 42 |
| 3.4.3 | Deep-water Depositional Styles | 45 |
| 3.4.3.1 | Hemipelagic Rain..... | 45 |
| 3.4.3.2 | Canyons..... | 46 |
| 3.4.3.3 | Turbidites | 47 |
| 3.4.3.4 | Mass Transport Deposits | 48 |
| 3.4.3.5 | Contourites | 52 |
| 4 | Data..... | 55 |
| 4.1 | Introduction..... | 55 |
| 4.2 | 3D seismic..... | 55 |
| 4.3 | Gravity | 63 |
| 4.4 | Well data | 64 |
| 4.5 | Interpretation methodology | 64 |
| 4.5.1 | Horizon Selection | 68 |
| 4.5.1.1 | Horizons | 68 |
| 4.5.1.2 | Mapping | 70 |
| 5 | Stratigraphy | 72 |
| 5.1 | Introduction..... | 72 |
| 5.2 | Horizon identification | 73 |
| 5.2.1 | The syn-rift (below Horizon 800)..... | 74 |
| 5.2.2 | Mid Albian Unconformity (Horizon 785) | 75 |
| 5.2.3 | The Senonian Unconformity (Horizon 680)..... | 77 |
| 5.2.4 | Campanian (Horizon 630)..... | 79 |
| 5.2.5 | Near base Cenozoic (Horizon 600)..... | 79 |
| 5.2.6 | Top of the regional mass transport complex (Horizon 510)..... | 79 |
| 5.2.7 | Deepest faulted event within the Cenozoic (Horizon 500)..... | 81 |
| 5.2.8 | Intra ridge surfaces (Horizons 470, 465, 429, 425) | 82 |
| 5.2.9 | The base of the Neogene (Horizon 420)..... | 82 |
| 5.2.10 | Unconformity within the Neogene (Horizon 400)..... | 84 |
| 5.2.11 | Upper limit of the levee system (Horizon 300) | 84 |
| 5.2.12 | Lower Miocene, base of the channel levee system (Horizon 200) | 85 |
| 5.2.13 | Middle Miocene Upper limit of main channel levee influx (Horizon 160)..... | 86 |
| 5.2.14 | Upper Miocene Base of low stand section (Horizon 130)..... | 86 |
| 5.2.15 | Pliocene (Horizon 100) | 87 |
| 5.2.16 | Seabed (Horizon 0) | 88 |
| 6 | Description of interpreted depositional setting..... | 90 |
| 6.1 | Introduction..... | 90 |
| 6.2 | Cretaceous..... | 90 |

| | | |
|-------------|---|-----|
| 6.2.1 | Syn-Rift | 90 |
| 6.2.2 | Early post rift | 95 |
| 6.2.3 | Drift..... | 99 |
| 6.3 | Cenozoic | 100 |
| 6.3.1 | Canyons | 100 |
| 6.3.1.1 | Lagos Canyon deposits..... | 101 |
| 6.3.1.2 | Avon-sourced deposits..... | 103 |
| 6.3.1.3 | Mahin Canyon-sourced deposits | 106 |
| 6.3.1.4 | Opuama/Benin Canyon-sourced deposits | 106 |
| 6.3.2 | Hemipelagic input..... | 109 |
| 6.3.3 | Turbidity flow deposits | 109 |
| 6.3.3.1 | Channel levee complex | 109 |
| 6.3.3.1.1 | Mahin-sourced channels..... | 110 |
| 6.3.3.1.2 | Opuama/Benin-sourced channels | 111 |
| 6.3.3.2 | Levees..... | 118 |
| 6.3.4 | Mass transport deposits..... | 127 |
| 6.3.4.1 | Headwall domain | 130 |
| 6.3.4.2 | Translational zone..... | 131 |
| 6.3.4.3 | Toe domain | 133 |
| 6.3.4.4 | Fluidised apron..... | 133 |
| 6.3.4.5 | Neogene mass transport intervals..... | 136 |
| 6.3.4.5.1 | Lower Miocene (Horizon 160 to 200) | 136 |
| 6.3.4.6 | Cretaceous mass transport deposits..... | 140 |
| 6.3.4.6.1 | Campanian (horizon 630 to 650) | 140 |
| 6.3.4.6.2 | Palaeocene (the detachment mass transport complex)..... | 142 |
| 6.3.4.6.2.1 | The western lobe | 143 |
| 6.3.4.6.2.2 | The central lobe | 147 |
| 6.3.5 | Confined debris flows | 157 |
| 6.3.6 | Sediment remobilisation | 161 |
| 7 | Structural deformation | 162 |
| 7.1 | Introduction..... | 162 |
| 7.2 | Tectonic history | 166 |
| 7.2.1 | Mid-Lower Cretaceous (Barremian to Early Albian) | 166 |
| 7.2.2 | Middle Cretaceous (Albian to Turonian)..... | 169 |
| 7.2.3 | Upper Cretaceous (Campanian to Maastrichtian) | 169 |
| 7.2.4 | Palaeogene | 172 |
| 7.2.4.1 | Shelf collapse and mass transport deposition | 172 |
| 7.2.4.2 | Intra-levee deformation..... | 175 |

| | | |
|-------------|---|-----|
| 7.3 | Structural elements..... | 176 |
| 7.3.1 | Introduction..... | 176 |
| 7.3.2 | Basal detachment..... | 178 |
| 7.3.2.1 | The interplay between structural deformation and mass transport deposits 183 | |
| 7.3.3 | Extension..... | 184 |
| 7.3.3.1 | Normal faulting | 185 |
| 7.3.3.1.1 | Fault geometries | 186 |
| 7.3.3.1.2 | Timing | 186 |
| 7.3.3.1.3 | Northern extensional zone | 190 |
| 7.3.3.1.4 | The western region | 192 |
| 7.3.3.1.5 | The eastern region..... | 195 |
| 7.3.4 | Compression | 205 |
| 7.3.4.1 | TA I to TA III..... | 205 |
| 7.3.4.1.1 | Thrusted anticline I (TA I)..... | 206 |
| 7.3.4.1.2 | Thrusted Anticline II (TA II) | 210 |
| 7.3.4.1.3 | TA III | 213 |
| 7.3.4.2 | TA IV | 213 |
| 7.3.4.3 | TA V and VI..... | 219 |
| 7.3.5 | Deformation of ridges | 225 |
| 7.3.5.1 | Internal..... | 225 |
| 7.3.5.1.1 | Fault characteristics..... | 228 |
| 7.3.5.2 | Lateral boundary fault zone..... | 233 |
| 7.3.6 | Fluid escape | 239 |
| 7.3.7 | Transcurrent faulting..... | 241 |
| 7.3.7.1 | Fault zone SS A..... | 241 |
| 7.3.7.2 | Mahin and Avon fault zone | 246 |
| 7.3.7.2.1 | Mahin fault zone..... | 247 |
| 7.3.7.2.1.1 | Measurement of lateral movement | 247 |
| 7.3.7.2.2 | Avon fault zone | 262 |
| 7.3.7.3 | Timing of movement..... | 263 |
| 7.3.7.3.1 | Recent movement..... | 263 |
| 7.3.7.3.2 | Early movement..... | 266 |
| 8 | Discussion | 269 |
| 8.1 | Mass transport apron as the Cenozoic detachment interval..... | 270 |
| 8.1.1 | Origin of the mass transport deposits | 270 |
| 8.1.2 | Nature of mass transport deposits | 274 |
| 8.1.2.1 | Composition of mass transport deposits..... | 274 |

| | | |
|---------|---|-----|
| 8.1.2.2 | Permeability in mass transport deposits | 275 |
| 8.1.2.3 | Overpressure generation | 276 |
| 8.2 | Origin of the large-scale levees | 277 |
| 8.2.1 | Contourites | 277 |
| 8.2.2 | Turbidites..... | 278 |
| 8.2.3 | Nature of the levees | 280 |
| 8.2.3.1 | Internal geometry | 280 |
| 8.2.3.2 | Intra-levee deformation..... | 281 |
| 8.3 | The origin of the Avon/Mahin fault zone..... | 285 |
| 8.3.1 | Is there a deep basement control?..... | 285 |
| 8.3.1.1 | Syn rift | 285 |
| 8.3.1.2 | Mid to Upper Cretaceous..... | 287 |
| 8.3.2 | Gravity imbalances in the Cenozoic..... | 290 |
| 8.3.3 | Evolution of the Avon/Mahin fault zone..... | 294 |
| 9 | Conclusions..... | 298 |
| 9.1 | Twin sources of sedimentation | 298 |
| 9.1.1 | Benin Basin | 299 |
| 9.1.2 | The Niger Delta | 300 |
| 9.2 | Structural styles | 300 |
| 9.2.1 | Deltaic styles | 300 |
| 9.2.1.1 | Extension..... | 300 |
| 9.2.1.2 | Transition | 301 |
| 9.2.1.3 | Toe Thrust Region | 301 |
| 9.2.1.4 | Transcurrent/Tear faulting..... | 301 |
| 9.2.2 | Fan/levee style | 302 |
| 9.3 | Mass transport complex as the detachment..... | 303 |

List of Figures

| | |
|---|----|
| Figure 1-1 Location of the study highlighted by the red polygon, superimposed on the bathymetry and digital elevation of the Gulf of Guinea derived from satellite altimetry (Sandwell et al. 2014). | 4 |
| Figure 1-2: Perspective view of a two-way time composite Miocene horizon illustrating the key structural elements within the survey area. The black dashed line marks the change in horizon – the horizon north-west of this line has been eroded by the influx of sediments from the Avon Canyon, which lies to the north. Warm colours represent short travel times. | 8 |
| Figure 1-3: Sea bed two-way time perspective view; warm colours represent shallow values. . | 11 |
| Figure 2-1: A regional seismic traverse through the Niger Delta highlighting the five structural domains (Corredor et al. 2005). | 14 |
| Figure 2-2: Map illustrating the distribution of the five structural regions of the Niger Delta; the area covered by this study is highlighted by the black rectangle (taken from (Corredor et al. 2005). | 15 |
| Figure 2-3: An example of the quality of imaging that gave rise to the concept of shale diapirism (taken from Bruce, 1973). | 17 |
| Figure 2-4: image illustrating the change in seismic data imaging, which allows for steeply dipping data to be correctly identified. | 17 |
| Figure 3-1 Vertical gravity gradient (in Eotvos) derived from satellite measurements of sea level in the Gulf of Guinea (Sandwell et al., 2014). The location of the survey is highlighted by the black rectangle. | 23 |
| Figure 3-2 Gravity Free Air anomaly (in colour) of the Gulf of Guinea in milligals; the contours are the bathymetry derived from satellite gravity data. | 24 |
| Figure 3-3 A reconstruction of the African and South American continental plates at 140 Ma, indicating the fit of the two plates prior to the separation that commenced in the Barremian (Heine et al. 2013). The key features are labelled in line with the list below. | 25 |
| Figure 3-4 Detailed view taken from Figure 3-3, indicating the location of the study area, which lies adjacent to the Potiguar Basin in South America and the Benue Trough in West Africa. | 26 |
| Figure 3-5 Isochrone of the Upper Cretaceous interval, which is defined as the section between the base Cenozoic and Senonian unconformity. | 29 |
| Figure 3-6 Tectono-stratigraphy of the Benin Basin region. | 32 |
| Figure 3-7 Lithostratigraphic subdivisions of the Cenozoic Niger Delta (Short and Stauble 1967). | 33 |
| Figure 3-8 The lithostratigraphic breakdown of the Benin Basin (Kaki et al. 2012). | 34 |
| Figure 3-9 Summary of the chronostratigraphy of the Benin Basin; the section runs from the shelf break in a north-south orientation. | 35 |
| Figure 3-10 Cross line 4700, both in the original form, top, and flattened at Base Cenozoic (the red horizon) in the bottom image. The vertical lines mark 5km intervals. | 37 |
| Figure 3-11 Crossline 5700, the upper image is the original; the lower one is flattened at the Base Cenozoic. | 38 |
| Figure 3-12 TWT map of the top of the syn-rift, showing location of Figures 3-7 and 3-8; the yellow dashed line is the location of the Mahin fault zone in the overburden. | 39 |
| Figure 3-13 Alternative stratigraphic description of the Cenozoic sediments of the Niger Delta, based upon geographical location and structural domains (Edjedawe 2012). | 41 |

| | |
|--|----|
| Figure 3-14 Surface geology of Nigeria taken from (Bonne 2014). | 44 |
| Figure 3-15 Free-air gravity anomaly, in milligals, illustrating the interpreted locations of canyons. | 46 |
| Figure 3-16 Illustration of the key components of a deep-water canyon-fed depositional system (Posamentier and Kolla 2003). | 48 |
| Figure 3-17 A vertical cross section through a mass transport complex, offshore Morocco (Dunlap et al. 2010). | 50 |
| Figure 3-18 RMS extraction of the MTD identified offshore Morocco (Dunlap et al. 2010). | 51 |
| Figure 3-19 Classification of contourite drifts (after (Faugères and Stow 2008). | 53 |
| Figure 3-20 Example of large-scale contourite drifts, the Eirik drift offshore southern Greenland (Nielsen et al. 2008) | 54 |
| Figure 4-1 Frequency spectrum | 56 |
| Figure 4-2 Phase spectrum of the data | 57 |
| Figure 4-3 comparison of two dip lines, showing the poor imaging quality in the steeply dipping interval in the left hand image | 58 |
| Figure 4-4 Comparison of original data (upper image) with the AGC compensated volume (lower image). | 60 |
| Figure 4-5 Portion of inline 5300 illustrating the over migration of reflectors below the Avon/Mahin fault zone | 61 |
| Figure 4-6 Two way time map of the base Cenozoic horizon, illustrating the location of anticlinal ridges (in white) mapped at the base of the Neogene. | 63 |
| Figure 4-7 vertical gravity gradient derived from satellite data, draped over topography (Sandwell et al. 2014) | 64 |
| Figure 4-8 Interpretation workflow | 65 |
| Figure 4-9 Extracted similarity from a grid of a Miocene horizon, which indicates in the dark colours the presence of faults – where the degree of similarity between traces is low. | 67 |
| Figure 4-10 Example of an RMS extraction from within a window between two middle Miocene horizons | 68 |
| Figure 4-11 Seismic cross section which indicates the reflection character of both high | 71 |
| Figure 5-1 two way time map of the break up unconformity (horizon 800), the dashed white line marks the approximate location of the boundary between reflective - to the east, and non-reflective - to the west, events below the unconformity. | 74 |
| Figure 5-2 Isochrone of the Albian to Cenomanian interval (between horizon 785 and 680). The white polygon indicates the location of the overlying Avon/Mahin fault zone. | 76 |
| Figure 5-3 portion of cross line 5000, which is flattened at the base of the Cenozoic (horizon 600), see Figure 5-2 for the location of the line. | 76 |
| Figure 5-4 Inline 3800, illustrating the interval below the Senonian Unconformity (horizon 680), which includes the wavy discontinuous seismic facies. | 78 |
| Figure 5-5 Isochrone of the mass transport complex (between horizons 510 and 600), the south eastern limit of the map is the location of the Avon/Mahin fault zone | 80 |
| Figure 5-6 portion of inline 3800, illustrating the chaotic interval, the mass transport complex (between horizons 600 and 510), and the overlying section which is tectonically modified (See Figure 5-7 for location) | 81 |
| Figure 5-7 similarity attribute extracted from horizon 500 | 82 |
| Figure 5-8 two way time map of the base Neogene (horizon 420) | 83 |

| | |
|--|-----|
| Figure 5-9 Isochrone of the thickness of the Palaeogene (between horizon 600 and 420) | 83 |
| Figure 5-10 random seismic line which passes over the western ridge and the adjacent moats | 84 |
| Figure 5-11 portion of inline 6480 which illustrates the horizon selection for the Miocene and Pliocene surfaces 200, 160, 130 and 100. Note that the character match across the major Y shaped fault zone (the Avon fault zone) is considered robust. | 85 |
| Figure 5-12 two way time map of upper Miocene low stand (horizon 130) | 87 |
| Figure 5-13 two way time map of Pliocene (horizon 100)..... | 88 |
| Figure 5-14 two way time map of the seabed | 89 |
| Figure 6-1: Cross line 7800; the top image is the original section, while the lower image is the same line flattened on the base Cenozoic (horizon 600); the break-up unconformity (purple event) has a fairly even topography..... | 92 |
| Figure 6-2: Cross line 4700; the top image is the original section, while the lower image is the same line flattened on the base Cenozoic event (horizon 600)..... | 93 |
| Figure 6-3: Two-way time map of the top syn-rift (horizon 800); the solid white lines refer to the locations of Figure 6-1 and Figure 6-2. The dashed white line indicates the division of the terrains that underlie the unconformity..... | 94 |
| Figure 6-4: Inline 3800, flattened on the base Cenozoic (horizon 600)..... | 96 |
| Figure 6-5: Inline 4600 flattened at the Base Cenozoic (horizon 600). | 97 |
| Figure 6-6: Two-way time map of the Senonian unconformity (orange, horizon 680), illustrating the location of the lines in Figure 6-4 and Figure 6-5. | 98 |
| Figure 6-7: Isochrone in twt of the Upper Cretaceous interval (between horizons 600 and 680). | 99 |
| Figure 6-8: Free-air gravity anomaly for the region, in mgal; the twt thickness of the Palaeogene is superimposed to illustrate its relationship to the canyons. | 102 |
| Figure 6-9: Isochrone of the interval between horizons 600 and 420..... | 102 |
| Figure 6-10: Seismic line across the Avon Canyon, taken from (Olabode and Adekoya 2008). | 103 |
| Figure 6-11: Interpreted version of Figure 6-10 (Olabode and Adekoya 2008)..... | 104 |
| Figure 6-12: Similarity attribute extracted some 200ms below the seabed. The black dashed lines are Avon-sourced channels, while the red is a Mahin-derived channel system..... | 104 |
| Figure 6-13: A phase rotated seismic envelope display of inline 6100, which illustrates the sediments derived from the Avon Canyon. | 105 |
| Figure 6-14: Isochrone of the interval between horizons 190 and 202..... | 106 |
| Figure 6-15: Similarity attribute extracted at the seabed; dark colours indicate low similarity. | 107 |
| Figure 6-16: Seismic amplitude of the seabed reflector. | 108 |
| Figure 6-17: 3D perspective of the similarity of a pseudo horizon 100ms below the seabed. . | 110 |
| Figure 6-18: Seismic line in the northern region of the 3D survey which illustrates the channel levee geometry in a cross section of the Mahin Canyon; highlighted in yellow are three separate channel complexes that are interpreted to have their origin in the outflow from the Mahin Canyon. | 111 |
| Figure 6-19: RMS amplitude extracted from a window within the Middle Miocene (between horizon 130 and a pseudo horizon 200 ms below), draped on a 3D perspective view of the twt surface of Horizon 130. | 112 |
| Figure 6-20: Portion of inline 3590, illustrating the discontinuous nature of the reflections within the Lower to Middle Miocene (below horizon 160 (green) and above 310 (orange)); line location is highlighted in Figure 6-21. | 113 |

| | |
|---|-----|
| Figure 6-21: RMS extraction of a Middle Miocene interval (between horizon 160 and a pseudo horizon 100ms below horizon 160). The red regions are interpreted to be channel complexes. | 114 |
| Figure 6-22: Similarity attribute extracted at a level 50 milliseconds below seabed; the present-day Mahin channel is highlighted in yellow. | 116 |
| Figure 6-23: Perspective view of an RMS extraction from an interval some 300-400 milliseconds below horizon 160, draped on horizon 160. | 117 |
| Figure 6-24: Perspective view of the base Neogene unconformity, in twt, illustrating the location of the western ridges and their relationship with the major tectonic elements within the survey. | 119 |
| Figure 6-25: Perspective view of an Upper Oligocene event (horizon 310) in twt, showing the relationship between the western ridges and the thrust anticlines. | 120 |
| Figure 6-26: Isochrone of the interval between horizons 300 and 400 (cold colours indicate thicker regions) – see Figure 6-27 for the cross section A-B. | 121 |
| Figure 6-27: Seismic line illustrating the geometry of the two major ridges and associated synclines in the western area of the survey. | 122 |
| Figure 6-28: Perspective view of horizon 300 showing the difference in the vertical expression of the thrust anticlines, compared to the levees. | 123 |
| Figure 6-29: Detailed view of Ridge A (from Figure 6-27), showing the location of several internal ridges within the overall body of Ridge A, highlighted in yellow. | 124 |
| Figure 6-30: Schematic depiction of a depositional system that could be an analogy for the levees (Reading and Richards 1994). | 126 |
| Figure 6-31: Seismic traverse with base of the mass transport complexes highlighted in red (the Base Cenozoic) illustrating the presence of two mass transport complexes. The inset map is an isochrone of the thickness of the mass transport complex (blue being thick). | 128 |
| Figure 6-32: The seismic traverse in Figure 6-31 flattened at the base Cenozoic (red horizon), which shows the relationship between the two mass transport deposits at the base of the Cenozoic. | 129 |
| Figure 6-33: Seismic profile from the headwall domain (Maloney et al. 2012). | 130 |
| Figure 6-34: Illustration of the scour at the base of the Upper Miocene. | 131 |
| Figure 6-35: Portion of seismic line that passes through the translational zone of two mass transport deposits. | 132 |
| Figure 6-36: Outcrop example of contorted beds within a mass transport deposit. | 133 |
| Figure 6-37: Schematic diagram of the key elements of a mass transport complex after (Galloway 1998). | 134 |
| Figure 6-38: Classification of fabrics associated with mass transport deposits, taken from Bull et al. (2009). | 135 |
| Figure 6-39: Illustration of the similarity attribute extracted from horizon 163. | 137 |
| Figure 6-40: Similarity attribute extracted from horizon 200. | 138 |
| Figure 6-41: Seismic line that is located along the axis of the western anomaly seen in Figure 6-40. | 138 |
| Figure 6-42: RMS amplitude extraction of a window between horizon 202 and 100ms below. | 139 |
| Figure 6-43: Similarity extraction at horizon 200, with the locations of the seismic line labelled C-D. | 140 |
| Figure 6-44: A vertical section through the Campanian sequence of high-angle seismic reflections. The inset map is a time slice at 6.24 seconds (the red line in the section) showing the arcuate nature of these dips in an areal sense. | 141 |

| | |
|---|-----|
| Figure 6-45: Isochrone map of the thickness of the basal Cenozoic mass transport deposit (between horizons 600 and 510); thickness is in two-way time in seconds. | 142 |
| Figure 6-46: RMS extraction of an interval 100ms above horizon 600. The green and yellow zones indicate intervals of higher amplitude; the blue, lower amplitude regions. | 143 |
| Figure 6-47: Seismic profile B-B` , (see Figure 6-46); a north-west to south-east traverse through the western mass transport complex (highlighted in yellow). | 145 |
| Figure 6-48: Seismic profile A-A` (see Figure 6-46) traversing the western mass transport deposit in a north-east to south-west orientation. | 146 |
| Figure 6-49: North-west to south-east traverse (see Figure 6-46 for location) of the main mass transport deposit. | 148 |
| Figure 6-50: North-east to south-west seismic traverse (see Figure 6-46 for location) showing the chaotic reflection character of the mass transport deposit. | 149 |
| Figure 6-51: Random line through the mass transport deposit, flattened at the base of the interval (horizon 600). | 150 |
| Figure 6-52: Illustration of the tip-out of faults at the surface of a mass transport deposit below horizon 470. | 152 |
| Figure 6-53: The RMS amplitude attribute of an interval within the mass transport interval, highlighting the presence of arcuate and linear anomalies. The imaging of the interval has been investigated by means of amplitude and coherence attributes derived from the seismic data. | 153 |
| Figure 6-54: Outcrop of mass transport complex, showing isolated competent strata within a mass transport deposit. This outcrop is within the Tres Pasos formation and is located along the Zamora River in southern Chile. | 155 |
| Figure 6-55: Seismic line illustrating the presence of competent blocks within the mass transport deposit. | 155 |
| Figure 6-56: A perspective view of the surface of the mass transport deposit, displayed along with a vertical section that shows the presence of the deformed overburden. The white dashed line is the trace of the Mahin fault. | 156 |
| Figure 6-57: RMS amplitude attribute for an interval within the Upper Oligocene. Note the absence of any channel-like geometries. The sections highlighted in the map are shown in Figure 6-58 and Figure 6-59. | 158 |
| Figure 6-58: Seismic cross-sections across the syncline between Ridges A and B. | 159 |
| Figure 6-59: Seismic cross-sections across the syncline to the east of Ridge B. | 160 |
| Figure 6-60: Outcrop view of mobilised, intruding clastics within a deep-water shale matrix. | 161 |
| Figure 6-61: Illustration of mounded features that are interpreted to represent extruded bodies of remobilised sediment; the figure is a perspective view of an horizon (see Figure 6-63) in the northern region of the survey; the faulted anticlines TA II, II, and IV are outlined in more detail in chapter 7. | 163 |
| Figure 6-62: Another view of the surface shown in Figure 6-61, along with a vertical section through the mounds. | 164 |
| Figure 6-63: Vertical section through the mounds shown in Figure 6-62. | 165 |
| Figure 7-1: Perspective view, looking from the north-east, of the base of the Upper Miocene twt surface, highlighting the change in structural style across the strike slip faults (dashed white lines). | 163 |
| Figure 7-2: Seismic line illustrating the significant difference in structural style above and below the red horizon that crosses the study area. | 164 |
| Figure 7-3: The same line displayed in Figure 7-2, with the contrasting tectonic styles highlighted on either side of the Mahin fault zone. | 165 |

| | |
|--|-----|
| Figure 7-4: Cross line 6100, which illustrates the complex faulting, highlighted in blue, within the interpreted sedimentary section below the syn rift unconformity (purple horizon). The location of the continental ocean boundary is interpreted to lie between the reflective sediments and the non-reflective section to the south-west..... | 167 |
| Figure 7-5: Free-air gravity anomaly map, with interpreted fracture zones and continent ocean boundaries marked. The location of Figure 7-4 is highlighted by the white line. The gravity map lends support to the possibility of the OCB being as shown in Figure 7-4. | 168 |
| Figure 7-6: Arbitrary seismic line showing the presence of several thrust anticlines in the section below the Base Cenozoic (red marker), the assumed base Cenozoic. | 170 |
| Figure 7-7: Seismic inline 5840 showing the thinning wedge of sediments within the Upper Cretaceous. | 171 |
| Figure 7-8: Isochrone map of the Lower Cenozoic interval, illustrating the north-east to south-west trending ridges and synclines; the ridge on the western edge of the map is bounded to the east by a complex fault zone. | 173 |
| Figure 7-9: Seismic line highlighted by line A-A` on the map shown in Figure 7-8, flattened on horizon 600 (the base of the Lagos mega slide), showing the thickening of the section below the blue horizon (420) towards the west. Notice also the presence of ridges that have accumulated post the blue horizon. | 174 |
| Figure 7-10: Perspective view of horizon 130 showing the key structural features in the survey area. | 177 |
| Figure 7-11: Portion of inline 3800 illustrating the location of the detachment. | 180 |
| Figure 7-12: Detail of Figure 7-11 illustrating the basal limit of the deformed overburden. | 181 |
| Figure 7-13: Portion of inline 4200, illustrating the discontinuity in structural deformation at horizon 500. | 182 |
| Figure 7-14: Illustration of the variation in fault throws on either side of the Mahin fault zone. | 188 |
| Figure 7-15: Isochrone of the interval between horizons 160 and 200..... | 189 |
| Figure 7-16: Isochrone of the interval between horizons 130 and 160..... | 190 |
| Figure 7-17: Similarity attribute extracted for horizon 202 (one loop lower than horizon 200). | 191 |
| Figure 7-18: Measurement of strain along the trace of fault plane NW1. | 193 |
| Figure 7-19: Contours of the vertical displacement vs. spatial location along the fault plane of fault NW9. | 194 |
| Figure 7-20: Similarity attribute extracted at horizon 160. | 195 |
| Figure 7-21: Plot of the throw of horizons 160 and 200 along fault NW1 | 196 |
| Figure 7-22: Fault NW 1, as it appears on either side of the Avon/Mahin fault zone. | 198 |
| Figure 7-23: Horizon 160 twt surface showing the location of fault NW1. | 199 |
| Figure 7-24: Perspective view of a composite horizon showing the location of fault NW1 on either side of the Mahin fault. | 200 |
| Figure 7-25: Illustration of the lateral displacement of fault NW1. | 201 |
| Figure 7-26: Similarity attribute extracted at horizon 160. | 202 |
| Figure 7-27: Cross line 5700 with the two faults referred to in the text highlighted. | 203 |
| Figure 7-28: Random traverse around the tip of fault NW9 showing the continuity of the events from the footwall to the hanging wall..... | 204 |
| Figure 7-29: Inline 6300 which illustrates the four thrust anticlines noted in the northern region. | 207 |
| Figure 7-30: Twt map of horizon 191, showing the location of the named faults. | 208 |

| | |
|---|-----|
| Figure 7-31: Plot of fault throw at horizons 160 and 200 along fault RA1. | 208 |
| Figure 7-32: Plot of throw of horizons 160 and 200 along the fault plane of RA3. | 209 |
| Figure 7-33: Twt map of horizon 420. | 210 |
| Figure 7-34: Fault throw measured along RB1. | 211 |
| Figure 7-35: Fault throw measured along fault RB2. | 212 |
| Figure 7-36: Fault throw measured along fault FB3. | 212 |
| Figure 7-37: Fault throws for three faults within TA II, including the combined displacement of the three faults. | 213 |
| Figure 7-38: Inline 5900 illustrating the location of TA IV. | 215 |
| Figure 7-39: Similarity attribute extracted at horizon 202. | 216 |
| Figure 7-40: Seismic profiles that cross the two strike-slip faults highlighted in Figure 7-39. ... | 217 |
| Figure 7-41: Similarity extraction at four horizons in the northern area. | 218 |
| Figure 7-42: Random line through the western half of the survey, illustrating the two high-relief anticlines TA V and VI. | 220 |
| Figure 7-43: Seismic line through the northern portion of TA VI. | 222 |
| Figure 7-44: Seismic line through the central portion of TA VI. | 223 |
| Figure 7-45: Seismic section through the southern portion of TA VI. | 224 |
| Figure 7-46: Twt map of horizon 470. The white dashed line is the interpreted location of the lateral fault zone. | 227 |
| Figure 7-47: Random line that passes down the ridge and across the lateral fault zone (see Figure 7-46 for location). | 227 |
| Figure 7-48: North-south traverse through the western-most ridge; refer to Figure 7-49 for location. | 229 |
| Figure 7-49: Similarity attribute extracted at horizon 470. In addition to the array of reverse faults that have been described above, there is a central fault belt within the levee that is comprised of both normal faults, as illustrated in Figure 7-51, and sub-vertical faults. | 230 |
| Figure 7-50: North-south line passing through the middle of the levee; refer to Figure 7-49 for location. | 230 |
| Figure 7-51: West-to-east section through Ridge A; refer to Figure 7-49 for location. | 231 |
| Figure 7-52: Photograph of a stack of reverse faults which verge up-dip, seen in outcrop. | 232 |
| Figure 7-53: Detail of the faulting that can be seen in the eastern margin fault zone from seismic line 4120. | 234 |
| Figure 7-54: Similarity attribute extracted at horizon 425. | 236 |
| Figure 7-55: Perspective view of the two-way time for horizon 425; the black line is the location of Figure 7-56. The black dashed line is the trace of the eastern margin strike-slip fault zone. | 237 |
| Figure 7-56: Cross section highlighted in Figure 7-55, which traverses the strike-slip fault at the eastern margin of Ridge A. | 238 |
| Figure 7-57: Illustration of a diatreme associated with the release of overpressure. | 240 |
| Figure 7-58: Perspective view of the Upper Miocene similarity (horizon 130) viewed from the north-east. Highlighted is the location of fault SS A in relation to the Avon/Mahin fault zone. | 243 |
| Figure 7-59: Amplitude extraction of the Upper Oligocene (horizon 200), showing the displacement of a pre-existing channel, offset by lateral movement along fault SS A. | 244 |

| | |
|---|-----|
| Figure 7-60: Three seismic lines which cross fault SS A, illustrating the sub-vertical nature of the transcurrent fault SS A. | 245 |
| Figure 7-61: Similarity attribute of horizon 130, showing the location of the key strike-slip faults in the survey area – in red the Mahin and in yellow the Avon. | 246 |
| Figure 7-62: Illustration of fault displacement estimation..... | 248 |
| Figure 7-63: Method for calculating the lateral extension. | 248 |
| Figure 7-64: Portion of two seismic lines on either side of the Mahin fault zone; the two lines are used to illustrate the varying degree of extension on either side of the strike-slip fault zone in the following figures..... | 249 |
| Figure 7-65: Portion of a random line that lies to the north of and runs parallel to the Mahin fault zone..... | 250 |
| Figure 7-66: Portion of a random track through the volume, which runs to the south of and parallel to the Mahin fault zone..... | 251 |
| Figure 7-67: Displacement of channels by lateral movement..... | 253 |
| Figure 7-68: RMS extraction of the interval between horizon 130 and 100ms above the horizon. | 254 |
| Figure 7-69: RMS extraction from horizon 130 to 100ms above the horizon, with the south-eastern block shifted 4km to the north-east. | 255 |
| Figure 7-70: RMS extraction of a window 100ms below horizon 160. The blue colours represent a series of slope channels..... | 256 |
| Figure 7-71: In this figure, the map has been split at the Avon/Mahin fault zone and moved approximately 5km. | 257 |
| Figure 7-72: RMS amplitude extracted from a window in the Lower Miocene, showing the location of two channel belts. | 258 |
| Figure 7-73: A reconstruction of the channel belts after shifting them by 7.8km in a dextral sense. | 259 |
| Figure 7-74: Isochrone map of the interval between horizons 160 and 200..... | 260 |
| Figure 7-75: Isochrone of thickness between horizons 160 and 200, with the south-eastern domain shifted by 7km to the north-east..... | 261 |
| Figure 7-76: Seismic cross section through the northern portion of the survey, showing the "negative flower structure" associated with the Avon fault. | 263 |
| Figure 7-77: Seismic Cross section through the Transpressional portion of the Avon Fault zone, showing a characteristic "pop-up" structure..... | 264 |
| Figure 7-78: Isochrone of the Pliocene to recent interval. | 265 |
| Figure 7-79: Seismic line running along the western side of the Mahin fault zone..... | 267 |
| Figure 7-80: Illustration of how the principle stress direction alters across the Niger Delta. | 268 |
| Figure 8-1: Early evolution of the mass transport complex: creation of the conditions that allowed the formation of the mass transport complexes. | 272 |
| Figure 8-2: regressive nature of the mass transport complex formation. | 273 |
| Figure 8-3: Illustration of a mass transport complex offshore Morocco (Dunlap et al. 2010). .. | 275 |
| Figure 8-4: Seismic line illustrating the upper surface of the mass transport deposit acting as a detachment layer..... | 277 |
| Figure 8-5: The process of mass transport emplacement can be related to the cannibalisation and focussing of outflow from a canyon system. | 279 |

| | |
|--|-----|
| Figure 8-6: The evolution of the large-scale levees; low sediment input into the canyon leads to low-energy deposits being fed from the canyon. | 280 |
| Figure 8-7: Illustration of multiphase levee construction; the various coloured intervals are indicative of several different phases of construction. | 281 |
| Figure 8-8: Isochrone of the interval between..... | 283 |
| Figure 8-9: Seismic line highlighted in Figure 8 9 that shows the faulting present at horizon 465, but absent at the top of the mass transport complex. | 283 |
| Figure 8-10: Similarity attribute for horizon 425, with inferred stress regime indicated. | 284 |
| Figure 8-11: Gravity free air anomaly map showing the location of oceanic fracture zones; the survey area is highlighted by the red polygon. | 286 |
| Figure 8-12: Upper Cretaceous isochrone, illustrating the presence of a structural nose running from the north-west to the south-east. | 287 |
| Figure 8-13: Seismic line illustrating the truncation of the Mid Albian (horizon 785) by the Senonian unconformity (horizon 680). | 289 |
| Figure 8-14: Thickness of the Albian to Turonian interval (between horizon 785 and 680) the location of Figure 8-13 is highlighted in red. | 290 |
| Figure 8-15: Cenozoic thickness in twt, note the thickening towards the south-east. | 290 |
| Figure 8-16: Thickness of the Palaeogene in twt..... | 292 |
| Figure 8-17: Thickness of the Neogene in twt. | 292 |
| Figure 8-18: Similarity attribute for Middle Miocene (horizon 160), showing the main strike-slip and compressional trends. | 293 |
| Figure 8-19: Thickness of the Pliocene to recent interval (between sea bed and horizon 100). | 294 |
| Figure 8-20: Isochrone of the Upper Miocene thickness (between horizons 100 and 130). | 295 |
| Figure 8-21: Perspective view of the isochrone of the thickness of the Middle Miocene interval (between horizons 130 and 160). | 296 |
| Figure 8-22: Perspective view of the Lower Miocene isochrone. | 297 |
| Figure 9-1 Seismic line illustrating the relationship between the upper surface of the mass transport complex (yellow horizon) and the tectonic deformation in the overburden | 304 |

List of Tables

| | |
|--|-----|
| Table 5-1 Horizon identification..... | 73 |
| Table 7-1: Calculated lateral displacement along the Avon/Mahin zone. | 262 |

Appendix A

| | |
|------------------------|-----|
| Two-way time maps..... | 323 |
|------------------------|-----|

Chapter 1

Contents

| | |
|---|----|
| 1. Introduction..... | 1 |
| 1.1 Rationale | 1 |
| 1.2 Hypothesis..... | 2 |
| 1.3 Structure of the thesis..... | 3 |
| 1.4 Overview | 4 |
| 1.5 What are the key focus areas? | 9 |
| 1.5.1 Mass transport deposits as the base of Cenozoic deformation | 9 |
| 1.5.2 Strike-slip faulting | 9 |
| 1.5.3 Levee construction | 10 |
| 1.5.4 Intra-levee deformation..... | 10 |

1. Introduction

1.1 Rationale

The nature of deltaic deformation has been studied in connection with the search for and production of oil and gas in Nigeria for well over a century (Short and Stauble 1967; Evamy et al. 1978; Haack et al. 2000). The majority of this time was devoted to the evaluation of the proximal regions that were accessible by onshore or shallow-water drilling rigs. In the past 25 years, the introduction of drilling rigs capable of operating in water depths of up to three kilometres has allowed the exploration of that portion of the Niger Delta previously beyond the reach of the drill bits.

The advent of deep-water drilling rigs was coincident with the growth in the use of 3D seismic technology that allowed previously unavailable spatial imaging of the sediments within the subsurface to be achieved. These two technologies – 3D seismic and deep-water drilling – has led to the widespread evaluation of many deep-water sedimentary settings among which Cenozoic deltas, such as the Niger Delta, form a significant proportion. In particular, the use of 3D seismic data has led to a greater understanding of the structure and sedimentology present in deep-water settings.

The economic significance of deep-water deposits has led to the need to gain a better understanding of the distribution of deep-water sediments and structural deformation. The bulk of the hydrocarbons found in deep-water settings are described as being reservoired in either slope-channel deposits, ponded amalgamated turbidites, or basin floor fans.

Among the sedimentary aspects of deep-water deposits that 3D seismic data has enabled is recognition of the role of turbidity currents and ocean-bottom currents in the distribution of sediments. An understanding of the interaction of deep-water sedimentary processes is required to gain a better understanding of the distribution of coarse-grained material, which is the target for exploratory drilling. The widespread distribution of mass-transport deposits has also been recognised as a result of the increased use of 3D seismic. In this study, the impact of these sedimentary processes on subsequent tectonic deformation has been investigated using information found within a 3D seismic volume.

In the Niger Delta, a number of commercially exploitable accumulations of oil and gas have been discovered within sediments of Miocene to Pleistocene age. The search for additional hydrocarbon accumulations may well involve drilling to deeper stratigraphic levels – to the Oligocene and perhaps the Cretaceous. A clearer understanding of the nature of the sediments at these deeper levels will, therefore, be of benefit to those involved in the study of the nature of deep-water depositional processes.

The nature of deltaic sediments is such that there is in general a coarsening upwards of the grains and bedding within the stratigraphic column. Drilling below the sand-rich, upper layers was often hampered by the presence of overpressures, which prevented deeper penetration of the subsurface. A better understanding of sediment distribution, tectonic stresses, and the nature of overpressure will be useful in a reduction of the risks involved in future exploration efforts.

1.2 Hypothesis

The Niger and Benue Rivers have deposited a thick sedimentary sequence, interpreted to reach in excess of 9,000 metres (Evamy et al. 1978), which has built out from the east and spread across an unconstrained sea floor in an arcuate pattern (Wu et al. 2015). The Delta is divided into two major lobes, one of which has built out towards the south (Doust and Omatsola 1990) and the other towards the west (Corredor et al. 2005). This western prograding lobe has a northern limit that is not constrained by the deltaic sediment budget but by the presence of a west-to-east striking shelf that marks the southern limit of the West African continental margin. This shelfal sequence and its associated deep-water apron is referred to as the Benin Basin (Kaki et al. 2012).

The sediments within the southern extent of the Benin Basin are poorly constrained due to the extreme water depths and consequent limited well penetration. A well-defined shelf margin is present, which has been a feature since the middle Cretaceous (Morgan 2003; Basile et al. 2005; Heine et al. 2013). This margin has been subjected to several

episodes of erosion and shelf collapse and is cut into by a number of canyons (Olabode and Adekoya 2008).

The sediments that have been shed from the episodic headwall erosion of the Benin Basin shelf have been deposited continuously since the Albian, whereas the deposits that have been derived from the Niger River have been laid down since the Eocene (Evamy et al. 1978). The presence of the Benin Basin sedimentary sequence is interpreted to have played a key role in the tectonic deformation of the later-deposited Niger Delta deposits.

It is the intention of this thesis to demonstrate that the structural configuration seen in the present day is a result of not only conventional deltaic tectonic deformation (Morley 2003; Wood 2011; Wu et al. 2015) but also the morphology and sedimentology of the pre-existing underlying strata.

The morphology of the section that predates the onset of sedimentation from the Niger River has been mapped, and it will be shown that this relates primarily to the influence of the presence of canyons along the Benin Basin shelf margin. In particular, the canyons have provided conduits for the focussed deposition into deeper waters of large-scale levees and mass-transport deposits. These levees and mass-transport complexes will be shown to play a key role in the deformation of the overlying Niger Delta-sourced sediments.

The nature of the subsequent Cenozoic deformation, both in terms of timing and magnitude, is examined in this thesis and in particular, the presence of a number of strike-slip fault zones will be described. Estimates of the degree of lateral displacement have been made using three separate approaches which indicate lateral displacements in excess of 7 kilometres.

1.3 Structure of the thesis

This thesis is broken down into five principle parts.

- A review of the current state of understanding of deltaic tectonics and the regional sedimentology and stratigraphy (Chapters 2 and 3).
- An outline of the data available and the methods used to evaluate the data (Chapter 4).
- A description of the results obtained from interpreting of the data (Chapters 5, 6, and 7).
- A summary of the observations that can be inferred from the results (Chapter 8).

- A suite of conclusions that can be reached, from the analysis (Chapter 9).

1.4 Overview

The area covered by the 3D volume, outlined in red in Figure 1-1, lies offshore Nigeria in the north-west region of the present-day Niger Delta Basin, some 70-100 kilometres to the south of Lagos. The present-day water depth ranges from approximately 800 metres to in excess of 2,500 metres. (Figure 1-3) The data were acquired as a non-exclusive survey by PGS in advance of the Nigerian government's 2005 licence round in which blocks OPL 315, 321, and 323 were offered for complete bids. In the licence blocks immediately to the south of the 3D survey area are three significant oil and gas fields – Bonga, Erha, and Bosi, reservoirised within Miocene-aged slope-channel deposits (Chapin et al. 2002; Morgan 2003, 2004; Deptuck et al. 2007). At the time of writing, the two southern blocks covered by the 3D data are subject to a legal dispute as to the ownership of the licence.

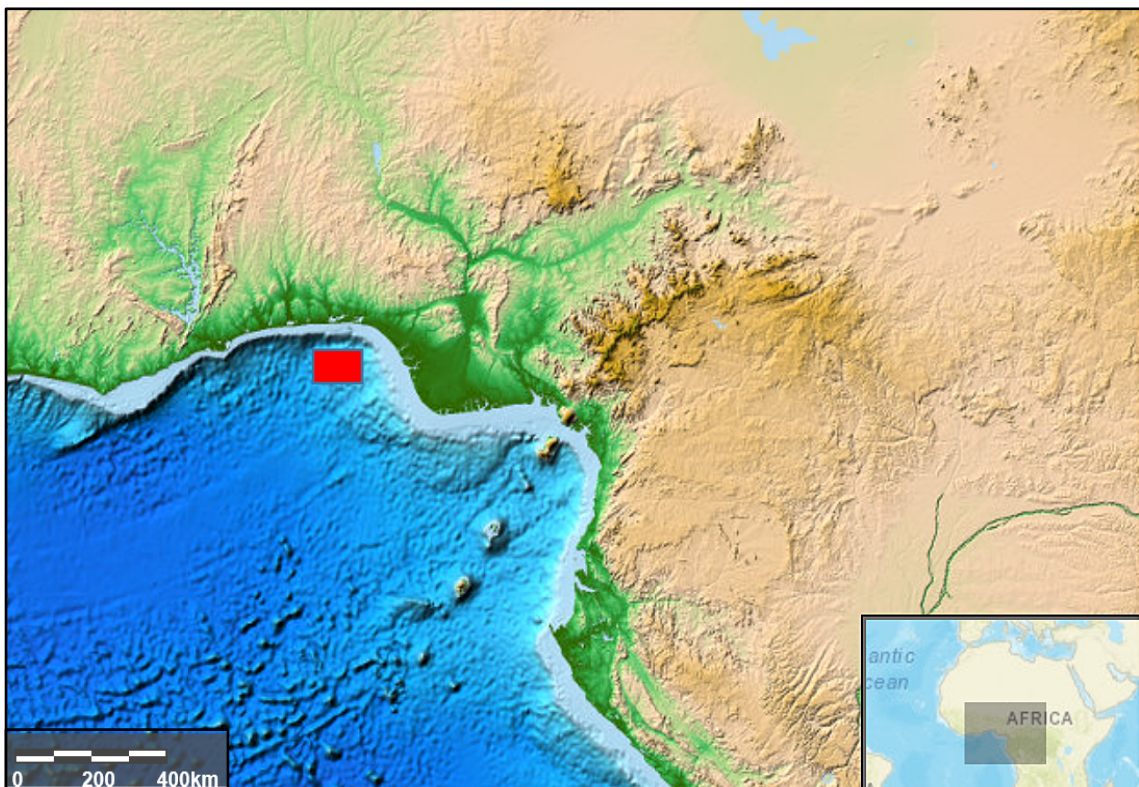


Figure 1-1 Location of the study highlighted by the red polygon, superimposed on the bathymetry and digital elevation of the Gulf of Guinea derived from satellite altimetry (Sandwell et al. 2014).

Exploration and production of hydrocarbons from the Niger Delta is well-established and widespread (Short and Stauble 1967; Evamy et al. 1978; Haack et al. 2000; Reijers

2011), with the early production being focussed onshore and along the present-day shelf. Deep-water exploration in the 1990s led to the discovery of a number of fields reservoired in turbiditic deposits (Chapin et al. 2002; Deptuck et al. 2007). These fields are defined by a combination of both structural and stratigraphic trapping; both the slope channels and ponded amalgamated intervals drape over anticlines that were formed post-deposition as a result of gravitational deformation (Deptuck et al. 2003; Corredor et al. 2005; Deptuck et al. 2007; Kostenko et al. 2008; Leduc et al. 2009). Lateral seal is limited by the stratigraphic nature of the channel margins and mini-basin margins, which are bounded by fine-grained levees. To the north of the survey area, a number of exploration wells, drilled both onshore and in the shallow waters close to Lagos, have encountered a Cenozoic and Cretaceous sequence of both clastic and carbonate composition (Adeleye 1975; Onuoha and Ofoegbu 1988). The Cretaceous-aged deposits now lie beneath a thick Cenozoic section, which is comprised of predominantly marine fine-grained material.

The sediments found in these northern wells lie in the eastern portion of the Benin Basin, a Cretaceous-to-Cenozoic basin that was initiated during the middle Cretaceous at the time of the break-up of Gondwana, which led to the separation of Africa from South America (Fairhead and Binks 1991; Guiraud et al. 1992; de Matos 1999; Guiraud et al. 2005). The oldest sediments that are present in the study area are assumed to be Syn-rift deposits of Barremian age, being the conjugate basin to the Potiguar basin in Brazil (de Matos 1999; Heine et al. 2013). The section can be identified within the 3D volume as a series of complexly faulted half grabens, truncated by an angular (break-up) unconformity.

Overlying the break-up unconformity within the area covered by the 3D is a section of probable Aptian to Turonian age; because there has been no well penetrations of the section, this cannot be confirmed. The section on-laps the break-up unconformity and is not present in the wells drilled into the Cretaceous shelf sediments to the north (Kaki et al. 2012). The section is separated by a bypass zone from the shelfal sediments. A regional tectonic episode in the Santonian gave rise to the Senonian unconformity (Guiraud and Bosworth 1997). The origin of this unconformity is linked to change in the pole of rotation of the African craton, following the initial separation of the African plate from the South American plate (Fairhead 1988; Heine et al. 2013). The effects of this episode of motion alteration led to a hiatus in sedimentation as the African Craton underwent localised uplift (Guiraud and Bosworth 1997).

Sedimentation resumed in the Campanian with a global sea-level rise (Haq et al. 1987). The presence in the outcrop of a marine and fluvio-deltaic sequence to the east of the present-day Niger Delta (Benkhelil et al. 1998) may indicate that there was a significant

delta present in the Upper Cretaceous that underlies the present-day Niger Delta. There is evidence within the seismic volume of Upper Cretaceous compressional features that may be related to the compressional toe of a palaeo Benue Delta.

The early Cenozoic (Palaeocene to Eocene) is found in the wells drilled on the shelf to the north of the studied region. This Palaeogene section is interpreted to have been cannibalised through a process of shelf collapse, which led to the widespread distribution of mass-transport deposits downslope and into the area covered by the 3D data (Maloney et al. 2012).

In the studied area, the Eocene to present-day section is dominated by the presence of the Niger Delta pro-delta slope, which has prograded westwards; the extent of the sediments fed into the Gulf of Guinea by the Niger River extends out to the abyssal plain, well to the west of the region of study (Davies et al. 2005; Wu et al. 2015).

There are a number of distinctive sedimentary facies recognised within the data. The most striking are a suite of ridges and synclines in the Palaeogene section and the slope channel complexes in the Neogene. In both intervals, a series of mass-transport complex deposits (MTC) are recognised. Canyons to the north of the study area, the Avon (Olabode and Adekoya 2008), Lagos, Mahin, and Seme are believed to be the source of a number of Palaeogene slope deposits in the western region of the study, whereas in the east, the slope channels appear to be derived from an eastern canyon system, assumed to be either the Benin or Opuama canyons (Petters 1984; Deptuck et al. 2007). The slope deposits within the Neogene are known to be prolific hydrocarbon reservoirs. There are no known Palaeogene hydrocarbon accumulations within the deltaic section.

In the study area, a number of slope channel systems can be mapped, along with late stage structural modification. However, in the area covered by the 3D volume, there is a distinct structural difference when compared to the tectonic styles found to the south (Bilotti and Shaw 2005; Cobbold et al. 2009; Leduc et al. 2012).

The main structural feature that cuts through the strata is a north-east to south-west lineament, which is interpreted to be the result of right-lateral movement within the Cenozoic interval (Leduc et al. 2012). This lineament, herein referred to as the Avon/Mahin fault zone, is sometimes referred to as the north-western limit of the Niger Delta. This definition is misleading because the sediments that originate from the Delta are present to the west of the lineament. In chapter 6, concerning sedimentology, it will be demonstrated that the slope channels that originate from the Niger Delta pass through the survey area and cross this lineament. There are several other faults present to the west of the Avon/Mahin strike-slip fault zone that are also interpreted to be strike-slip faults. This structural deformation is discussed in chapter 7.

In addition to the transcurrent lineament, there is a marked vertical separation of the sedimentary section, with a relatively undisturbed deep section of presumed Cretaceous age and a younger tectonically modified section of Cenozoic strata. The upper deformed interval is separated from the deeper section at the top of a mass-transport deposit.

Previous authors have offered a number of explanations as to the nature of the detachment; all assume a degree of overpressure is required to facilitate the dislocation (Poblet and McClay 1996; McClay et al. 2003; Rowan et al. 2004; Shaw et al. 2004; Corredor et al. 2005; Wiener et al. 2009). Overpressures result from the excess loading by the overburden of confined water trapped within the sedimentary section due to low permeability. Among the causes of overpressure are the rapid deposition of fine-grained sediments that prevent the escape of bound water, the generation of hydrocarbons, and their expulsion and clay diagenesis. In this thesis, the role of mass-transport deposits in the generation of overpressures is added to the list of possible detachment enablers.

The principle stress acting in the deep-water sediments is thought to be horizontal. This occurs due to the thick sediment pile in the proximal delta setting exerting a greater gravitation force than the water layer and thinner sediment package in the deep water (Damuth 1994; McClay et al. 2003; Rowan et al. 2004; Cartwright and Jackson 2008; Mulder 2011). The presence of a gently dipping slope coupled with a lateral stress gradient between rocks at a similar depth triggers lateral movement down-slope (gravitational sliding). The sliding takes place along the surface with the lowest frictional resistance (Schultz-Ela 2001) and the lowest shear strength (Twiss and Moores 2007).

In the case of the MTC, there are no coherent bedding planes observed and a high frictional resistance within the MTC is interpreted; hence, the sliding takes place in the deepest laterally continuous sediments with accompanying low-frictional stress that immediately overlie the MTC, which also coincides with the over-pressured zone.

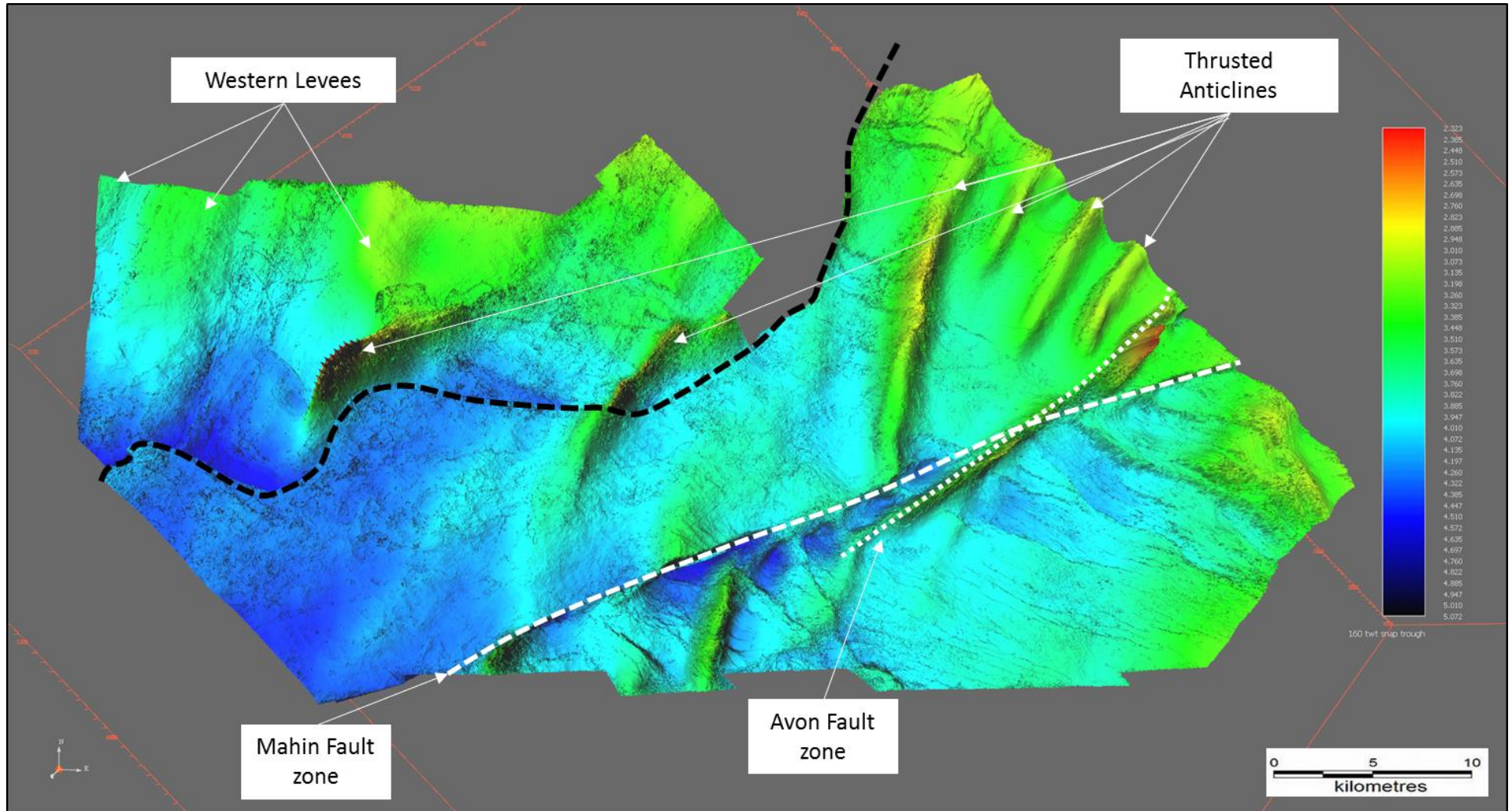


Figure 1-2: Perspective view of a two-way time composite Miocene horizon illustrating the key structural elements within the survey area. The black dashed line marks the change in horizon – the horizon north-west of this line has been eroded by the influx of sediments from the Avon Canyon, which lies to the north. Warm colours represent short travel times.

1.5 What are the key focus areas?

The four main topics that have been examined in this study are linked by the sedimentary influence on the tectonic history of the region. The mass-transport deposits, large-scale levees, and Niger Delta sediment thickness all contribute to the subsequent structural deformation. This framework has been used to study the sedimentary inputs and structural deformation.

1.5.1 Mass-transport deposits as the base of Cenozoic deformation

The Cenozoic deformation observed within the data is interpreted to be linked to the presence of an apron of mass-transport deposits that are assumed to be early Cenozoic in age. The extent of these mass-transport deposits goes beyond the extent of the 3D survey. However, within the 3D volume, it has been possible to map a number of these features. In the western half of the study area, two distinct mass-transport complexes are mappable, having their sediment source to the north of the survey. The base of the mass-transport complex is a regionally extensive seismic reflection. This regionally widespread basal surface appears to correspond to a possible forced regression (Posamentier et al. 1992) and may be related to the cessation of sediment supply at the end of the Cretaceous at a time of a relatively high sea level. The upper surface of the complex has an irregular top, with the surface infilled by pelagic sediments. A number of authors (Bull et al. 2009; Richardson et al. 2011; Shipp et al. 2011; Alves 2015) have made observations about the morphology and kinematics of mass-transport complexes; the similarity to the referenced mass-transport deposits has been used to reinforce the interpretation in this study. In this thesis, the influence of the upper surface of the complex as a key component for later structural deformation will be outlined.

1.5.2 Strike-slip faulting

There is a major transcurrent fault zone (christened the Avon/Mahin fault zone in this thesis) that passes through the survey (Figure 1-2); however, there are other examples of presumed fault-related lateral displacements observed within the data. The quality of the data is such that the imaging of these fault zones enables some detailed mapping to take place, which suggests a multi-stage history of movement. Estimating the lateral displacement along these strike-slip faults has been attempted; the results are inconclusive as to the total amount of lateral displacement because the survey does not extend to the limits of the fault zone. Estimates of lateral displacement within the limits of the survey have been made using piercing points of

both structural as well as sedimentary intersections with the fault zones. It would appear that a dextral displacement in the region of 7 kilometres can be demonstrated for the south-western portion of the fault zone. In the following chapters, this deformation will be discussed in detail, with examples of the structural styles and the displacement calculations.

The displacement does not take place along a single through-going fault but by via a combination of extensional and compressional fault assemblages. Examples of the structural style will be presented in chapter 7.

1.5.3 Levee construction

The outflow of sediment from the canyons that are known to be present to the north of the survey boundary are inferred to have focussed sediment supplied into the study area (Olabode and Adekoya 2008); this has contributed to the construction of a number of elongate ridges whose elongate axis are approximately orthogonal to the palaeo-shelf margin.

The presence of large-scale depositional bodies in deep-water settings have been the subject of several recent studies that have focused on the role of both turbidity currents and bottom-circulating currents. This has led to the recognition of geometries within seismic data that are interpreted to be indicative of both levees and contourite drifts. The ridges noted in the section above share some geometric similarities with levees but also the contourites. This geometry and the nature of the ridges is covered in chapters 6 and 7.

1.5.4 Intra levee deformation

In the western half of the survey area, where the section is less affected by the Miocene tectonic overprint, there are a number of elongate ridges, as noted above, which have been structurally modified during the Palaeogene. What is striking about these ridges is the unusual internal deformation, which is also assumed to be influenced by gravity-driven lateral movements. In this case, the internal deformation is not necessarily related to the gravitational influence of the Niger Delta, which during the Palaeogene was modest in comparison to its current extent. It is likely that the deformation is due to local downslope movements within the ridges arising from variable overburden loading. The tectonic deformation that took place is predominantly compressional and trans-tensional and will be described in detail in chapter 7.

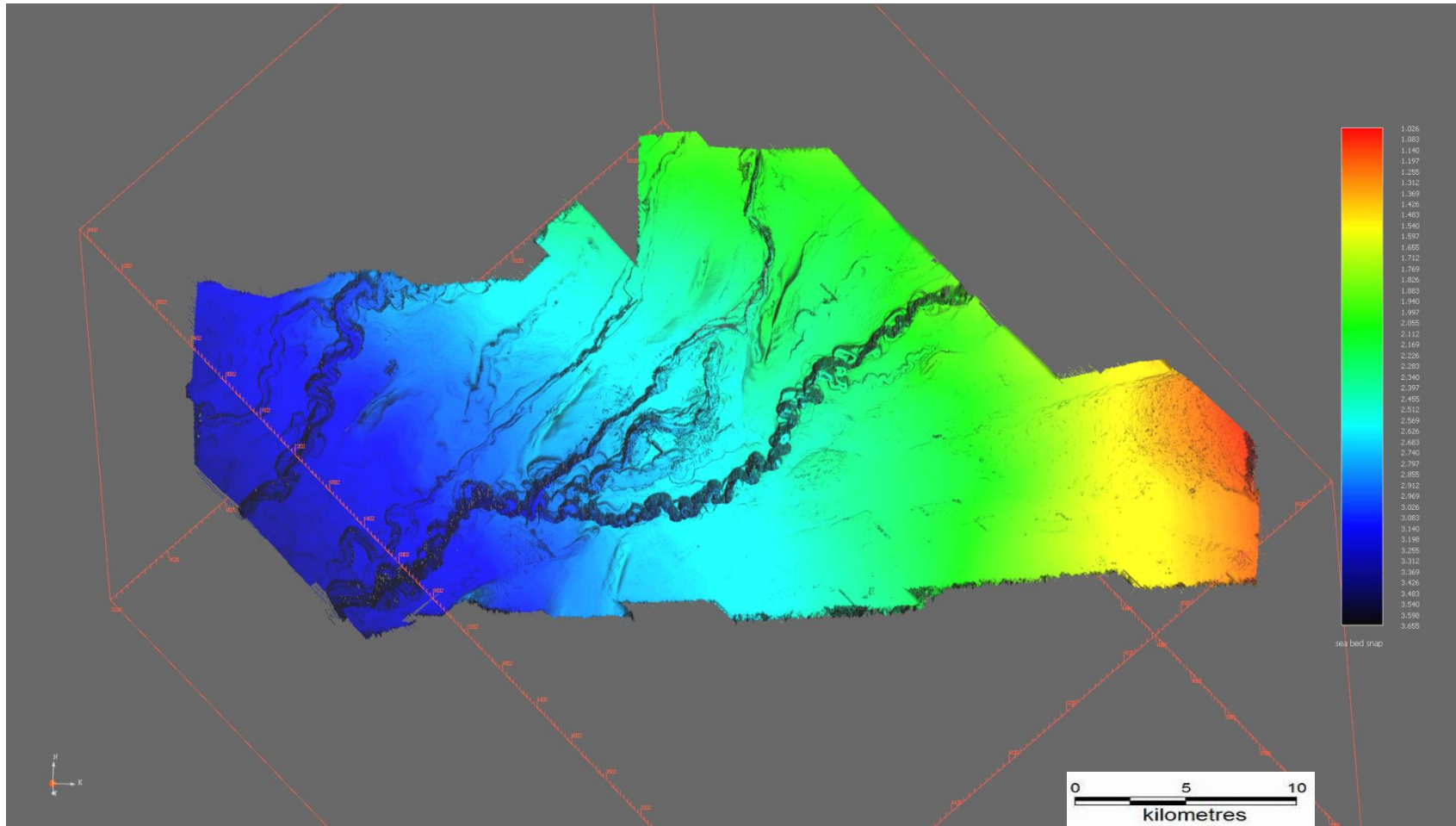


Figure 1-3: Sea bed two-way time perspective view; warm colours represent shallow values.

The meandering channels seen in the above illustration are sourced from the Mahin Canyon in the north-east and the Avon canyon to the north of the survey.

Chapter 2

Contents

| | | |
|-----|---|----|
| 2 | Deltaic deformation..... | 12 |
| 2.1 | Introduction..... | 12 |
| 2.2 | Extensional zone | 13 |
| 2.3 | Transition zone | 15 |
| 2.4 | Compressional zone (outer thrust belt)..... | 15 |
| 2.5 | Diapir zone | 16 |
| 2.6 | Inner thrust belt..... | 18 |
| 2.7 | Detachment surface..... | 18 |

2 Deltaic deformation

2.1 Introduction

The major focus of this study has been the structural deformation present within Cenozoic sediments in the deep water region of the present day Niger Delta. In order to explain the observations that have been made, they have to be placed within the context of what is already understood about deformation in deltas such as the Niger. In this chapter, the current view of deltaic tectonics is reviewed.

The Cenozoic strata in the Niger Delta, similar to other large deltas worldwide, can be divided into three main regions of structural styles (Crans and Mandl 1980; Crans et al. 1980; Crans and Mandl 1981). These three regions are the proximal, extensional belt, the distal compressional belt and an intervening transition zone (Lehner and De Ruiter 1977; Doust and Omatsola 1990; Damuth 1994; Corredor et al. 2005).

In the case of the Niger Delta, a further subdivision of the delta into five structural domains is put forward to explain observations, the two additional domains being the diapir zone and the inner thrust belt (Bilotti and Shaw 2005; Corredor et al. 2005). A further component, the strike slip or tear faulting, is noted at the margins of the sediment cone, which is formed by the outbuilding of clastic sediments. One additional component that exists in the Niger Delta is the presence of fossil transform faults, which are present in the oceanic crust that underlies the distal portion of the delta (Davies et al. 2005; Wu et al. 2015). The role of transcurrent faulting within this deltaic setting was recently addressed in a paper by Leduc (2012). The nature of this strike slip faulting was studied

further in this thesis and insights into the kinematics and appearance of this strike slip fault zone are presented in section 7.3.7. One of the main observations in the literature is the ubiquitous assumption of a basal detachment layer (McClay et al. 2003; Morley 2003; Wiener et al. 2009). Although the detachment layer is an integral part of the deformation narrative, little is known about its true nature, as it generally lies in the zone where seismic imaging is either poor or the vertical resolution is low. In this study, it was possible to examine in some detail the seismic expression of the basal detachment (Mourgues et al. 2009). These observations will be outlined in section 7.3.2.

In Figure 2-1, taken from papers by Kostenko (2008a) and Corredor (2005), the lower sections are a non-interpreted version of the seismic cross section through the key structural domains. The upper cross section is a drawing that outlines the deformation that has been interpreted using data of similar quality to that seen in the lower image. The non-interpreted image highlights the difficulty of assigning a reliable set of observations about the nature of the detachment layer that lies at the base of the section.

2.2 Extensional zone

The extensional zone is characterised by large, down-to-the-basin growth faults that are described as listric, implying that they flatten at depth and sole out on a basal slippage surface (Imber et al. 2003). In addition to the down-to-the-basin, synthetic faults, counter regional faults are often also present (Sapin et al. 2012) that hade in the opposite direction to the synthetic faults (Bruce 1973; Doust and Omatsola 1990; McClay et al. 2003; Morley 2003; Sapin et al. 2012). This combination of synthetic and antithetic faulting has been used to divide the onshore Niger Delta into “depobelts” (Doust and Omatsola 1990). Typically, coarse grained material is deposited in the hanging wall of the down to the basin faults, with thousands of feet of sand aggrading in close proximity to the fault. The sands are assumed to have a higher density to the distal clays, which adds to the overburdened stress imbalance (Evamy et al. 1978).

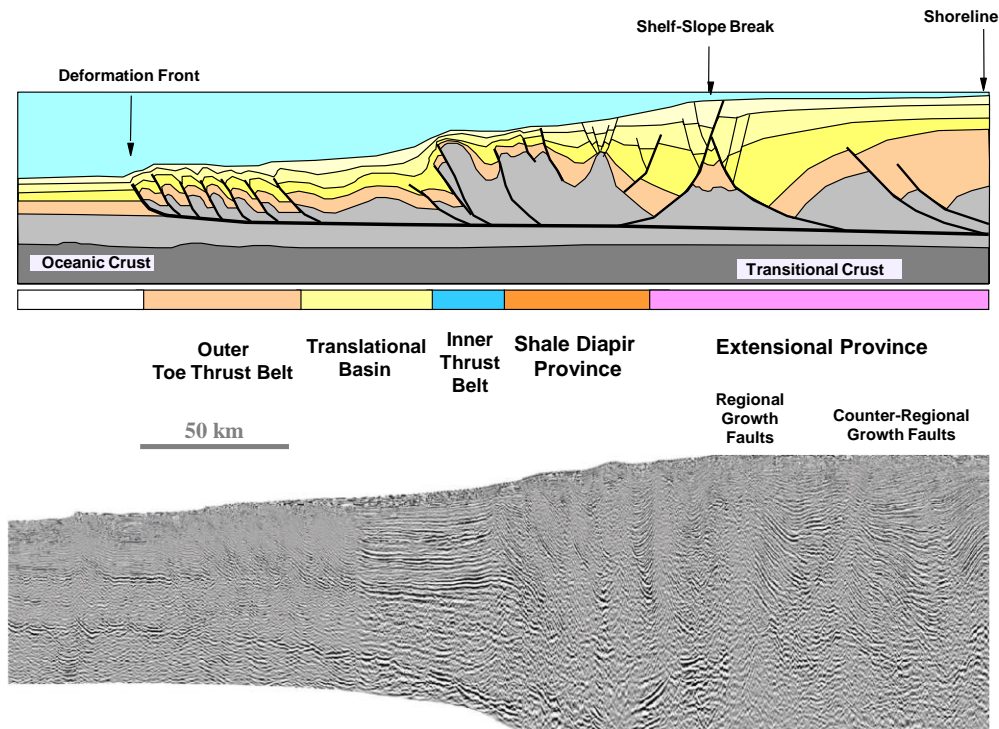


Figure 2-1: A regional seismic traverse through the Niger Delta highlighting the five structural domains (Corredor et al. 2005).

2.3 Transition zone

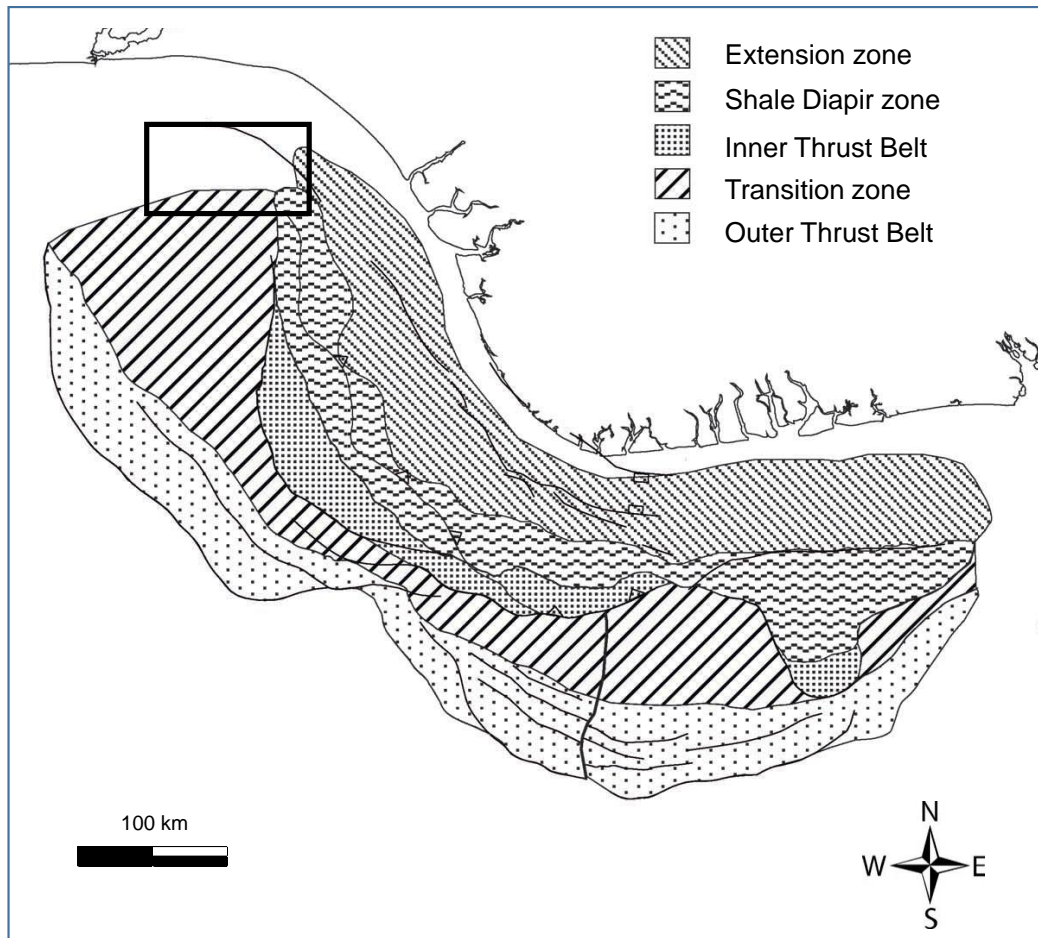


Figure 2-2: Map illustrating the distribution of the five structural regions of the Niger Delta; the area covered by this study is highlighted by the black rectangle (taken from (Corredor et al. 2005)).

The transition interval is largely unaffected by significant structural deformation. As the lateral stress regime ranges from extensional in the proximal region to compression in the distal region, the intervening interval passes through a zone of little effective lateral stress (Damuth 1994; Morley and Guerin 1996; Bilotti and Shaw 2005).

2.4 Compressional zone (outer thrust belt)

The outer compressional belt can be recognised by the presence of a series of imbricate thrust anticlines, which are well imaged with both 2D and 3D seismic data and appear to sole out into a common detachment layer (Bilotti and Shaw 2005; Corredor et al. 2005; Kostenko et al. 2008; Maloney et al. 2010). In deep water, the quality of seismic data is of a considerably higher quality than data acquired in both shallow water and onshore.

This is primarily due to the absence of multiple reflections and relatively slower velocities that provide higher resolution. However, there are still lateral velocity variations in the section, which can, if not correctly depth migrated, lead to image distortions under the apex of the anticlines.

In the case of the Niger Delta, the three part subdivision has been further refined by Corredor (Corredor et al. 2005) to include an inner thrust belt and a shale diapir province, based on the interpretation of a regional grid of 2D seismic data. These regions are highlighted in Figure 2-2. The location of the outer thrust belt has been the subject of study by a number of authors, among the more recent (Bilotti and Shaw 2005; Tuitt et al. 2012). The variation in the shear strength of the basal surface and the critical angle that exists at the toe region of the sediment wedge have been invoked to explain the nature of these compressional features (Cobbold et al. 2009).

2.5 Diapir zone

In the more proximal regions of the delta, seismic data is less well imaged, although improvements in migration algorithms are leading to better imaging of deeper and more complex sections. The poor imaging of reflections has been interpreted as indicating no internal bedding being present and as such, these reflection free zones have been considered to be an amorphous zone of fluidised shale, as illustrated in Figure 2-3 (Bruce 1973; Mascle 1973; Cohen and McClay 1996). Improvements in migration algorithms have allowed coherent seismic horizons to be imaged in regions previously considered to be comprised of mobile shale (Van Rensbergen et al. 1999; Aikulola et al. 2010; Maloney et al. 2010; Elsley and Tieman 2011).

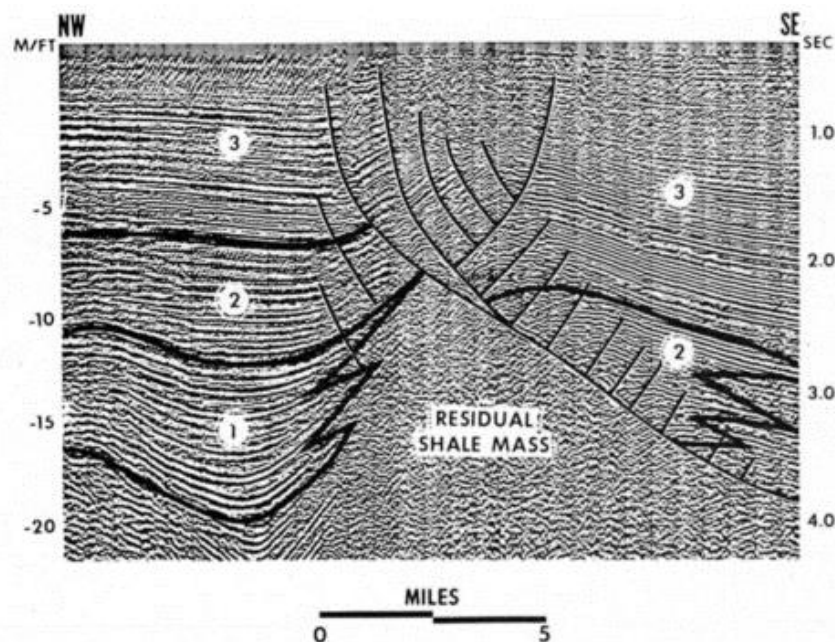


Figure 2-3: An example of the quality of imaging that gave rise to the concept of shale diapirism (taken from Bruce, 1973).

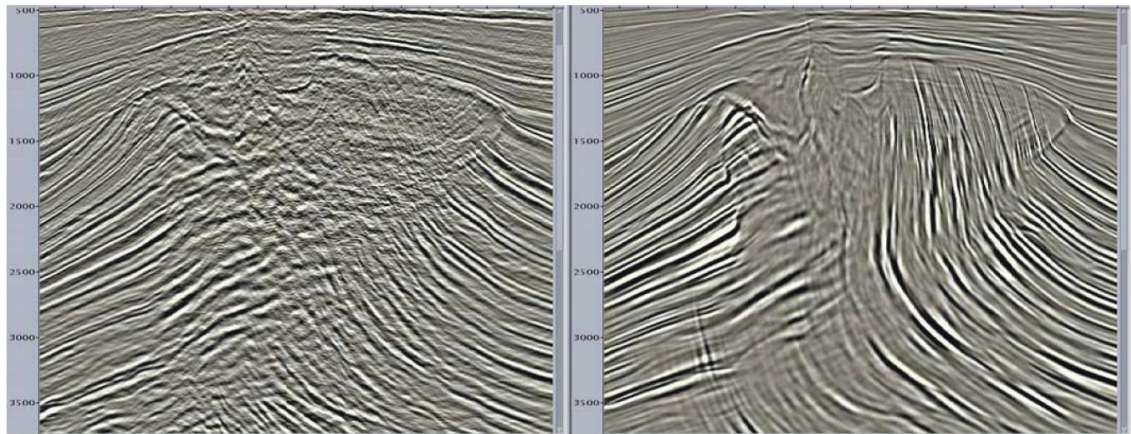


Figure 2-4: image illustrating the change in seismic data imaging, which allows for steeply dipping data to be correctly identified.

The images above illustrate improvements in seismic imaging that has led to the recognition of steeply dipping reflectors in an interval previously interpreted to be a shale diapir (Elsley and Tieman 2011).

The nature of mobile shale is poorly understood, and outcrops of supposed mud diapirs are few and far between (if any). Cases of shale diapirism quoted often refer to Brunei (van Borren et al. 1996) and Trinidad (Moscardelli et al. 2006). What is common to both of these regions is the presence of mud diatremes (volcanoes) and fault planes filled with mobilised mud; what is not observed are masses of amorphous structureless shale.

These diatremes represent the surface expression of a pressure release in the subsurface of pore pressures in excess of the fracture gradient of the overburden. Numerous examples of such “mud volcanoes” have been observed in the Niger Delta (Graue 2000).

Typically, these diatremes are located at the apex of subsurface structures, where there is a lateral pressure difference between fault compartments that cut through the structure. The fluid escapes that take place often have a detrimental effect on seismic data (through which the fluids have passed), adding to the difficulty of interpreting these diapiric features. The large scale deformation of supposedly ductile mud is more difficult to characterise, as there are no outcrops that can be employed to represent a large scale shale diapir.

The assumed mechanism for the presence of mud diapirs is related to the overpressured nature of under-consolidated shale with a high water content, which rises through the subsurface under the effect of buoyancy (Masclé 1973; Damuth 1994; Cohen and McClay 1996). The absence of any surface expression of such mobile shale has been attributed to the process whereby overpressure bleeds off as the shale mass rises to a point of hydrostatic equilibrium (Vendeville and Jackson 1992).

2.6 Inner thrust belt

Inboard of the transition zone is a region of high angle thrust anticlines, which several authors refer to as the inner thrust belt (Corredor et al. 2005; Cobbold et al. 2009; Maloney et al. 2009). The origin of this structural terrain is not well documented. One possible explanation for the presence of this zone is outlined in Chapter 6 of this paper. As noted in both the depositional and structural description chapters, there is evidence of a Cretaceous delta that preceded and currently underlies the present day Niger Delta (Benkhelil et al. 1998; Guiraud et al. 2005).

2.7 Detachment surface

In large deltas, lateral and vertical stresses originate from the variation in thickness between the proximal, thick, section and the distal relatively thinner section (Chapple 1978; Morley 2003; Rowan et al. 2004). The overburden stress relates to the gravitational force associated with the thickness and density of the overlying interval, which comprise both sediment grains and intergranular water. In the proximal setting, the overburden at a given depth is predominantly porous lithified rock, whereas the distal portion of the delta sediments are often less well lithified and consequently, have a higher water content and lower density, and are covered by a column of water. At similar depths, the vertical stress is therefore significantly different between the proximal and distal regions. In the presence of a dipping set of strata, this imbalance gives rise to lateral stress that is sufficient for inducing (sub) horizontal movement along an assumed basal detachment zone (Short and Stauble 1967; Masclé 1973; Damuth 1994; Cohen and McClay 1996; Morley and Guerin 1996; Onuoha 1999; Graue 2000; Schultz-Ela 2001; McClay et al. 2003; Bilotti and Shaw 2005; Corredor et al. 2005; Briggs et al. 2006; Maloney et al. 2012).

The nature of the basal detachment layer is poorly understood in the case of the Niger Delta, as no wells have been drilled through it to date. Wells that have been drilled into the thrust anticlines encounter overpressure with depth, typically around 2500m below

the sea bed (Bilotti and Shaw 2005); the wells, located in the deep water region, have been terminated above the detachment (Bilotti and Shaw 2005; Kostenko et al. 2008).

For the majority of the Niger Delta, the basal detachment layer is not well imaged on seismic data. In order to explain the behaviour of the thin skinned deformation, the nature of the basal detachment has been modelled (Chapple 1978; Mitra 2002; McClay et al. 2003; Bilotti and Shaw 2005; Corredor et al. 2005; Cobbold et al. 2009; Zhang 2013). All models for explaining deformation invoke a basal layer that has lower frictional resistance to motion due to low shear stress. The nature of this basal zone and its origin have been theorised and there is consensus that an overpressured interval is involved that acts as a lubricant for the lateral motion of the overburden. The origin of the overpressure, which lowers the effective stress in the detachment layer, is poorly understood; explanations for the phenomenon include the rapid burial of sediments that entrap water in low permeability rocks (Osborne and Swarbrick 1997; McClay et al. 2003), as well as the generation and expulsion of hydrocarbons (Cobbold et al. 2004; Cobbold et al. 2009).

The deformation observed in the Niger Delta and other regions of thin-skinned tectonic deformation can be explained in terms of the critical taper theory, which has been employed by a number of authors to explain the geometries observed (Chapple 1978; Dahlen 1990; Bilotti and Shaw 2005).

The critical taper assumption is based on the observation that a body will glide over a basal layer with an associated low frictional resistance, but once the resistance to basal motion reaches a critical level, the moving body will deform internally. In large scale deltas, this effect is observed where the thin-skinned interval terminates in the toe thrusting region, at the point where sliding is inhibited either by a change in slope or in vertical stress.

The critical taper theory invokes the need for a basal layer of low shear strength that allows for the glide of the overlying section when the overburden is of a certain thickness. In addition, a rise in shear strength or a decrease in overburden can cause the sliding to cease. In addition, the angle of dip of the basal layer and the angle of dip of the upper surface of the overburden also play important roles. The taper observed as the sediment wedge thins into the distal region of the Niger Delta sediments adheres to the above criteria, and lateral motion is inhibited as the thickness and basal stress conditions change.

The subsequent lateral motion can be reactivated should the overburden thickness increase, leading to multiphase deformation (Bilotti and Shaw 2005). This repeating process of lateral movement and subsequent lock up can lead to imbricated thrust zones.

Chapter 3

Contents

| | | |
|----------|-------------------------------------|-----------|
| 3 | Outline | 20 |
| 3.1 | Introduction..... | 20 |
| 3.2 | Plate tectonic aspects..... | 21 |
| 3.2.1 | Rifting | 21 |
| 3.2.2 | Drifting..... | 23 |
| 3.2.3 | Senonian Unconformity | 28 |
| 3.2.4 | Thermal Subsidence..... | 28 |
| 3.3 | Regional Stratigraphy | 30 |
| 3.3.1 | Lithostratigraphy..... | 32 |
| 3.3.2 | Chronostratigraphy | 34 |
| 3.3.3 | Sequence Stratigraphy | 41 |
| 3.4 | Regional Sedimentology..... | 41 |
| 3.4.1 | Niger Delta | 42 |
| 3.4.2 | Benin Basin | 42 |
| 3.4.3 | Deep-water Depositional Styles..... | 45 |

3 Outline

3.1 Introduction

To gain an understanding of the elements within the geological history of the region that impact upon this study, a review of published material was undertaken. A summary of the regional aspects are outlined in this chapter.

The location of the area of interest lies offshore south-west Nigeria at the junction of two present-day basin settings. The origin of these basins is linked to the separation of Africa from South America as a result of the plate tectonic activity that led to the formation of the South Atlantic Ocean (Lehner and De Ruiter 1977; Fairhead 1988; Nürnberg and Müller 1991; Basile et al. 2005; Heine et al. 2013). The motion of the African continent and its relationship to the oceanic spreading is one of the key components in gaining an understanding of the geological history of the region studied.

As a result of the opening of the South Atlantic Ocean, the region transitioned from a continental rifted domain to an open marine one (Basile et al. 2005; Heine et al.

2013). The resulting sediment dispersion that accompanied this transition is outlined within this chapter.

The survey area can be divided into four vertically separated mega sequences. The uppermost zone can be further divided into two laterally differing tectonic regions. The lowermost of the four vertically separated levels is the syn-rift of Neocomian age (de Matos 1992; Haack et al. 2000). The interval that overlies the syn-rift is a section that is assumed to be of Albian to Turonian age and is capped by the Senonian unconformity (Guiraud and Bosworth 1997); above this is an interval that is comprised of a sequence that is largely unaffected by large-scale tectonic deformation; the upper limit of this sequence is the basal detachment of the thin-skinned overburden (Morgan 2003; Bilotti and Shaw 2005; Cobbold et al. 2009). The upper interval has undergone a large amount of structural modification. Within this upper interval, the section is divided by a north-east to south-west trending lineament, the Avon/Mahin fault zone (Leduc et al. 2012).

3.2 Plate tectonic aspects

The West African region has its origins in the break-up of Gondwana during the early to middle Cretaceous. Prior to the break-up of the Gondwana super continent, the area that is now located in the Gulf of Guinea was attached to the north-east region of present-day Brazil (Wilson 1965; Fairhead 1988; Nürnberg and Müller 1991; Basile et al. 1993; Heine et al. 2013). A period of rifting preceded the break-up of the continent; during this rifting phase a number of basins were created, which were modified by the subsequent drifting apart of the two newly formed continents (Lehner and De Ruiter 1977; de Matos 1992).

3.2.1 Rifting

The separation of Africa from South America occurred in a number of stages and has been described by several authors (Hedberg 1970; Lehner and De Ruiter 1977; Austin and Uchupi 1982; Fairhead and Binks 1991; Heine et al. 2013). The earliest stage of tectonic activity that led to the separation of the two continents occurred in the lower Cretaceous (Fairhead and Okereke 1987; Fairhead 1988; Fairhead and Binks 1991; de Matos 1992), with the initiation of rifting. The evidence of the rifting is found in an outcrop in the Benue Trough, which lies to the east of the study area (Benkheilil et al. 1998) and in the Potiguar Basin of the conjugate margin in Brazil (de Matos 1999). Exploratory drilling has also confirmed the presence of Aptian-aged sediments within the rifted section in the onshore area around Lagos (Haack et al. 2000) and offshore in the recently discovered Aje and Ogo fields (Adeleye 1975; Haack et al. 2000). Further to the west in

Benin, exploratory drilling in the Seme field has also revealed a similar Neocomian section (Kaki et al. 2012).

The rifted basins observed in south-west Nigeria are the conjugate equivalent of the Potiguar Basin in Brazil (de Matos 1999; Heine et al. 2013). In the Nigerian/Benin continental region, the syn-rift basin is recognised on 2D and 3D seismic data, as a series of tilted fault blocks, which are truncated by an angular unconformity (Morgan 2003). The conjugate Potiguar basin is comprised of several half grabens, which have the controlling faults along the southern margin of the grabens. This geometry is observed in the rifted interval in the Benin Basin also, and this orientation fits well with the two sides of the ocean having been contiguous prior to the commencement of ocean spreading (Figure 3-3).

The interpreted rifted basin terrain is approximately 90 km from north to south, a similar extent to the Potiguar Basin (de Matos 1992, 1999). The southern limit of the basins visible within the seismic data may well be limited by the presence of a fossil fracture zone similar to the Chain fracture zone seen further to the south (Davies et al. 2005).

The onshore exploration of this syn-rift section has been carried out via the drilling of the Ise-1 and -2 wells and Afowo-1 well (Onuoha and Ofoegbu 1988; Haack et al. 2000); the interval is also known to have been found in the recent exploration wells Aje-4 and Ogo-1. The age assigned to the interval is Barremian or older. This interval in the Ise wells is interpreted to be the basal portion of the rift infill with the younger Aptian section having been eroded at the time of the break-up (Haack et al. 2000).

Within the study area there is evidence of deep rifting where there is strong evidence for the presence of a thick succession of sediments that fill the accommodation space created by the rifting. The top of this interval is marked by an angular truncation of the deeper section in the seismic volume. The section is up to two seconds thickness two-way time (Figure 3-10 and Figure 3-11).

In addition to the rifting observed in the Benin Basin, a significant rift system was formed to the east of the study area in the Benue Trough. Although not directly related to this study, the Benue Trough is interpreted to have been the location of a major delta that preceded the evolution of the Niger Delta (Benkhelil et al. 1998; Guiraud et al. 2005; Bonne 2014).

3.2.2 Drifting

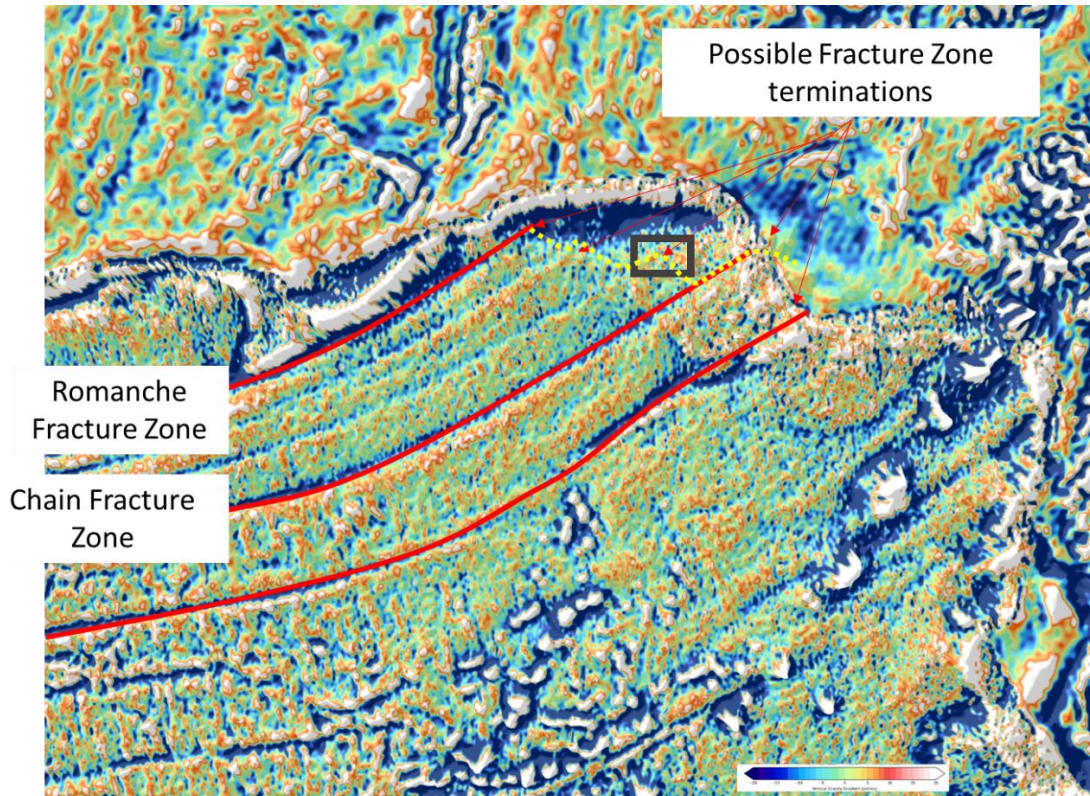


Figure 3-1 Vertical gravity gradient (in Eotivos) derived from satellite measurements of sea level in the Gulf of Guinea (Sandwell et al., 2014). The location of the survey is highlighted by the black rectangle.

The southern margin of West Africa is commonly referred to as a transform margin due to the relative motion of the continent with respect to South America being in a lateral rather than an orthogonal sense via the action of transform faults (Wilson 1965; Freund 1974; Basile et al. 2005).

In Figure 3-2, the striking SW-NE lineaments are interpreted to represent changes in the density of the basement fabric across oceanic fracture zones. The termination of the lineaments is assumed to lie close to the continental ocean boundary, highlighted by the mauve dashed lines. It can be seen that the survey area lies at the north-eastern termination of the second from top fracture zone. The map picks out the location of the present-day shelf break and the location of an interpreted thick low-density continental suite of rock in the blue region.

The main fracture zones, along which the West African plate moved relative to South America in this portion of the Equatorial Atlantic, are the Romanche and Chain fracture zones, (Fairhead and Okereke 1987; Fairhead 1988; Nürnberg and Müller 1991; Benkhelil et al. 1998; Basile et al. 2005; Bonne 2014). Recently published vertical gravity gradient values (Sandwell et al. 2014) following the updated work on marine satellite bathymetry are shown in Figure 3-1. The map illustrates the connection of the Gulf of Guinea with South America along the Chain and Romanche fracture zones. The focus of this study lies at the eastern end of the region lying between the Chain and the Romanche fracture zones.

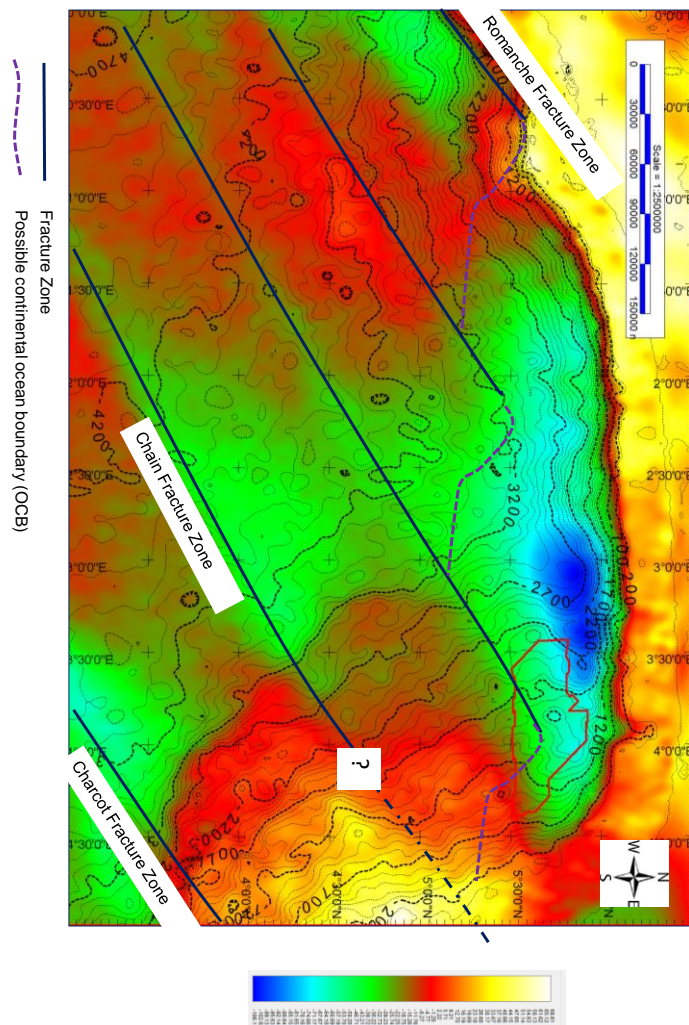


Figure 3-2 Gravity Free Air anomaly (in colour) of the Gulf of Guinea in milligals; the contours are the bathymetry derived from satellite gravity data.

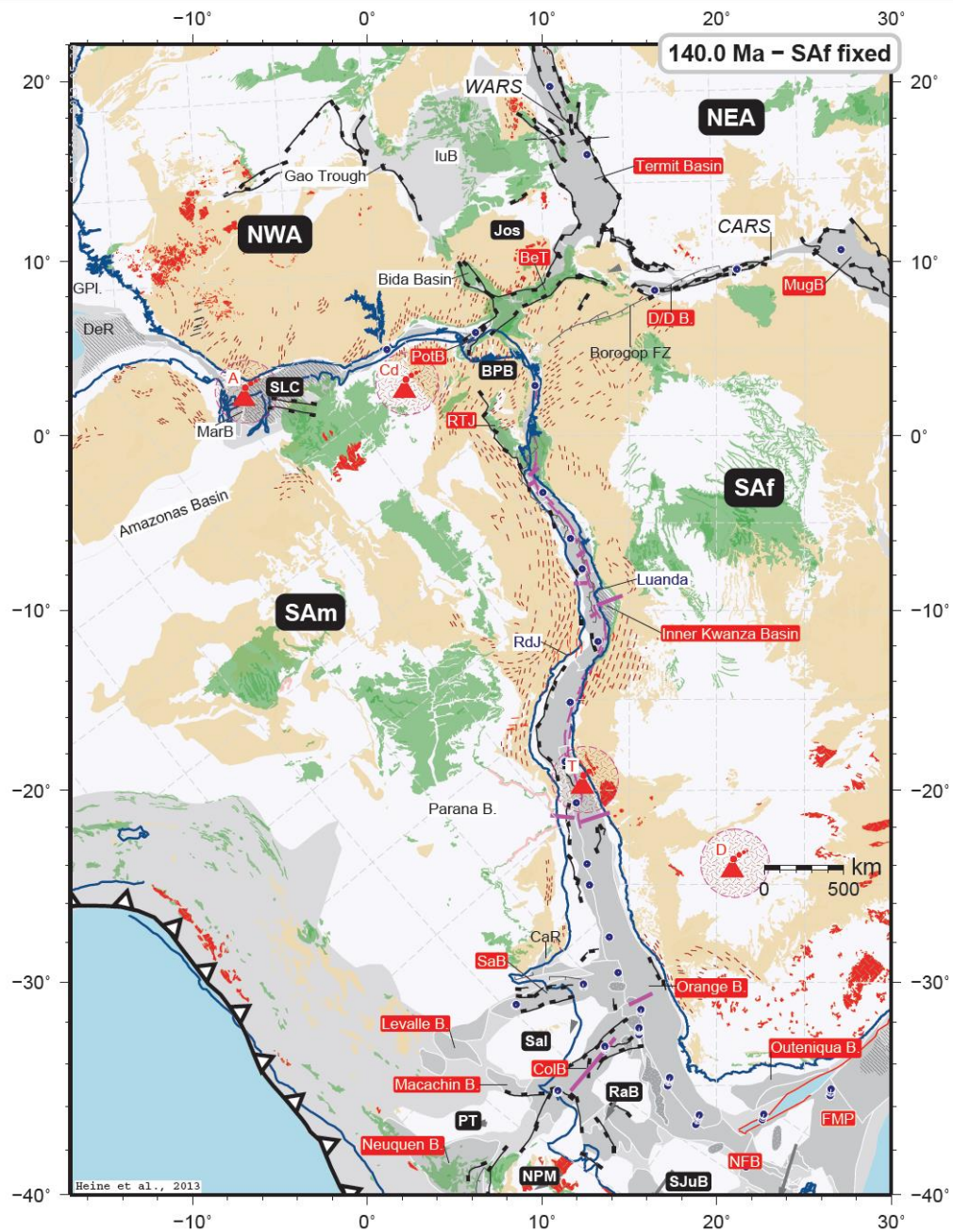


Figure 3-3 A reconstruction of the African and South American continental plates at 140 Ma, indicating the fit of the two plates prior to the separation that commenced in the Barremian (Heine et al. 2013). The key features are labelled in line with the list below.

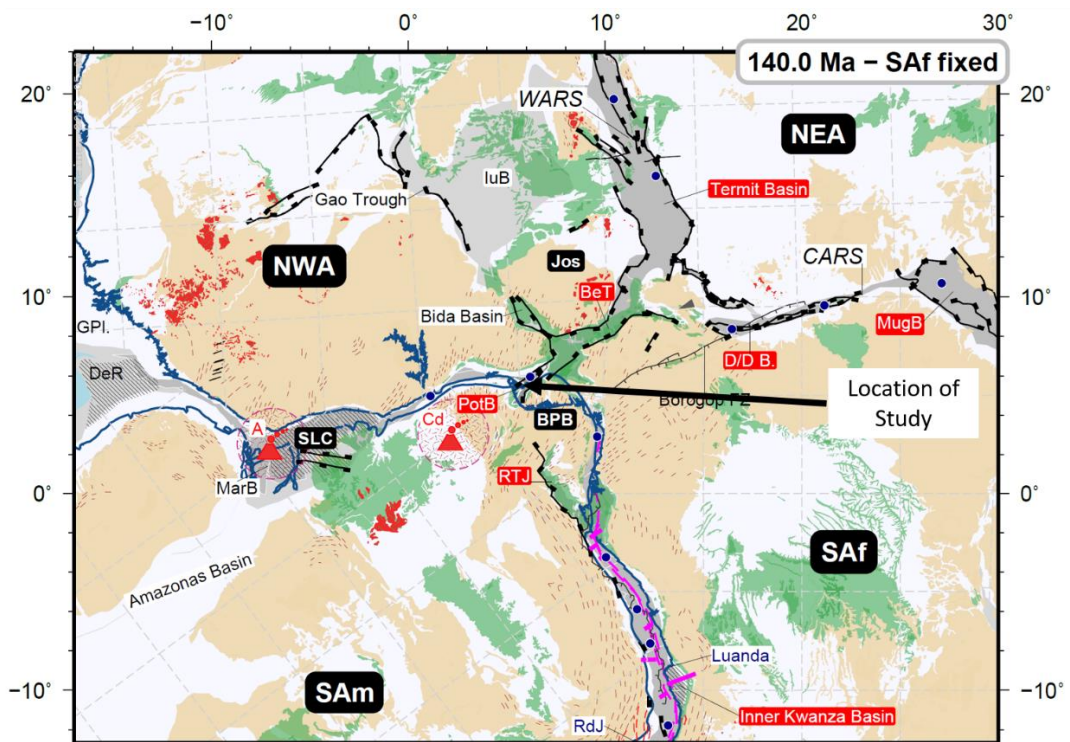


Figure 3-4 Detailed view taken from Figure 3-3, indicating the location of the study area, which lies adjacent to the Potiguar Basin in South America and the Benue Trough in West Africa.

Rigid lithospheric blocks denoted by black labels: SAf – Austral African plate; BoP – NE Brazilian Borborema Province plate; Jos – Jos Plateau sub-plate; NEA – NE African plate; NPM – North Patagonian Massif; PT – Pampean Terrane; RaB – Rawson Block; Sal – Salado sub-plate; SAm – main South American plate; SJuB – San Julian Block; SLC – São Luis Craton block. Actively extending basins are indicated by red background in label; post-rift basins are indicated by light grey background in label; abbreviations: BeT – Benue Trough; CaR – Canelones rift; D/D B. – Doba and Doseo basins; CoIB – Colorado Basin; LuB – Lullemeden Basin; marB – Marajo’ Basin; MugB – Muglad Basin; NFB – North Falkland Basin; PotB – Potiguar Basin; TRJ – Reconavo, Jatoba and Tucano basins; SaB – Salado Basin. Other abbreviations: RdJ – Rio de Janeiro; B. – basin; GPI. – Guyana Plateau; DeR – Demerara Rise. Present-day hotspots are shown as volcano symbol and plotted with 400 km diameter (dashed magenta-coloured circle with hachured fill), assuming that they are stationary over time: A – Ascension; B – Bouvet; Ch – Chad/Tibesti; Ca – Mount Cameroon; Cd – Cardno Seamount; D – Discovery; T – Tristan da Cuñha.

The regional gravity data (Sandwell et al. 2014) indicates that there are several fracture zones that appear to terminate in close proximity to the area being studied. The fracture zones juxtapose continental crust against oceanic crust in the vicinity of the ocean-continental boundary (OCB) (Davies et al. 2005). Visible within the 3D data are deep reflections that are interpreted as possible seaward dipping reflectors (SDR), a possible indication of oceanic crust. Elsewhere, the deeper section appears to show sedimentary character (see chapter 6). It would appear from this observation that the study area is underlain by the landward termination of a fossil transform zone. It is not as clearly seen as in the paper by Davies et al. (2005), but the gravity data along with the seismic reflections suggest that this is indeed the case. The complex faulting seen within the

section underlying the break-up unconformity would require further analysis to establish if this is the case.

Overlying this syn-rift section are sediments ranging in age from the Albian to the present day. They comprise a sequence of shallow marine to deep-water sediments that have been collectively assigned the name of the Benin Basin. This definition is a geographical one since there are sediments derived from the Niger Delta (and perhaps the Benue Delta), which are present within the Benin Basin as defined.

The Benin Basin, as noted in the literature, is confined to the interval that lies to the south of the Romanche fracture zone (Brownfield and Charpentier 2006) and its continental extension; the basin is bounded to the east by an uplifted region, the Okitipupa high, which separates the Benin Basin from the Benue Trough lying to the east of this regional high (Onuoha 1999). The depositional history of the sediments within this interval record a history of subsidence that corresponds with the thermal subsidence of the region following the separation of Africa from South America (Onuoha and Ofoegbu 1988). This may be a limit placed upon the basin by lack of data to the south; it may well be that the Albian to Turonian section wraps around the Okitipupa high and into the Benue Trough, where there is evidence of strata with a similar age and marine affinity (Adeleye 1975). In addition, the gravity and magnetic interpretation presented by Haack (Haack et al. 2000) may support this assumption.

Following the initial separation and with the distance between the two continents growing, the region became tectonically quiet during this drift stage, with the gradual thermally induced subsidence creating a marine environment, following the establishment of the proto-South Atlantic Ocean. An east-west orientated shelf along the southern margin of West Africa (Emery et al. 1975; Benkhelil et al. 1998; MacGregor et al. 2003) was established during the Albian and persisted until the Turonian. A number of wells have been drilled into this interval and confirm a laterally extensive shallow marine sequence (Onuoha and Ofoegbu 1988; Onuoha 1999; Basile et al. 2005; Olabode and Adekoya 2008; Kaki et al. 2012). The Cretaceous section pinches out onto basement to the north of Lagos in a continental facies. Numerous oil seeps have been observed at this pinch-out. The presence of the seeps led to the drilling of a number of onshore wells, but with little success, primarily due to the lack of a trapping mechanism. Although good source rocks were found within the syn-rift section (Haack et al. 2000), the section that overlies the syn-rift is essentially a dipping monocline with little or no faulting or dip reversal. It would appear that all of the oil generated has migrated to the outcrop.

3.2.3 Senonian Unconformity

A regionally important unconformity (the Senonian) is recognised along the western coast of Africa, which affected the Turonian and older sediments (Guiraud and Bosworth 1997). A significant relative fall in sea level occurred towards the end of the Turonian. This forced regression (Posamentier et al. 1992) exposed the Albian, Cenomanian, and Turonian sections, which were present to sub-areal erosion.

The relative drop in sea level is interpreted to have been associated with uplift of the region due to late-stage movements along transform faults and a shift in the pole of rotation of the African continent (Fairhead 1988; Fairhead and Binks 1991; Guiraud et al. 1992). A noticeable gravity high (Sandwell et al. 2014) is present to the north-east of the study area and most likely links to the onshore Okitipupa high (Onuoha and Ofoegbu 1988; Onuoha 1999; Haack et al. 2000).

The Senonian unconformity resulted in the separation of the South Atlantic from the Tethys Ocean, which lay to the north (Fairhead and Binks 1991; Guiraud et al. 1992; Bonne 2014). The closure of the seaway between the two oceans led to the establishment of a fluvio-deltaic system in the region of the Benue Trough (Guiraud et al. 1992; Genik 1993).

3.2.4 Thermal Subsidence

The post break-up sequence that is present within the bounds of the 3D survey is separated from the shelfal sequence by a bypass zone. Within the bounds of the 3D survey, the section that overlies the syn-rift unconformity is a package of seismic reflectors that are seen to thin towards the north and onlap the break-up unconformity. This onlapping section is capped by an angular unconformity, assumed to be the Senonian unconformity. If this is a correct assumption, then the section that lies above the break-up unconformity must be older than the Campanian and younger than the Aptian (Morgan 2003; Kaki et al. 2012).

The upper Cretaceous interval identified in the 3D volume appears to be thickening towards the south and east (Figure 3-5), indicating the presence of a significant amount of accommodation space being present in this region. Under the present-day Niger Delta, the seismic data is not well imaged and the interpretation of the Cretaceous is conjectural. Indirect evidence may point, however, to the presence of an underlying Upper Cretaceous delta.

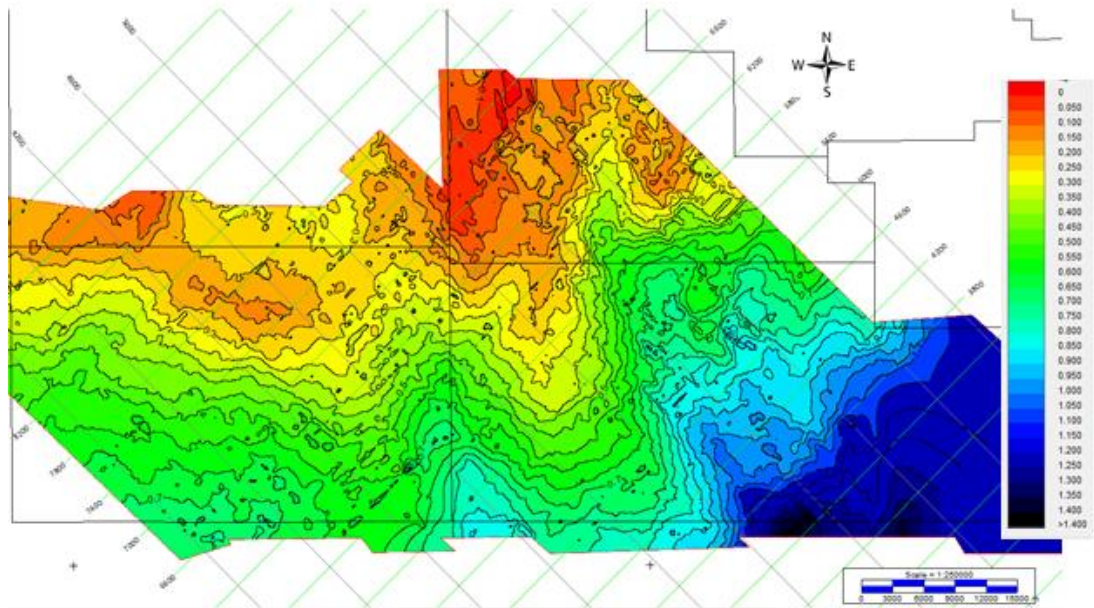


Figure 3-5 Isochrone of the Upper Cretaceous interval, which is defined as the section between the base Cenozoic and Senonian unconformity.

The map in Figure 3-5 indicates that the Upper Cretaceous interval thickens towards the south-east. The irregular thickness may be interpreted to indicate that the base of this interval was affected by canyonisation at the time of the Senonian event.

Reconstruction of the Upper Cretaceous palaeogeography of the region is hampered by the poor quality of seismic data and limited well penetrations or outcrops. The Upper Cretaceous has been documented by Benkhelil et al. (1998), but there is a gap between the onshore Benue Trough and the study area, so no tie can be definitively made between the two areas. The role of the Benue Trough and the rifted basins in the Upper Cretaceous sediment distribution is significant (Avbovbo et al. 1986; Genik 1993; Benkhelil et al. 1998). The palaeogeographical reconstruction of the region indicates that during the late Cretaceous a deltaic system was present, being fed from the proto-Benue River. Given the presence of littoral deposits in the Maastrichtian and marine sediments in the Campanian, it is possible to assume that they represent the regression of a delta into the Gulf of Guinea in the Upper Cretaceous.

In addition to the Benue Delta, the global rise in sea level that commenced in the early Campanian (Vail et al. 1977; Haq et al. 1987) resulted also in the spread of this deltaic system to the region, which lies to the north of the study area (in a similar manner to the later Niger Delta); this sequence prograded towards the south and eventually led to the gradual drowning of the entire region in deep water. The predominantly fine-grained sediment of Maastrichtian age, found in the Aje and Seme fields (Olabode and Adekoya 2008; Kaki et al. 2012), directly overlies the Cenomanian and Turonian shore-

face sands and form the top seal for the accumulations. It is postulated, therefore, that the section below, the assumed base Cenozoic, may well be sourced from the Benue River Delta.

The location of the Benin Basin shelf edge is difficult to locate as it has been cannibalised by slope instability and mass wastage during the Oligocene until the present day.

The deep-marine conditions in the 3D survey area, which were established in the late Cretaceous, have persisted to the present day. A feature of the region, which is associated with an oscillating shoreline/shelf, is the presence of several canyons. The canyons have been active repeatedly (Burke 1972; Olabode and Adekoya 2008) and have played a significant role in the sediment budget, which is supplied to the bathyal region.

The Niger Delta basin comprises a regression sequence of clastics, which is assumed to have prograded from the east via the western extension of the Benue Trough from the Eocene onwards (Avbovbo 1978; Evamy et al. 1978). The Benue Trough was formed initially at the time of the continental break up (Fairhead and Okereke 1987; Fairhead 1988). This rifted basin, which strikes in an east to west direction, became the location of sedimentation in the accommodation space that was created. A change in the drainage system of the continent led in the Pleistocene to the capture of sediments from the Niger basin, which superseded the Benue as the main sedimentary supply (Bonne 2014).

3.3 Regional Stratigraphy

A number of approaches to the subdivision of the stratigraphic breakdown of the study area have been used in the past to characterise the succession of strata found in this region.

The use of lithostratigraphy by several authors (Short and Stauble 1967; Adeleye 1975; Avbovbo 1978; Evamy et al. 1978) has led to some confusion of formation names given the diachronous nature of lithological formations. The large-scale subdivision of the subsurface into chronostratigraphic units is useful in the presence of age-dating methods. Within the region covered by the 3D survey used in this study, there is no means of establishing the age of the sediments since there is no age-diagnostic data available.

The extrapolation of regionally known stratigraphic boundaries has been used to identify the major unconformities seen within the data; however, the age of the section that lies between these major unconformities cannot be defined with certainty.

Sequence stratigraphy relies on the recognition of variations in relative sea level (or degree of coastal onlap). This methodology is useful for the definition of depositional sequences in shallow marine settings, but more problematic in deep-water settings. The principle that underpins this approach is that a body of rock that is bounded by unconformities at the upper and lower surfaces of the correlative conformity can be treated as a depositional cycle; the cycle is broken into tracts that are related to fluctuations in relative sea level. In deep water, the sequence-bounding unconformities are hard to recognise as they fall into the categories of correlative conformities (Mitchum Jr. et al. 1977; Vail et al. 1977).

| Period | Epoch | Age Ma | Horizon ID | Depositional Setting | Eustatic Events | Global/Regional Events |
|-----------------|------------------|--------|---------------------------|---------------------------------------|---|--|
| TERTIARY | Pliocene -Recent | 5 | 100 | Slope channel deposition | Ice House Conditions | Series of high stands and low stands resulting from glaciation cycles |
| | Miocene | | 200 | | | |
| | | 300 | | | | |
| | Oligocene | 25 | 400 | Chattian Unconformity | | Circum Antarctic circulation established |
| | | | 420 | | | |
| | Eocene | 36 | 510 | Levee deposition | Sea level drop | Continued thermal subsidence, Canyonisation of shelf margin |
| | | | | 54 | | |
| Palaeocene | 54 | 510 | Mass transport deposition | | | |
| Maastrichtian | 66 | 600 | | | | |
| LATE CRETACEOUS | Campanian | 71 | (Hemi) Pelagic deposition | Rising Sea Level | Establishment of Benue Delta associated with uplift and erosion along southern margin of the Benue Trough | |
| | | 83 | | | | |
| | Santonian | 85 | 680 | Senonian Unconformity | | Change in African Plate pole of rotation, closure of the Atlantic to Tethys seaway, prior fluvial catchment areas altered |
| | Coniacian | 88 | | | | |
| | Turonian | 92 | 785 | Canyonisation of shelf | Thermal subsidence | Linkage of South Atlantic to Tethys Ocean, continued deposition along the West African coast |
| | Cenomanian | 97 | | Mid Albian Unconformity | | |
| | EARLY CRETACEOUS | Albian | 108 | Establishment of shallow marine shelf | Thermal subsidence | Establishment of proto South Atlantic Ocean, thermal subsidence of the newly created oceanic crust. Shallow marine environment established along the southern margin of West Africa. Benue Rift formed |
| Aptian | | 121 | | | | |
| Barremian | | 127 | 800 | Break Up Unconformity | | Initial separation of Africa from South America, the syn rift half grabens were tectonically modified by the influence of the ocean spreading transform faulting |
| Hauterivian | | 132 | | | | |
| Valanginian | | 137 | Lacustrine deposition | | Intra-cratonic rifting within Gondwana, formation of lacustrine filled half grabens | |
| Ryazanian | | 142 | | | | |

Figure 3-6 Tectono-stratigraphy of the Benin Basin region.

3.3.1 Lithostratigraphy

3.3.1.1 Niger Delta

The Cenozoic section in the Niger Delta is often broken into three major lithostratigraphic units (Short and Stauble 1967; Avbovbo 1978; Doust and Omatsola 1990). Figure 3-7 illustrates the subdivision based upon a rough division into lower coastal plain (Benin formation), shallow marine (Agbada formation), and pro-delta deep water (Akata formation) sediments. This division implies a diachronous age range for formations of a

similar name. Confusion occurs when some authors (MacGregor et al. 2003; Morgan 2003; Cobbold et al. 2009) ascribe the name Akata to the deepest section only, whereas, by definition, the formation is present up to the current sea bed. The Cretaceous interval has not been encountered in the deep-water portion of the Delta and assignment of a lithostratigraphic formation name is problematic as the lithology is unknown.

The use of lithostratigraphy has, therefore, led to a confusion in the literature when referring to the section being described. A further example is the use of the term Agbada to describe the sand within slope channel complexes. The Agbada formation as defined by Doust (Doust and Omatsola 1990), Short et al., and Evamy and Avbovbo (Short and Stauble 1967; Avbovbo 1978; Evamy et al. 1978) is a shallow marine sequence of sands and shales.

NIGER DELTA

| SUBSURFACE | | | SURFACE OUTCROPS | | |
|-----------------------|---|------------------|-------------------------|--|---------------------|
| YOUNGEST KNOWN AGE | | OLDEST KNOWN AGE | YOUNGEST KNOWN AGE | | OLDEST KNOWN AGE |
| RECENT | BENIN FORMATION Afam Shale Member | OLIGOCENE | PLIO/ PLEISTOCENE | BENIN FORMATION | MIOCENE? |
| RECENT | AGBADA FORMATION | EOCENE | MIOCENE EOCENE | OGWASHI-ASABA FORMATION AMEKI FORMATION | OLIGOCENE EOCENE |
| RECENT | AKATA FORMATION | EOCENE | L. EOCENE | IMO SHALE FORMATION | PALEOCENE |
| EQUIVALENTS NOT KNOWN | | | PALEOCENE | NSUKKA FM | MAESTRICHTIAN |
| | | | MAESTRICHTIAN | AJALI FORMATION | MAESTRICHTIAN |
| | | | CAMPANIAN | MAMU FORMATION | CAMPANIAN |
| | | | CAMP./MAEST. | NKPORO SHALE | SANTONIAN |
| | | | CONIACIAN/ SANTONIAN | AWGU SHALE | TURONIAN |
| | | | TURONIAN | EZE AKU SHALE | TURONIAN |
| | | | ALBIAN | ASU RIVER GROUP | ALBIAN |

Figure 3-7 Lithostratigraphic subdivisions of the Cenozoic Niger Delta (Short and Stauble 1967).

Given the confusion that surrounds the use of the lithology to define the various formations, the use of lithostratigraphy has been avoided in this study. In order to understand the palaeogeography of any region, the strata need to be broken out into age-equivalent sequences.

The Cenozoic stratigraphy of the Benin Basin is classified using a different lithostratigraphic scheme. This is partly due to the fact that the Palaeogene and Cretaceous section found in the Benin Basin has not been penetrated in the Niger Delta,

but primarily because the simple three-part subdivision that can be applied in the Niger Delta does not lend itself to the description of the sediments encountered in this region. There is a more complex geological history underpinning the stratigraphic record in this coastal to outer shelf region.

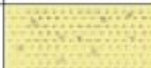
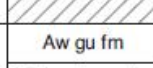
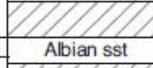
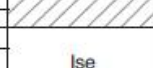
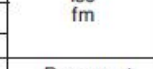
| System Period | Epoch | | Age | Formation | Lithology |
|------------------|-----------|-----------|---|---|---|
| Quaternary | | | Present to pliocene | Benin/ idjebu fm |  |
| | Tertiary | Neogene | | Miocene | |
| Palaeogene | | Oligocene |  | | |
| | | Eocene | Oshoshun fm | | |
| | | Paleocene | Imo shale | | |
| Cretaceous | | Late | Senonian | Maastrichtian | Araromi shale chenal |
| | Campanian | | |  | |
| | Santonian | | |  | |
| | Coniacian | | | Aw gu fm | |
| | Early | | Turonian | Turonian sst Abeokuta | |
| | | | Cenomanian |  | |
| | | | Albian | Albian sst | |
| | | | Aptian |  | |
| | Late | | Barremian |  | |
| | | | Hauterivian | Ise fm | |
| | | | Valanginian | | |
| | | | Berriasian | | |
| Jurassic | Early | | | | |
| Paleozoic | Late | | | | |
| | | | Cambrian | Basement |  |

Figure 3-8 The lithostratigraphic breakdown of the Benin Basin (Kaki et al. 2012).

The Benin Basin has been explored both on- and offshore in the search for hydrocarbons. Using the data gathered from this activity, the Cretaceous section that has been drilled can be described, in contrast to the Niger Delta, where there is no data that can be tied to the Cretaceous (Evamy et al. 1978; Olabode and Adekoya 2008; Kaki et al. 2012).

3.3.2 Chronostratigraphy

The subdivision of the subsurface into age-equivalent sequences has been investigated as a means to better understand the overall geological history of the region. There are a number of well-recognised unconformities in the succession. Of particular note are the sedimentary hiatus noted in the Mid Oligocene, the Cenomanian (Adeleye 1975), and the Middle Albian.

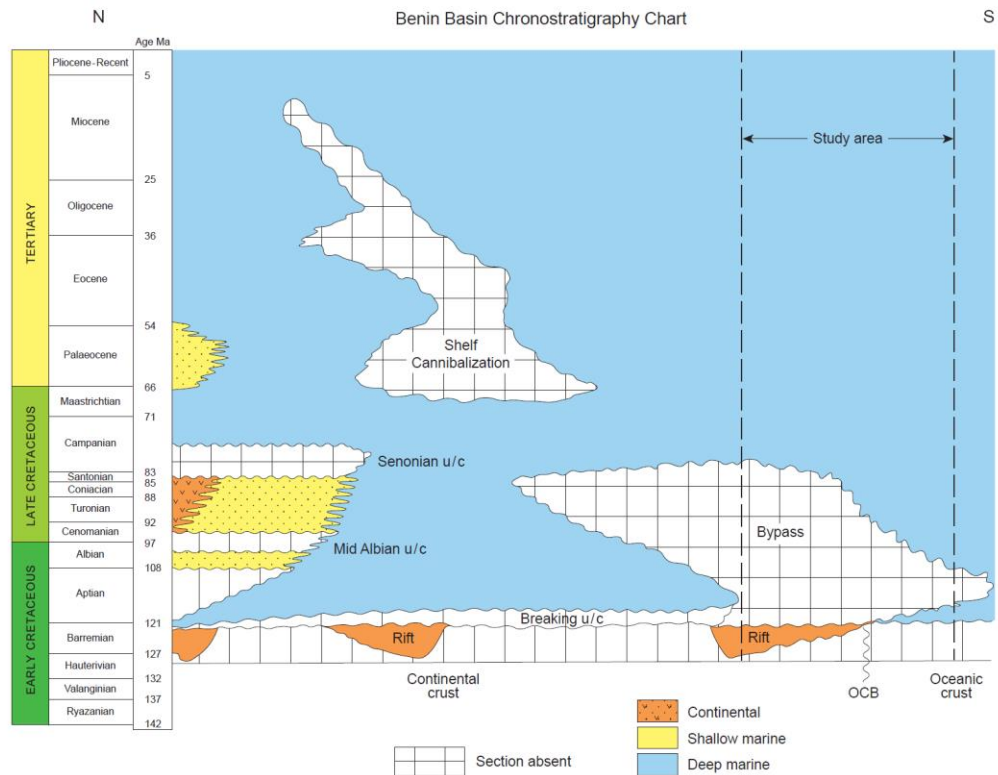


Figure 3-9 Summary of the chronostratigraphy of the Benin Basin; the section runs from the shelf break in a north-south orientation.

3.3.2.1 Syn-rift (Barremian to Aptian)

The faulting within the syn-rift is complex and, due to the distortions in the overburden, the imaging of the syn-rift sedimentary interval is compromised. Some major fault trends can nonetheless be identified, which would indicate that the section is comprised of a series of tilted half grabens, with the graben bounding faults heading towards the south and the strata within the grabens dipping towards the north. The grabens are truncated by the syn-rift break-up unconformity and are seen to be absent at the southern margin of the 3D survey area.

In the eastern region of the survey area, there are well-imaged events that lie below the break-up unconformity truncating the syn-rift section (Figure 3-10 and Figure 3-11). The morphology of the break-up unconformity surface, when mapped, indicates that there are a number of west to east trending ridges. They are seen to die out towards the east as the section gets deeply buried. The eastern termination of these ridges is an approximately north-south lineament.

The western limit of the seismically reflective package that sits beneath the unconformity is poorly defined in detail; however, in broad terms, the western limit is also

interpreted to be a north-south lineament, which separates the reflection-rich interval from one that is devoid of any coherent reflections.

When the African and South American plates are reconstructed at the pre-break-up age (Heine et al. 2013), the extension of the Potiguar Basin half grabens across the break-up line matches up with the half grabens seen in the 3D volume. This evidence supports the interpretation in the paper by Heine et al. (2013).

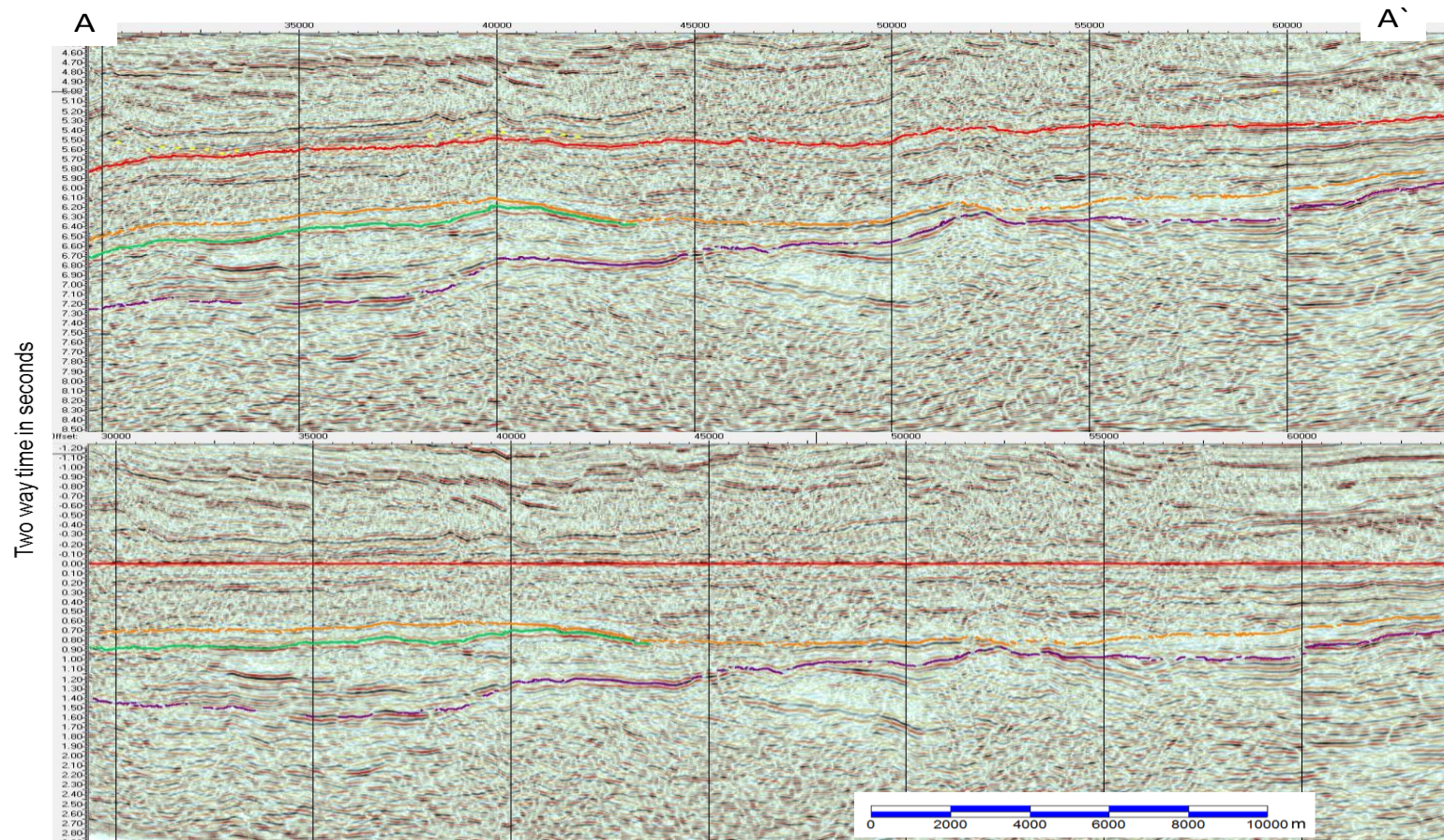


Figure 3-10 Cross line 4700, both in the original form, top, and flattened at Base Cenozoic (the red horizon) in the bottom image. The vertical lines mark 5km intervals.

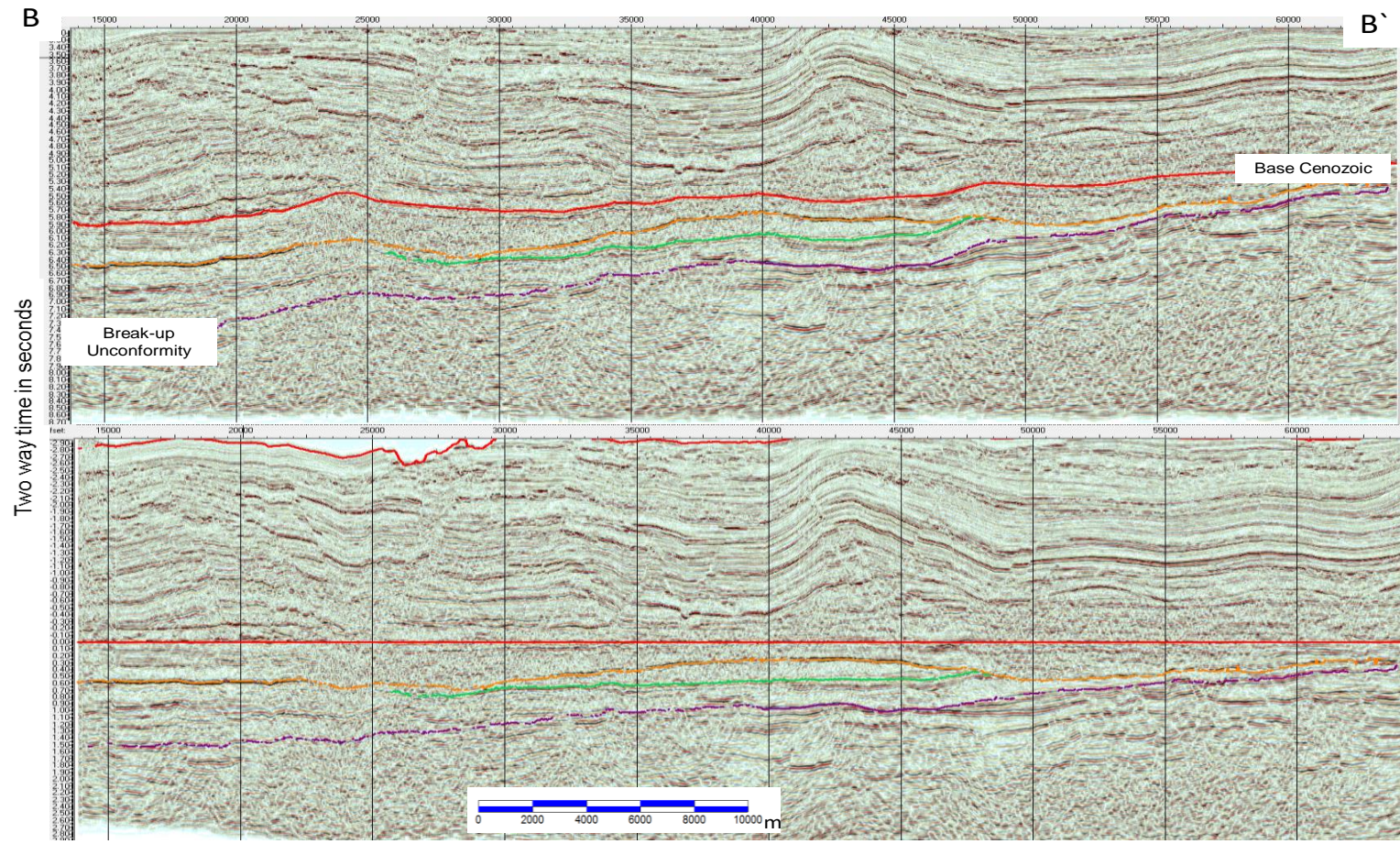
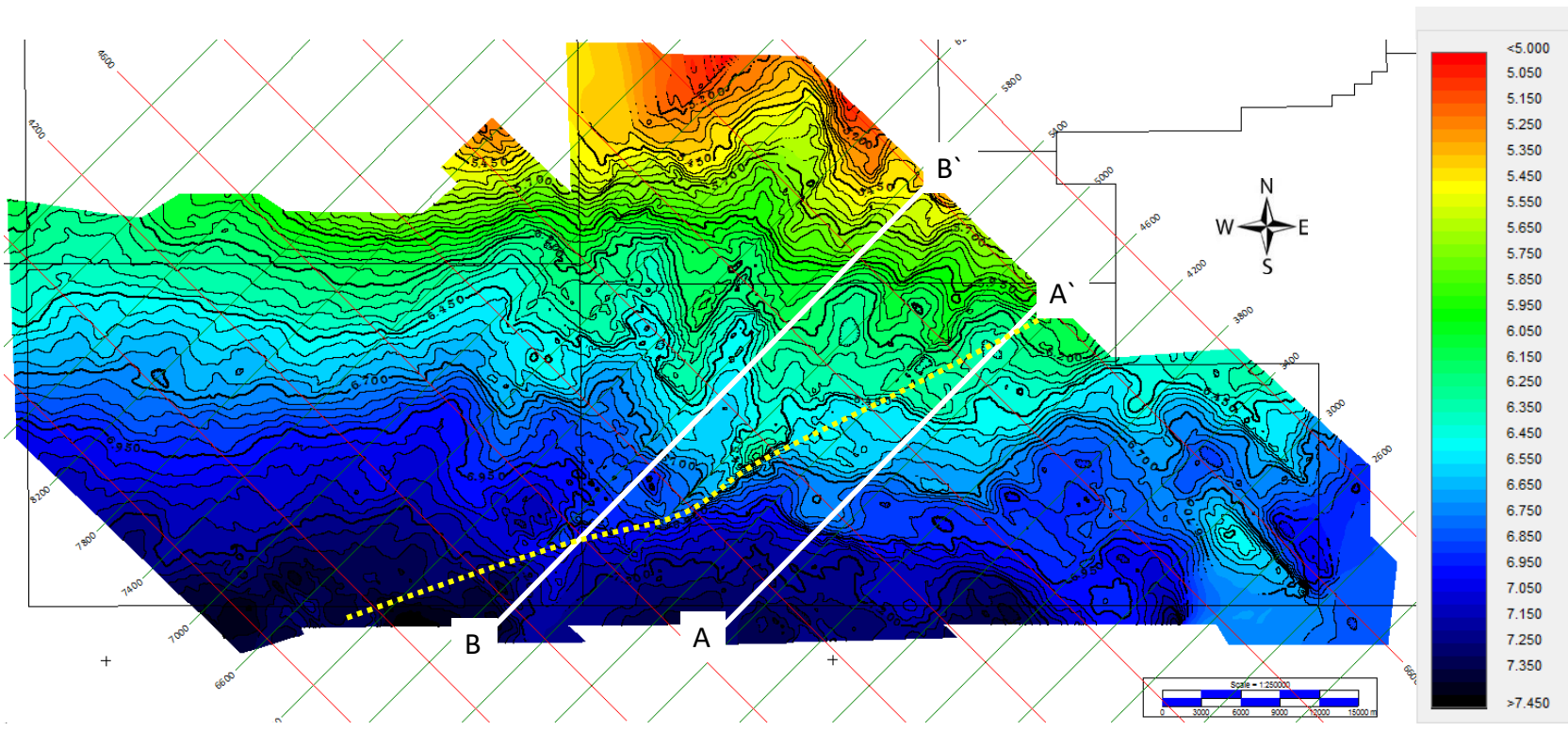


Figure 3-11 Crossline 5700, the upper image is the original; the lower one is flattened at the Base Cenozoic.



Horizon 800

Figure 3-12 TWT map of the top of the syn-rift, showing location of Figures 3-7 and 3-8; the yellow dashed line is the location of the Mahin fault zone in the overburden.

3.3.2.2 Pre-Senonian Interval (Albian to Turonian)

The sequence that lies between the top syn-rift unconformity and the Senonian unconformity does not appear to be heavily faulted. The laterally discontinuous nature of the seismic reflectors in the west of the survey are interpreted to represent a high-energy depositional setting.

3.3.2.3 Post-Senonian (Campanian to Maastrichtian)

This interval is comprised of primarily distal deltaic sediments derived from the palaeo-Benue and the present-day Niger Deltas, which are located to the east of the survey. The exception to this simplified model is the presence of sediments derived from the north, which are linked to both present-day and older canyons that are known to exist (Olabode and Adekoya 2008).

3.3.2.4 Cenozoic

The tectonic deformation within these sediments is directly linked to the growth of the deltas. The gravity-induced deformation has created three distinct structural provinces within the studied area. In the east, the predominant tectonic style is that of extension, with the majority of the faults striking in an east-west orientation; the western half of the survey is characterised by predominantly compressional deformation.

In the greater Niger Delta, the use of biostratigraphy to break out the Neogene section into zones of similar age is widespread. This has enabled the breakdown illustrated in Figure 3-13. This is useful as a means of showing the overall westwards migration of the Niger Delta shoreline since the Eocene. It does not, however, offer any subdivision of the deep water other than the use of the lithostratigraphic nomenclature. In addition, this description places the sediments older than the Eocene into a blanket group of deep-marine shale.

The use of a chronostratigraphic approach to the distribution of sediments within the Niger Delta has been outlined by Edjedawe (Figure 3-13). This subdivision of the delta is based upon the lateral (including the structural terrains observed) distribution of the sediments with changing time, rather than just the rock type.

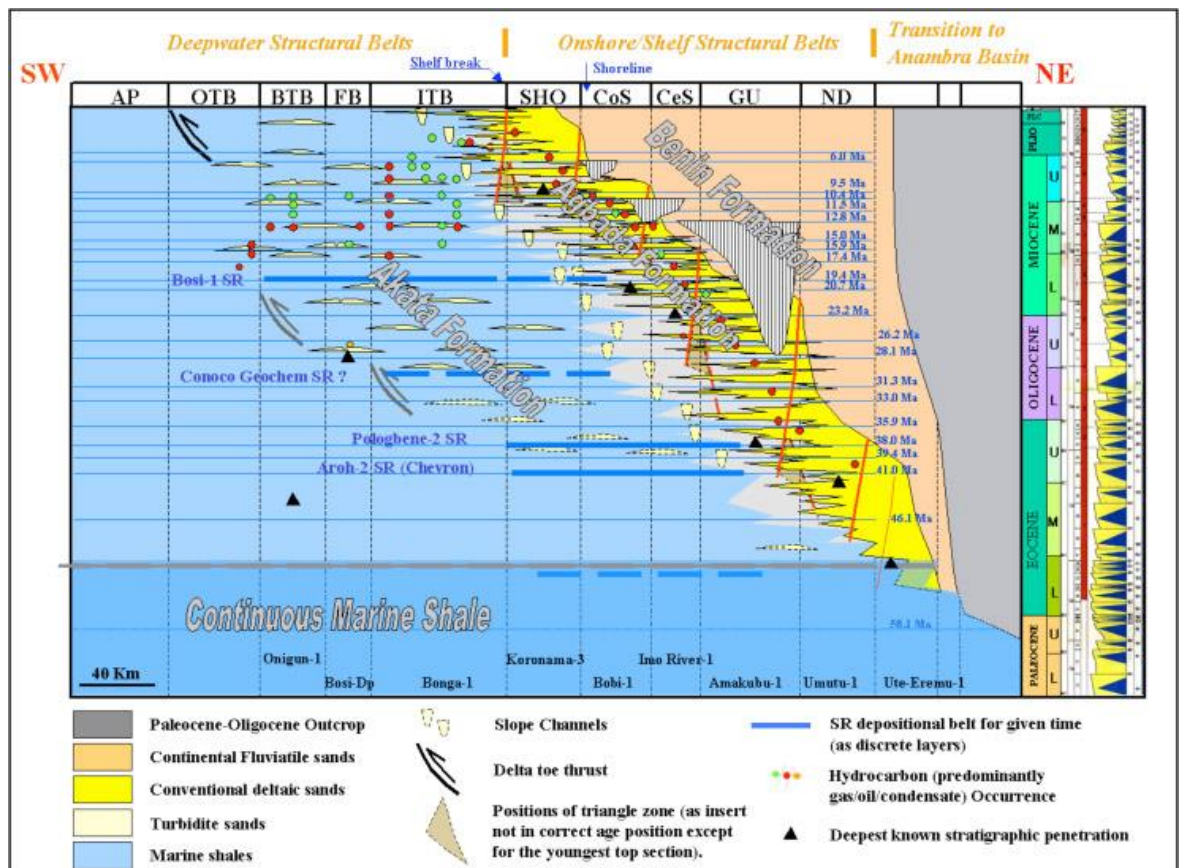


Figure 3-13 Alternative stratigraphic description of the Cenozoic sediments of the Niger Delta, based upon geographical location and structural domains (Edjedawe 2012).

3.3.3 Sequence Stratigraphy

The principles of sequence stratigraphy as a means of subdividing the sub-surface has not been widely used to describe the region. However, the principles of seismic sequence stratigraphic methods (Mitchum Jr. et al. 1977; Vail et al. 1977) proved useful for the breakdown of large sequences, whereas sequence stratigraphy in a strict sense is more useful as a tool for analysing small-scale variations in sedimentary patterns in shallow water and slope settings (Magbagbeola and Willis 2007). For example, in deep water, it is difficult to define the maximum flooding surface. In this study, indirect evidence of coastal onlap variations are recognised; these are outlined in chapter 4.

3.4 Regional Sedimentology

The location of the study lies in a region of overlapping basins, the Benin Basin and the Niger Delta, and is dominated by marine to deep-marine sedimentary processes.

3.4.1 Niger Delta

The portion of the Niger Delta that is present within the area covered by the 3D data is outboard of the lower coastal fluvial and alluvial regions and shallow-water deposits, which are present to the east. The fluvial and alluvial sediments are derived from the Niger and Benue river catchment areas (Evamy et al. 1978; Doust and Omatsola 1990; Bonne 2014). This catchment area has evolved throughout time to reach its present-day extent (Bonne 2014).

The shallow-water sediments are comprised of aggrading shore face to barrier bar sands interlaced with shelfal muds, which have been assigned the lithostratigraphic affinity of the Agbada formation (Avbovbo 1978; Evamy et al. 1978; Magbagbeola and Willis 2007). The width of the present-day shelf, from today's coast to the shelf break, is in the region of 35km. The dip of the shelf is in the region of one degree from the horizontal.

Outboard of this shallow-water setting, the slope is comprised primarily of pro-delta shales; this shale-prone interval is referred to as the Akata formation. The shales are interbedded with sand-prone slope channels and amalgamated ponded turbidites (MacGregor et al. 2003; Heiniö and Davies 2007; Kostenko et al. 2008); these sand-prone intervals are known to be productive hydrocarbon-producing reservoirs (Chapin et al. 2002; Morgan 2004). The dip of the present-day slope is calculated to be in the region of 1.5° (Bilotti and Shaw 2005).

Slope channel deposits within the Niger Delta have been a focus of study, in order to understand reservoir behaviour in these complex bed forms (Clark and Pickering 1996; Deptuck et al. 2007; Leduc et al. 2009). The characteristics of this depositional environment have been described by a number of authors (Reading and Richards 1994; Galloway 1998; Posamentier 2003; Kolla et al. 2007). The work that these authors have undertaken has allowed the presence of similar deposits to be established within the 3D volume used in this study.

3.4.2 Benin Basin

The northern limit of sediments within the Benin Basin succession lies to the north of Lagos, where the Cretaceous interval pinches out onto metamorphic basement (Adeleye 1975). At this pinch-out margin, the sediments are comprised of coarse-grained conglomerates. The interface between the basement and the overlying sediments is the site of active oil seeps (Haack et al. 2000). The oil has been geochemically typed to have been derived from a source rock of Neocomian to Albian age (Haack et al. 2000; Kaki et al. 2012). The interpreted depositional environment that has been assigned to the syn-

rift (referred to as the Ise formation) is lacustrine. Immediately overlying the syn-rift sediments is a transgressive clastic interval of Albian age, which is found in the wells drilled in the offshore region (Onuoha 1999). The northern limit of this transgressive interval is unknown, but as there are no Albian-aged sediments present in the onshore Afowo-1 well (Onuoha and Ofoegbu 1988), the northern limit of this interval is interpreted to lie to the south of the present-day coastline.

The exploration drilling that has taken place in the coastal region has encountered the syn-rift section directly overlain by Albian-aged shallow-marine sediments. In the Aje and Seme (Kaki et al. 2012) fields, the Albian-aged section contains both shallow-water sands and limestone deposits.

The Cenomanian to Turonian interval, which has been penetrated in the wells drilled offshore on the present-day shelf, are known to have encountered thick sand-prone intervals (Onuoha and Ofoegbu 1988; Kaki et al. 2012). These are interpreted to be a representation of widespread shore face and littoral deposition that occurred as the thermal subsidence, which commenced in the Albian, and led to the establishment of an east-west trending shoreline of the proto-Atlantic Ocean. The provenance of these sediments responsible for the deposition on the palaeo shelf is unknown. The rearrangement of the continent at the time of the Senonian unconformity led to the erosion of the hinterland and has, therefore, obscured evidence of local fluvial inputs to the region (Guiraud and Bosworth 1997).

The Upper Cretaceous interval deposited following the Senonian unconformity is seen as a transgressive sequence of shallow-marine sands and shales, which spread towards the north as the relative sea level rose throughout the Campanian and Maastrichtian. One observation that is noted by Kaki et al. (2012) is the presence within the Maastrichtian of deep-marine organic-rich black shales. This interval is considered to be a key to understanding the later thin-skinned deformation that took place along the margin within the Cenozoic. It is unclear as to the explanation of the presence of bathyal sediments, such as those described by Kaki, in an otherwise shallow-marine setting. One possibility is the presence of steep-sided canyons, known to be present along this margin, which were infilled by deep-marine-filled basins.

The bulk of the onshore Cretaceous section in the vicinity of the study area is covered by younger Cenozoic sediments (Figure 3-14). The limited amount of outcrop data that has been studied (Olabode 2006) has led to an interpretation of the observed sediments (which are not age specific – being lithostratigraphically defined as part of the Abeokuta formation) to be siliciclastic slope deposits.

The Cenozoic portion of the Benin Basin has been penetrated by a number of wells, drilled both on- and offshore (Onuoha 1999; Olabode and Adekoya 2008; Kaki et al. 2012). The sedimentary succession reveals a gradual shallowing of the water depth through time. The deep marine Upper Cretaceous is overlain by shales that are described as being deep-water to slope in the Palaeocene and evolving to outer shelfal in the Eocene.

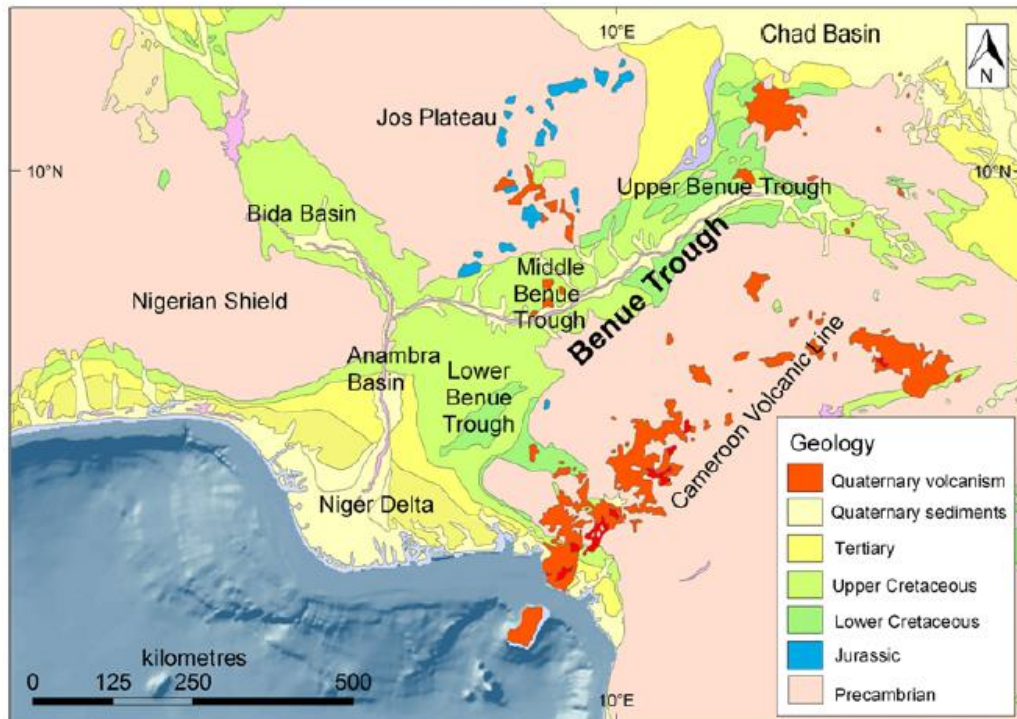


Figure 3-14 Surface geology of Nigeria taken from (Bonne 2014).

The Eocene Imo shale is described as being present along the entire Benin Basin margin (Benkhelil et al. 1998; Haack et al. 2000; Kaki et al. 2012). The cannibalisation of this shelf throughout the Cenozoic by a process of headward erosion and canyon formation led to the redistribution of the fine-grained sediments, which were deposited on the shelf being redeposited down the slope.

The Neogene interval, present within the wells drilled in the present-day shallow water shelfal region, has encountered two apparent unconformities within the Oligocene and the Miocene (Avbovbo 1978; Morgan 2003; Kaki et al. 2012). These unconformities are interpreted to represent the shelf and shelf margin regions that have been removed by the action of shelf margin collapse during sea level low-stand periods. Overlying and underlying each of these unconformities is a sequence of shelfal shales and minor sandstones.

The location of the shelf-to-slope break has remained relatively constant throughout the depositional history of the post rift sediments. The Albian shelf edge is only some 15km further south than the location of the present-day shelf edge. The present-day shelf break lies some 30 km from today's shore line. The seawards dip of the shelf is less than 1° from the horizontal, whereas the dip of the slope is in the region of 5–6°. The slope extends for some 22 km to the point at which the gradient decreases again to approximately 1.5°, where it becomes the continental rise. The dip of the shelf and of the rise are of the order of magnitude seen in many other continental margins (Galloway 1998; Hodgson et al. 2011). The angle of dip of the slope is, however, larger than the average slope seen elsewhere. As noted in the previous section, the dip of the slope in the Niger Delta is in the region of 1.5°. The dip of the slope in the Benin Basin is one possible cause of the instability that led to the collapse of the shelf and the associated distribution of the apron of mass transport and levees down the slope.

The provenance of the sediments within the stratigraphic succession found in the Benin Basin is unclear. There are no records of significant fluvial systems that drain southwards towards the east-west trending shoreline and shelf. The distribution of sediment that flows out from the tributaries within the Niger Delta have been studied by Allen (1965). In the Holocene, the distribution of material that reached the coast was dispersed in a coast-parallel manner as a result of wave action and the accompanying longshore drift. Sediments that are found in the region of Lagos are interpreted to have been sourced from the outflow of the Niger coupled with influence from minor rivers that flow from the north. This system of sedimentation may have been active since the Upper Cretaceous.

3.4.3 Deep-water Depositional Styles

The deposits found in the studied area can be broken down into five primary deep-water sedimentary settings. These are outlined in the following paragraphs.

3.4.3.1 Hemipelagic Rain

In the absence of high-energy lateral sediment input into the basin, the majority of the deposits are laid down via the gradual settling out of fine-grained material carried in suspension out into the deep-water regions combined with a low-energy lateral input. The seismic character of these deposits is of laterally continuous events, generally draping the pre-existing morphology. In the presence of active tectonic activity, these pelagic sediments are seen to thin but not onlap onto the emergent highs (Brown Jr and

Fisher 1977; Henrich and Hüneke 2011; Hüneke and Henrich 2011). Within the 3D survey area, the presence of hemipelagic sediments is recognised as being widespread.

3.4.3.2 Canyons

A significant aspect of the regional sedimentary system is the presence of a number of canyons that have formed along the shelf margin that lies to the north and east of the 3D survey area. The best documented canyon is the Avon canyon (Olabode and Adekoya 2008). The age of the initial formation of the canyon is unknown and has remained active intermittently up to the present day. There are a number of additional canyons, notably the Seme, Mahin (Burke 1972), and Opuama (Petters 1984), and the Lagos and Benin canyons (Deptuck et al. 2007). The canyons have been the source of focused sediment supply into the lower slope and abyssal plain. Sediment supply into the study area can be identified, which is interpreted to have been derived from the Mahin, Avon, and Benin/Opuama canyons. There is less confidence in the recognition of input from the Lagos canyon.

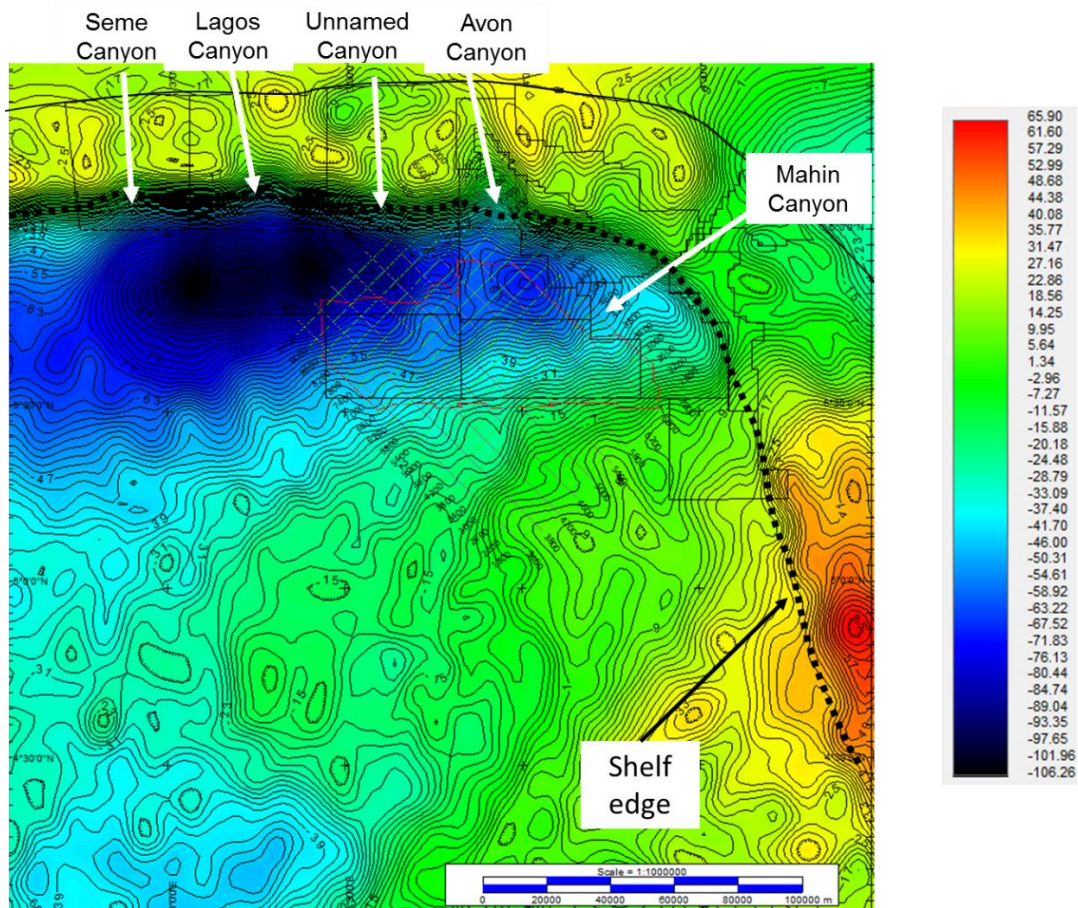


Figure 3-15 Free-air gravity anomaly, in milligals, illustrating the interpreted locations of canyons.

In Figure 3-15, the white arrows indicate the location of inferred canyons within the shelf that lies to the north of the survey area. The present-day shelf edge is highlighted by the dashed black line. The Northern canyons, Seme, Lagos, and Avon, are interpreted to have been active as sediment input points since the Cretaceous; the unnamed Canyon is interpreted to be present on the basis of the gravity data, but there is little published to support its presence. The Mahin canyon is a recent development of likely Pleistocene age.

Canyons are known to be the entry points for sediments into deep-water settings, funnelling both fluvial bed load and cannibalised canyon margins via turbidity currents that transport the suspended sediment particles down the slope (Middleton 1993; Galloway 1998; Hodgson et al. 2011; Talling et al. 2012; Wijono et al. 2015).

3.4.3.3 Turbidites

Turbidity flows are described as being rapid flows of sediment-laden water that travel down slopes within a body of clean water (Middleton 1993; Galloway 1998). Sediment-laden water is denser than the surrounding fluid and, as a consequence, gravity aids in the process such that the turbidity flow travels down the slope. As the turbiditic flow travels down the slope its velocity changes and slows at the base of the slope or at a change in gradient on the slope. It can also speed up if the gradient should steepen. In general, the first grains to drop to the underlying surface are the largest (heaviest) with the finest-grained material remaining within the flow until it ceases to move.

The study of turbiditic flows in deep-marine settings has been aided by both 3D seismic and well data (Normark et al. 1993; Stow and Mayall 2000; Posamentier and Kolla 2003; Adeogba et al. 2005; Talling et al. 2012; Talling 2014).

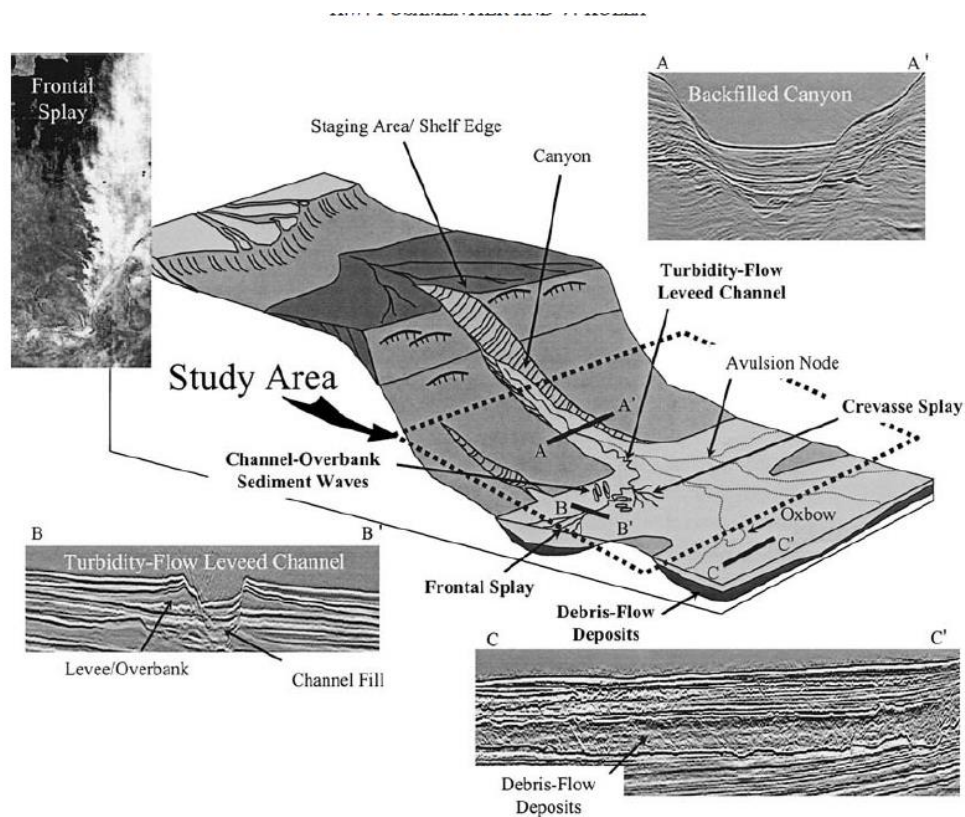


FIG. 1.—Schematic depiction of principal depositional elements in deep-water settings.

Figure 3-16 Illustration of the key components of a deep-water canyon-fed depositional system (Posamentier and Kolla 2003).

Although turbidity flows are often associated with headward erosion of the shelf and the formation of canyons in the shelf margin, the flows can also originate in the upper reaches of the slope, or outer shelf. Sediment is captured within the up-dip canyon axis and, due to the higher density of the material that flows out of the canyon, the sediment-laden water flows down the dip from the mouth of the canyon. Several distinct facies are associated with turbidity current deposits, including levee channel, overbank sediment waves, frontal splays or distributary channel complexes, crevasse splays, and debris flows (Posamentier and Kolla 2003). There are several examples of turbidite deposits found within the 3D data volume; they are discussed in more detail in chapter 6.

3.4.3.4 Mass Transport Deposits

The widespread presence of mass transport complexes at the base of the Cenozoic interval along the southern edge of the West African margin will be shown to play a significant role in the later structural deformation of the Cenozoic deposits.

The input of sediment into deep water is known to occur when the shelf collapses (Shipp et al. 2011; Talling 2014). The collapse can have a number of causes, but the effect is to deposit, often over a large area, a complex melange of chaotically organised sediments. The presence of mass transport deposits in deep water has been known for some time (Carter 1975); the analogue for the description of the submarine deposits was initially by comparison to landslides, which share many causal mechanisms. With the advent of 3D seismic data, the ability to study these deposits has been enhanced. The interpretation of 3D seismic data to analyse these deposits has been undertaken by a number of authors (Carter 1975; Kvalstad et al. 2005; Frey-Martínez et al. 2006; Faereth and Saetersmoen 2008; Bull et al. 2009; Alves 2010; Shipp et al. 2011). To date, there has been a limited amount of published material that relates to mass transport deposits in the Niger Delta and the Benin Basin (Adeogba et al. 2005).

Numerous examples of mass transport complexes have been described in the literature (Moscardelli and Wood 2016). Among these are examples from recent slope failures such as the Storegga Slide offshore Norway (Bryn et al. 2005a; Faereth and Saetersmoen 2008), Miocene examples in the Espirito Santo Basin in Brazil (Alves 2010; Gamboa et al. 2010), offshore Morocco (Dunlap et al. 2010), and in the deep water offshore eastern Trinidad (Moscardelli et al. 2006).

The seismic expression in both the vertical cross sections and RMS amplitude extractions of the Moroccan example shown in Figure 3-17 and Figure are similar to those observed in the main mass transport deposits seen within this survey. In this study, the presence of mass transport deposits is considered a major component of the sedimentary history of the region. A more detailed examination of the interpreted mass transport deposits is presented in section 6.3.4.

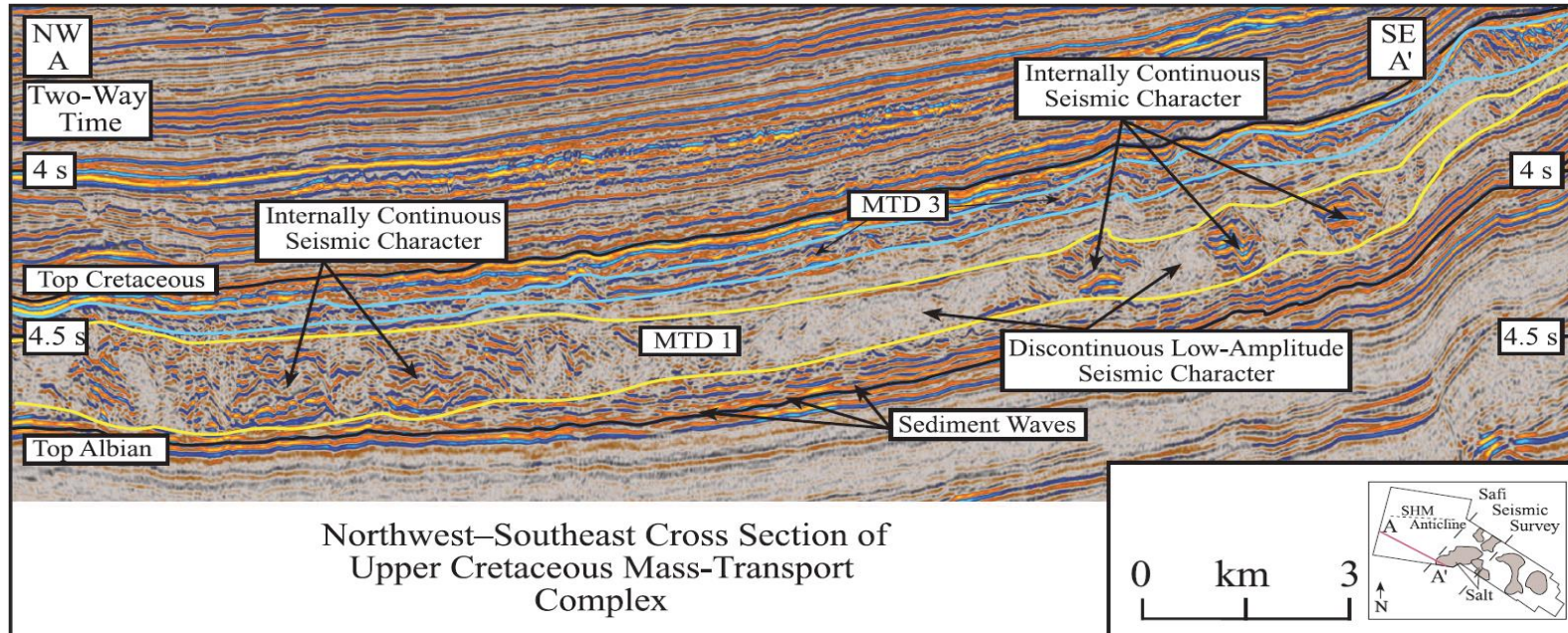


Figure 17. Northwest–southeast cross section of the Upper Cretaceous mass-transport complex. Mass-transport deposit (MTD) 1 bounded by yellow top and base shows two distinct facies: a high-amplitude, internally continuous blocky character within a chaotic, low-amplitude seismic facies. MTD 3 bounded by blue top and base is deposited after MTD 1 and below the top Cretaceous unconformity. MTDs 2 and 4 are not present in this section. SHM = Safe Haute Mer.

Figure 3-17 A vertical cross section through a mass transport complex, offshore Morocco (Dunlap et al. 2010).

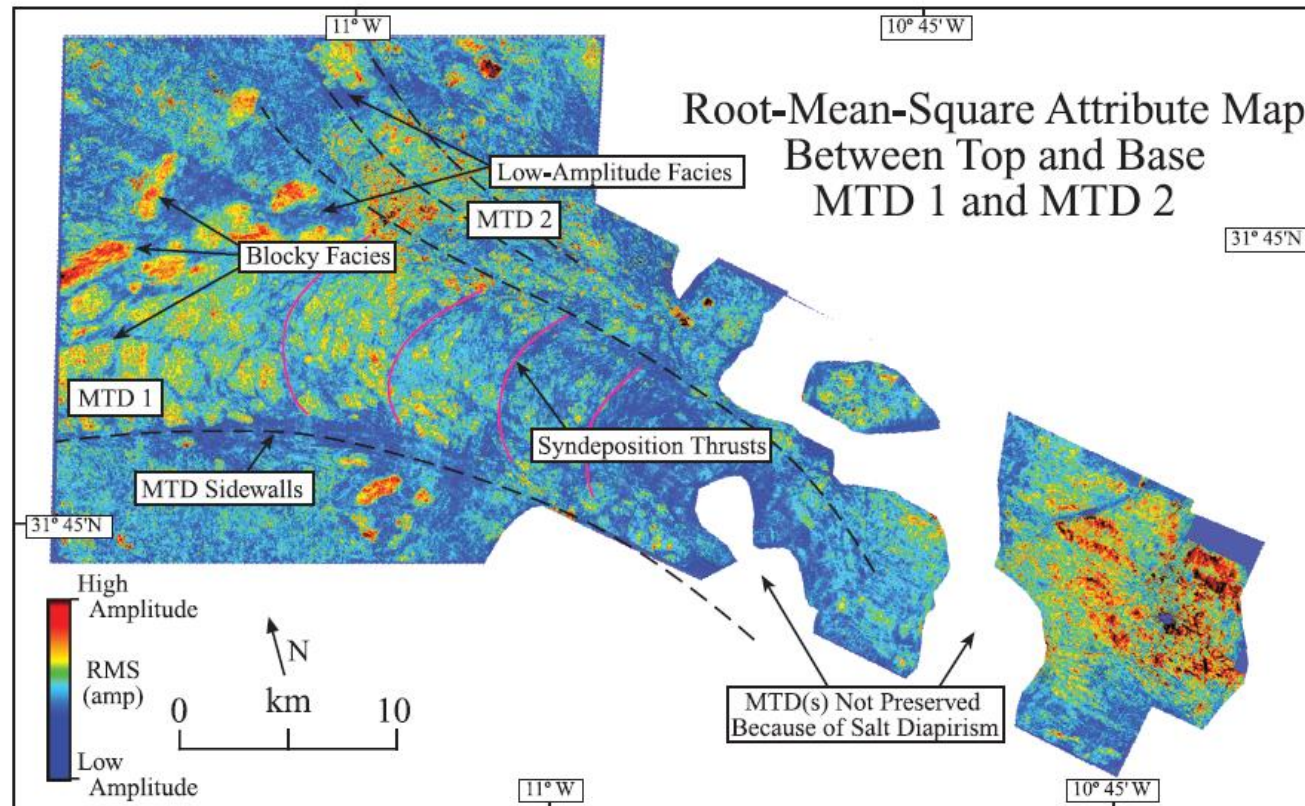


Figure 19. Root-mean-square attribute map of the interval between the merged tops and bases of mass-transport deposit (MTD) 1 and MTD 2. The map shows the distribution of high-amplitude MTD blocks within fluidlike, low-amplitude, chaotic facies. Syndepositional thrusts and distinct sidewalls are visible. Postdepositional salt diapirism has partly displaced the mass-transport complex in the east part of the study area.

Figure 3-18 RMS extraction of the MTD identified offshore Morocco (Dunlap et al. 2010).

3.4.3.5 Contourites

The recognition of seismic reflection geometries that indicate the influence of sea-bottom currents on the deposition of sediments has become a topic of recent investigation (Faugères and Stow 2008; Nielsen et al. 2008; Zenk 2008; Rebesco et al. 2014). Contourites are characterised by the presence of drifts, which are bodies of sediment in general having an anticlinal form, with the internal reflectors seen to down lap or pinch out at the edges of the feature. The adjacent regions, often infilled with horizontally layered reflections, are known as moats. The nature of these sediments is such that they appear as long wavelength sediment waves that can be divided into the constructional portion of the fabric as drifts, and the intervening bypass or erosional regions as moats.

Contourites have been interpreted as being present in a variety of locations around the globe, including, but not limited to, Norway (Bryn et al. 2005b), Brazil (Duarte and Viana 2007), Antarctica (Lucchi and Rebesco 2007), Denmark (Surlyk and Lykke-Andersen 2007), and Greenland (Hunter et al. 2007).

A classification of the geometries typically associated with contourite deposits outlined by Rebesco and Faugeres (Faugères and Stow 2008) has been used in this study to compare the seismic responses seen in the 3D volume with those attributed to contourite deposition.

The variety of bed forms that are attributed to deep-water ocean currents as classified by Faugeres et al. (2008) is illustrated in Figure 3-19.

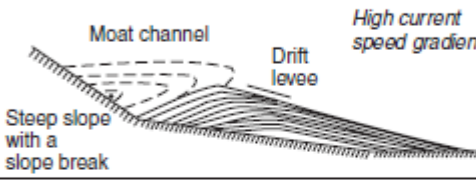
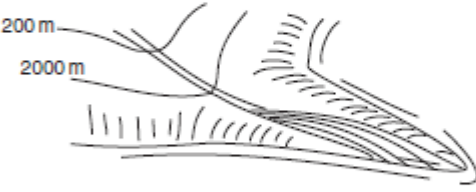
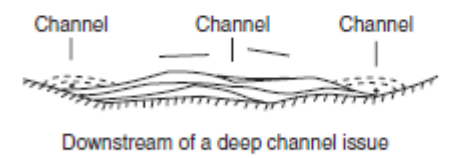
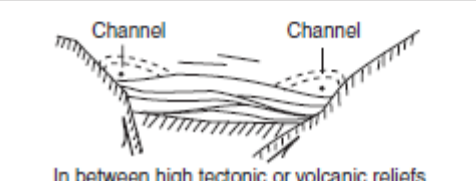
| Mounded drifts: migration and aggradation any type of reflections, except horizontal/parallel reflections | | |
|---|--|--|
| Giant elongated drifts | Plastered drift - along-slope migration (downstream of the current flow) - down-and up-slope migration Example: Gardar drift |  <p style="text-align: right;"><i>Low current speed gradient</i></p> |
| | Separated drift - along-slope migration (downstream of the current flow) - up-slope migration E.g. Faro drift |  <p style="text-align: right;"><i>High current speed gradient</i></p> |
| | Detached drift - predominant down-slope migration Example: Eirik drift |  |
| channel-related drifts | - predominant down-current migration - random lateral migration Example: Vema contouritic fan |  <p style="text-align: center;">Downstream of a deep channel issue</p> |
| Confined drifts | - predominant down-current migration - limited lateral migration Example: Sumba drift |  <p style="text-align: center;">In between high tectonic or volcanic reliefs</p> |

Figure 3-19 Classification of contourite drifts (after (Faugères and Stow 2008)).

The morphology of the channel-related drifts noted in Figure 3-19 is noted to be similar to some of the geometries recognised within the 3D volume.

A good seismic example of contourite deposits is seen in Figure 3-20. The presence of large-scale ridges cut through by erosional scours is highlighted by Nielsen et al. (2008). This reflection pattern is similar to that observed in the western half of the 3D survey, which is discussed in chapter 6. Of note is the scale of the bodies identified in the image, as the lateral extent of the large-scale depositional units is in the order of tens of kilometres.

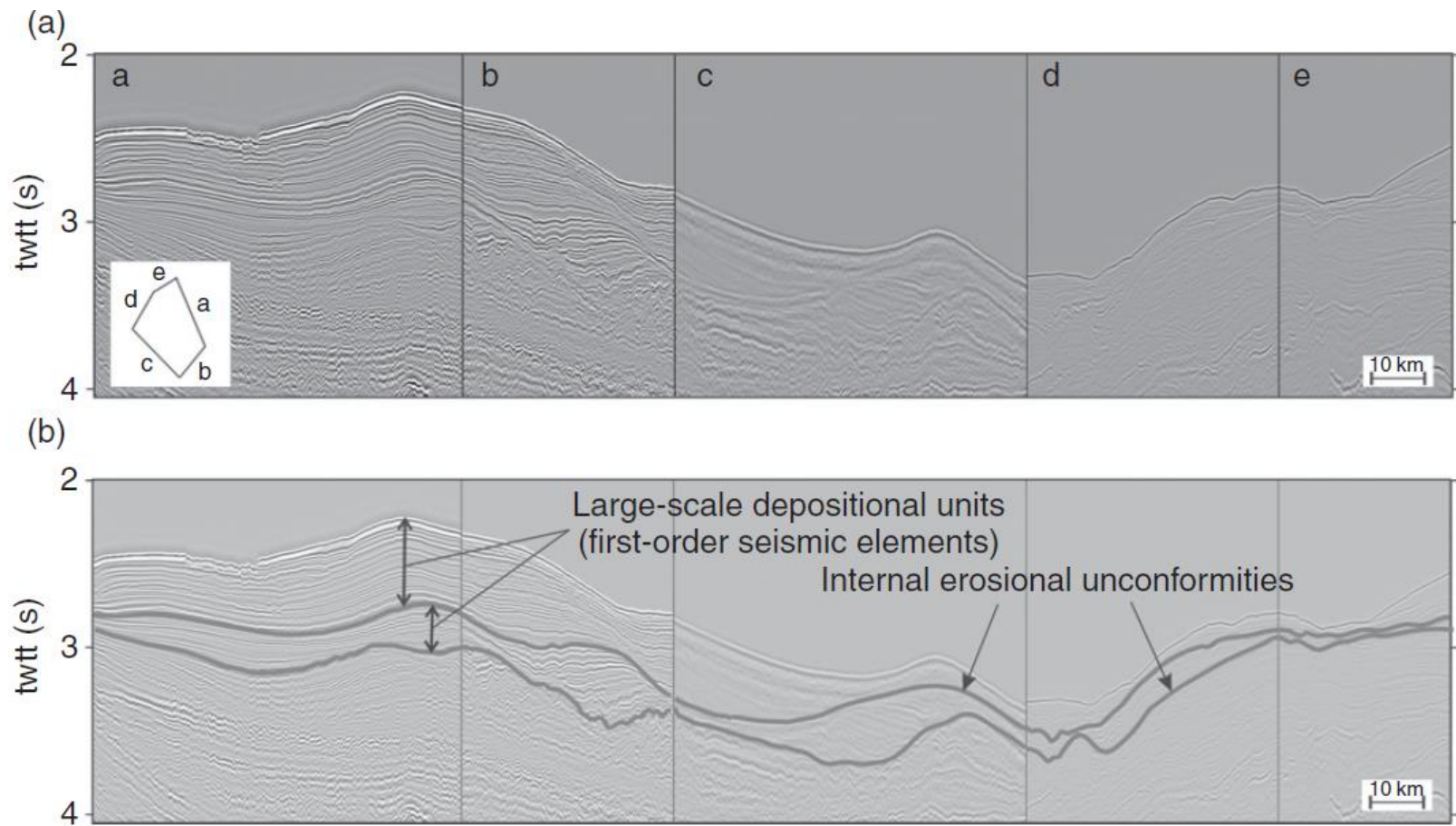


Figure 3-20 Example of large-scale contourite drifts, the Eirik drift offshore southern Greenland (Nielsen et al. 2008).

Chapter 4

Contents

| | | |
|-------|----------------------------------|----|
| 4 | Data..... | 55 |
| 4.1 | Introduction..... | 55 |
| 4.2 | 3D seismic..... | 56 |
| 4.3 | Gravity..... | 63 |
| 4.4 | Well data | 64 |
| 4.5 | Interpretation methodology | 65 |
| 4.5.1 | Horizon Selection | 68 |

4 Data

4.1 Introduction

The primary source of data used in this study is a 3D seismic survey, which was provided by Petroleum Geo-Services (PGS). The seismic data was provided as a true amplitude time migrated stack volume. No additional volumes, such as partial offset stacks were available, hence the data cannot be used for amplitude versus offset (AVO) analysis in deciding the nature of the lithology from the 3D seismic.

The study has been performed without access to publicly available well data. The well data in Nigeria is not released to the public and is held as proprietary information by licence holders of exploration and production acreage.

The Niger Delta has been covered with widespread 3D seismic data; the images of the deep water that have been published indicate that the imaging of deep data of Cretaceous age is in general poorly imaged (Corredor et al. 2005; Maloney et al. 2009). Particularly in regions of complex folded structures, the imaging is poor (Graue 2000). However, the seismic data in the northern region of the Niger Delta and the Benin Basin indicate the presence of good quality data in the pre Cenozoic interval (Morgan 2003).

4.2 3D seismic

The 3D data covers an area of close to 3,330 sq. km and lies in an area where the water depth ranges from 800 meters to 2600 meters. The data was supplied without any indication of the acquisition parameters, such as cable length, gun depths, cable depths and fold of stack. The volume was processed to a two way travel time (twl) of 8.7 seconds. The sample rate is 4 milliseconds giving a Nyquist frequency of 125 Hz (Yilmaz and Doherty 2000). No

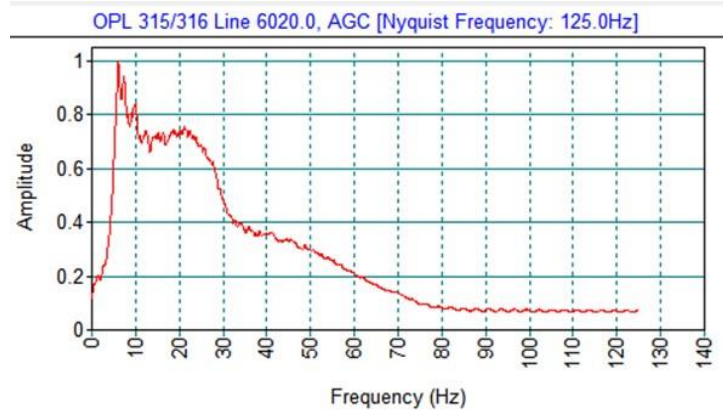


Figure 4-1 Frequency spectrum

further information concerning the processing of the data was provided. However, analysis of the data suggests that the data is dominated by frequencies in the 5-30 Hz range (Figure 4-1). This limitation on bandwidth is time variant, with higher frequencies present in the shallow section.

Seismic resolution is defined by the tuning thickness, the thickness below which it is not possible to resolve bed separation. The tuning thickness is usually calculated from the equation:

$$\lambda = v/4f$$

Where v is the average velocity within the bed, f is the dominant frequency (in Hz) within the wavelet and λ is the bed thickness (Brown 1996; Yilmaz and Doherty 2000).

In the shallow section, the frequency ranges up to 80 Hz and the velocity is often less than 1600 ms⁻¹. This implies a tuning thickness of around 5m close to the sea bed. In the deeper section, the velocity is anticipated to be in the region of 4000 ms⁻¹ and the frequency closer to 20 Hz. At these depths, the resolution increases to 50m.

As a result of the acquisition geometry, the resultant bin size is 37.5m (inline) x 25m (cross line), which is not unusual for a regional 3D seismic survey. Typically a high resolution survey would be acquired with a bin size of 12.5 x 12.5m. This large bin size limits the degree of lateral resolution and the dip angles that are imaged. The maximum dip that can be imaged without aliasing is a function of the velocity and the lateral sampling interval. In this case, the dips in the cross line direction are better sampled than the inline.

The maximum dip that can be sampled is derived from the equation below (Brown 1996):

$$\frac{v}{2f\Delta x} \leq \sin\Theta$$

Where Θ is the angle of dip of the reflection being adequately imaged, Δf is the dominant frequency and v is the average velocity in the overlying medium. Δx is the trace spacing. As an example with 4ms sampling (with an implied Nyquist frequency of 125Hz) and an overburden velocity of 2000 ms⁻¹ a trace spacing of 25m would be sufficient to image dips up to around 20 degrees. However, given the nature of the data, in that it is also an amplitude varying data set rather than a monochromatic one, the character of the data is such that dips can be mapped up to 70 degrees. Nonetheless, in areas of steep dip, apart from one recognisable horizon it is not possible to map any dips greater than about 45 degrees (Figure 4-3).

The phase of the data does not appear to be zero. The sea bed is a clear acoustic boundary and since it corresponds to an increase in acoustic impedance a zero phase response would be represented by a symmetrical wavelet. The peak/trough actually observed is assumed to indicate that the data is non-zero phase. Analysis of the phase/amplitude spectrum of the data also indicates the data to be mixed phase. Figure 4-2

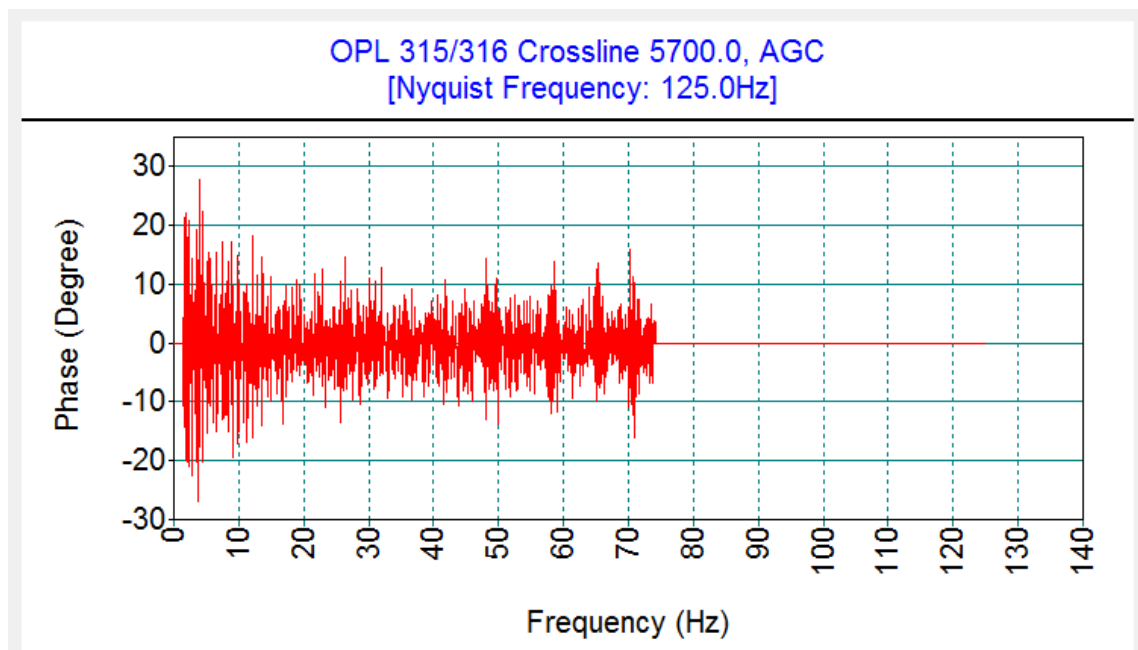


Figure 4-2 Phase spectrum of the data

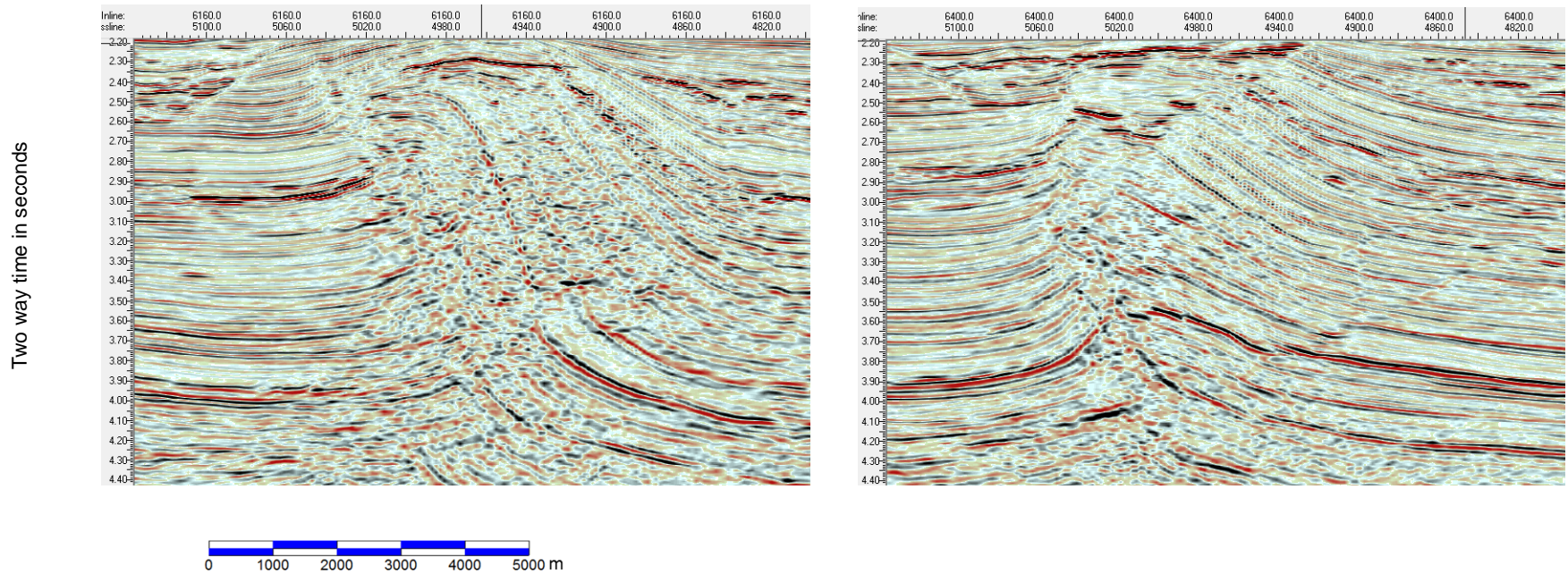


Figure 4-3 comparison of two dip lines, showing the poor imaging quality in the steeply dipping interval in the left hand image

No processing report was available as the data were produced as a non-exclusive product. The data is migrated in time and hence there are still distortions within the data set, which could be rectified with depth migration. Nonetheless, the key stratigraphic and structural elements of the region can still be obtained from this data set.

The data supplied was processed to obtain a true amplitude set, in order to highlight potential hydrocarbon related anomalies. Within the shallow portion of the data, there is an interval with large acoustic contrasts. As a consequence of the shallow anomalies within the section, the first inspection of any amplitude work indicated that the shallow amplitude effects were masking the deeper information. A 1000ms automatic gain control (AGC) was applied to the data for the purpose of interpretation. The contrast between the original data and the AGC volume is shown in Figure 4-4. In areas of very high amplitudes in the shallow section the deeper data is masked, such that even the application of an AGC does not recover the amplitudes.

In addition to the AGC dataset, a volume was generated using the SMT Kingdom software's similarity algorithm; this similarity volume proved to be extremely useful in identifying a number of geological features, which are less obvious in the conventional amplitude data. The similarity attribute commonly referred to as the coherency attribute (Li and Zhao 2014) is used to compare adjacent traces within the dataset. Where two adjacent traces have a similar character, the value of the similarity is high; where the two traces differ in character, the similarity is low. When viewed in map form either as a time slice or an extraction at a gridded horizon, this attribute is good for identifying lateral discontinuities, such as faults and channel margins.

There is an inherent distortion within the data in terms of structural and sedimentary information. The data is processed through a time migration and the imaging is therefore dependent upon the velocity field used for stacking and migration. An example (Figure 4-5) illustrates the presence of non-geological features caused by the time and velocity limitations. Structural maps generated from the data are presented here as two way time contour displays. As a consequence a number of apparent artefacts are observed; this could be due to velocity variations.

Should further work be undertaken to better understand the detailed structural history of the region, then a depth migrated volume should be used. The use of isochrones, however, is less compromised as the velocity distortions affect all the horizons to more or less a similar degree. Within this thesis, the seismic vertical cross sections are

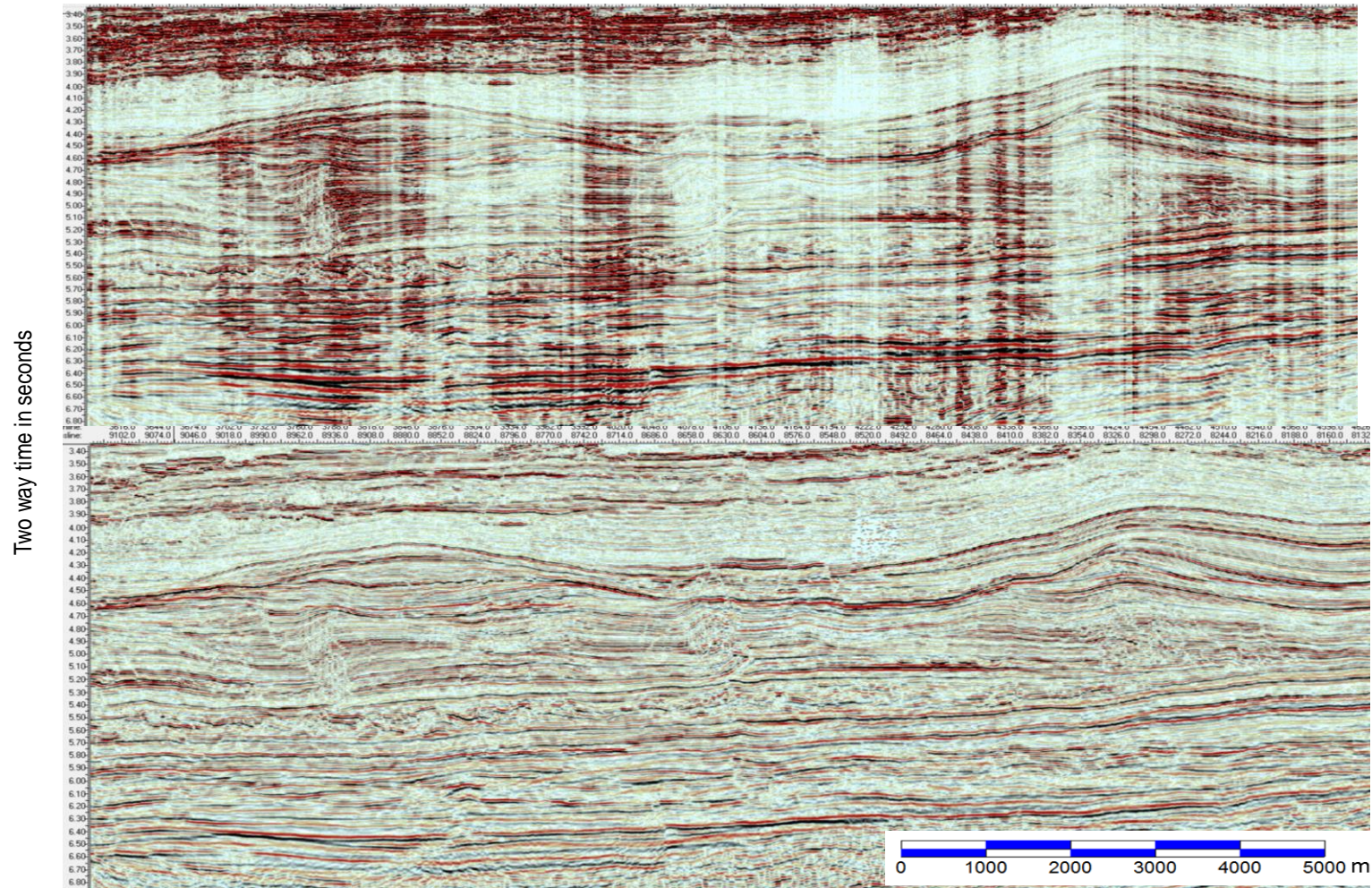


Figure 4-4 Comparison of original data (upper image) with the AGC compensated volume (lower image).

displayed at a number of vertical and horizontal scales. Where a scale is not included in the figure, the distance between the vertical black lines is 5 kilometres as in Figure 4-4. All sections are displayed in two way travel times in seconds.

Of particular note is the synclinal nature of the section underlying a series of anticlinal structures in the overburden. This “push down” has been recognised by other authors (Tucker 1982; Kostenko et al. 2008). The velocity push down has been ascribed to the lowering of compressional acoustic velocities arising from the presence of overpressured mobile shale and the associated shale diapirism (Bruce 1973; Tucker and Yorston 1973).

The data in this survey are imaged quite well within these anticlinal ridges and where visible a complex structural deformation is observed. The map in Figure 4-6 is a two way time contour map of the base Cenozoic horizon (Figure 4-6). Overlain on this map are the locations of the anticlinal ridges in the overlying interval taken from the two way time map of the base Neogene horizon. What is striking is the alignment of the anticlines with the apparent depressions in the base Cenozoic twt map. This suggest there is indeed a strong link between the ridges and the lowering of lateral velocity, relative to the surrounding sediments, within the anticlinal features.

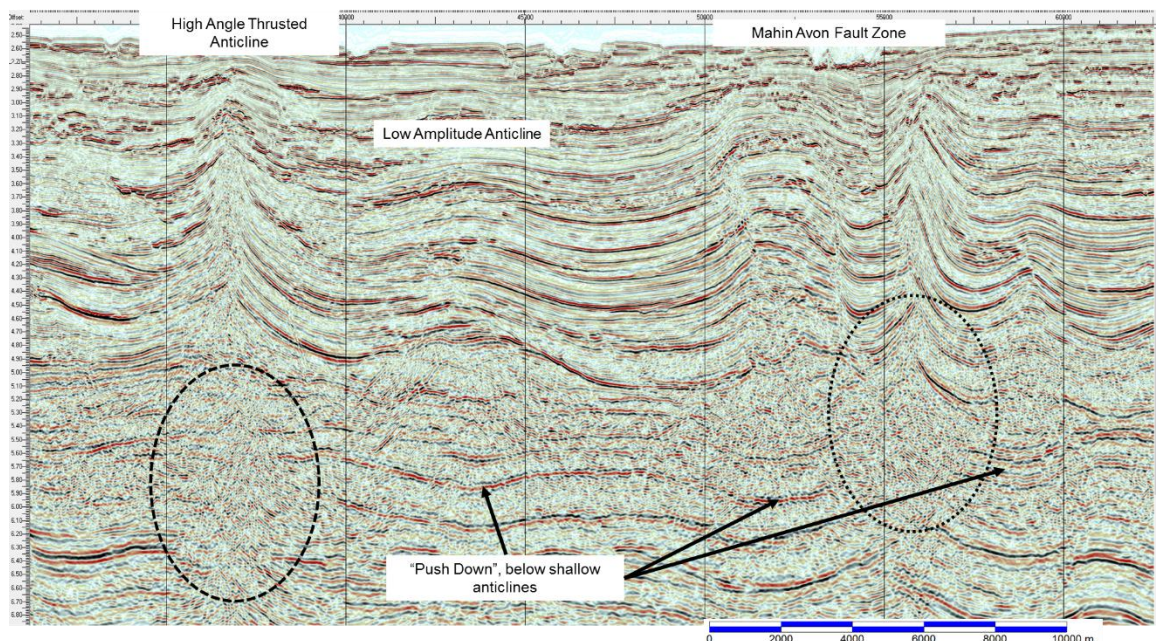


Figure 4-5 Portion of inline 5300 illustrating the over migration of reflectors below the Avon/Mahin fault zone

The apparent lowering of the velocity can be linked to a number of factors as follows:

Overpressures: when sediment is unable to expel fluids due to rapid loading or hydrocarbon generation, the pore fluids become overpressured relative to the

hydrostatic pressure for the equivalent depth. This overpressure lowers the effective stress of the rock, which in turn is reflected in a lowering of velocity (Yilmaz and Doherty 2000). In addition, the presence of a larger percentage of pore water within a rock lowers the velocity due to the higher percentage of low velocity water within the overall body of rock (Cobbold et al. 2009).

Ray path irregularities: the assumption of the hyperbolic behaviour of move out is only valid for non-dipping isotropic media. In dipping beds with lateral velocity variations and a highly anisotropic medium, the normal move out assumptions are no longer valid (Hubral 1980). In theory this effect should be catered for in the migration process. Ideally a pre stack depth migration (PSDM) with the correct velocity model would rectify the distortions but in this case the data is not in this form. As a result of this, the deeper data in particular is poorly imaged in areas of structural complexity, such as the zone that lies below the Avon/Mahin fault zone.

Sediment composition: it may be that the sediment composition within the anticlines is such that the acoustic properties of the sediments vary considerably from the surrounding rocks.

Anisotropy: one other possible explanation for the “push down” is the effect of anisotropy on the travel paths of the acoustic energy through the subsurface. Shales are known to be anisotropic in their acoustic properties and therefore this needs to be accounted for in the processing (Tsvankin and Thomsen 1992).

Counteracting the effect of velocity depression is the impact of velocity hysteresis, whereby sediments buried to a certain depth inherit a velocity due to lithification and compaction. When uplifted, the acoustic properties of the rocks do not return to their values at an equivalent depth; they tend to retain the values reached at maximum burial. Intuitively therefore the uplifted axis of these ridges should have a higher average velocity (Japsen 1993).

It is beyond the scope of this thesis to investigate this issue further as access to the data other than in a migrated time volume is not possible.

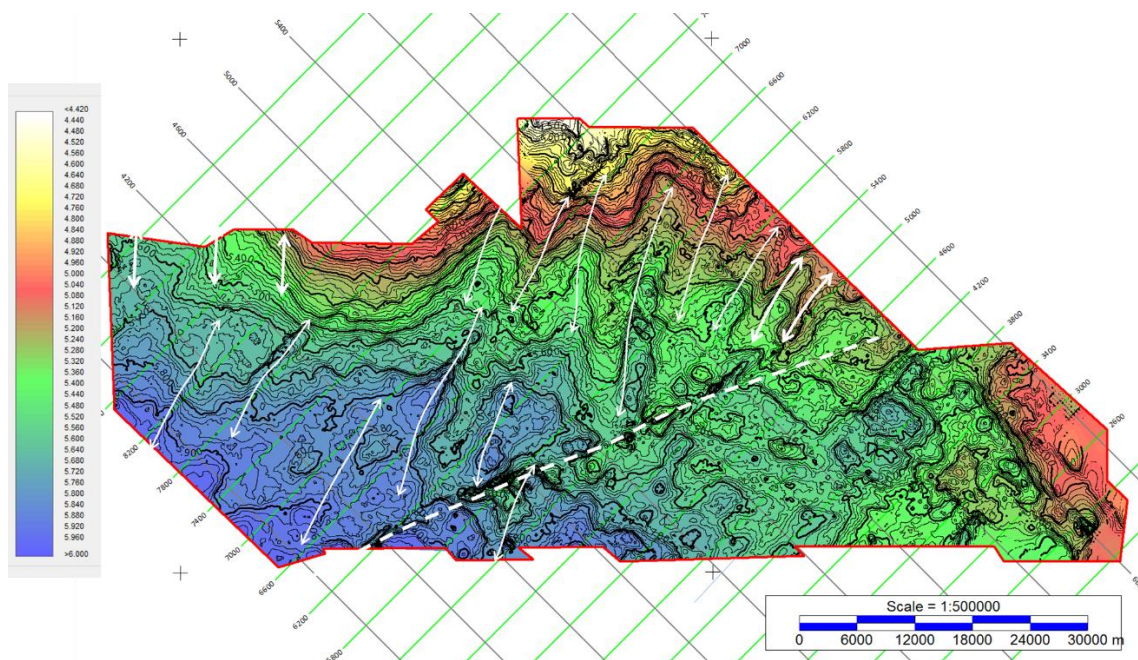


Figure 4-6 Two way time map of the base Cenozoic horizon, illustrating the location of anticlinal ridges (in white) mapped at the base of the Neogene.

In Figure 4-6, the white arrows are indicative of the location of the late stage anticlinal features; the darker colours in the two way time map indicate depressions. The correlation between the shallow anticlines and the underlying depressions in the map are considered to be the cause and effect of velocity distortions within the overburden. The white dashed line is the approximate location of the Mahin/Avon fault zone.

A common cause of data degradation is the presence of multiple energy within the data. Multiples result from repeated reflections from acoustic boundaries. The most obvious multiple observed within marine seismic data is that of the sea bed. In places where there is a high amplitude even in the shallow section the multiple can also cause interference with the primary data.

Additional noise contamination arises from the migration of noise, which if not catered for correctly produces “smiles” within the data. This is particularly noticeable in low signal to noise regions of the data, such as the zone that lies under the Avon/Mahin fault zone

4.3 Gravity

Satellite gravity data covering the gulf of Guinea is available to download from Scripps Institute of Oceanography, University of California, and San Diego. This global data set has proven to be useful in establishing the plate reconstructions that reunite Africa and South America (Fairhead 1988; Nürnberg and Müller 1991; Basile et al. 1993). The most recent update to the published material is the inclusion of a vertical gravity gradient image. In Figure 4-7, (Sandwell et al. 2014) the transform faults that traverse the Atlantic

Ocean are clearly visible. The use of the gravity data has allowed the recognition of the presence of canyons present along the shelf margin of the Benin Embayment.

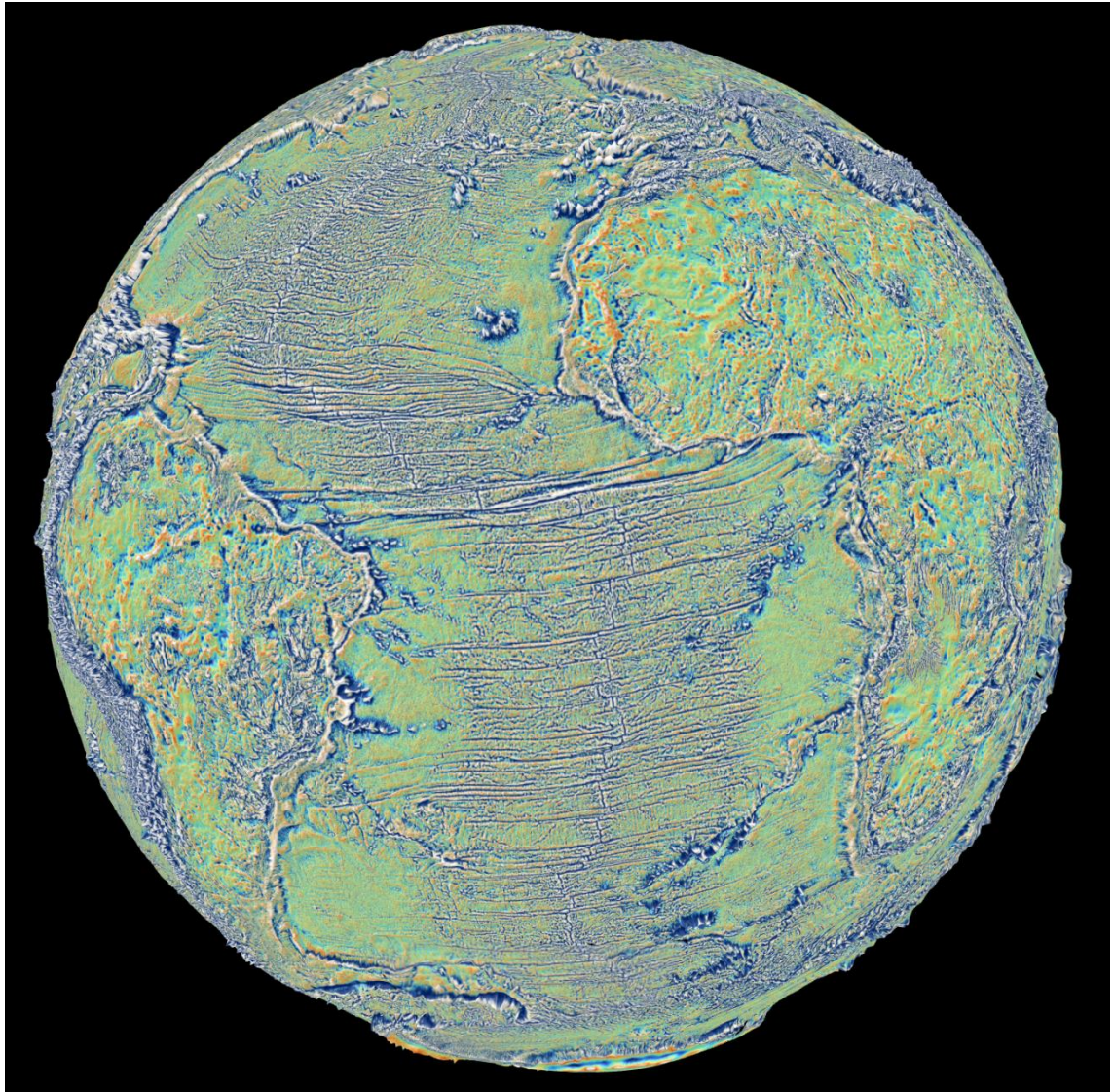


Figure 4-7 vertical gravity gradient derived from satellite data, draped over topography (Sandwell et al. 2014)

4.4 Well data

Primary well data (wireline logs, cuttings and core) is the property of the Nigerian government and is limited in use to the licence owners of the permit in which the well has been drilled or another permit holder who has traded the data. Therefore in this study the references to well data come from published material and cannot be verified at their source.

4.5 Interpretation methodology

Interpretation was performed using the seismic micro technologies (IHS/SMT) Kingdom suite of software and was carried out using primarily a laptop PC. The functionality of this suite of software allowed the major observations to be reached.

Interpretation was carried out on the basis of picking every tenth in line, spaced 375 meters apart and tied via means of every fiftieth cross line, spaced 1250 meters apart. In places of complex geology, the picking of cross lines was reduced to every tenth line and every fifth inline. In addition, the option to select random lines through the survey proved to be useful in confirming both structural picks and horizon continuity. The ability to create random lines that run orthogonally to major faults is a particularly helpful tool. The random line selection and the finer cross line spacing of lines interpreted helps with the interpretation of the more complex faults and the steeply dipping ridges. In areas of laterally continuous horizons, automatic picking was used, however given the laterally varying geology, both structural and sedimentary, this technique had limited use in this study.

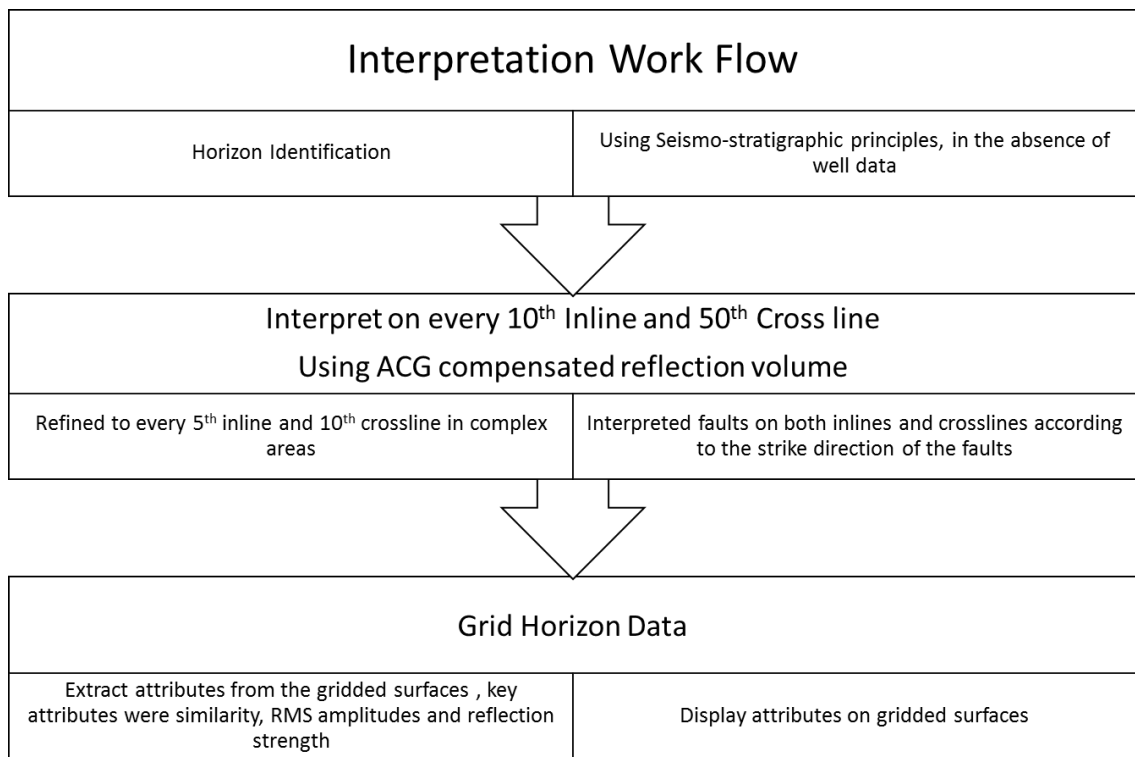


Figure 4-8 Interpretation workflow

One aspect of the area that limits the degree to which horizons can be carried to any great lateral extent is the influence of the Avon Canyon (Olabode and Adekoya 2008). The canyon`s most recent manifestation, which has shed sediments into the deeper water via turbidity currents, has led to the erosion of a number of horizons in the western

half of the survey as noted in section 6.3.1. Nonetheless, the key structural features can still be mapped.

In areas of distorted overburden arising from lateral velocity variations in the overburden noted earlier in this chapter, the use of the flattening option within the software proved useful in gaining an understanding of the geology. This was particularly true for the interpretation of the Cretaceous section.

Faults were initially picked on vertical sections without any assignment. In order to correlate the key faults, horizontal slices were used to identify continuity. Of particular use are the similarity slices that pick out discontinuities more readily than conventional amplitude slices. One method which proved valuable in identifying fault patterns is outlined below.

The interpreted horizon picks were gridded and the interpreted grid was converted to a horizon. Amplitudes and similarity values were then extracted at the generated horizon. The extraction of the similarity at the horizon picks out faulting clearly in areas of the data that are often complex, as can be seen in Figure 4-9

The image in Figure 4-9 is the similarity attribute extracted along the surface of horizon 130. The lighter colouring indicates regions where adjacent traces have similar reflection characteristics. The darker lines indicate a difference in the character of adjacent traces, such as that found at fault intersections. Additionally, to enhance the understanding of the lateral distribution of sedimentary features, a series of attributes were extracted in windows either hung upon specific horizons or between horizons. The use of the root mean square (RMS) sum of amplitudes within an interval proved to be a useful means of identifying channel deposits in particular. In Figure 4-10 the lighter colours indicate the presence of higher amplitudes within a window of 150 milliseconds above a middle Miocene horizon. The presence of meandering channel belts can be inferred from this image.

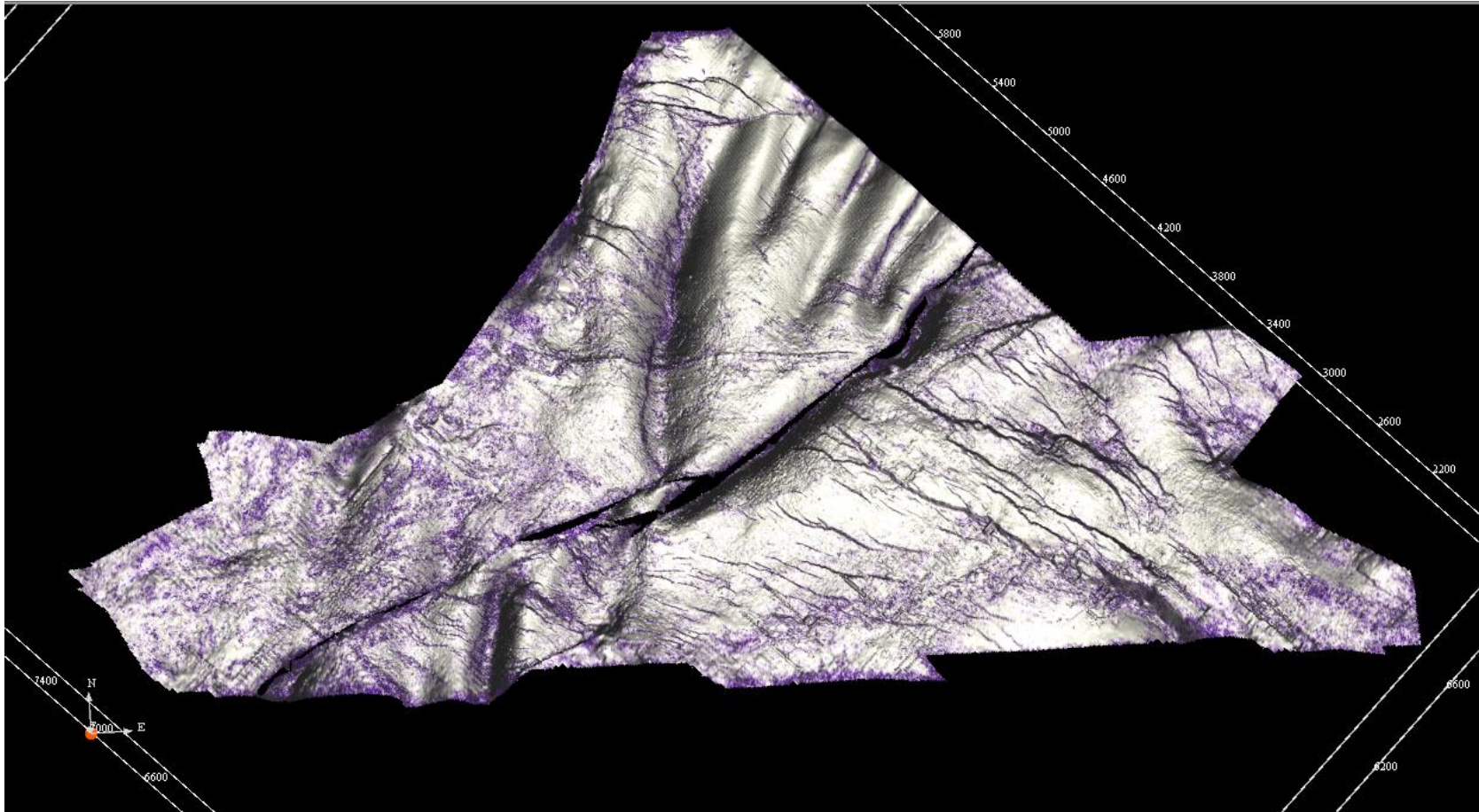


Figure 4-9 Extracted similarity from a grid of a Miocene horizon, which indicates in the dark colours the presence of faults – where the degree of similarity between traces is low.

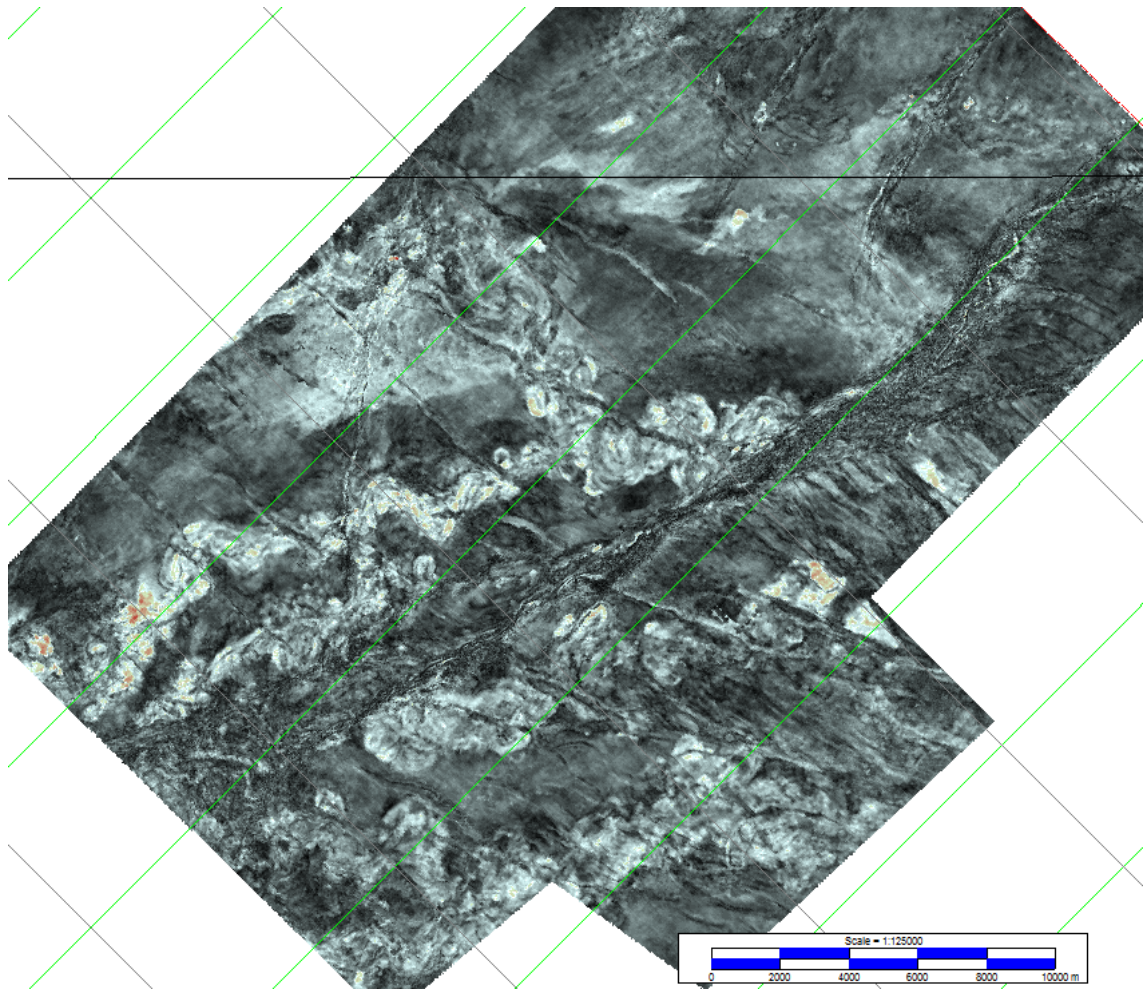


Figure 4-10 Example of an RMS extraction from within a window between two middle Miocene horizons

4.5.1 Horizon Selection

4.5.1.1 Horizons

There is no available well data that can be used to tie the reflectors seen within the 3D data limits. As a consequence, a seismostratigraphic approach has been used to identify various sequences. This breakdown was then tied in a broad sense into the known depositional history of the region as described in chapter 3. In chapter 5, the key horizons and their stratigraphic significance are outlined. With no data available to definitively tie the picked horizons to a specific sequence boundary, the use of a numbering system in which the oldest horizons were assigned a high number was implemented, with the sea bed being the youngest and labelled horizon 0.

The basis for selecting the chosen horizons was primarily based upon the recognition of seismic sequences, following the principles as outlined in AAPG memoir 26 (Mitchum Jr. et al. 1977; Vail et al. 1977). The sedimentary section can be broken down into several major sequences, which are bounded by regionally known unconformities: the break up unconformity which is linked to the separation of Africa from South America, the Senonian unconformity which is linked to the change in the pole of rotation of the African plate during the Upper Cretaceous. (Guiraud and Bosworth 1997; de Matos 1999) and a significant unconformity within the Cenozoic, linked to the global drop in sea level during the Oligocene (Vail et al. 1977).

The large scale regional unconformities are related to significant tectonic movements that altered the gross geographical setting; they are regionally limited to the African margin. Within these regional scale sequences a number of lower order sequences are recognised, which are primarily linked to changes in eustatic sea level changes; these are mostly global in significance.

In deep water sediments, the effects of eustatic sea level fluctuations are not directly visible. However, the recognition of sea level high and low stands relies upon the change of sedimentation within the deep water deposits, which are associated with the rise and fall of relative sea level. The breakdown of depositional units controlled by eustatic sea level fluctuations can be broken down into a number of tracts within a sequence, which describe the process of deposition. In general there are three phases of deposition, which are classified as low stand tracts, transition tracts and high stand tracts (Van Wagoner et al. 1990).

In general, the input of coarse sediments into deep water occurs at time of a relative sea level low stand (Galloway 1975, 1998). During the period during which the sea level drops, the coast line moves seawards and exposes the coastal section to erosion. The product of the erosion is shed down the slope into the basin. During periods of high sea level, the coast moves landward and the degree of erosion drops as the provenance area becomes drowned. The presence of both mass transport deposits and slope channels in the section are considered to represent periods of relative low sea level.

Within the seismic volume, the regional unconformities are seen as angular truncations of reflectors. This is particularly noticeable at the top of the syn-rift interval, which is marked by the truncation of the underlying dipping and faulted sediments and the deposition of the overlying un-faulted reflections.

The recognition of the high stand and low stand intervals in the shallow section is based upon the recognition of reflection character and geometries (Mitchum Jr. et al. 1977). High stand intervals are represented by a set of parallel horizons with lateral continuity.

The nature of the high and low stand sequences within the seismic data is illustrated in Figure 4-11. The low stand intervals are characterised by the influx of material, which either cuts into the layered sediments or is deposited over these high stand section. In this study, the low stand intervals contain both mass transport deposits (including debris flows) and slope channels.

4.5.1.2 Mapping

Survey wide mapping of horizons was carried out, in the main without the inclusion of faults, so that the gross form of the structure could be observed.

For more detailed mapping of selected areas, the faults were incorporated to show the local tectonic arrangement. If the large number of faults present within the 3D volume (in excess of five hundred) had been included in all of the maps, they would have obscured some of the larger scale elements of the region.

All of the maps are presented as two way time maps, with the exception of the sea bed (where a water velocity of 1500ms⁻¹ was used to depth convert). With no well control or velocity data available, it was thought best to leave the data in time rather than use an erroneous depth conversion.

Gridding of the picked horizon data was used to generate surfaces, which were then used for isochrones calculations and amplitude and similarity extractions.

In order to assist in the understanding of the evolution of the region, a number of isochrones of the intervals between horizons were generated. The maps generated are broad representations of the thickness variations, as no attempt has been made to compensate for structural thickening and thinning in the presence of faulting and folding.

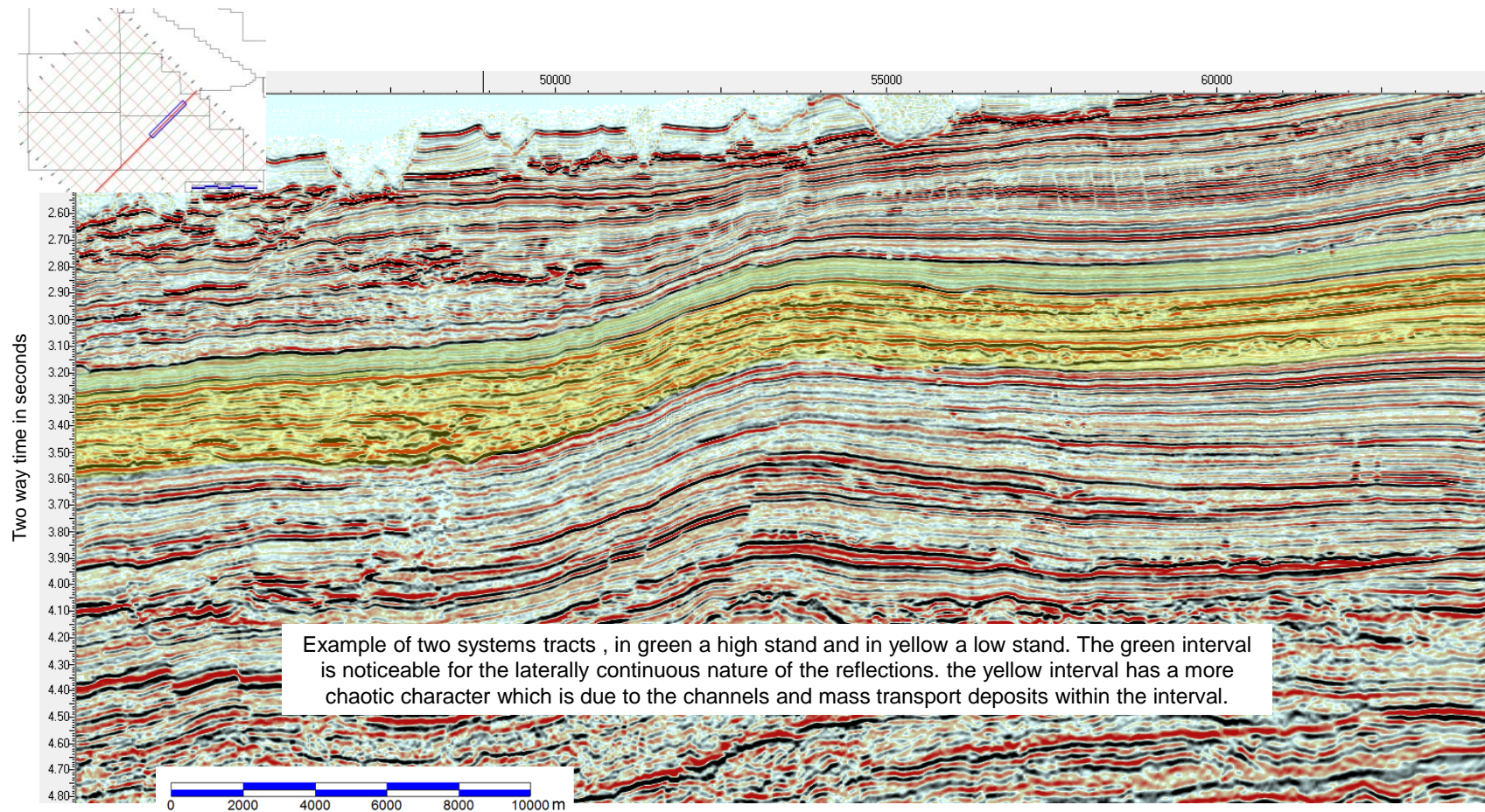


Figure 4-11 Seismic cross section which indicates the reflection character of both high and low stand deposits

Chapter 5

Contents

| | | |
|--------|--|----|
| 5 | Stratigraphy | 72 |
| 5.1 | Introduction..... | 72 |
| 5.2 | Horizon Identification | 73 |
| 5.2.1 | The syn-rift (below Horizon 800)..... | 74 |
| 5.2.2 | Mid Albian Unconformity (Horizon 785) | 75 |
| 5.2.3 | The Senonian Unconformity (Horizon 680)..... | 77 |
| 5.2.4 | Campanian (Horizon 630)..... | 79 |
| 5.2.5 | Near base Cenozoic (Horizon 600)..... | 79 |
| 5.2.6 | Top of the regional mass transport complex (Horizon 510)..... | 79 |
| 5.2.7 | Deepest faulted event within the Cenozoic (Horizon 500)..... | 81 |
| 5.2.8 | Intra ridge surfaces (Horizons 470, 465, 429, 425) | 82 |
| 5.2.9 | The base of the Neogene (Horizon 420)..... | 82 |
| 5.2.10 | Unconformity within the Neogene (Horizon 400)..... | 84 |
| 5.2.11 | Upper limit of the levee system (Horizon 300) | 84 |
| 5.2.12 | Lower Miocene, base of the channel levee system (Horizon 200) | 85 |
| 5.2.13 | Middle Miocene Upper limit of main channel levee influx (Horizon 160). | 86 |
| 5.2.14 | Upper Miocene Base of low stand section (Horizon 130)..... | 86 |
| 5.2.15 | Pliocene (Horizon 100) | 87 |
| 5.2.16 | Sea Bed (Horizon 0)..... | 88 |

5 Stratigraphy

5.1 Introduction

The breakdown of the sedimentary section into sequences, using the methods described in chapter 4 resulted in the identification of a number of key seismic horizons and their assumed stratigraphic significance. Using the regional description outlined in chapter 3, the selection of seismic horizons follows the same stratigraphic divisions highlighted in that chapter. The use of the seismostratigraphic approach (Brown Jr and Fisher 1977; Mitchum Jr. et al. 1977) has proven to be useful in linking the events mapped to the regional stratigraphy outlined in Chapter 3.

The key sequences are the syn rift, the Albian to Cenomanian, the Campanian to Maastrichtian, the Palaeogene, and the Neogene. Within the Paleogene, a number of horizons were selected to demonstrate the structural deformation. The Neogene was subdivided into further sequences. These are based upon the seismic character, which is tied to the rise and fall of relative sea levels.

Isochrones of the intervals between the major mapped surfaces indicate that, in general, the post rift Cretaceous section thickens from north to south, while the Palaeogene is thickest in the west and the Neogene thickest in the east. The Palaeogene is thickest in the west due to the input of sediment from a source in the north, which is probably associated with a canyon system. The Neogene is dominated by the influence of sediment supply from the Niger delta.

5.2 Horizon identification

A chronostratigraphic breakdown of the Benin Basin was used as a guide to recognise the key geological events within the region.

Table 5-1 Horizon identification

| Horizon | Horizon Identification | Age | Pick ID | Key |
|----------------------------|---|-----|---------|-----|
| Sea Bed | | 0 | 0 | |
| Base Pliocene | Base of parallel transparent package | 5 | 100 | |
| Base Upper Miocene | Base of shallow mass transport complex | 9 | 130 | |
| Top Middle Miocene | Top of slope channel suite | 12 | 160 | |
| Top Lower Miocene | Mapped mass transport level | 17 | 200 | |
| Top Oligocene | Top Ridge/Levee sequence and Onset of channel levee deposition | 25 | 300 | |
| Mid Oligocene | Sediment hiatus, top of lower tectonised interval | 27 | 400 | |
| Base Neogene | Base of tectonised section | 58 | 420 | |
| Top Mass Transport Complex | Top regional mass transport complex | 60 | 510 | |
| Top Maastrichtian | Base regional mass transport complex | 66 | 600 | |
| Top Campanian | Top of interval which contains both thrusts and a major mass transport complex. | 72 | 630 | |
| Senonian Unconformity | Angular unconformity, which cuts down into the underlying horizon 785 | 83 | 680 | |
| Mid Albian Unconformity | High amplitude event seen to be truncated by down cutting erosional event | 102 | 785 | |
| Syn Rift Unconformity | Near top Syn-Rift, angular unconformity | 120 | 800 | |

The initial identification of the seismic horizons was made without reference to any age association and hence a numeric ID was used. However, during the project it became possible to assign tentative ages to the selected horizons.

For example, the recognition of angular unconformities can be tied to major regional or global geologic episodes. The recognition of gross depositional sequences was also used to identify the more significant horizons to map. The key horizons mapped are listed

in Table 5-1 along with the colour key that can be used to identify the age of the horizons in the cross sections within this document.

5.2.1 The syn-rift (below Horizon 800)

The deepest regionally mappable event is the angular unconformity, which marks the upper limit of the syn-rift (horizon 800). It is recognised as an angular unconformity that separates an underlying section of tilted and faulted sediments from an overlying section, which is largely un-faulted; this underlying interval is assigned a syn-rift affinity. As the horizon marks an unconformity, it is interpreted to represent a hiatus in deposition and a period of sediment erosion and is diachronous in nature. By analogy with the Brazilian margin the rifted section would be the conjugate to the rifted elements of the Potiguar Basin (de Matos 1992, 1999). The age of the rifted sediments in the Potiguar Basin are Barremian and older in age.

In the western half of the area covered by the 3D survey, the reflective package of events, which are interpreted to be syn-rift deposits are absent. This may be the result of poor seismic imaging or the absence of sediments below the unconformity. The two way travel time (twt) map of horizon 800 (Figure 5-1) shows an overall west to east striking surface, which dips to the south. The anticlinal and synclinal trends seen in the eastern half of the survey are interpreted to be related to the velocity distortions seen in the overburden.

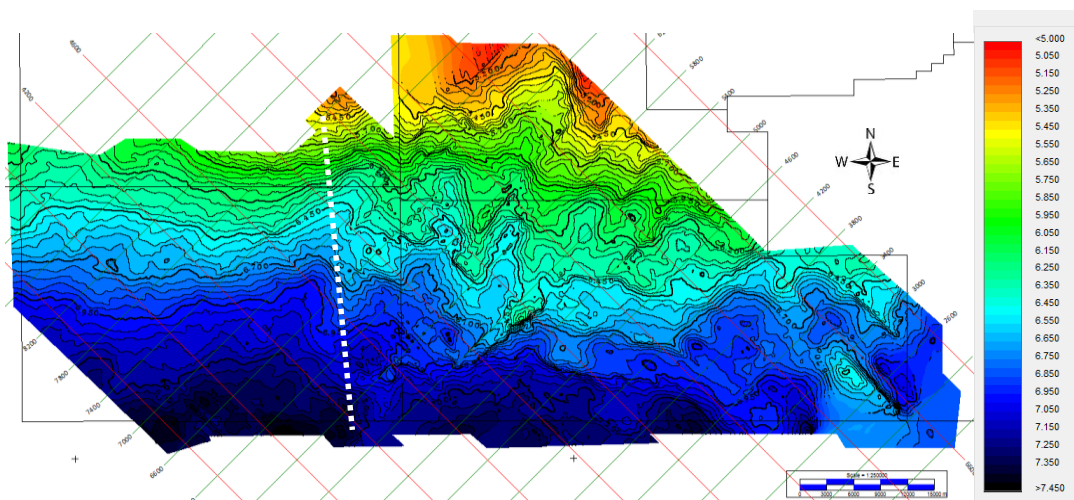


Figure 5-1 two way time map of the break up unconformity (horizon 800), the dashed white line marks the approximate location of the boundary between reflective - to the east, and non-reflective - to the west, events below the unconformity.

Underlying the unconformity is an interval, which is separated into two geographical regions. One is characterised by an interval up to two seconds twt in thickness, in which there are reflections interpreted as representing sediments, which are heavily faulted. The second region is devoid of any continuous reflectivity. The dividing line between the two sub unconformity facies is marked by the dashed white line in Figure 5-1.

The region with the marked reflectivity is assumed to be comprised of sediments deposited during the rifting whereas the region with little or no reflectivity may be devoid of sediments and may be comprised of continental, igneous, or metamorphic rocks or transitional oceanic crust.

In places, the data is of good enough quality in the syn rift region to recognise the major fault trends, which have left their mark in the remnant morphology of the unconformity surface. The key faults strike in a north west to south east direction, with the major throws being down to the south west.

Overlying this unconformity is an interval, capped by the Base Cenozoic event I in which the sediments appear to be unaffected by major tectonic activity; they fill the accommodation space created when the rifting ceases and thermal subsidence commences. The interval thins towards the north. Within this interval two horizons have been mapped which are of regional significance.

5.2.2 Mid Albian Unconformity (Horizon 785)

Within the section, which overlies the syn rift unconformity, a number of seismic reflectors can be seen. These fall into two categories; there is a sequence in the west, described in the next section, which contains seismic horizons that are limited in lateral extent. Towards the east, there is one mappable event displaying good lateral continuity. This horizon is limited to the east following the effect of subsequent erosion. This truncation runs in a north to south orientation. The imaging of the event is poor beneath the Avon/Mahin fault zone, but the character match allows a confident jump correlation to be made (Figure 5-3). The fact that the truncation is not displaced in a lateral sense below the Avon/Mahin fault zone is interpreted to imply that there is no transcurrent displacement at this level. In Figure 5-2 the thickness of the Middle Cretaceous interval (between horizon 785 and horizon 680) thins to the east as a result of the down cutting erosion associated with the effects of the Senonian unconformity. Also highlighted in this figure is the location of the Avon/Mahin fault zone (the white polygon). The western limit of the mapped horizon results from a change in the reflection character outlined in the following section.

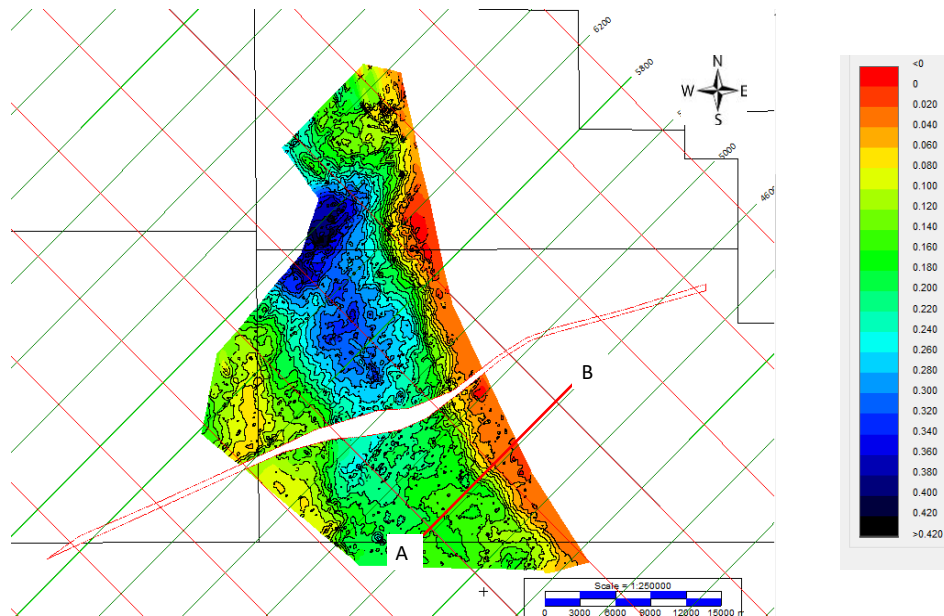


Figure 5-2 Isochrone of the Albian to Cenomanian interval (between horizon 785 and 680). The white polygon indicates the location of the overlying Avon/Mahin fault zone.

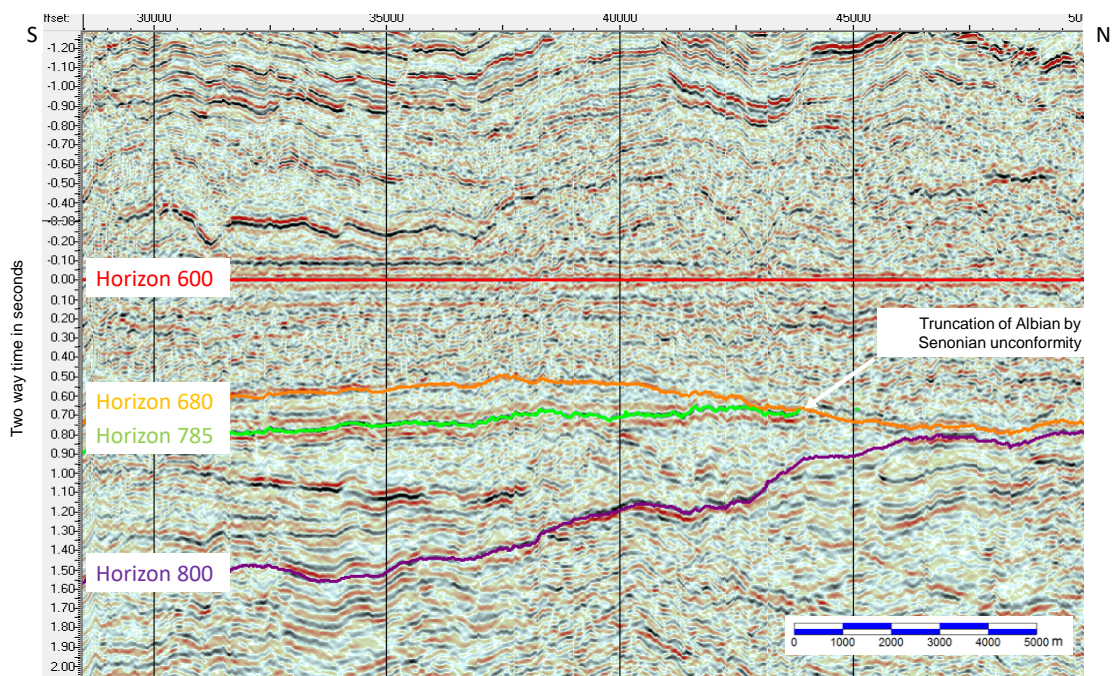


Figure 5-3 portion of cross line 5000, which is flattened at the base of the Cenozoic (horizon 600), see Figure 5-2 for the location of the line.

Figure 5-3 illustrates the truncation of the mid Albian Unconformity (horizon 785) by the Senonian Unconformity (horizon 680). The high amplitudes seen below the Albian horizon may represent igneous intrusions, as their geometries are irregular and in places resemble the saucer shape associated with igneous sills.

5.2.3 The Senonian Unconformity (Horizon 680)

A horizon, which is interpreted to correspond to the Senonian unconformity was interpreted and mapped; the horizon marks the boundary between either an overlying parallel set or onlapping set of reflections and by the truncation of underlying events via assumed erosion (Figure 5-3). In the eastern half of the survey, the event is very clearly identifiable. The onlapping interval appears to be a section of parallel-presumed marine sediments. In the western half of the survey, the overlying sediments are largely parallel and continuous. The section beneath the unconformity in the west, where the imaging is good, is laterally discontinuous with varying dips. As the unconformity, by its nature, is a varying acoustic boundary the character of the surface varies across the survey. In the region close to the Avon/Mahin fault zone the quality of the data breaks down.

Within the interval, which lies below the unconformity in the western region of the survey, the reflection geometries are irregular. The orientation of the internal reflectors is not confined to a single azimuthal direction; there is an apparent progradation from north to south, but also mounded geometries in an east to west orientation. The overall package of events suggests that it is comprised of a shelfal sequence, which has either been cut by canyons or an apron of deep water turbiditic deposits sourced from canyonised shelf which lay to the north. The laterally limited extent of any one reflector would indicate that the depositional setting was high energy. Low energy environments tend to leave deposits with laterally extensive seismic reflectors.

The shelfal interpretation would fit a regional depositional history of a gradually deepening sea/proto ocean in the Albian to Turonian with a southwards shift in the location of the shelf during a relative sea level drop. The turbiditic interpretation would indicate that the sediments are separated from the palaeoshelf by a bypass.

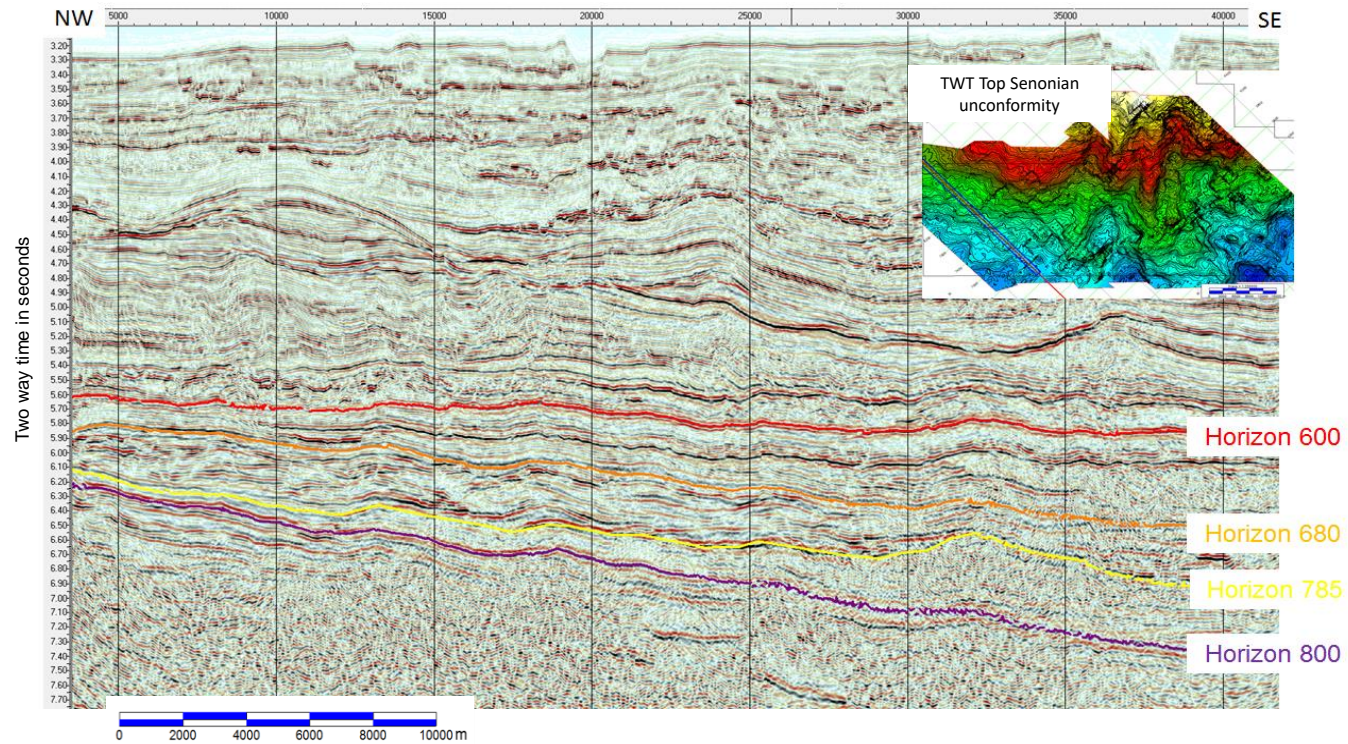


Figure 5-4 Inline 3800, illustrating the interval below the Senonian Unconformity (horizon 680), which includes the wavy discontinuous seismic facies.

5.2.4 Campanian (Horizon 630)

This event is mapped in the western half of the survey. It corresponds to the top of an interval which contains both parallel continuous events but also a section which is characterised by a series of high angle dipping reflectors. These suite of events are spatially distributed in a broad arc which points in a westerly direction. The significance of this seismic geometry will be discussed in Chapter 6.3.4. The section which overlies this horizon is parallel and continuous in nature. This horizon also marks the upper limit of a group of thrust anticlines observed in the south east of the survey.

5.2.5 Near base Cenozoic (Horizon 600)

The most regionally mappable event is the base of the Cenozoic (horizon 600). This reflector is present across the entire survey area and marks the base of the tectonically modified overburden. The underlying interval is largely undisturbed by tectonic activity; the horizon corresponds to the top Akata pick of late Cretaceous to Early Cenozoic age noted by other authors (Morgan 2003; Briggs et al. 2006; Cobbold et al. 2009). This is a key horizon to consider in the structural evolution of the region. Flattening of the horizon on the workstation helps to eliminate some of the velocity distortions which are seen in the volume. The nature of this acoustic interface is not well understood. It is not clear why this horizon should mark the base of the region wide shelf collapse. One possible explanation is outlined in chapter 8. The horizon appears to be faulted in three regions, however it is thought that this may be an artefact of the processing and lateral velocity variations in and around the major anticlines observed in the overburden. The horizon extends well beyond the extent of the 3D survey and is interpreted to represent the top of the Cretaceous marine shales found in the Aje and Seme wells (Kaki et al. 2012).

5.2.6 Top of the regional mass transport complex (Horizon 510)

A chaotic set of reflections are noted in the section immediately overlying the Base Cenozoic (horizon 600). It is capped by a high seismic reflection strength horizon with an irregular topography. The horizon is readily identifiable in the southern half of the survey, where it is a clear reflector. Towards the north of the survey, the event which can be mapped in the south becomes difficult to follow. The interval between this event and the base Cenozoic (horizon 600) is interpreted to be comprised of a large scale mass transport complex. In the survey area, the interval shows two distinct lobes emanating from the north. An isochrone map of the interval illustrates this (Figure 5-5). Towards the north of the survey, the horizon becomes less well defined due to the presence of

assumed younger mass transport assemblages being deposited. The eastern limit of the map is defined by the Avon/Mahin fault zone.

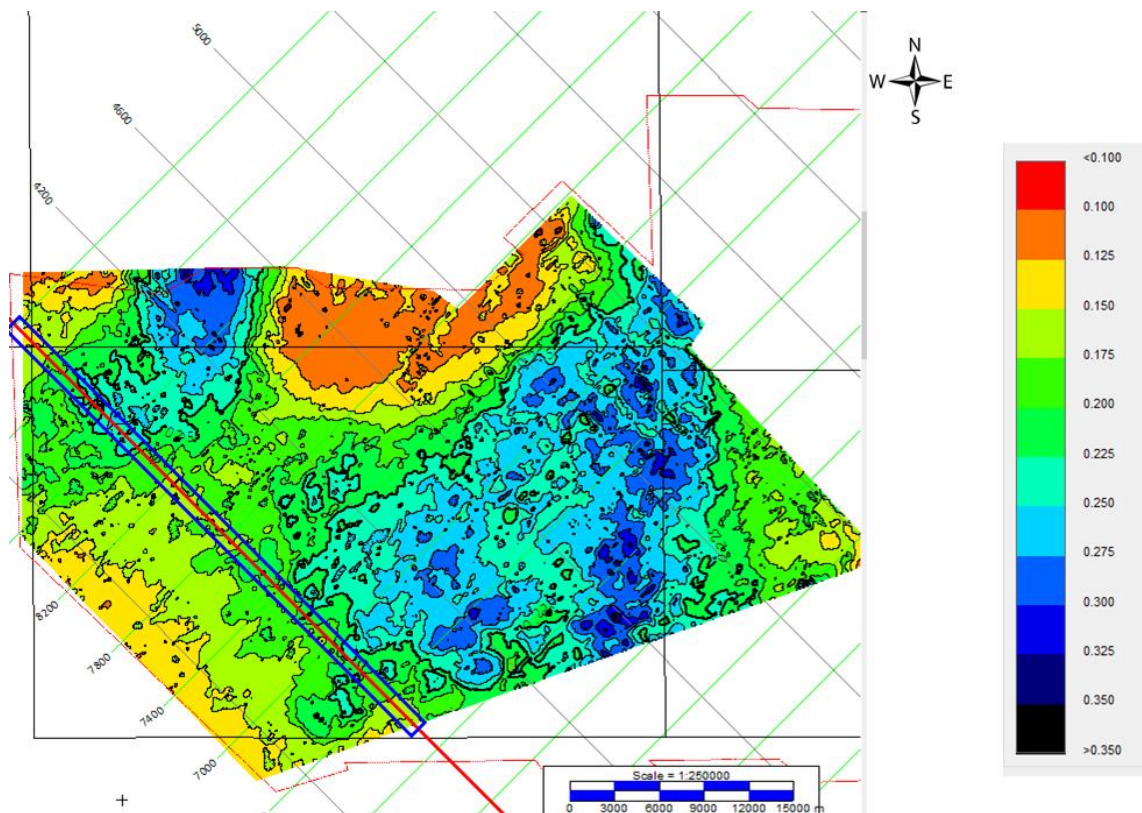


Figure 5-5 Isochrone of the mass transport complex (between horizons 510 and 600), the south eastern limit of the map is the location of the Avon/Mahin fault zone

The internal character of this interval has been compared to other published examples of mass transport complexes and the similarities observed support the interpretation of this interval being of a similar nature (Moscardelli et al. 2006; Faersth and Saetersmoen 2008; Alves 2010; Dunlap et al. 2010). One aspect which is not observed is the linear striations which are typical for the basal surface, suggesting that in the mapped area the interval is in the run out facies (Galloway 1998). The data becomes more difficult to interpret towards the north but the interpreted northern equivalent of the mapped interval is characterised by a series of southwards verging reverse faults indicative of the thrust toe of a mass transport interval.

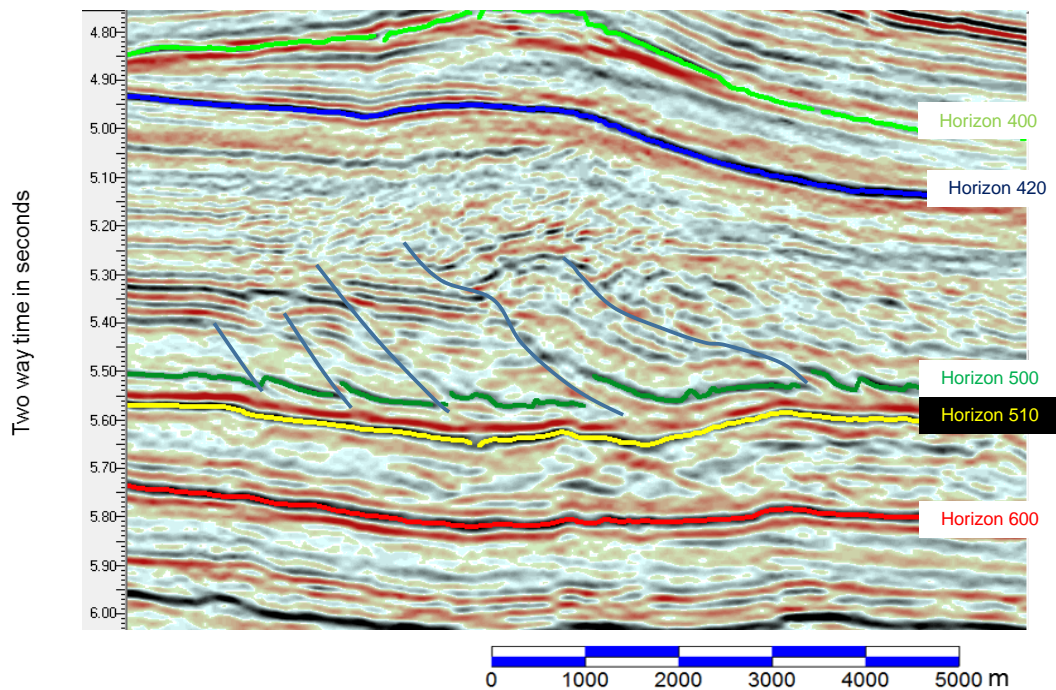


Figure 5-6 portion of inline 3800, illustrating the chaotic interval, the mass transport complex (between horizons 600 and 510), and the overlying section which is tectonically modified (See Figure 5-7 for location)

In Figure 5-6 it can be observed that the faulting overlying horizon 510 does not penetrate into the chaotic interval. The detachment is therefore interpreted to be at the interface between the mass transport interval and the later deposited hemipelagic section.

5.2.7 Deepest faulted event within the Cenozoic (Horizon 500)

The layer immediately overlying horizon 510 is the deepest event, which can be mapped, that is affected by the tectonic disturbance in the overburden. A coherency attribute extracted at this horizon indicates a large amount of faulting, which cannot be seen at horizon 510 (Figure 5-7). This surface in turn becomes a glide surface for later deformation. In the western portion of the 3D volume, the horizon marks the top of a minor mass transport deposit, which overlies the interval which contains the chaotic seismic facies referred to above.

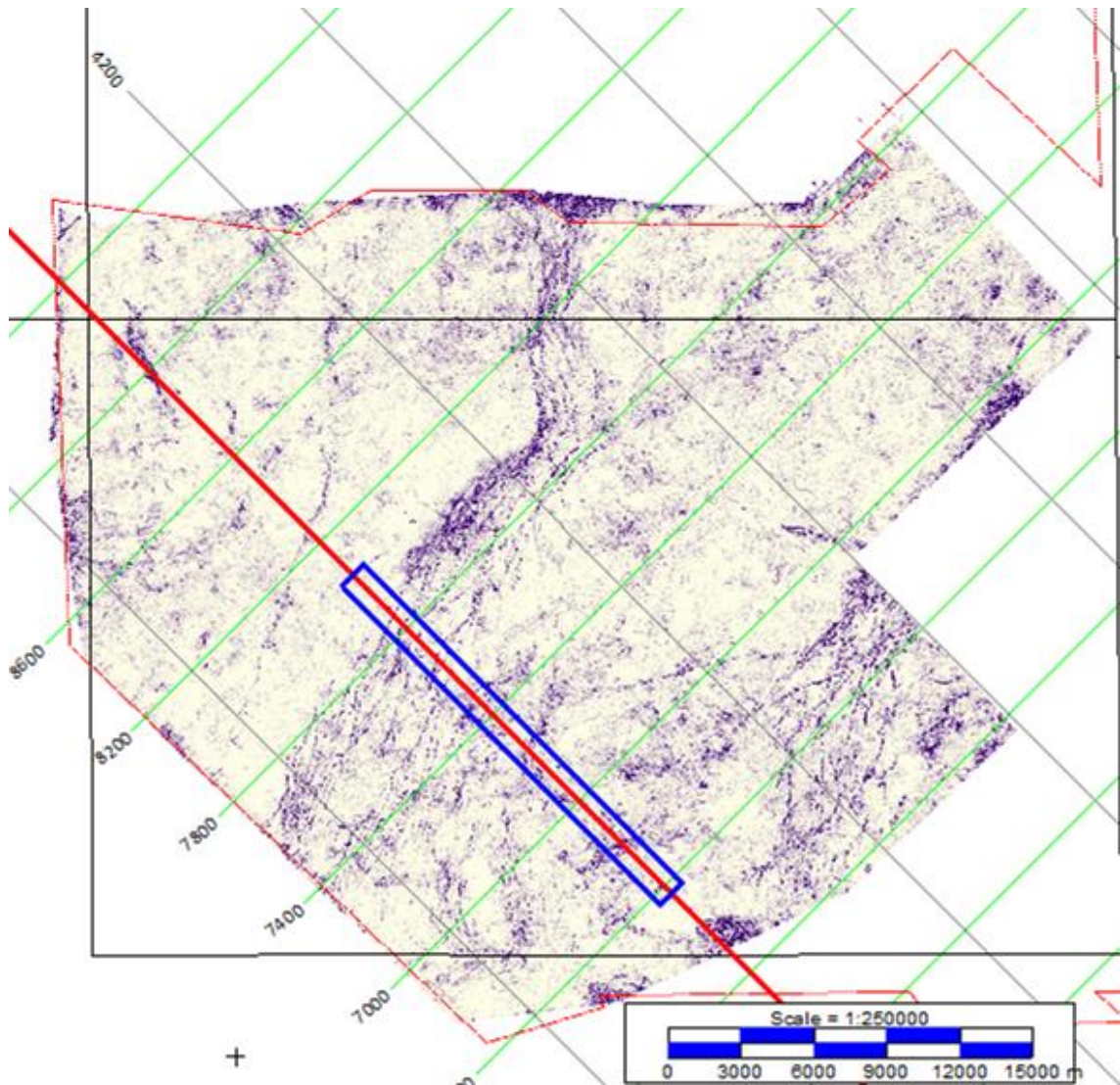


Figure 5-7 similarity attribute extracted from horizon 500.

5.2.8 Intra ridge surfaces (Horizons 470, 465, 429, 425)

In the core of the western most ridge there is a large amount of faulting. The faults, where they are well imaged in the seismic, have been mapped at a number of levels to define the structural configuration. Both amplitude and coherency extractions serve to illustrate the fault geometries. This fault pattern will be discussed in chapter 7 (structural deformation). The horizons are interpreted to represent over bank deposits within the levee of a turbidite unit.

5.2.9 The base of the Neogene (Horizon 420)

This event appears to represent a widespread unconformity, which is interpreted to be related to the major sea level drop in the Oligocene (Mitchum Jr. et al. 1977; Vail et al. 1977). It is clearly identifiable over large parts of the survey, where it is seen as a high amplitude peak within the data. This peak is absent in regions of later erosion where the

seismic reflector has been removed. The morphology of the mapped surface is notable for the presence of a series of north to south trending anticlines and synclines.

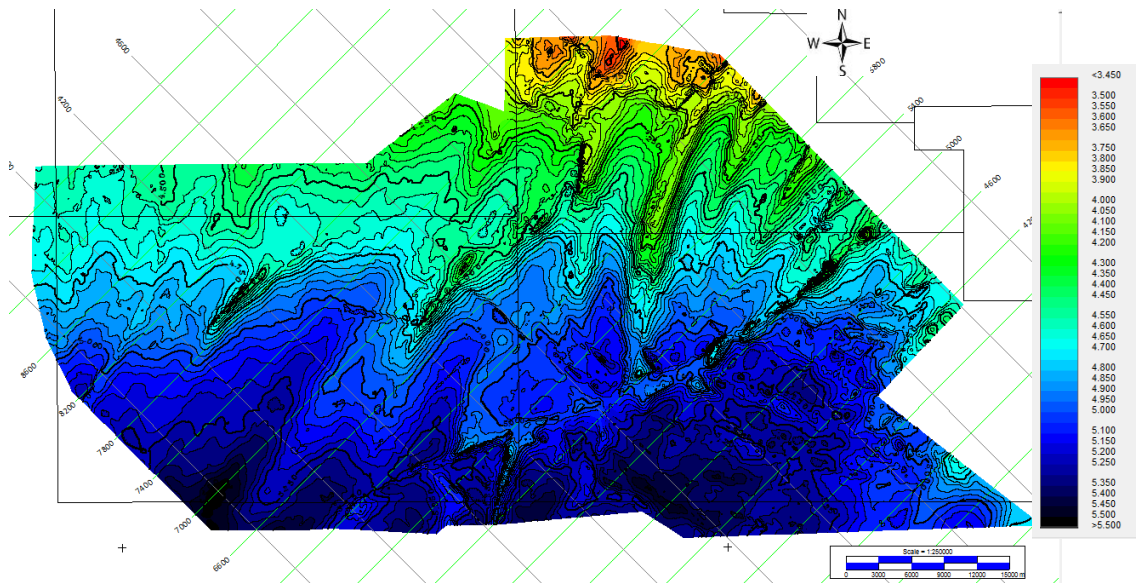


Figure 5-8 two way time map of the base Neogene (horizon 420)

Below this base Neogene unconformity (horizon 420), but above the base Cenozoic (horizon 600), the section is seen to thicken towards the west within the 3D volume. The isochrone of the interval between horizons 420 and 600 illustrates this variation in thickness (Figure 5-9).

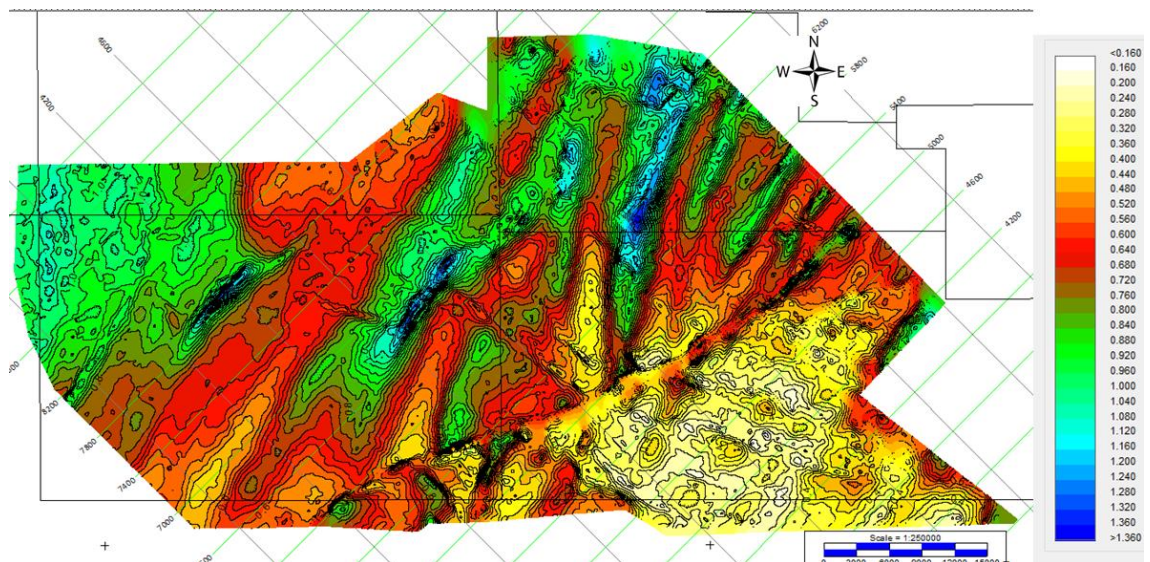


Figure 5-9 Isochrone of the thickness of the Palaeogene (between horizon 600 and 420)

The above map (Figure 5-9) illustrates the thinning of the Palaeogene interval towards the south east. The thick intervals seen in the west are interpreted to be due to the influx of sediments from the north during this period. Of particular note are the variations in the

thickness, which appear to be linear in form. This geometric form is interpreted to be a result of turbiditic flows funnelled from canyons along the shelf margin, which is present to the north of the survey area.

5.2.10 Unconformity within the Neogene (Horizon 400)

This event was mapped as it is persistent across the western half of the survey. Over the crest of the western ridge, the surface is noted as being irregular in morphology (Figure 5-10) which is a possible indicator of a depositional hiatus. The similarity attribute extracted at this surface indicates a number of arcuate discontinuities on the flank of the ridge. This may indicate the presence of collapse of unstable sediment into the adjacent syncline.

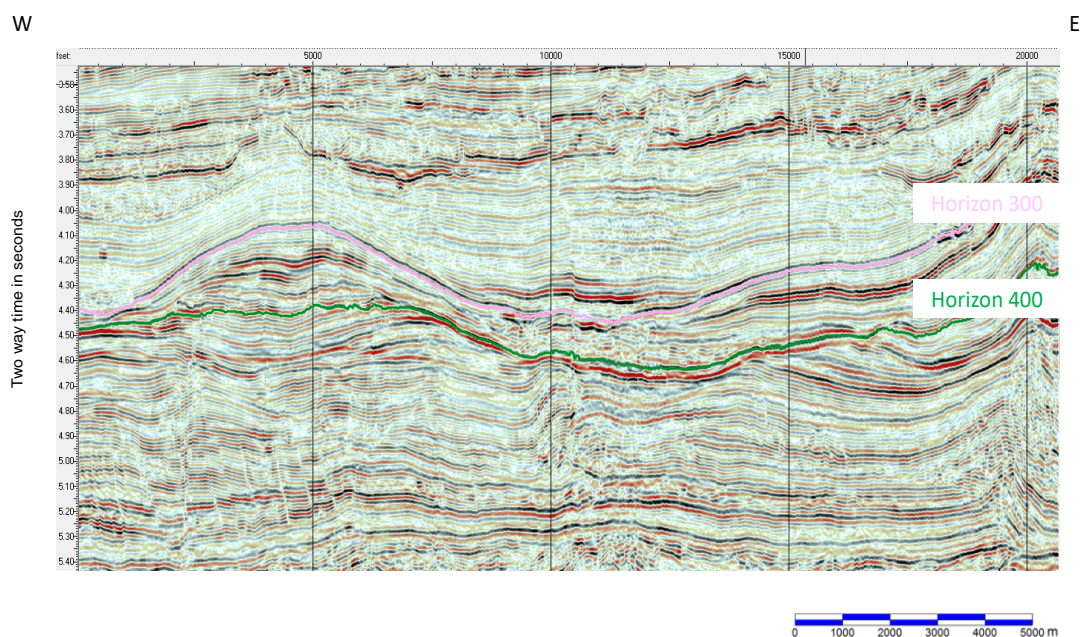


Figure 5-10 random seismic line which passes over the western ridge and the adjacent moats

5.2.11 Upper limit of the levee system (Horizon 300)

This reflection (Figure 5-10) is a laterally continuous horizon over the western half of the survey, apart from the interval cut out by the later Avon canyon sourced channel cuts. It adequately describes the prevalence of ridges and synclines in the western portion of the data. The reflector is both overlain and underlain by low amplitude sub parallel horizons, which are seen to thin down the flanks of the north south oriented ridges found in the west of the survey area. In the synclines, which lie between the ridges, the horizon loses its high amplitude continuity and becomes irregular. This irregularity is attributed to the presence within the syncline of sediments, which are not hemipelagic in origin, but most likely debris which has collapsed into the syncline or has been transported along

the axis under gravitational forces. It is interpreted that this horizon represents a change of the predominant sediment influx, from being primarily shed from the northern shelf margin of the Benin Basin to the large scale influx of sediments from the Niger Delta.

5.2.12 Lower Miocene, base of the channel levee system (Horizon 200)

This horizon was selected, as it is the highest amplitude event identified within the Cenozoic interval (Figure 5-11). It is not present over the entire survey as a recognisable reflector. Additionally, the western extent of the horizon is limited by the later erosion of the section in which it is found, by the down cutting action of younger channelised sediments, which originated to the north of the survey. To the east, the amplitude diminishes and merges into a sequence of parallel low amplitude reflectors, which have been heavily faulted post deposition.

The mapped horizon was used to map out the fault pattern associated with the major lineament, which cuts through the survey area. Correlation across the major fault was not possible via mapping around the tips of the fault and hence a jump correlation was required. The anomalously high amplitude, which characterises the picked event, was used as one of the key correlation surfaces that enabled the cross fault linkage. In addition, the faulting is so intense in the depression to the east of the lineament that a regional map was not possible to generate. Nonetheless, mapping was possible in the region immediate to the east and west of the lineament.

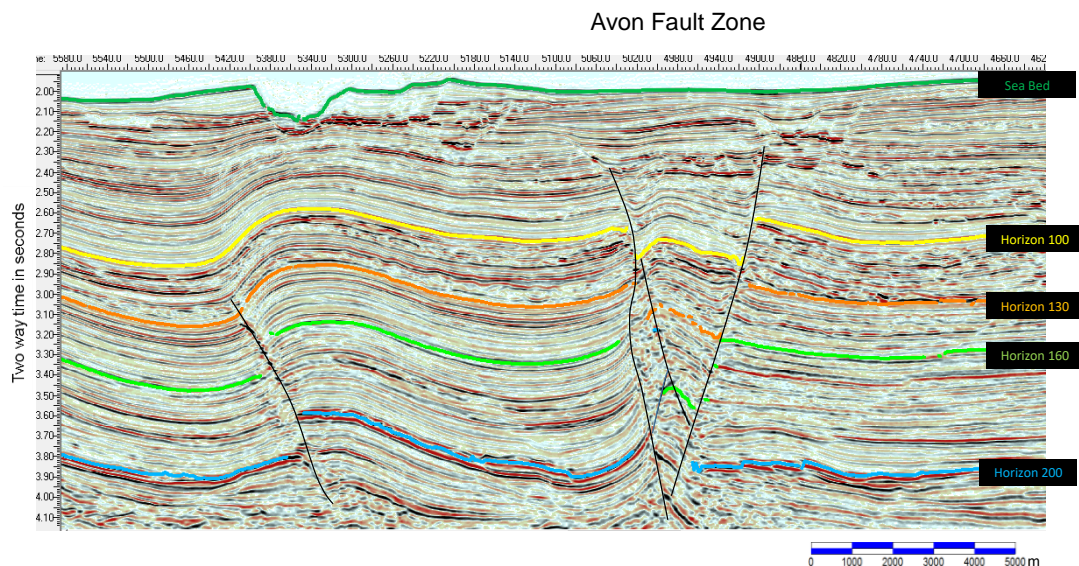


Figure 5-11 portion of inline 6480 which illustrates the horizon selection for the Miocene and Pliocene surfaces 200, 160, 130 and 100. Note that the character match across the major Y shaped fault zone (the Avon fault zone) is considered robust.

The faulting observed in Figure 5-11 is associated with the Avon/Mahin strike slip fault zone. The nature and timing of displacement within this fault zone is outlined in Chapter 7. The amplitude extraction and the similarity attribute extracted from this horizon display two regions, which can be interpreted as mass transport or debris flows. This is further discussed in chapter 6. Overlying this horizon is an interval, which contains a number of anomalous seismic events, which will be discussed in the next section. The mapped surface, since it is mapped as being coeval with mass transport activity, is interpreted to represent the onset of a period of relatively low sea level.

5.2.13 Middle Miocene Upper limit of main channel levee influx (Horizon 160)

This horizon marks the boundary between an underlying interval, which contains a seismic facies containing high amplitude discontinuous seismic reflections when viewed in vertical cross sections and an overlying sequence of parallel continuous reflections. RMS extractions from various intervals below the pick were used to establish the spatial nature of the high amplitude discontinuous events seen on the vertical displays. This led to the recognition of a number of sinuous amplitude trends, interpreted as channels when compared to similar facies noted elsewhere (Clark and Pickering 1996; Kolla et al. 2007; Cross et al. 2009; Talling et al. 2012). The slope channels which were identified in the section below the picked event are seen to originate in the east and alter their direction of flow to a more north east to south west direction, west of the Avon/ Mahin fault zone (Leduc et al. 2009). The initial direction of flow, which is mapped as being in the east, indicates that they have been sourced from the Opuama/Benin canyon system (Petters 1984; Deptuck et al. 2007).

The mapped horizon marks the cessation of the inflow of these channelised deposits, which is interpreted to indicate that a relative rise in sea level occurred at this time, terminating the supply of turbidity current derived sediment reaching this region.

In the region, which lies to the north of the channel belt, the attribute extractions indicate periodic input of material from the north in the form of debris flows.

5.2.14 Upper Miocene Base of low stand section (Horizon 130)

This event marks a break between an underlying sequence of parallel continuous reflectors, which are interpreted to be the result of pelagic sedimentation and an overlying interval of discontinuous reflectors. The mapped horizon has a marked v shaped erosional base which runs in a roughly east west orientation west of the Avon/Mahin fault zone. The interpretation of this horizon was possible across the majority of survey (being eroded in the west by the later channels related to the outwash from the Avon canyon) and proved useful in demonstrating the difference in tectonic style on

either side of the lineament which cuts through the survey. A series of RMS amplitude and similarity extractions were performed on the interval between this horizon and the overlying Pliocene (Horizon 100). It appears that an east west trend of channel and sediment dispersal is present, indicating that the slope of the seabed was probably dipping towards the west into the nascent Avon canyon flume. The interval which lies between this horizon and the shallower Pliocene (Horizon 100) is interpreted to have been deposited during a period of relative low sea level, which led to the increase in the input of sediments from the shelf and shelf margins.

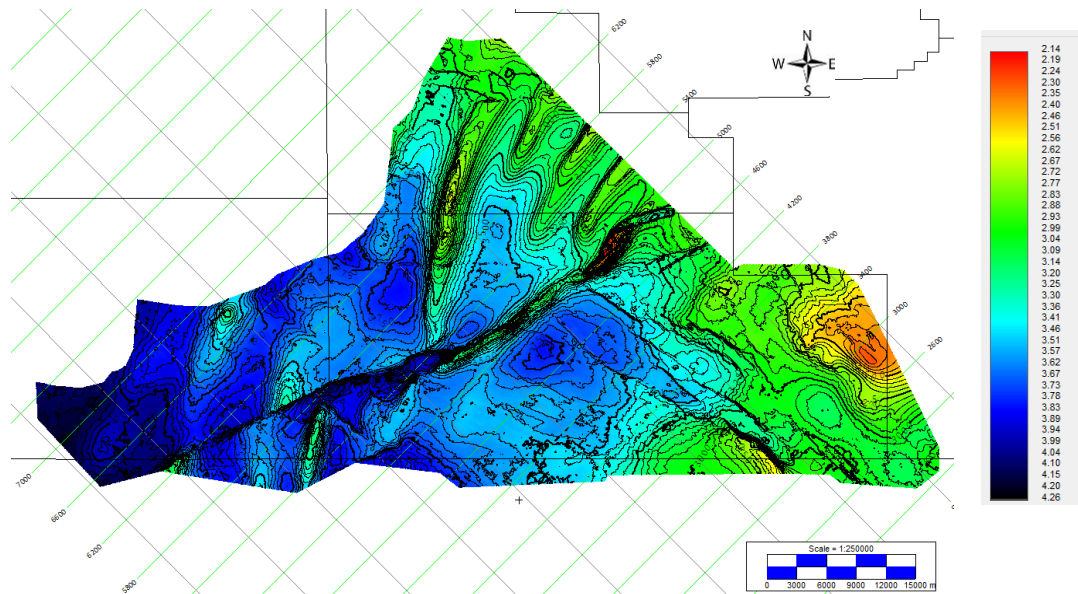


Figure 5-12 two way time map of upper Miocene low stand (horizon 130)

5.2.15 Pliocene (Horizon 100)

This event marks the upper limit of an interval, which contains a sequence of laterally discontinuous events and is the base of a sequence of under formed parallel continuous reflections. This surface is indicative of the commencement of a period of low lateral sediment input into the region, which is interpreted to represent the onset of a high stand. The two way time map of the surface Figure 5-13 highlights the location of the Avon/Mahin fault zone running through the region in a north east to south west direction.

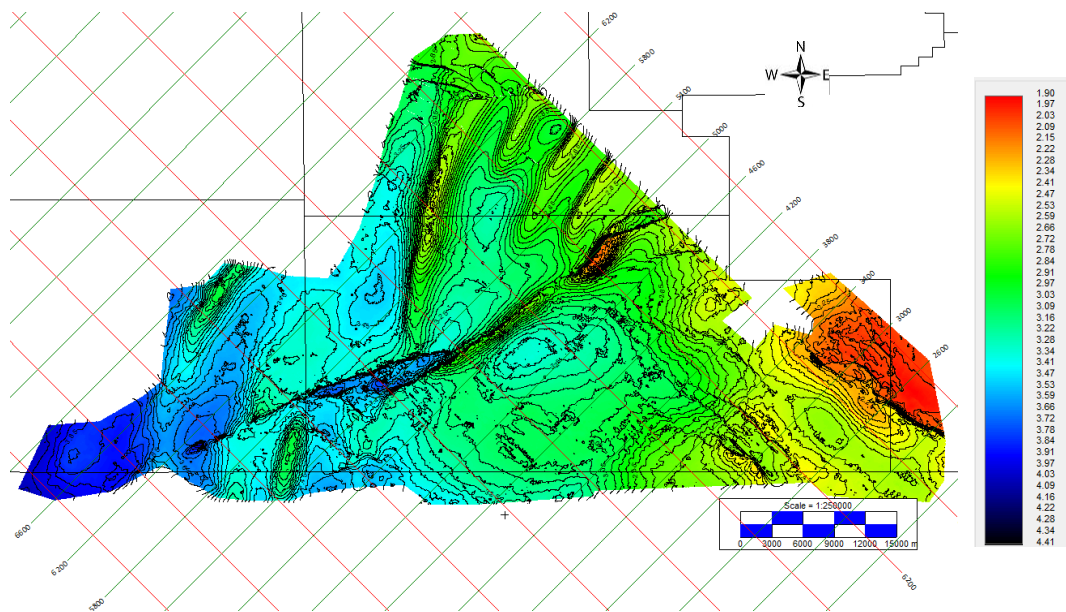


Figure 5-13 two way time map of Pliocene (horizon 100)

5.2.16 Seabed (Horizon 0)

This reflector is readily mappable over the entire survey. The seabed topography is characterised by an arcuate dipping surface which trends north south in the west of the survey area and east west in the east of the survey area. It is cut by a number of channels, the most prominent of which is the down slope extension of the Mahin Canyon. The channels cut by the Mahin canyon can be seen running north east to south west through the middle of the map.

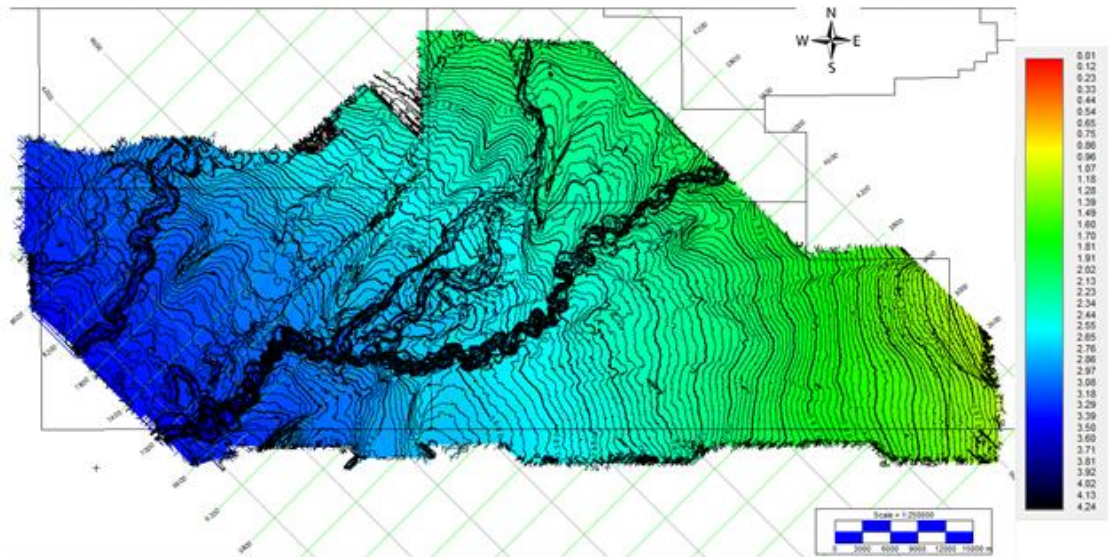


Figure 5-14 two way time map of the seabed

Chapter 6

Contents

| | | |
|-------|--|-----|
| 6 | Description of interpreted depositional setting..... | 90 |
| 6.1 | Introduction..... | 90 |
| 6.2 | Cretaceous..... | 90 |
| 6.2.1 | Syn-Rift..... | 90 |
| 6.2.2 | Early post rift..... | 95 |
| 6.2.3 | Drift..... | 99 |
| 6.3 | Cenozoic..... | 100 |
| 6.3.1 | Canyons..... | 100 |
| 6.3.2 | Hemipelagic input..... | 109 |
| 6.3.3 | Turbidity flow deposits..... | 109 |
| 6.3.4 | Mass transport deposits..... | 127 |
| 6.3.5 | Confined debris flows..... | 156 |
| 6.3.6 | Sediment remobilisation..... | 160 |

6 Description of interpreted depositional setting

6.1 Introduction

The region that is the focus of this study is interpreted to have been submerged beneath deep water since the post-break-up subsidence commenced in the Aptian (Lehner and De Ruiter, 1977). In the absence of well data, the depositional settings that are described in this chapter have been derived exclusively from an examination of the 3D seismic data volume. The use of analogues to compare features that have been observed in other deep-water regions has proven useful in constraining the interpreted facies.

6.2 Cretaceous

6.2.1 Syn-Rift

The oldest Cretaceous sediments in the study area are confined to rifted basins and are generally comprised of siliciclastic rocks deposited in a lacustrine or alluvial/fluvial setting (Adeleye, 1975; Fairhead, 1988; de Matos, 1999; Haack et al., 2000; Burke et al., 2003). There have been limited well penetrations of the syn-rift interval in Nigeria. Recent drilling

activity in and around the Aje and Ogo discoveries has encountered the syn-rift section close to the up-dip pinch out. Little is therefore known about the youngest portion of the section, which was subsequently eroded in the vicinity of these exploration wells.

Examination of the 3D seismic suggests that there is a significant thickness of syn-rift section, within which two distinct seismostratigraphic units can be recognised. One package is characterised by high-amplitude continuous reflections and the other by more discontinuous and lower amplitude reflections. The significance of this is not known because no wells have been drilled into the two intervals. In Figure 6-1 and Figure 6-2, the syn-rift package lies below the purple horizon (the interpreted break-up unconformity). The map in Figure 6-3 can be divided into two distinct regions. The first lies to the west of the dashed white line and is characterised by a relatively smooth southwards dipping surface; the second is located to east of the white dashed line, which is topographically more undulating. The undulations in the map, which is a two-way travel time map, are in part due to the distortions that arise from the velocity-induced artefacts noted in chapter 4. However, by flattening the data at the level of interpreted Base Cenozoic (the red horizon) level, these velocity related distortions can be minimised.

The illustrations in figures Figure 6-1 and Figure 6-2 indicate the effect of this flattening procedure.

Figure 6-1 illustrates the region in which there is little or no coherent reflection energy noted, below the break-up unconformity. This part of the study area, which lies in the western portion of the survey area, coincides with the uniform southerly dipping region of the horizon 800 map (Figure 6-3). The dipping events identified towards the southern edge of the section Figure 6-1 may be seaward dipping reflectors (SDR) associated with the margins of the proto-Atlantic Ocean.

In contrast, the images in Figure 6-2 illustrate the presence of a number of coherent reflection packages, which are interpreted to be the faulted sediments that were deposited during the rifting episode that preceded the separation of Africa from South America. It is also noted that the purple horizon (the break-up unconformity) in this section has a topographic expression that is uneven when compared to the unconformity, as identified in Figure 6-1. This uneven topography would suggest that the underlying interval is comprised of lithologies of a heterogeneous nature, whereas the section below the unconformity in Figure 6-1 is interpreted to be of a more homogeneous nature because the surface does not exhibit the marked topographic changes seen in Figure 6-2. The layered nature of the reflections in the syn-rift interval may be indicative of either marine or lacustrine sedimentation.

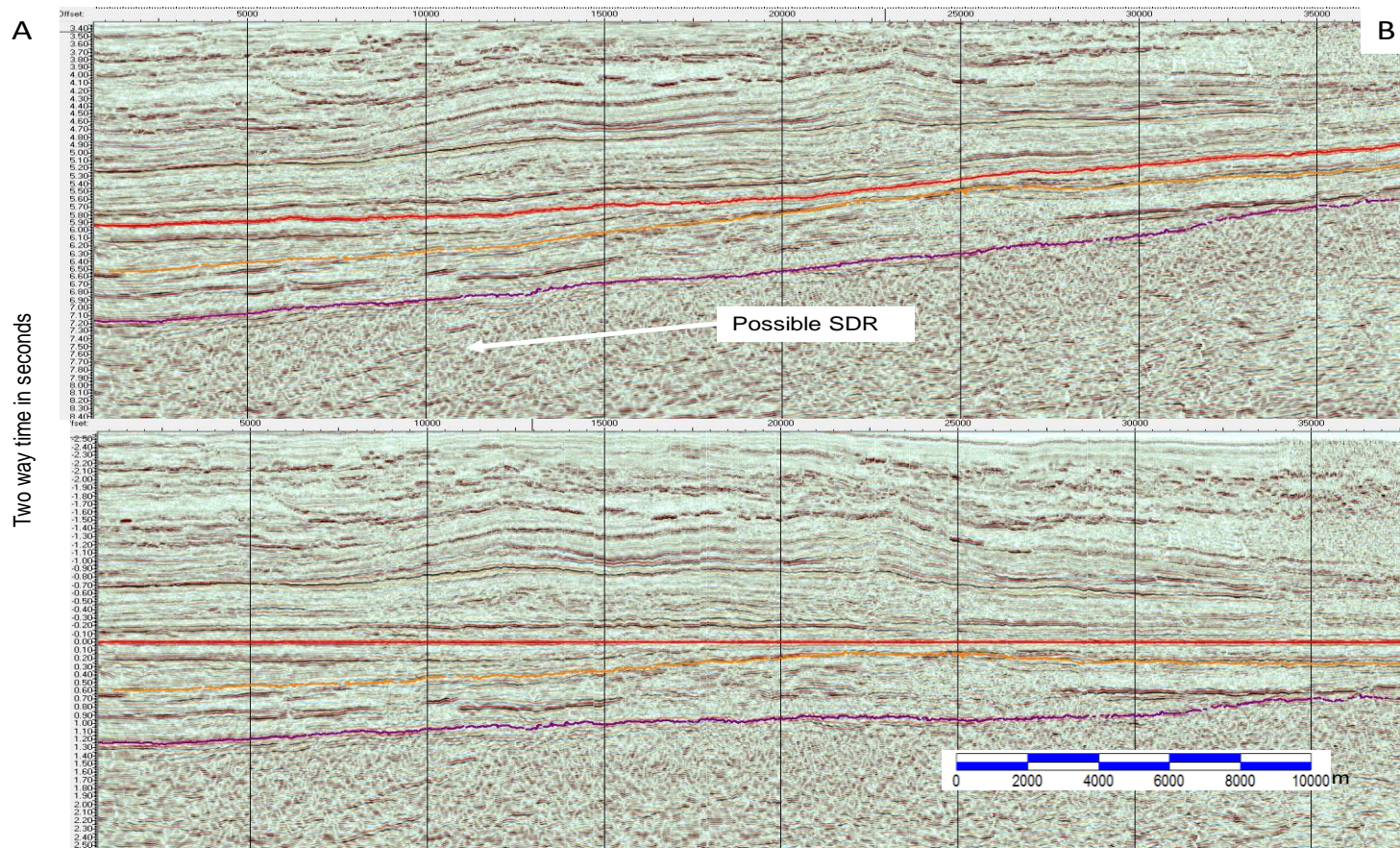


Figure 6-1: Cross line 7800; the top image is the original section, while the lower image is the same line flattened on the base Cenozoic (horizon 600); the break-up unconformity (purple event) has a fairly even topography.

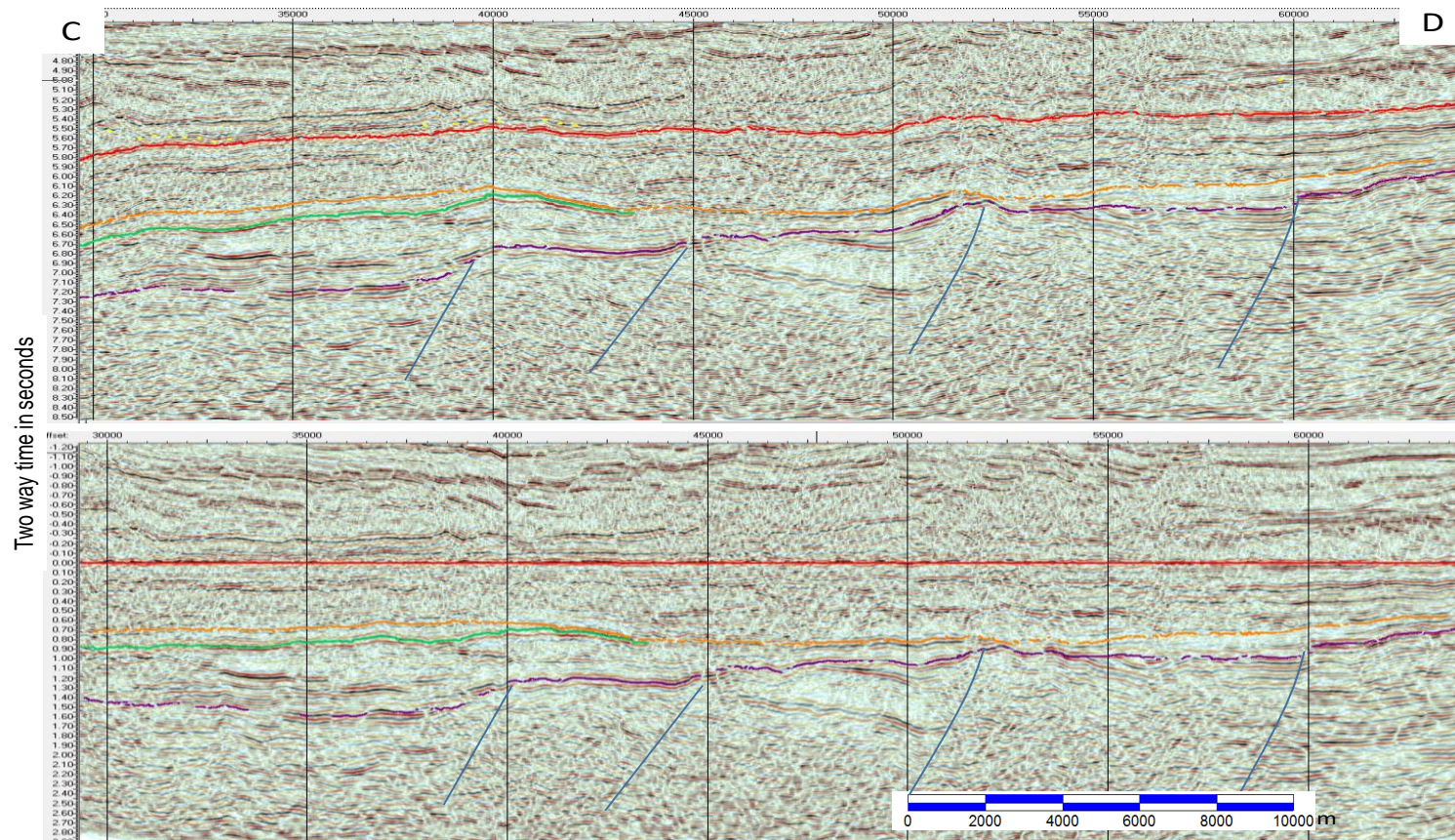


Figure 6-2: Cross line 4700; the top image is the original section, while the lower image is the same line flattened on the base Cenozoic event (horizon 600).

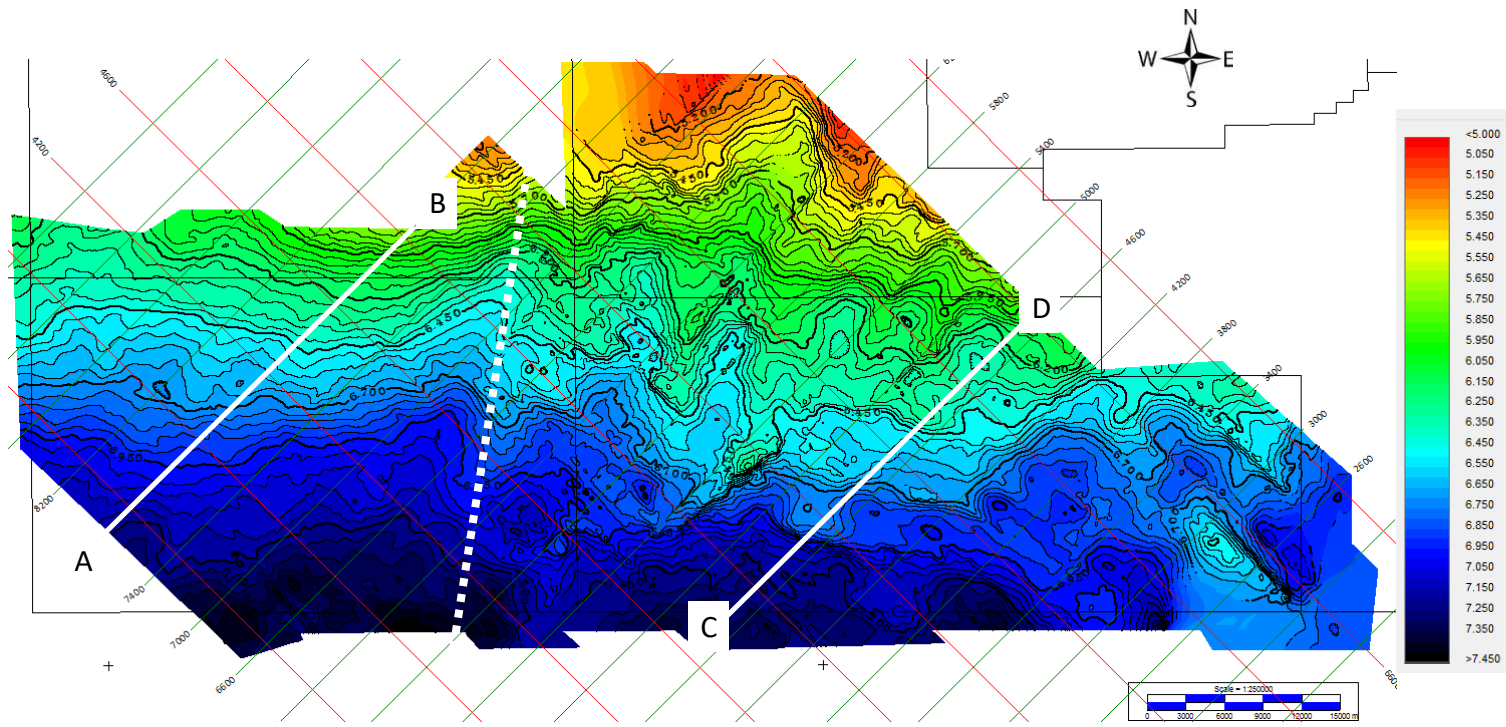


Figure 6-3: Two-way time map of the top syn-rift (horizon 800); the solid white lines refer to the locations of Figure 6-1 and Figure 6-2. The dashed white line indicates the division of the terrains that underlie the unconformity.

6.2.2 Early post rift

The post-rifting section is poorly constrained in terms of well data in the region of the 3D volume. To the north of the studied area, well data indicates that the oldest sediments that overlie the break-up unconformity are Albian-aged shallow marine sands and carbonates (Kaki et al., 2012). This observation indicates that during the Albian, a shallow marine environment was established with a shelf running in a west-east strike direction. The preserved remnants of this shelf are present to the north of the study area (Brownfield and Charpentier, 2006).

The age-equivalent section that is covered by the 3D volume has not been drilled. The Aptian to Cenomanian section (which lies between horizons 800 and 680) is assumed to lie downslope of the shelfal sediments, and is interpreted to be separated from the shelfal deposits by a bypass zone. The section remains unknown in terms of the sedimentology of the interval. Further work using the 3D data could help to better understand this interval.

The seismic character within this interval is divided into two regions in terms of the geometries observed (Figure 6-4, Figure 6-5, Figure 6-6). To the west, the interval is comprised of a series of laterally limited events, with undulating morphology. The limited amount of horizon-mapping that can be accomplished, due to the rapidly varying reflectivity, indicates that the internal surfaces are a series of stacked and laterally compensating north-south trending ridges.

The suite of foresetting events seen in Figure 6-5 may represent the lateral infill of a canyon because it shares some resemblance with the seismic reflection patterns seen at the margins of the present-day Avon Canyon (Figure 6-10) (Olabode and Adekoya, 2008). The limit of this undulating reflection facies is difficult to ascertain with certainty due to the degradation in data quality beneath the overlying steep-sided structures within the Cenozoic. Nonetheless, a clearly different reflection geometry is present towards the east. In the eastern region, the reflections within this interval are more laterally continuous. It is interpreted that the foresetting reflections at the margin of the laterally continuous reflections may indicate that the eastern region was a low-energy, possibly shelfal region, while the western area could have been a canyonised terrain. In this section (see Figure 6-6 for location), a clear difference in seismic character below the Senonian unconformity (horizon 680) can be seen between the western region, with an apparent foresetting set of reflections (in the yellow shaded region) and the east, where the reflections are more laterally continuous. This discontinuous reflection configuration is observed to be similar to that seen in the region of the Avon Canyon (Olabode and Adekoya, 2008) (Figure 6-11).

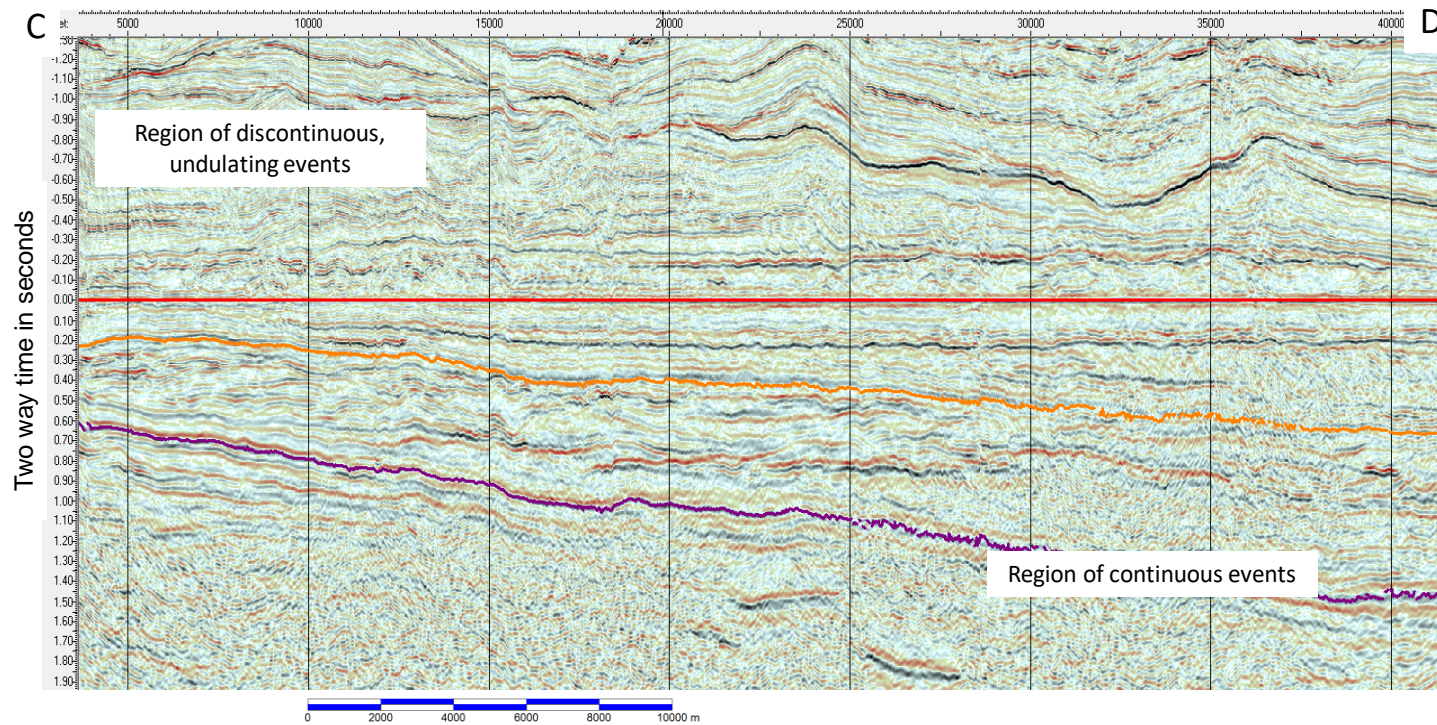


Figure 6-4: Inline 3800, flattened on the base Cenozoic (horizon 600).

The interval that lies below the interpreted Senonian unconformity (the orange event) is seen to be comprised of a discontinuous facies when compared to the eastern region (for the location of the line, see Figure 6-9).

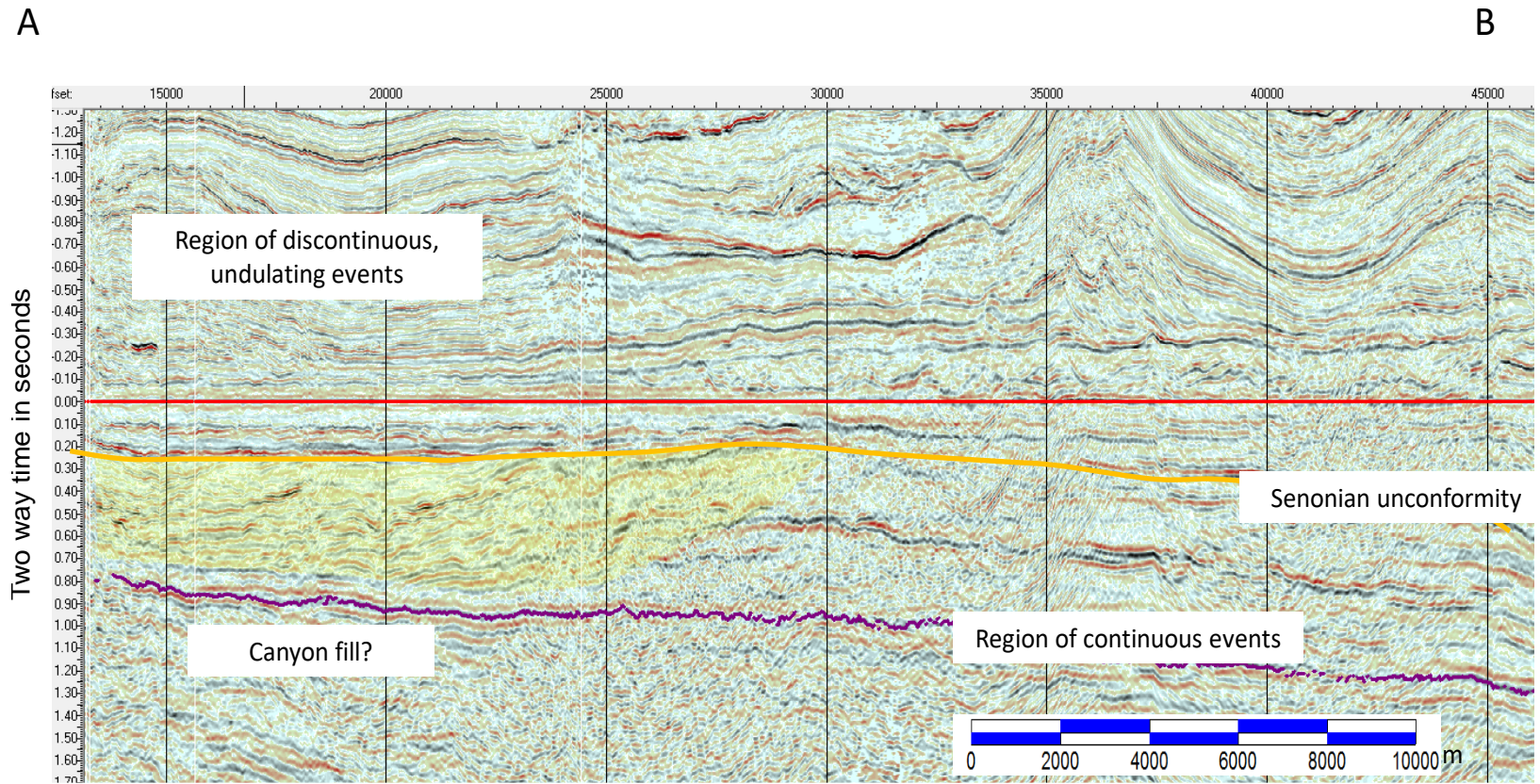


Figure 6-5: Inline 4600 flattened at the Base Cenozoic (horizon 600).

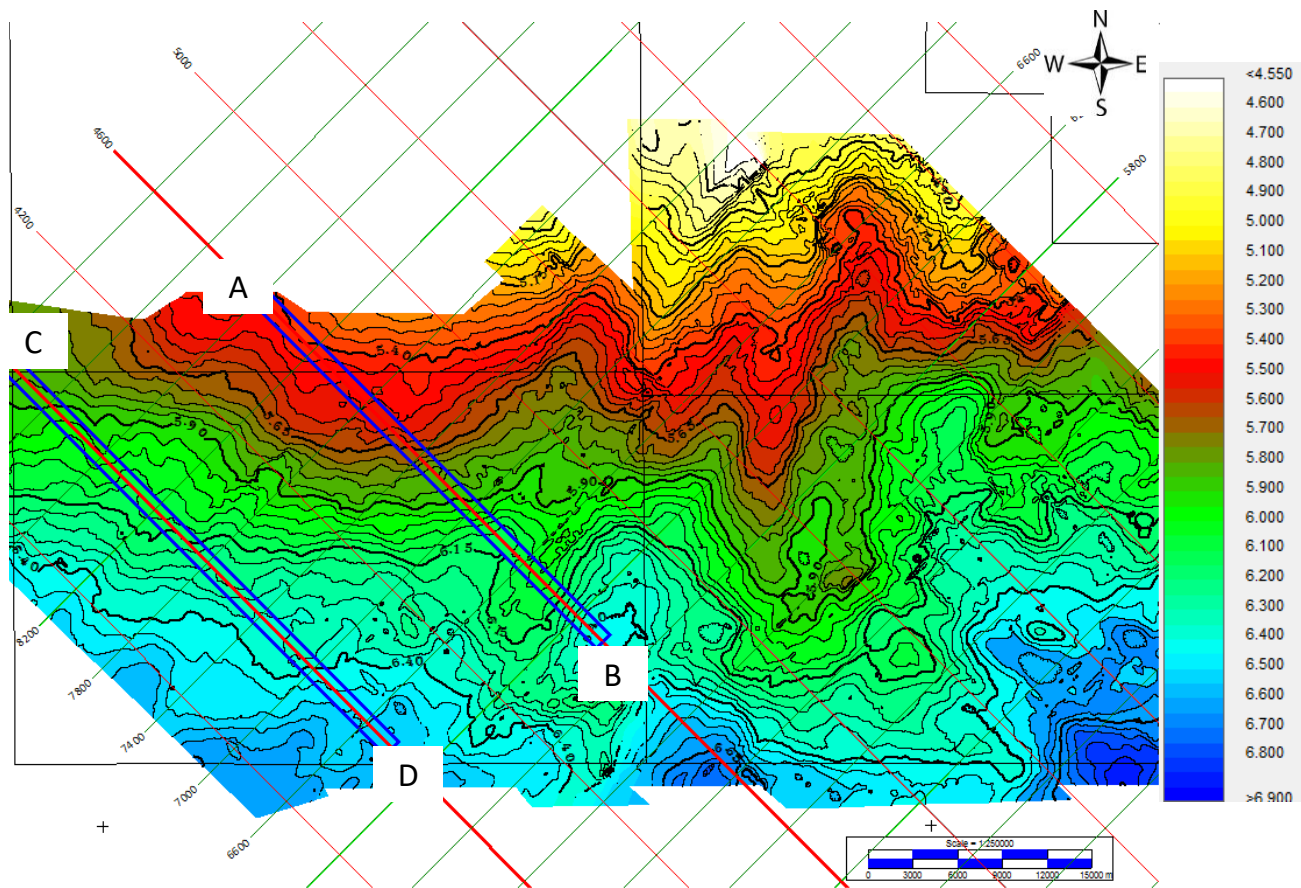


Figure 6-6: Two-way time map of the Senonian unconformity (orange, horizon 680), illustrating the location of the lines in Figure 6-4 and Figure 6-5.

6.2.3 Drift

The section that lies between the interpreted Senonian unconformity and the Base Cenozoic (between horizons 680 and 600) is seen to thicken from the north-west towards the south-east. In Figure 6-7, an isochrone of this interval, the thickest section lies to the south-east. Visible within the map is the presence of a broad nose surrounded by two synclines. This thickness variation is interpreted to represent the effects of erosion of the pre-existing sedimentary section at the time of the Senonian hiatus.

Within this section, which is interpreted to be the Upper Cretaceous (Campanian to Maastrichtian) interval, the lower portion is interpreted to infill the remnant topography that was left after the effects of the Senonian event (Guiraud and Bosworth, 1997). This onlapping sequence is interpreted to represent the distal portion of a delta which preceded the Niger Delta (the postulated Benue River Delta). The Benue Rift, which lies to the south-east of the survey area, is the site of Upper Cretaceous sediments that indicate that it was a fluvio-deltaic setting (Benkhelil et al., 1998) in the region of the present-day Niger River. The deep-water age equivalent of these continental- and shallow-water sediments would, if present, be expected to be present in the region of the 3D survey. The distal Benue Delta sediments, if present, should now be buried below the Niger Delta cone; the distal portion of the assumed delta would have spread into the accommodation space that was created at the end of the Senonian hiatus.

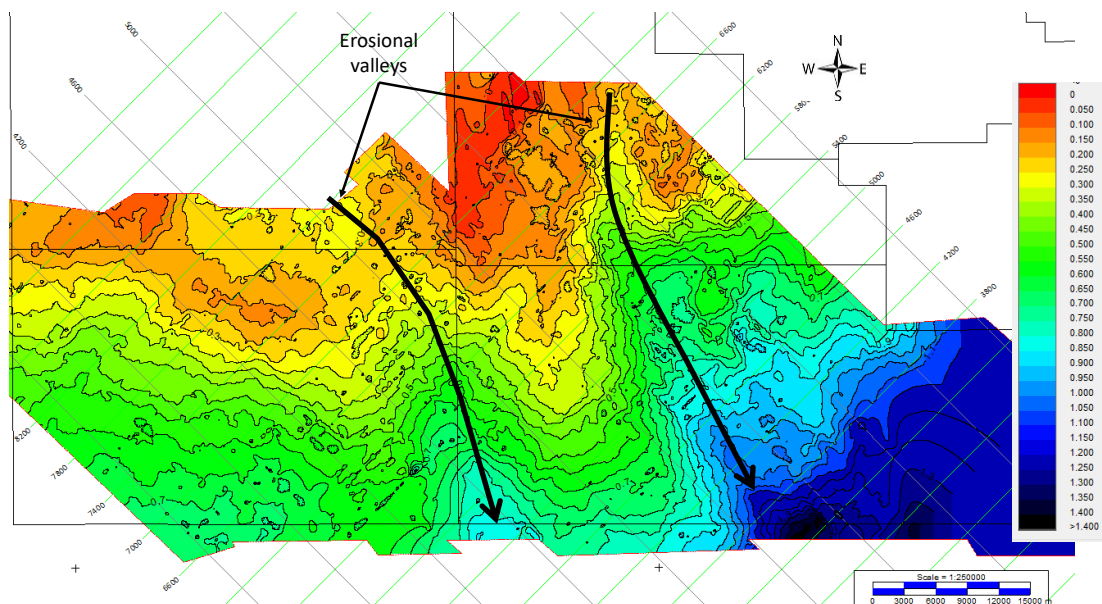


Figure 6-7: Isochrone in twt of the Upper Cretaceous interval (between horizons 600 and 680).

It is interpreted, therefore, that the sediments that onlap and subsequently overlie the Senonian unconformity are distal pro-delta shales. This deep-water environment fits with the observation that the overlying Cenozoic sediments are also deep-water deposits.

6.3 Cenozoic

The Cenozoic sedimentary section in the region covered by the 3D survey is dominated by deep-water deposits. The provenance of the clastic material is not known with certainty, but it is likely that the fine-grained material was sourced initially from the Niger/Benue Delta. The Niger Delta is of a classic wave-dominated nature (Wright and Coleman, 1973). Sediments emerging at the mouth of the river are deflected along the shoreline via means of wind-induced wave action (Galloway, 1975). Shallow-water, coarse-grained sediments were fed by longshore currents along the continental margin (Burke, 1972). The outbuilding of the delta is a function of sediment supply and accommodation space. The Niger Delta is notable for the tectonic control that creates the accommodation space (Evamy et al., 1978; Doust and Omatsola, 1990). Thick aggradational intervals of sand accumulated in the hanging-walls of down to the basin listric faults, with the finer-grained material deposited distally in the deeper water adjacent to the hanging-wall of counter-regional faults (Evamy et al., 1978). The controlling faults, both listric and counter regional, have been interpreted as having their origin in vertical and lateral movement over a deep detachment layer of low shear strength (Cohen and McClay, 1996; McClay et al., 2003; Cobbold et al., 2004). This interpretation is often hindered by the lack of seismic reflections within the deeper section that underlies the well-imaged shallow deformation.

Seven distinct deep-water seismic facies are defined, having been fed into the deep-water region via four sediment transport mechanisms, as follows: pelagic rain, turbiditic flows (slope channel fill, channel levee, terminal fan lobes, and sheet turbidites), slope or shelf failure (debrites and mass transport deposits), and contourites (Galloway, 1998).

6.3.1 Canyons

The bathymetry and, in particular, the gravity data of the coastal region of Nigeria highlight the presence of a number of canyons. As noted earlier in section 3.4.3.2, there are two present-day canyons, which lie to the north and north-east of the survey area. The presence of the canyons has played a significant role in the input of sediments into the deep-water realm that is the focus of this study. The nature of the sediments within the canyons cannot be ascertained in this study because the 3D data do not extend far enough to the north. Oloabode and Adekoya (2008) include two seismic lines that traverse the Avon Canyon. In the seismic sections (Figure 6-11, Figure 6-10), the flanks

of the canyon are seen to be comprised of a series of foresetting dipping events that prograde into the axis of the canyon. This seismic geometry would suggest that the canyon is infilled with sediment that is derived from both up-dip and lateral headwall erosion.

6.3.1.1 Lagos Canyon deposits

The regional gravity data indicates the presence of a number of canyons (Figure 6-8) which have eroded into the shelf margin to the north. The density of the sediments and water within the canyons when contrasted with the sediments that are undisturbed by the canyon activity gives rise to a series of anomalies along the shelf margin. These anomalies are aligned with both known and postulated canyons. In addition to the documented Avon Canyon, (Burke, 1972; Olabode and Adekoya, 2008) to the north-west of the 3D survey area, there are known to be two canyons – the Seme and the Lagos – and one additional interpreted unnamed canyon. The closer of these canyons to the 3D survey are the Lagos Canyon and the unnamed canyon. A Palaeogene fan-like accumulation of sediments is interpreted to be present to the south of the Lagos Canyon and have its eastern flank covered by the 3D volume. The inset map within Figure 6-8 is an isochrone of the Palaeogene interval, shown in more detail in Figure 6-9; the colder colours indicate a thicker section. It can be observed that there is a thick interval at the western margin of the 3D survey.

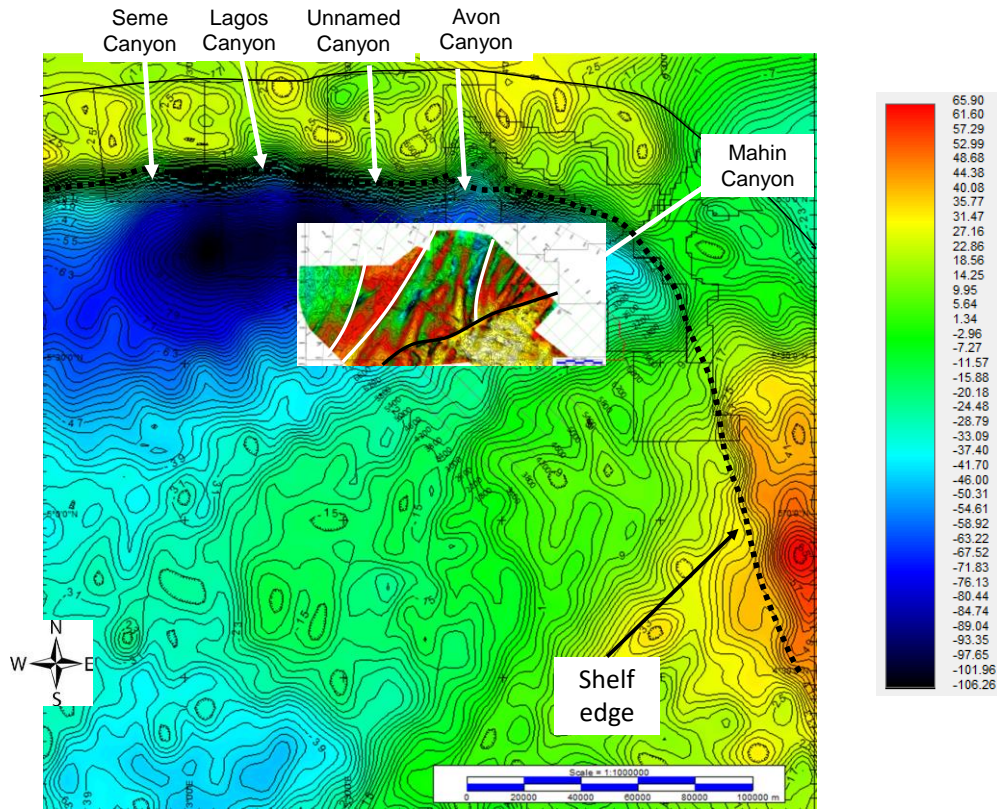


Figure 6-8: Free-air gravity anomaly for the region, in mgal; the twt thickness of the Palaeogene is superimposed to illustrate its relationship to the canyons.

The isochrone of the Palaeogene (the interval between horizon 600 and 420), in twt, illustrates the location of the eastern margin of the Lagos Canyon fan (Figure 6-9) and the levee system that appears to have emanated from the Avon Canyon.

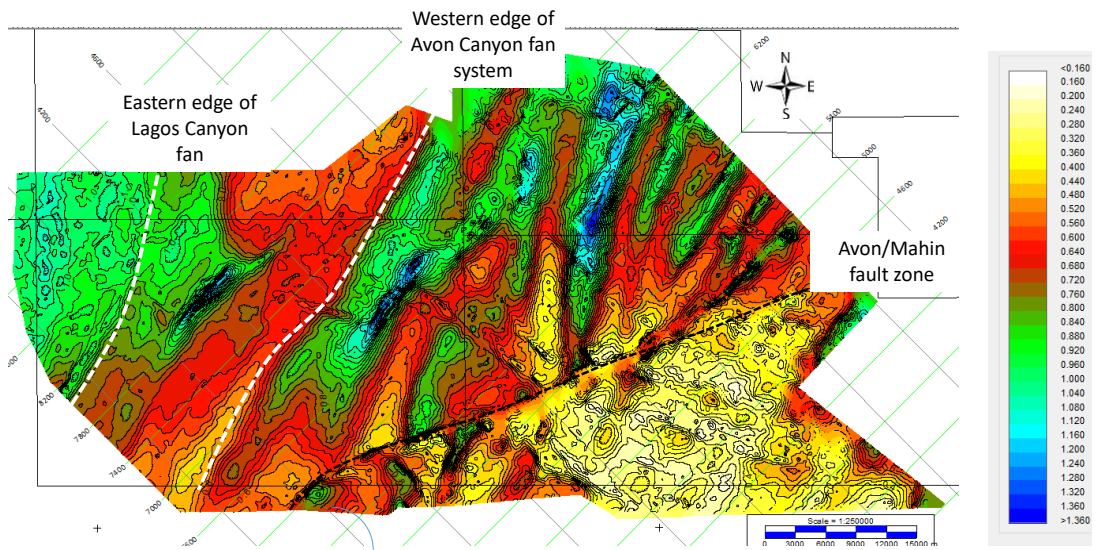


Figure 6-9: Isochrone of the interval between horizons 600 and 420.

The Avon Fan system is affected by post-depositional tectonic activity to a much greater degree east of the Avon/Mahin fault zone than that seen in the west. Nonetheless, a significant thinning of the section towards the east is observed. The alternating thick and thin lineaments within the Avon Fan system, which are oriented in a north-east to south-west direction, are interpreted to arise from the deposition of levees and the associated intra-levee bypass zones at the outflow of the canyon.

6.3.1.2 Avon-sourced deposits

The Avon Canyon, as described by Olabode et al. (2008), is filled with a Miocene-to-recent sequence of sediments. The sides of the canyon are defined by the erosion of a series of parallel continuous seismic events, which implies that the erosion postdates the deposition of the parallel section, which is interpreted to be comprised of shelfal muds and minor amounts of sand and carbonates. This dates the bulk of the canyonisation as Miocene or younger. The base of the canyon can be seen to have eroded into the Cretaceous sediments, which could indicate that there was a canyon present prior to the Miocene and a younger canyon that was removed by the Miocene activity.

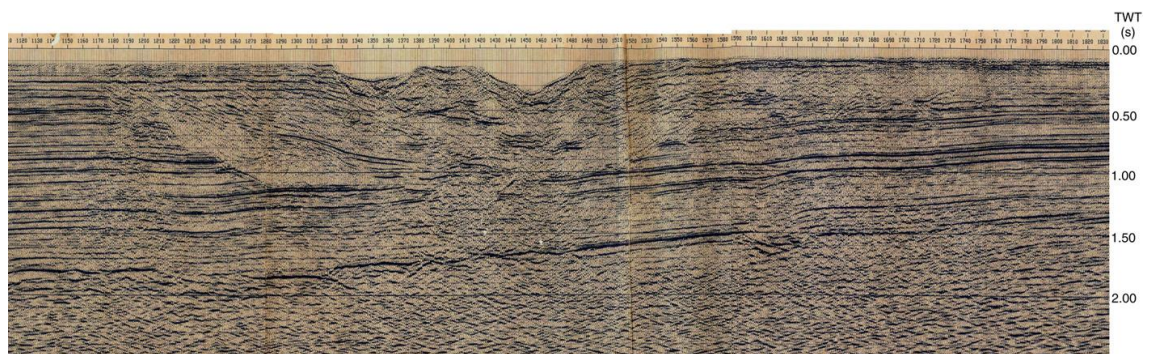


Figure 6-10: Seismic line across the Avon Canyon, taken from Olabode and Adekoya (2008).

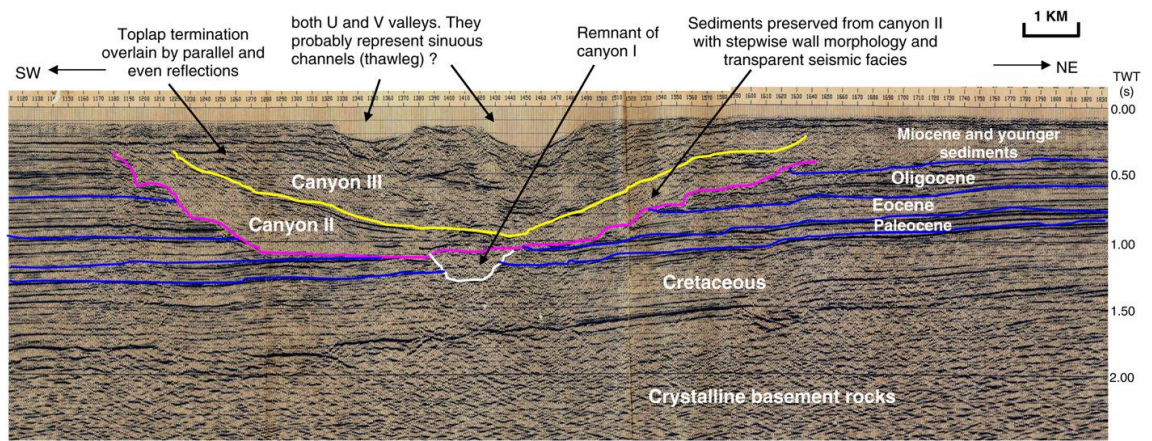


Figure 6-11: Interpreted version of Figure 6-10 (Olabode and Adekoya, 2008).

The Miocene and Plio/Pleistocene outflow from the Avon Canyon can be recognised within the 3D volume as a fairway of sinuous geometries that are present over the western half of the survey. The similarity attribute extracted at a number of intervals below the present-day seabed highlights the sinuous nature of these deposits. In Figure 6-12, there are a number of channel fairways (the regions of darker colouration) that are highlighted by the red dashed arrows. By tracing the orientation of the arrows, they are seen to be converging to a point north of the survey area at the mouth of the present-day Avon Canyon.

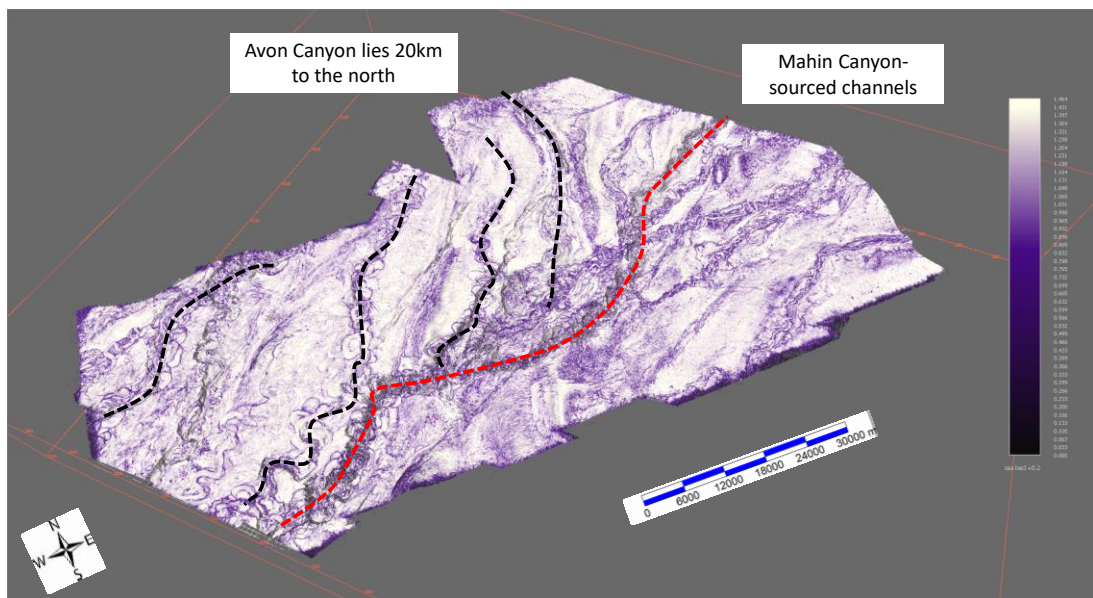


Figure 6-12: Similarity attribute extracted some 200ms below the seabed. The black dashed lines are Avon-sourced channels, while the red is a Mahin-derived channel system.

There are interpreted to have been a number of separate phases of deposition that originated as a result of the flow of sediments from the outflow from this canyon.

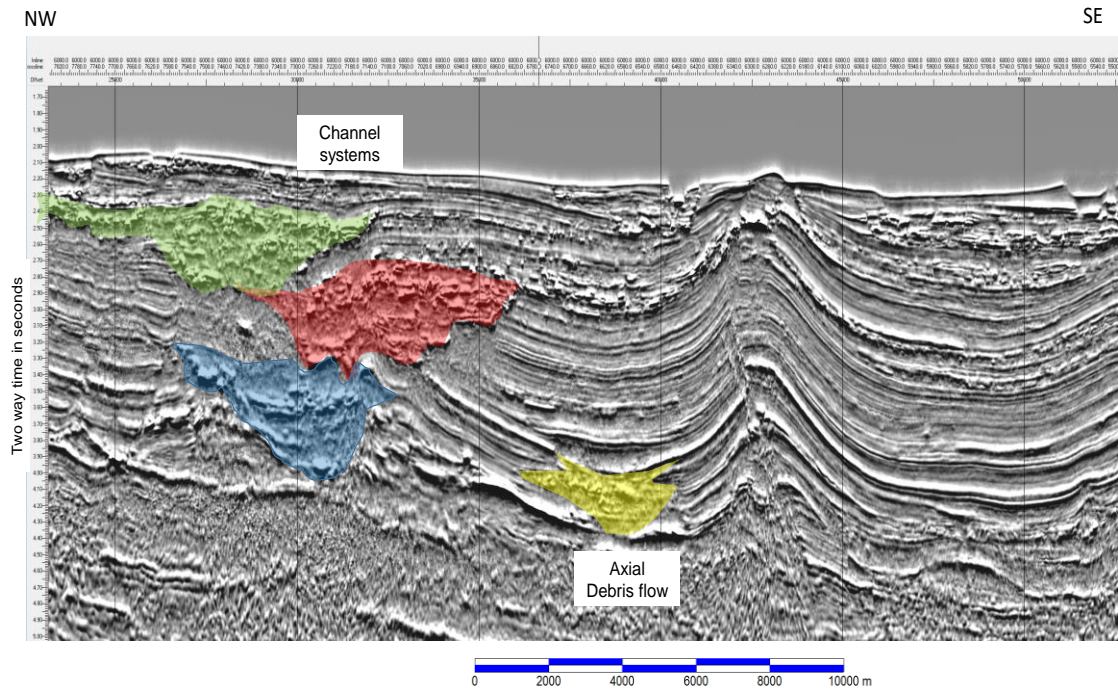


Figure 6-13: A phase rotated seismic envelope display of inline 6100, which illustrates the sediments derived from the Avon Canyon.

In Figure 6-13, the display emphasises the contrast between the low-energy and high-energy deposits. Three regions are highlighted (in red, blue, and green) that are interpreted to be deposits that have been avulsed from the Avon Canyon in the form of meandering channels. The three intervals are seen to truncate the semi-continuous reflections that are assumed to represent low-energy, deep-water deposits. The discontinuous nature of the reflections within this vertical cross section, when viewed in a spatial manner, are seen to be sinuous in nature. The blue interval would represent the oldest of the Neogene outflows, it is seen to have cut down into the parallel bedded sediments that existed prior to the deposition of the discontinuous facies. The red interval, which is younger, partially erodes the blue section. The green interval is representative of the more recent depositional unit.

In addition to the sinuous deposits highlighted above, there is evidence within the deeper sediments of north-south trending valleys, which are filled with a combination of chaotic seismic facies and parallel draped events. One of these valleys is also seen in the above figure, highlighted in yellow. This facies is discussed in section 6.3.5.

Isochrone maps of the interval between a number of Miocene horizons were created in the northern region of the survey area. Of particular note are the isochrone between horizon 202 and 190. In this figure, four isochrone thick intervals are observed that run from the northern edge of the survey, highlighted by the black arrows in Figure 6-14.

These four thick intervals represent the infill of valleys that resulted from turbidity outflows from the Avon and the unnamed canyon.

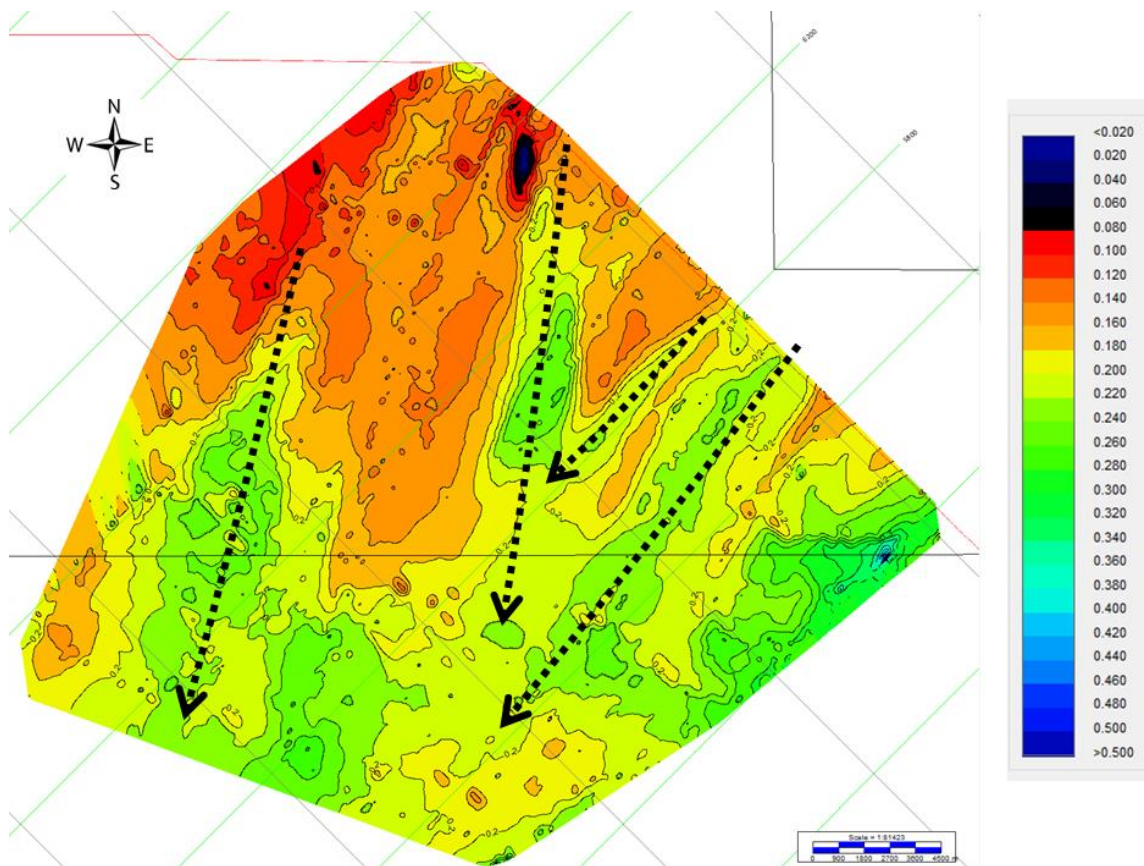


Figure 6-14: Isochrone of the interval between horizons 190 and 202.

6.3.1.3 Mahin Canyon-sourced deposits

In Figure 6-12, Figure 6-15, and Figure 6-16, the meandering belt of sinuous amplitude anomalies, highlighted by the blue arrow, are evidence of sediments that have been derived from a source that lies to the north-east of the survey. This channelised feature is traceable back to the present-day Mahin Canyon.

The presence of channels with similar orientation to the present-day Mahin Channel are not recognised in the Middle Miocene strata below horizon 130. This may place a limit on the age at which this canyon was initiated.

6.3.1.4 Opuama/Benin Canyon-sourced deposits

Turbiditic, slope channel deposits from the east of the survey boundary are found within the sediments from the present-day seabed down to at least the Lower Miocene (horizon 200). Below this horizon, there is limited evidence of the meandering seismic facies. The green arrow that is located at the south-eastern margin of the survey in Figure 6-12 indicates the direction of flow of sediments that have been derived from the east.

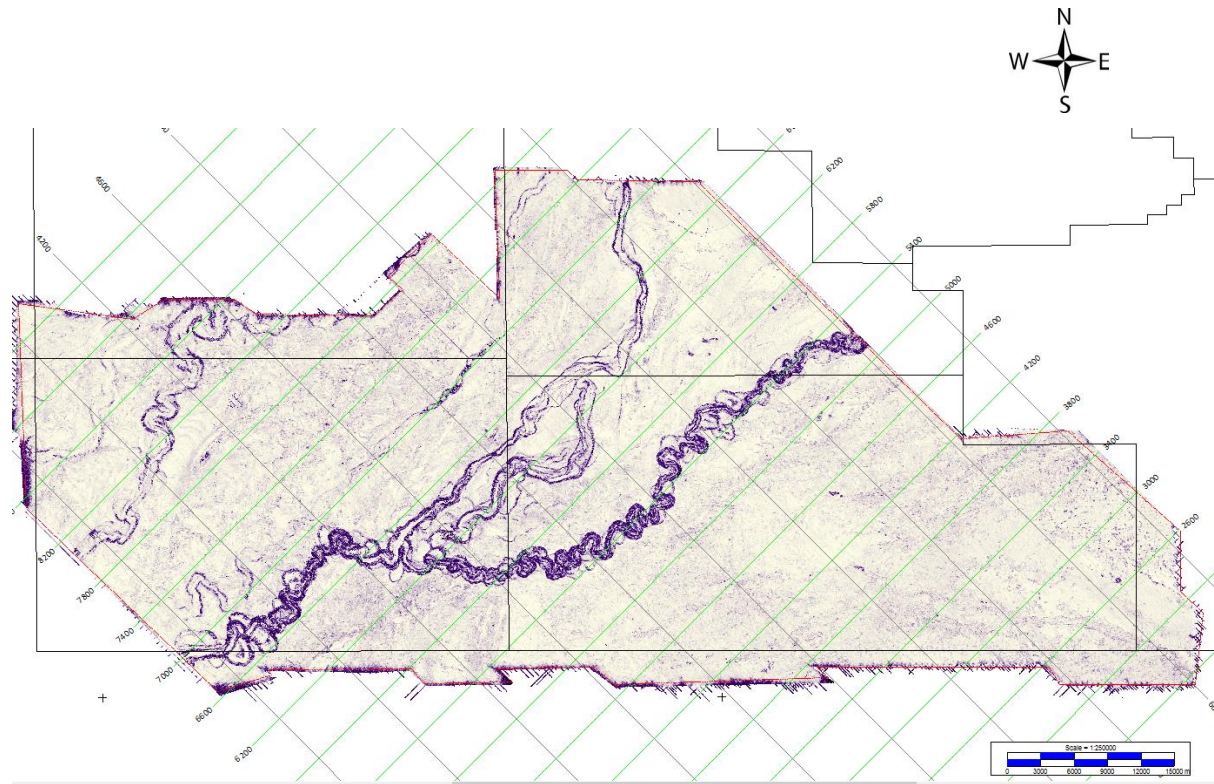


Figure 6-15: Similarity attribute extracted at the seabed; dark colours indicate low similarity.

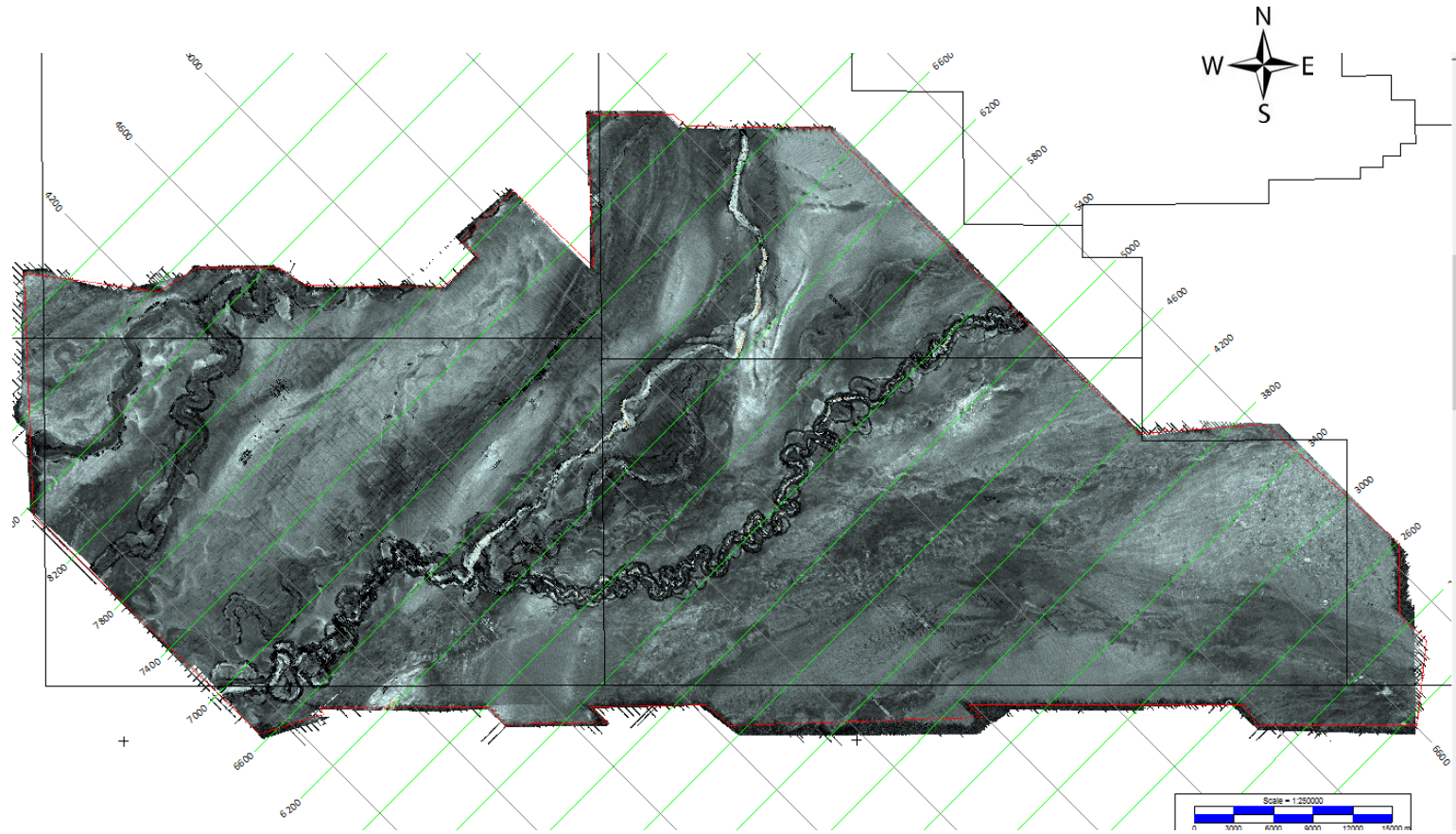


Figure 6-16: Seismic amplitude of the seabed reflector.

6.3.2 Hemipelagic input

Within the 3D volume are a number of intervals that exhibit parallel continuous seismic reflectors. This seismic facies is a characteristic of the deposition of fine-grained pelagic and hemipelagic material in a deep-water setting. These intervals represent periods of diminished lateral sediment input, often associated with a relative high stand of sea level (Brown Jr and Fisher, 1977).

6.3.3 Turbidity flow deposits

The input of sediment into deep water, from the updip slope and nearby shelf, can result primarily from turbidity current activity (Kane et al., 2010; McHargue et al., 2011). The content of the turbidity flow – a mix of water and rock fragments – can vary from a coarse-grained rich mix to a fine-grained rich mix. The flows with high levels of coarse grains lead to the subsequent deposition of sand rich turbidites. Flows with high amounts of fine-grained constituent particles can travel further than sand-rich ones and are typically found in the levees that build on the flanks of the flow. Within the 3D volume, a number of turbidite deposits are recognised and described in the following paragraphs.

6.3.3.1 Channel levee complex

The most visible turbidite deposits are the slope channels and associated levees, which are similar to those observed in other deltaic environments (Middleton, 1993; Galloway, 1998; Posamentier and Kolla, 2003; Talling et al., 2012). They are recognised as being present in the Miocene sediments that are present within the 3D survey area. The mapping of these channel systems has proven useful in the estimation of lateral displacement along the main transcurrent fault zone.

Three suites of channel slope systems are recognised within the data (Figure 6-17). They are interpreted to be sourced from canyons that lie outside the 3D survey area. The provenance of the sediments within the channels is thought to have been derived from the Mahin, Opuama/Benin, and Avon Canyons, respectively.

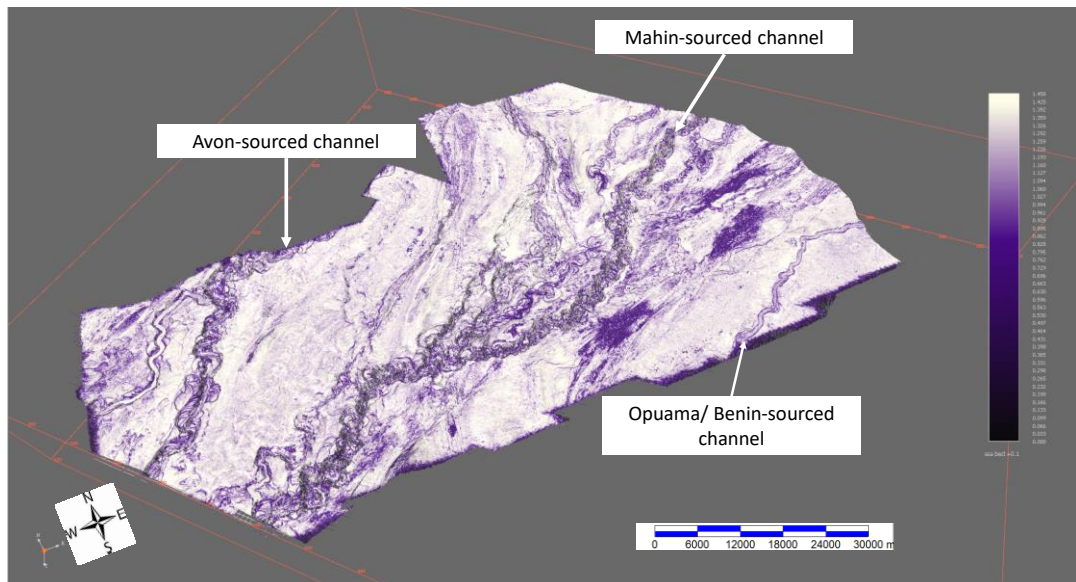


Figure 6-17: 3D perspective of the similarity of a pseudo horizon 100ms below the seabed.

6.3.3.1.1 Mahin-sourced channels

The best image of a slope channel, the outflow from the Mahin Canyon, is found at the present-day seabed. The Mahin channel runs in a north-east to south-west direction through the middle of the survey. The channel is characterised by a broadly linear swath of meandering channel cuts. It is comprised of a number of channels that have migrated laterally and vertically, with the younger channels cannibalising the sediments that were pre-existing (Figure 6-18). In Figure 6-15 and Figure 6-16, the location of the Mahin channel is clearly visible. The amplitude extraction in Figure 6-16 points to the presence of other channels at or close to the present-day seabed. A series of similarity attributes were extracted at levels parallel to the seabed at intervals of 25 milliseconds below the seabed. One example of this is shown in Figure 6-12; this extraction illustrates the presence of a number of channels that are interpreted to have their provenance outside of the boundaries of the 3D survey.

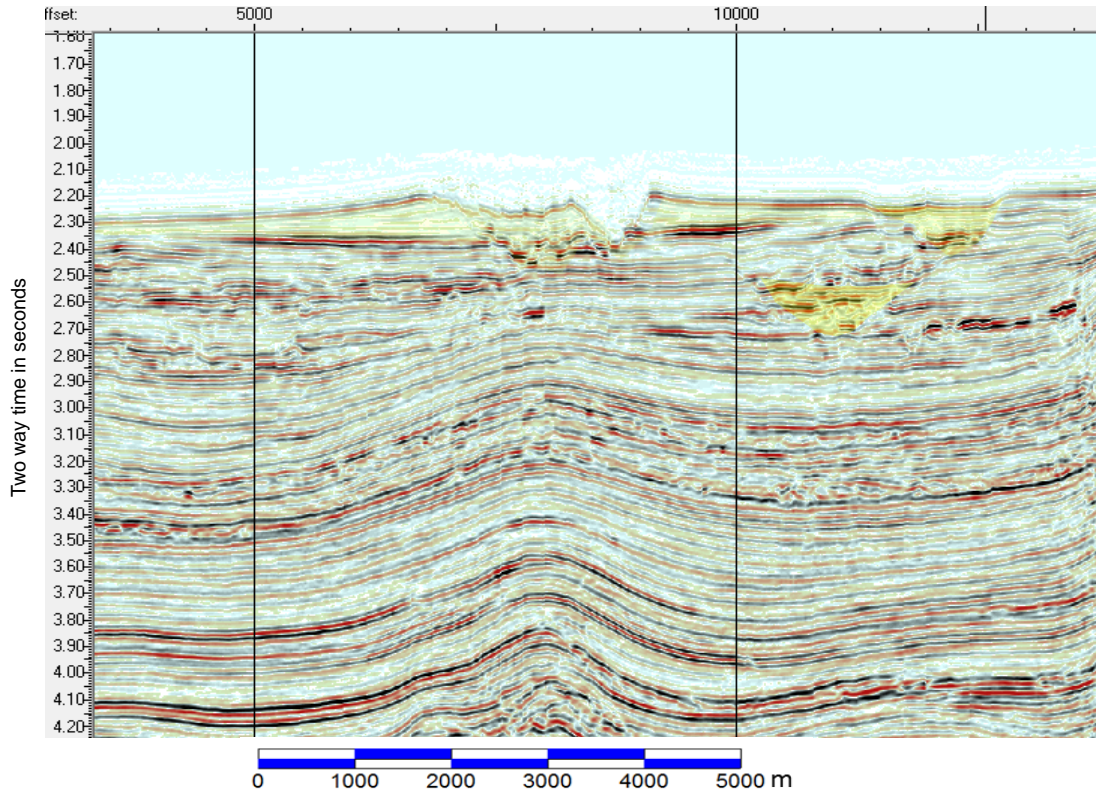


Figure 6-18: Seismic line in the northern region of the 3D survey which illustrates the channel levee geometry in a cross section of the Mahin Canyon; highlighted in yellow are three separate channel complexes that which are interpreted to have their origin in the outflow from the Mahin Canyon.

6.3.3.1.2 Opuama/Benin-sourced channels

Those that originate in the east and have their provenance in the Niger Delta are possibly related to the presence of the Opuama/Benin Canyon system (Petters, 1984; Deptuck et al., 2007). These channels run in an approximately east-to-west direction and the commencement of deposition is interpreted to have originated during the Lower to Middle Miocene; they are still active at present.

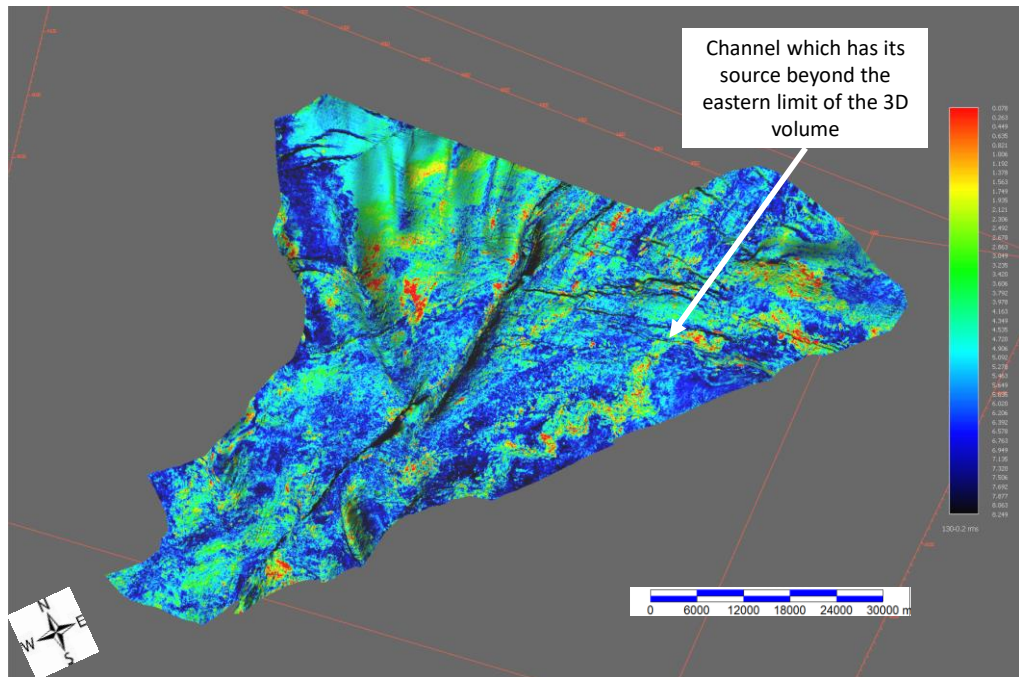


Figure 6-19: RMS amplitude extracted from a window within the Middle Miocene (between horizon 130 and a pseudo horizon 200 ms below), draped on a 3D perspective view of the twt surface of Horizon 130.

A good example of one of the eastern-sourced channel deposits is shown in Figure 6-19. The warmer colours indicate the higher amplitudes that are associated with the assumed heterogeneous sediments within the channels, when compared to the lower amplitude reflectivity that is present (cold colours) in the background deposits within the 200 ms window.

The third suite of channels comes from the north and is assumed to be related to the outflow from the Avon Canyon (Olabode and Adekoya, 2008). This channel complex has a narrow lower interval and expands laterally into the shallow portion of the data. The onset of the deposition of these channel levees might have commenced at the same time as the Opuama-sourced system, at the time of a drop in relative sea level.

The two systems interfinger in the survey area, with the higher volume of sediments from the north often eroding the sediments that have come from the east. Avon Canyon-sourced channels are also evident at the seabed and are seen to merge with the Mahin channel (Figure 6-15).

The length of channel systems can exceed several hundred kilometres and carry sediment out towards the abyssal plain (Kostenko et al., 2008). At the south-eastern margin of the 3D survey, the Mahin channel complex is over 100km from the present-

day Mahin Canyon. The orientation and scale of the channels is similar to those observed to the south of the study area (Morgan, 2004; Heiniö and Davies, 2007).

The character of the channels varies with the dip of the slope; in the shallow portion of the data, this can be seen quite clearly. When the gradient is low, the channels develop highly sinuous meanders; however, in regions of higher gradient, they become more linear. This behaviour can be seen in Figure 6-22 (a similarity extraction at a level some 50 milliseconds below the sea bed reflector); in this image, several linear channels that emanate in the north are seen to alter their course to a more meandering nature towards the south. This is interpreted to indicate that the gradient of the slope was greater in the north than towards the north-east.

The slope channels that have their provenance in the east are found throughout the Lower Miocene to recent section but are most abundant in the intervals immediately below the seabed and between horizons 160 and 200, which correspond to an assumed low stand within the Miocene. Because the provenance of these channel levee complexes is outside the 3D survey limits in the east, it is not possible to estimate the overall length of these particular systems.

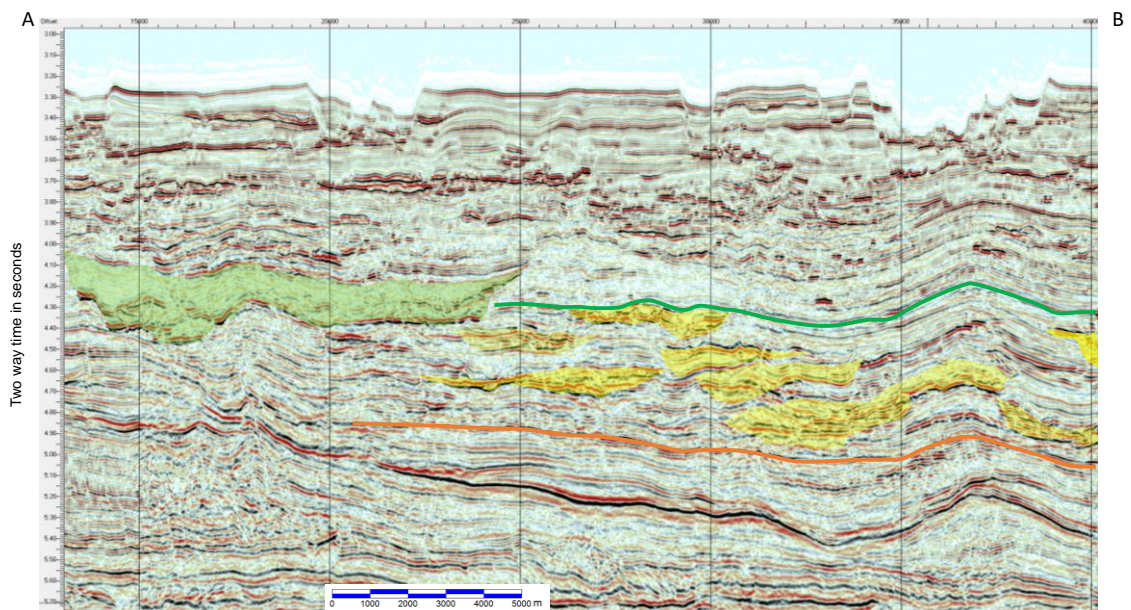


Figure 6-20: Portion of inline 3590, illustrating the discontinuous nature of the reflections within the Lower to Middle Miocene (below horizon 160 (green) and above 310 (orange)); line location is highlighted in Figure 6-21.

The yellow intervals are interpreted to be Opuama-sourced channels, while the green interval is an Avon-sourced channel system.

An examination of the vertical seismic displays provide an indication of the presence of anomalies within the section (Figure 6-20). It is by examining the anomalies in an areal sense that leads to the recognition of the presence of channel fairways.

The image in Figure 6-21 is a RMS amplitude extraction from an interval below the green horizon (horizon 160) in Figure 6-20. This map provides evidence of two channel levee systems passing through the survey area. The lighter colours indicate the presence of higher amplitudes in the window, which are associated with the presence of meandering channels within a channel complex. In this image, the channels run in two orientations, east to west and north-east to south-west.

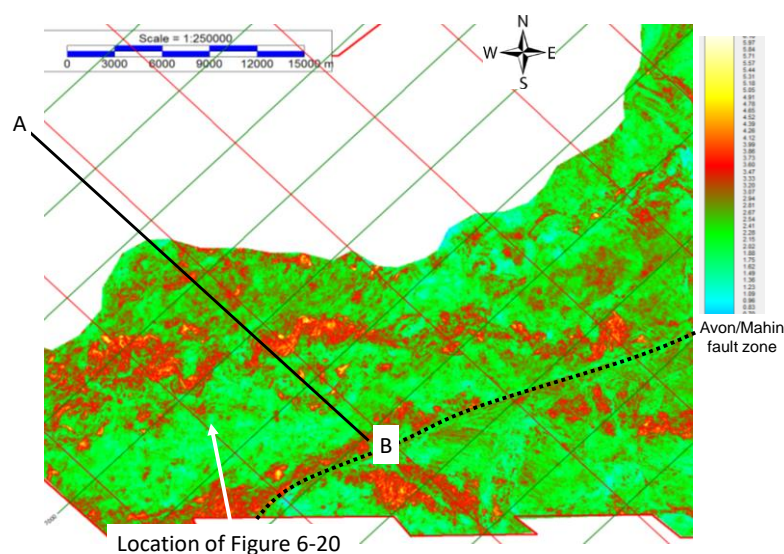


Figure 6-21: RMS extraction of a Middle Miocene interval (between horizon 160 and a pseudo horizon 100ms below horizon 160). The red regions are interpreted to be channel complexes.

The offset of the two channel complexes across the major transcurrent fault zone has been used to estimate the amount of lateral displacement; this is discussed in more detail in chapter 7.

The majority of the slope channels pass through the survey; the up-dip and down-dip portions lie outside the survey boundaries. In the Lower Miocene there is evidence that one of the channels may have terminated in close proximity to the Avon/Mahin fault zone. Examination of the RMS extraction of an interval between 300 and 400 milliseconds below horizon 160 shows an amplitude form that resembles a terminal

fan (Middleton, 1993; Galloway, 1998). This geometry is displayed in Figure 6-23, where there is a petal-shaped geometrical pattern visible. This is interpreted to represent the superposition of a number of terminal fans located in a local depression that was created as a result of trans-tensional accommodation space creation adjacent to the Mahin fault zone. The later transpressional movements attributed to displacement along the strike slip fault zone have led to this sedimentary feature being draped over a present-day local compressional pop-up structure.

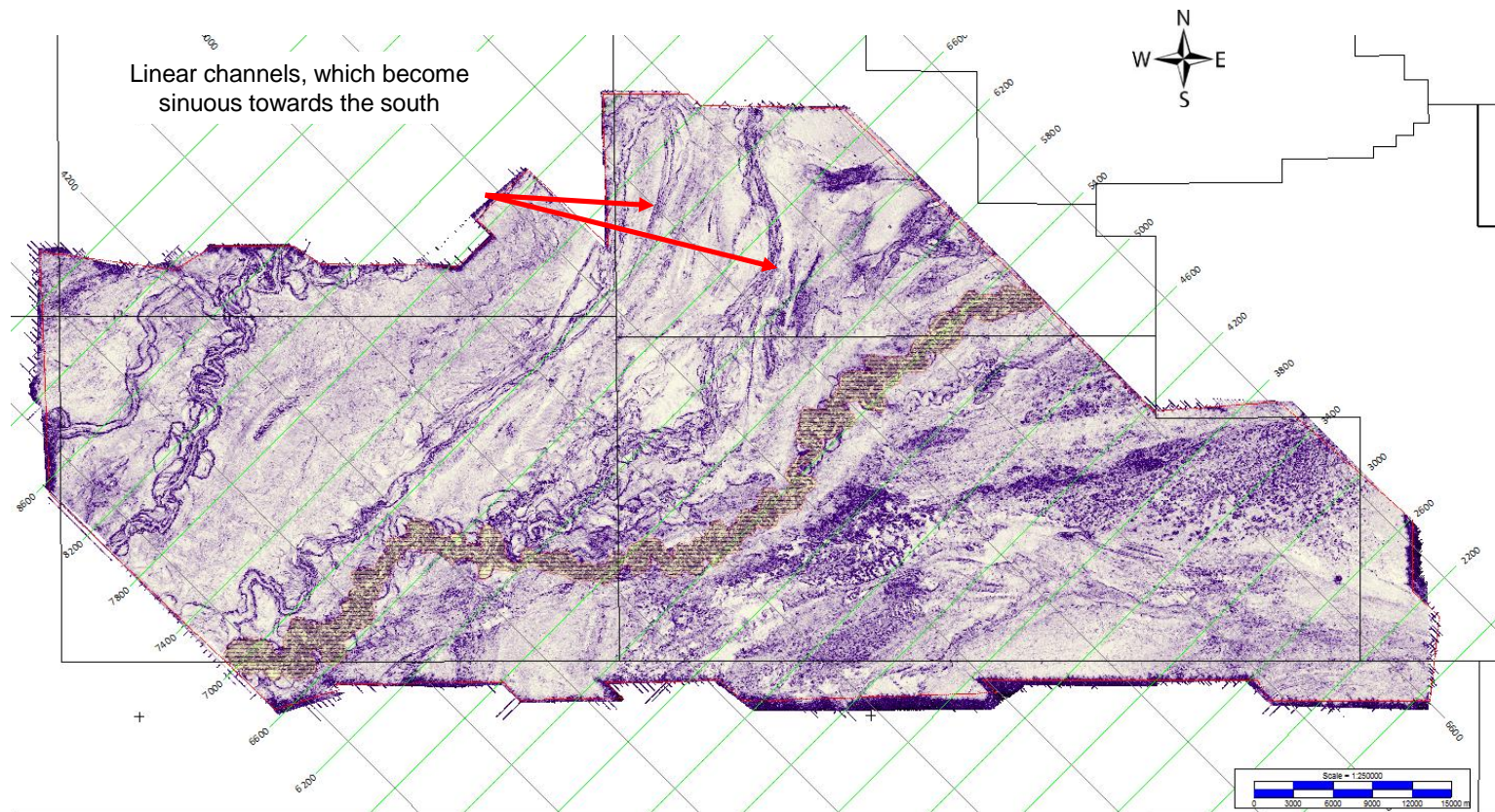


Figure 6-22: Similarity attribute extracted at a level 50 milliseconds below seabed; the present-day Mahin channel is highlighted in yellow.

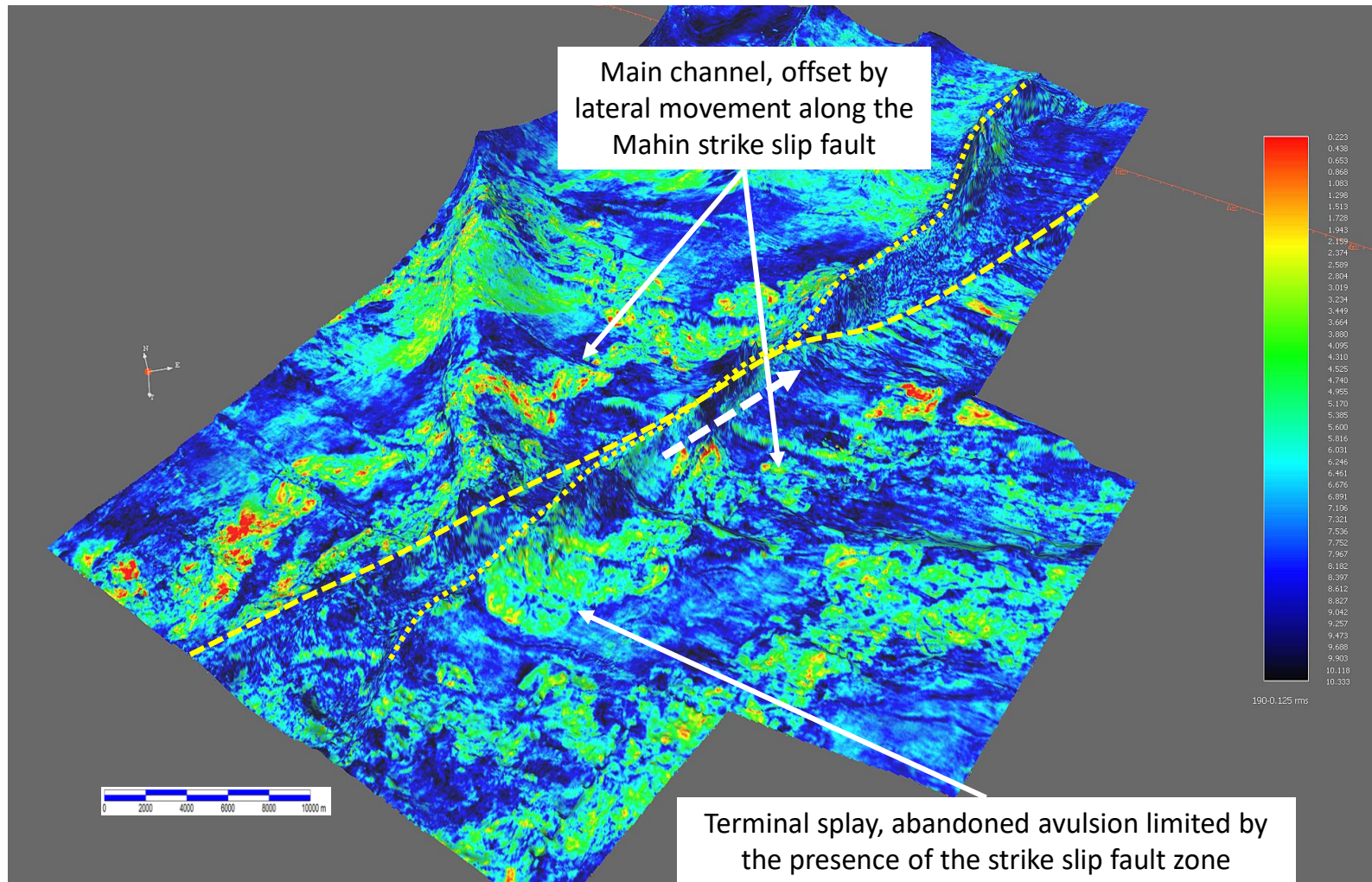


Figure 6-23: Perspective view of an RMS extraction from an interval some 300-400 milliseconds below horizon 160, draped on horizon 160.

6.3.3.2 Levees

The Palaeogene section, which lies between horizons 500 and 400, is dominated by a series of roughly coast-orthogonal elongate ridges that exhibit complex internal deposition and post-depositional deformation. To the west of the Avon/Mahin fault zone, the ridges are well-imaged within the 3D volume. Figure 6-27 illustrates the location and nature of the two most westerly ridges that are imaged in the data. Two high-relief folded anticlines, TA V and TA IV, are present in this region of the survey; the imaging at the core of these anticlines is degraded by the high degree of tectonic deformation. The two ridges at the western margin of the survey area, Ridge A and Ridge B, are well-imaged compared to the high-relief structures and were the focus of study in this chapter.

The ridges are separated from each other by linear synclinal valleys that run in an approximately north-to-south direction at the western limit of the survey, but in a more north-east-south-west direction to the east of these two ridges. The width of the ridges ranges from 10 to 14km and their length exceeds 40km. The wavelength between ridge crests is in the order of 4-12km. The elevation range of the ridges is up to 1.1 seconds two-way time (approximately 1,000m, assuming a seismic velocity of $2,000\text{ms}^{-1}$ for the interval), prior to subsequent tectonic modification.

The base of the antiforms is observed to lie at, or close to, the top of the underlying mass transport complex (MTC west), which will be discussed in section 6.3.4. The upper limit of the ridges is interpreted to be close to horizon 300 (Figure 6-27), where the overlying sediments are largely continuous and parallel. Below horizon 300, the mapped reflectors are limited in lateral extent, either downlapping within the ridge or onlapping within the adjacent synclines.

In Figure 6-25, the two western ridges are illustrated with an east-west seismic profile. They are separated by a syncline in which the seismic facies is chaotic at the base and overlain by parallel continuous events that are seen to onlap the adjacent ridges. The western ridge (A) is bounded to both west and the east by linear tectonic disturbances that are complex in detail; this faulting is reviewed in section 7.3.5.

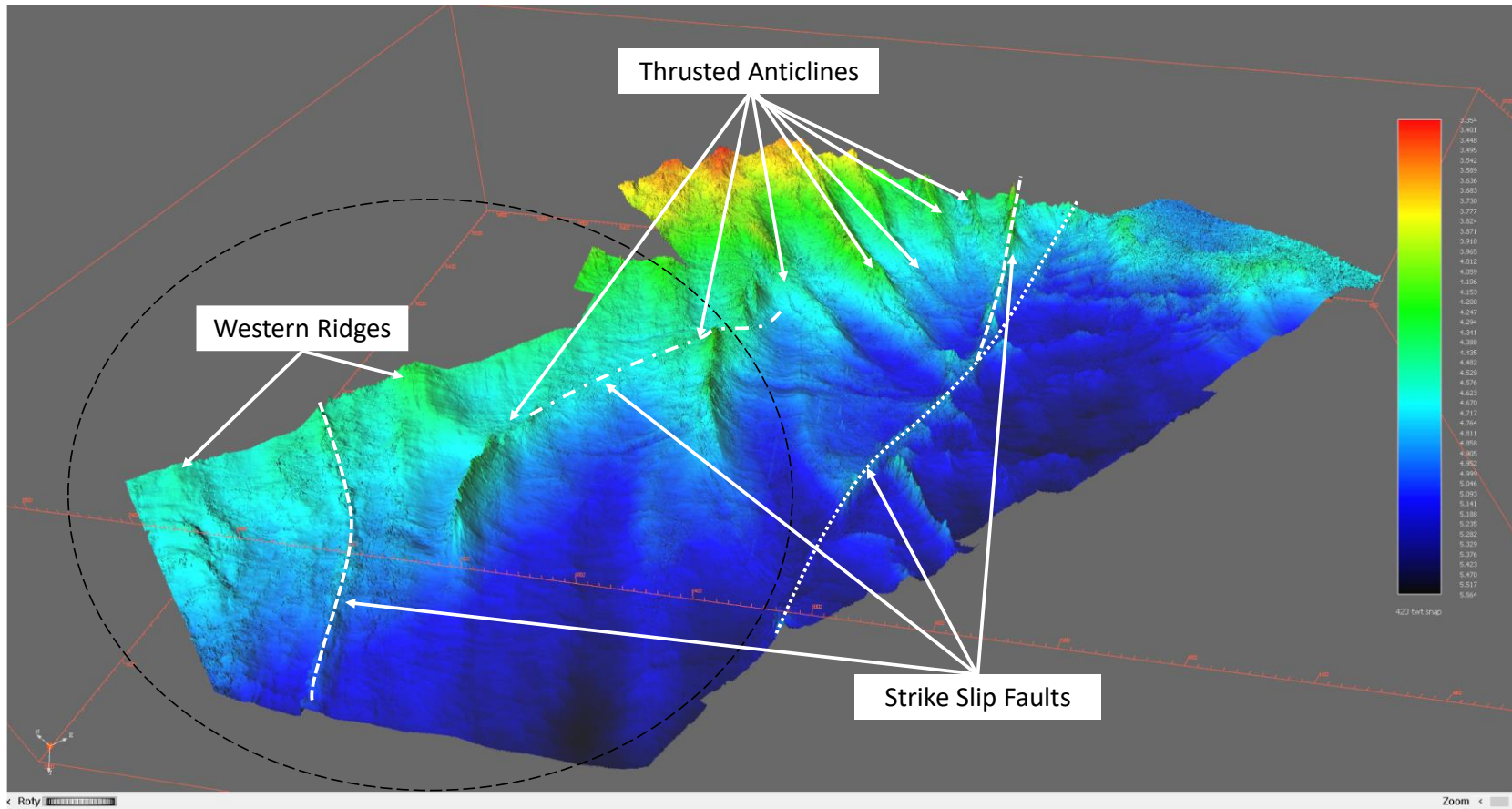


Figure 6-24: Perspective view of the base Neogene unconformity, in twt, illustrating the location of the western ridges and their relationship with the major tectonic elements within the survey.

The internal reflection patterns within the two ridges are comprised of high amplitude, high-frequency reflectors stacking up vertically but pinching out laterally either by erosion or non-deposition.

The vertical relief is greatest in the westernmost ridge, with a decrease in the vertical relief noted progressively in the ridges towards the east. The western ridges are interpreted to be comprised of a number of laterally compensating units. In Figure 6-27, the internal build-up of sediment can be seen to shift laterally as well as vertically. The individual units within this large body of sediments are in the region of 5-7km in width and up to 600ms vertically. The slopes of the beds on the flanks of the units lie in the range of five to six degrees.

The shallow portion of the ridges are relatively undeformed by tectonic activity. Isochrones highlight the location of the ridges, notably the interval between horizons 400 and 420 and 300-400 (Figure 6-26). The orientation of the three synclines noted in Figure 6-27 alters from a north-east to south-west direction in syncline C to north-south in syncline A and B. In syncline B, the axis of the syncline is filled with a chaotic package of reflectors. This arises from both along-axis debris flows and mass wastage from the flanks of the ridges. This seismic character is discussed in section 6.3.5.

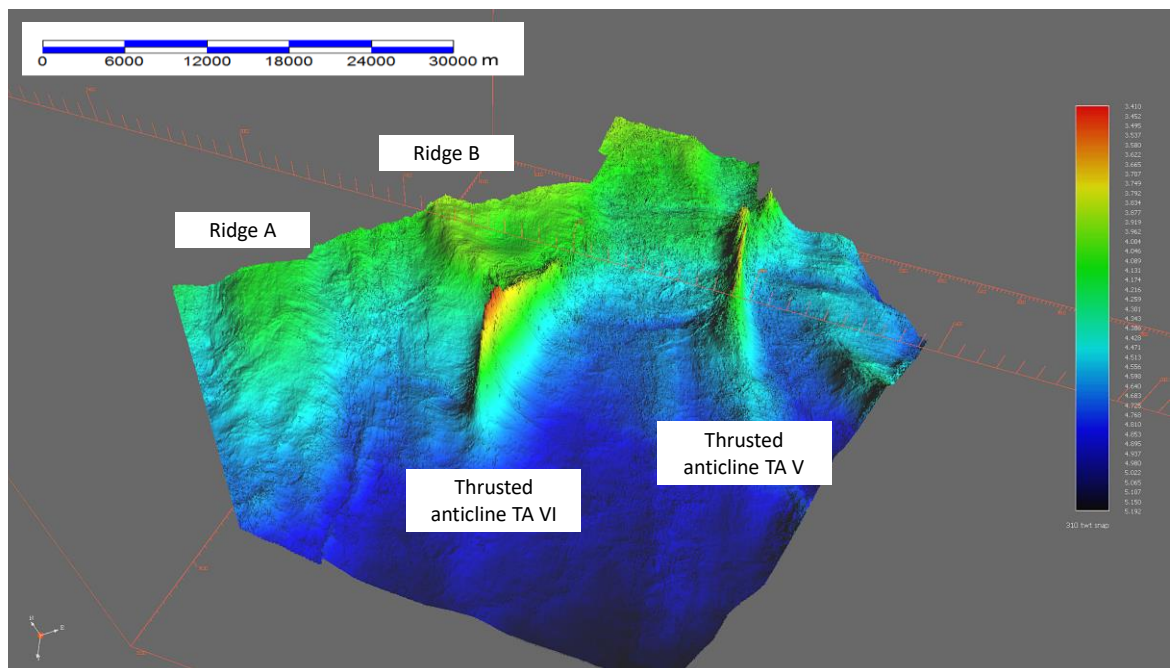


Figure 6-25: Perspective view of an Upper Oligocene event (horizon 310) in twt, showing the relationship between the western ridges and the thrustured anticlines.

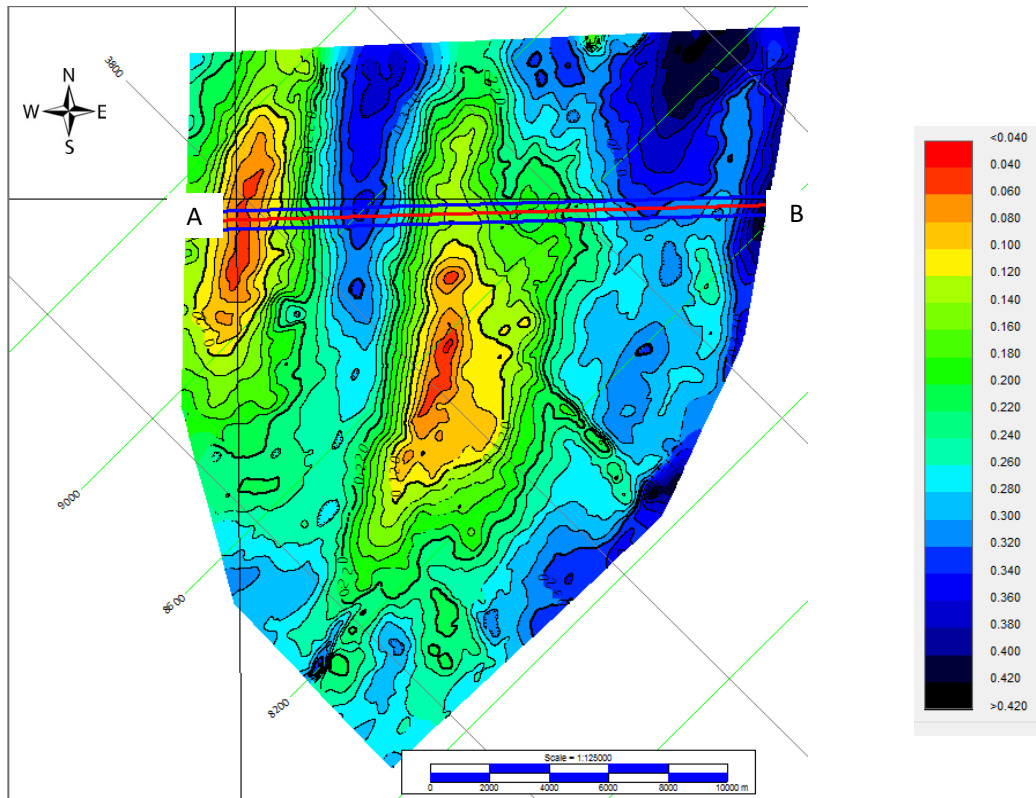


Figure 6-26: Isochrone of the interval between horizons 300 and 400 (cold colours indicate thicker regions) – see Figure 6-27 for the cross section A-B.

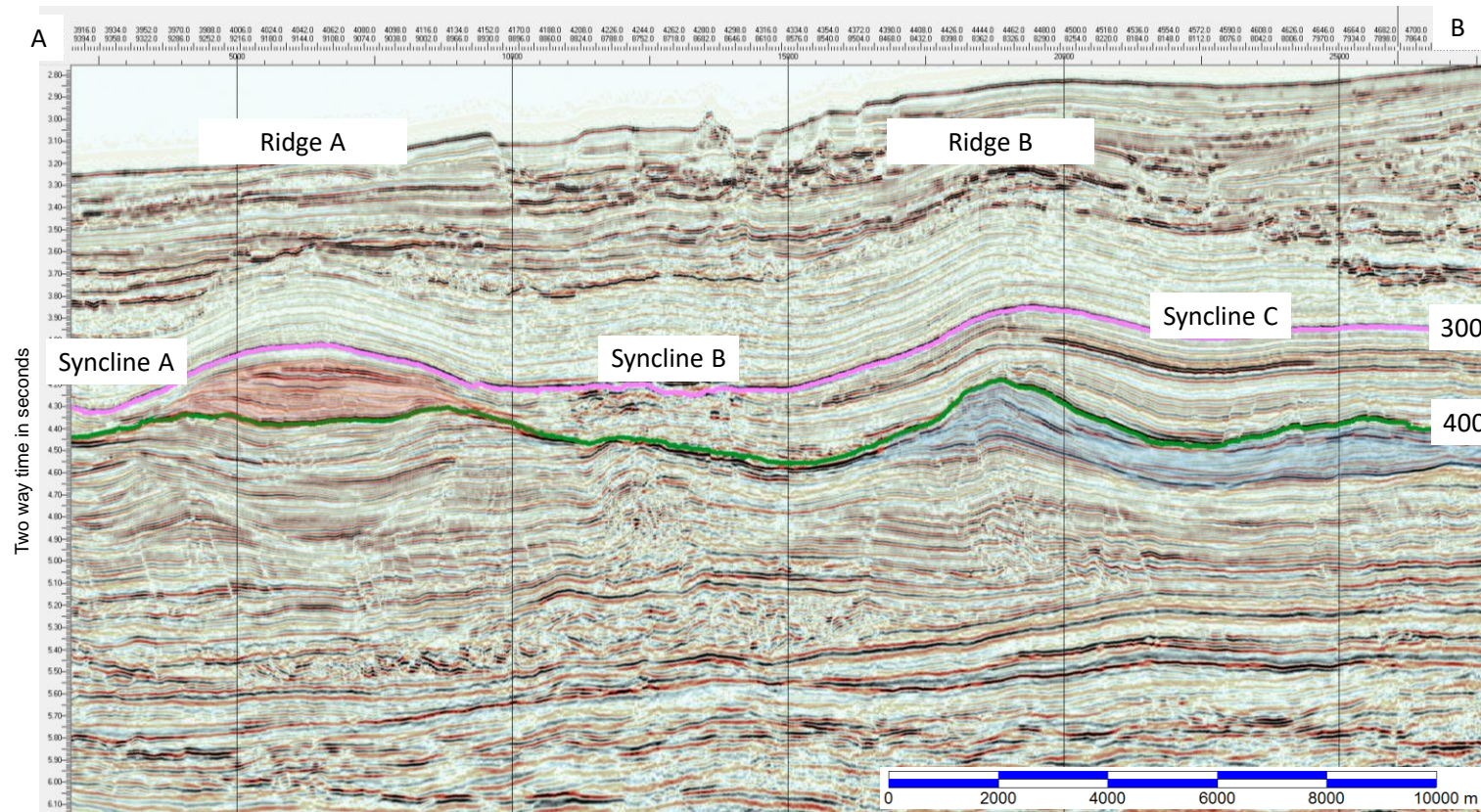


Figure 6-27: Seismic line illustrating the geometry of the two major ridges and associated synclines in the western area of the survey.

In Figure 6-27, the pink horizon is close to the upper surface of the levee system, while the green horizon is representative of an internal surface within the levee system. Highlighted in red and blue are two examples of accreting bodies unaffected by later tectonic deformation. A number of other accreting intervals are present below the green horizon, but they have been modified by later compressional faulting.

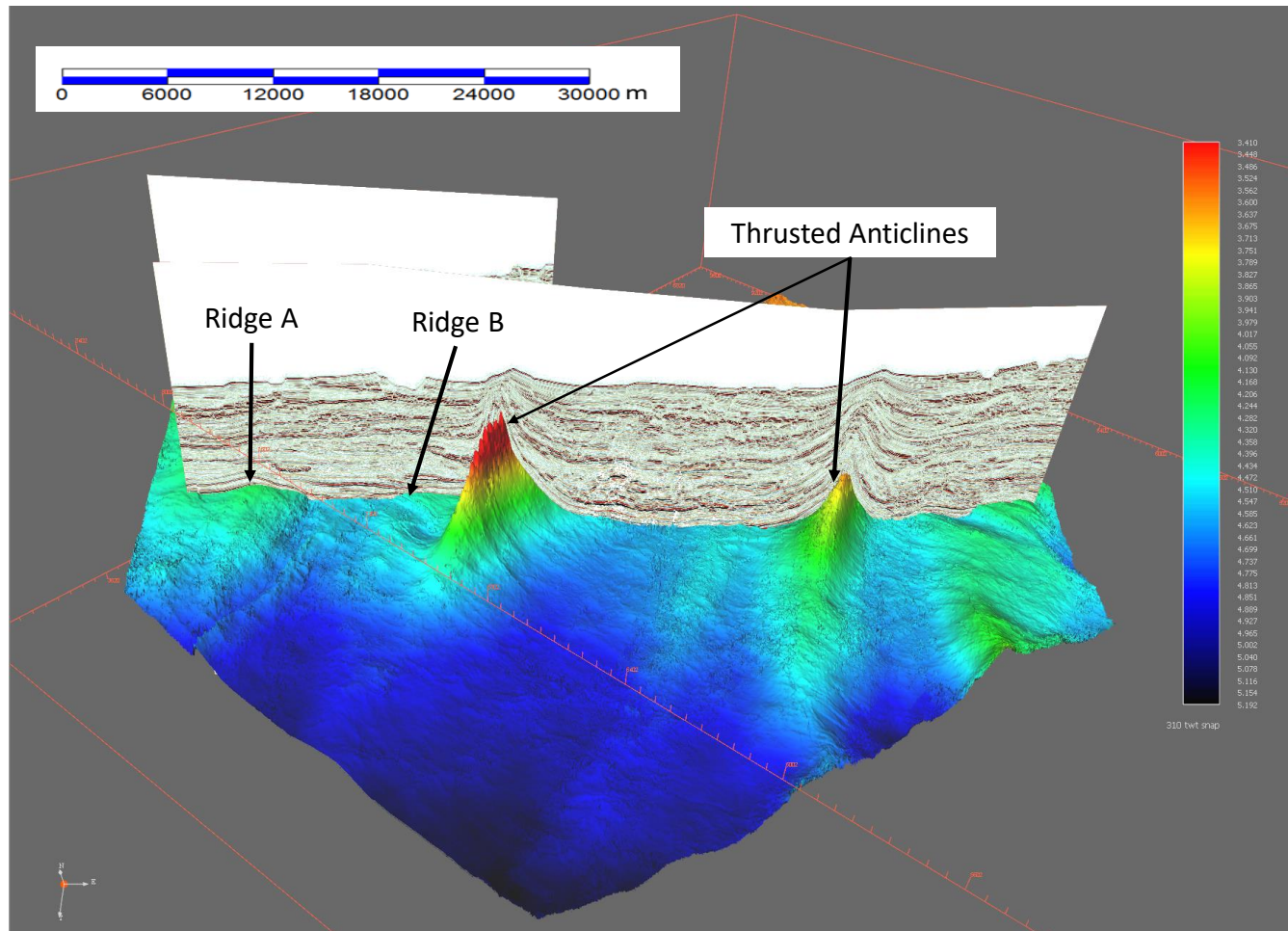


Figure 6-28: Perspective view of horizon 300 showing the difference in the vertical expression of the thrust anticlines, compared to the levees.

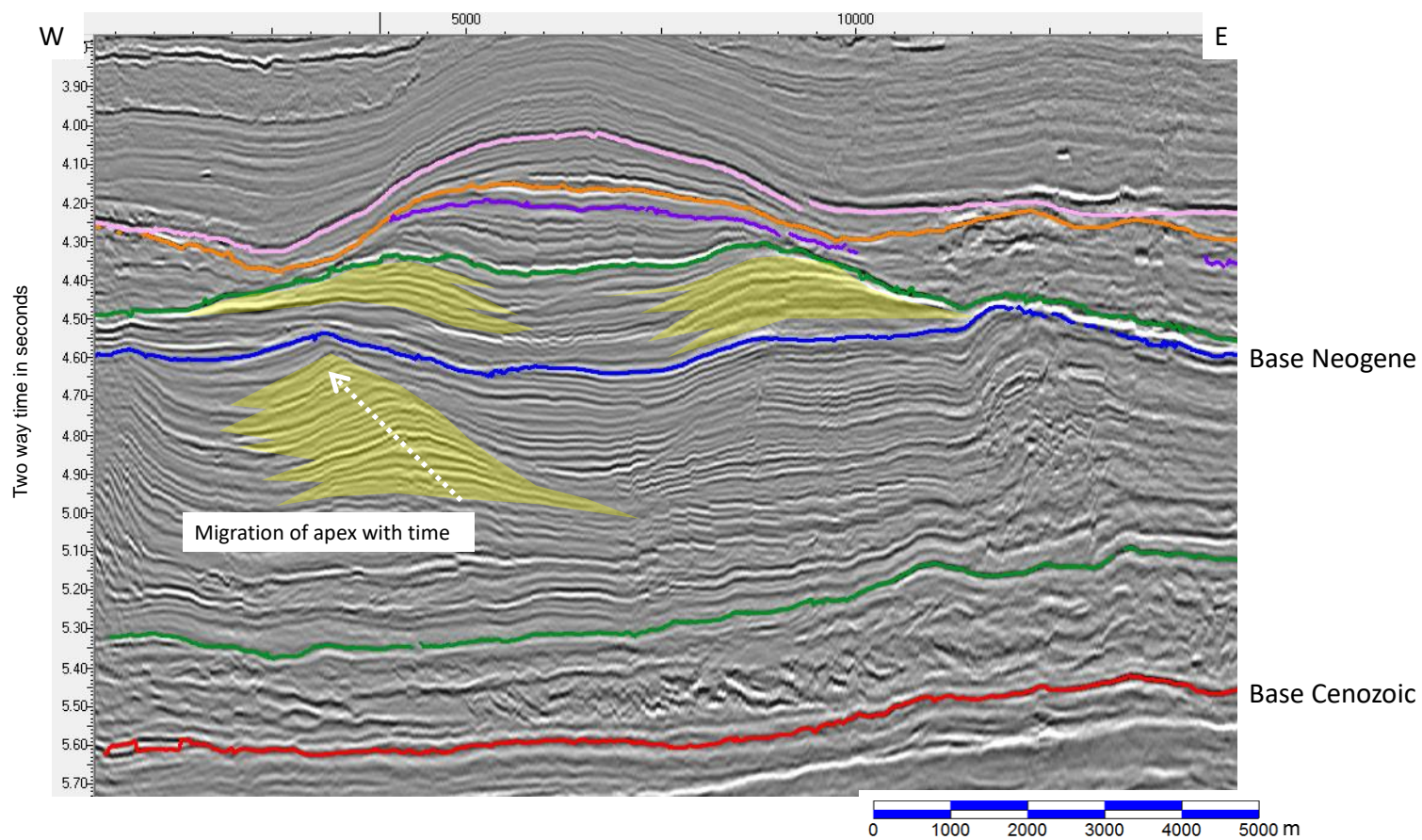


Figure 6-29: Detailed view of Ridge A (from Figure 6-27), showing the location of several internal ridges within the overall body of Ridge A, highlighted in yellow.

The geometry of the reflectors within the ridges are illustrated in Figure 6-29; the areas highlighted in yellow have approximately triangular cross sections. The upper layers are narrower than the basal horizons; in addition, the crests of these triangular intervals are seen to move laterally with time.

This reflection geometry is similar to that observed in the levees that accompany slope channel deposits (Kneller, 1995; Posamentier and Kolla, 2003; Kolla et al., 2007; Rabelo et al., 2007; Cross et al., 2009).

The following observations can be made about the ridges:

The length of these ridges exceed 40km and if tied to the Avon Canyon, they could extend for over 60km in length.

The ridges are constructed from an amalgamation of smaller ridges. The largest of the ridges in the west is an aggrading stack of compensating levees, which indicates a long-lived supply of sediments from the north.

The slope channels identified in this study area are observed to alter course along their course, which is interpreted to result from a change in the dip of the surface, over which the turbidity currents travel. In the case of the ridges referred to in this chapter, they exhibit linear downslope orientations, with no apparent meandering.

There are intervals of higher seismic amplitude discontinuous reflections within the base of the synclines. Attempts to extract depositional information from both attribute analysis (including similarity) and the RMS extraction of the amplitude within a window that includes the high-amplitude events were made. The results indicated that the intervals have no recognisable patterns that could be associated with channels. The discontinuous seismic facies is present throughout the length of the synclines. Overlying this chaotic interval, the bulk of the infill is comprised of parallel bedded deposits.

Two possible explanations for the presence of these features have been considered; they are either the result of predominantly downslope turbidity current activity or they have been formed as a result of ocean-bottom currents. The closest analogy to the elongate linear levees is that described by Reading (1994), which would suggest that there is a region to the south of the survey area where a basin floor fan may have developed.

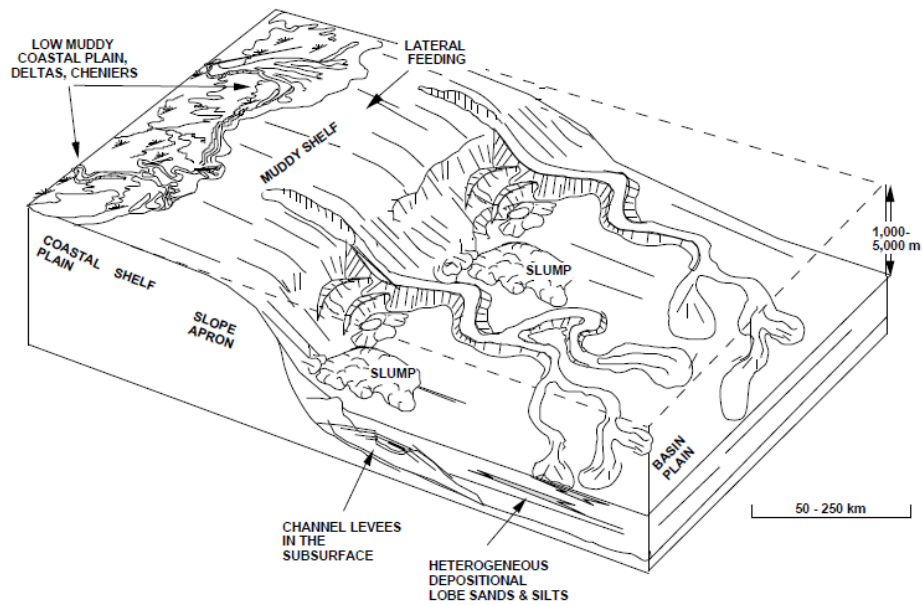


Figure 11—Depositional model for a multiple-source mud-rich ramp.

Figure 6-30: Schematic depiction of a depositional system that could be an analogy for the levees (Reading and Richards, 1994).

This geometrical arrangement of seismic reflectors is compared to other deep-water regions in order to establish the origin of these particular deposits. The region that appears to resemble most closely the arrangement of coast-orthogonal elongate ridges are those described from the Antarctic Peninsula (Rebesco et al., 2014). The ridges in the Antarctic case are associated with the interaction of bottom-circulating currents with downslope current motion. However, the symmetry of the ridges seen in this study does not match that observed within contourite drifts. The nature of these ridges is dealt with in the observations in chapter 8.

The location of Ridge A at the end of the western edge of the survey limits the evaluation of the entire feature of which this is a constituent part.

6.3.4 Mass transport deposits

3D seismic data has been valuable in the study of deep-marine sedimentary processes, not least in the recognition of the morphology and geometry of mass transport deposits. Prior to the advent of 3D data sets, 2D data was unable to image in a spatial manner the nature of these deep-water fabrics. What may be unusual in this study is the depth below the seabed of the mass transport complexes. Most studies focus on imaging in the shallow subsurface where the vertical resolution in the data is better (Deptuck et al., 2003; Deptuck et al., 2007). In this study, the interval is present at depths in the order of 4-5km; this makes the internal resolution lower than that observed in the recent slides. Nonetheless, the key aspects of the deposits are recognisable, and these have been studied; the results of this analysis is presented below.

The nature of large-scale mass transport deposits has been described by several authors (Carter, 1975; Galloway, 1975, 1998; Moscardelli et al., 2006; Bull et al., 2009; Alves, 2010; Mulder, 2011; Richardson et al., 2011; Shipp et al., 2011). These assemblages are the product of slope failure (Canals et al., 2004) and downslope movements of fluidised sediment and coherent blocks of formerly competent strata. There are few outcrop examples of deep-water mass transport deposits due to the limited number of former deep-water sedimentary basins being sufficiently uplifted to be exposed. However, one example – the Tres Pasos formation of southern Chile – does provide surface outcrop exposures of deep-water slope deposits that included both slope channels and mass transport complexes (Schultz and Hubbard, 2005).

The bulk of the descriptions of mass transport complexes comes from the examination of 3D seismic data and high-resolution seabed surveys. Among the best documented are the Storrega slide offshore Norway (Bryn et al., 2005; Kvalstad et al., 2005; Solheim et al., 2005); Brunei (Gee et al., 2007); Trinidad (Wood, 2011); the Gulf of Mexico (Cardona et al., 2016); Azerbaijan (Richardson et al., 2011); Brazil (Viana et al., 2003); Morocco (Dunlap et al., 2010); and Spitzbergen (Nemec, 1988).

Within the 3D seismic volume that forms the basis of this study, a number of intervals are interpreted as being mass transport complexes. The majority of these generic units are derived from the north. They display many of the typical characteristics described by a number of authors (Galloway, 1998; Bryn et al., 2005; Kvalstad et al., 2005; Gee et al., 2007; Faereth and Saetersmoen, 2008; Bull et al., 2009; Alves, 2010; Shipp et al., 2011). In this study, the three domains described by Bull have been used to compare what is observed within the data to the models described by both Bull et al. (2009) and Galloway (1998). The localised diagnostics that support the interpretation of the mapped entities as mass transport deposits are taken from Bull et al. (2009).

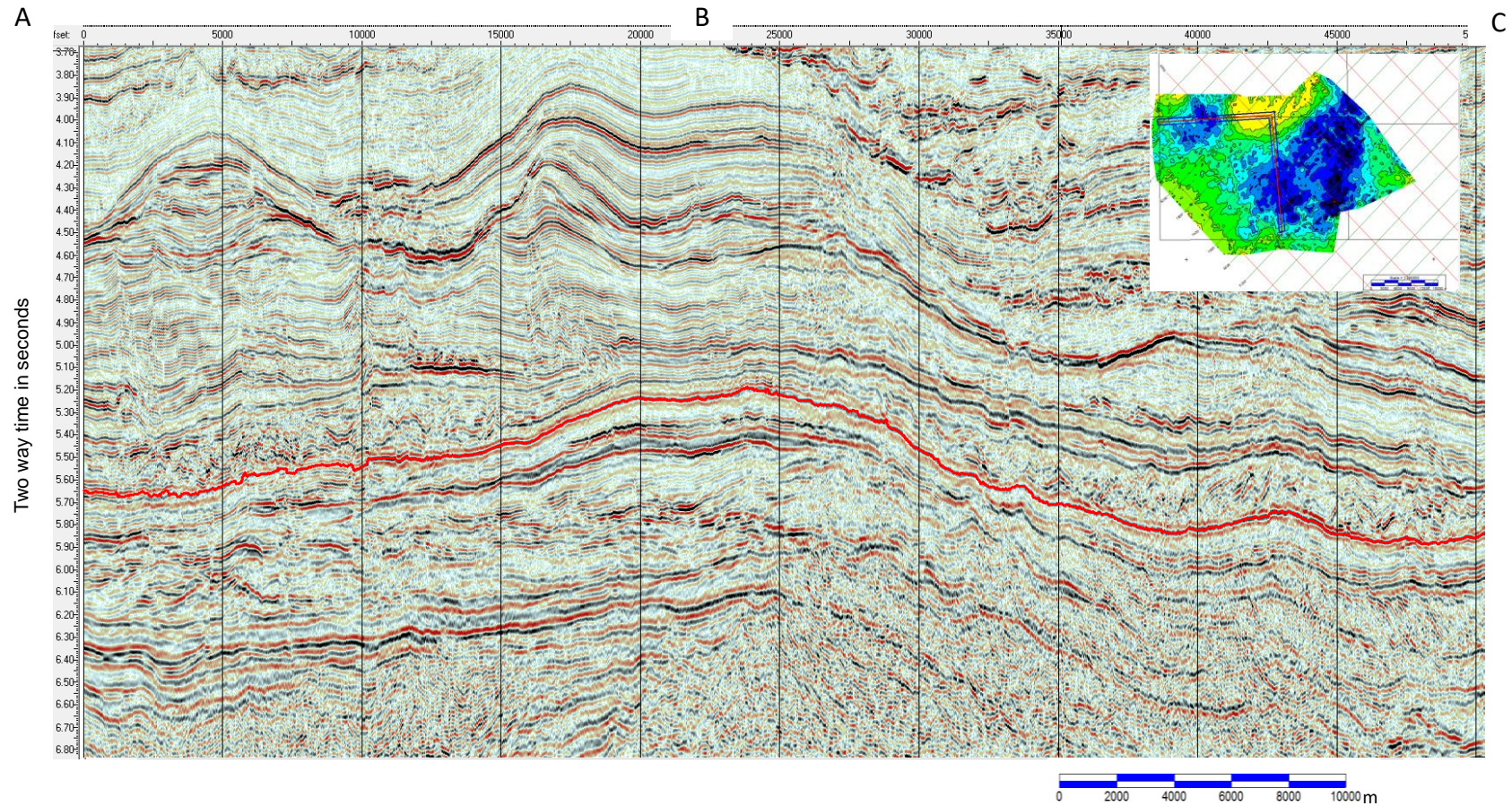


Figure 6-31: Seismic traverse with base of the mass transport complexes highlighted in red (the Base Cenozoic) illustrating the presence of two mass transport complexes. The inset map is an isochrone of the thickness of the mass transport complex (blue being thick).

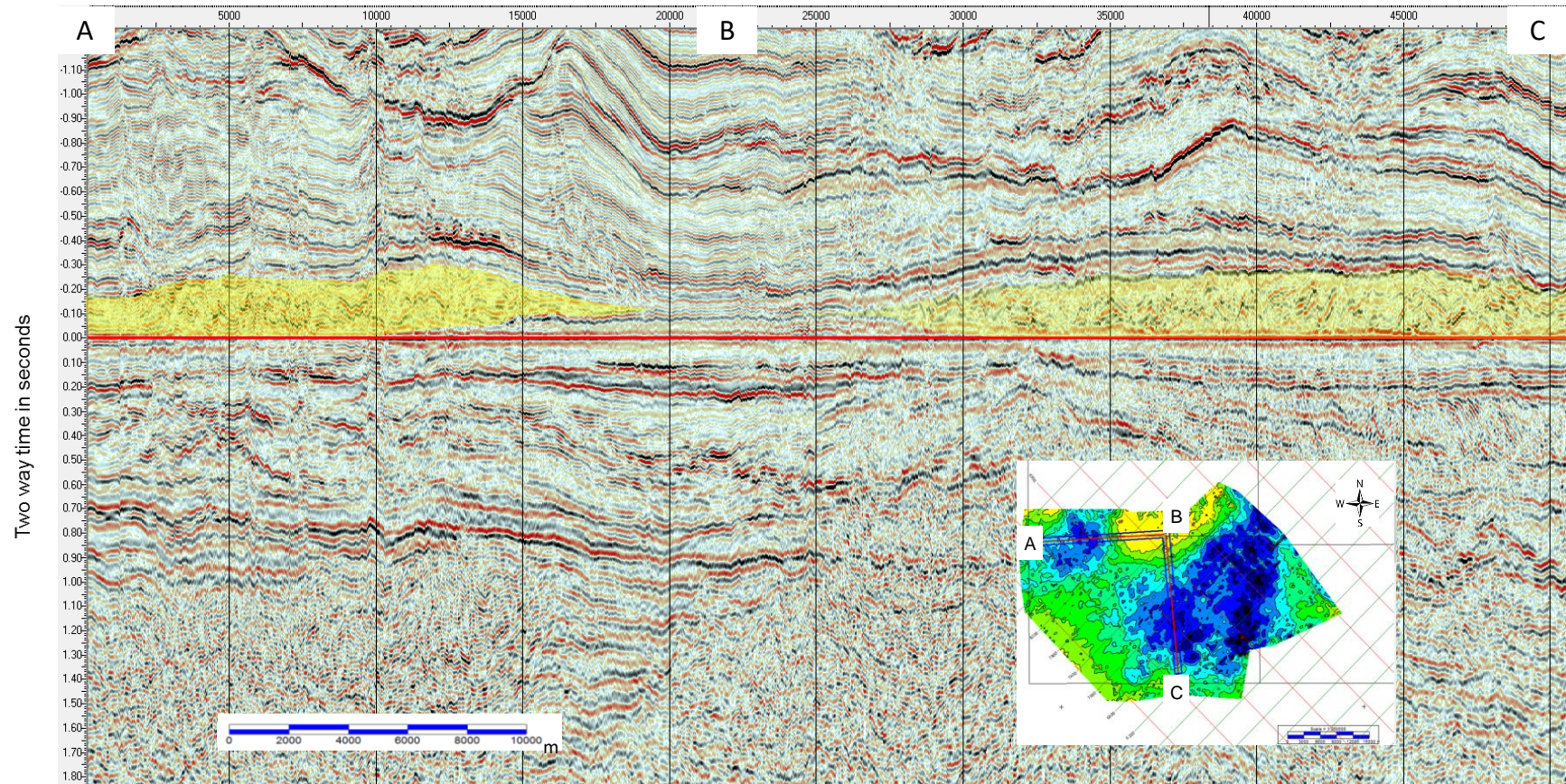


Figure 6-32: The seismic traverse in Figure 6-31 flattened at the base Cenozoic (red horizon), which shows the relationship between the two mass transport deposits at the base of the Cenozoic.

In Figure 6-32, the seismic expression of the mass transport complex at the base of the Cenozoic is highlighted. The seismic also highlights the distinct separation of depositional and structural nature between the section that underlies the base of the mass transport complex and that which overlies the upper surface of the mass transport deposits. The presence of two separate intervals of chaotic internal reflection character is highlighted by the yellow colouring.

6.3.4.1 Headwall domain

The headwall domain (up-dip extension and slip) for the flows seen in the 3D data set lie to the north and north-east of the survey area, where they have been described by Maloney et. al. (2012). This suite of down-to-the-basin listric faults sole out on a clear detachment layer (Figure 6-33). The detachment surface mapped by Maloney is interpreted to be the lateral equivalent to the Base Cenozoic, within the 3D survey area.

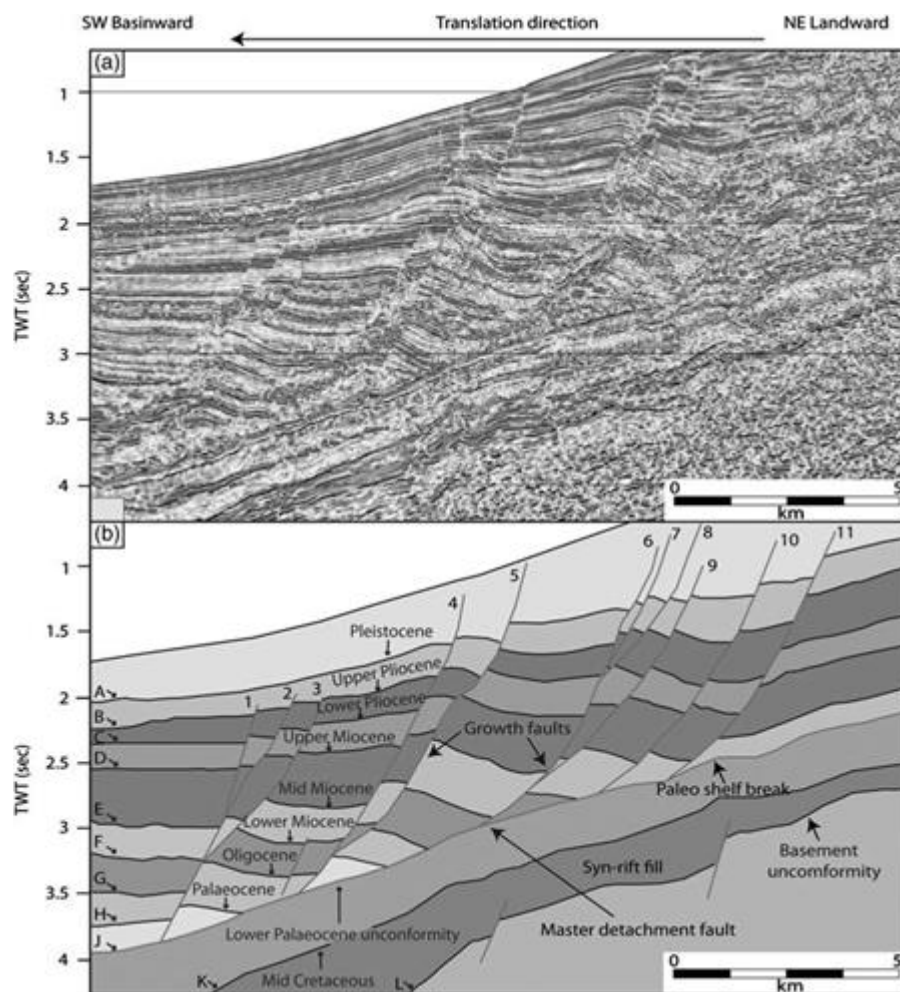


Figure 6-33: Seismic profile from the headwall domain (Maloney et al., 2012).

It is interpreted from the above section that the initial period of shelfal collapse was initiated at or around the end of the Cretaceous. In Figure 6-34 intervals G-J are absent at the northern limit of the cross section, indicating that growth took place during this period at the distal portion of the shelf system.

6.3.4.2 Translational zone

Among the diagnostic elements that should be visible in the accumulation/translation domain are basal scours and striations; only one of the intervals that has been mapped exhibits evidence of a basal scour and no evidence of striations; it is at the base of the Upper Miocene low stand interval (Figure 6-34). It may be that at depth, the vertical and lateral resolution within the band-limited dataset is too low to image the scours.

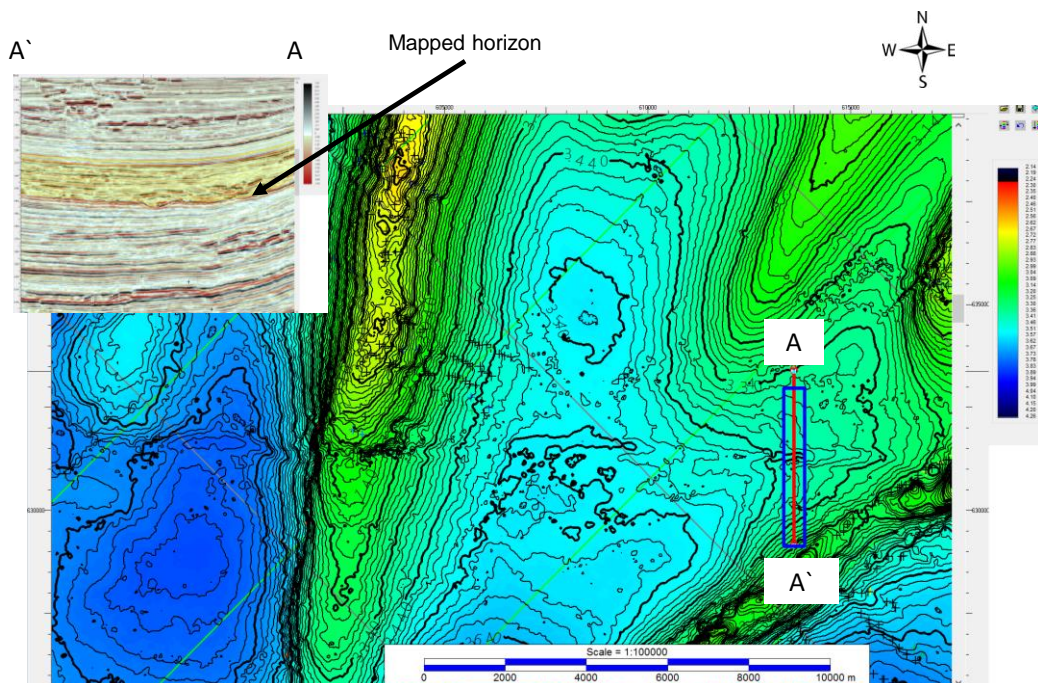


Figure 6-34: Illustration of the scour at the base of the Upper Miocene.

The lateral margins of the chaotic zones are not sharply defined, most likely due to the fact that the well-imaged portion of the zones are interpreted to be in the run-out region. The upper reaches of the complex are poorly imaged and in all likelihood, the complex is constructed from several amalgamated episodes of downslope motion.

The internal character of the deposits range from folded and thrust regions to chaotic isolated blocks.

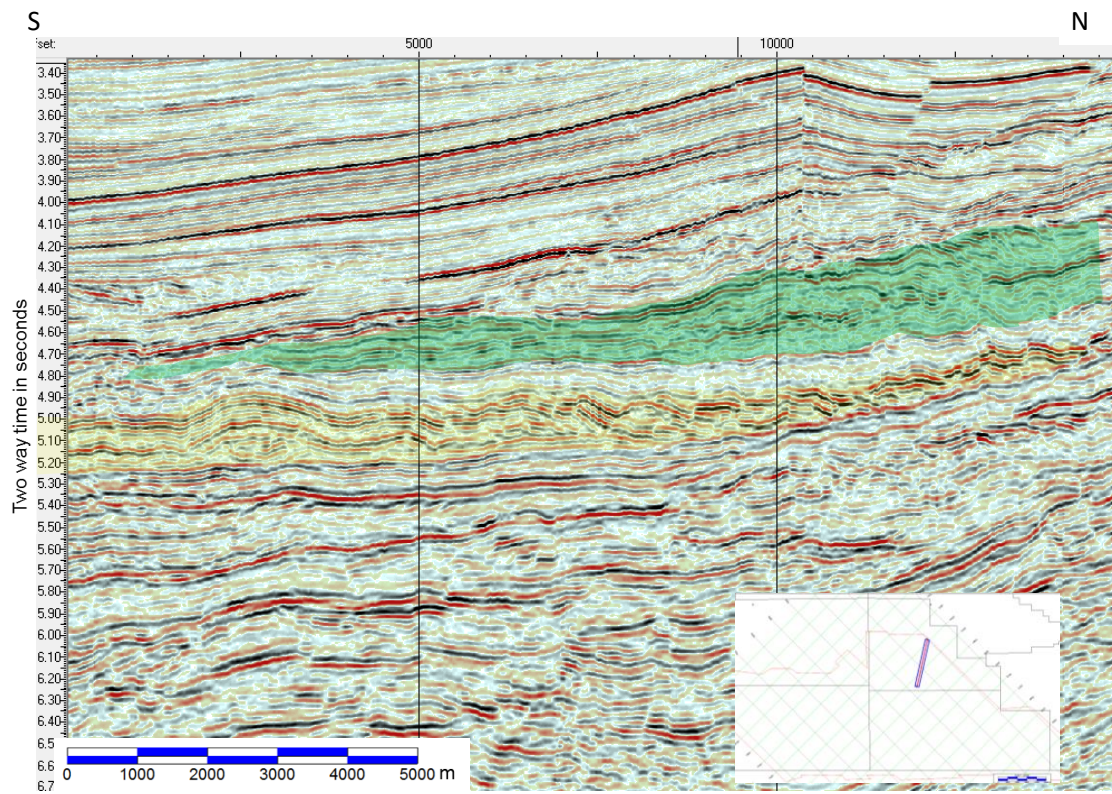


Figure 6-35: Portion of seismic line that passes through the translational zone of two mass transport deposits.

The translational domain of Bull et al. (2009) can be recognised by the stacking of a set of folded strata that exhibit a folded geometry with reverse faults that verge towards the south (Figure 6-35). The strike of the fold axes of the folds within this interval are aligned in an east-to-west orientation. This matches the slump fold description seen in Figure 6-38.

In Figure 6-35, the intervals highlighted in yellow and green are interpreted to be representative of the translational zone of a mass transport deposit. Within these zones, the basal section is comprised of a series of apparently thrust and folded sediments. The green interval represents a younger episode of deposition of a mass transport complex, with a series of thrusts apparent at the upper limit of the zone towards the northern end of the line.

Mass transport deposits in outcrop display contorted bed forms that are below the resolution of seismic such that even transparent seismic facies can be comprised of originally competent strata.



Figure 6-36: Outcrop example of contorted beds within a mass transport deposit.

Figure 6-36 is located within the Tres Pasos formation within the Magallanes Basin in southern Chile (Shultz et al., 2005; Macauley and Hubbard, 2013). The image above contains an example of a set of contorted beds sandwiched between two sand-filled channels.

6.3.4.3 Toe domain

The compressional toe is a region in which coherent blocks of strata are deformed in a manner that generates widespread thrusting and reverse faulting or pressure ridges. The best example of the pressure ridge fabric is that observed in the deepest mapped chaotic interval within the Campanian (below horizon 630).

6.3.4.4 Fluidised apron

In addition to the characteristics described by Bull et al. (2009), there is a region beyond the compressional toe, where the mass transport deposits run out over the sea floor (Galloway, 1998). In the run-out region, the internal reflection character becomes diffuse, with lower amplitude discontinuous reflections noted.

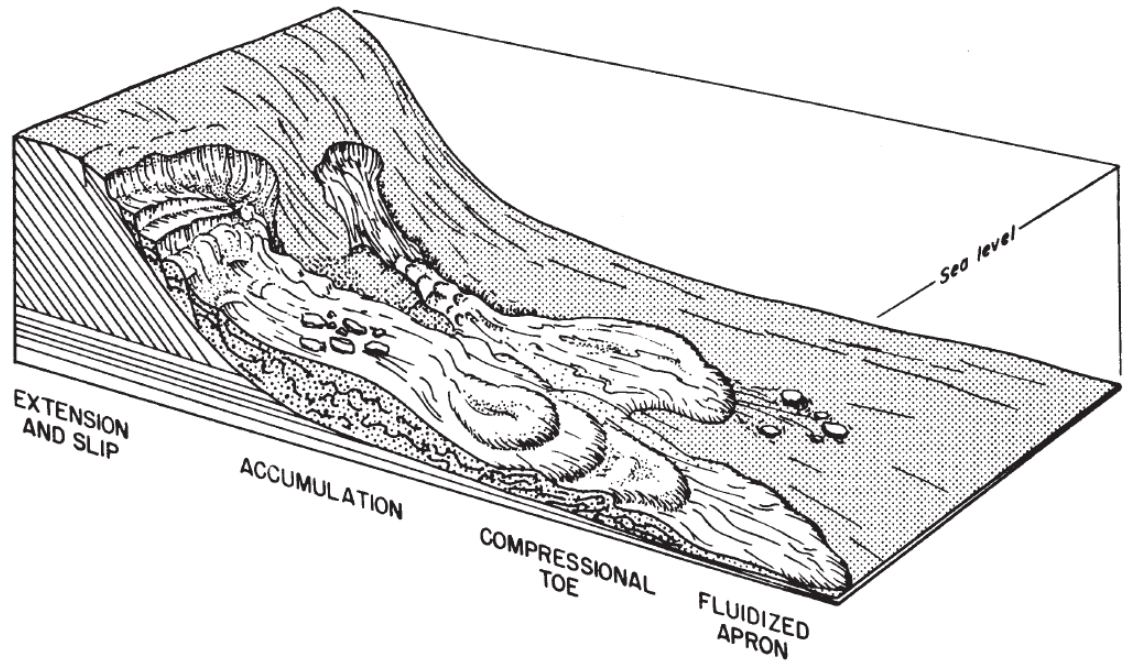


Figure 6-37: Schematic diagram of the key elements of a mass transport complex after Galloway (1998).

The input of sediment from the north via the process described above appears to have commenced during the late Cretaceous to early Cenozoic. This process is interpreted to have been active up until the early Miocene. Sedimentation in the study area from the early Miocene onwards appears to have been predominantly influenced by the growth of the Niger Delta in the east.

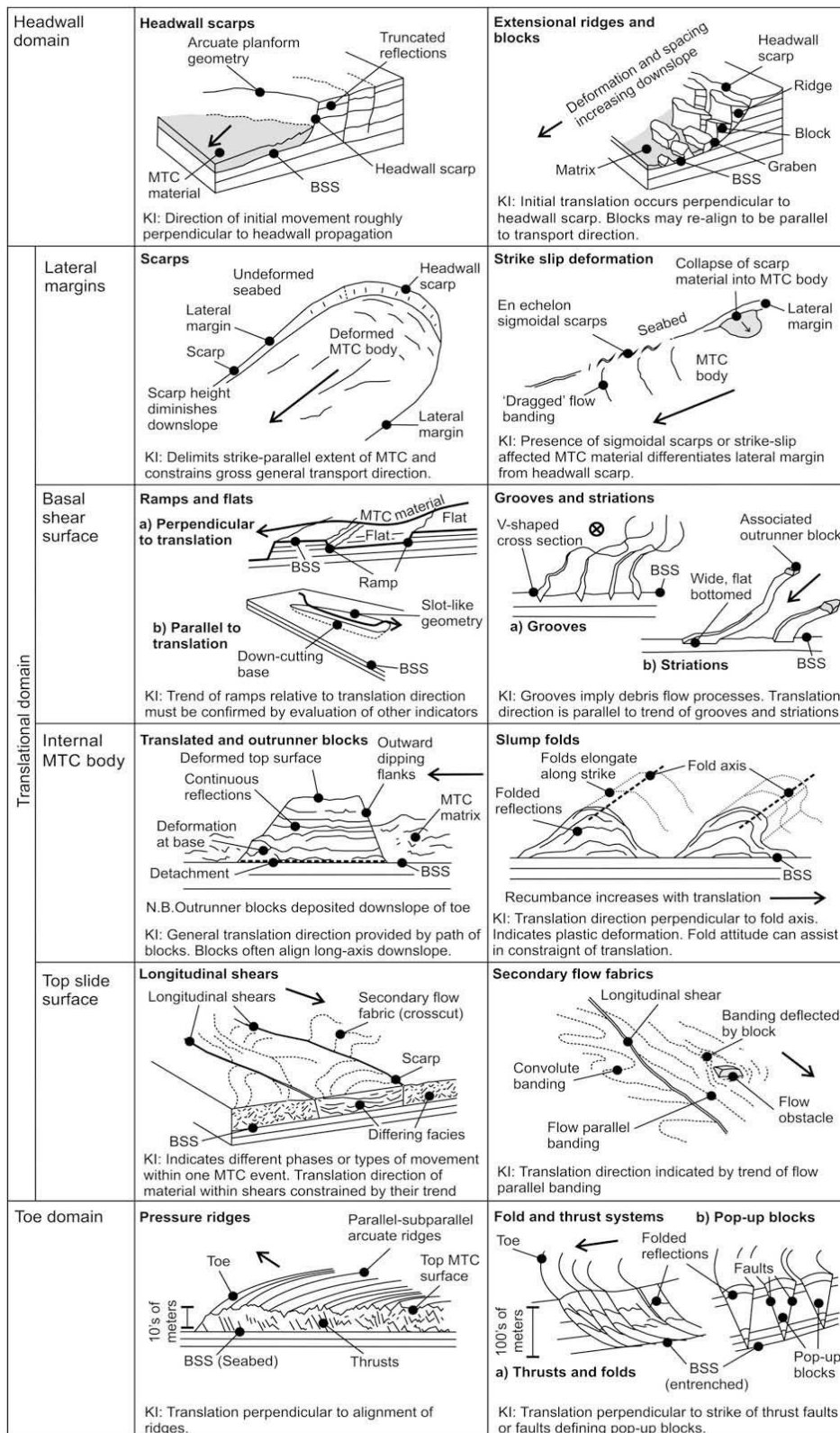


Figure 6-38: Classification of fabrics associated with mass transport deposits, taken from Bull et al. (2009).

Using the above diagnostics, the chaotic intervals identified within the 3D volume have been interpreted to be the result of the emplacement of mass transport deposits, which in the main have been sourced from outside the survey to the north.

6.3.4.5 Neogene mass transport intervals

There are a number of intervals recognised within the shallow portion of the seismic volume, which exhibit chaotic internal reflection geometries. They are particularly well-imaged in the region to the west of the Avon/Mahin fault zone. This region has therefore been the focus of the analysis. The younger the section, the further north they are seen.

The following set of examples is used to demonstrate these properties. Unfortunately, the Miocene to recent tectonic distortion does not enable clear imaging of a complete mass transport complex from its up-dip provenance to the basin.

6.3.4.5.1 Lower Miocene (Horizon 160 to 200)

Within this sequence, the chaotic intervals are in general located within the remnant synclines that were created during the Palaeogene. There are a number of well-imaged such zones that were mapped.

Horizon 160 is notable for the fact that it appears to represent not only a change in structural modification but also a change in sedimentology. Immediately above this horizon there is limited evidence of slope channel deposition; below it, a series of slope channel complexes have been mapped, which appear to originate from the east (Deptuck et al., 2007; Leduc et al., 2009). Although there are no slope channels observed to have been sourced from the north, within this interval, there are a number of layers that contain chaotic seismic facies which do have their origin in the north.

Within the interval that underlies horizon 160, a seismic event that represents the top of an assumed mass transport complex, horizon 163, was mapped and amplitude extractions of the interval of 100 milliseconds that lay beneath the event were performed. The similarity attribute that was obtained from horizon 163 (Figure 6-39) exhibits the overall shape of the anomaly, which resembles that of a teardrop with a thin neck in the north, and broadens to the south.

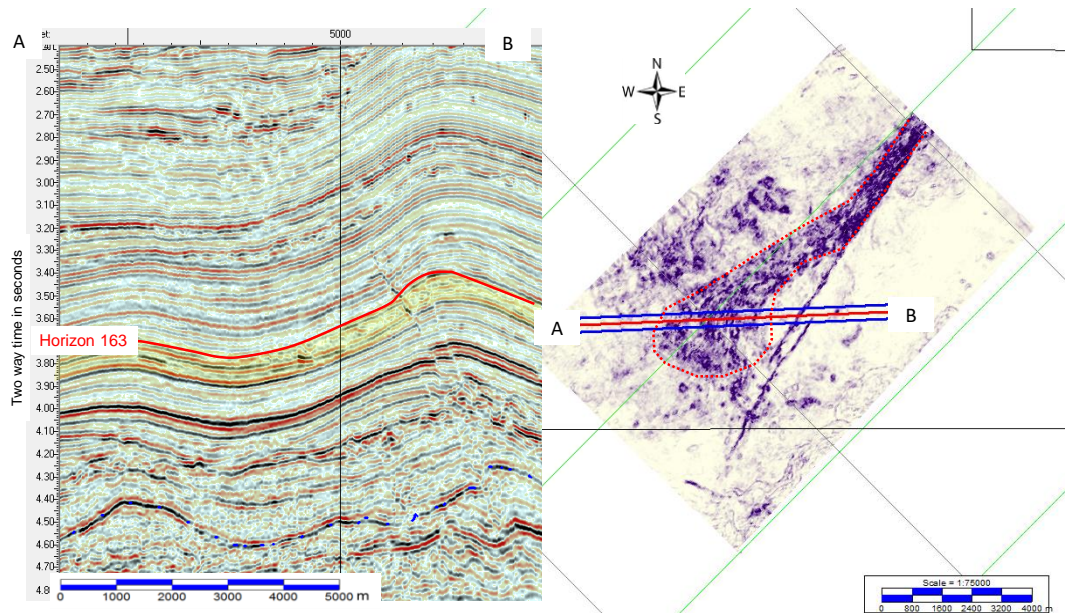


Figure 6-39: Illustration of the similarity attribute extracted from horizon 163.

A map of the similarity attribute of horizon 200 highlights two separate features (Figure 6-40). The more westerly one also exhibits a teardrop areal extent, with a thin northern neck, which expands down-dip into an arcuate form. The internal nature of the interval between horizon 200 and 190, which includes the mass transport complex, has very little coherent reflection energy and overall, a low amplitude. The upper limit of the flow is outside the 3D survey area. However, in the main body of the flow, there is very little coherent energy. Towards the toe, in the south, a number of reflectors can be seen, which are interpreted to be associated with a set of toe thrusts. The interval passes southward into a region of undeformed continuous reflections (Figure 6-41).

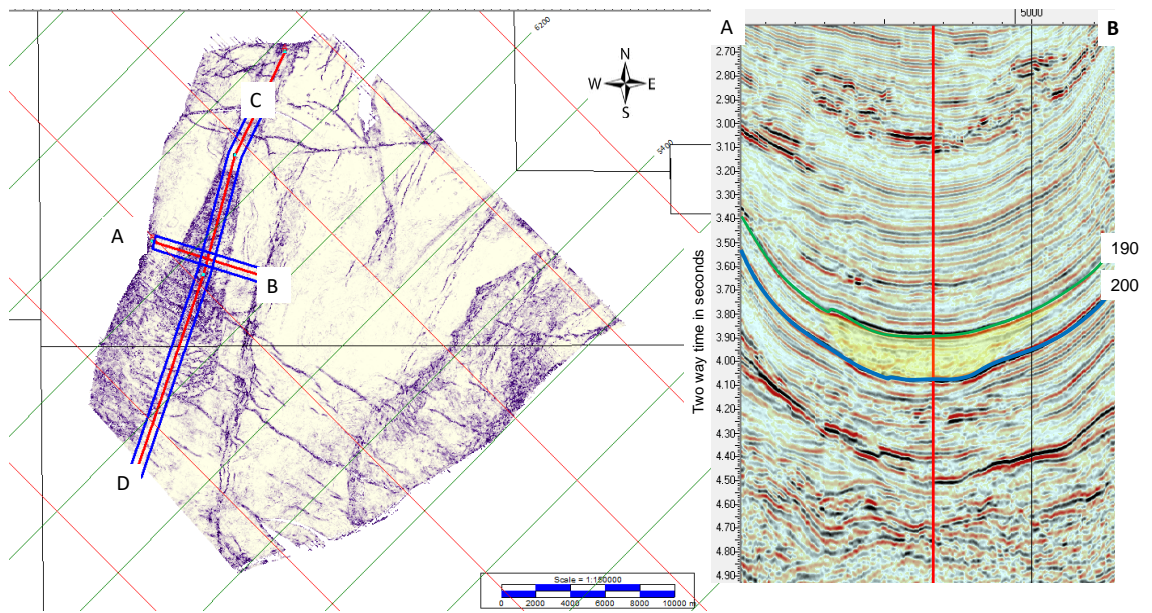


Figure 6-40: Similarity attribute extracted from horizon 200.

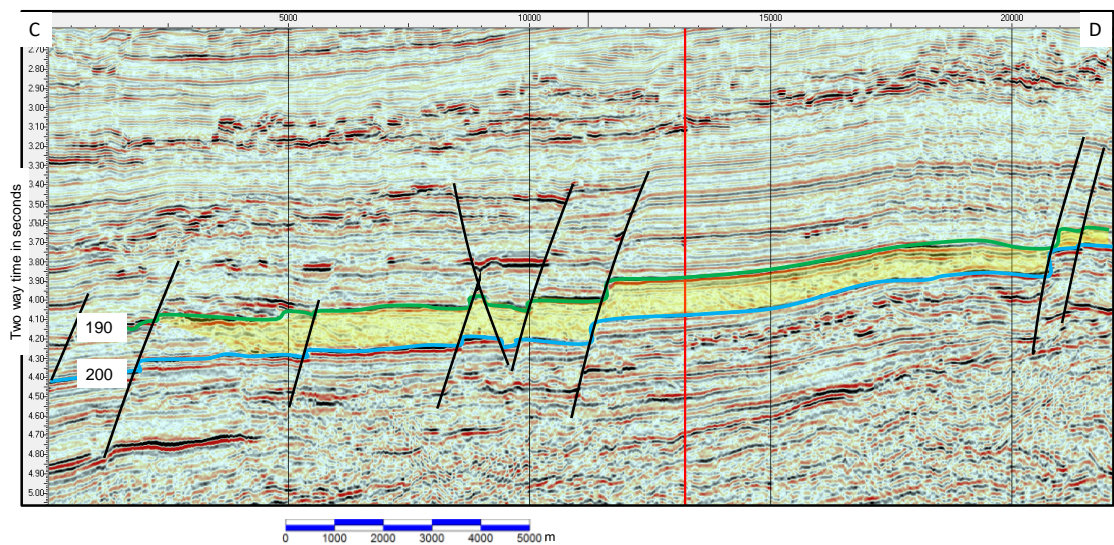


Figure 6-41: Seismic line that is located along the axis of the western anomaly seen in Figure 6-40.

This western teardrop-shaped anomaly is interpreted to result from the flow of sediments down the axis of a pre-existing valley. An amplitude extraction of the interval that underlies the base of this chaotic zone picks out the presence of a deeper layer of high-amplitude discontinuous events. In addition to the interval underlying the western anomaly, at the level below horizon 200, there are two additional zones of randomly

oriented discontinuous seismic amplitudes highlighted by the dashed red lines in Figure 6-42.

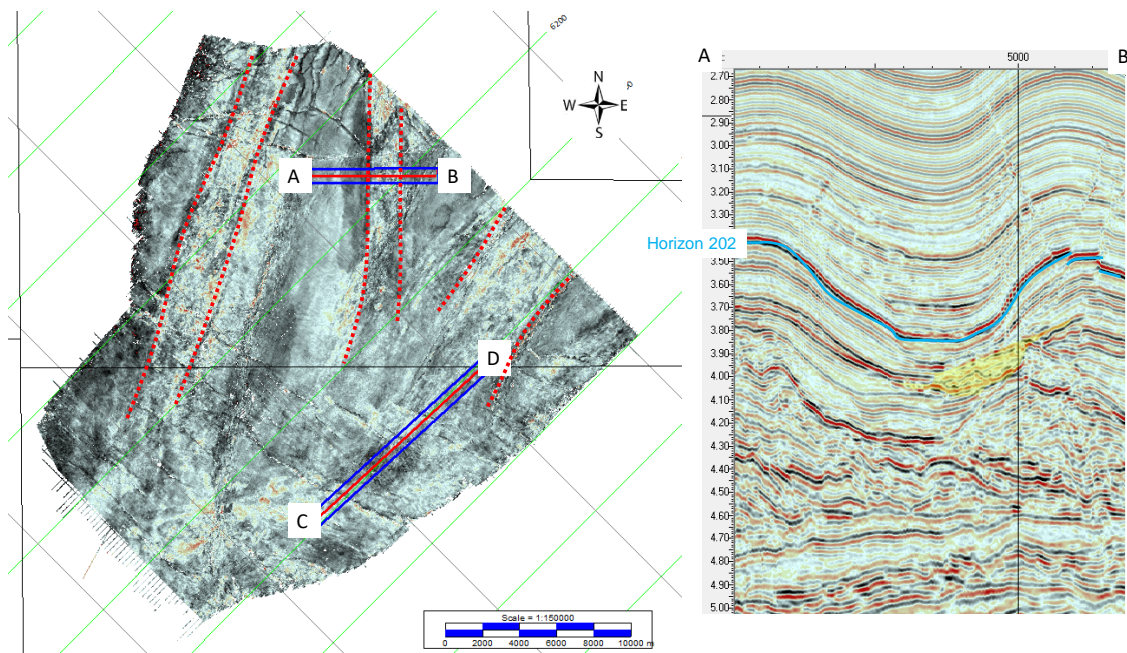


Figure 6-42: RMS amplitude extraction of a window between horizon 202 and 100ms below.

The regions between the dashed red lines are interpreted to be confined debris flows that were restricted in a lateral sense by the pre-existing valleys which they occupy.

The eastern anomaly seen in Figure 6-40 overlies the eastern anomaly seen in Figure 6-42. This anomaly, as illustrated in Figure 6-43, is highlighted in yellow. The source of this flow is also located beyond the margin of the survey to the north. The interval is marked by a series of apparent compressional thrusts, typical of the toe of a mass transport deposit, as noted in the Bull et al. paper (2009).

The central anomaly in Figure 6-42 runs in an orientation that crosses at an oblique angle to one of the recently formed thrust anticlines, whereas the western anomaly shares the same orientation as the adjacent anticline. By following the axis of the two westernmost valley fills to the north, beyond the survey boundary, the junction of the two would occur close to the mouth of the Avon Canyon.

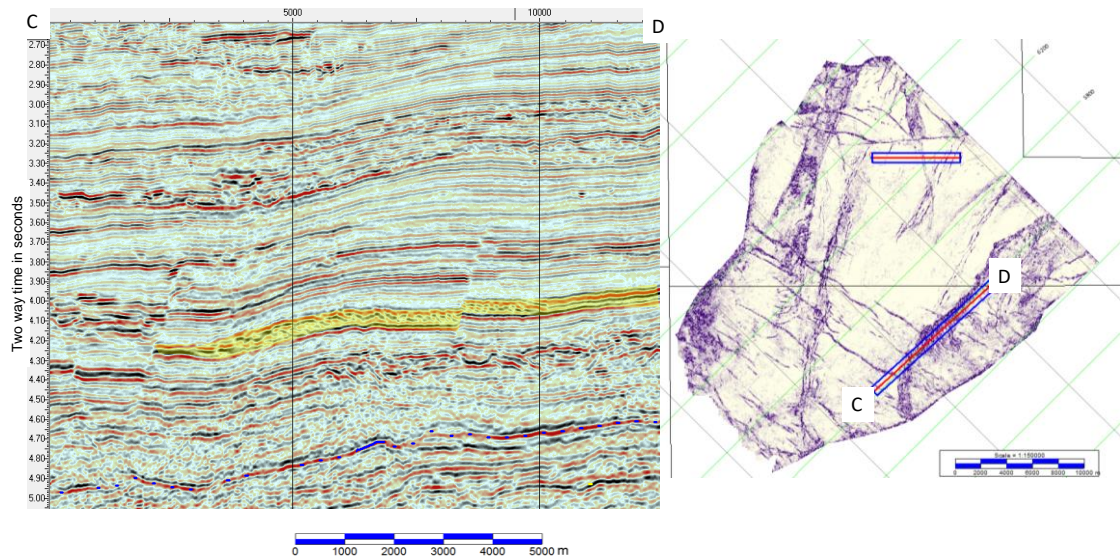


Figure 6-43: Similarity extraction at horizon 200, with the locations of the seismic line labelled C-D.

6.3.4.6 Cretaceous mass transport deposits

6.3.4.6.1 Campanian (horizon 630 to 650)

In addition to the numerous occurrences of mass transport deposits that have been identified in the thin-skinned portion of the region, there is at least one interval below the detachment in which there is evidence of sediment modification which resembles that of a mass transport complex. The deepest mappable such sequence lies in the southern part of the survey area in the Campanian (below horizons 630).

The reflection characteristics are comparable to the compressional toe region associated with mass transport deposits identified elsewhere (Bryn et al., 2005; Kvalstad et al., 2005; Solheim et al., 2005; Frey-Martínez et al., 2006; Bull et al., 2009; Shipp et al., 2011).

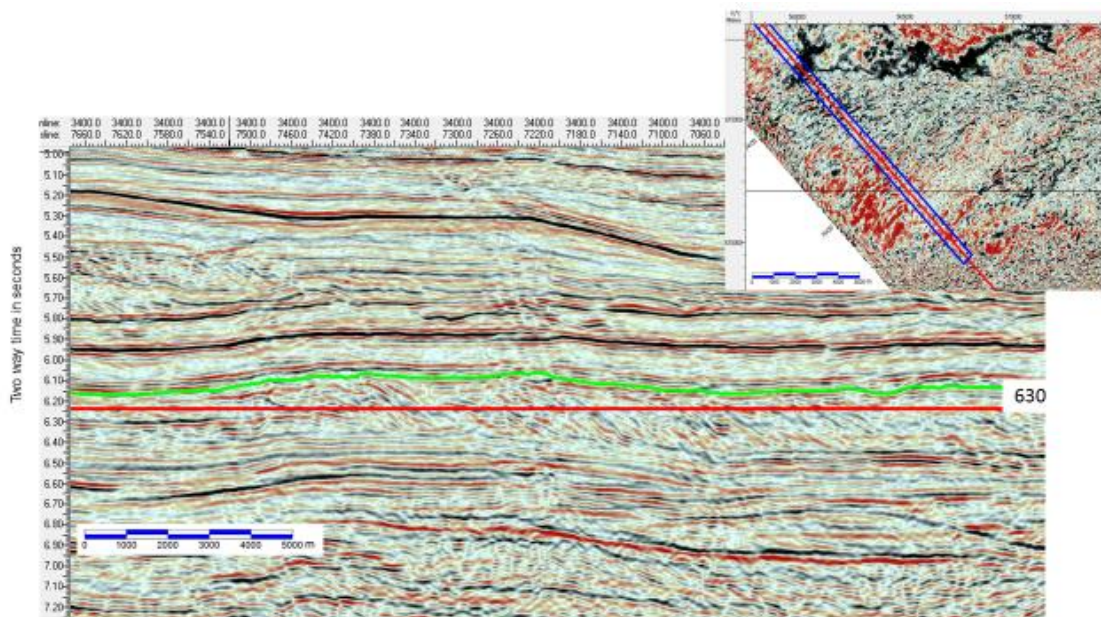


Figure 6-44: A vertical section through the Campanian sequence of high-angle seismic reflections. The inset map is a time slice at 6.24 seconds (the red line in the section) showing the arcuate nature of these dips in an areal sense.

As noted in Figure 6-44 a number of arcuate lineaments are observed. The arcuate nature of the spatial distribution would indicate that may be the toe-end of a major slide. Unfortunately, the 3D data does not extend sufficiently far to the east such that this can be confirmed. The high-angle reflectors below the top Campanian (horizon 630) verge in a north-westerly direction. This would also suggest lateral compression from the south-east, where the assumed proto-Niger (Benue Delta) Delta was building at this time (assumed to be late Cretaceous in age). This fits with the observation made concerning fossil toe thrusts described above. It is possible, however, that this is a large feature and that what is observed is a lateral lobe of a body that may have its origin to the north-west.

The location of the hypothesised Cretaceous Benue Delta (Benkhelil et al., 1998) is now buried beneath the Niger Delta sedimentary pile. It is therefore unknown where the shelf edge would have been at the time that the interval which contains this seismic facies was generated.

6.3.4.6.2 Palaeocene (the detachment mass transport complex)

A widespread interval of disorganised seismic reflectors which is seen to lie at the base of the Cenozoic (between horizons 600 and 510) is interpreted to represent the presence of a large-scale mass transport complex. The base of the interval (horizon 600) is mappable across the entire survey; however, the upper surface (horizon 510) of the chaotic interval – although clearly mappable in the southern half of the survey – cannot be traced across the whole survey area. The evidence for this interval being a mass transport complex is presented in the following paragraphs.

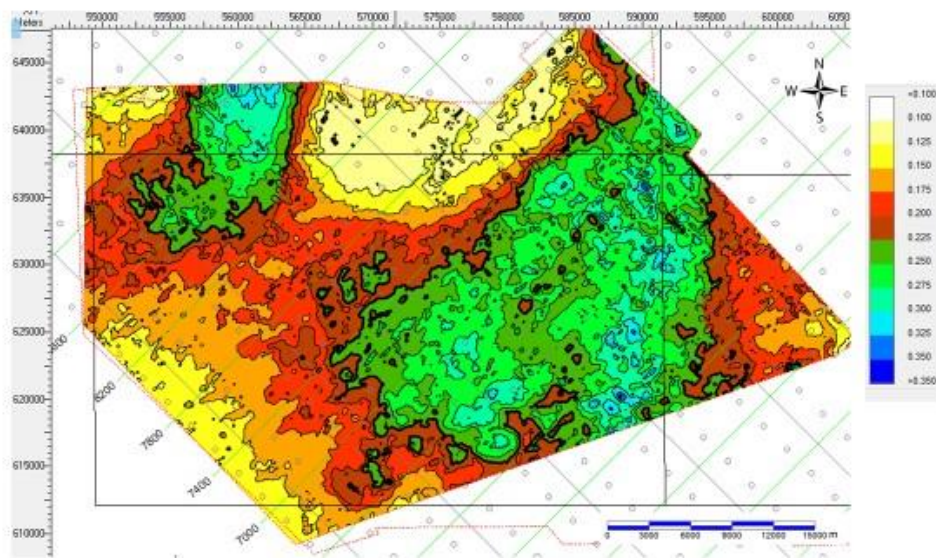


Figure 6-45: Isochrone map of the thickness of the basal Cenozoic mass transport deposit (between horizons 600 and 510); thickness is in two-way time in seconds.

The isochrone of the thickness of the interval indicates the presence of a fan-like geometry spreading from north-east to south-west and an additional north-south trending thick at the western margin of the survey (Figure 6-45). It is interpreted from this figure that the deposits are derived from two source areas; one to the north of the western edge of the survey (MTC west) and the larger of the two (MTC central) to the north of the centre of the survey area. The imaging beneath the highly faulted region to the east of the Avon/Mahin fault zone is poor and it was not possible to map with confidence the upper surface of this mass transport complex.

Attribute analysis of the interval was undertaken and internal reflection fabric recognised. This fabric supports the interpretation of the section being a mass transport deposit (Figure 6-46).

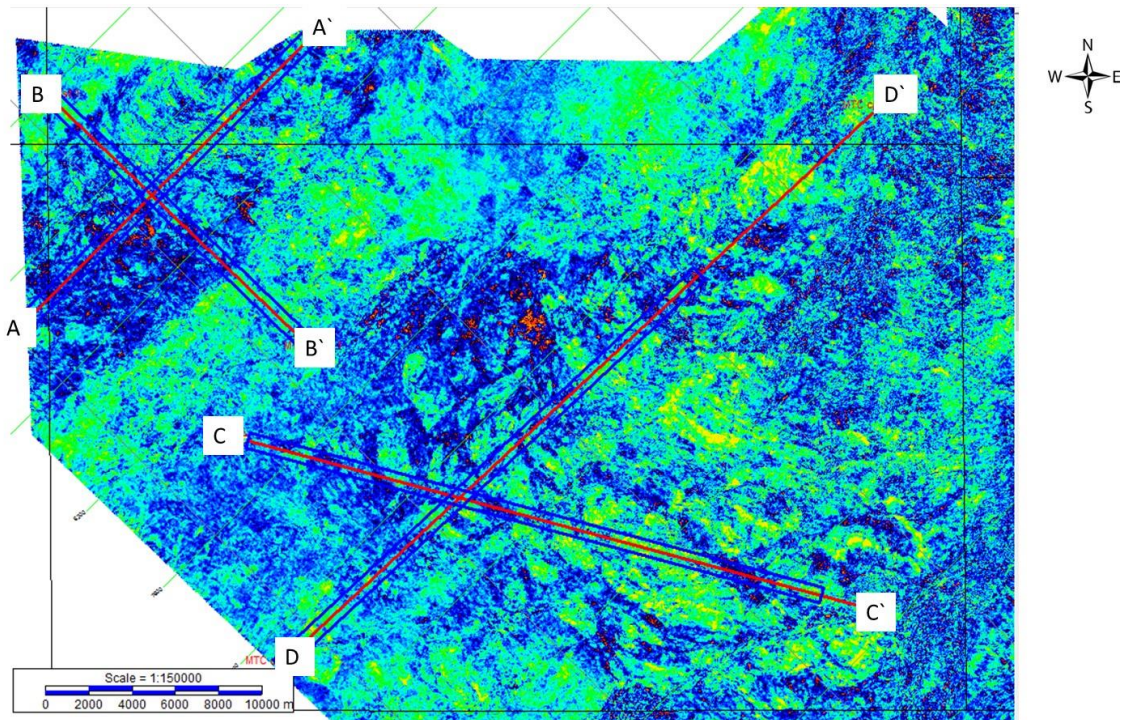


Figure 6-46: RMS extraction of an interval 100ms above horizon 600. The green and yellow zones indicate intervals of higher amplitude; the blue, lower amplitude regions.

6.3.4.6.2.1 The western lobe

The western lobe is interpreted to have approximately parallel linear margins, which run in a north, north-east to south, and south-west direction. The internal character of this western lobe is illustrated in Figure 6-47 and Figure 6-48

Figure 6-47 and Figure 6-48, which are an axial and a transverse section. There are regions within the overall chaotic section of limited coherent reflections that can be interpreted as competent blocks of sediment flowing within a heterolithic flow. The RMS extraction is presented both as an uninterpreted and interpreted image. The patterns within the image indicate several of the same characteristics that are present in the image shown in the paper by Dunlap et al. (2010); in particular, the presence of syn-depositional thrusts, the lateral limit, and the presence of regions with both low- and high-amplitude values that correspond to the region of coherent blocks. The western lobe covers an area of over 250 sq.km within the boundary of the survey, but is undoubtedly larger than this in totality because it clearly extends beyond the extent of the 3D data.

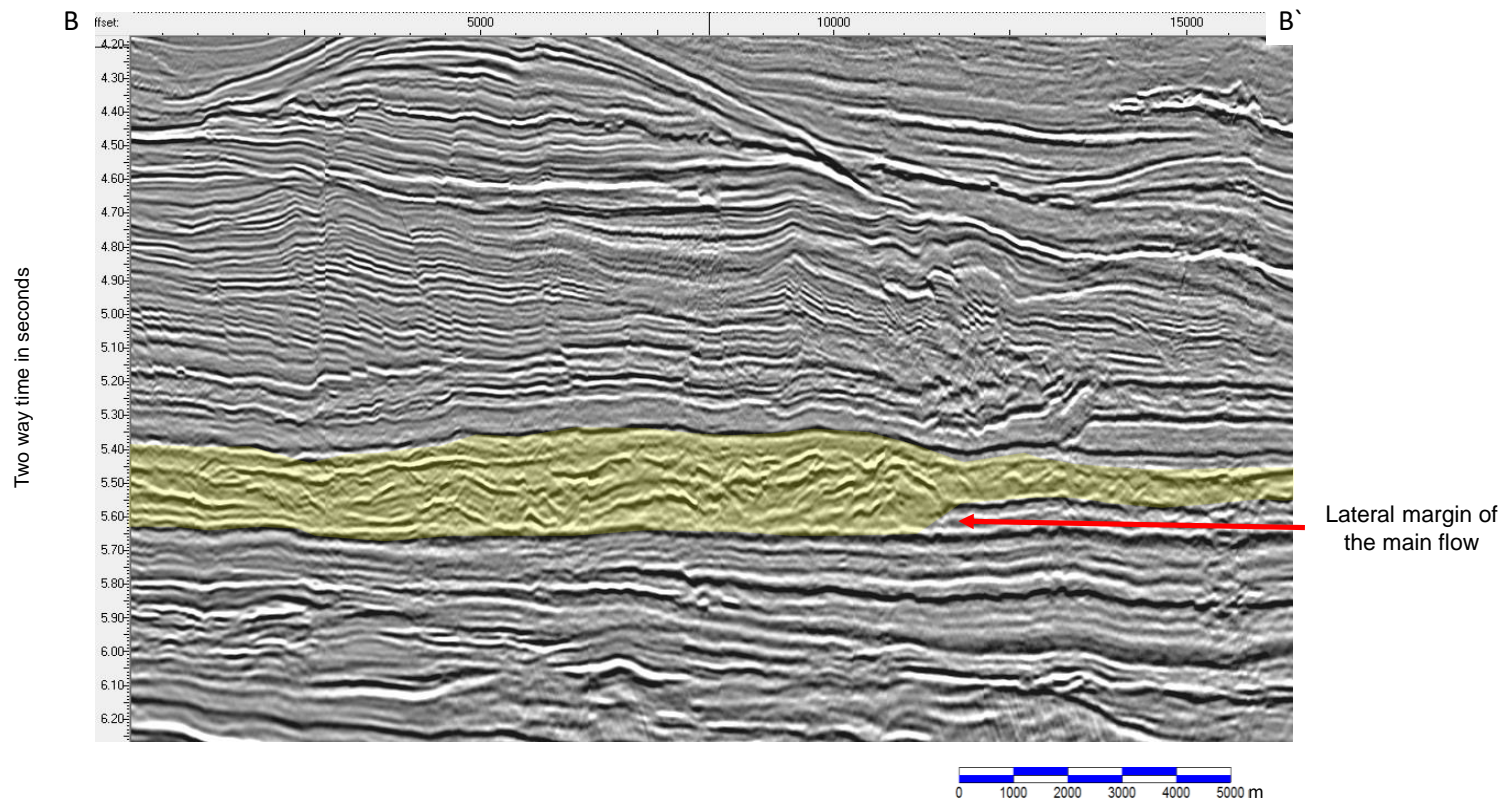


Figure 6-47: Seismic profile B-B', (see Figure 6-46); a north-west to south-east traverse through the western mass transport complex (highlighted in yellow).

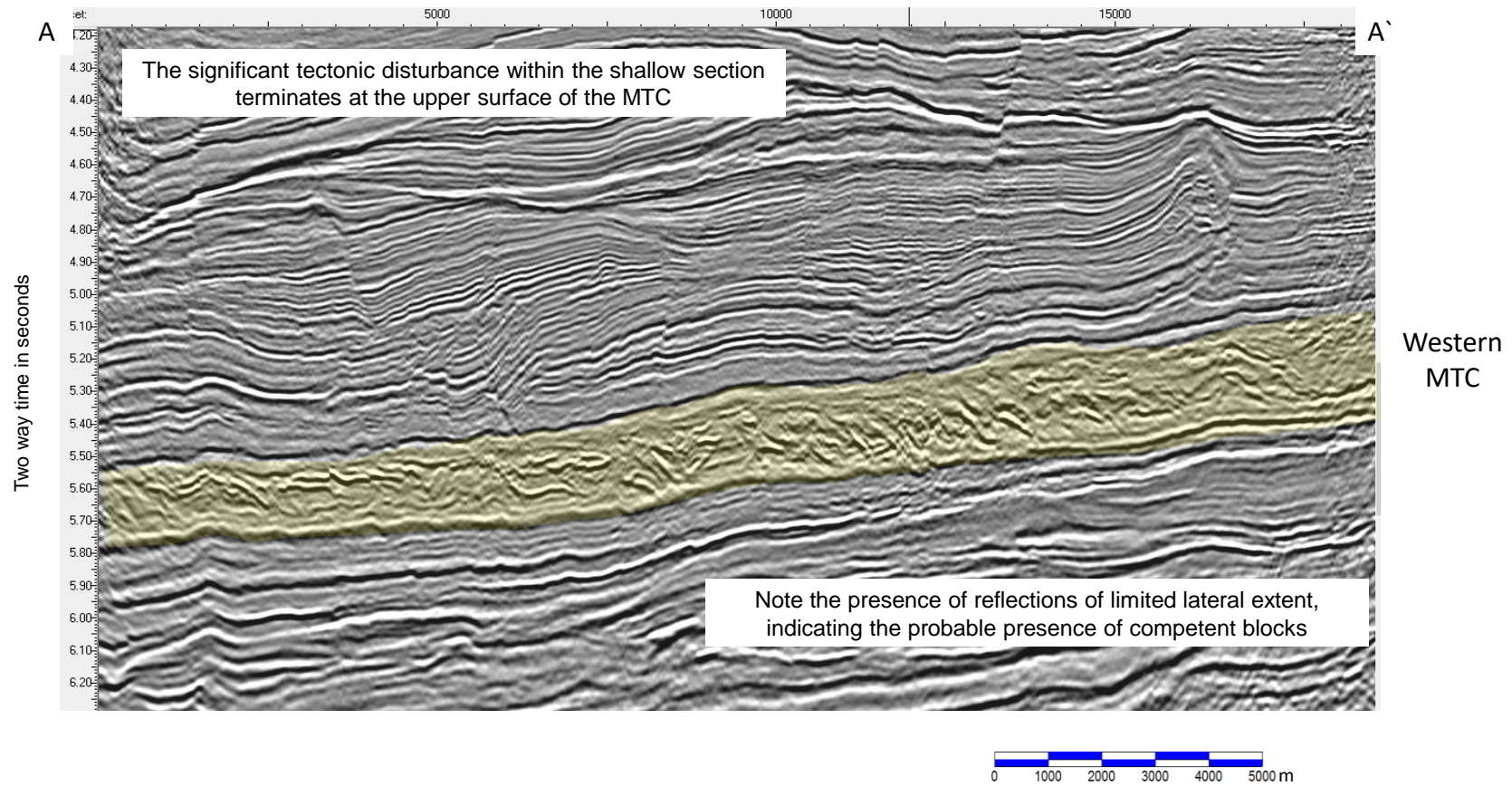


Figure 6-48: Seismic profile A-A` (see Figure 6-46) traversing the western mass transport deposit in a north-east to south-west orientation.

The western lobe is interpreted to be comprised of two distinct stacked deposits, with the sediments being derived from a source to the north of the survey. This north-western source area is also interpreted to be the provenance for the younger mass transport complex recognised in the interval between horizons 490 and 470.

6.3.4.6.2.2 The central lobe

The central lobe measures in excess of 1,000 sq. km. within the limits of the 3D volume. The thickness of both lobes ranges up to an excess of 300 milliseconds in two-way time (over 400m, if the assumed interval velocity is in the region of $3,000\text{ms}^{-1}$); this would imply a total volume within the two lobes in the region of 500 cubic kilometres of material contained within the region covered by the survey alone. For comparison, the Storrega slide is estimated to be comprised of somewhere between 2,500 and 3,500 cubic kilometres (Bryn et al., 2005). Other large-scale mass transport deposits are known to be present on the north-western margin of Africa with a similar age affinities (Moscardelli and Wood, 2016).

As noted above, the reflector that marks the upper surface becomes less clear towards the north; this is interpreted to be due to the input of younger flows, whose basal surface may have eroded the pre-existing upper surface of the existing body of sediments. Overall, the complexity of the section in the north-western portion of the data set makes it difficult to map with certainty the up-dip portion of the central mass transport deposit. In Figure 6-51, the top of the mass transport apron that has been mapped is the yellow horizon.

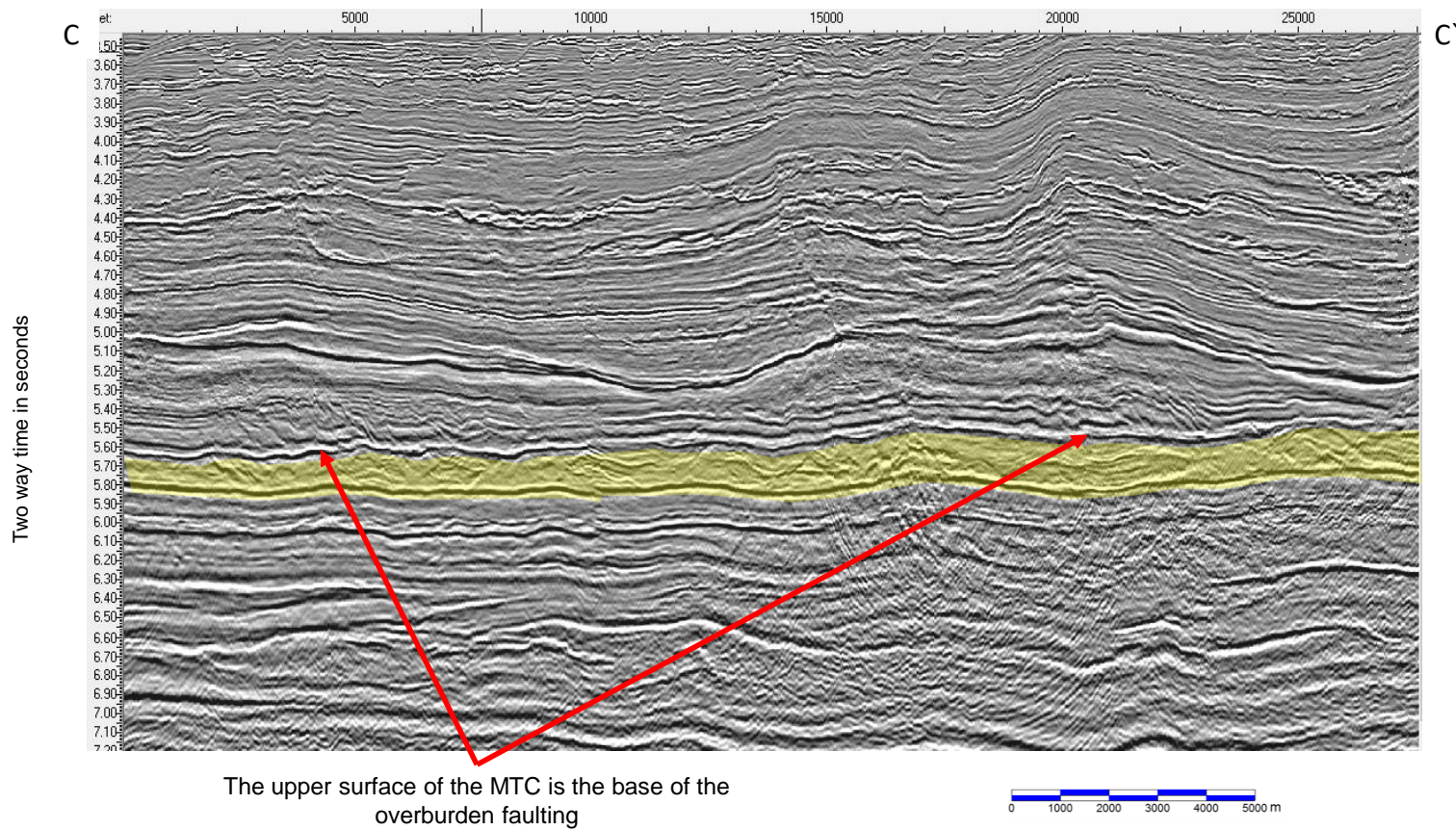


Figure 6-49: North-west to south-east traverse (see Figure 6-46 for location) of the main mass transport deposit.

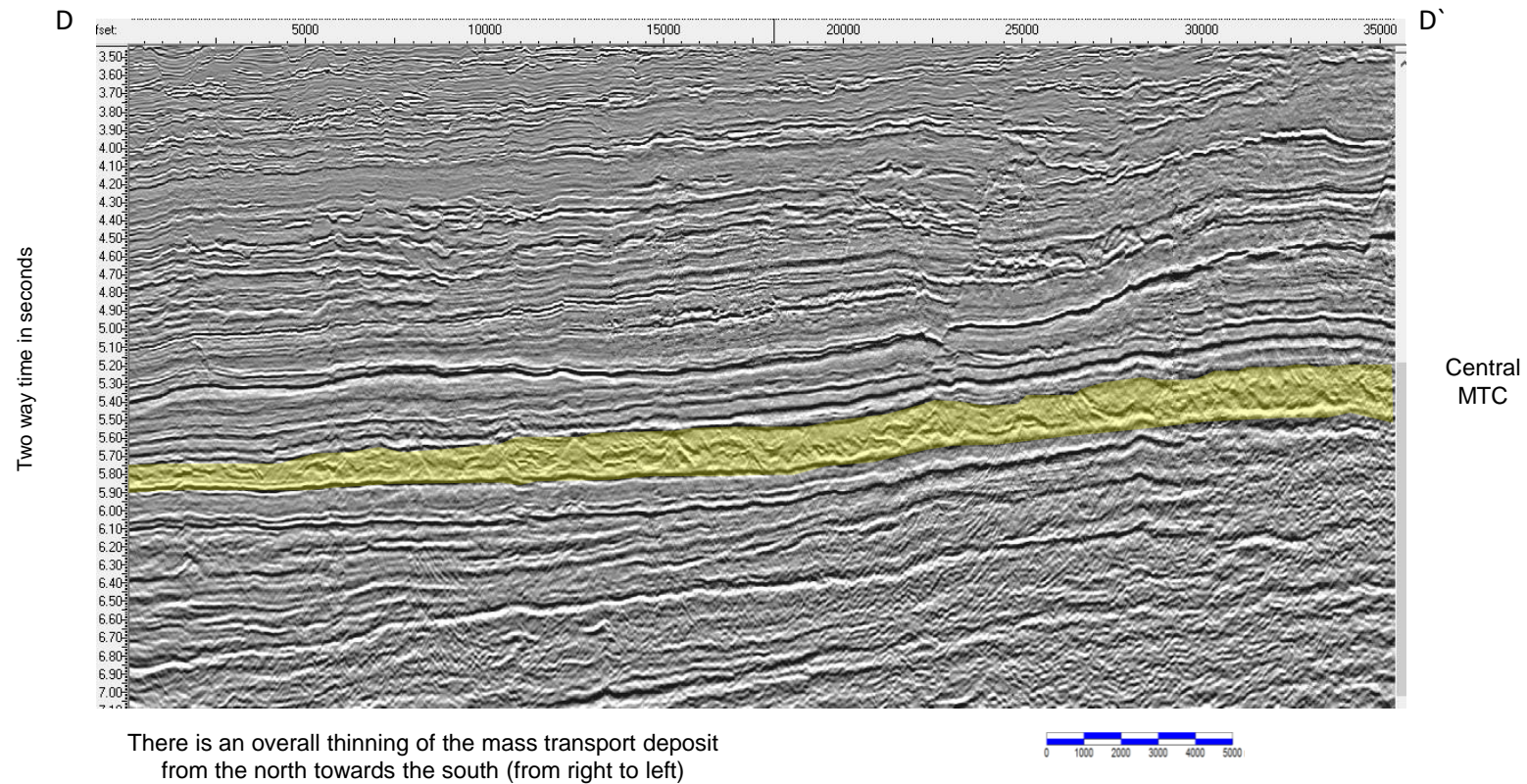


Figure 6-50: North-east to south-west seismic traverse (see Figure 6-46 for location) showing the chaotic reflection character of the mass transport deposit.

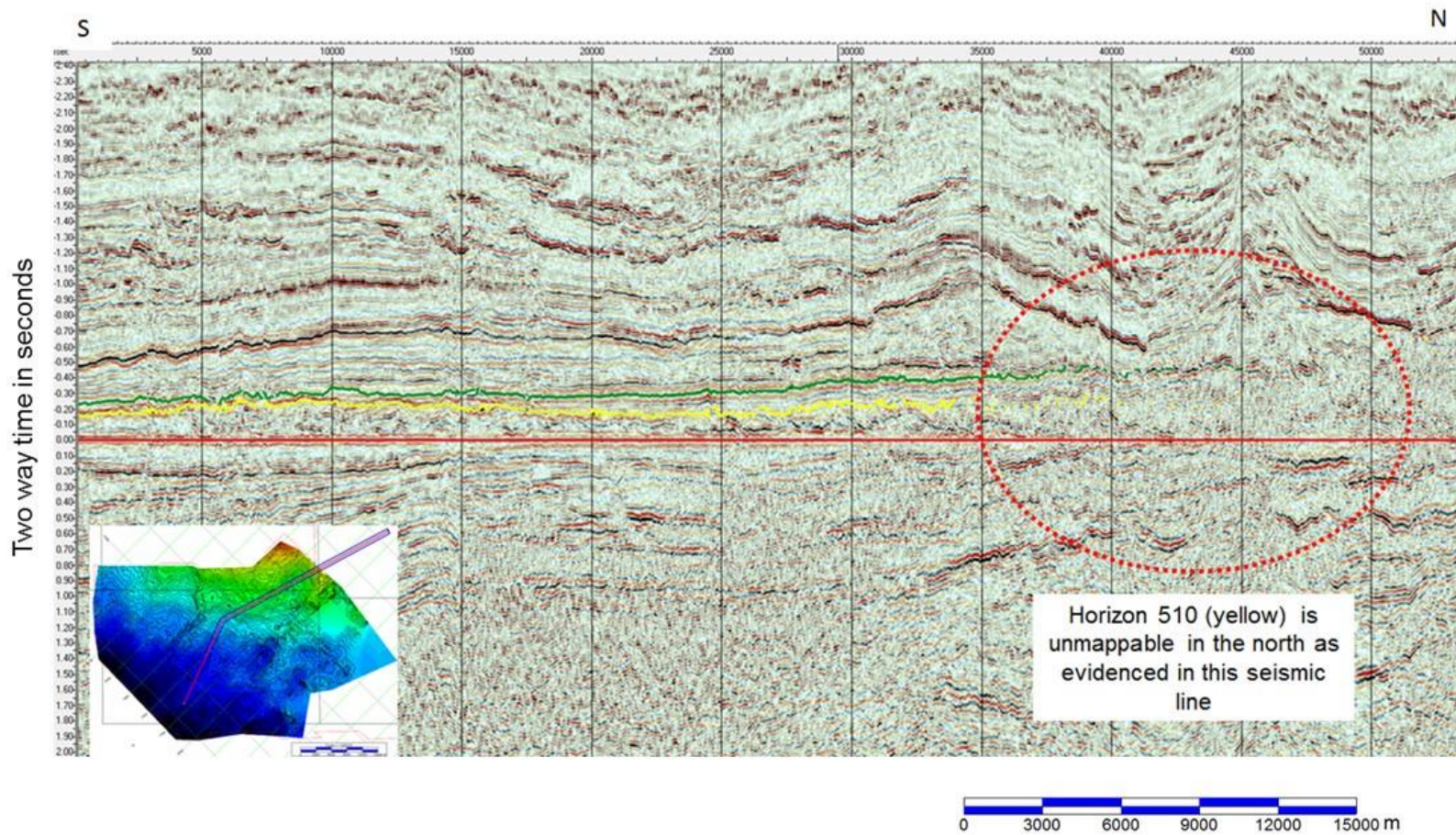


Figure 6-51: Random line through the mass transport deposit, flattened at the base of the interval (horizon 600).

The larger central mass transport (MTC Central) deposit has a very clear seismic reflection that corresponds to its upper surface (horizon 510). This event can be mapped with confidence in the southern half of the western half of the survey – the region of primarily compressional tectonic deformation. To the east of the Avon/Mahin fault zone, this event is difficult to trace because it is affected by the poor imaging associated with the high degree of faulting in the overlying section.

An additional, shallower mass transport complex was recognised in the western region, lying between horizons 490 and 470 (Figure 6-52); this interval is interpreted to have had its sediments supplied from the same northern area as the western lobe.

The upper surface of both lobes as well as the upper surface of the shallower interval (horizon 470) coincide with the vertical discontinuity that marks the separation of the tectonically modified overburden from the underlying interval. It is this observation that leads to the assumption that the mass transport complexes play a significant role in the establishment of the detachment layer.

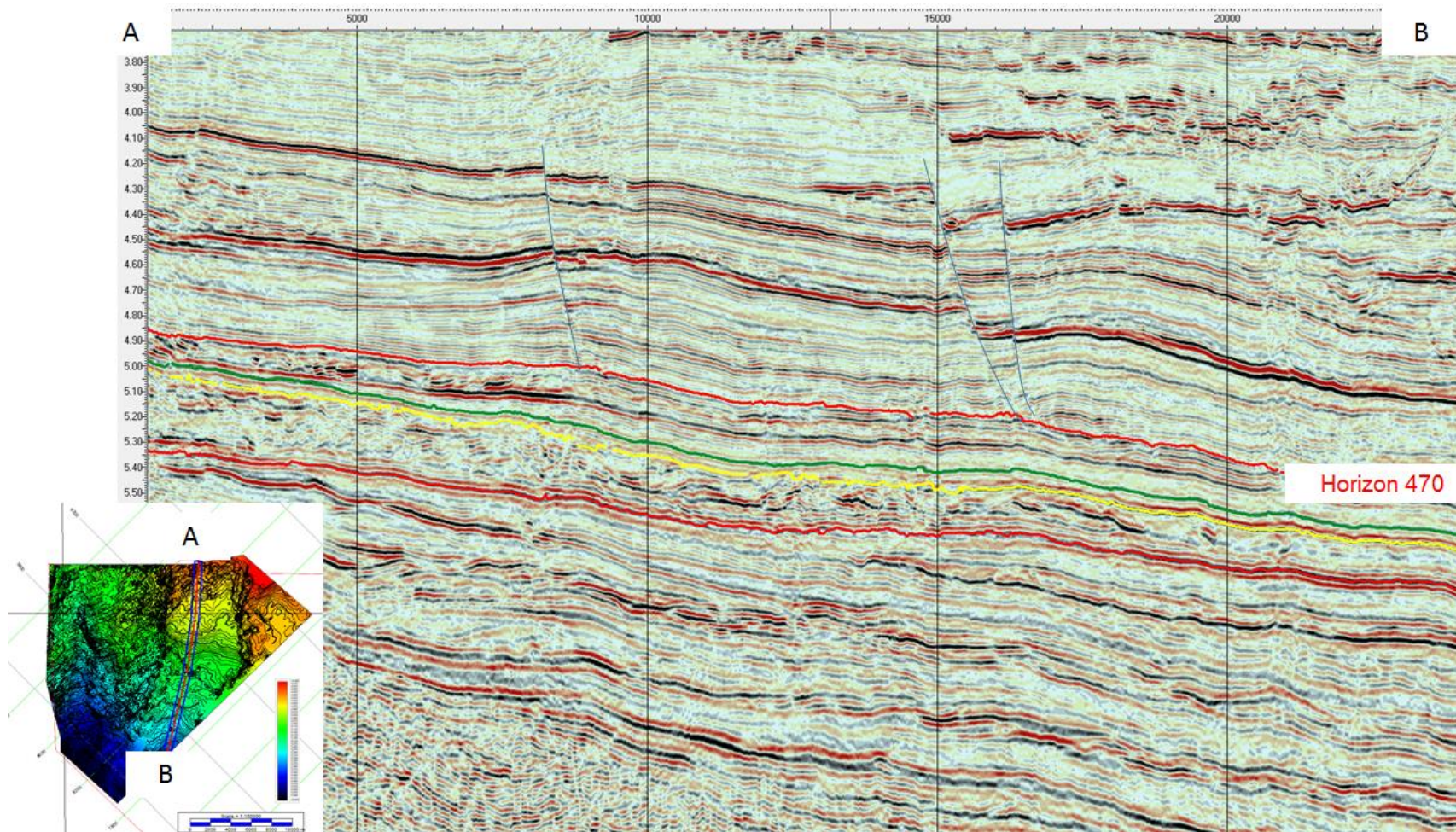


Figure 6-52: Illustration of the tip-out of faults at the surface of a mass transport deposit below horizon 470.

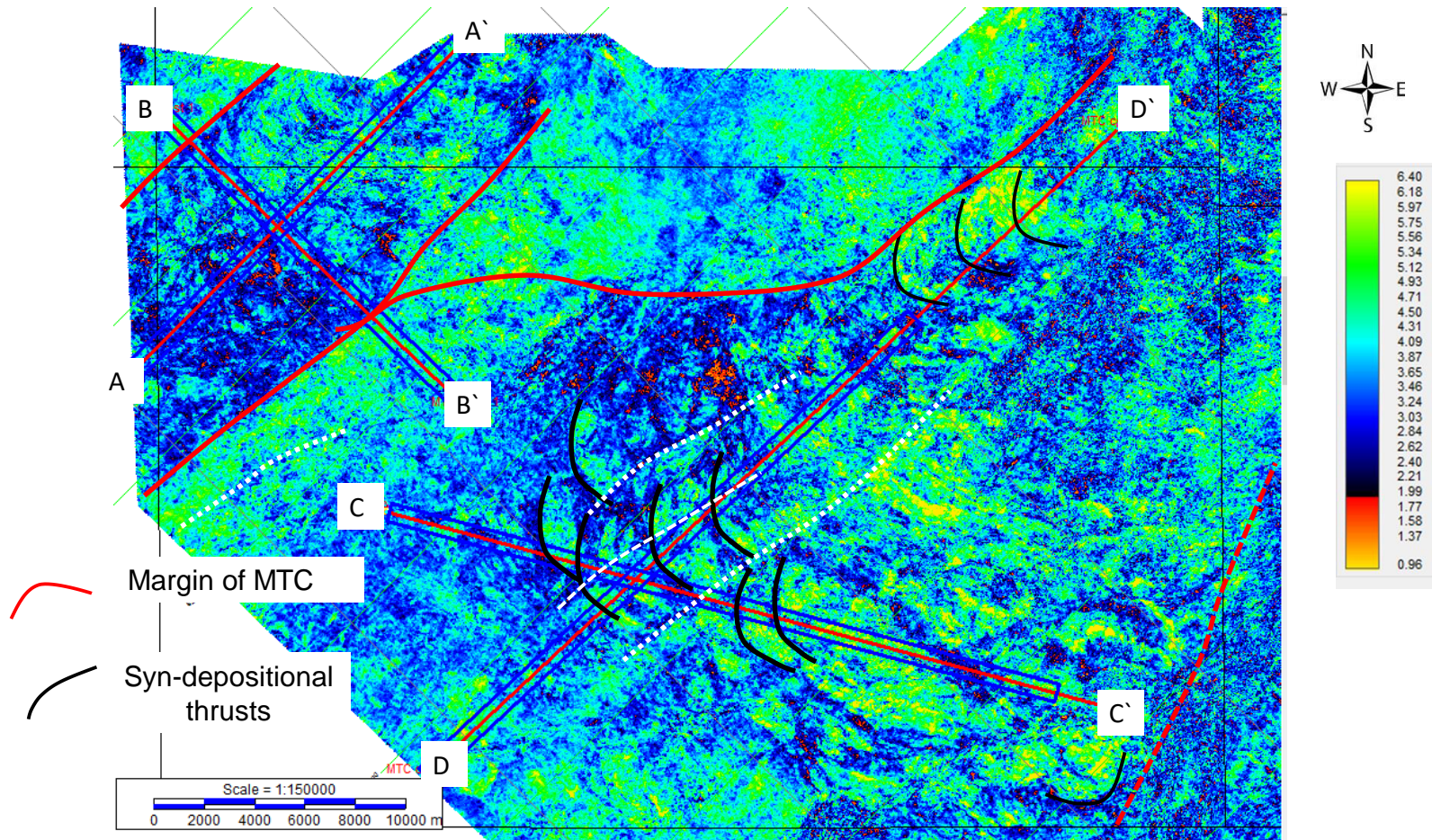


Figure 6-53: The RMS amplitude attribute of an interval within the mass transport interval, highlighting the presence of arcuate and linear anomalies. The imaging of the interval has been investigated by means of amplitude and coherence attributes derived from the seismic data.

Although there is little coherent energy, there is evidence of a number of arcuate lineaments, which are interpreted as pressure ridges associated with individual flows (Figure 6-53); there are a number of blocks within the body of the mass transport interval with kilometre-scale dimensions in the region of the survey area. The sediments within the mass transport deposits are interpreted to have been derived from a shelfal area to the north, which was subject to episodic margin collapse. This diachronous activity implies that the mass transport complexes are composite bodies resulting from many inflows from the north. The retreat of the shelf due to the mass wastage and the likely diminution of material that could be shed from the shelf could explain the observation that the southern limits of the mass transport deposits moves northwards as the sediments become younger.

There are several regions within the overall complex where coherent reflection data can be identified. These are interpreted to represent competent lithified strata that have maintained their competent nature, while being caught in the flow downslope. Similar characteristics are noted in outcrop sections of mass transport deposits; as illustrated in Figure 6-54, the two areas highlighted by the yellow dashed lines are competent strata that have been caught up in a mass transport deposit. The outcrop is found in the Cerro Toro formation of the Magallanes basin in southern Chile (Shultz et al., 2005).

This image is of the upper 15m of a mass transport complex measured to be in excess of 60m in vertical extent. The upper surface of this mass transport complex is seen to be undulating, with the post depositional topography infilled by channel sands.

The upper surface of the mass transport deposit is a morphologically undulating surface (Figure 6-56), as is recognised in the photo from Chile (Figure 6-54). In this field example, the topography of the upper surface, which was created by the mass transport motion, is infilled with a down-cutting, sand-filled channel. In the absence of a coarse-grained depositional event following the settling of the mass transport deposit, a hemipelagic rain of sediments can drape over the surface of the complex. It is interpreted that this is the case in this region of the Niger/Benin Basin.

It is clear from Figure 6-56 that the overlying structural deformation does not conform to the upper surface of the mass transport complex. The structural dislocation leads to the interpretation that the upper surface is a key component in the basal detachment process.

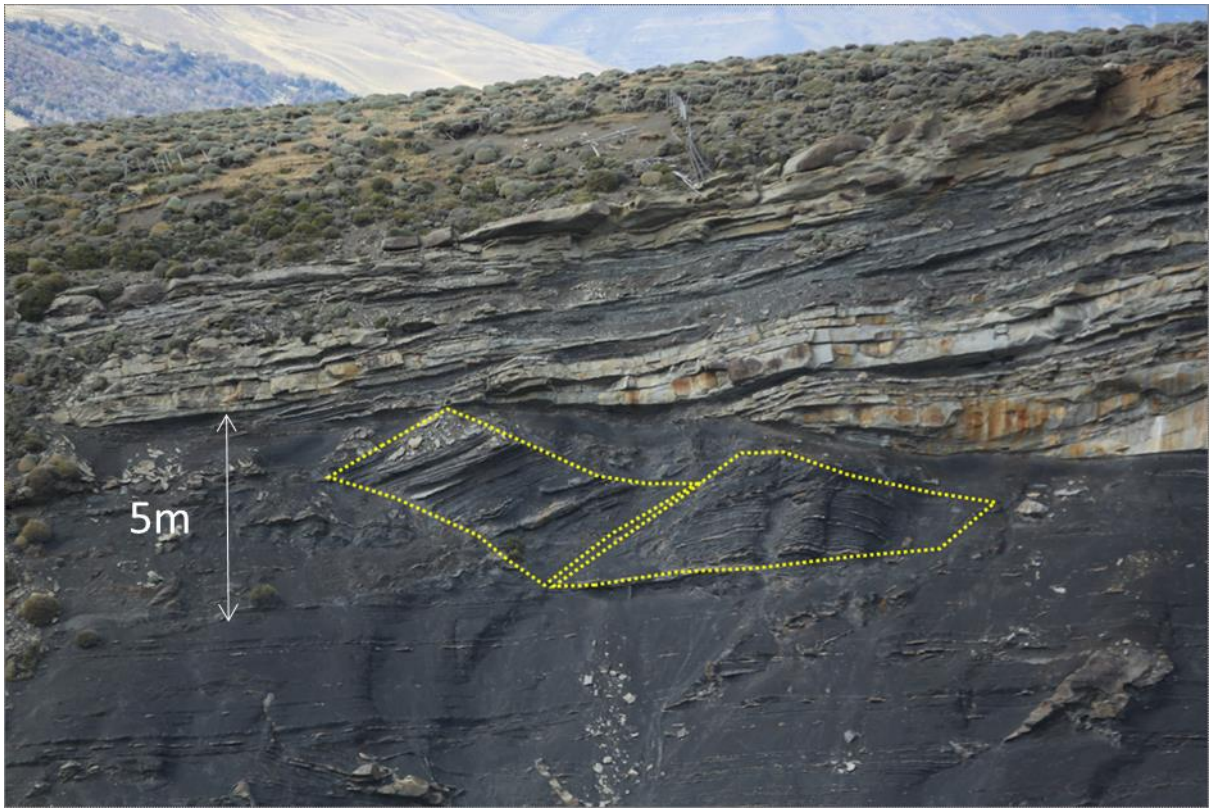


Figure 6-54: Outcrop of mass transport complex, showing isolated competent strata within a mass transport deposit. This outcrop is within the Tres Pasos formation and is located along the Zamora River in southern Chile.

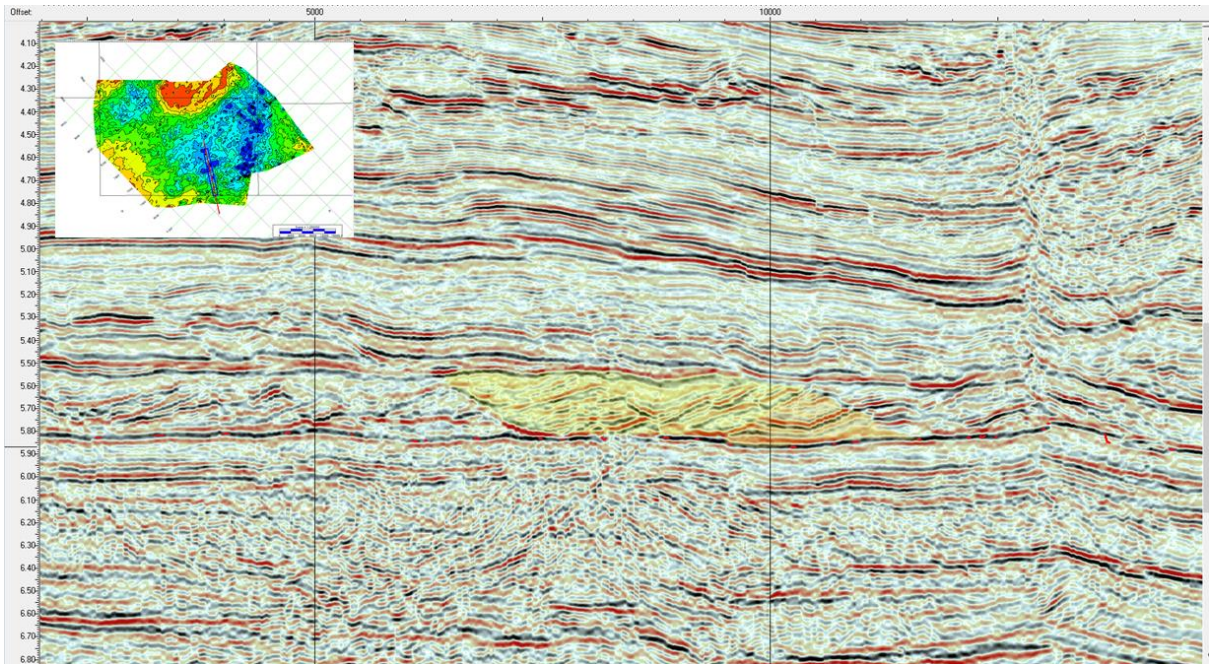


Figure 6-55: Seismic line illustrating the presence of competent blocks within the mass transport deposit.

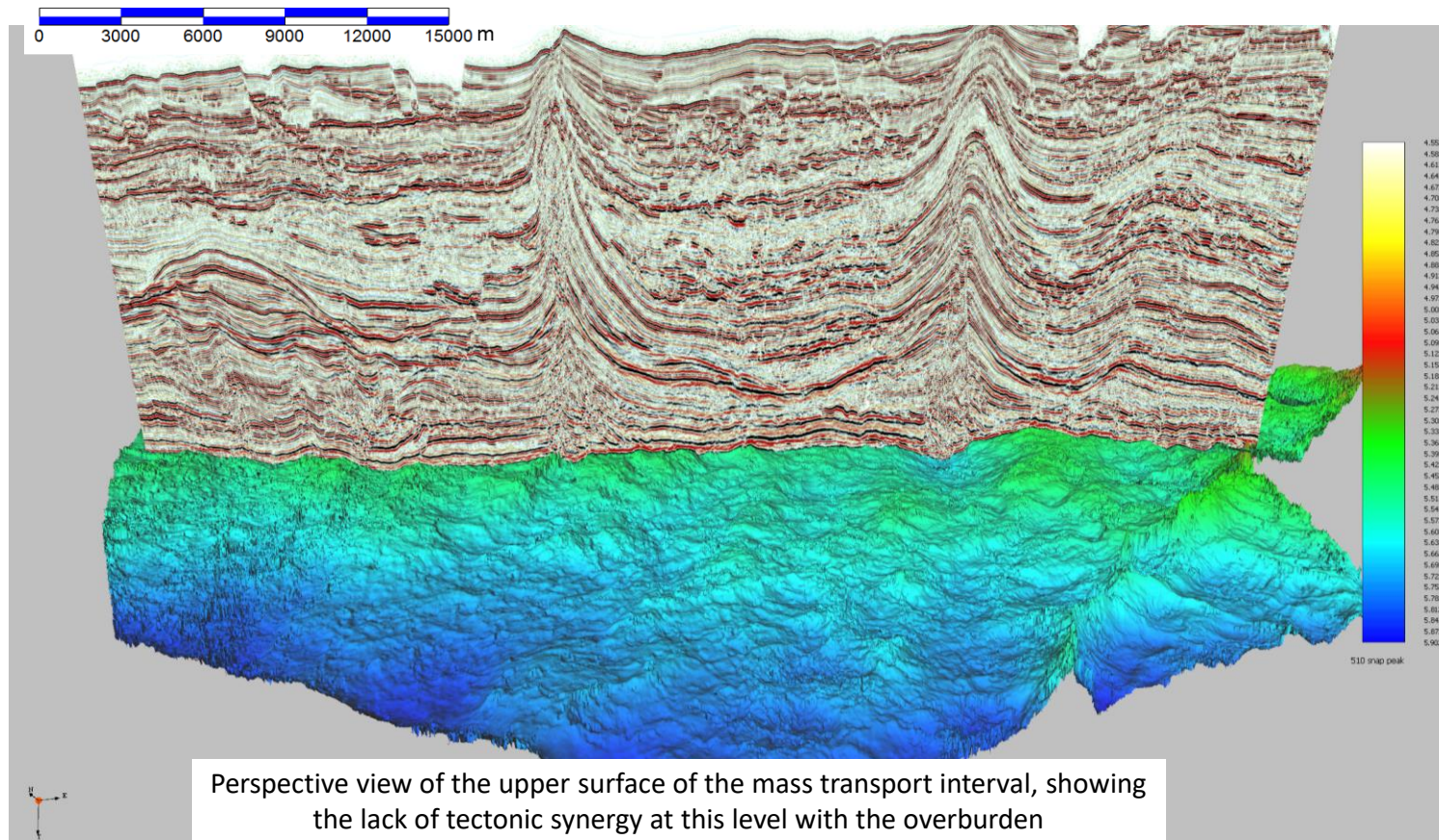


Figure 6-56: A perspective view of the surface of the mass transport deposit, displayed along with a vertical section that shows the presence of the deformed overburden. The white dashed line is the trace of the Mahin fault.

In Figure 6-56, the surface of the MTC exhibits an undulating topography, whereas the overlying section displays a number of high-relief structural features that do not affect the top of the mass transport complex.

Thin-skinned deformation relies upon a weak basal layer with low shear strength (Twiss and Moores, 2007). Within a volume of rock, the dislocation between the shallow and deep layers requires a detachment (or decollement) surface that has low shear strength to be present (Chapple, 1978; Stewart, 1999; McClay et al., 2003). Examples of such surfaces include evaporites, coals, and overpressured shales/mudstones (Poblet and McClay, 1996; Rowan et al., 2004; Tuitt et al., 2012). In this study area, there is no evidence for either evaporites or coal within the section. It is, therefore, assumed that the detachment layer is linked to the presence of an overpressured interval that lies at the surface of the mass transport deposit (King and Cartwright, 2010).

6.3.5 Confined debris flows

The mass transport deposits described above are interpreted to have spread out over a largely planar basal surface, which could have provided an unconfined area into which the material can be deposited.

In addition to these unconfined flows, there are at least three well-defined elongate synclines that run in a north-south direction within the survey area, within which chaotic seismic reflection geometries are seen. In the western half of the survey area, two such synclines are visible; the westernmost u-shaped valley has a chaotic interval at the base of the section and the overlying infill is comprised of parallel reflections. The nature of the infill is illustrated by means of an RMS amplitude extraction of a window of 100ms below horizon 310.

The central valley has a smooth base; the upper portion of the infill is, however, a chaotic interval. The chaotic interval is restricted by the sides of the syncline and can be seen from the RMS amplitude attribute maps to be limited in the lateral extent.

A similar suite of laterally confined debris flows are present in the northern region of the survey. The best example is that mapped at horizon 200; however, as outlined in section 6.3.4, these deposits exhibit compressional toe regions. In the two cases noted in this section, there is no evidence of a compressional toe region.

The ridge and syncline morphology that is mapped at horizon 420 was infilled by a combination of debris flows and low-energy hemipelagic sediments.

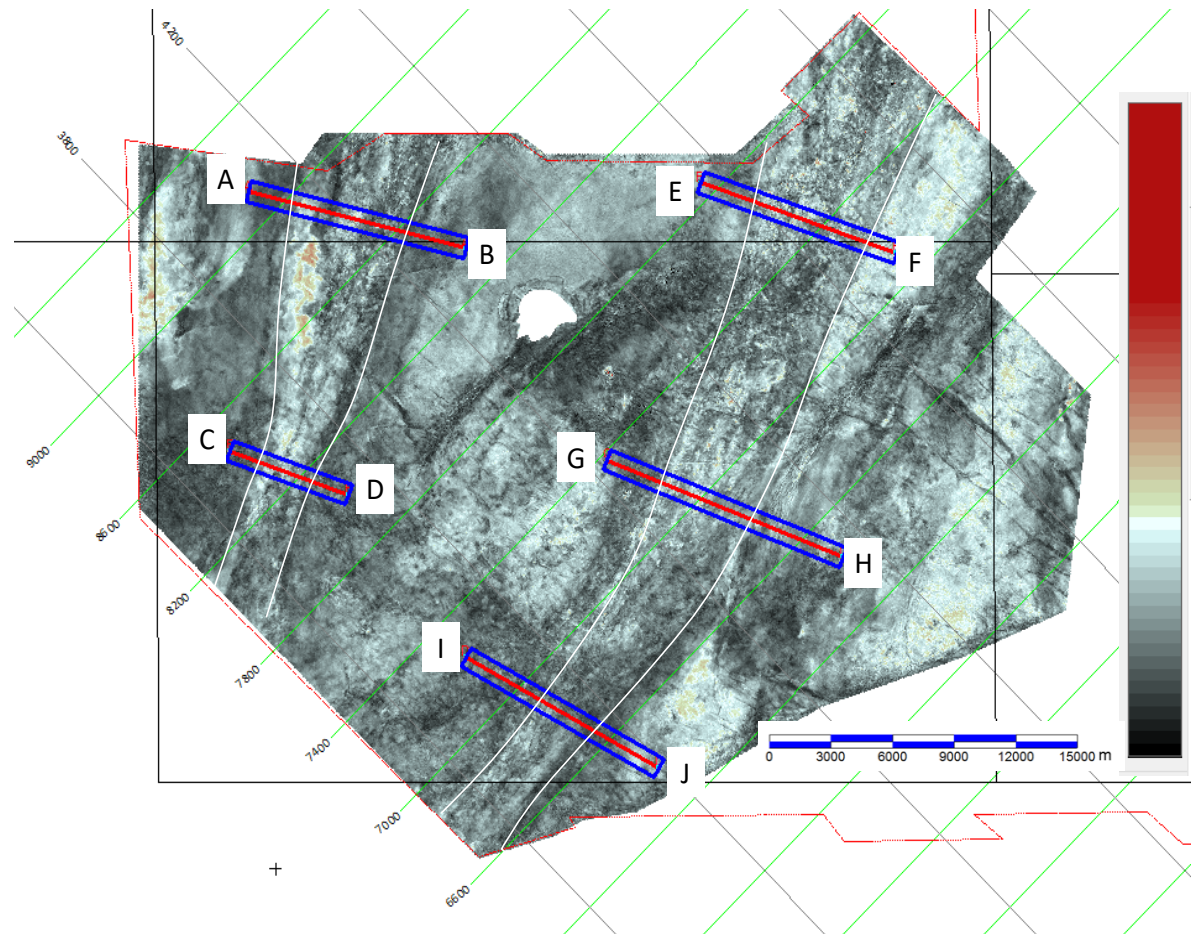


Figure 6-57: RMS amplitude attribute for an interval within the Upper Oligocene. Note the absence of any channel-like geometries. The sections highlighted in the map are shown in Figure 6-58 and Figure 6-59.

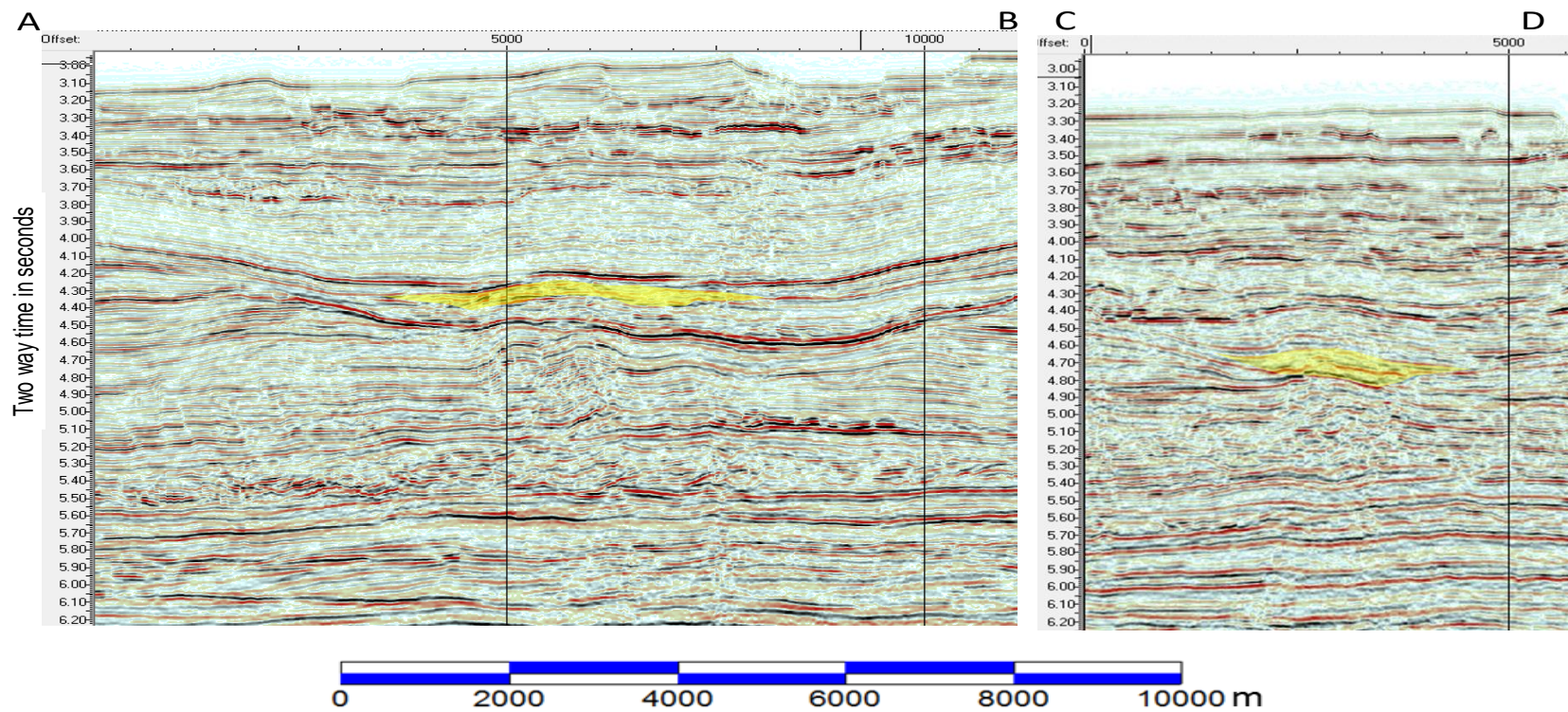


Figure 6-58: Seismic cross-sections across the syncline between Ridges A and B.

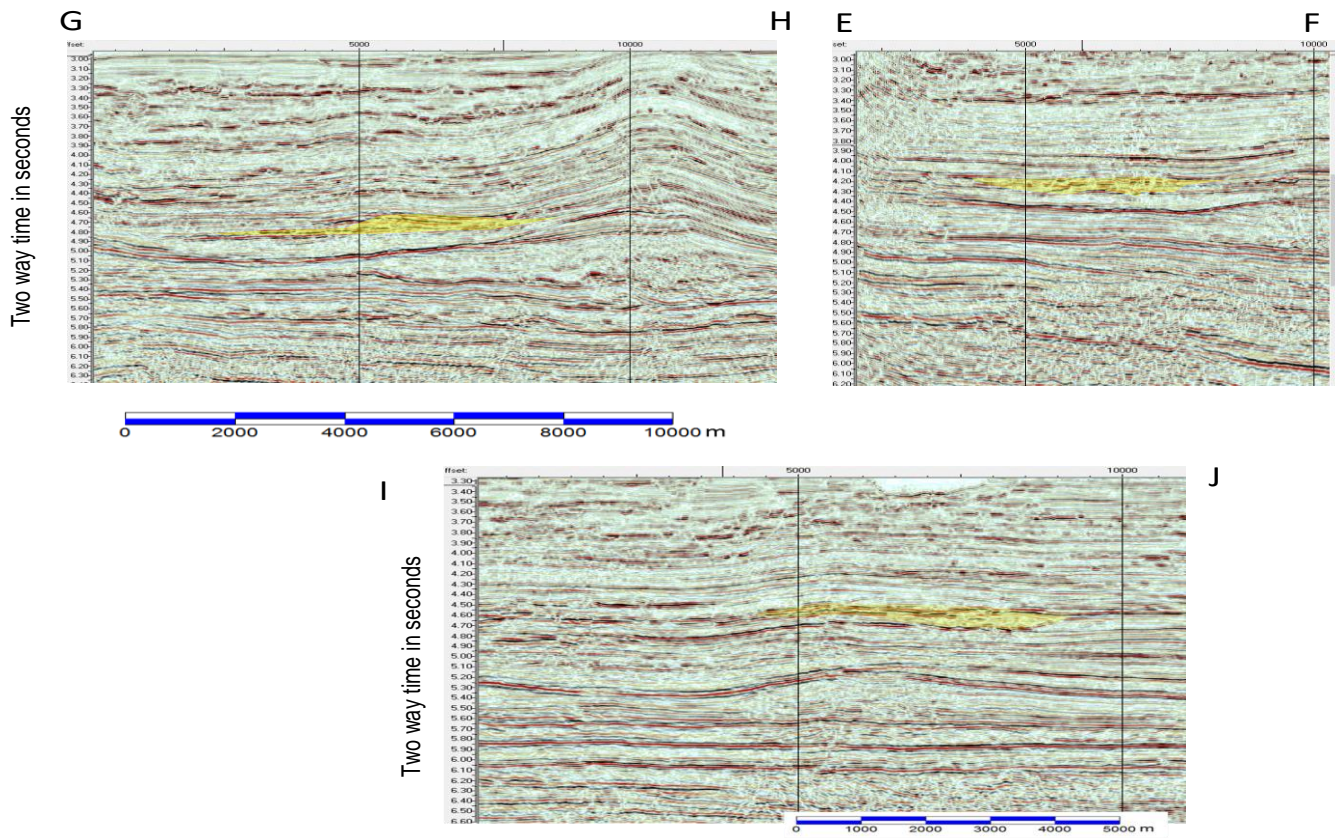


Figure 6-59: Seismic cross-sections across the syncline to the east of Ridge B.

6.3.6 Sediment remobilisation

Unconsolidated sediments are prone to remobilisation under anisotropic stress conditions. Examples of the kind of deformation that can arise as a result of this sedimentary activity have been documented, notably in relation to the remobilised sands in an number of North Sea fields (Hurst et al., 2007). The extrusion of sands and shales at the seabed as a result of the remobilisation of unconsolidated sediments gives rise to so-called extrudites and injectites. These can be seen in outcrops within deep-water sediments and have been documented as possible breaches of seal for hydrocarbon accumulations (Cartwright et al., 2007). The presence of remobilised sediments allows the passage of fluids through strata that might otherwise be considered as permeability barriers. The presence of remobilised sediments within mass transport deposits has been described by Strachan (2002), which raises the possibility that mass transport complexes could allow the flow of fluids through an apparently low-permeability interval.



Figure 6-60: Outcrop view of mobilised, intruding clastics within a deep-water shale matrix.

In the figure above (Figure 6-60), from the Tres Pasos formation in the Magallanes Basin in Southern Chile, the light-coloured, dipping, sediments are remobilised sands within a deep-marine, shale-prone setting (the dark background interval) in which there are known to be extensive mass transport deposits.

At the time of deposition, the mass transport complexes described above are likely to have been unconsolidated and the internal stresses within the chaotically assembled body would have been anisotropic. Under these circumstances, the presence of remobilised sediment would not be unexpected. A case in point that has been observed within this data set is interpreted to be a manifestation of the phenomenon.

The features illustrated in Figures 6-56 to 6-57 are used to show the presence of surface-related mounds that are interpreted to be created as a result of the remobilisation of sediments. These features line up parallel to and in the footwall of one of the major faulted anticlines in the northern region of the survey. Their presence is hard to explain other than by local deformation.

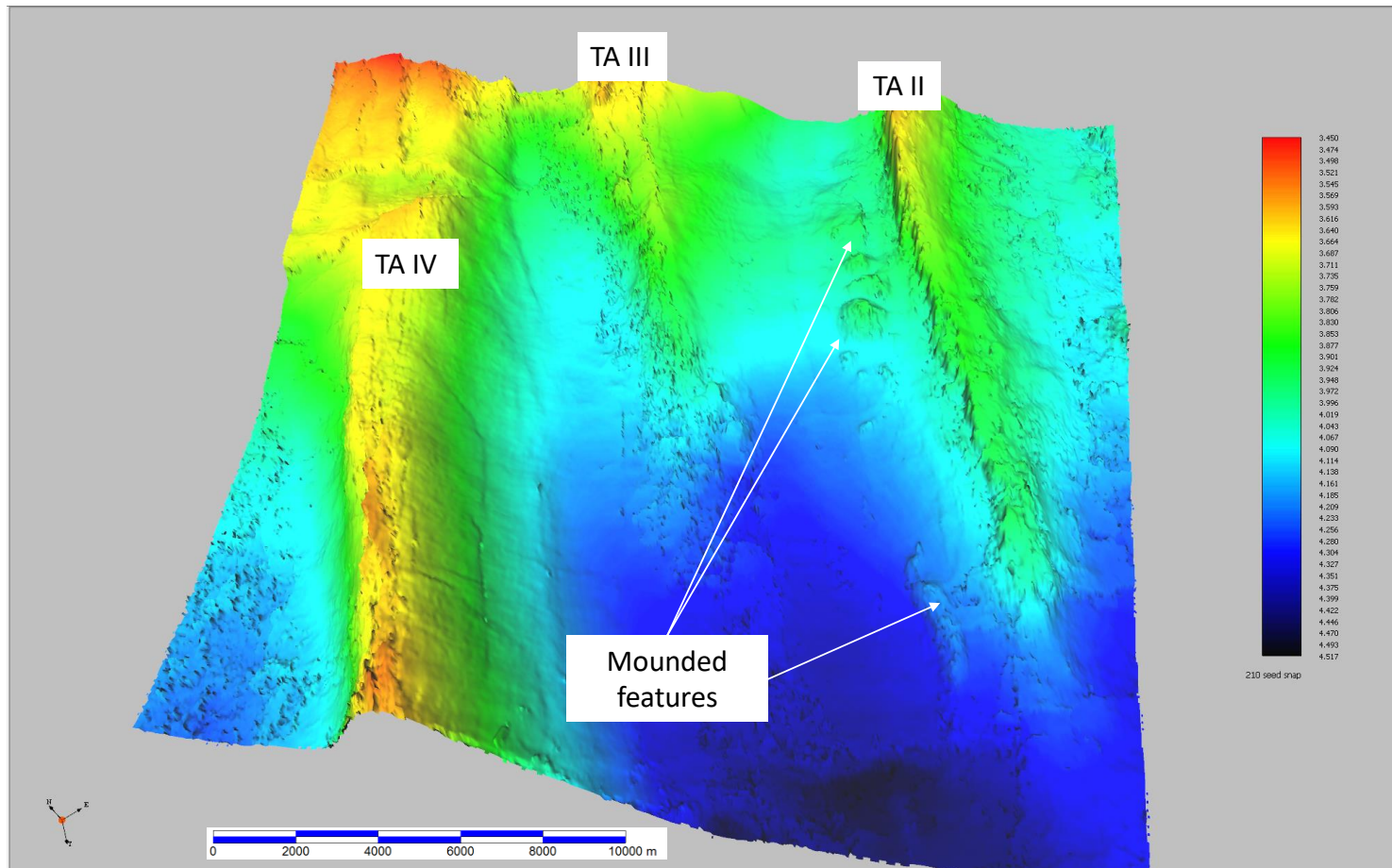


Figure 6-61: Illustration of mounded features that are interpreted to represent extruded bodies of remobilised sediment; the figure is a perspective view of an horizon (see Figure 6-63) in the northern region of the survey; the faulted anticlines TA II, II, and IV are outlined in more detail in chapter 7.

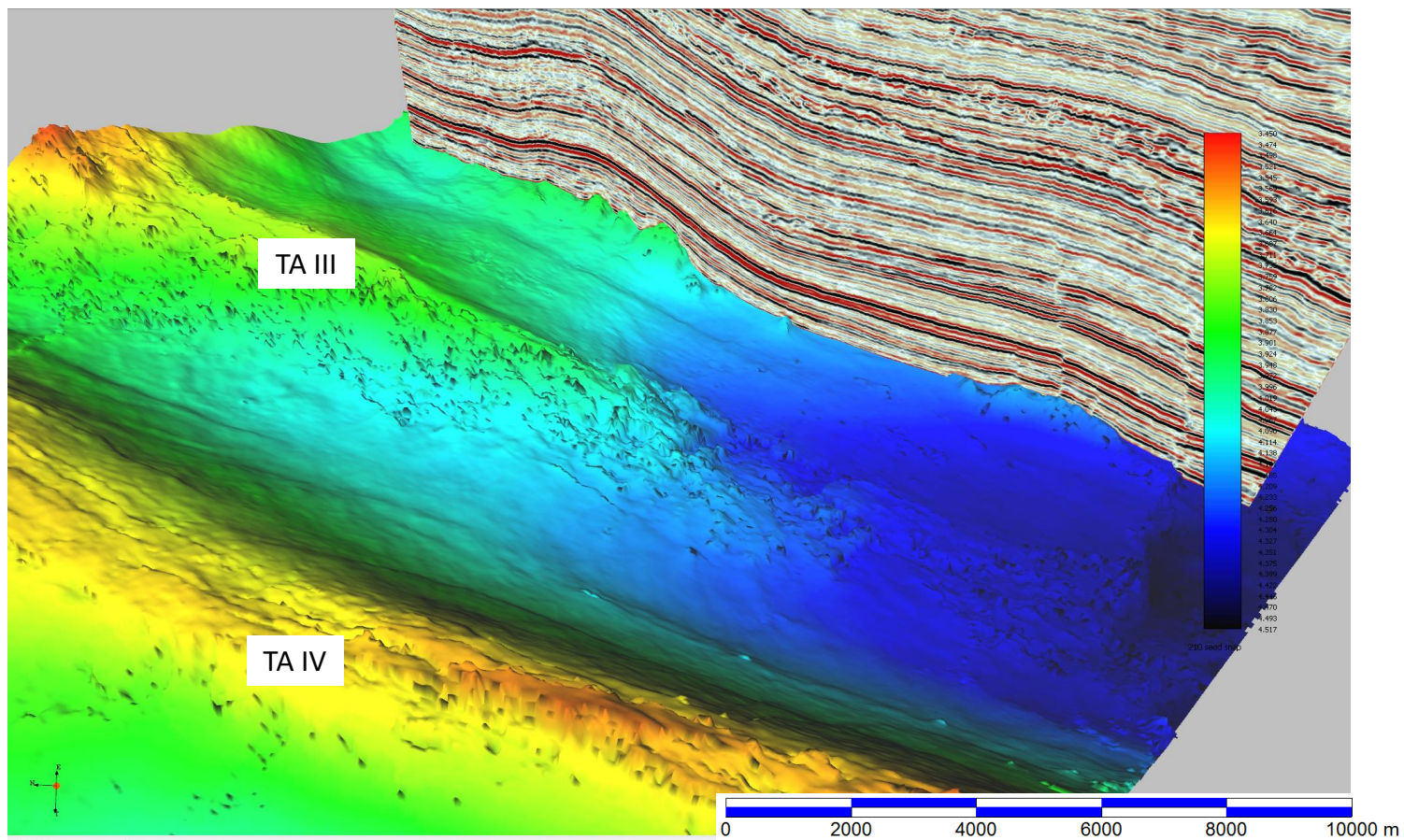


Figure 6-62: Another view of the surface shown in Figure 6-61, along with a vertical section through the mounds.

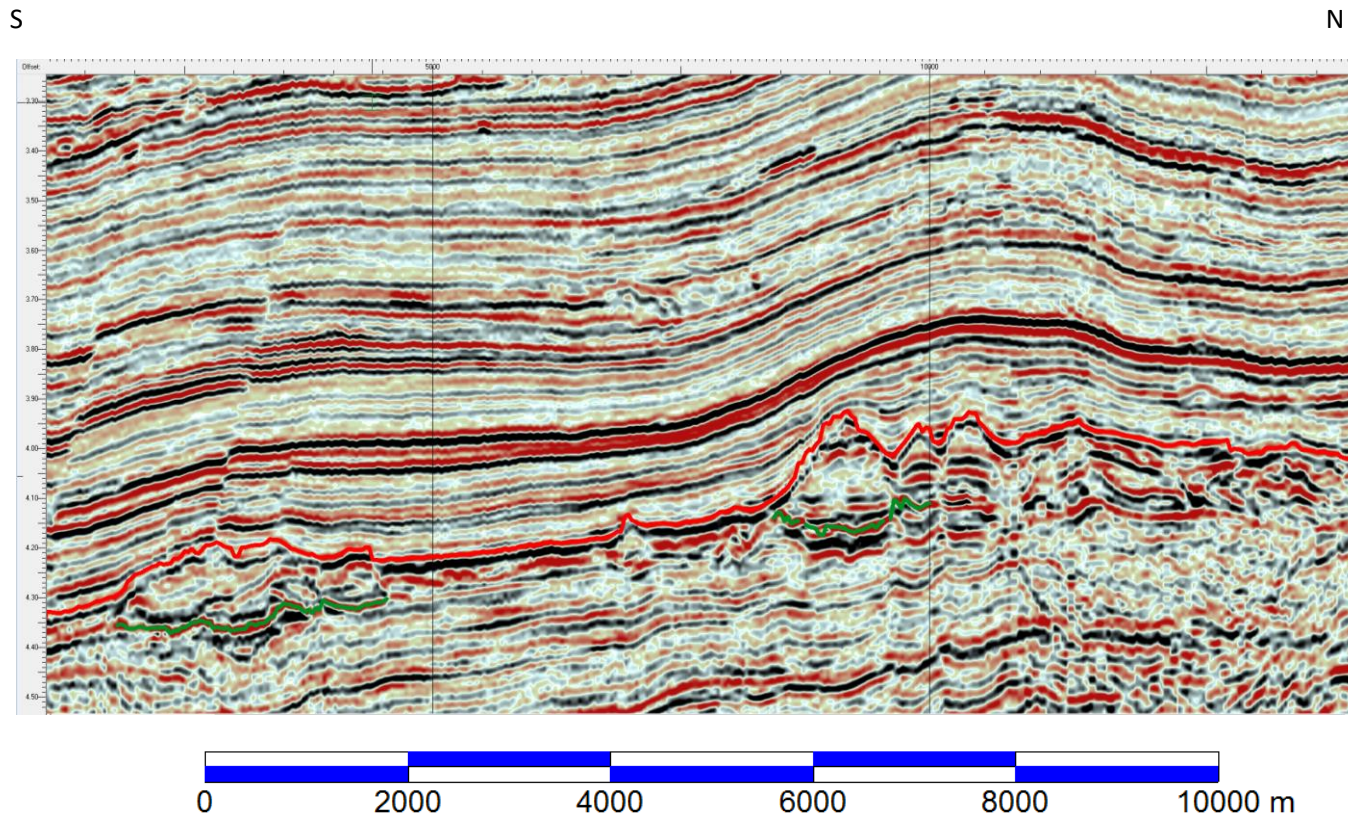


Figure 6-63: Vertical section through the mounds shown in Figure 6-62.

Chapter 7

Contents

| | | |
|----------|--|------------|
| 7 | Structural deformation | 165 |
| 7.1 | Introduction..... | 165 |
| 7.2 | Tectonic history | 169 |
| 7.2.1 | Mid-Lower Cretaceous (Barremian to Early Albian) | 169 |
| 7.2.2 | Middle Cretaceous (Albian to Turonian)..... | 172 |
| 7.2.3 | Upper Cretaceous (Campanian to Maastrichtian) | 172 |
| 7.2.4 | Palaeogene | 175 |
| 7.3 | Structural elements..... | 179 |
| 7.3.1 | Introduction..... | 179 |
| 7.3.2 | Basal detachment..... | 181 |
| 7.3.3 | Extension..... | 187 |
| 7.3.4 | Compression | 207 |
| 7.3.5 | Deformation of ridges | 227 |
| 7.3.6 | Fluid escape | 241 |
| 7.3.7 | Transcurrent faulting..... | 243 |

7 Structural deformation

7.1 Introduction

The interplay of the sediments that have been derived from the Benin Embayment and those from the Niger Delta has created a tectonic framework that has not been studied previously.

There are a number of studies that have focussed on the deltaic deformation relating to the growth of the Niger Delta. However, there is no study that the author is aware of which links the structural modification to the interplay of sediments derived from the two basins.

In this chapter, the nature of the structural deformation is outlined. The faulting within the syn rift section is complex and has not been investigated in any detail in this study. The major focus has been the thin-skinned Cenozoic portion of the subsurface. Within this upper interval, evidence of extensional compressional and strike-slip motion is observed.

The extensional faulting has been investigated in order to establish the timing of fault movement as part of the reconstruction of the tectonic history. The nature of the extensional faults and the spatial variation in throw was used to gain an understanding of how the faults interact with the underlying detachment zone.

The imaging of the shallow data allows some insight into the nature of a transcurrent fault zone. The nature of the Avon/Mahin fault zone is such that there is a variation in the throw of the fault along its length. These variations are illustrated in the section on transcurrent faulting.

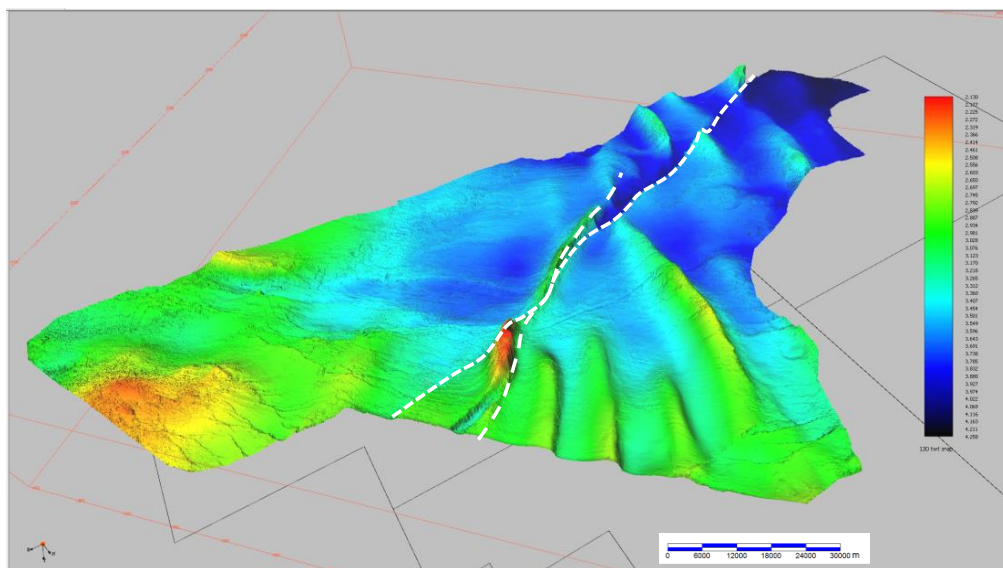


Figure 7-1: Perspective view, looking from the north-east, of the base of the Upper Miocene twt surface, highlighting the change in structural style across the strike slip faults (dashed white lines).

In order to verify the degree of strike slip that has taken place, three methods have been used to estimate the amount of lateral offset. The methods are calculating the amount of apparent extension on either side of the fault zone, the measurement of the displacement of slope channels which intersect the fault zone, and the correlation of isochrones to match intervals of similar thickness that are present on either side of the fault zone. This isochrone matching was accompanied by the fault-throw analysis of one of pre-existing faults that has been offset by the later lateral motion.

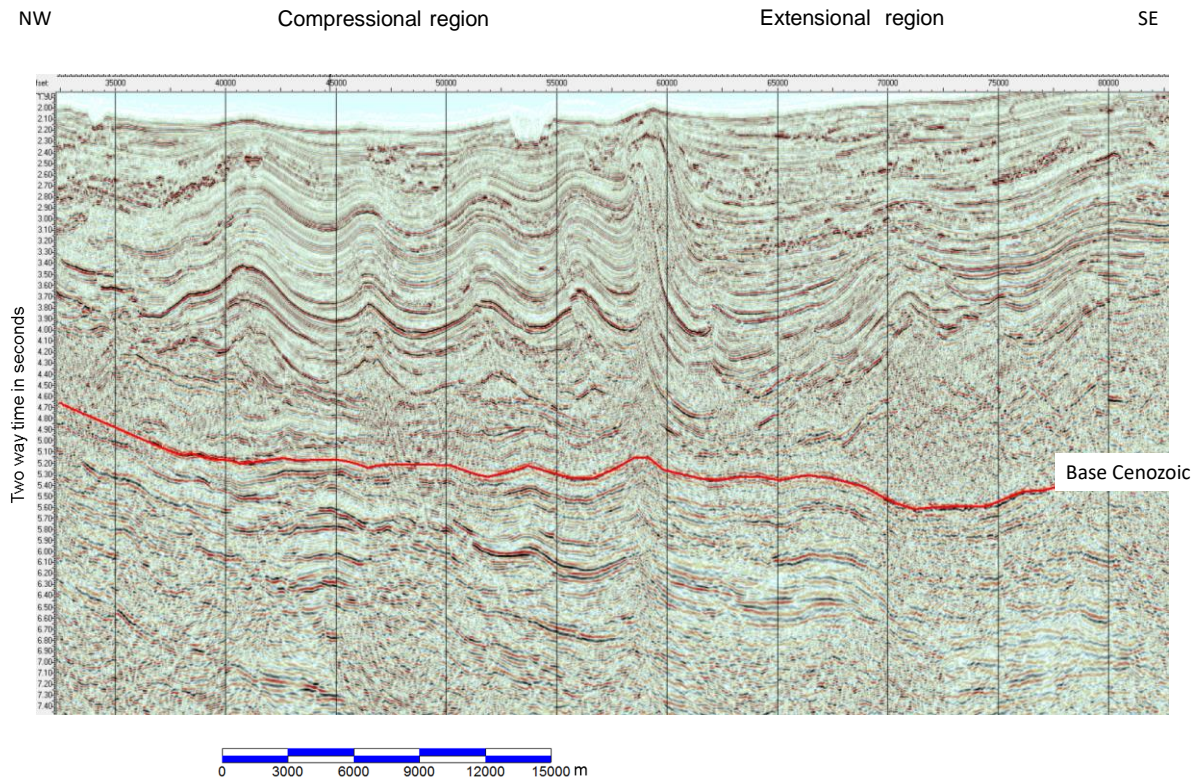


Figure 7-2: Seismic line illustrating the significant difference in structural style above and below the red horizon that crosses the study area.

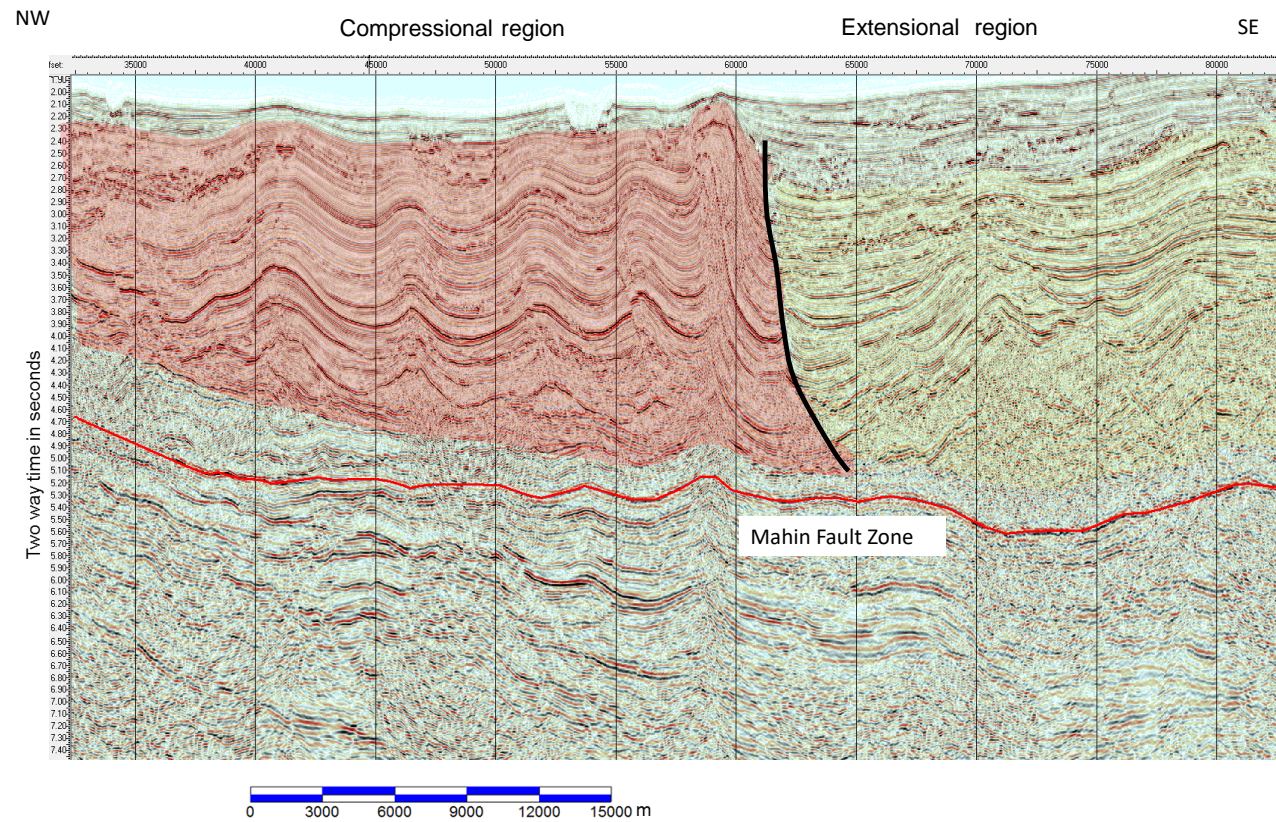


Figure 7-3: The same line displayed in Figure 7-2, with the contrasting tectonic styles highlighted on either side of the Mahin fault zone.

In Figure 7-3, the section to the east of the Mahin fault zone is comprised of largely extensional tectonic elements, whereas the interval that lies to the west (in red) is largely deformed by compressional stress.

The studied region is divided into several structural domains, which can be seen in Figure 7-2 and Figure 7-3; the shallow section is heavily deformed, whereas the deeper section is less affected by faulting. The shallow section can be further divided into western and eastern regions, with markedly different structural styles of deformation. The western region is dominated by high-relief folded anticlines, and the eastern is predominantly subject to widespread extension and normal faulting. Underlying the whole region is a rifted-basin terrain infilled with sediments, which have been subject to deformation associated with the break-up of the south Atlantic. This rifted interval is in turn overlain by a sequence of sediments that are largely unaffected by major tectonic activity.

7.2 Tectonic history

7.2.1 Mid-Lower Cretaceous (Barremian to Early Albian)

The oldest sediments in this area are within the syn rift (section 5.20). The strata in this interval have been subjected firstly to the extension accompanying the rifting (De Matos, 1999) and then to the transcurrent stress that led to the separation of the two continents (De Matos, 1992). As a result of these two tectonic episodes, the rifted section is folded and faulted in a complex fashion. The quality of the 3D seismic data used in this survey in the rifted section is poorly imaged, primarily due to velocity distortion in the overburden. By flattening the Base Cenozoic (horizon 600) and compressing the horizontal-to-vertical aspect ratio, the syn-rift section is better visualised. It is possible to see clear faulting within the interval (Figure 7-4). The region highlighted in blue is assigned an affinity with the syn-rift sedimentary section that has been tectonically modified.

The faulting appears complex, primarily due to the two-fold nature of the stresses that have acted upon this interval. It has not been part of this study to map this deeper interval, other than in gross terms. The tilted fault blocks identified within the sedimentary section are similar to those seen elsewhere along the transform margin, in Ghana and Cote D'Ivoire (Basile et al., 1993).

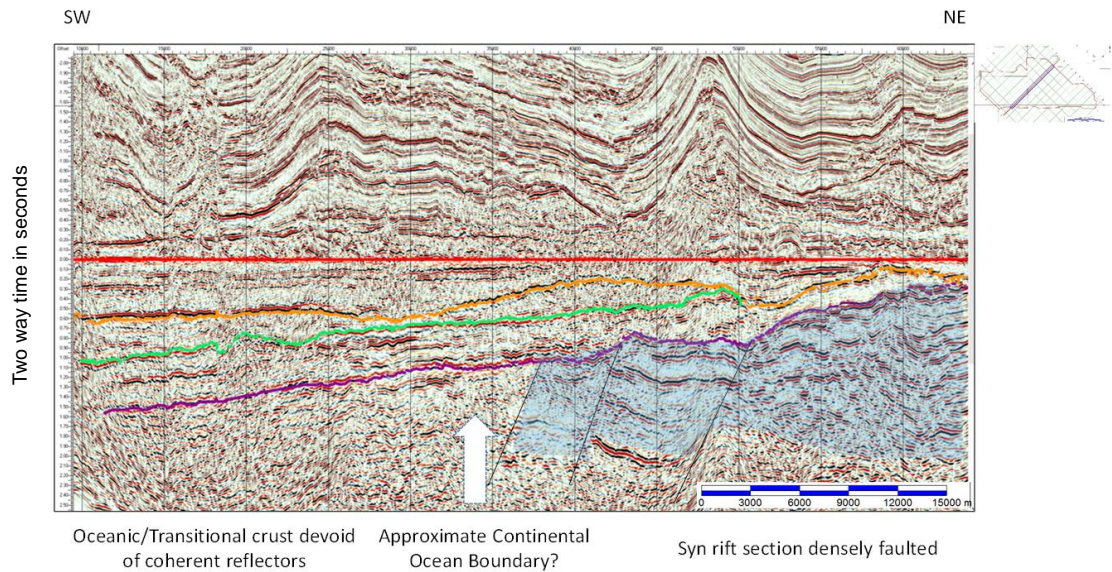


Figure 7-4: Cross line 6100, which illustrates the complex faulting, highlighted in blue, within the interpreted sedimentary section below the syn rift unconformity (purple horizon). The location of the continental ocean boundary is interpreted to lie between the reflective sediments and the non-reflective section to the south-west.

Gravity data indicate that a fossil transform fault may pass through the area; in Figure 7-5, the black lines are interpreted to be transform faults. The presence of such a fossil transform has been identified within the limits of a 3D survey to the south of this study area (Davies et al., 2005). It is interpreted that the survey area is likely to have been affected by the tectonic deformation that accompanied the initial opening of the south Atlantic.

In Figure 7-5, the location of known (named) fracture zones are identifiable in the free-air gravity data (Sandwell et al., 2014). Two additional fracture zones with free-air gravity data lie between the Romanche and Chain fracture zones are interpreted; the more southerly one may extend into the area that is the focus of this study.

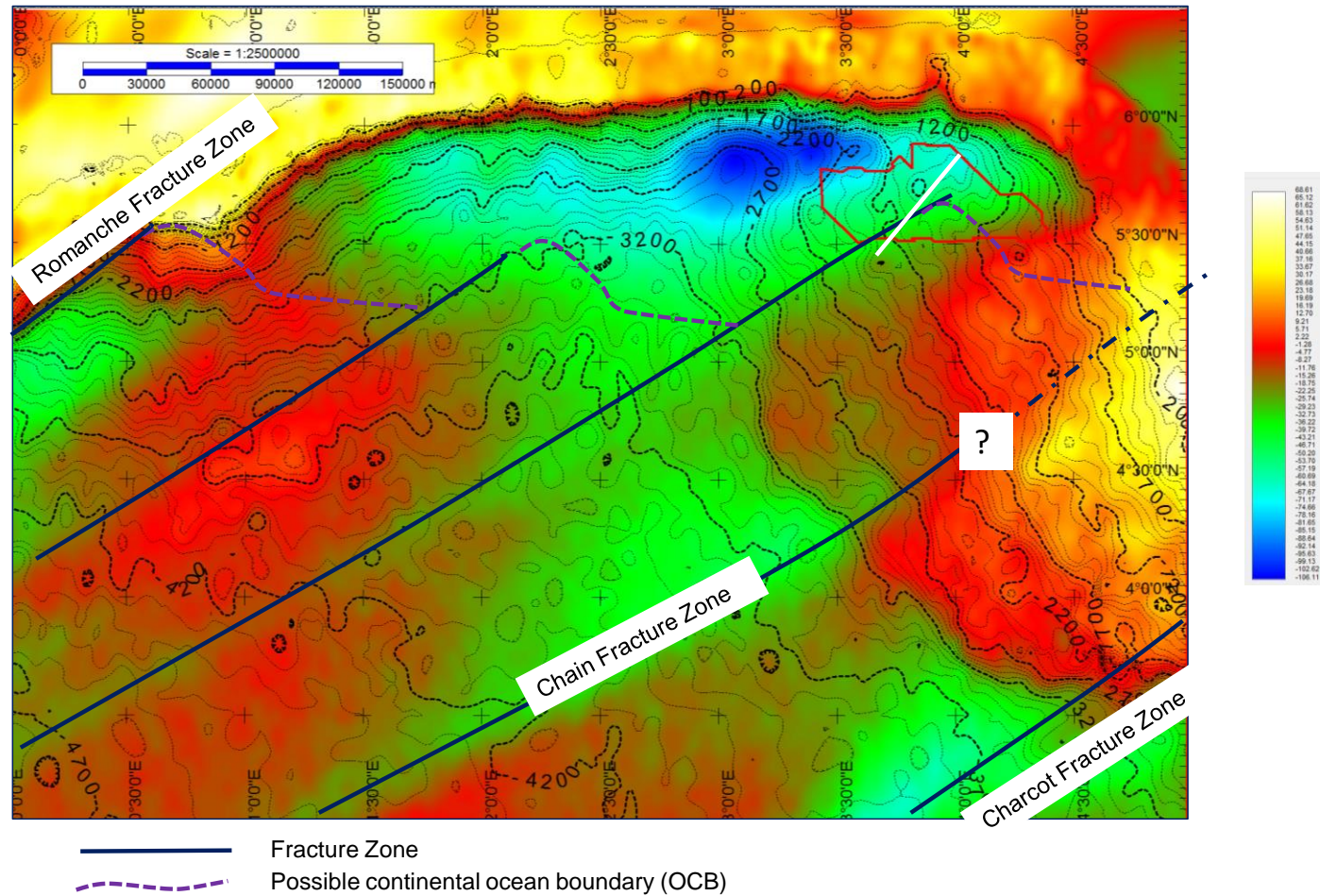


Figure 7-5: Free-air gravity anomaly map, with interpreted fracture zones and continent ocean boundaries marked. The location of Figure 7-4 is highlighted by the white line. The gravity map lends support to the possibility of the OCB being as shown in Figure 7-4.

7.2.2 Middle Cretaceous (Albian to Turonian)

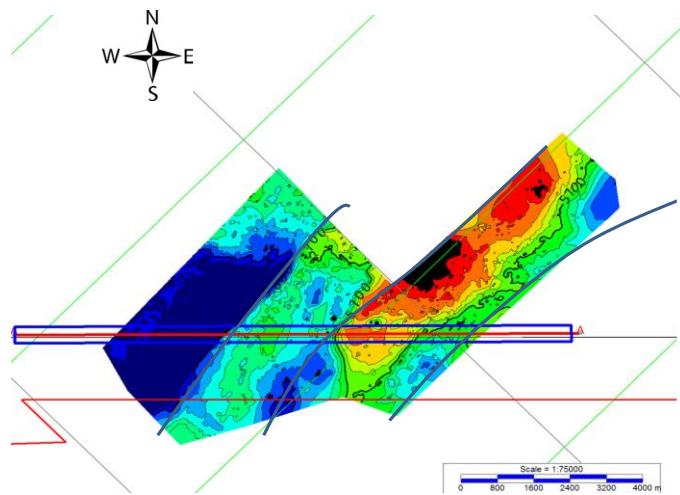
The primary tectonic control on the region during this period is the thermal subsidence of the oceanic crust following the separation of Africa from South America and the creation of the proto-Atlantic Ocean. Periodic relative sea-level fluctuations led to a number of erosional unconformities as the shoreline oscillated. A significant unconformity is recognised regionally – the Senonian unconformity. This unconformity, which is recognised across West Africa and was discussed in section 3.2.3, led to the erosion of older Albian to Turonian sediments (Guiraud and Bosworth, 1997; Benkhelil et al., 1998).

7.2.3 Upper Cretaceous (Campanian to Maastrichtian)

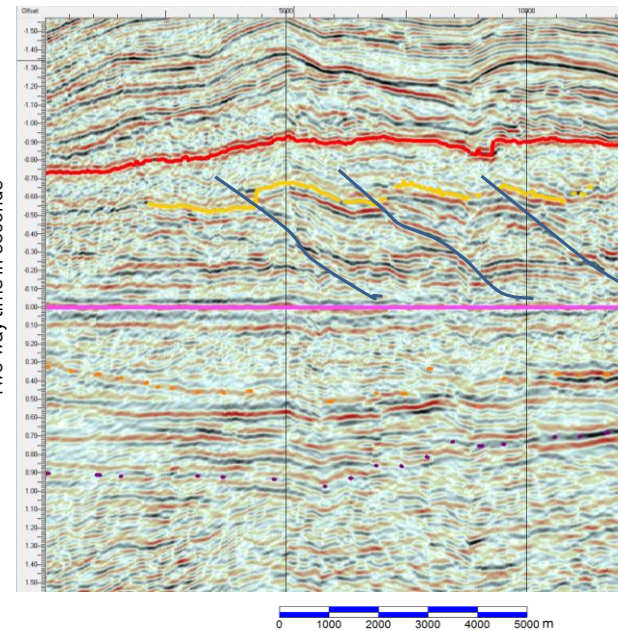
If the assumption that horizon 600 marks the base of the Cenozoic, then the section above the Senonian unconformity (horizon 680) is of Upper Cretaceous age. Little is known about this interval that underlies the Cenozoic section in the present-day deep water. The oldest deltaic penetrations both onshore and offshore are Eocene in age. However, although the data are not of the highest quality, it is possible to map some structural features within this interval.

Towards the south-eastern end of the 3D volume, there are reflections that indicate a series of thrust anticlines, (Figure 7-6), which bear a resemblance to the Mio-Pliocene thrust observed in the present-day outer thrust belt (Corredor et al., 2005). The crests of the anticline strike in a north-east to south-west direction, suggesting that the compression acting on these sediments was from the south-east. The wavelength of the folds is of the order of 1.5 to 2km; the lateral extent is not possible to map due to the poor data quality to the north and the edge of the survey to the south, but they are at least 8km in length in a strike direction.

The orientation of the thrust features would suggest that the compression which led to their formation was a result of lateral stress that was oriented in a south-east to north-west direction. One explanation for this stress would be the presence of a thick sediment wedge of clastics derived from an Upper Cretaceous precursor to the Niger Delta. The palaeo-shoreline is now somewhere buried beneath a thick Cenozoic overburden. If this thrust fault trend is traced towards the south, it is possible to make an interpretation that this compressional zone is related to the inner thrust belt mentioned earlier (Bilotti and Shaw, 2005).

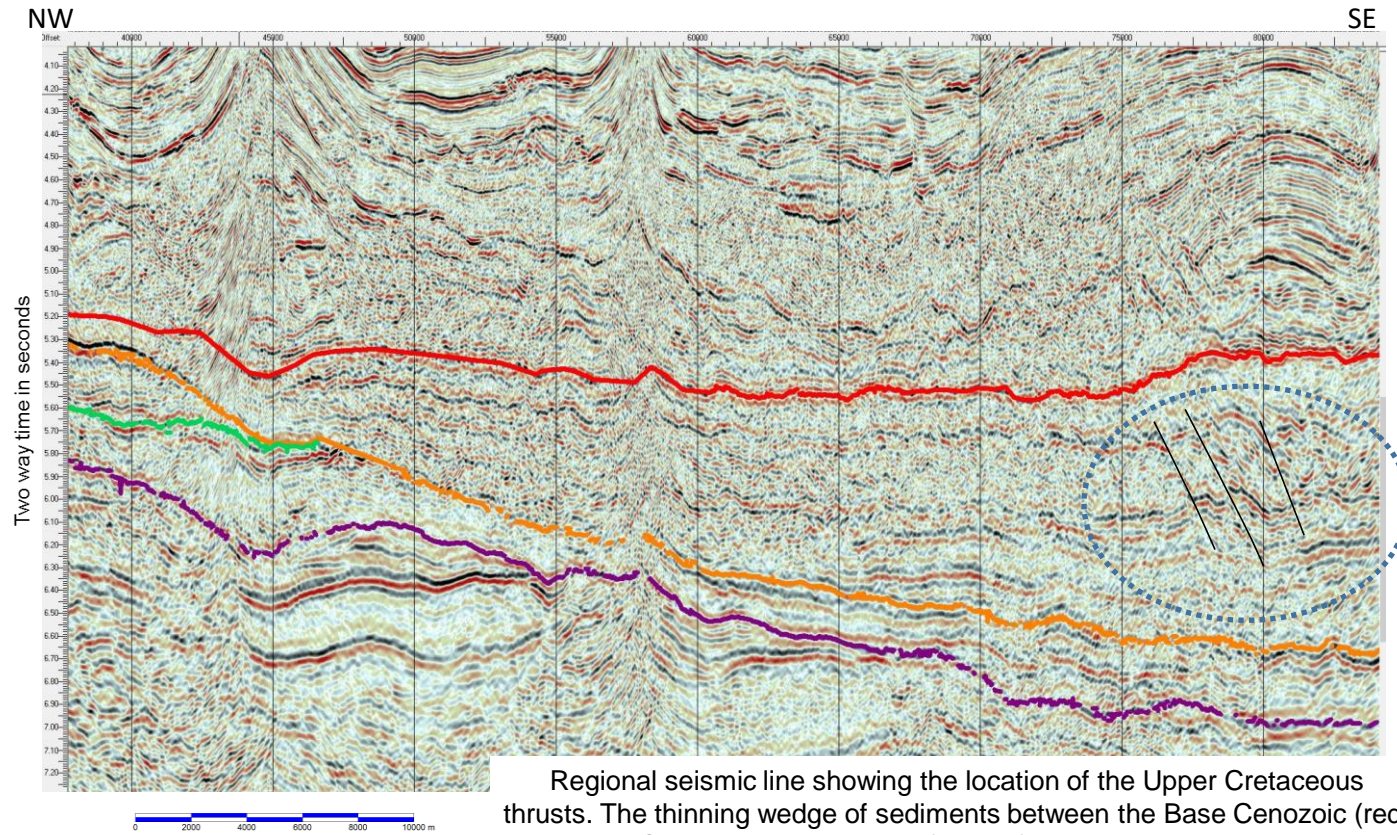


Two way time map of the sandy-coloured horizon in the adjacent image (close to the upper surface of the thrust interval).



Section across the thrust region which lies below the base Cenozoic event (red horizon), flattened at the interpreted basal detachment.

Figure 7-6: Arbitrary seismic line showing the presence of several thrust anticlines in the section below the Base Cenozoic (red marker), the assumed base Cenozoic.



Regional seismic line showing the location of the Upper Cretaceous thrusts. The thinning wedge of sediments between the Base Cenozoic (red) and the Senonian unconformity (orange) could be responsible for the critical taper behaviour of the sedimentary sequence.

Figure 7-7: Seismic inline 5840 showing the thinning wedge of sediments within the Upper Cretaceous.

The image in Figure 7-7 highlights the presence of a wedge of sediments within the Upper Cretaceous. The critical taper theory could be used to explain why the thrusting is present in this wedge. The Cenozoic delta has been modelled as such and it is possible that a Cretaceous delta would have been subject to the same mechanical deformation (Dahlen, 1990; Bilotti and Shaw, 2005; Frey-Martínez et al., 2006).

7.2.4 Palaeogene

The Cenozoic interval has been subjected to a large amount of structural deformation. The tectonic evolution of this interval has been the subject of a number of papers that have studied the deep-water section of the Niger Delta. (Short and Stauble, 1967; Mascle, 1973; Evamy et al., 1978; Doust and Omatsola, 1990; Cohen and McClay, 1996; Morley and Guerin, 1996; Onuoha, 1999; Graue, 2000; Morgan, 2004; Corredor et al., 2005; Briggs et al., 2006; Heinio and Davies, 2006; Heiniö and Davies, 2007; Kostenko et al., 2008; Leduc et al., 2012; Maloney et al., 2012; Sapin et al., 2012). These studies have focused on the overall deltaic deformation or most recently, on the outer thrust belt. There have been limited amounts of study concerning the confluence of the Benin and Niger Basins (Leduc et al., 2012). The bulk of the deformation described relates to Miocene and younger tectonic activity. Little is known about the Palaeogene structural activity in the Niger Delta.

7.2.4.1 Shelf collapse and mass transport deposition

The presence of an assumed apron of mass transport deposits that is immediately overlying the Base Cenozoic is interpreted to have been the result of the cannibalisation of the Benin basin shelf margin during the early Cenozoic. This has been described in some detail in chapter 6.3. This shelfal collapse has been described by Maloney et al. (2012). Following the cessation of the shelf collapse, a period of low-energy deposition is interpreted to have been established. The shelfal region lies beyond the extent of the 3D seismic data boundary and therefore it was not possible to examine this region in any meaningful way.

Within the levees mapped in the western region of the survey, there is a good deal of faulting recognised.

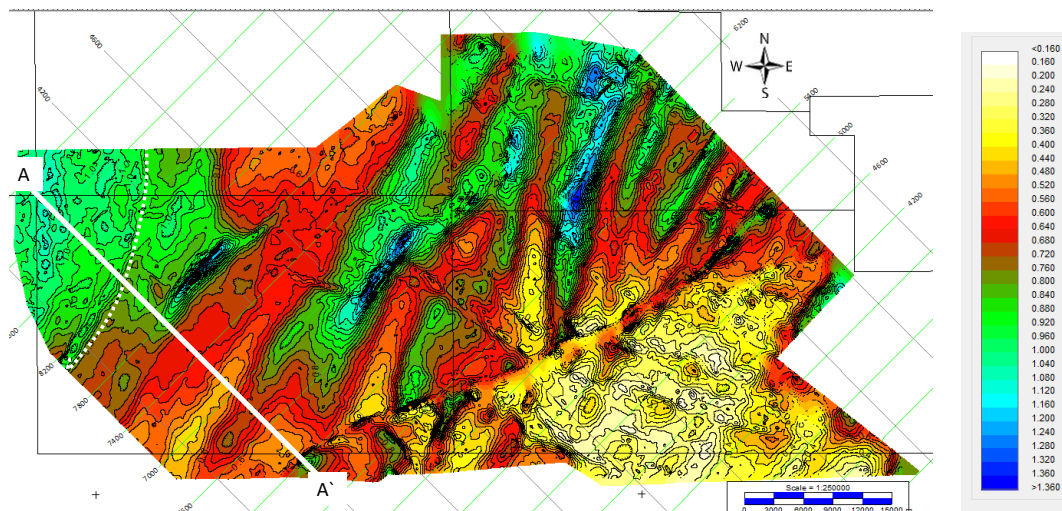


Figure 7-8: Isochrone map of the Lower Cenozoic interval, illustrating the north-east to south-west trending ridges and synclines; the ridge on the western edge of the map is bounded to the east by a complex fault zone.

The elongate north-east to south-west synclines (the blue regions in the map) seen in Figure 7-8 are interpreted to be the downslope portion of a turbidity flume, with adjacent levees that are linked to the Avon canyon. The synclines are areas of limited deposition because the sediment carried down the synclines is interpreted to have been deposited primarily in the flanking levees by the action of downslope currents or dispersed laterally by the action of ocean-bottom currents (section 6.3.3).

The mass-transport sequence is recognised along the entire shelf margin, and has been referred to as the Dahomey Wedge (MacGregor et al., 2003; Morgan, 2003), and has been interpreted as a channelised system. The volume of sediment deposited in the mass-transport complexes exceeds 500km³ alone within the 3D survey area. Given that it stretches at least 60km from the shelf towards the south and in excess of 100km to the west, along with an unknown distance to the east, this makes it one of the largest such features globally. Similar-scale events have been documented along the margins of Norway, Brunei, Trinidad, and Morocco (Bryn et al., 2005; Gee et al., 2007; Dunlap et al., 2010; Shipp et al., 2011; Moscardelli and Wood, 2016).

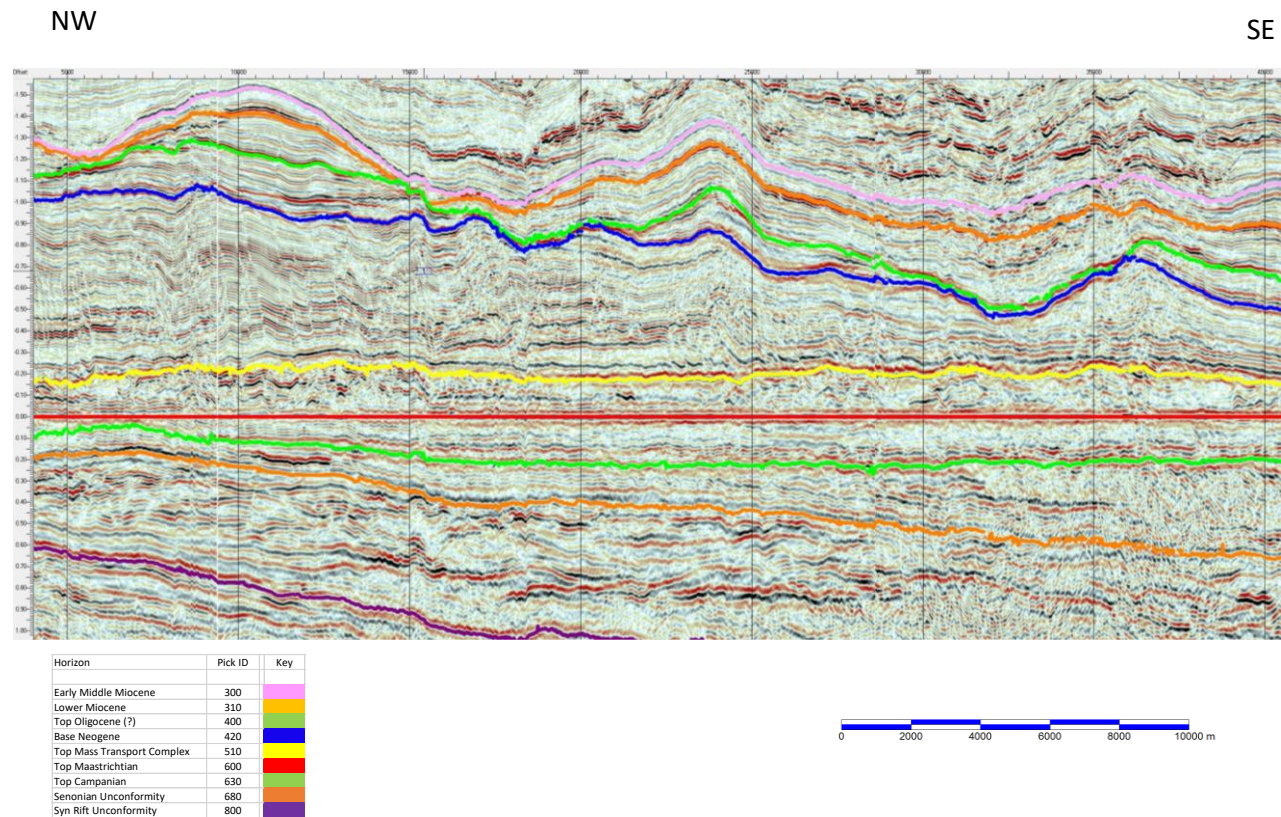


Figure 7-9: Seismic line highlighted by line A-A' on the map shown in Figure 7-8, flattened on horizon 600 (the base of the Lagos mega slide), showing the thickening of the section below the blue horizon (420) towards the west. Notice also the presence of ridges that have accumulated post the blue horizon.

Large-scale tectonic deformation of this kind requires a regional cause. Among the possibilities that have been put forward for other large-scale slides are scale-regional tectonic events such as the initiation of the Alpine Orogeny (Dunlap et al., 2010), or the retreat of the glaciers after the last ice age (Bryn et al., 2005; Solheim et al., 2005), or even extra-terrestrial impacts (Dunlap et al., 2010).

There is no evidence of a large-scale regional tectonic event that can be used to explain the trigger for this activity. There is little evidence of a significant regional tectonic episode such as that which occurred at the time of the Senonian unconformity (Guiraud and Bosworth, 1997). It is possible that the trigger for the collapse could be related to eustatic sea-level changes because this is the only regional geological event that is known to have occurred at the end of the Cretaceous. A number of Atlantic margin basins are known to have been subject to widespread shelfal erosion around the end of the Cretaceous (Dunlap et al., 2010). A possible explanation for this shelf collapse may be related to the differential compaction of sediments over the palaeo shelf margin, which created a stress imbalance at the shelf margin; this is discussed in chapter 8.

7.2.4.2 Intra-levee deformation

In the western half of the survey, within the Palaeogene (Figure 7-9) there is a region of structurally deformed strata. Overlying this horizon, the tectonic deformation is markedly reduced. It is, therefore, interpreted that the deformation that is present in this interval occurred during the Palaeogene. In Figure 7-8, the mapped Palaeogene thickness exhibits, in addition to the north-east to south-west linear synclines, that there is a thick section mapped at the western edge of the survey. Within this sedimentary thick, there is an unusual style of faulting recognised, which is discussed in section 7.3.5.

7.3.5. Neogene

The spread of the Niger Delta from the east led to the accumulation of a thick section of clastics in the proximal region (see chapter 2), from the Eocene up to the present day. The lateral stress that accumulated as a result of his progradation generated the tectonic regime that led to the present structural configuration. The deformation in this Neogene sequence is divided into distinct domains with markedly different structural styles. The classic deltaic deformation that has been described by several authors (Morley and Guerin, 1996; McClay et al., 2003; Bilotti and Shaw, 2005; Corredor et al., 2005; Briggs et al., 2006) has focused on the tectonic activity that has occurred during the Neogene.

The main depocentre of sediments that have been fed from the Niger lies to the south of the study area. The area covered by the 3D survey used in this study lies at the north-western margin of the thick sediment wedge that has been deposited since the Eocene. The structural alterations that have occurred in the delta during the Neogene have impacted upon the studied area, but this tectonic activity has been affected by the section that was deposited and deformed during the Palaeogene.

7.3 Structural elements

7.3.1 Introduction

The region covered by the 3D survey encompasses a wide variety of structural deformation styles. In this chapter, the key structural deformation styles will be discussed. Examples of extension, compression, and strike-slip movement are interpreted to be present; the nature of these structural styles is presented below.

The region is divided into two terrains by a tectonic lineament that strikes in a north-east to south-west direction through the study area (Figure 7-10). To the west of this fault zone is an area that is comprised of a number of thrust anticlines of compressional origin; this is discussed in section 7.3.4. The eastern half of the survey is characterised by widespread extension and normal faulting, which is described in 7.3.3. The major lineament – the Avon/Mahin fault zone – which traverses the block is interpreted to be a dextral strike slip zone of faulting; the evidence to support this is presented in section 7.3.7. The deformation is linked to a predominantly strike-slip stress regime, with the principle stress orientation being south-east to north-west in orientation. Within the data set, there are also examples of conjugate strike-slip motion that also fit the interpreted stress orientation. The nature of this fault zone and the evidence that is used to support the interpretation of dextral strike-slip motion is outlined in section 7.3.7.

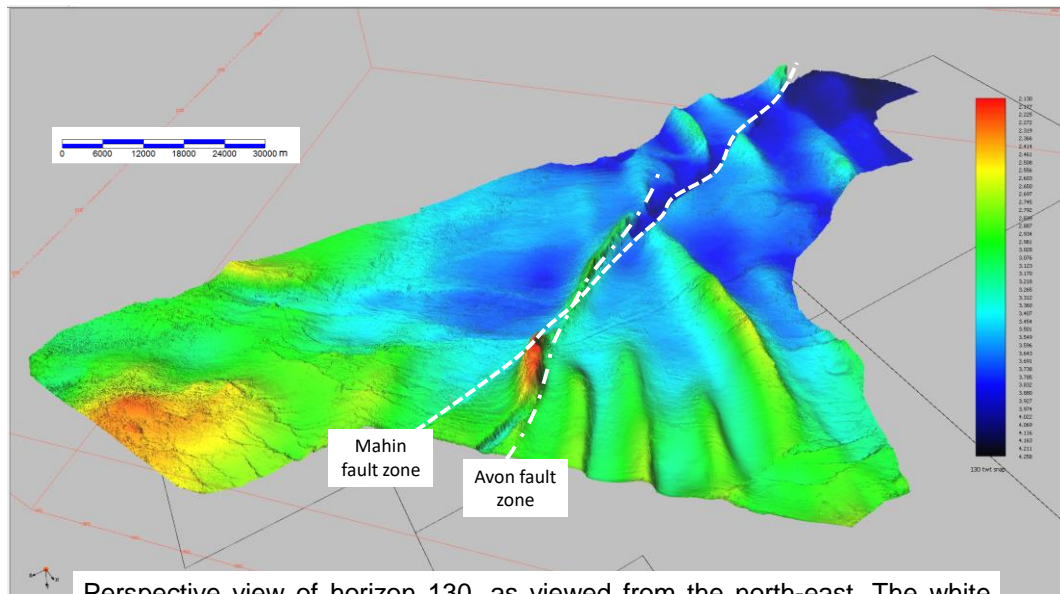


Figure 7-10: Perspective view of horizon 130 showing the key structural features in the survey area.

The strike-slip deformation seen in the Avon/Mahin fault zone is interpreted to have commenced in the middle Miocene. The mapping of several events from the Miocene until the present has established lateral displacements that are seen to have increased with time. The Mahin fault zone is inferred to have been the earlier active zone of deformation; the Avon fault zone is a recent feature. A more detailed description of this strike slip motion is outlined in section 7.3.7.

In addition to these large-scale structural domains, there are deformation styles that are more localised. One such area lies at the western margin of the survey area. In this area, a deformation style not previously described in the Niger Delta has been identified. The faulting, which is restricted to the limits of elongate levee/ridges, resembles a reverse fault version of the bookcase style of extensional faulting. This is described in section 7.3.5.

The separation of the thin-skinned interval from the underlying stable section is marked by a detachment zone. The nature of the detachment zone and its link to the presence of an interval of chaotic seismic reflections, which is interpreted to be a mass transport deposit, was outlined in section 6.3.4 and the observations are outlined in section 7.3.2.

Large-scale examples of strike-slip motion are found at a number of plate boundaries such as at the west coast of the US (the San Andreas and associated faults) (Wilcox et al.,

1973; Harding, 1985), Sumatra (Malod and Kemal, 1996), New Zealand (Little and Jones, 1998), the Jordan Valley in the Levant (Wilcox et al., 1973; Harding, 1985), and Papua New Guinea (Abers and McCaffrey, 1988; Ali and Hall, 1995; Pubellier and Ego, 2002). Other examples of large-scale transcurrent faulting include Thailand and Vietnam (Molnar and Tapponnier, 1975), which although not located at the continental boundary is a result of the Himalayan orogeny leading to the extrusion of south-east Asia along major strike slip fault zones – the Red River, Mae Ping, Klong Marui, and Ranong faults (Molnar and Tapponnier 1975)

All of the above wrench fault zones are associated with significant plate boundary motion and involve basement movements. Examples of extensive strike-slip faults not linked to the relative motion of tectonic plates are less common; those with no basement involvement are rare. This is due in part to the fact that for the principle stress to exceed the overburden stress requires large forces to be applied in a horizontal manner, which is often the case at plate boundaries.

Strike-slip fault zones have been studied with the aid of surface geological mapping, experimental sand box and clay models, and seismic data (Emmons, 1969; Wilcox et al., 1973; Freund, 1974; Harding, 1974, 1985; Naylor et al., 1986; Leduc et al., 2012). A number of common styles have been observed and given generic names such as “flower structures,” pull-apart basins, and pop-ups. Within the 3D volume, all of these styles are observed; in addition to these common descriptions there are a number of additional characteristics that this study has identified including an unusual “snake-bite” structural style.

The most obvious characteristic of the strike-slip faulting is the fact that the faults are sub-vertical in cross section and linear in map view (Figure 7-10). Although the strike slip faults are sub-vertical, in detail the hade of the fault alters with depth and also sense of throw. The variation of faulting along the length of a strike-slip zone ranges from trans-tensional, including the creation of pull-apart basins, to transpressional, where the apparent motion of the strata is akin to reverse faulting (Freund, 1974).

7.3.2 Basal detachment

The presence of mass transport deposits within the 3D volume of data has been described in chapter 6. The interval in which the mass transport deposits are most widespread is in the interval between horizons 600 and 500/510. Overlying this interval, the strata have been subject to widespread structural modification. It is notable that the faults in the overlying interval are interpreted to tip out, with depth, either close to or at the surface of the mass transport deposits (Figure 7-11, 7-8, and 7-9).

In the compressional region, to the west of the Avon/Mahin fault zones the deformation noted in the Palaeogene is well-imaged within the 3D volume. The horizon that marks the top of the mass transport deposit is unbroken, whereas the sediments immediately overlying this horizon are heavily deformed. The tipping-out of faulting at the surface of the chaotic interval is seen to be widespread, where the data quality is good enough to image the surface well.

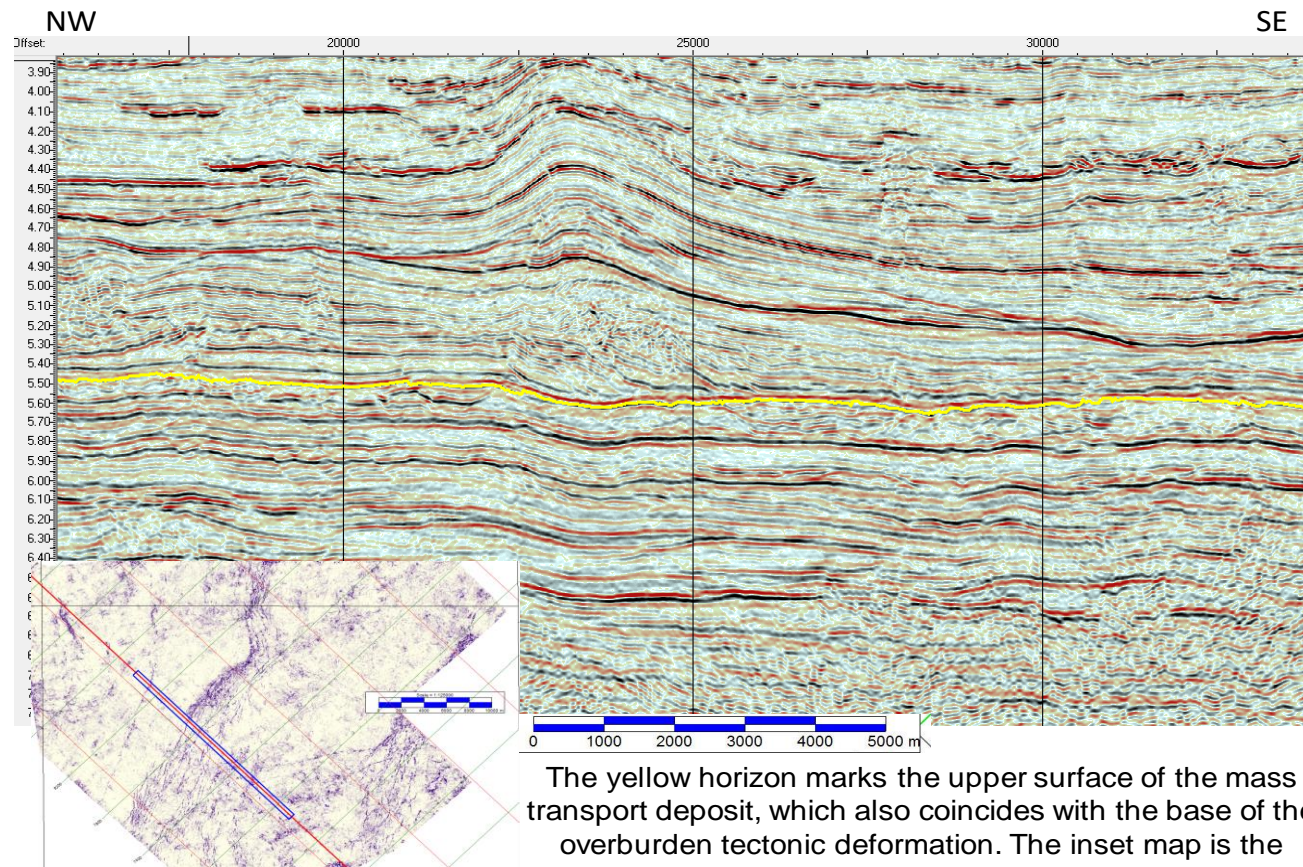
In Figure 7-11 and Figure 7-12, the top of the mass transport deposit is interpreted as a peak (black reflector). This horizon (510) is a continuous reflector and marks the top of the underlying chaotic interval. The horizon that immediately overlies the mass transport complex (horizon 500 – green) is distorted as a result of compressional deformation. The inset map is the similarity attribute that was extracted at this horizon. The faulting that is observed in the vertical section extends to the north in a belt of reverse faults, which is picked out as the series of dark lines on the similarity map.

In the western region of the survey area, horizon 500 marks the top of a younger mass transport complex that directly overlies horizon 510. In this region, the overburden deformation terminates at depth at this horizon (Figure 7-13).

The basal reflector that marks the lower boundary of the mass transport complex is also mapped as a peak amplitude. The horizon is present across the entire survey and is underlain by a predominantly parallel series of reflectors that are mildly deformed by small-scale faulting. The surface appears to be devoid of any basal scouring, although the lateral and vertical resolution of the data at the depth of the horizon is limited; it is therefore equivocal as to whether scouring is present.

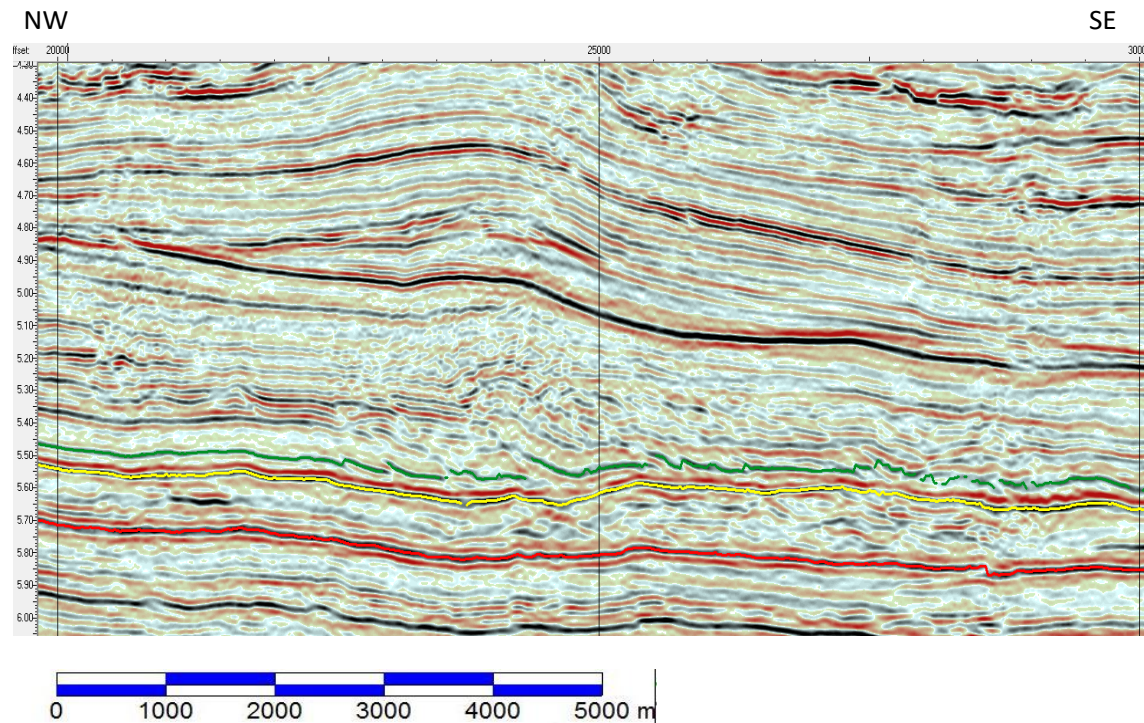
This surface is known regionally to mark the base of the chaotic seismic facies, which has been referred to as the Dahomey Wedge (Morgan, 2003; Briggs et al., 2006). The nature of the faulting that is present in the thin-shinned shallow section and which soles out at the top of this mass transport complex is described in the later paragraphs.

The seismic imaging of the basal detachment referred to in the deep-water Niger Delta is distorted by the imaging of the horizon under a complexly disturbed overburden. In the deep-water region covered by the studies of the outer trust belt, the undeformed section beneath the detachment can be readily identified.



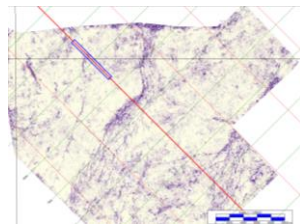
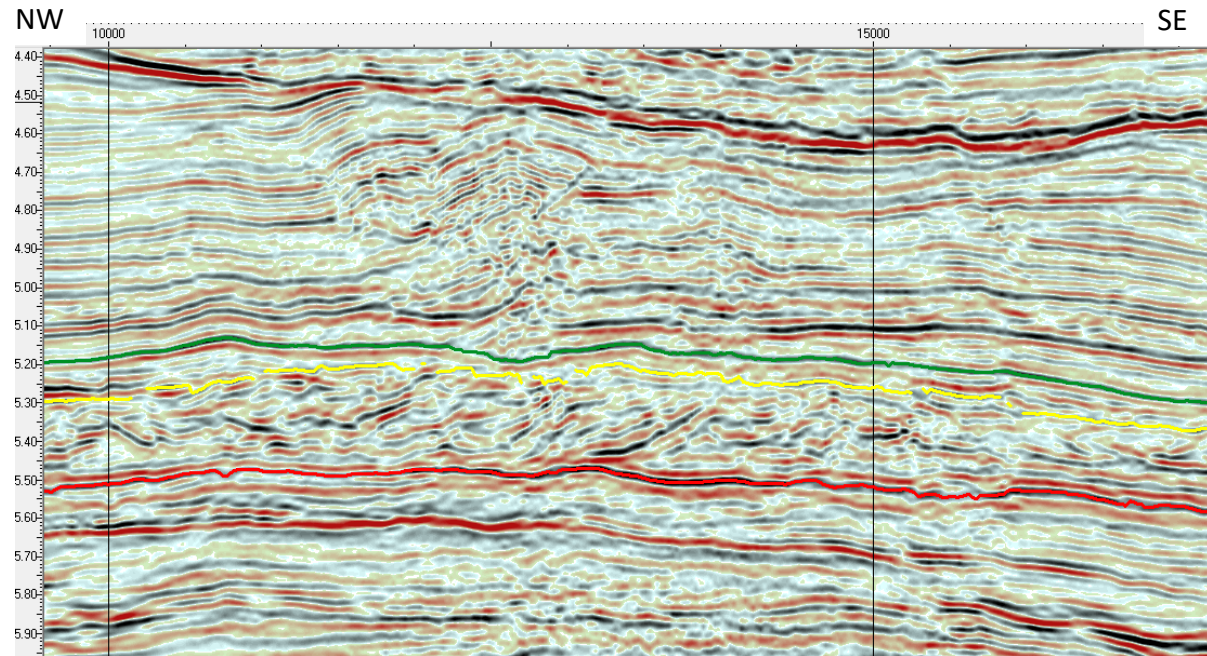
The yellow horizon marks the upper surface of the mass transport deposit, which also coincides with the base of the overburden tectonic deformation. The inset map is the similarity extraction at the horizon immediately overlying the yellow pick.

Figure 7-11: Portion of inline 3800 illustrating the location of the detachment.



A magnified view of a portion of the previous figure, illustrating the contrast in the continuity of the top of the mass transport deposit (yellow) and the overlying event (green). Also evident is the base of the mass transport complex (red).

Figure 7-12: Detail of Figure 7-11 illustrating the basal limit of the deformed overburden.



Towards the western margin of the survey, the green horizon becomes the basal limit of the overburden tectonic deformation. It is interpreted that in this western region, the green horizon is the upper surface of a younger mass transport deposit.

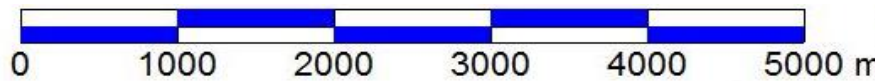


Figure 7-13: Portion of inline 4200, illustrating the discontinuity in structural deformation at horizon 500.

The actual nature of the detachment zone is unclear (Bilotti and Shaw, 2005; Corredor et al., 2005; Briggs et al., 2006; Butler and Iacopini, 2009) because the internal resolution of the interval noted as the upper detachment layer by Briggs (Briggs et al., 2006; Maloney et al., 2009) is limited by the frequency content of the data. The multiple detachment layers referred to by Briggs may in fact be the upper and lower surfaces of the lateral equivalent of the mass transport complex.

The seismic imaging in these studies is hampered by the limitations of time-migrated data. An additional complication is the presence of overpressure within the vicinity of the basal detachment layer (Bilotti and Shaw, 2005; Kostenko et al., 2008). Overpressured shales have low acoustic compressional wave velocities when compared to normally pressured shales. The lowering of velocity gives rise to a lowering of frequency content – lowering the vertical resolution.

The interval between horizons 510 and 600 that corresponds to the Dahomey Wedge (Morgan, 2003; Briggs et al., 2006) would, if buried and subjected to overpressure, also lose resolution and the zone would appear seismically nebulous. However, the imaging of the top of this wedge in this data set is of a high quality and the upper surface is seen to be the layer at which the separation of the overburden deformation from the underlying sediments is located.

7.3.2.1 The interplay between structural deformation and mass transport deposits

Throughout the 3D volume, it is recognised that there is a link between the thin-skinned structural deformation and the upper surface of mass transport deposits. The folding and faulting in the Cenozoic section appears to be contained in the layers immediately overlying the apron of mass transport deposits that has been identified in chapter 6.3.4 and the present-day seabed. It is evident that the mass transport deposits play a role in controlling the deformation of the overburden.

Evidence

Mass transport complexes are interpreted at a number of levels within the survey (section 6.3.4). Those that appear to have the largest impact upon the deformation of the shallow section are those between horizons 600 and 500/510 and between 490 and 470. It is at the upper boundaries of these two intervals that the structural deformation of the shallow section can be seen to terminate with depth.

Horizon 510 (as seen in Figure 7-11 and Figure 7-12) is a good seismic event, which can be mapped with confidence across the western half of the survey. It is an unfaulted horizon with an irregular topographic shape. Below this horizon, the chaotic interval displays the hallmarks of a mass transport deposit (section 6.3.4). There does not appear

to be any post-depositional modification of the sediments within the chaotic interval, although this cannot be stated unequivocally. The seismic evidence would indicate, therefore, that horizon 510 in the south of the survey is the detachment layer. If this is the case, then the reason for this being the case needs addressing.

In section 6.4.3, the nature of the basal detachment was discussed, in which the role of overpressure was highlighted as the means by which a low shear strength layer can form.

A number of mechanisms for the generation of overpressure within a sedimentary section have been documented (Mann and Mackenzie, 1990; Osborne and Swarbrick, 1997). These include the rapid burial of sediments, the diagenetic alteration of sediments in situ, the generation of hydrocarbons (Cobbold et al., 2009), the uplift of fossilised pressured intervals lateral transfer from deep connected basins (Yardley and Swarbrick, 2000), and excessive heat flow (Barker, 1972), amongst others.

Mass transport deposits are comprised of a heterolithic mixture, with a wide variety of constituent particles; the particles range in size from fine-grained clay to kilometre-scale blocks of competent strata (Carter, 1975; Moscardelli et al., 2006; Bull et al., 2009; Alves, 2015). Added to this heterolithic mix is a significant quantity of interstitial water that is transported with the solid material.

The resulting sediment pile may remain stable under deep-water conditions, with the water within the mass transport deposit remaining while additional pelagic sediments are deposited over the top. As with conventional shale deposition, bound and interstitial water remains within the sediments and is gradually bled off. The rate of the bleed-off of pressure is a function of the permeability of the rock. Shales have low permeability, whereas the permeability of a mass transport deposit will be variable.

It is postulated, therefore, that water released from the mass transport deposit may be expelled at a greater rate than can be absorbed by the overlying shale, creating an abnormal pressure at the surface of the two layers. Evidence of post-emplacement fluid flow within mass transport deposits (Strachan, 2002) indicates that fluid flow through a mass transport deposit is present at rates that could indicate higher overall permeability than that found in shales (Cartwright et al., 2007).

7.3.3 Extension

In this section, the nature of the normal faulting will be outlined, along with a description of the regional variations in both timing and deformation. Extensional faulting is recognised throughout the interval that overlies the basal detachment and is

characterised by a series of approximately east-west striking horsts and grabens with both down to the south synthetic faults and the corresponding antithetic faults (Sapin et al., 2012). The faults are seen to tip out at depth, at or close to the top of the Base Cenozoic mass transport complex. There is a notable difference in the orientation of the strike of the faults on either side of the Avon/Mahin fault zone. To the west, the faults share a similar strike orientation whereas to the east, they have varying strike directions.

7.3.3.1 Normal faulting

To the north of the 3D survey area lies a region of large-scale extensional faulting. This extensional region has been noted by both Leduc (Leduc et al., 2012) and Maloney (Maloney et al., 2012). This extensional zone is characterised by fault planes that are present at the sea bed and flatten out at depth where they sole out at a regional detachment layer.

Within the 3D survey bounds, the extensional faulting is widespread. There are two distinct regions of normal faulting recognised within the 3D volume; they are separated from each other by the Avon/Mahin fault zone (see chapter 6.1).

Normal faults occur when the principle stress is vertical; displacements are primarily vertical, with some minor dip slip occurring. The displacement of strata between the foot wall (up-thrown) and the hanging wall (down-thrown) that occurs as a result of normal faulting varies both vertically and laterally. Faults of this kind can occur either syn-depositionally or post-deposition.

The high quality of the data, notably in the shallow section, allows the reliable correlation of reflections across faults. In the deeper intervals, the imaging becomes less reliable and additionally – particularly in the eastern half of the survey – the degree of faulting increases such that it becomes difficult to map individual fault blocks, with confidence. A check on the reliability of cross-fault correlation was performed with the use of random tracks through the data. The use of random tracks through the 3D volume allows continuous horizon correlation between the footwall and hanging wall around the tips of faults (Figure 7-28, Figure 7-27). With the degree of confidence this provides, it was therefore possible to carry out the analysis of the variation in throw and to establish both the change in throws and the growth intervals.

The variation in displacement of stratigraphically continuous events across the fault has been plotted for a typical normal fault and indicates that the strain changes in a manner that is consistent with observations of normal faulting elsewhere (Imber et al., 2003; Baudon and Cartwright, 2008) As with the examples outlined in Baudon and Cartwright (2008), the use of two-way travel-time as a proxy for depth was used to plot the

displacements versus depth. For blind normal faults, the maximum displacement of the fault is at the centre of the fault plane, both laterally and vertically. The plot of an idealised blind normal fault would resemble an ellipse, with the edge of the ellipse marking the tip of the fault and the maximum throw located at the centre of the ellipse.

An additional complication in tracing the fault planes at depth in this 3D volume is the nature of the strata that are present. In the shallow interval, the majority of the reflectors are laterally continuous; however, at depth, the influence of mass transport deposits is evident and therefore there are few, if any, laterally extensive acoustic boundaries that can be mapped within the seismically chaotic intervals associated with the mass transport deposit. However, the surface of the mass transport complex can be mapped over a significant portion of the survey and where it is mapped, the faulting seen in the overburden does not offset the reflection that is the upper limit of the mass transport interval.

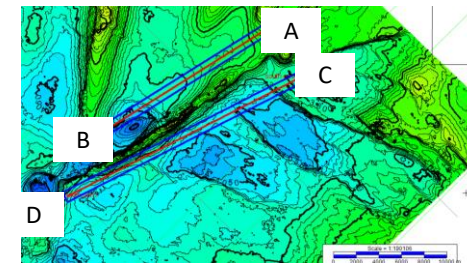
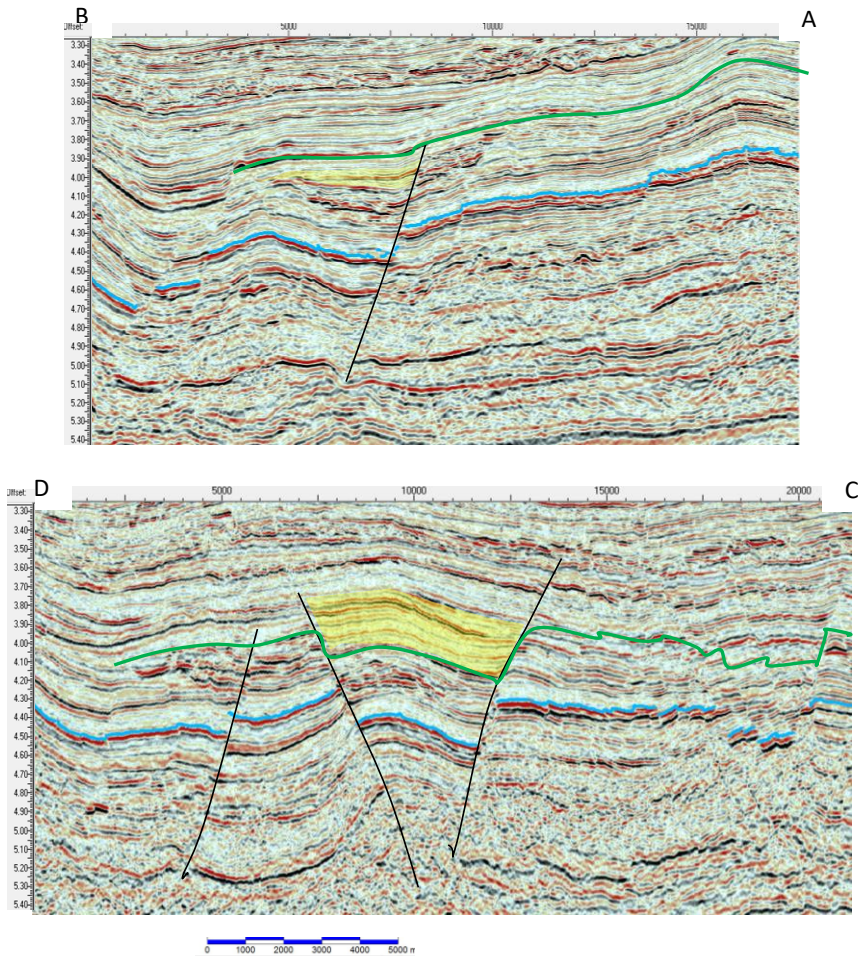
7.3.3.1.1 Fault geometries

In the main, the normal faults planes that have been studied in the region covered by the 3D survey exhibit linear and planar geometries. They do not appear to behave as listric faults, even though they tip out at depth. With no depth control or velocity data available to remove any distortion, the true fault plane geometries cannot be unequivocally described.

7.3.3.1.2 Timing

In order to establish the timing of the faulting, a number of approaches have been used. Ideally, any faults that can be seen to have been active at the palaeo-seabed would allow the dating of the cessation of faulting to be established. This recognition is possible where additional strata are present in the hanging wall compared to the footwall because the accommodation space in the hanging wall is filled with sediment deposited during active growth. To establish this relationship, it is necessary to be able to confidently map strata on both the up- and down-thrown portion of the fault. It is more difficult to establish the onset of the extensional fault activity. In the case of blind faults, as noted above the onset is as uncertain as the cessation. If the faulting is syn sedimentary, then the onset of deformation must occur prior to the deposition of the oldest strata within the growth package in the hanging wall.

By using this approach, it was possible to determine that the extensional faulting immediately to the west of the Avon/Mahin fault zone was confined to the period up to but no younger than horizon 160. However, in the eastern region the faulting has persisted to the present day.



Twt map of horizon 160

The two sections to the left are located on either side of the Mahin fault zone. The upper section lies to the north of the fault zone. The throw on the highlighted fault exhibits limited syn-depositional growth (highlighted in yellow).

In the lower section the amount of syn depositional growth is much greater. The major growth observed in this section, post-dates the deposition of the section between the blue and green (160) horizons.

Of note is the presence of a slope channel complex between these horizons which can be identified on either side of the strike slip fault zone. This observation is useful in determining the amount of lateral displacement along the fault zone.

Figure 7-14: Illustration of the variation in fault throws on either side of the Mahin fault zone.

In the case where the faults do not exhibit significant vertical dilation and exhibit no additional section in the hanging wall, the dating becomes problematic. Such blind faults could have been active at any time during the period following the deposition of the strata (Imber et al., 2003). Another way of establishing the timing of the faulting is to examine the isochrones between several intervals. The isochrones highlight the location of the increase in accommodation space that occurs through time but also the thickening of the intervals in the grabens, which form as a result of the normal faulting. This method has been used to investigate the timing of graben formation.

To the west of the Avon/Mahin fault zone, the isochrones indicate that there was growth in the interval below horizon 160, but very little additional growth on these faults after the deposition of horizon 160.

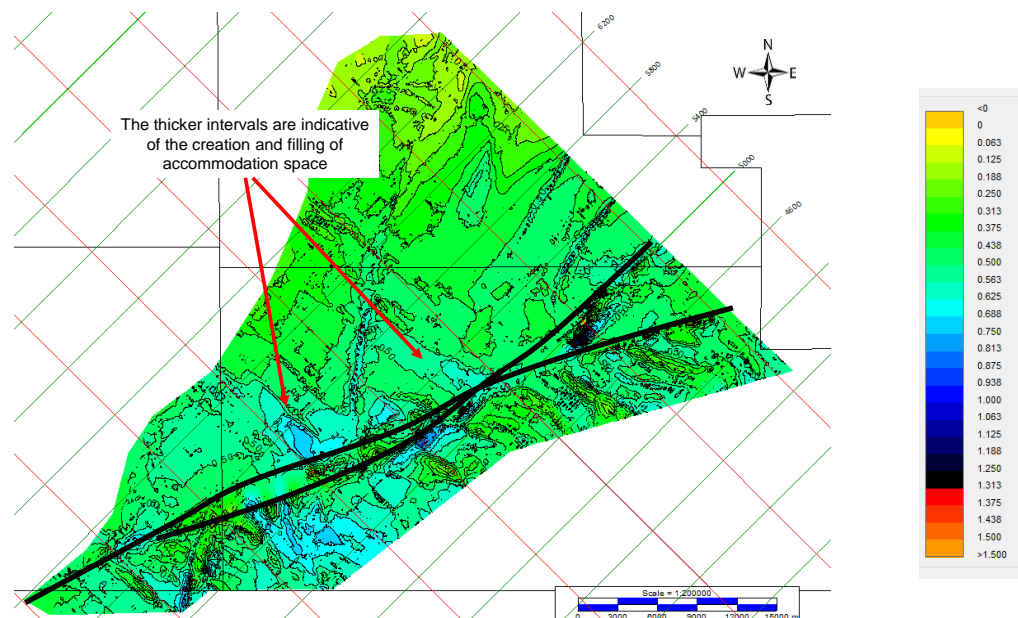


Figure 7-15: Isochrone of the interval between horizons 160 and 200.

In Figure 7-15, the thickening mapped between horizons 200 and 160 clearly indicates that accommodation space was being created during this period, by recognising the increase in the isochrones in the grabens. The isochrones that were generated for the interval between 160 and 130 – Figure 7-16, for example – does not indicate additional fault related accommodation space being present to the north of the Avon/Mahin fault zone.

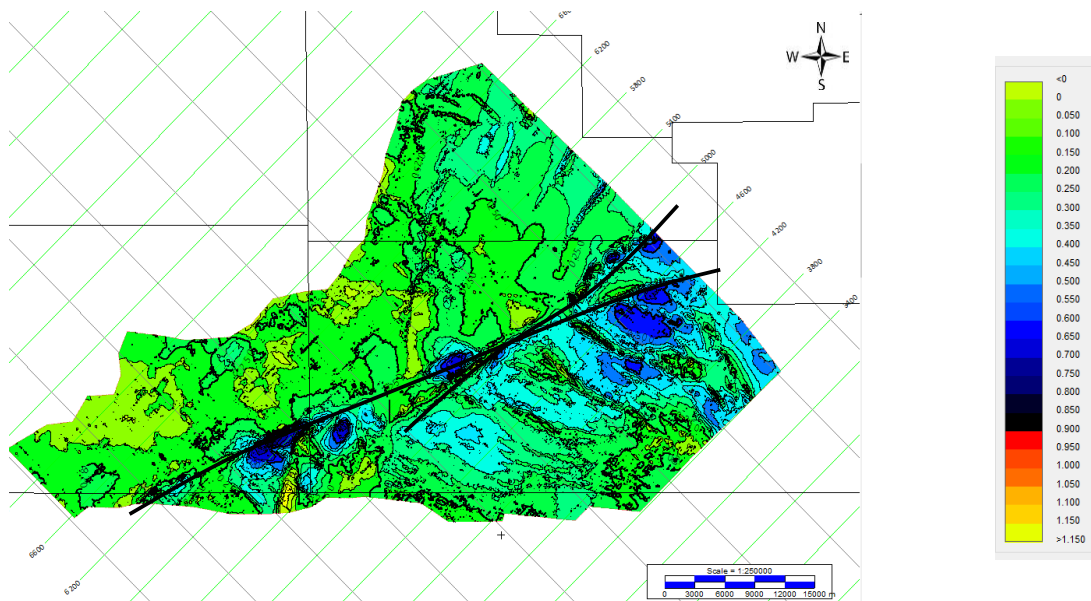


Figure 7-16: Isochrone of the interval between horizons 130 and 160.

The region to the south-east of the Avon/Mahin fault zone has been subject to greater accommodation space being created and there are also distinct zones of thickening associated with the ongoing extensional faulting.

7.3.3.1.3 Northern extensional zone

An area of large scale down to the basin normal faulting is present outside the limits of the 3D survey to the north of the study area (Morgan, 2004; Leduc et al., 2012; Maloney et al., 2012). This large-scale extensional fault zone indicates that in this region, faulting has been active from the early Cenozoic up to the present day. The faults sole out at depth, within a complex, tectonically disrupted section that overlies an undeformed Cretaceous interval. In the Maloney paper (Maloney et al. 2012), the base of the tectonically altered interval is noted as a master detachment fault. The faults in this region do appear to exhibit listric geometries, having steep fault planes in the shallow section and increasingly lower dip with depth. Listric faulting is a common deltaic characteristic (Chapple, 1978; McClay et al., 2003; Rowan et al., 2004).

This detachment “fault” can be traced into the 3D volume and is mapped as horizon 600. The extension in the thin-skinned interval that is implied from the faulting described by Maloney et al. (2012) indicates that a significant amount of accommodation space was present in the region of the 3D study.

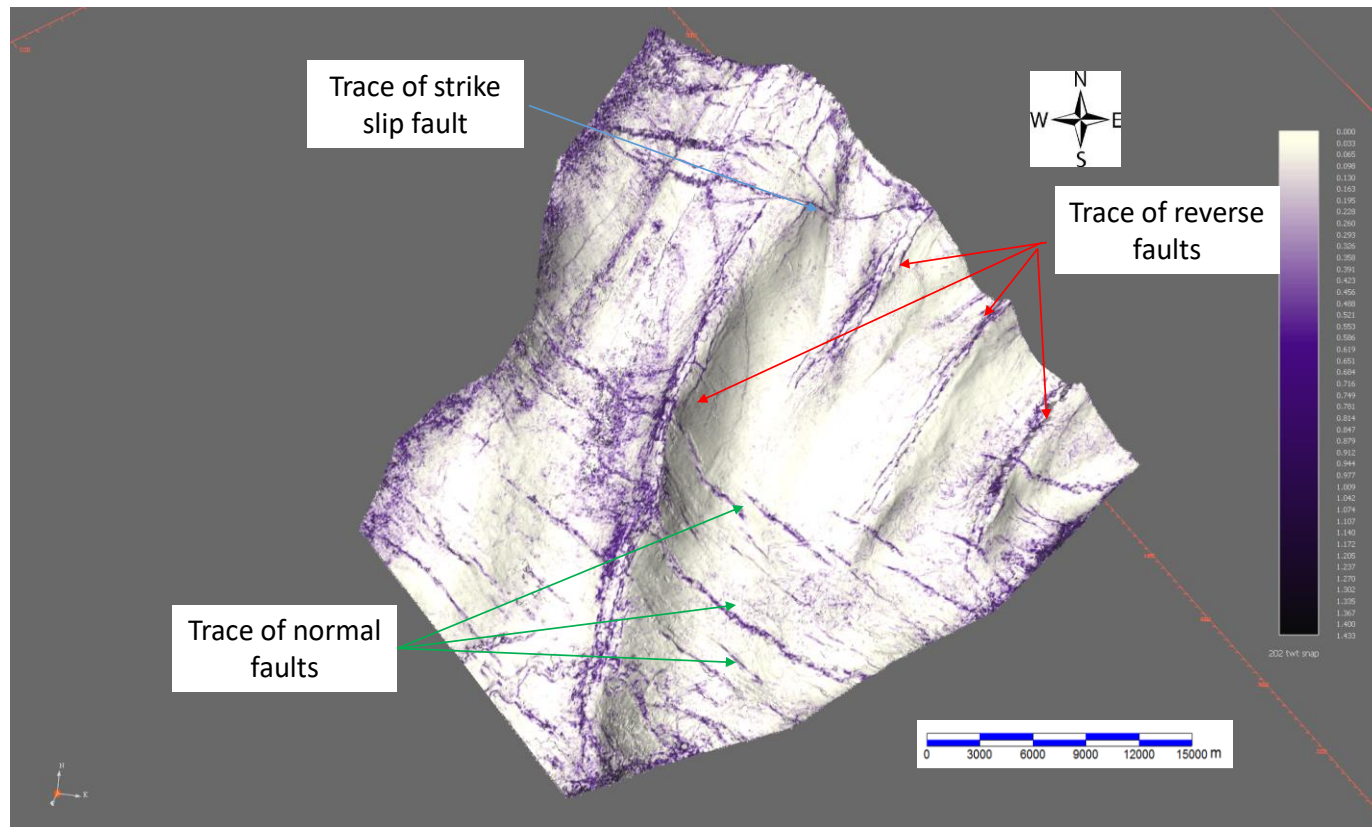


Figure 7-17: Similarity attribute extracted for horizon 202 (one loop lower than horizon 200).

7.3.3.1.4 The western region

The spatial distribution of the faults can be recognised from the similarity attribute extracted at selected horizons.

The normal faulting in this region is predominantly characterised by north-west to south-east striking faults, which are seen to tip out above the mass transport complexes described in chapter 6. The major extensional faults in the region adjacent to the Avon/Mahin fault zone are also limited vertically and in general, do not affect any horizons shallower than horizon 160. (Figure 7-27). Where later compressional activity has taken place (see chapter 6.3), a number of the faults have been reactivated and tension fractures generated.

The length of the seismically identifiable faults ranges from the order of 1km up to 10km. However, in the case of fault NW1, which is the fault with the largest lateral extent in the western region, the lateral extent prior to the onset of transcurrent movement along the Avon/Mahin fault zone is thought to be longer than the 10km seen. The vertical displacements on the larger faults lie in the region of 150ms twt or approximately 200m, assuming an interval velocity of approximately 2500 ms⁻¹. This ratio is similar to that noted by Cartwright et al. (1995).

It is observed that the faulting is not uniformly distributed in the western domain and has been modified by later compressional activity. The north of the survey area is largely devoid of normal faulting; the main deformation style in this region is late-stage folding and reverse faulting (Figure 7-17).

As noted above, the majority of the extensional faulting is found below horizon 160 in the western region. The degree of faulting with depth is such that in this western region, there is a good deal of faulting at horizon 202 (Figure 7-17), which can be seen in the similarity attribute that has been extracted at the horizon. However, the similarity attribute extracted for shallower horizons exhibits less fault activity. The other aspect of the similarity attribute extraction for horizon 202 is the strike-slip fault zone in the north and the limited amount of normal faulting in the north.

The structural configuration of the western region is characterised by a series of horsts and grabens. The synthetic (southward-hading) faults are more common, but a number of antithetic (northward-hading) faults are recognised. The amount of extension at the intersection of the synthetic and antithetic faults is minimal; the degree of lateral extension increases at shallower depths.

Fault NW 1

This fault is the largest synthetic fault in terms of both lateral extent and vertical throws measured. It is truncated to the east by the Avon/Mahin fault zone. The western tip of the fault plane coincides with the apex of thrust anticline IV. The fault throw that was measured is still significant at the point where it intersects the Avon/Mahin fault zone (Figure 7-18). In this figure, the throw measured at a number of reliably picked horizons was plotted against the mid-point depth (in two-way time) between the footwall and hanging wall cut of the horizons. The displacement of a normal fault when measured in this manner can provide insight into the nature of the fault. Idealised normal faults exhibit an elliptical shape, with the maximum strain located at the centre of the ellipse. In the case of fault NW1, the fault throw diagram indicates a broadly elliptical shape, truncated to the east by a sharp boundary. This distribution of strain is interpreted to indicate that the fault was initiated as a normal extensional one and subsequently cut by the later movement of the Avon/Mahin fault zone.

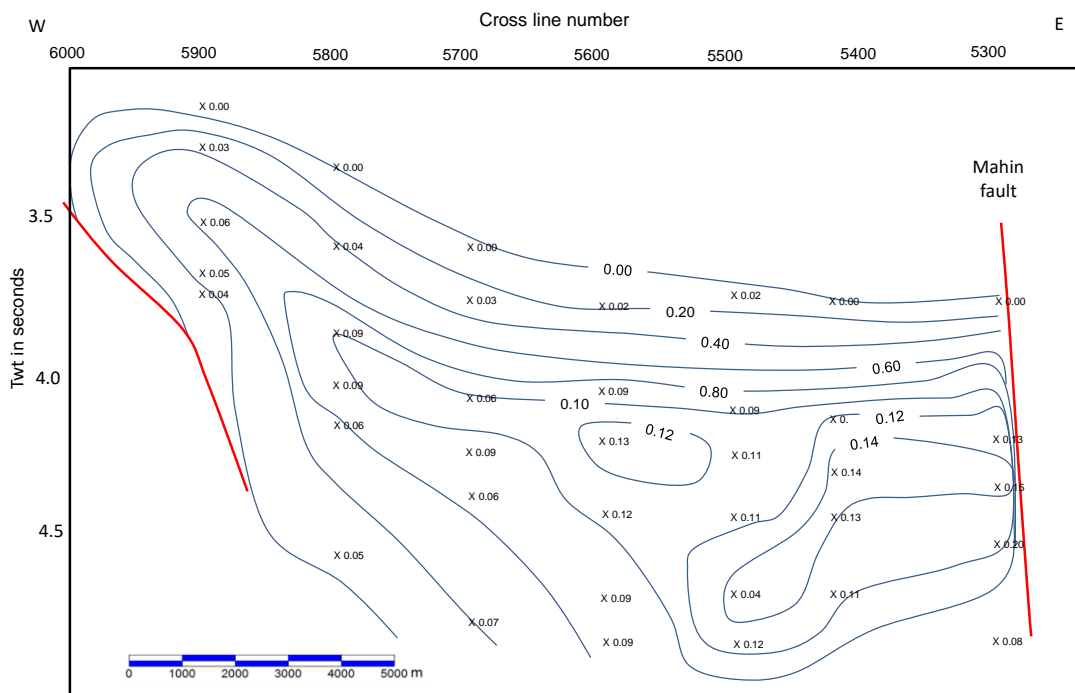


Figure 7-18: Measurement of strain along the trace of fault plane NW1.

Fault NW 9

This fault was also quantitatively studied to examine the behaviour of the displacement, both vertically and laterally. The displacement of several horizons across the fault at regular intervals along the strike of the fault plane has been measured. The accuracy of the measurements is rounded to the nearest 10ms two-way travel time. The displacements measured indicate that unsurprisingly, the throw of the fault is greatest at

the mid-point and gradually decreases laterally towards the tip point, where the fault ceases to exist. In a vertical sense, the fault tips out at or around horizon 160. This upper tip point is relatively well-constrained. The basal tip of the fault plane is interpreted to lie at a detachment layer and the maximum throw of the deepest horizon (420) is close to the basal tip. The rapid drop-off in throw at the upper tip is a characteristic of syn sedimentary faulting. In the case of this fault, the upper tip coincides with horizon 160. This supports the interpretation that the normal fault was active no later than the deposition of this horizon.

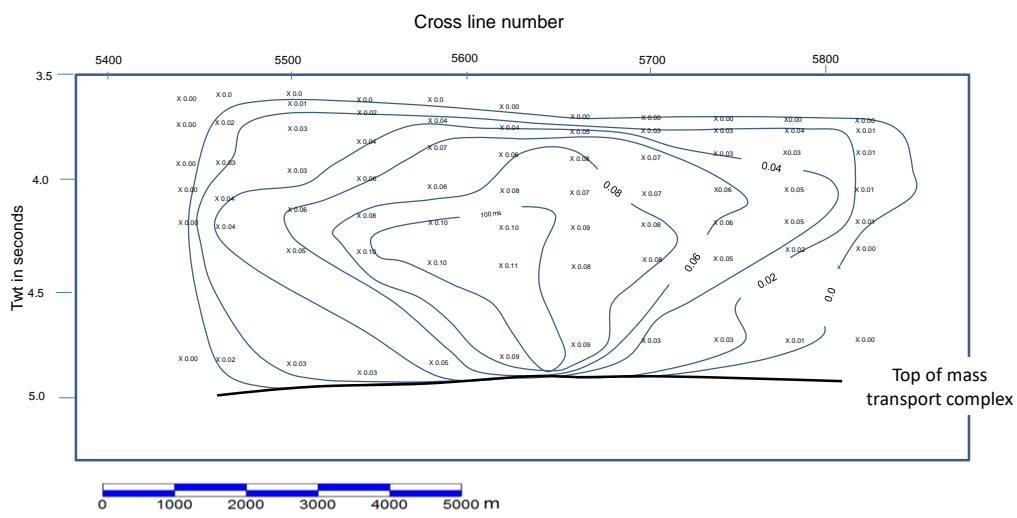


Figure 7-19: Contours of the vertical displacement vs. spatial location along the fault plane of fault NW9.

For an idealised blind normal fault, an elliptical shape points towards the fault nucleating at the centre of the ellipse, where the change in the strain is greatest. In the case of this particular fault, it appears that the maximum strain is close to the base of the fault, indicating that the fault may well have nucleated at the base and propagated vertically and horizontally from there. The basal tip of the fault is coincident with the upper surface of a mass transport deposit.

The throw of the fault in the shallower intervals indicate that the amount of displacement falls off more rapidly than the throw at depth. This again points to the fault not being a typical blind normal fault. It may indicate that the fall-off in the throw was less than currently mapped, but if the fault was active at the seabed, then the amount of throw

would have been diminished due to there being insufficient overburden to accommodate the extension at the sea bed.

7.3.3.1.5 The eastern region

To the east of the Avon/Mahin fault zone, the faulting is much more intensive. The faults also tip out at the detachment layer. They do, however, affect horizons up to the present day. The similarity attribute extracted from horizon 160 (Figure 7-26) shows the intensity of faulting to the east of the Avon/Mahin fault zone, when compared to the west.

The faulting appears to be grouped into a number of deep-seated grabens. Unlike the extension observed in the northern region, the amount of lateral extension calculated for the eastern region is much larger than that observed to the west of the Avon/Mahin fault zone. The fault pattern that has been identified in the eastern half of the survey is characterised by apparent fanning of the strike of the faults from north-west to south-east at the northern margin of the survey to a more west-to-east strike direction at the southern margin of the survey area. This is interpreted to be the result of an apparent rotation of the eastern region that has occurred as a result of the dextral movement of the Avon/Mahin fault zone.

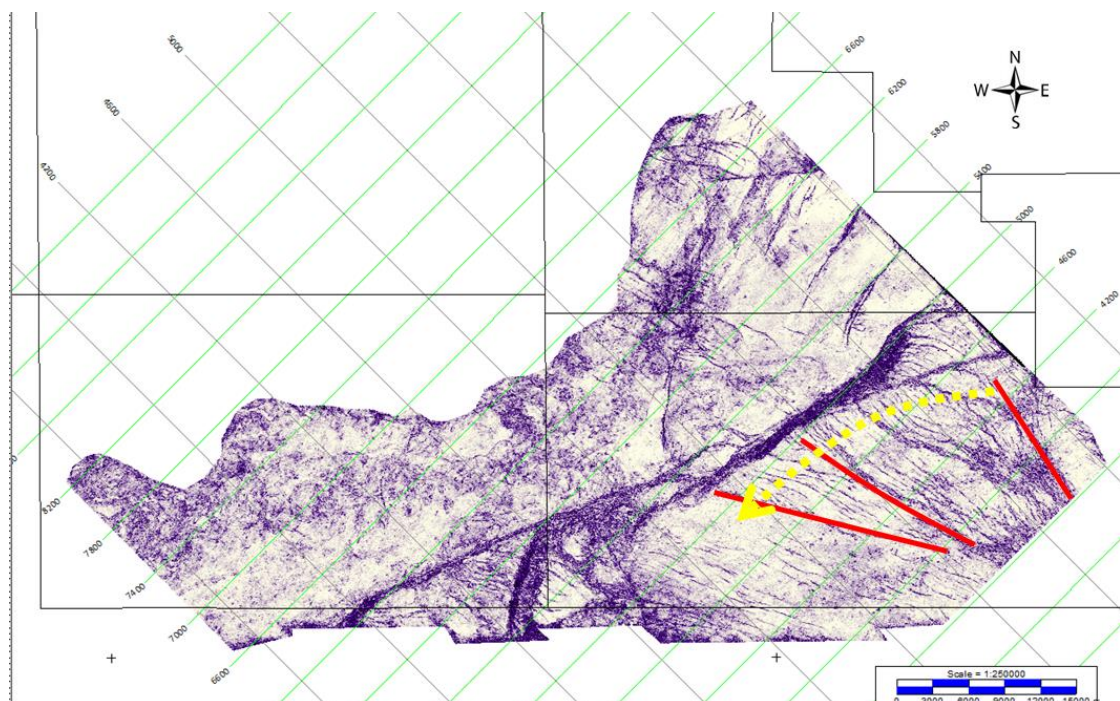


Figure 7-20: Similarity attribute extracted at horizon 160.

In Figure 7-20, the strikes of the major faults are highlighted in red. The variation in strike can be seen to rotate, as indicated by the yellow arrow. This rotation is interpreted to have arisen as a result of the right lateral movement of the eastern region.

The Avon/Mahin fault zone, which is discussed in more detail in section 7.3.7.2, is interpreted to be a dextral strike-slip fault zone. Using this assumption, fault NW1, which is described above, is interpreted to have been displaced laterally. The displacement that has been estimated from the restoration of the isochrones of the interval between horizon 160 and 200 places the severed portion of this fault some 6.2km south-west of the intersection with the Avon/Mahin fault zone. The synthetic fault that is found at this offset has been modified by late stage inversion. In addition, there is significant offset of horizon 160 on this side of the fault zone.

A plot of the throw of horizon 200 along the combined halves of the fault shows that the throw is larger on the eastern half of the fault zone. However, if the throw observed at horizon 160 is subtracted from the throw measured at horizon 200, the displacement is seen to tip out in a manner that suggests that the fault may have been a normal fault with the behaviour expected of a normal fault in the distribution of strain, subsequently reactivated during the interval between horizons 160 and 200. The apparent throw of the fault (the green line in Figure 7-21) is the net throw at horizon 200 after the throw at horizon 160 is removed.

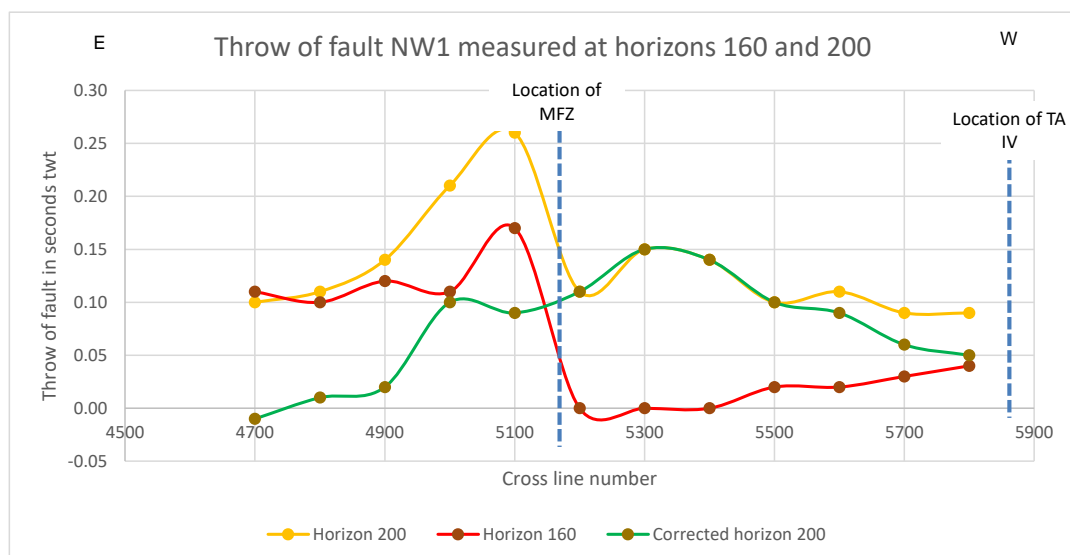


Figure 7-21: Plot of the throw of horizons 160 and 200 along fault NW1

In Figure 7-22, two seismic lines on either side of the Avon/Mahin fault zone are displayed. The fault highlighted in black is interpreted to be fault NW 1; the right-hand image, located to the east of the Avon/Mahin lineament, is seen to have additional section between horizons 160 and 200 (highlighted in yellow), when compared to the left-hand image. It is also seen to have been active at least up until the deposition of horizon 130. For the two red faults to be fault NW 1, a right lateral displacement of approximately 5.2km is required to match the two halves. This is in line with the observations made in section 7.3.7.

The two lines in this display are located on either side of the Mahin fault zone. The fault highlighted in the left-hand image, taken from the western side of the Mahin fault, does not displace horizon 160. The fault in the right hand side image, taken from the eastern side of the Mahin fault, does displace horizon 160.

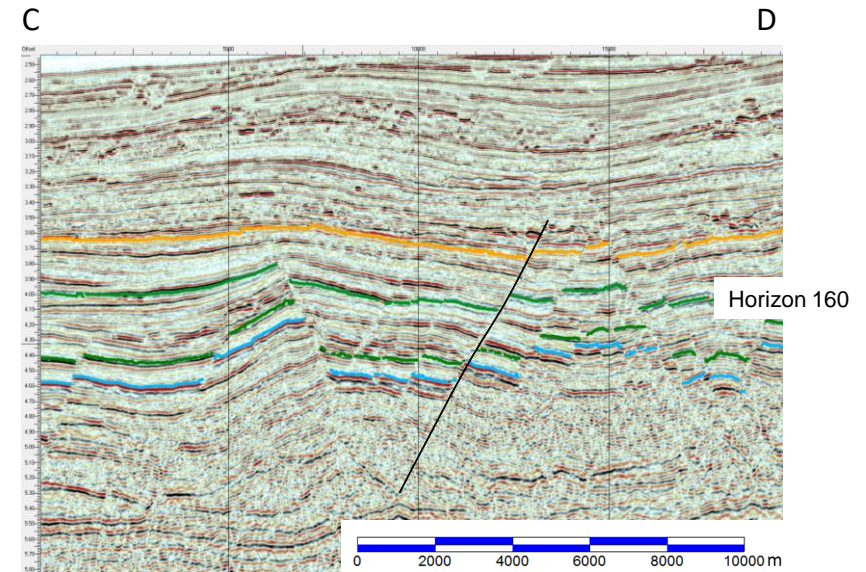
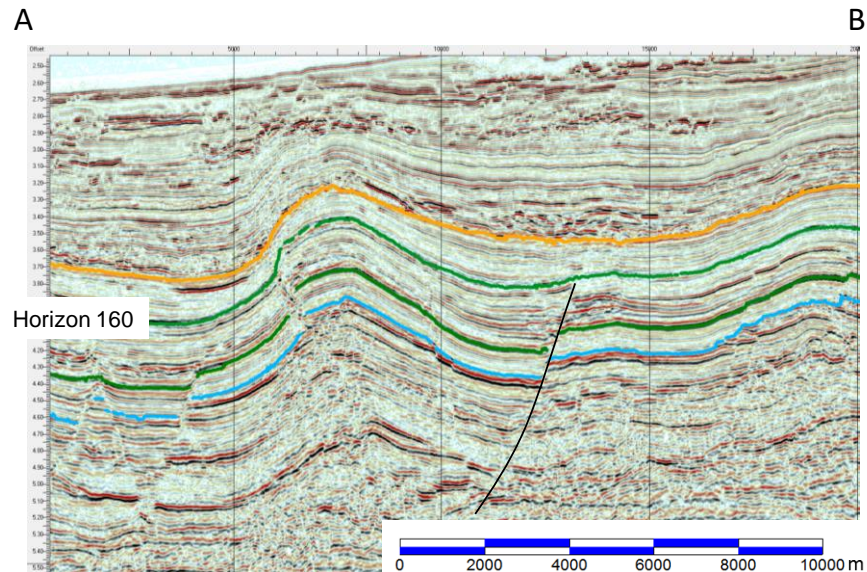
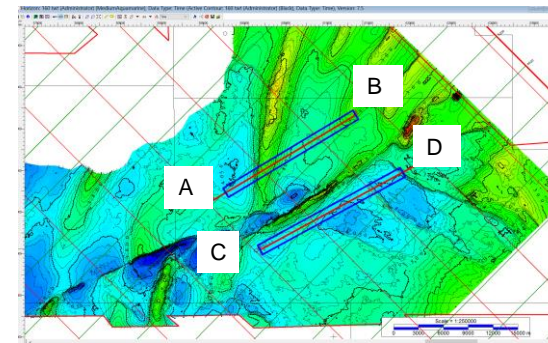


Figure 7-22: Fault NW 1, as it appears on either side of the Avon/Mahin fault zone.

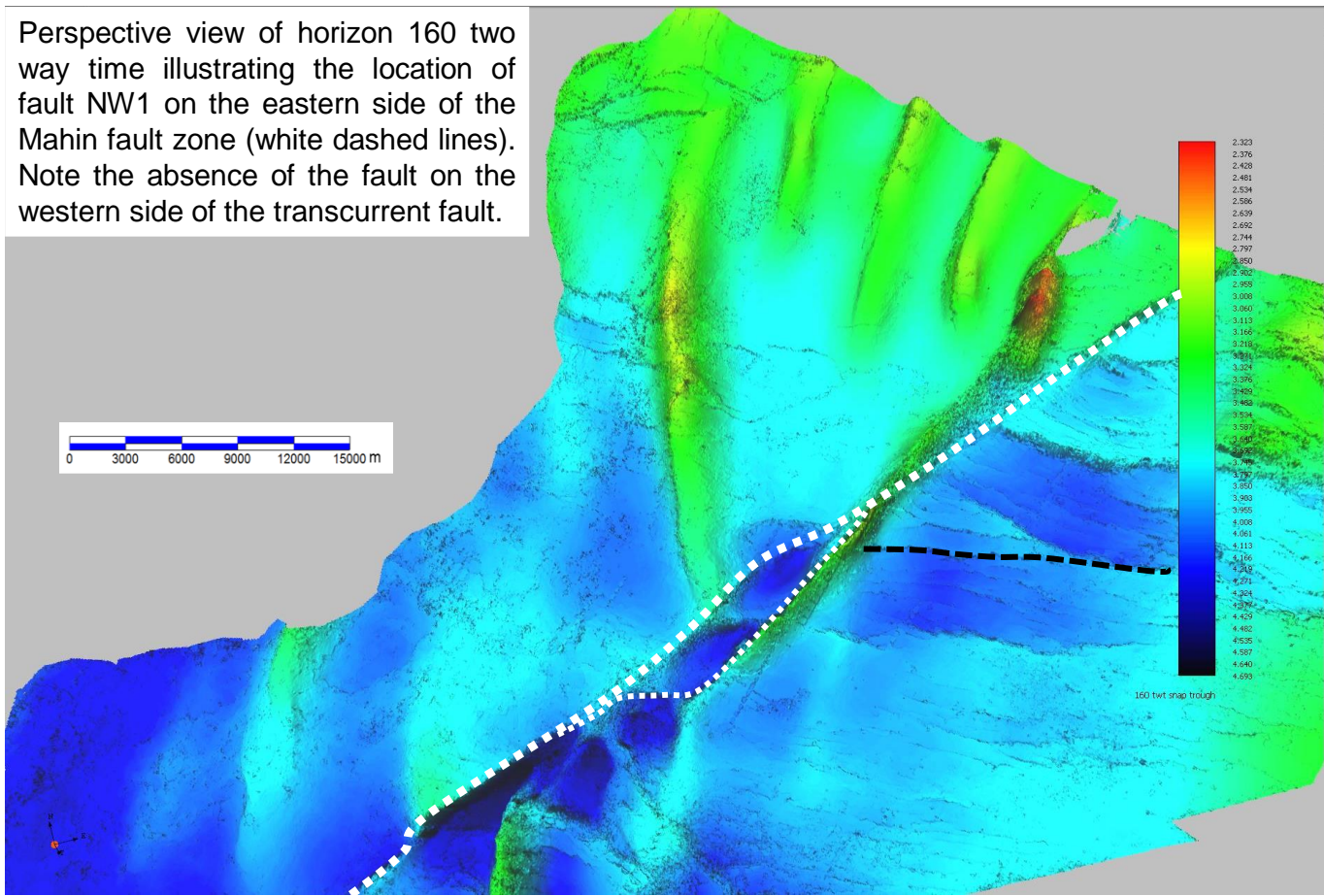


Figure 7-23: Horizon 160 twt surface showing the location of fault NW1.

Composite surface showing the location of fault NW1 (dashed black lines) on either side of the Mahin fault zone. The surface to the west of the strike-slip fault zone is horizon 200, that to the east is the younger horizon 160.

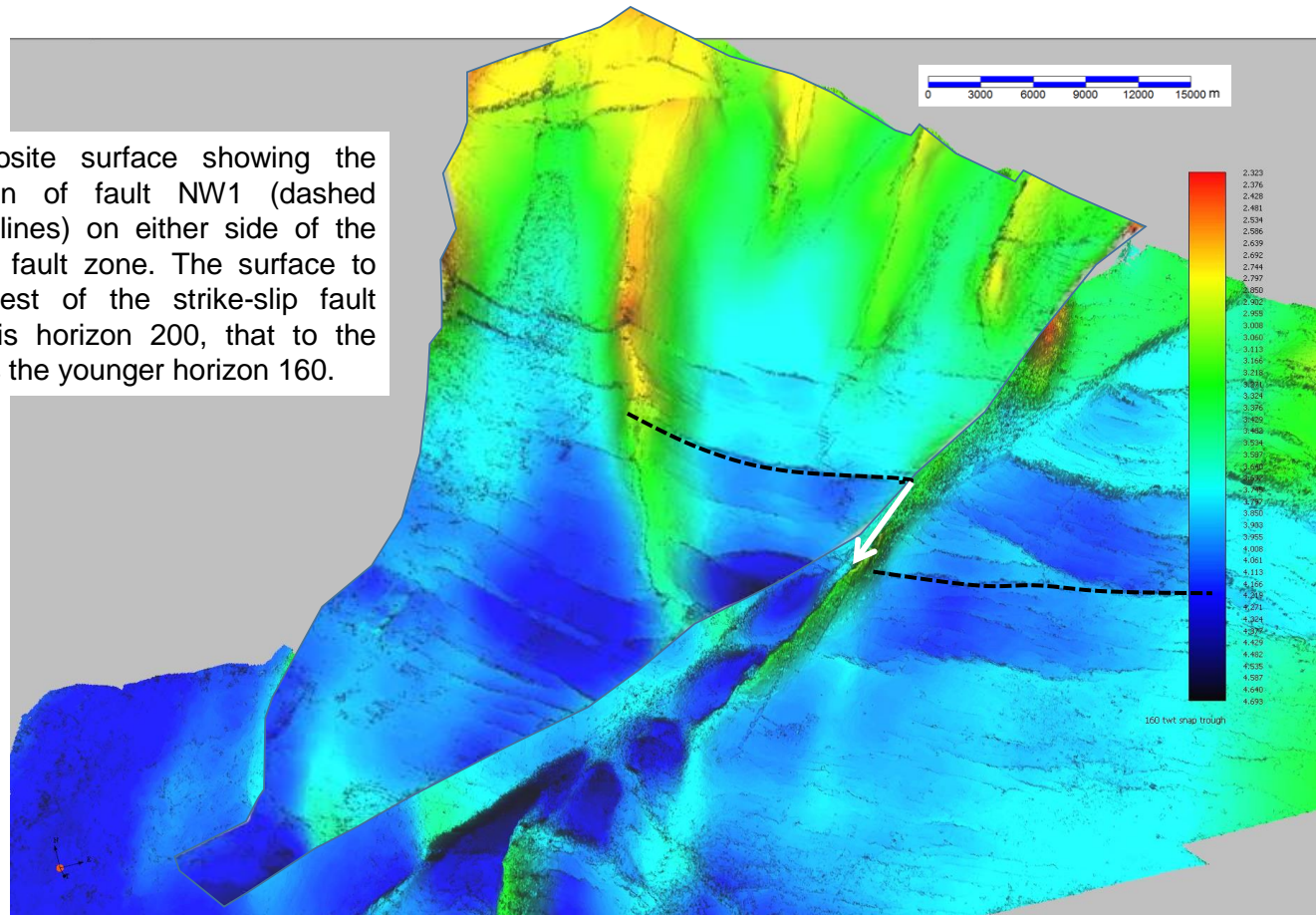


Figure 7-24: Perspective view of a composite horizon showing the location of fault NW1 on either side of the Mahin fault.

Assuming that lateral movement has taken place, then the pre-existing fault to the west will have been displaced by later dextral strike-slip motion.

A relative movement of the two surfaces along the fault zone by 7km leads to the alignment of the fault.

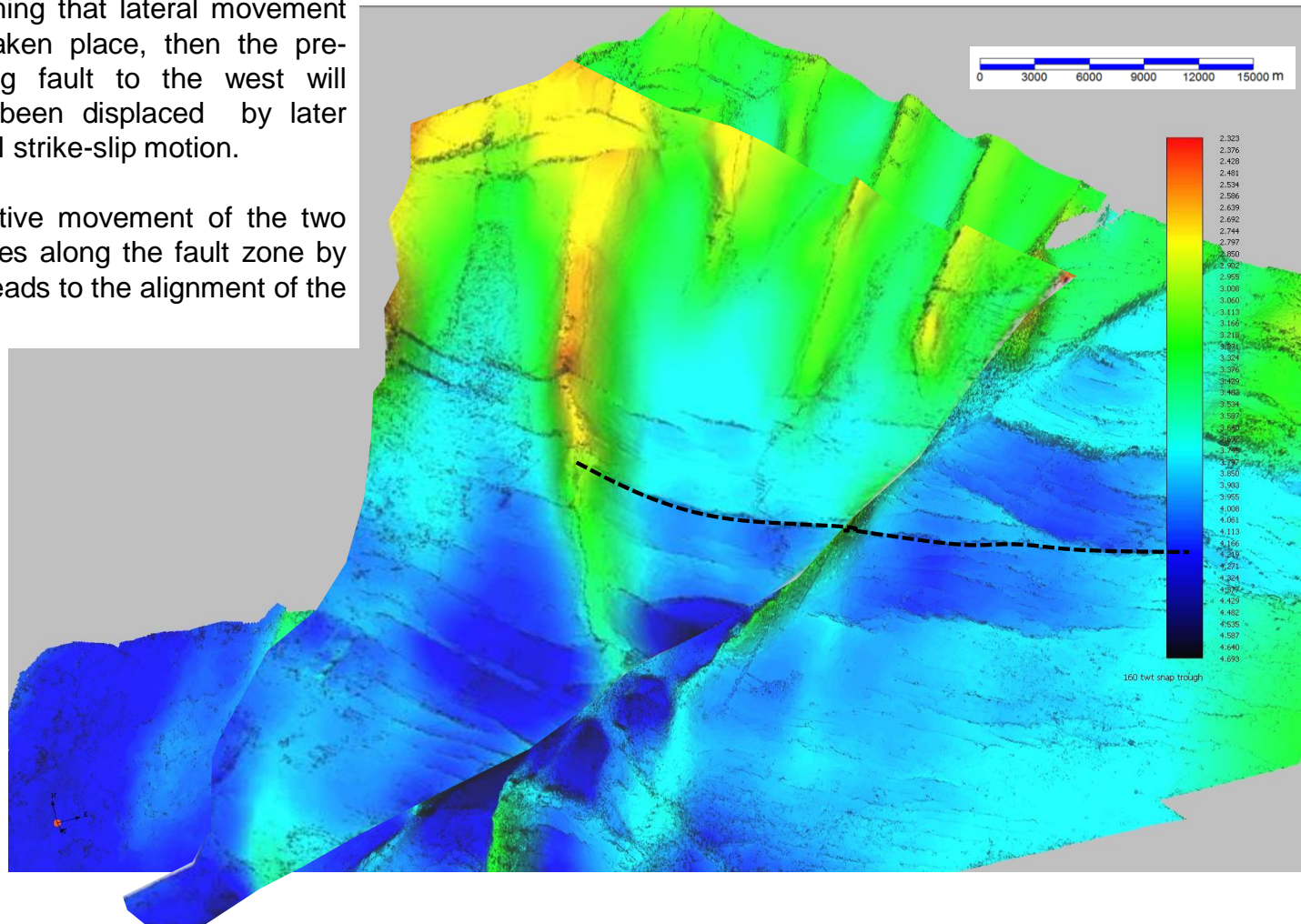


Figure 7-25: Illustration of the lateral displacement of fault NW1.

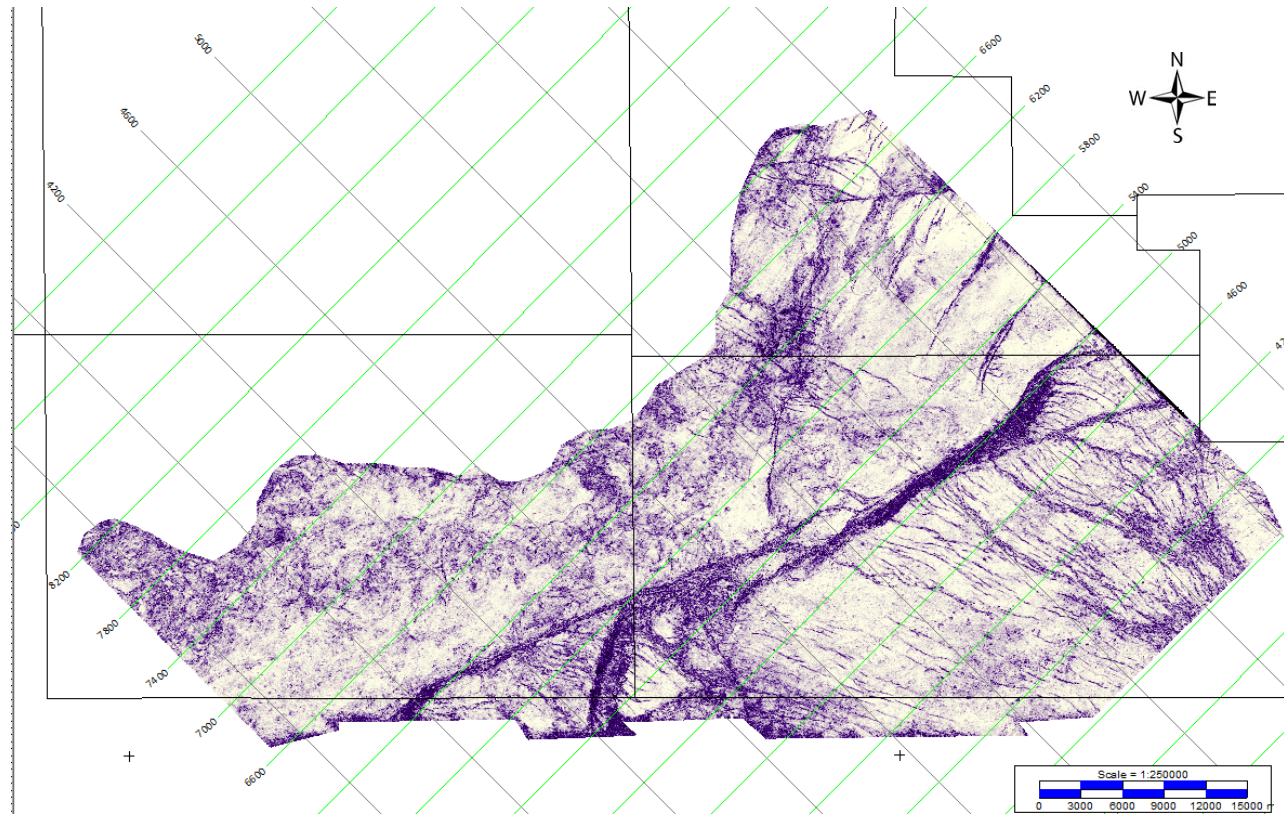


Figure 7-26: Similarity attribute extracted at horizon 160.

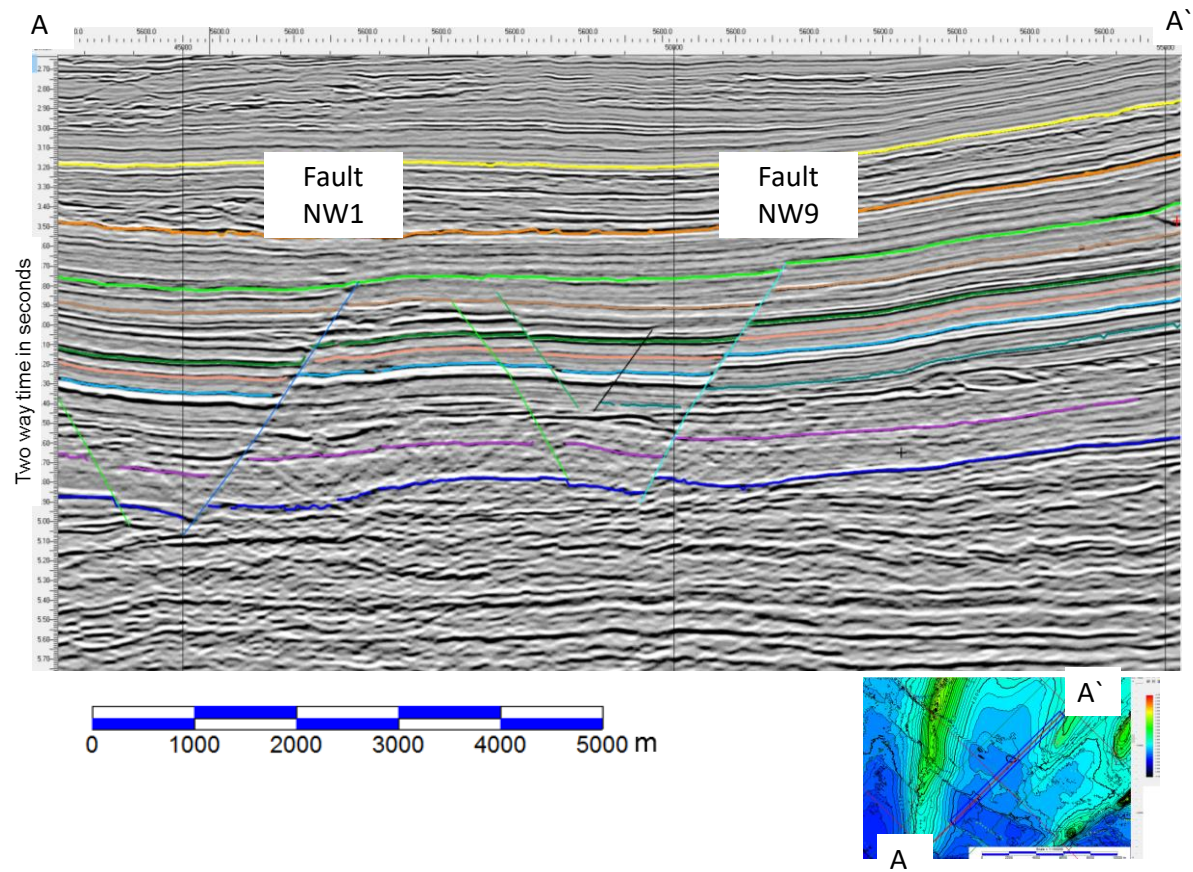


Figure 7-27: Cross line 5700 with the two faults referred to in the text highlighted.

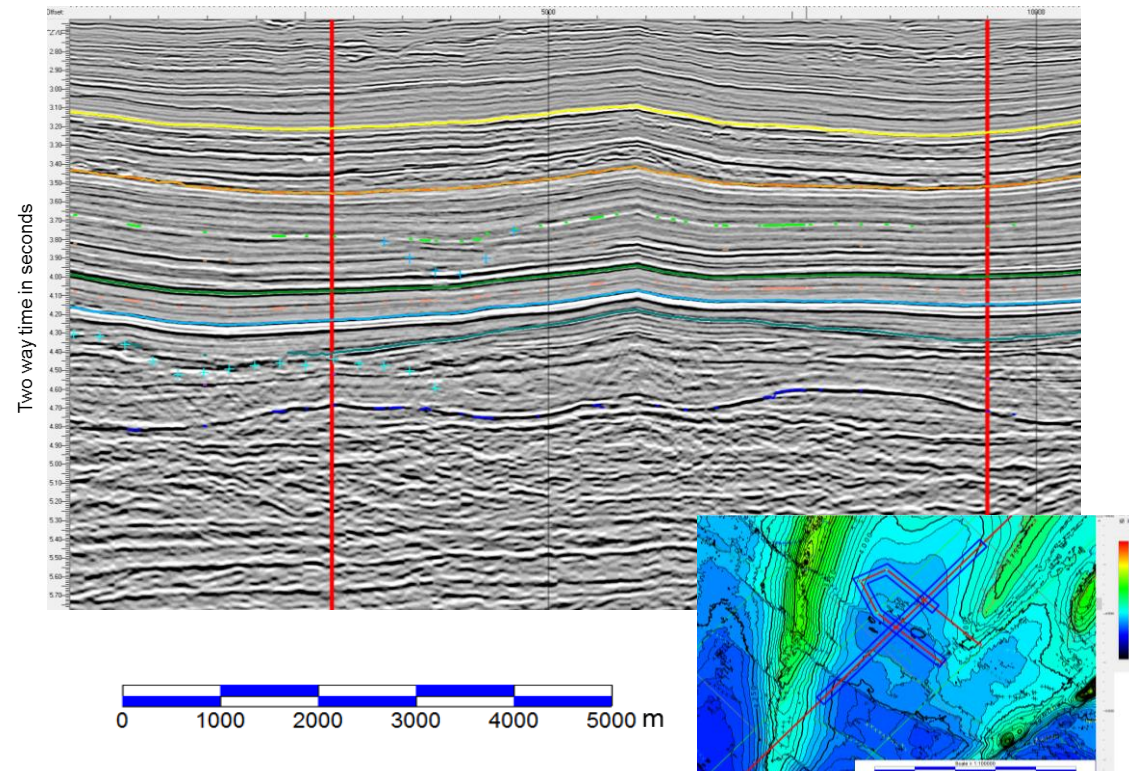


Figure 7-28: Random traverse around the tip of fault NW9 showing the continuity of the events from the footwall to the hanging wall.

7.3.4 Compression

Compressional faulting

Within the study, there are a number of number of thrust anticlines that have been formed as a result of compressional stress. The mapping of shallow horizons clearly identifies the location of these structures; the imaging in the core of the anticlines varies between each of the structures, making the detailed mapping of the internal deformation unreliable for the majority of the anticlines. The best-imaged anticlines are in the north of the 3D survey area (Figure 7-29). These have been studied in some detail and the results of the analysis will be presented in this chapter.

There are three categories of compressional deformation recognised in the western half of the survey, which lies to the west of the Avon/Mahin fault zone. The internal faulting within anticlines TA I-III is characterised by modest amounts of faulting, having between four and ten significant reverse faults cutting through the axis of the structures. Anticline TA IV, however, displays a more complex degree of faulting; the reverse faults are found to be shorter in lateral extent within the core, but there is also a complex fault pattern recognised within the shallow horizons that is not evident elsewhere.

The two westerly anticlines TA V and VI differ again in the internal structuration; the faulting within these structures resembles a saw-tooth pattern when viewed in a vertical cross section.

7.3.4.1 TA I to TA III

These three elongate structures lie between; in the east the Avon/Mahin fault zone and to the west, a fault zone that is interpreted to be a tear fault zone SS A. The style of faulting is interpreted to be the result of fault propagation (Mitra, 2002; Twiss and Moores, 2007). The faults identified in the seismic are most likely complex fault zones, but the resolution that is an inherent limit of the data does not allow the detail to be seen. The fault throw analysis in this section is based upon the visible faults being a single fault.

The three labelled TA – I, II, and III – exhibit similar structural styles of deformation. The three anticlines are asymmetric, with the western flanks being steeper than the eastern flanks. They are cored by reverse/thrust faults, which in general verge towards the west (Figure 7-29). It is not possible to determine the lateral extent of TA I and II because the 3D survey does not cover the northern termination of these two structures. Mapping of the reverse/thrust fault throws of several faults within these anticlines was carried out to understand the lateral and vertical variability of displacement.

7.3.4.1.1 Thrusted anticline I (TA I)

TA I is comprised of an elongate ridge that extends in a north-south direction for over 15km. The northern limit is not covered by the 3D volume. It is interpreted that the anticline terminates at the intersection with the extension of strike-slip fault SS A beyond the limit of the data. The shallow interval, between seabed and horizon 200, is well-imaged. Within this interval, there are a series of en echelon reverse faults, which verge to the west. The variation in the throws on the two faults (RA1 and RA3) was measured for horizons 160 and 200 and plotted in Figure 7-31 and Figure 7-32. The vertical displacement measured in two-travel time (which is considered to be representative of the depth in meters assuming an interval velocity in the region of 200 ms^{-1}) along the fault is plotted against the inline position of the fault plane. The distance between the plotted points is 375m.

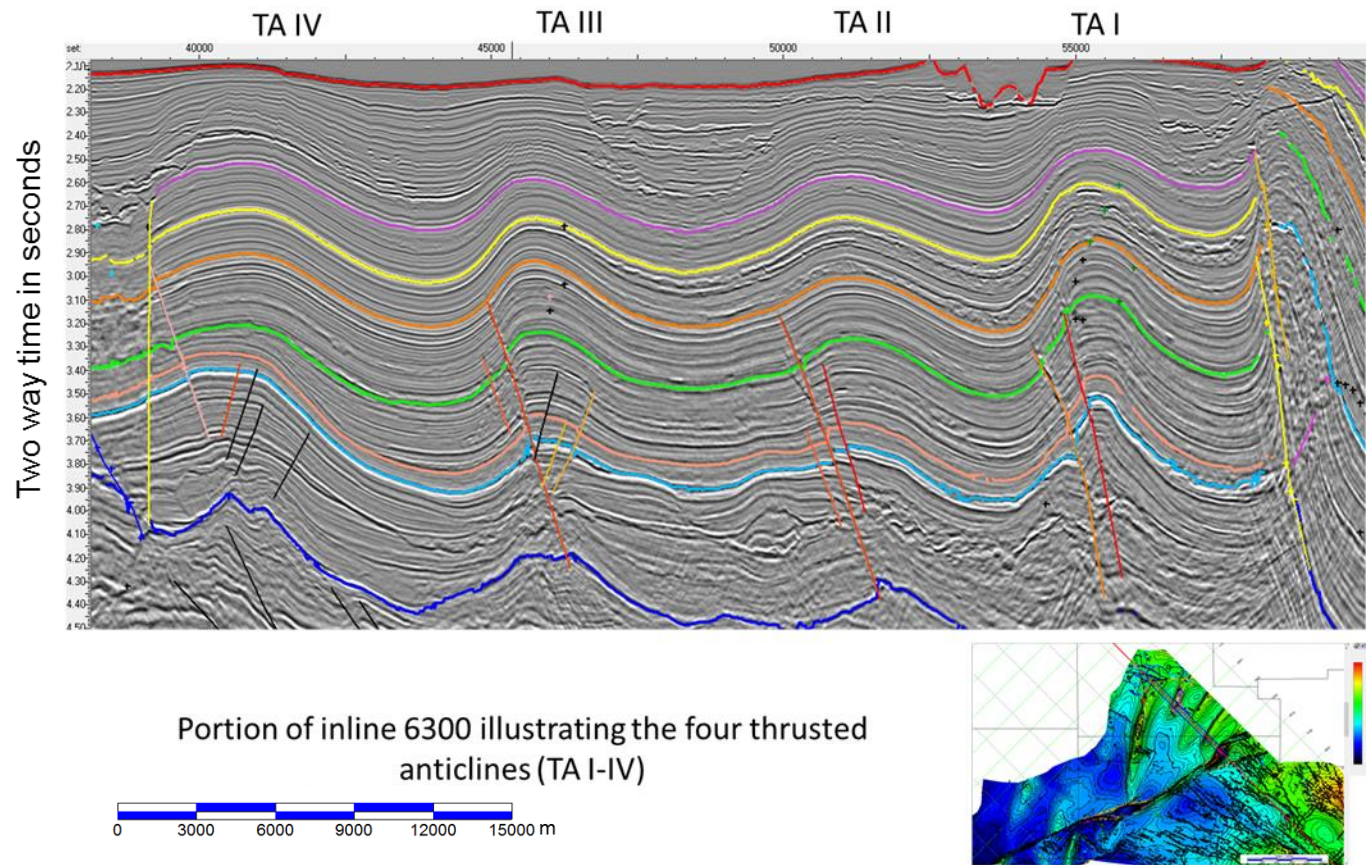


Figure 7-29: Inline 6300 which illustrates the four thrust anticlines noted in the northern region.

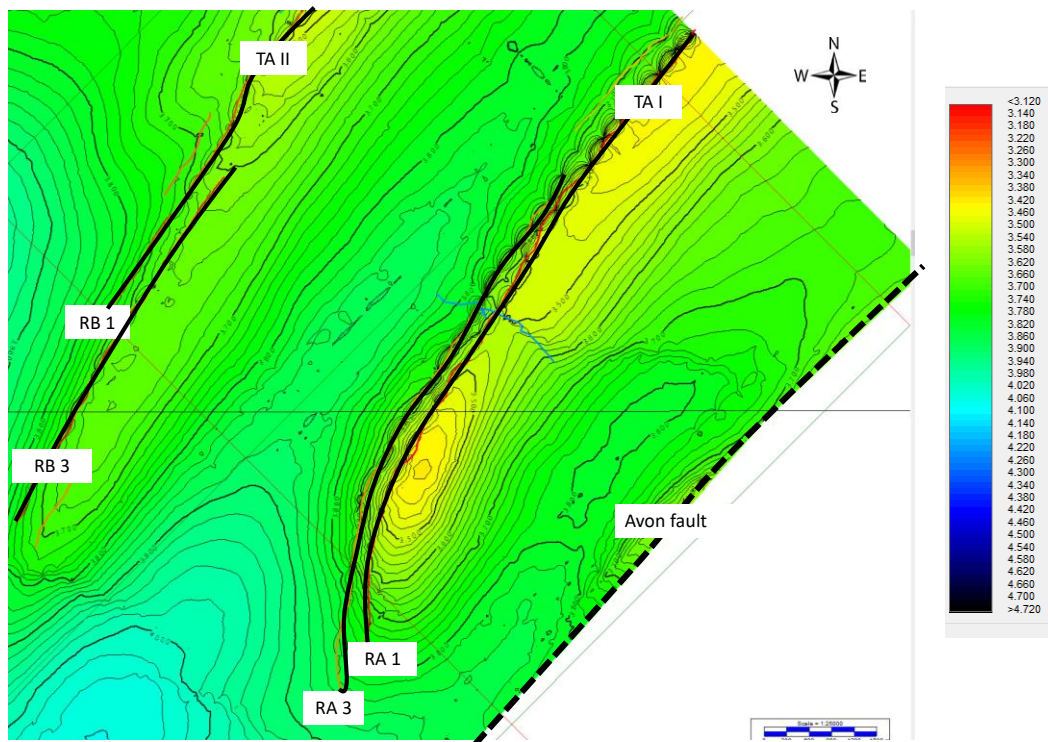


Figure 7-30: Twt map of horizon 191, showing the location of the named faults.

The average rate of fault throw growth is 30m/km for the southern part of fault RA1.

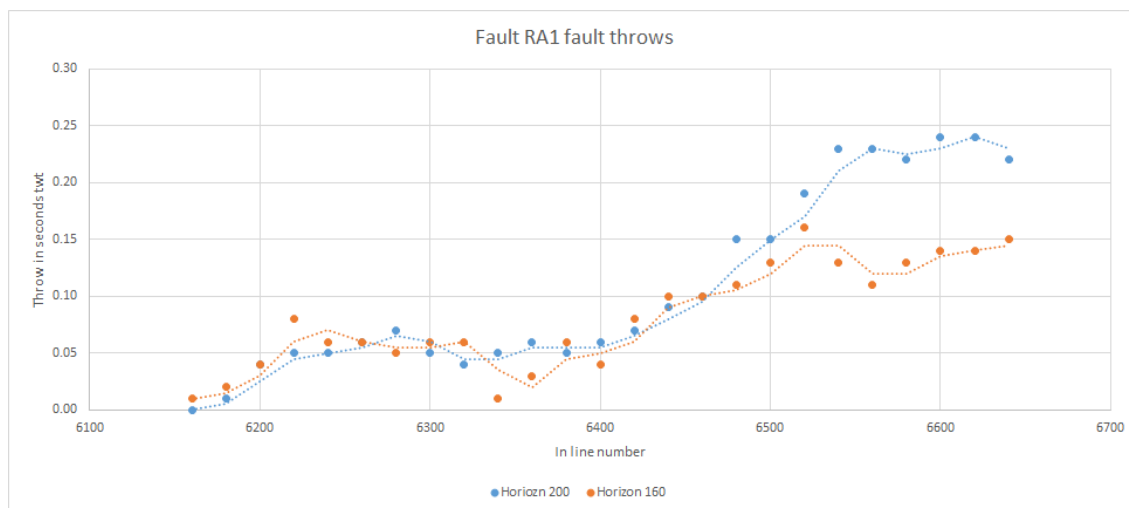


Figure 7-31: Plot of fault throw at horizons 160 and 200 along fault RA1.

There is a marked change in the displacement noted at around inline number 6380; this coincides with the presence of a north-west to south-east-striking normal fault. The normal fault is interpreted to have predated the compression; however, it may be that the presence of this pre-existing fault acted as a tear fault.

Fault RA3 is contained within the 3D survey and therefore the lateral extent of the fault can be captured in the analysis. A characteristic of the fault is the asymmetric distribution of vertical displacement; the throw grows from its southern tip at line 6140 to the maximum throw of 120ms at line 6420 – a distance of 5.25km – whereas the throw decreases to the northern tip at line 6500, a distance of 1.5km. The rate of fault growth is 22m/km for the southern half of the fault, whereas the northern portion of the fault has a gradient of 80m/km. This uneven throw along the fault is similar to that identified by Butler et al. (2009). This may indicate that the fault moves episodically, with growth unevenly distributed as a result.

Unlike extensional faults, the throws do not follow a predictable pattern because there are variations in the dips of both the footwall and hanging wall and in the relay ramps that lie between adjacent fault planes.

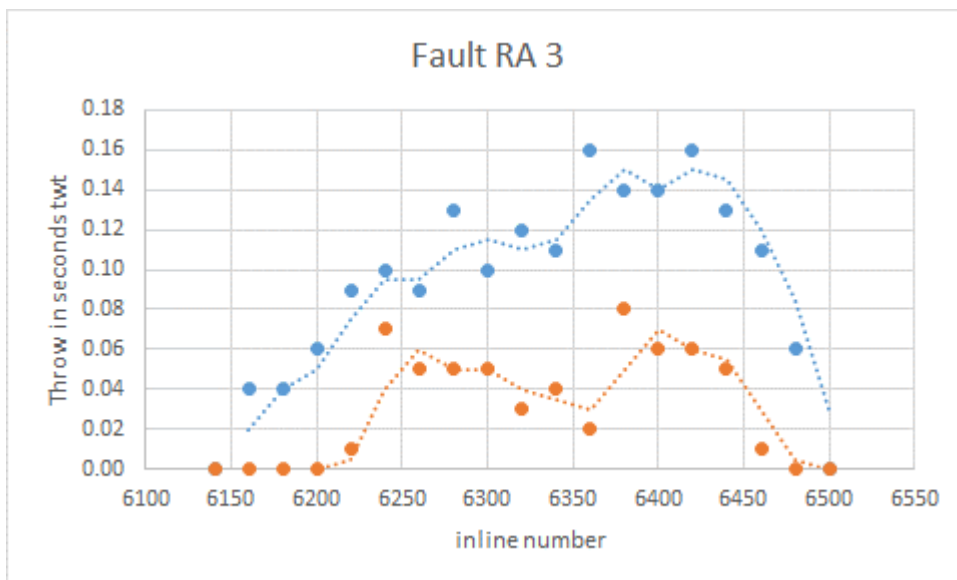


Figure 7-32: Plot of throw of horizons 160 and 200 along the fault plane of RA3.

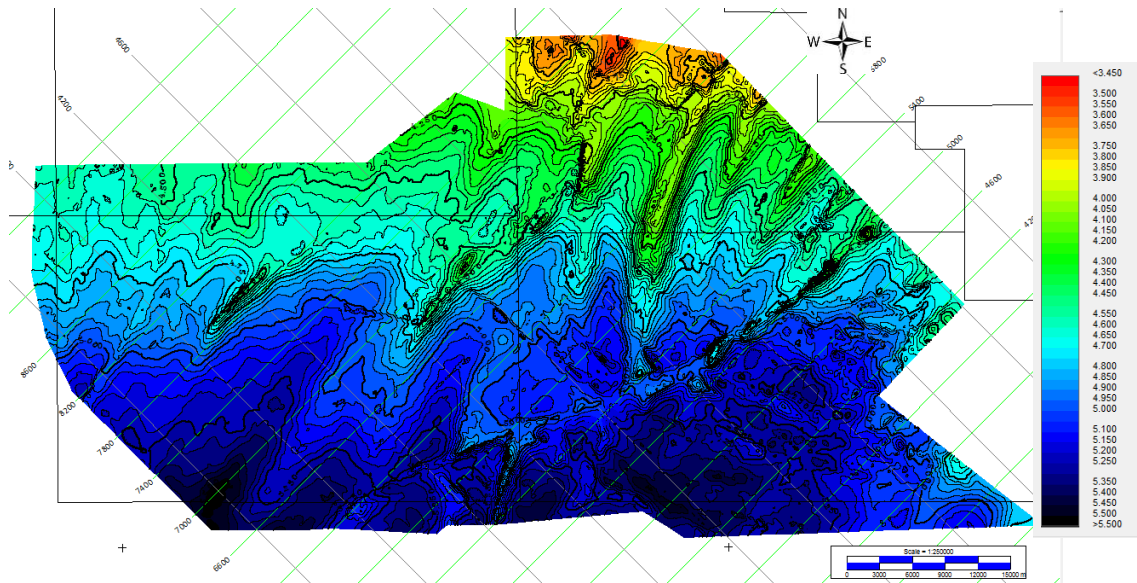


Figure 7-33: Twt map of horizon 420.

The deeper portion of the structure is poorly imaged, in part because below horizon 200 and above horizon 420, the section is largely composed of earlier disturbed sediments. The interval is interpreted to be primarily formed by the deposition of mass transport deposits from the north.

A structure map of horizon 420 (Figure 7-33) illustrates the presence of a number of north-south-trending ridges. The apex of the ridges coincide with the root of the reverse faults that are present in the shallower section. The imaging within these ridges is fair to poor. As a consequence, it is not possible to map in detail the internal structure of these deeper anticlines. There is evidence, however, of compressional faulting in the regions where the imaging is of a reasonable quality.

7.3.4.1.2 Thrusted Anticline II (TA II)

Three faults were examined within TA II. The three faults are parallel and arranged in an en-echelon manner.

Fault RB 1 is not captured completely within the 3D volume, hence it is not possible to define the fall-off in throw for this fault, but what portion of the fault there is has been

analysed.

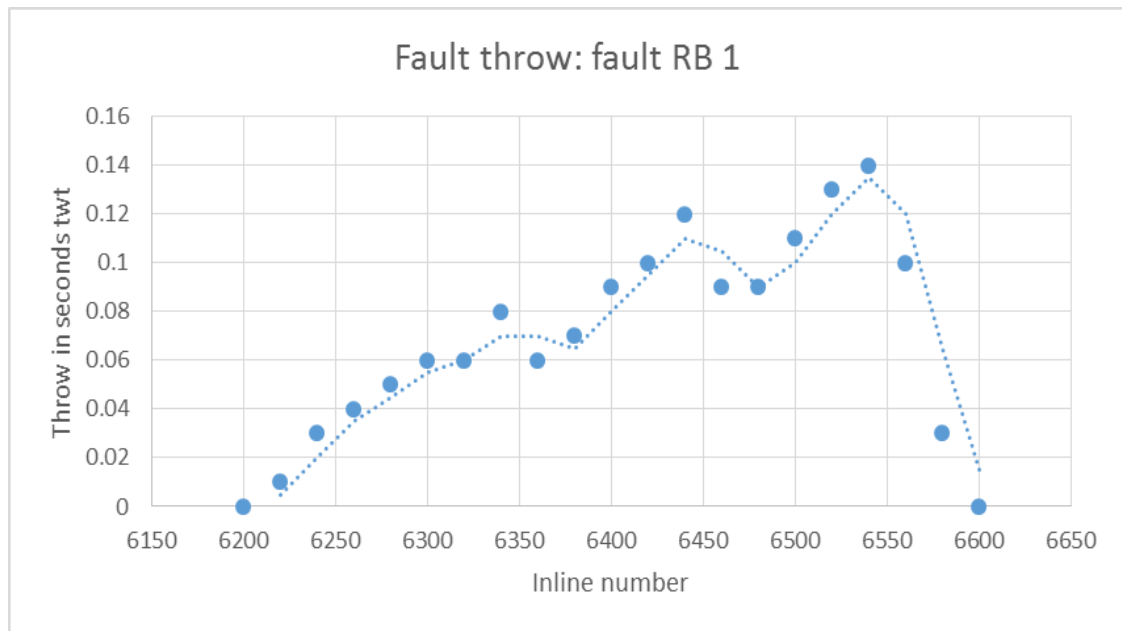


Figure 7-34: Fault throw measured along RB1.

As an additional check that the fault had been interpreted in a consistent manner, fault plane maps were created, which indicate that the fault planes are linear and planar in nature. There is no evidence of major bends or kinks in the fault planes. The dip of the fault plane was calculated by measuring the vertical and horizontal components of the mapped surface. In the case of fault RB1, the dip of the fault is in the region of 30 degrees.

However, the lateral throw variation for fault RB 2 is asymmetric, with the throw increasing in a relatively consistent manner from south to north, but the northern end of the fault displays a rapid fall-off in throw. This asymmetry is assumed to be the result of the change in the forelimb of the hanging wall block. In the south, the amplitude of the fold in the hanging wall is less than in the north. In the north, the rapid drop-off in throw is accommodated by an increase in dip of the fore limb.

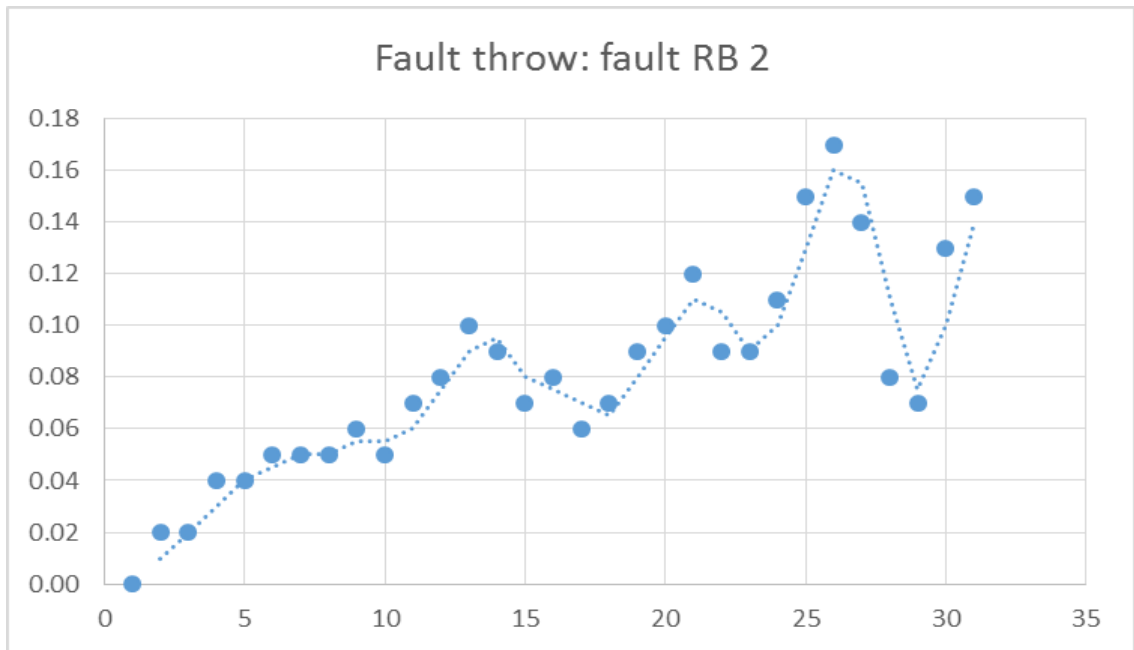


Figure 7-35: Fault throw measured along fault RB2.

In addition, the variations along strike in the amount of throw can be accounted for by the degree of westward motion of the hanging wall.

For fault RB3, the throw exhibits a similar pattern to that found in normal faults, with a relatively uniform increase in throw from the tip to the centre.

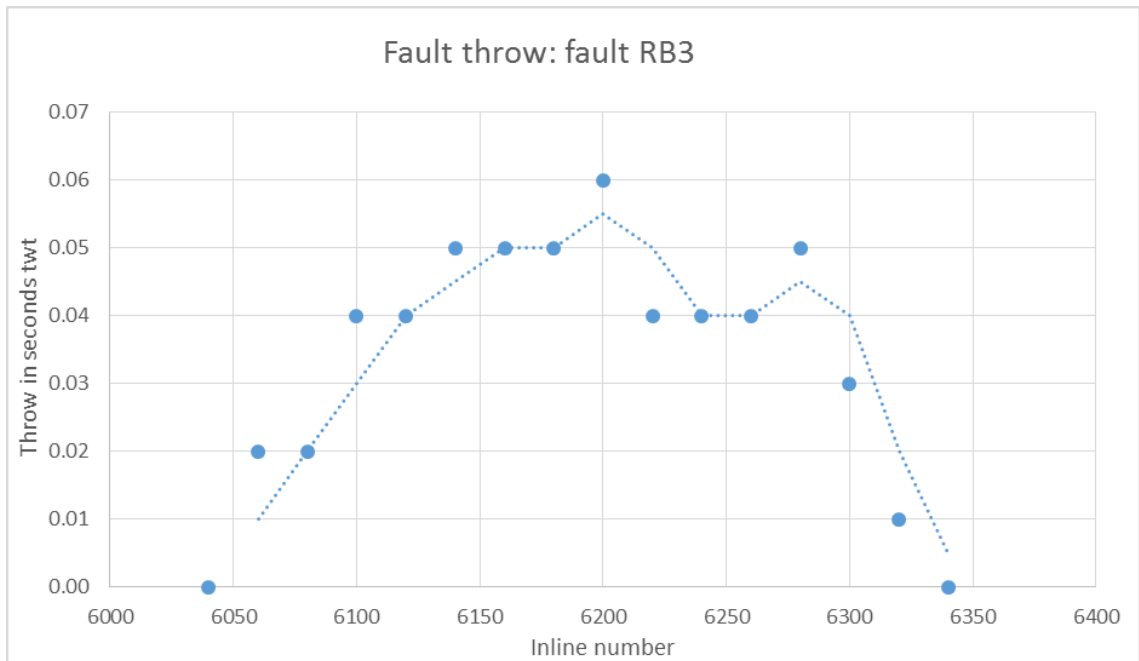


Figure 7-36: Fault throw measured along fault FB3.

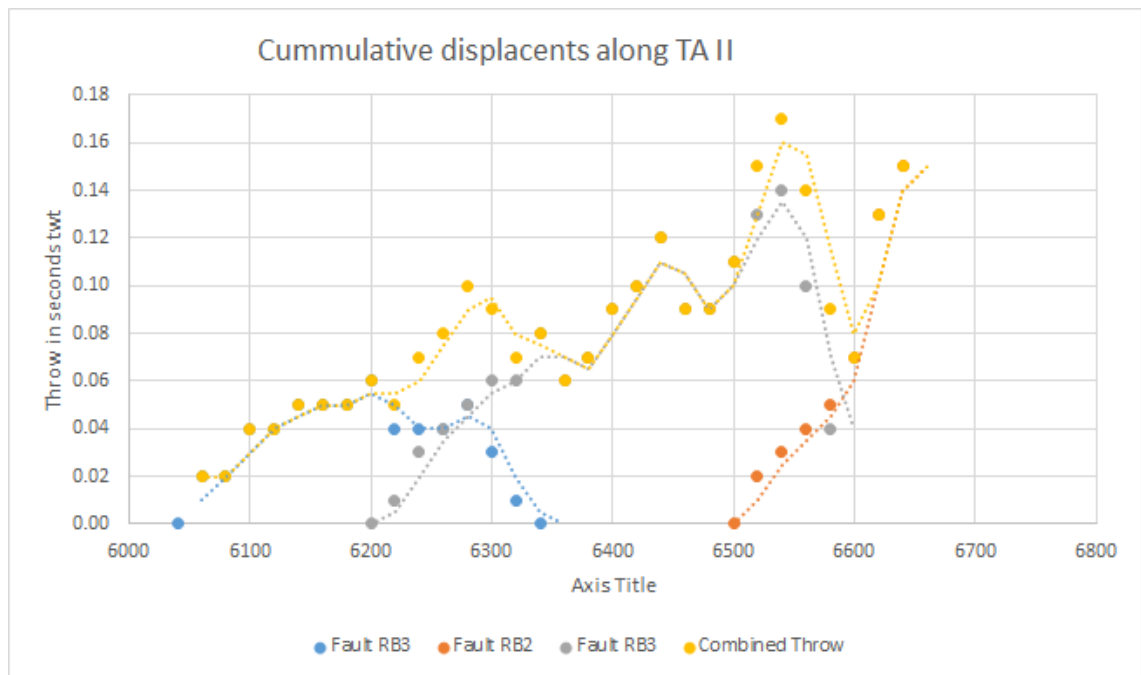


Figure 7-37: Fault throws for three faults within TA II, including the combined displacement of the three faults.

7.3.4.1.3 TA III

TA III is the smallest of the three, being approximately 10km from north to south. It terminates against the strike-slip fault zone that is present in the north of the survey area (SS A). TA III is comprised of two culminations.

7.3.4.2 TA IV

The largest of the four northern anticlines, in the lateral extent, is TA IV, which is the western-most of the mapped features. It is approximately 25km in length, from north to south. It terminates in the north at fault SS A and in the south at the Avon/Mahin fault zone (Figure 7-38). The vertical amplitude of this feature is approximately 600 ms twt. Unlike the other three anticlines, the faulting within this structure is comprised of a larger number of small scale faults rather than a few large scale faults. Additionally the axis of the anticline runs in a slightly different orientation to the three anticlines which found to the east.

The faulting within the anticline can be divided into two key suites of faults. The compressional, reverse faults strike in a north-east to south-west direction and are seen to be en-echelon in form. The second suite of faults are primarily extensional in nature and strike in a north-west to south-east orientation. In the northern region of the structure,

close to its termination against fault SS A, there is a sub-vertical fault recognised that strikes in a north-south direction.

In the three anticlines which are labelled TA I, II and III, the fault patterns at the deeper horizons (190 and 202) which are picked out are linear and trend in a north-east to south-west direction. The fault pattern in TA II in particular is clearly identified at horizon 202 by en-echelon linear faults. In the shallower section (Horizon 100) over these three anticlines, the faulting is limited to some minor normal faults that strike in a north-west to south-east direction (Figure 7-41).

In contrast, TA IV is characterised by dense faulting along the crest in the shallow layers, with the faulting ranging in strike azimuth from north-south to north-west to south-east. In contrast to this fault pattern in the shallow section, the faulting at the deep horizon (202) is similar to that observed in TA I-III, with linear parallel faults running in a north-east to south-west direction.

There are two additional observations concerning this anticline. The western boundary of the anticline is coincident with the location of a syncline that is filled with a chaotic seismic facies (section 6.3.4.4); in addition, a sub-vertical fault labelled SS B is present, which terminates the western limit of fault SS A. Additionally, there is a region in the centre of the anticline in which a sub-vertical fault is also observed. The sub-vertical faults are interpreted as late-stage strike-slip movement.

It is interpreted from these observations that this structural feature has a different origin to the TA I, II, and III; the presence of the syncline predates the late-stage compression, indicating that the deformation is linked to the pre-existing morphology. The fault propagation folding seen in TA I, II, and III is not as evident in TA IV, which appears to show evidence of strike-slip movement. This strike-slip motion is interpreted to have occurred because the horizontal stress which was active, and which was responsible for the growth of the structures, was at an oblique angle to the levee that marked the eastern boundary of a turbidite-derived syncline.

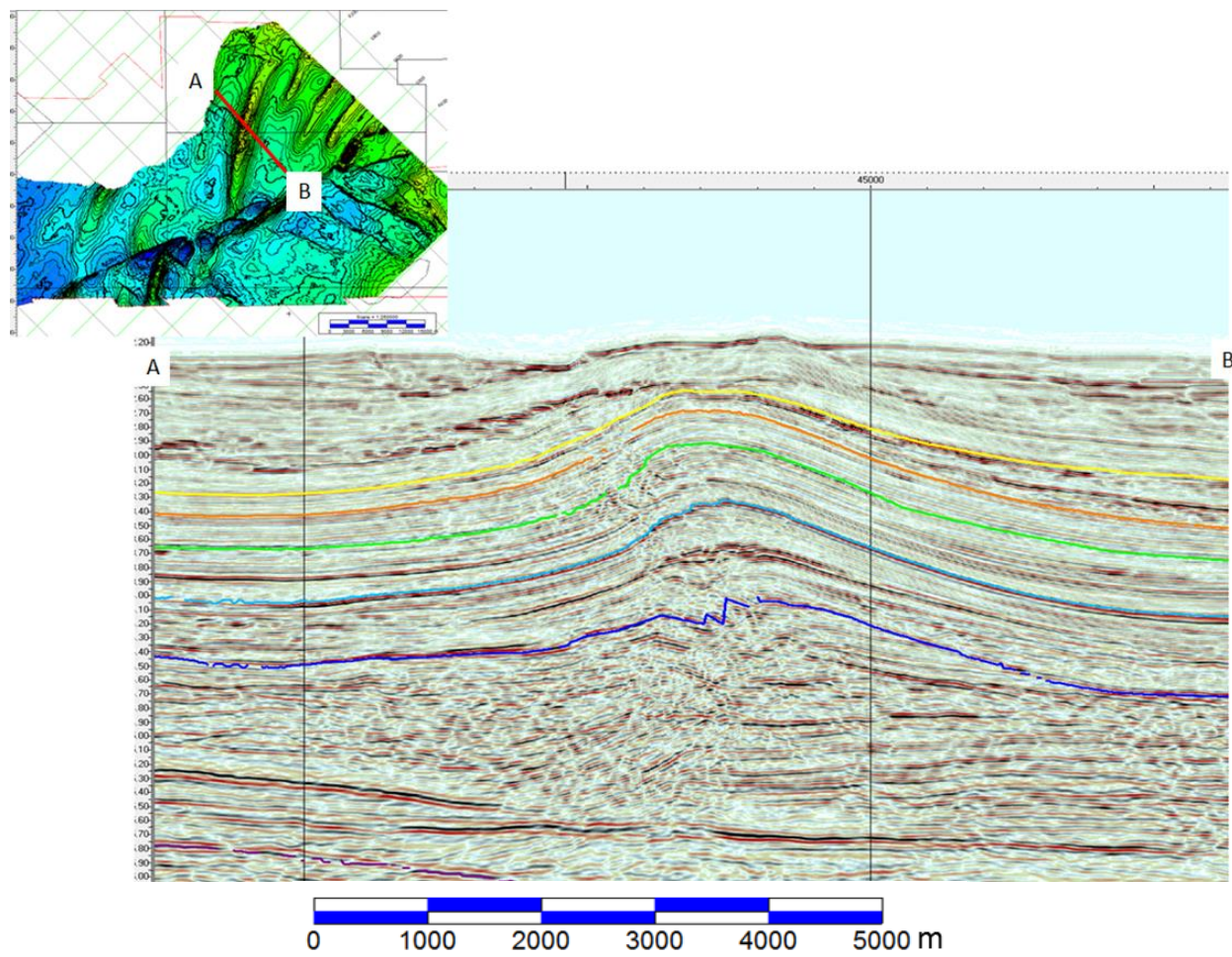


Figure 7-38: Inline 5900 illustrating the location of TA IV.

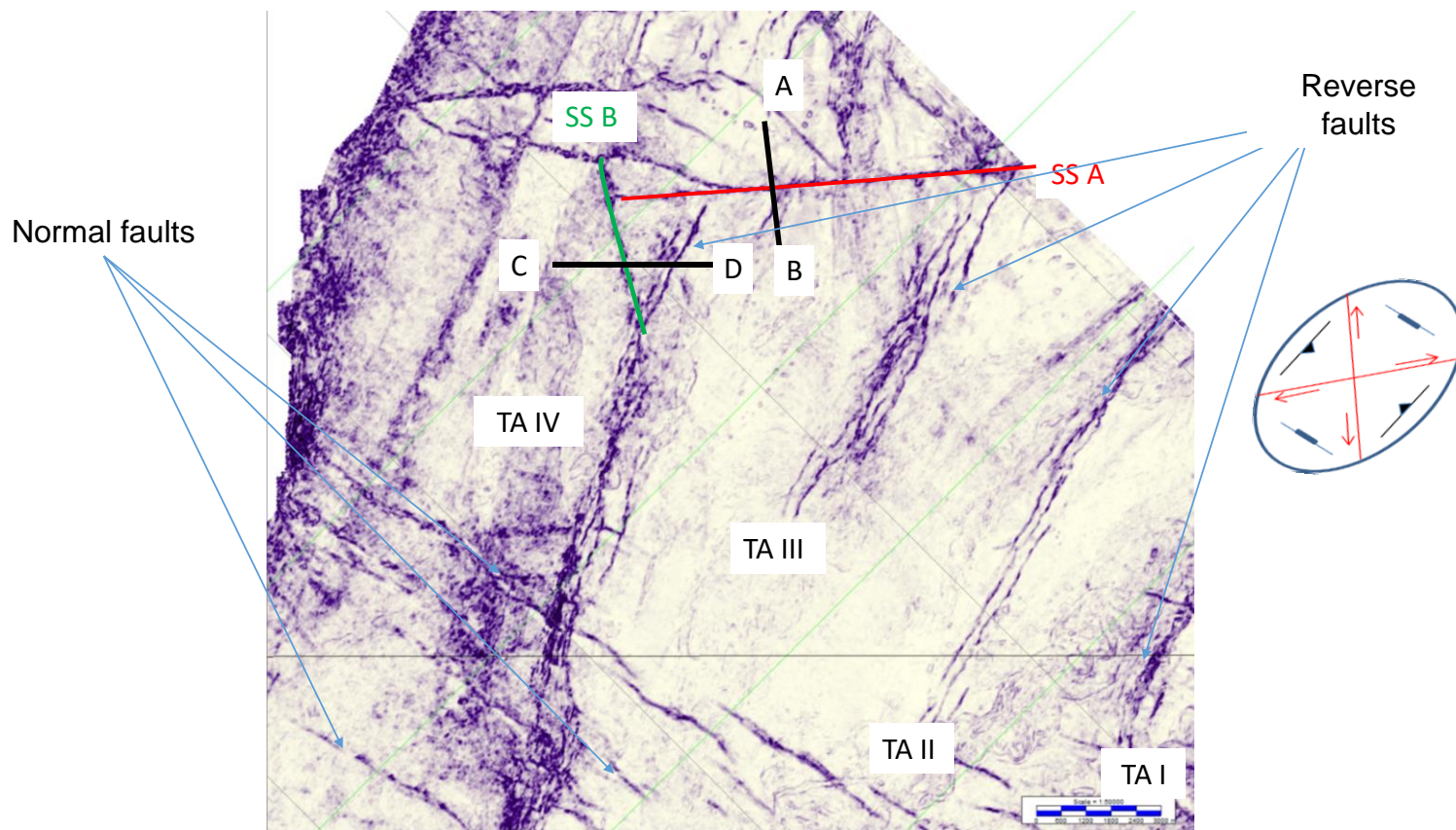


Figure 7-39: Similarity attribute extracted at horizon 202.

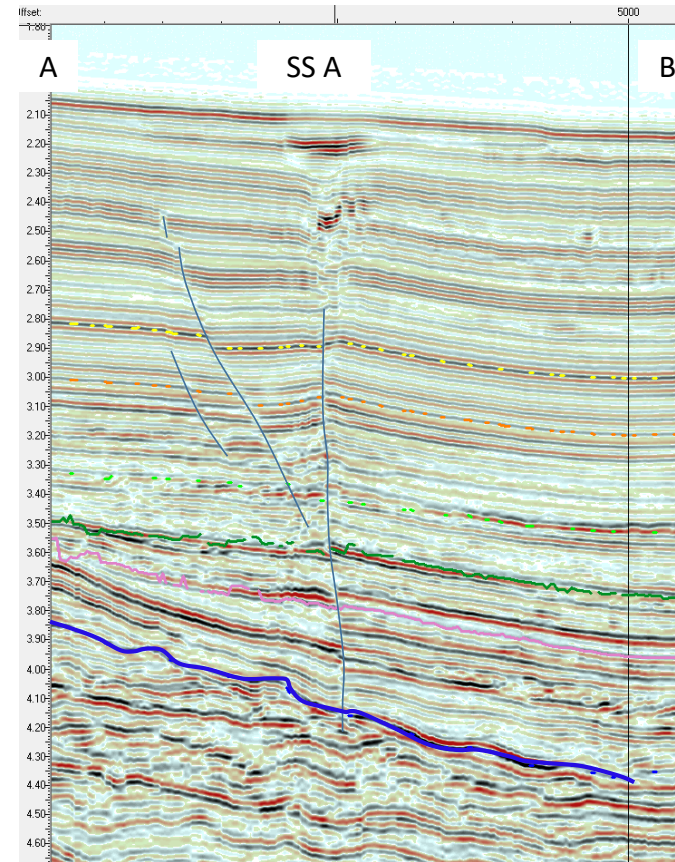
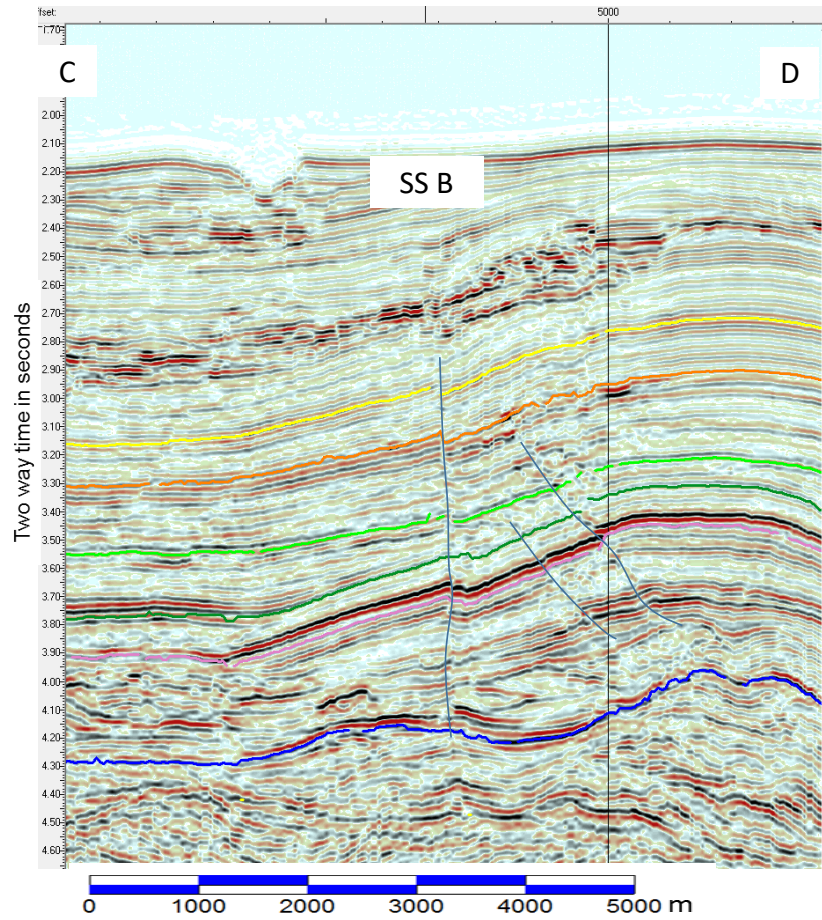
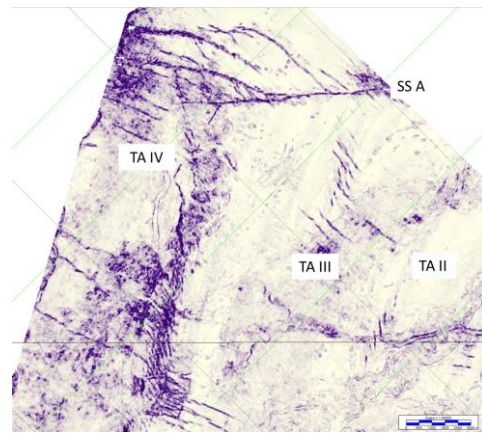
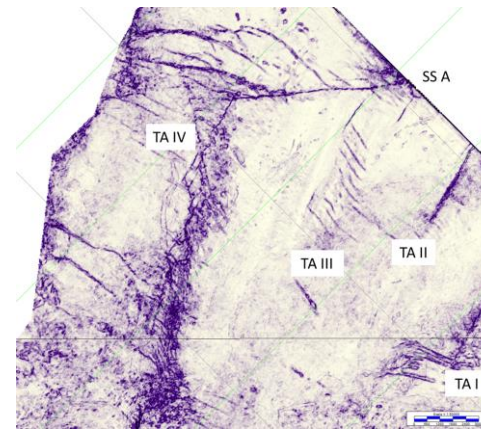


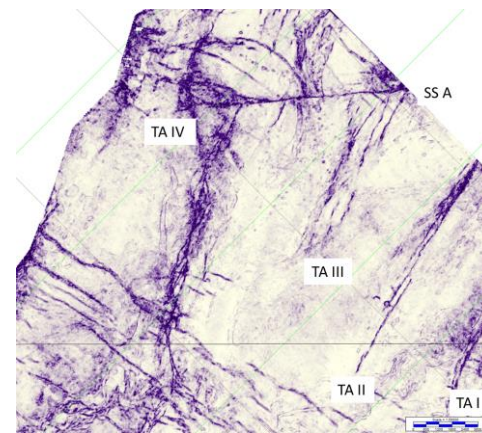
Figure 7-40: Seismic profiles that cross the two strike-slip faults highlighted in Figure 7-39.



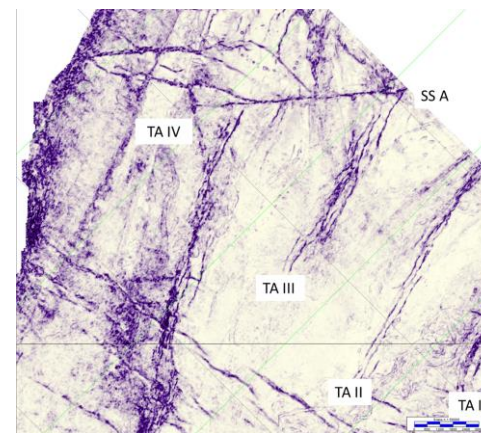
Horizon 100



Horizon 130



Horizon 190



Horizon 202

Figure 7-41: Similarity extraction at four horizons in the northern area.

Timing

The four anticlines described above have formed recently. The intervals below the Pliocene (horizon 100) do not display any syn-sedimentary thickening or thinning over the crest of the anticlines, with the exception of TA IV. The thinning observed over the crests of TA I, II, and III results from flexural slip. In the case of TA IV, the isochrones for the intervals below horizon 130 indicate the presence of an interpreted turbidite levee, with the axis of the central syncline filled with mass transport deposit (see section 6.3.4.2). In addition to the syncline that lies to the west of TA IV, a smaller debris-filled syncline is mapped as having been formed at the same time, which has been uplifted and cuts TA III at an angle.

The structures are still actively growing, with the sea bed exhibiting evidence of the growth by the presence of anticlines at the present day. The sea bed topography has influenced the location of channels which have been deflected by the presence of these sea-bed structures.

The structures are interpreted to be related to dextral motion along the strike-slip fault (SS A), as noted above. In addition, the timing of movement on the Avon strike-slip fault is interpreted as being coeval with the compressional deformation.

7.3.4.3 TA V and VI

In addition to the four anticlines outlined above, there are two high-relief anticlines that are found in the western half of the survey. In the two anticlines illustrated in Figure 7-42: , the central portion of both is characterised by a sub-vertical disturbance zone; the vertical dip of the beds is beyond the resolution of the seismic data resolution. However, by examining a series of lines that are located in an orthogonal direction to the structures, the evolution of the structures can be estimated.

The more westerly anticline TA VI is a north-east to south-west-oriented anticline, which is over 20km in length. The vertical relief at the mapped level (horizon 310) shown in Figure 7-42: is over one second two-way time. The structure has a sharply dipping western flank, with a less steeply dipping eastern flank – a property it shares with the four anticlines described in the previous sections. Unlike TA I-IV, the faulting in the core of the anticline is less well-imaged.

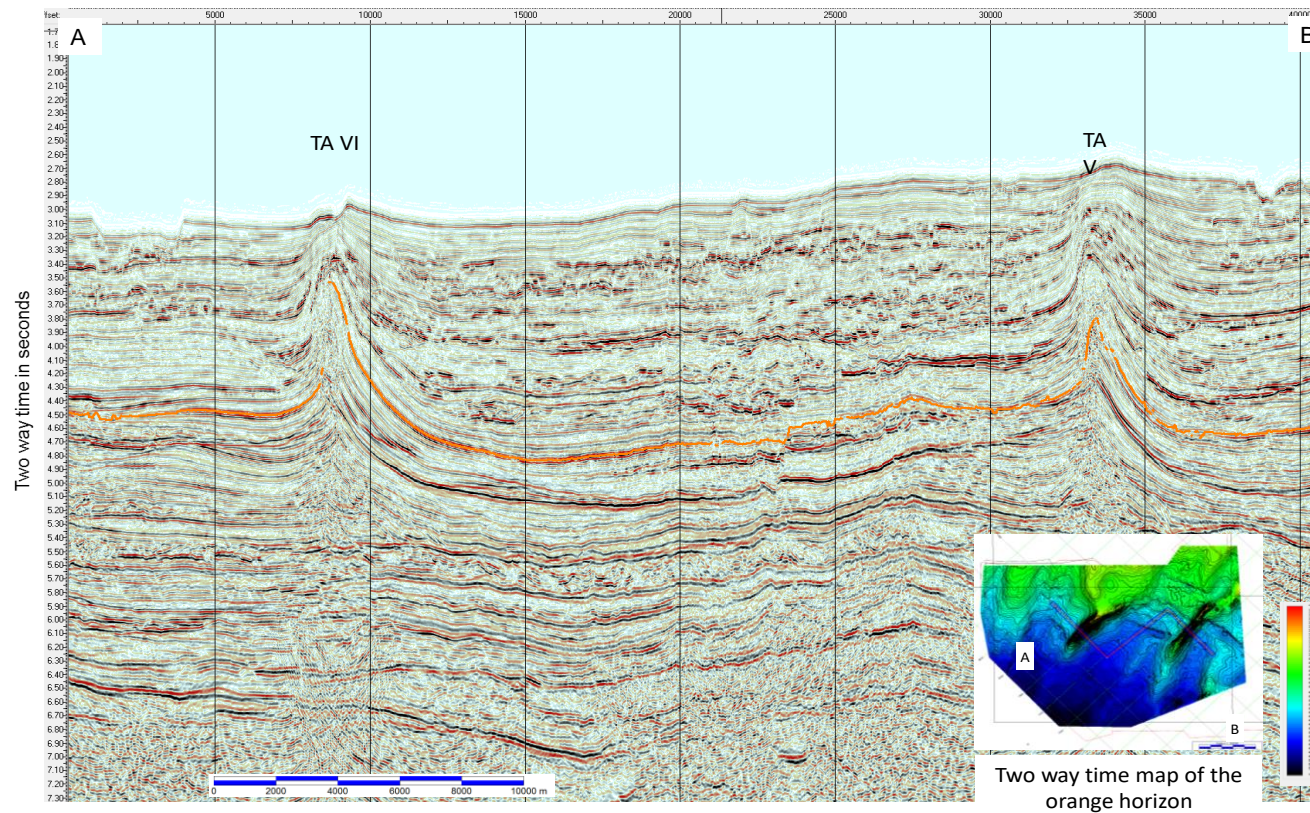


Figure 7-42: Random line through the western half of the survey, illustrating the two high-relief anticlines TA V and VI.

At the southern end of the western anticline, the deformation that is present is limited to the interval that lies between horizons 420 and 510 (Figure 7-45). There is a minor anticlinal feature that is present at the level of horizon 420 and the overlying horizon 310. The lower limit to the deformation is horizon 510, which exhibits a synclinal aspect. The structural style found within the interval that lies between horizons 510 and 420 is interpreted to be predominantly compressional, with a series of low-angle thrusts that verge towards the west. What limited faulting there is in the section between horizons 420 and 310 is also compressional, with the thrusts verging towards the east.

In the core of the anticline, the image is compromised by the steep dips, and the extraction of meaningful structural information is therefore limited (Figure 7-44). The simplified fault pattern in this figure suggests an interlocking of the faults in a “saw tooth” manner. This style of faulting is also recognised in the lateral margin fault complex that is described in section 7.3.5.

At the northern end of the anticline, it is interpreted that the structural deformation took place on at least two stages (Figure 7-43). The lower portion of the anticline exhibits a compressional set of faulting that is offset from the younger suite of compressional faulting.

In the case of both anticlines TA V and VI, the seismic imaging at depth is complex; however, in both of these cases there is a clear break at the level of the underlying mass transport deposit. It is unclear if this is a genuine structural dislocation or a function of the velocity distortion surrounding these high-relief features.

The sea bed is affected by the growth of these structures, indicating that they are still growing at the present day, under an assumed compressive stress regime that is acting in a south-east to north-west orientation.

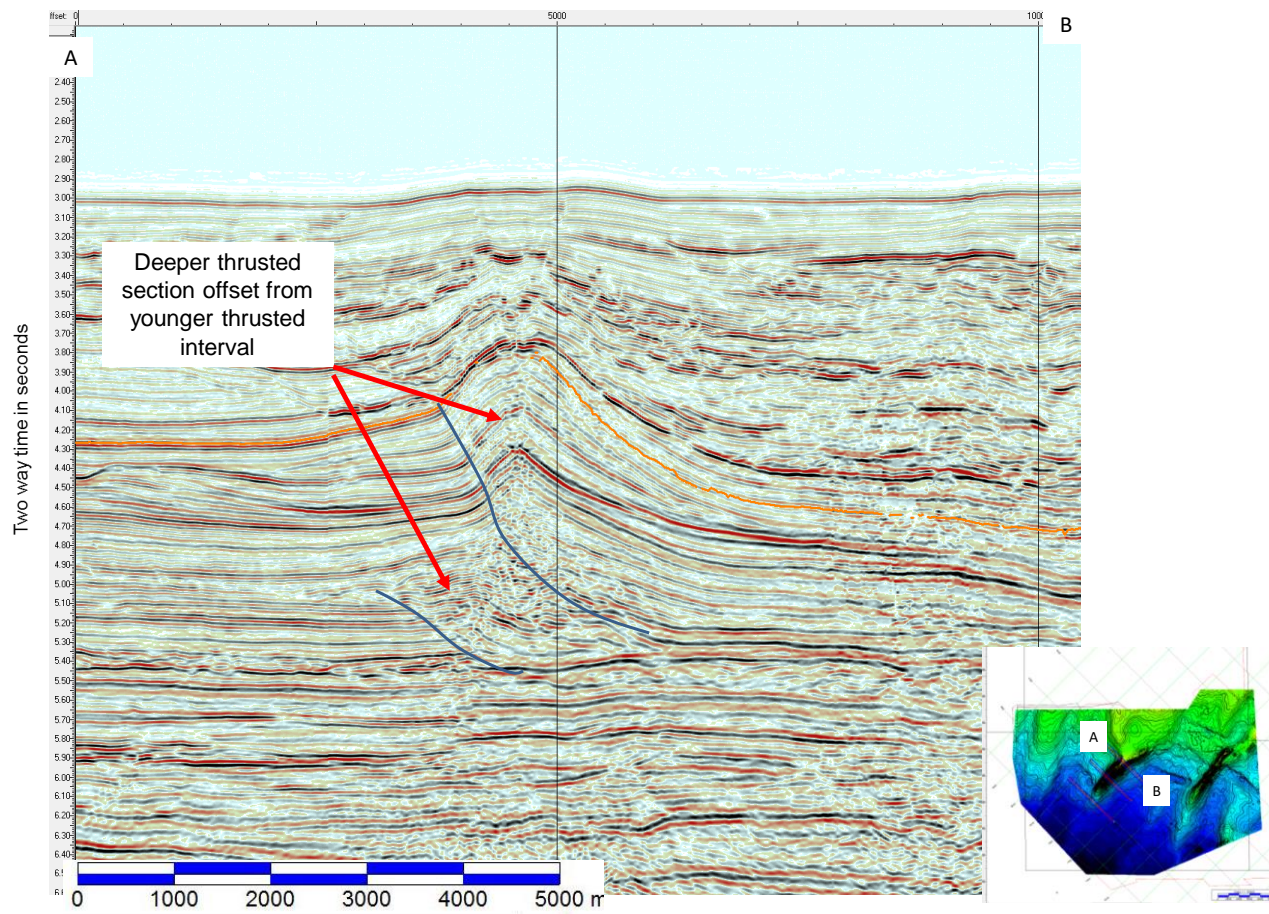


Figure 7-43: Seismic line through the northern portion of TA VI.

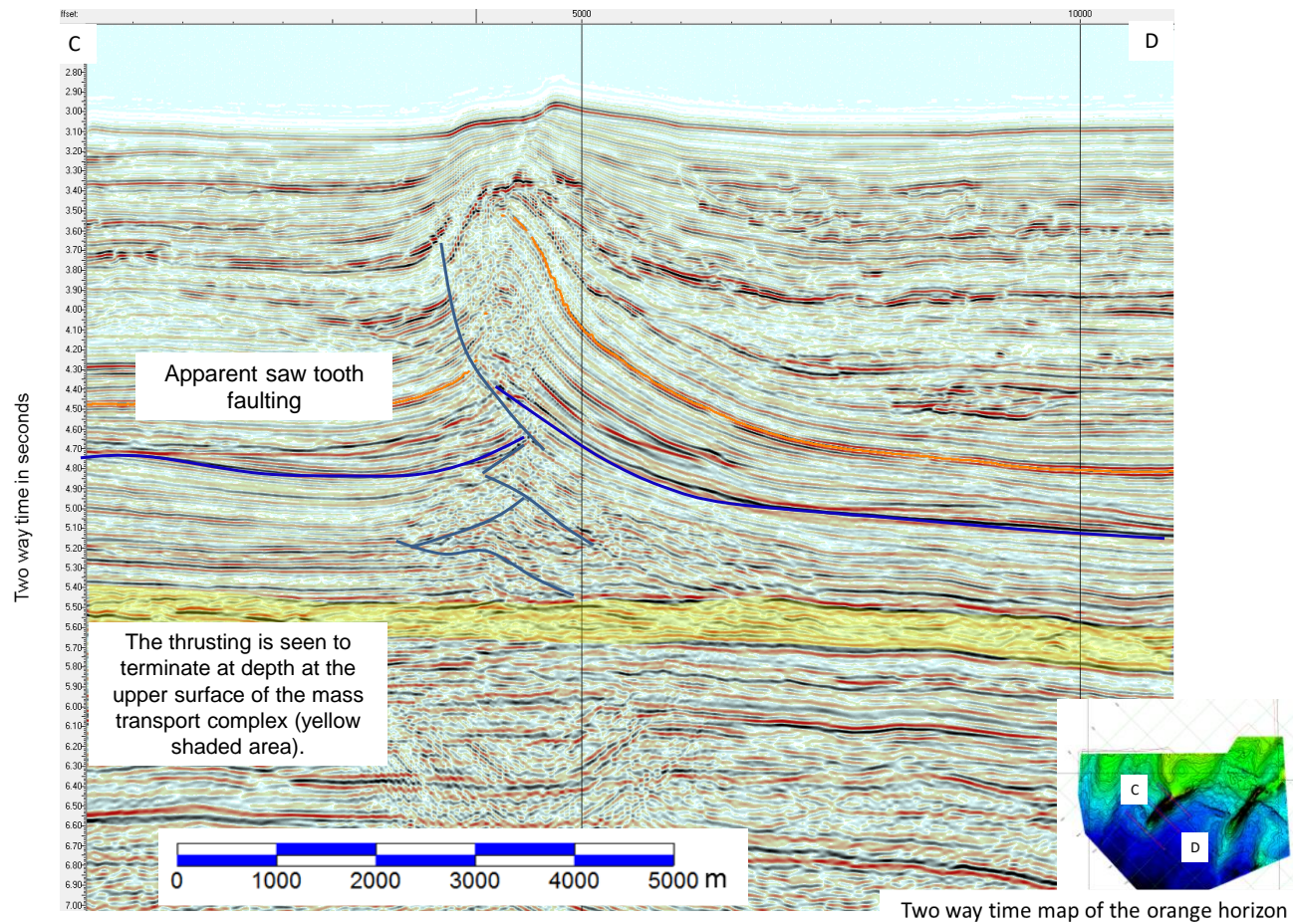


Figure 7-44: Seismic line through the central portion of TA VI.

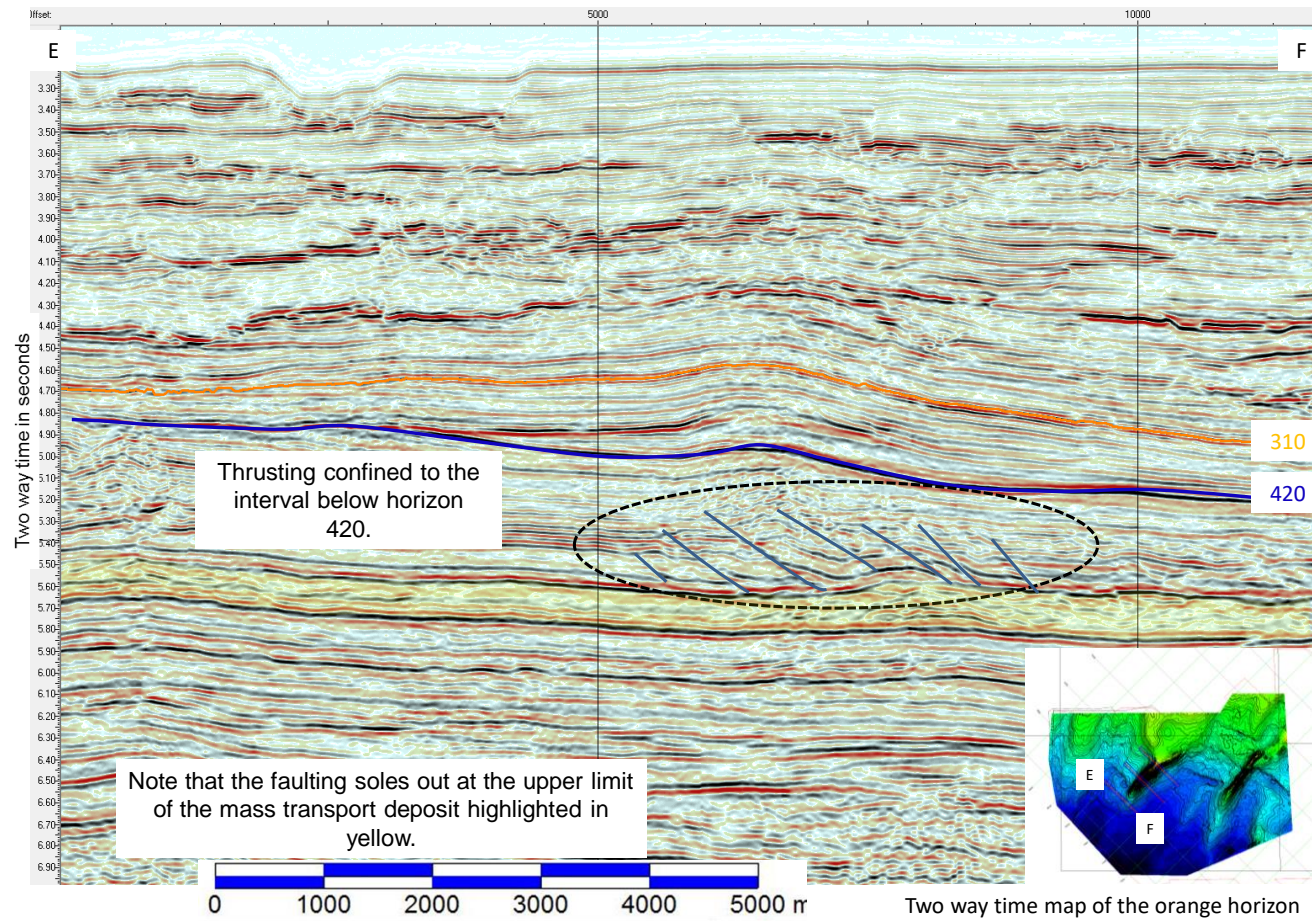


Figure 7-45: Seismic section through the southern portion of TA VI.

7.3.5 Deformation of ridges

7.3.5.1 Internal

As noted in chapter 6, there are a number of ridge/levees that are interpreted to have been built up as result of sediment flows via turbidity currents from the north. Within these ridges, there are a number of later structural deformation styles recognised. The westernmost ridge – DA -is the one with the largest relief within the survey area. It appears to be a composite body comprised of several separate episodes of construction. Each of the internal ridges within the overall major body appears to exhibit its own internal deformation. The lower portion of the composite ridge is intensely faulted, with mainly reverse faults, whilst the upper portion remains largely unaffected by tectonic activity; what faulting there is, is extensional.

In Figure 7-46, a map of one of the horizons within the DA build-up, the lateral change in structural style across the lateral boundary fault (highlighted in white) can be seen. To the west of the white line is a zone of intense faulting, which is not present to the east of this line.

Within the intensely faulted interval, there are distinct vertical as well as lateral changes in tectonic style. This suggests that the faulting took place in several phases, with the lower interval being probably deformed within the period during which the upper interval was not present. If this is the case, then the deformation is not likely to be a result of the gravitational impact of the Niger Delta, which at the time was a distant influence off to the east.

The origin of this deformation is unclear because the 3D volume does not encompass the entirety of the fan, of which this deformed region is the eastern limit. The motion of sediments downslope, as is the case for most gravitation slides, is a result of sediment accumulation in the proximal regions of a delta. In the absence of a large-scale delta, other triggers may be inferred. Amongst those that might be considered in this instance could be the increase in tilt of the continental margin (Dooley et al., 2013) as a result of increased thermal subsidence. Alternatively, a change on the slope of the margin may account for the inability of the sediment pile to slide unhindered across a basal detachment surface.

Analogue studies of transcurrent faulting highlight the presence of trans-tensional and transpressional faulting associated with strike-slip motion. (Naylor et al., 1986; Wu et al., 2009; Dooley and Schreurs, 2012). A variety of structural patterns have been generated using clay and sand box experiments, which have been summarised by Tchalenko

(1970) and Dooley and Schreurs (2012). Experiments are all based upon a laterally homogeneous set of pseudo-deposits overlying a movable base plate. Relative displacements of the base plate along a linear boundary between two halves of the base plate have been used to generate within the pseudo-sediments fault patterns which can then be analysed. The fault patterns observed in these experiments are noted to be similar to the faults seen within the 3D survey. In these modelled cases, the early stages of faulting can be studied; however, in the case of this study, only a single snapshot in time (the present day) is available.

In the case of this study, the deposits on either side of the strike slip fault zone are not homogenous and the basal layer upon which the two conjugate sides of the fault move is, in all probability, not horizontal. Consequently, these studies do not capture the coeval deformation that takes place on either side of the strike-slip zone of deformation.

The deformation seen in these levees are interpreted to have derived from the lateral, downslope motion of the Palaeogene section, with the thicker interval moving downslope at a greater rate than the thinner interval that lies to the east of Ridge A. As noted in chapter 3, the uneven distribution of a proximal thick sedimentary pile leads to lateral stress imbalances (McClay et al., 2003). It is, therefore, interpreted that the difference in lateral stress between a thick levee and thin moat will lead to a lateral contrast in the rate of downslope motion and the creation of a strike-slip fault zone in between the two sediment thicknesses.

The analogue studies (Dooley and Schreurs, 2012) that have been conducted do not address the concept of uneven loading; however, the presence of tear/strike-slip faults have been observed in the modelling of the Niger Delta by Wu et al. (2015), who have observed that these dislocations do occur at the lateral margins of the delta, where variations in the thickness of the overburden become significant.

In addition, what is not modelled in the analogue studies is the presence of conjugate shear zones that can create significant tectonic variety in the zone of the master fault zone. The interplay of the synthetic and conjugate shears remains to be investigated. Nonetheless, the similarity of faulting described in the analogue studies with the fault patterns observed within the 3D data are striking.

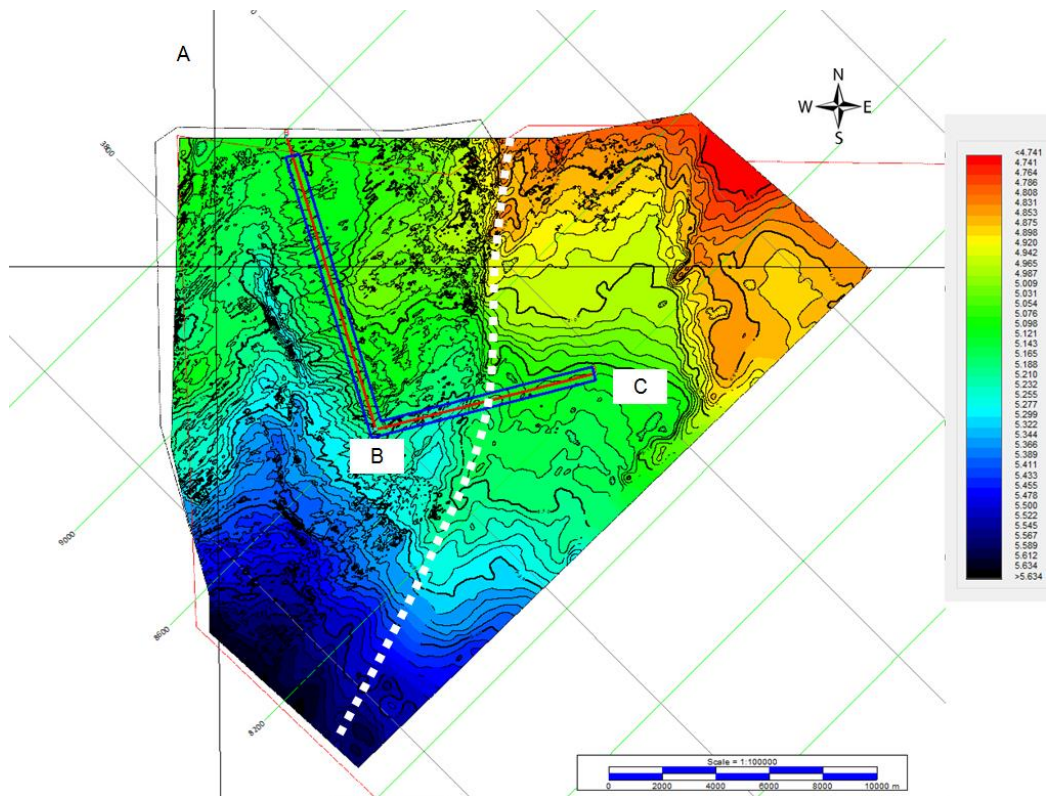


Figure 7-46: Twt map of horizon 470. The white dashed line is the interpreted location of the lateral fault zone.

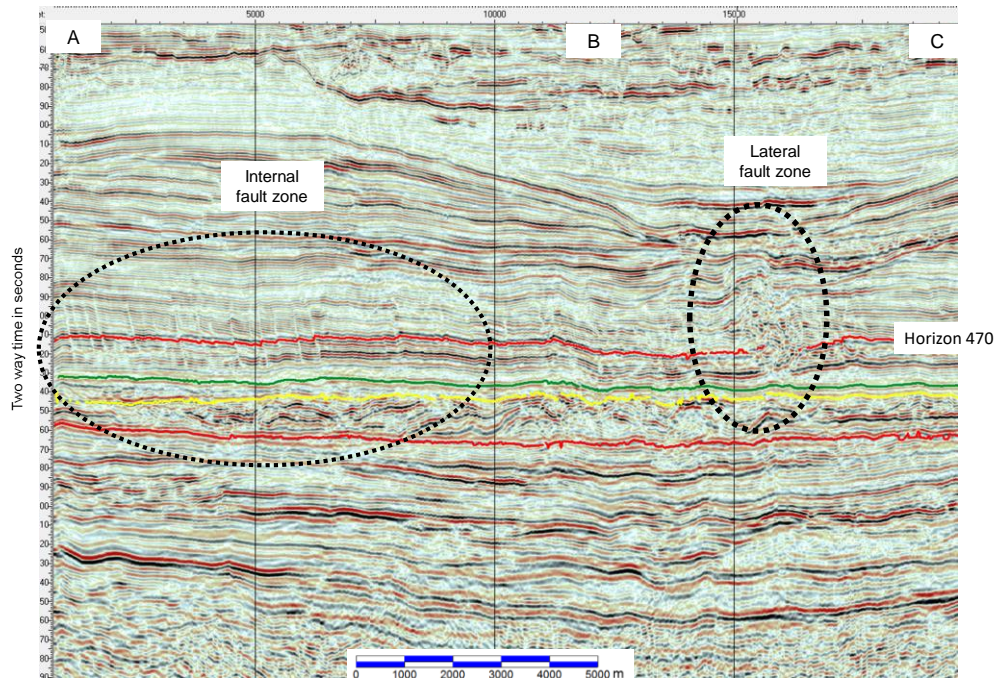
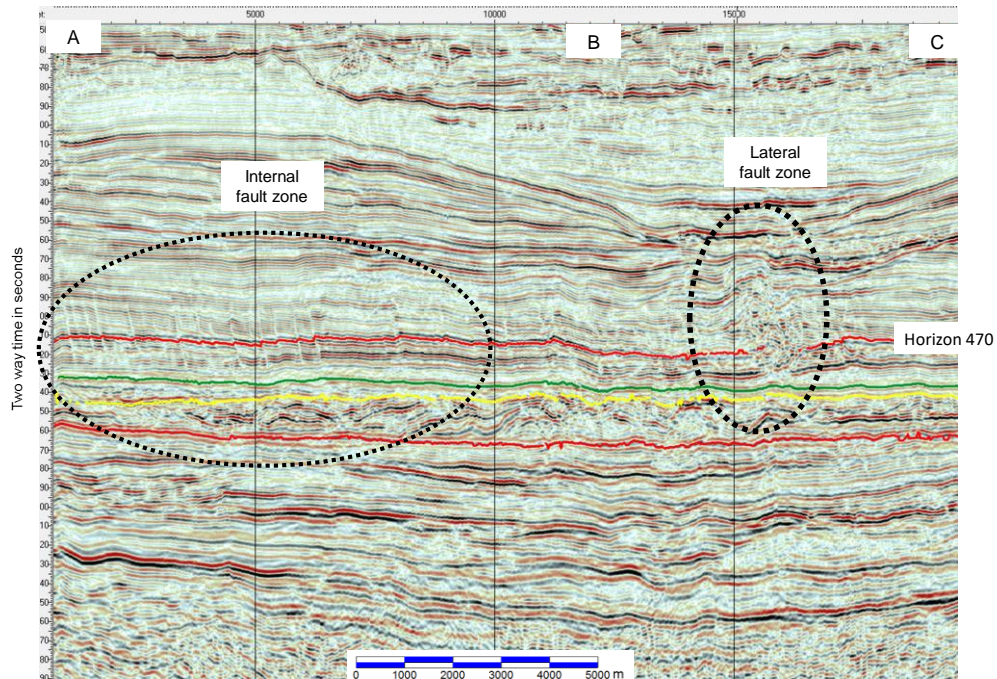


Figure 7-47: Random line that passes down the ridge and across the lateral fault zone (see Figure 7-46 for location).

The eastern margin of the deformed ridge/levee is a linear fault zone that is comprised of a complex set of compressional and extensional features that indicate it may be a transcurrent fault zone (



Figure

7-47).

7.3.5.1.1 Fault characteristics

The most obvious suite of faults within the ridge are the reverse faults, which generally strike in a north-east south-west direction (Figure 7-48). In ridge DA (see section 6.3.3.2), there are at least three suites with slightly different strike orientations. The vergence of the faults is generally towards the north-west, which is an unusual arrangement because this is in an up-dip orientation. This zone of deformation is confined to the body of the ridge/levee and bounded to the east by a complex fault zone. The western boundary of the ridge-related deformation lies beyond the western limit of the 3D survey. Nonetheless, there are hints that at the western margin of the survey, there may also be a north-south-trending fault zone based upon the deformation seen at the margin of the data.

The throws on the reverse faults are typically modest, in region of 5-20 milliseconds (10-40 meters), and their lateral extent is in the range of 1km to 3km. The spacing between the faults is in the order of 25 to 1000 meters. Faults with smaller throws are almost certainly present, but they are below the vertical and lateral resolution of the seismic data. The fault planes generally dip at angles in the region of 50-60 degrees but can become sub-vertical in places. There is some uncertainty in the true vertical extent

because the velocity is unknown, but assumed to be in the region of 3000ms^{-1} , at the depth of the deformation. The faults tip out at depth close to the mapped surface of the underlying interpreted mass transport complex. This reverse faulting is limited to the interval between horizons 420 and 500 (Figure 7-50).

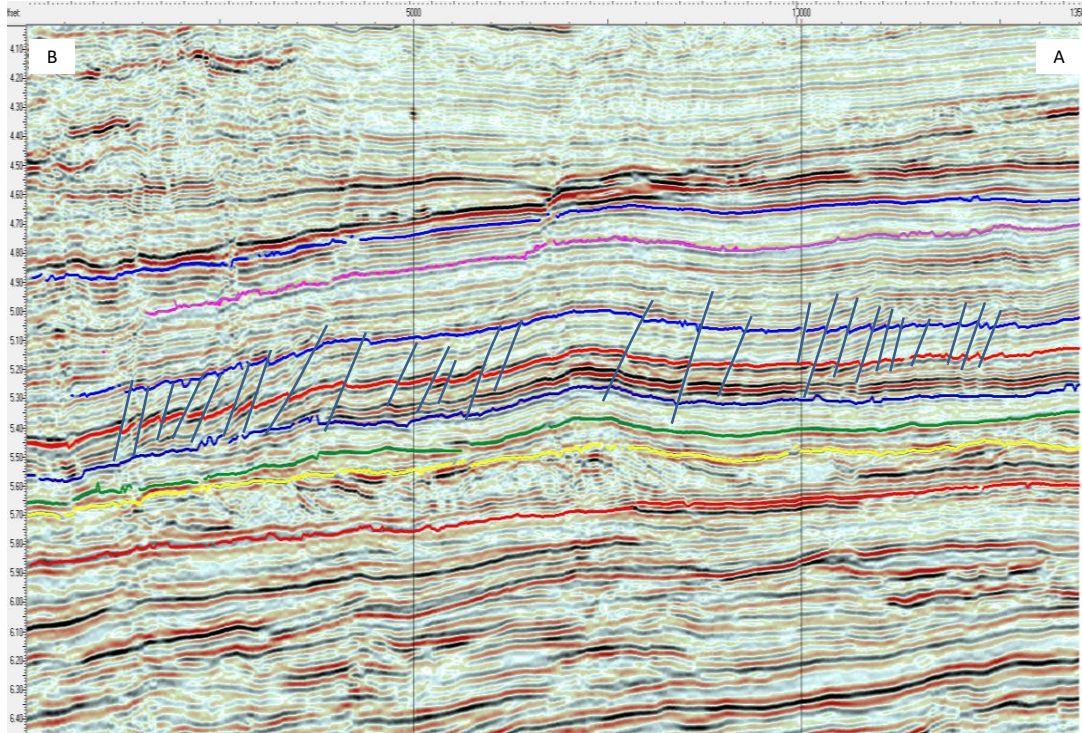


Figure 7-48: North-south traverse through the western-most ridge; refer to Figure 7-49 for location.

As noted above, the faults are limited in their lateral extent to the ridges, with the adjacent synclines unaffected. In the centre of ridge DA there is a north-west to south-east trend of en-echelon faults. These faults display both normal and sub vertical geometries. The section in Figure 7-51 illustrates the apparently normal fault that is found in the centre of the build-up. In Figure 7-49, the fault patterns can be picked out by the dark lines in the similarity extraction from the horizon 470 surface. The yellow dashed line indicates the location of the eastern boundary fault zone.

At the western margin of the dataset, the set of parallel faults strike in a south-west to north-east direction. This suite of faults is illustrated in Figure 7-48. The faults are limited in vertical extent and are not present at the level of horizon 423 and tip out at depth in the interval between horizon 490 and 500.

Moving westwards, in the map in Figure 7-49, the set of parallel faults that strike in a more east-to-west direction is illustrated in Figure 7-50. These faults are seen to tip out

at depth within the section between horizons 500 and 490. The upper limit of the faulting lies just below horizon 420.

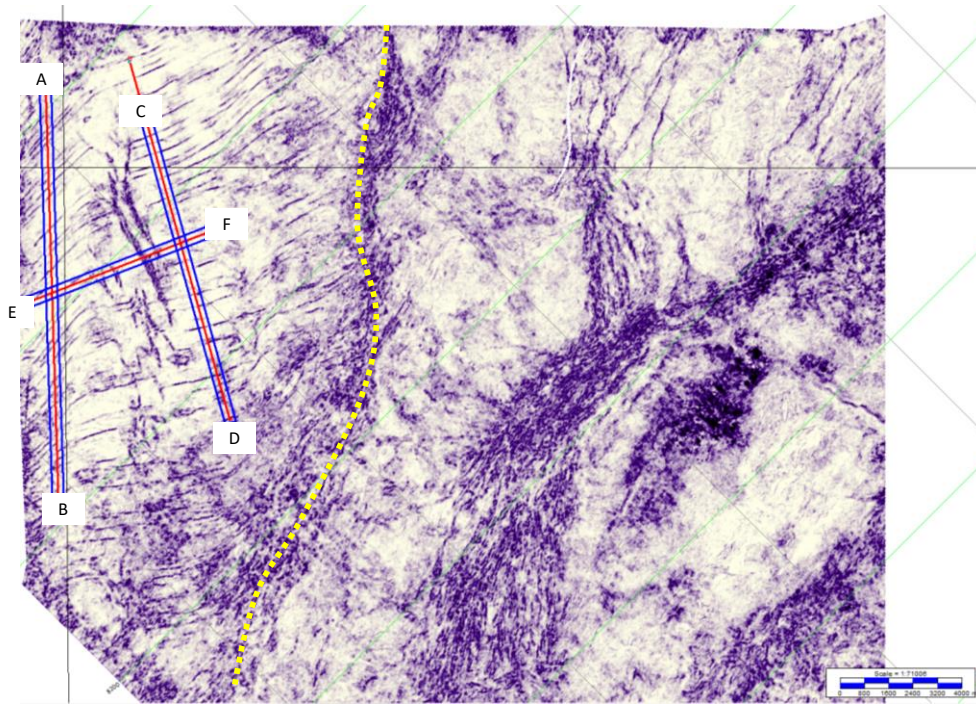


Figure 7-49: Similarity attribute extracted at horizon 470. In addition to the array of reverse faults that have been described above, there is a central fault belt within the levee that is comprised of both normal faults, as illustrated in Figure 7-51, and sub-vertical faults.

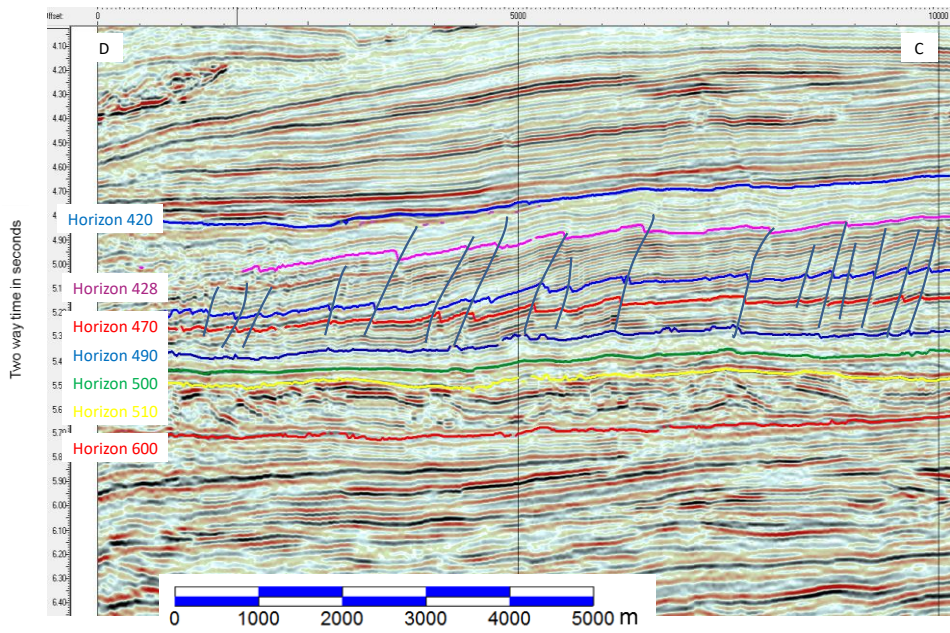


Figure 7-50: North-south line passing through the middle of the levee; refer to Figure 7-49 for location.

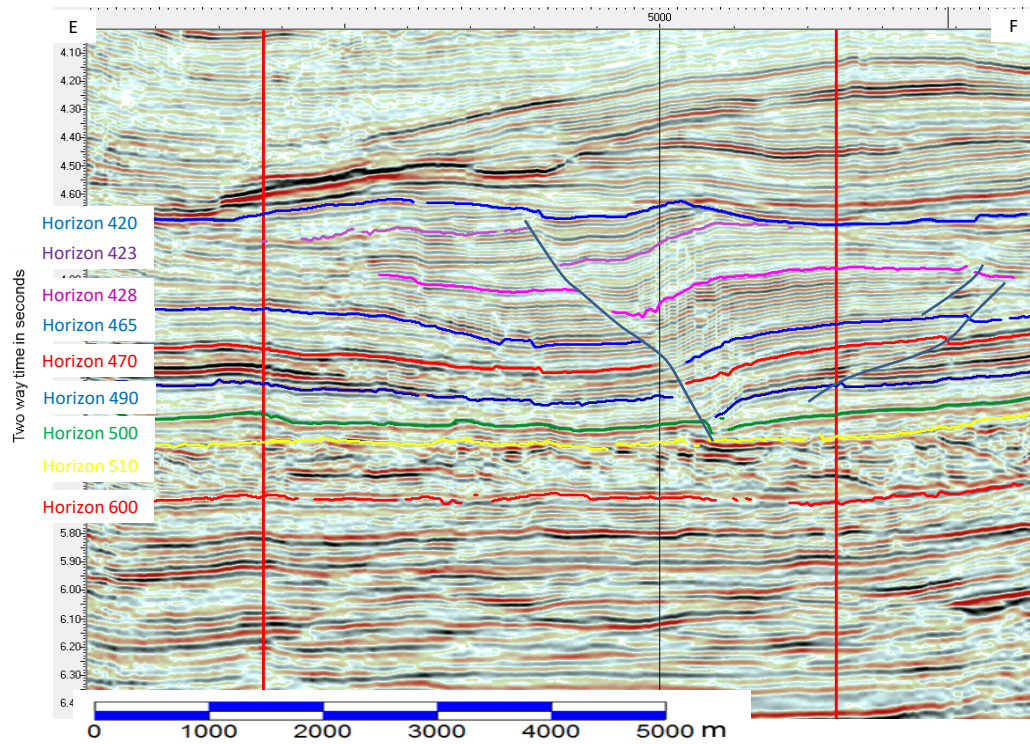


Figure 7-51: West-to-east section through Ridge A; refer to Figure 7-49 for location.

The three suites of faults are limited to specific regions within the overall ridge. In the west, the deformation is restricted to the deepest sub-ridge.

Analogues for similar arrays of reverse faulting are difficult to find in the literature; the author has seen a small-scale example in the field (Figure 7-52) from the Tres Pasos formation in the Magallanes Basin in southern Chile. This locality is within a deep water slope setting, in which there are a number of mass transport deposits, as well as slope channels (Schultz and Hubbard, 2005). The palaeo-slope dipped from the north to the south, from the left to the right in this picture.

Within the outer thrust belt of the Niger Delta (Bilotti and Shaw, 2005; Briggs et al., 2006; Maloney et al., 2010), the majority of the thrust anticlines are seen to be controlled by reverse/thrust faults that verge downslope. There are, however, some of the thrust anticlines in which the vergence of the reverse faults is up-dip towards the coast (Bilotti and Shaw, 2005).



Figure 7-52: Photograph of a stack of reverse faults which verge up-dip, seen in outcrop.

In the case of the outer thrust belt example, the structural deformation has been linked to the presence of a weak basal layer (McClay et al., 2003; Bilotti and Shaw, 2005; Wu et al., 2015), which allows the lateral movement of a body of rock. In the presence of a basal layer with unusually low shear strength, the sense of vergence of the faults in the overburden is unconstrained and vergence both up- and down-dip can be expected. The

weak basal layer would allow unlimited lateral movement, if the shear strength of this detachment was constant. Once the shear strength of the basal layer alters to become relatively less weak, the lateral motion is halted. This termination of lateral motion results in a contraction of the mobile strata and subsequent compressional deformation.

The point at which the detachment no longer allows the lateral movement of the overlying strata is a function of the properties of the detachment layer and the amount of overburden that lies above the detachment.

The isochrone of the interval between horizons 500 and 600 indicates that there was a mounded feature present on the slope post the emplacement of the mass transport deposit, based on the assumption that the base of this interval – horizon 600 – was essentially a planar surface dipping towards the south. The addition of sediments to the section overlying the basal detachment layer, at or close to the top of the underlying mass transport complex, is a surface that also dips towards the south and south-east.

Unlike the two dimensional models that are used to account for the toe thrusts in the literature (Corredor et al., 2005; Maloney et al., 2009), the presence of both a down-dip and a lateral ramp turns the deformation of the ridge/levee into a three-dimensional case. The thickness of sediment that overlays the mounded topography was asymmetrically laid down, as evidenced by the geometry seen within Ridge A. The thickness of the sediment pile that accumulated in the levees was greater than the thickness over the crest of the MTC. This variation in thickness created a gravitational imbalance in the effective stress found at the top of the MTC.

The combination of the extensive reverse faulting and the apparent extensional faults would indicate that the principle stress orientation is oriented in a north-west to south-east direction. (An alternative is that the area is subject to a north-east to south-west extension, which has the same effect as a north-west south-east compression.) As noted above, the age of the faulting predates the rapid build-up of sediments in the Niger Delta to the east; as a consequence, the orientation is not related to the stresses generated by the Niger Delta growth but to the local stress that was present during the Palaeogene. The accumulation of a thick sedimentary pile at the mouth of a canyon that thins downslope would generate an imbalance in the local horizontal stress regime. In the presence of a weak detachment layer at the base of the body of sediments, it becomes possible for the mass to slide downslope. The cessation of this downward motion comes at the point where the basal detachment becomes stronger or the lateral stress diminishes.

7.3.5.2 Lateral boundary fault zone

The eastern boundary fault zone is interpreted to have been active in the period between horizons 500 and 420; in addition, there is no evidence of the fault zone being active in the sediments that are younger than this. The unconformity that horizon 420 represents is seen to have removed the upper surface of this fault zone through erosion. These two strands of evidence support the interpretation that the timing of this deformation is limited to the time that corresponds to the interval between horizons 500 and 420.

Laterally, the deformed interval is bounded by a complex fault zone (Figure 7-46). This fault runs in an approximately north-south direction and exhibits a number of compressional “pop ups” along its length. In the core of the fault, the 3D data becomes difficult to interpret due to the high density of faulting; in the southern portion of the fault zone, the data is masked by the high amplitude events in the shallow section. Nonetheless, the overall form of the fault zone displays the elements of a strike-slip regime (see section 7.3.7).

The map in Figure 7-46 of horizon 470 indicates the contrast in structural styles across the eastern boundary fault zone. However, in detail, the fault zone is a complex array of interlocking reverse faults (Figure 7-53). In the image below, which is one of the better images of the fault zone, a reverse fault can be seen at the level of horizons 500 and 490 that verges towards the east. The section above this, however, is faulted such that the sense of vergence is towards the west. This structure appears to show the decapitation of a thrust that soles at the top of the mass transport deposit (horizon 510) by another thrust that soles out at horizon 470 – the upper surface of another mass transport deposit.

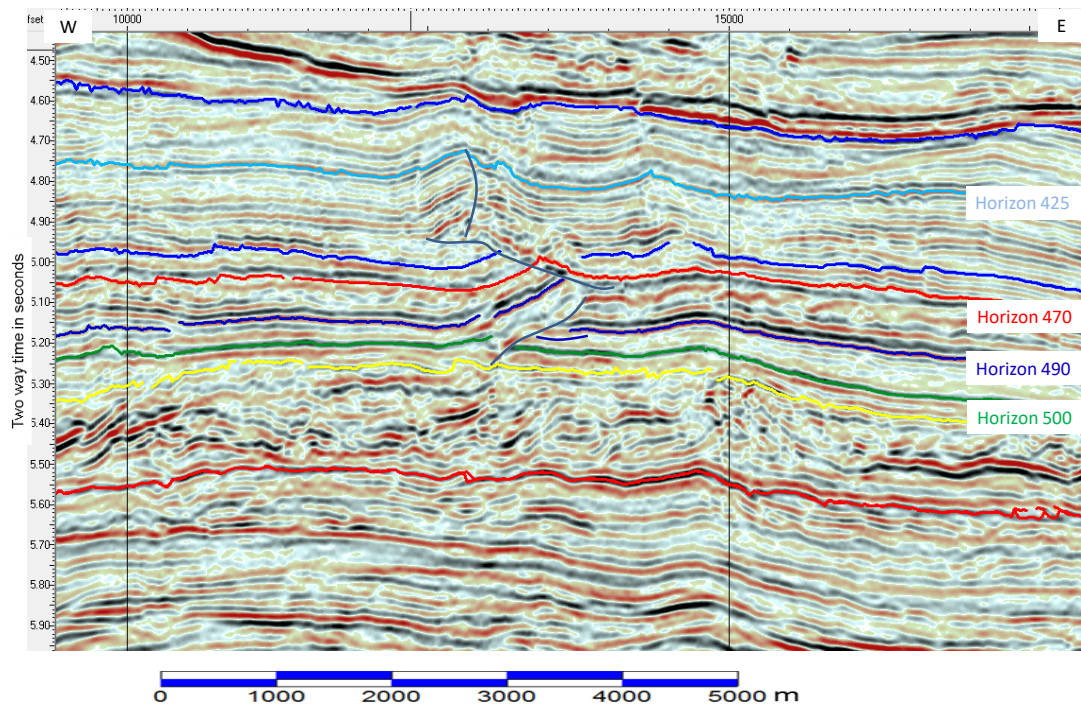


Figure 7-53: Detail of the faulting that can be seen in the eastern margin fault zone from seismic line 4120.

The apex of the deformation at horizon 425 is offset from that seen at horizons 490 and 500.

The deformation associated with this fault zone is truncated by a later unconformity (horizon 420/400), indicating that the tectonic activity associated with this levee deformation had ceased prior to the onset of the Niger Delta sediment influx.

The orientation of the faults within the body of the build-up suggests a compressional direction of stress that is somewhere between north-to-south and north-west to south-east. This assumption – when combined with the orientation of the extensional faults within the ridges – makes it possible to impose an assumed palaeo-stress regime on this area.

In Figure 7-54, the faulting is highlighted by the dark lines. The compressional, reverse faults strike in an east-to-west direction, while the extensional faults strike more north-south. This orientation of faults when compared to the strain ellipsoid indicate that the eastern boundary fault fits with it being a sinistral strike-slip fault zone.

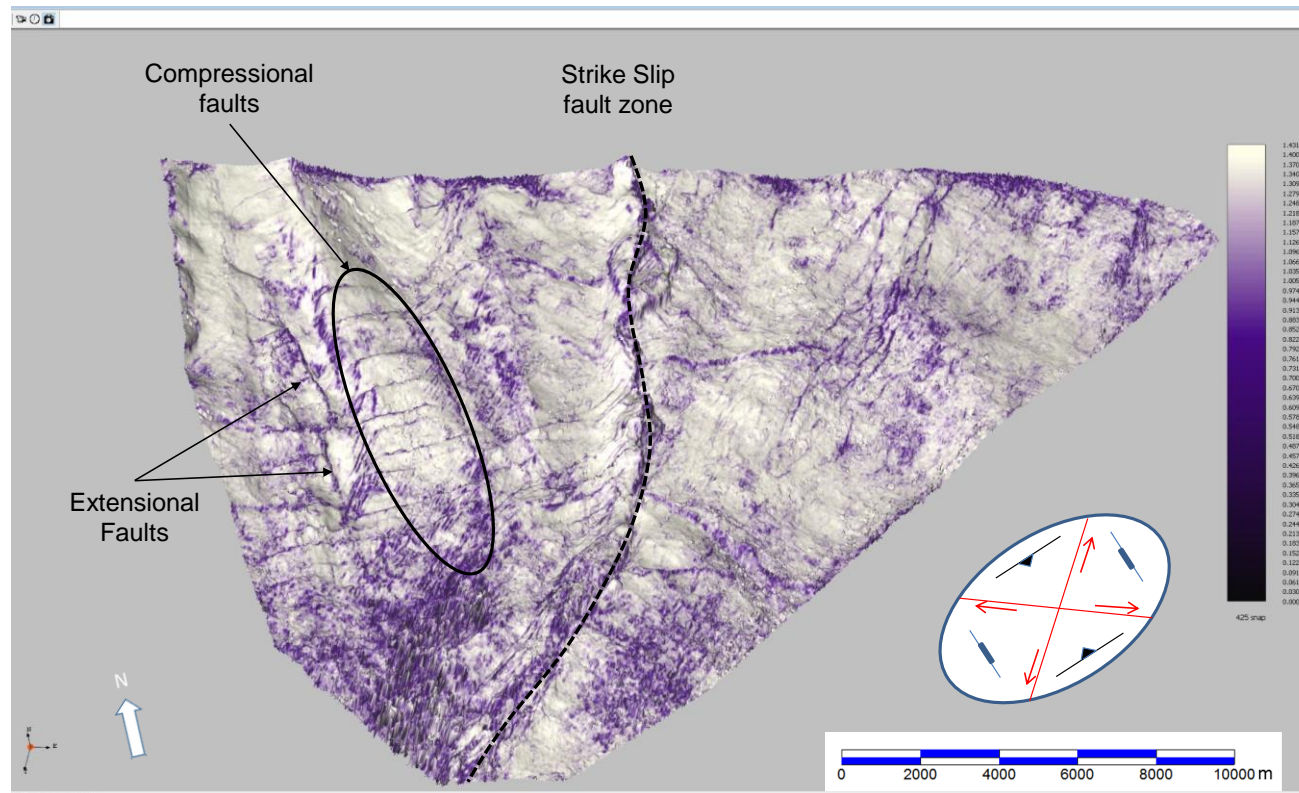


Figure 7-54: Similarity attribute extracted at horizon 425.

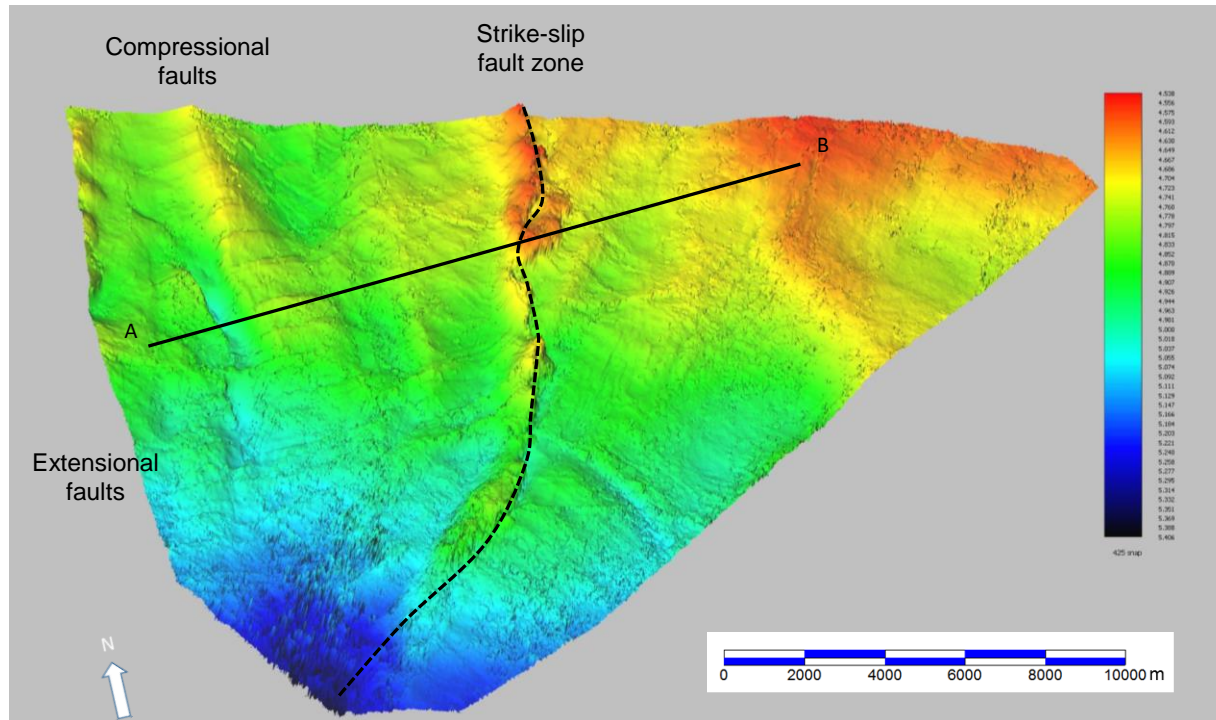


Figure 7-55: Perspective view of the two-way time for horizon 425; the black line is the location of Figure 7-56. The black dashed line is the trace of the eastern margin strike-slip fault zone

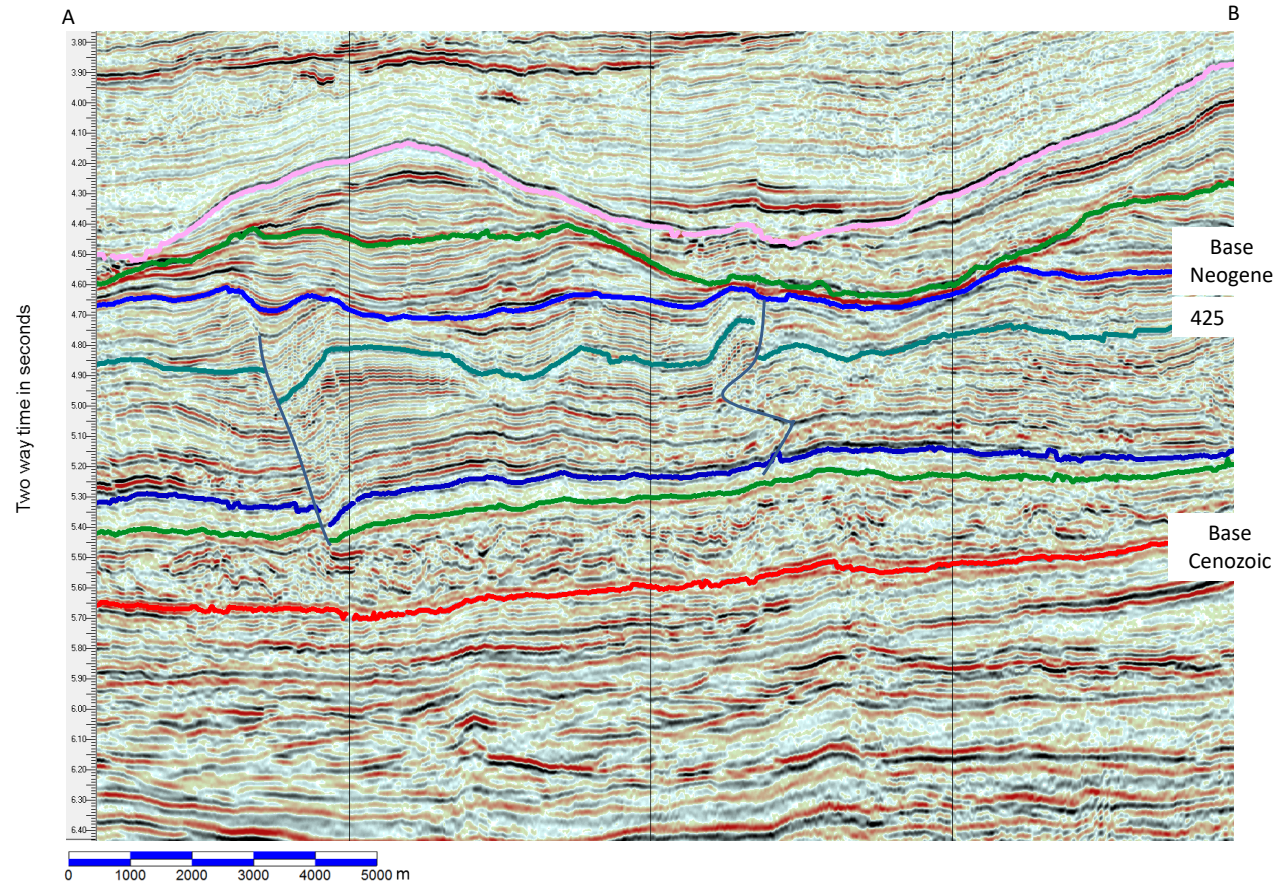


Figure 7-56: Cross section highlighted in Figure 7-55, which traverses the strike-slip fault at the eastern margin of Ridge A.

7.3.6 Fluid escape

When initially deposited, sediments contain large amounts of interstitial water. With increasing overburden loading as result of subsequent sediment deposition, the load is supported by a combination of both grains and water. With good permeability between grains, the water can flow freely, such that the water within the pore space remains in contact with the overlying water column. The pore pressure therefore remains hydrostatic. In the case where the permeability is low, the water in the pore space is unable to move quickly enough to maintain hydrostatic equilibrium. Rapid burial of the section with the low permeability prevents the water in the low permeability rocks from escaping in a timely manner and the trapped water, as part of the substrate, then assumes a greater share of the overburden stress.

In the event that the pore water pressure reaches a level equivalent to approximately 90% of the lithostatic overburden pressure, the rock can fracture and allow the water to escape (Boult et al., 2005). This release of pressure via the fracturing of the overburden is manifested by diatremes (mud volcanoes). One good example of such a diatreme is present in the eastern half of the survey area, shown in Figure 7-57.

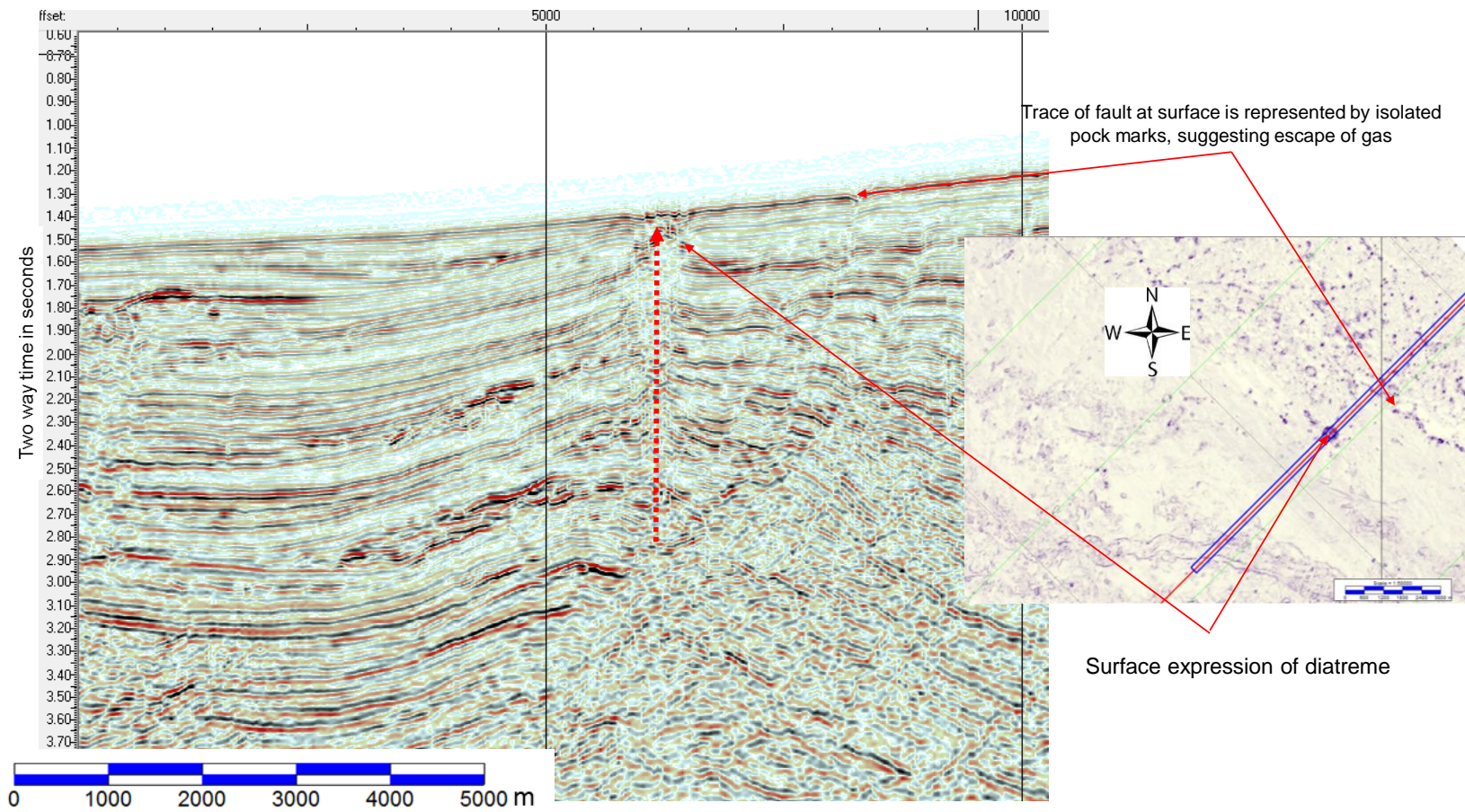


Figure 7-57: Illustration of a diatreme associated with the release of overpressure.

7.3.7 Transcurrent faulting

There are a number of linear faults mapped which when viewed in a horizontal sense are apparent within the data, but they do not conform to either normal or reverse dip-slip faulting; they are interpreted to be the result of strike-slip movement. The most striking of these fault zones is the Avon/Mahin fault zone, described in section 7.3.7.3. However, the best-imaged fault zone – labelled SS A (Figure 7-58) – is located in the north of the survey area, as noted in section 7.3.4.

Strike-slip or wrench faulting occurs when two adjacent masses of rock move primarily in a lateral manner with respect to each other. This occurs when the principle stress orientation that acts on the body of rock is horizontal rather than vertical. Under steady state conditions, with stress applied to a body, any fracture deformation will be related to the principle stress direction. Normally, the major stress is vertical and when the vertical stress is of sufficient magnitude, the body of rock will fracture according to Coulomb fracture criteria; this is usually manifested as normal faulting.

Examination of the structure maps of the suite of horizons from the sea bed to horizon 200 provides an indication of the principle stress orientation. The north-to-south oriented extension and approximately east-to-west compression indicates that the principle stress orientation within the rock volume is horizontal and is aligned south-east to north-west. Under this stress regime, the major lineament that traverses the survey area, the Avon/Mahin fault zone, is interpreted to be the result of right lateral movement within the thin-skinned deformed section. The offset along fault SS A is also interpreted to be dextral, as evidenced by the lateral displacement of both isochrones and seismic amplitudes.

7.3.7.1 Fault zone SS A

This fault zone is some 10km in length within the 3D volume, but extends beyond the boundary of the survey area (Morgan, 2004; Leduc et al., 2012; Maloney et al., 2012). It appears to terminate with two main structural trends taking up the displacement. To the north, the section is extended via means of a set of normal southward-hading faults (Maloney et al., 2012), while to the south of the fault zone, the change in lateral extent of the section is accommodated via reverse faulting, which hades in an east-to-west orientation.

When viewed in cross section, fault SS A is sub-vertical, as can be seen in the three lines that traverse the fault in Figure 7-60, but the hade of the fault alters with depth, giving rise to a nonlinear appearance when viewed in more detail. The displacement

along the fault can be estimated by measuring the offset of piercing points on either side of the fault. The presence of a number of valleys filled with debris flows can be used as means of tracing the offset. The displacement between the northern and southern half of the white line (SS A) is measured at 350 meters. The fault terminates within the survey, where the displacement is taken up by an extensional imbricate fan.

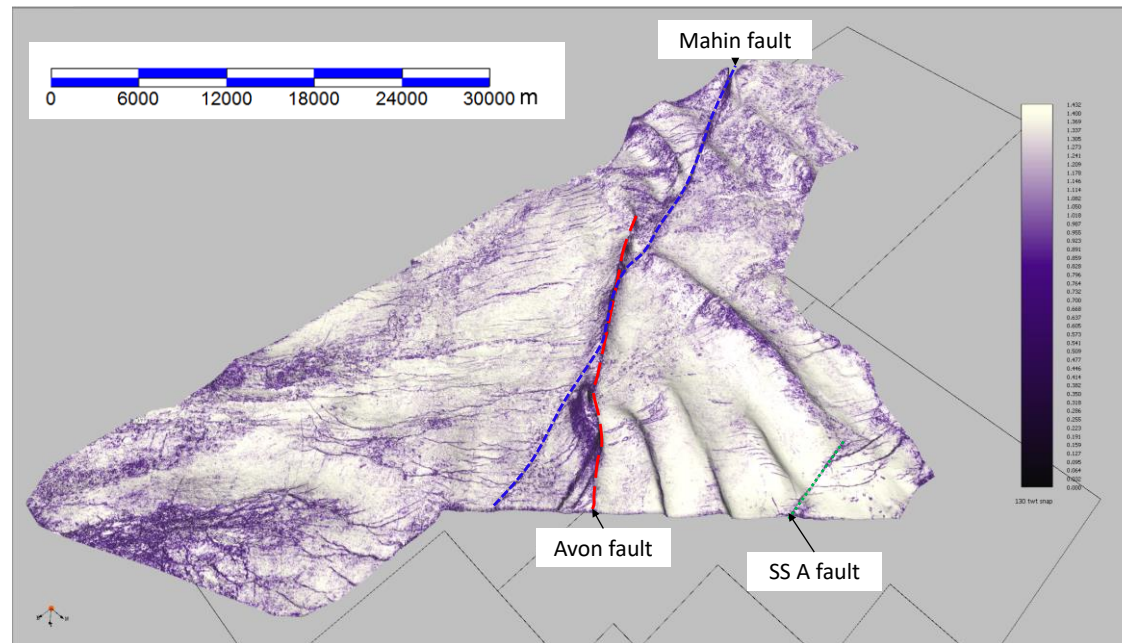


Figure 7-58: Perspective view of the Upper Miocene similarity (horizon 130) viewed from the north-east. Highlighted is the location of fault SS A in relation to the Avon/Mahin fault zone.

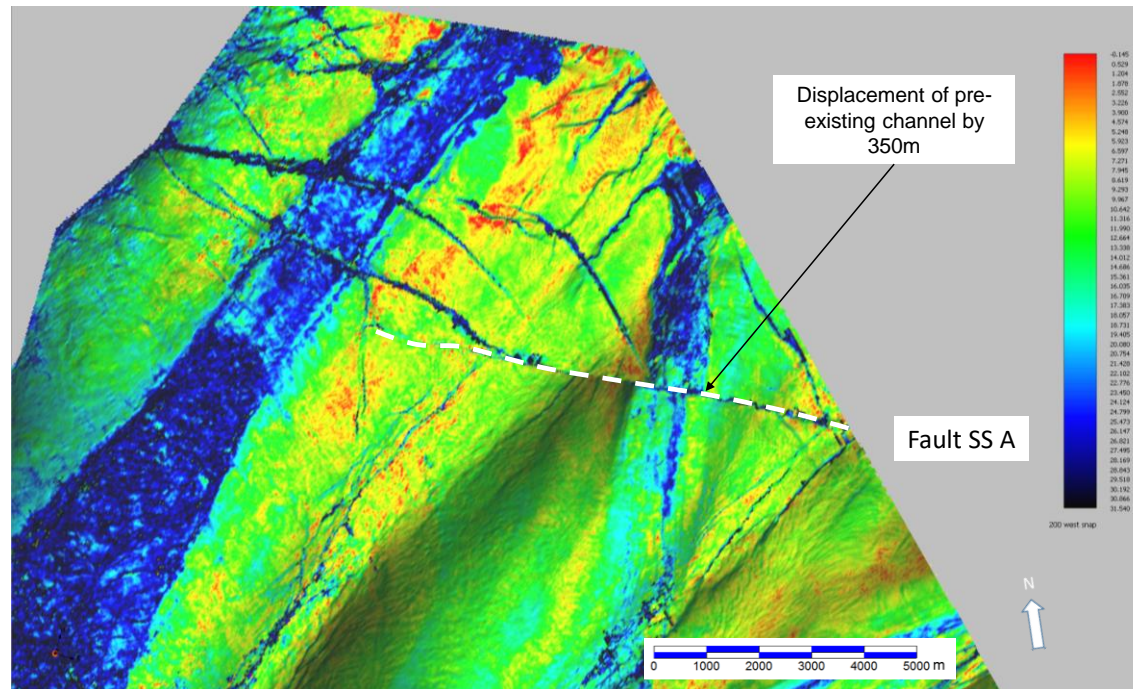


Figure 7-59: Amplitude extraction of the Upper Oligocene (horizon 200), showing the displacement of a pre-existing channel, offset by lateral movement along fault SS A.

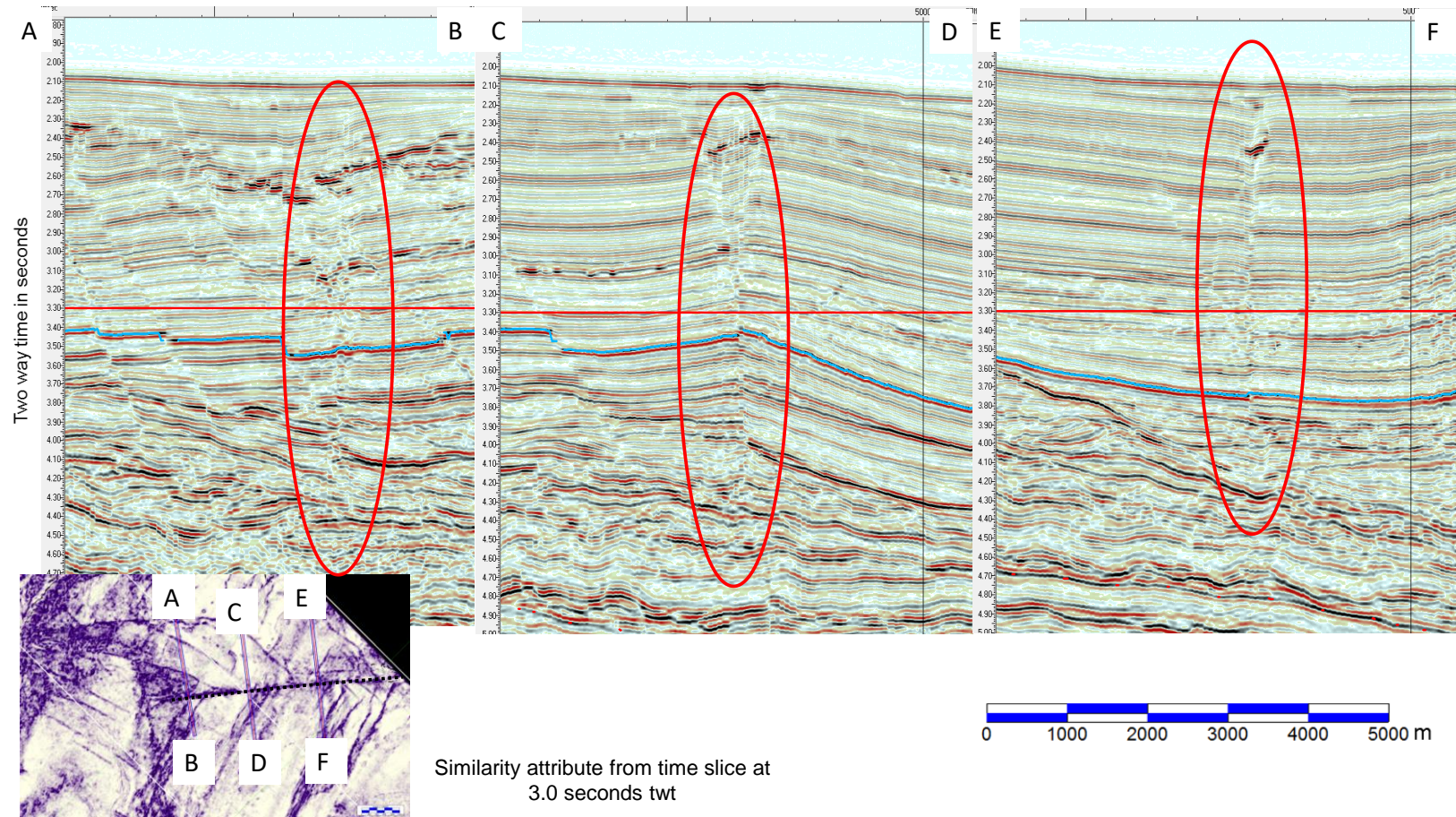


Figure 7-60: Three seismic lines which cross fault SS A, illustrating the sub-vertical nature of the transcurrent fault SS A.

7.3.7.2 Mahin and Avon fault zone

There are two major linear fault zones that intersect in the survey area: A north-east to south-west lineament labelled the Mahin fault zone and a more northerly linear zone that is labelled the Avon fault zone. The mapping that has been carried out suggests that the two faults were active at different times.

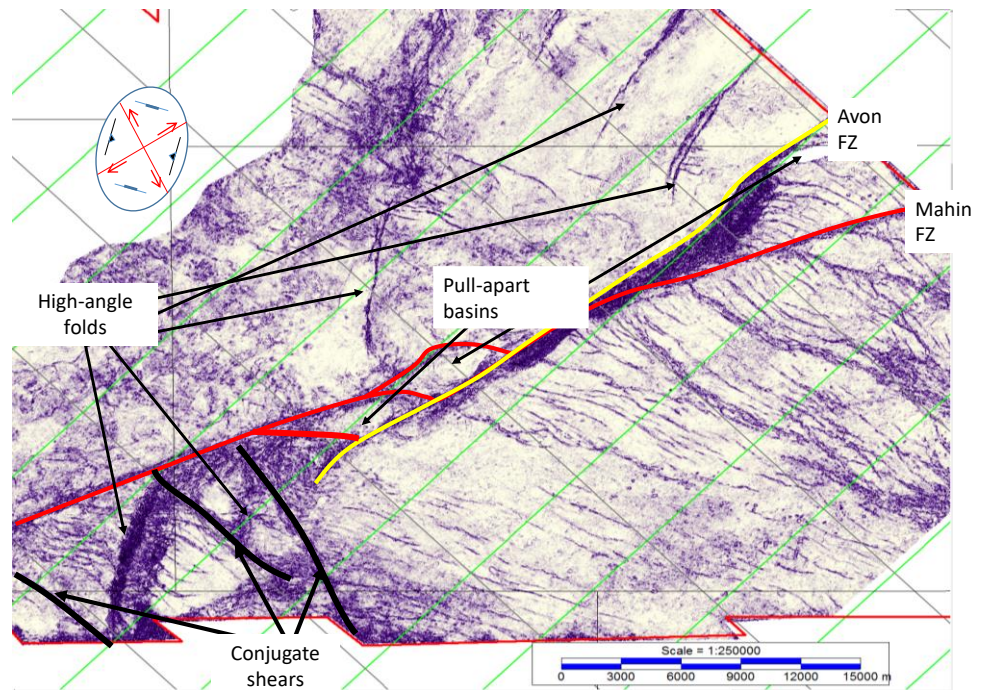


Figure 7-61: Similarity attribute of horizon 130, showing the location of the key strike-slip faults in the survey area – in red the Mahin and in yellow the Avon.

The Avon fault zone is interpreted to have its southern termination within the area covered by the 3D survey; this southern termination is accompanied by a number of possibly conjugate strike-slip faults, highlighted in red in Figure 7-61. The Avon fault zone extends northwards beyond the limits of the survey. The fault zone is best imaged at the northern edge of the 3D volume. The most striking aspect of the fault zone in this region is the steeply dipping high-relief anticline that is present. The growth of this anticline is interpreted to have been a relatively recent episode. The shallow horizons (100, 130, 160, and 200) can be character-matched across the fault zone and the growth is noted

in the interval that lies above horizon 100, as evidenced by the thinning of the section onto the flanks of the structure in the section overlying this horizon.

7.3.7.2.1 Mahin fault zone

7.3.7.2.1.1 Measurement of lateral movement

The Mahin fault zone extends for a distance in excess of 100km, with its south-western limit at the outer thrust belt zone (Morgan, 2004; Briggs et al., 2006; Wiener et al., 2009; Leduc et al., 2012). The north-eastern limit is associated with a series of extensional horse-tail faults, close to the present-day shelf. The fault zone ranges in width from around 5km at its widest to around 1km where it is thinnest. The fault zone extends to the present-day sea bed; at depth, the seismic imaging is compromised due to the complex ray paths that are present in the structurally complex fault zone, but it appears that the faults terminate at depth at or above the major mass transport deposit complex at the base of the Cenozoic.

Mapping of a number of Miocene horizons has been carried out over both the eastern and western regions of the Mahin fault zone in order to understand the more detailed fault configuration and timing and degree of lateral movement within the disturbed zone. In general, the shallow data is of a high-enough quality to trust the fault patterns that are mapped. However, at depth, the imaging of the data becomes less reliable and consequently, the deeper faulting is less well-constrained.

The spatial distribution of the faults highlights the fact that extension and compression are present on either side of the fault zone; however, the amount of extension to the east is far greater than that to the west and equally, the degree of compressional folding to the west is much larger than in the east. Figure 7-61 shows the similarity attribute extracted at horizon 130; the faulting to the west of the Mahin fault zone is more pervasive than the faults seen in the west.

A series of vertical profiles that intersect the strike-slip faults illustrate the variation in vertical displacement along the strike of the fault zone. Although the fault zone is generally vertical in cross section, there is a complex local fault arrangement when looked at in detail.

In the eastern half of the region, where the extension is greatest, an estimate of the amount of lateral (north-south) extension was made using the correlation polygons to reconstruct the original pre-displacement configuration. In Figure 7-63, the method used to calculate the approximate amount of extension is outlined. The Kingdom software

allows the correlation of portions of vertical sections. This is a very useful tool in examining the degree of extension that has occurred on either side of the strike-slip fault zone.

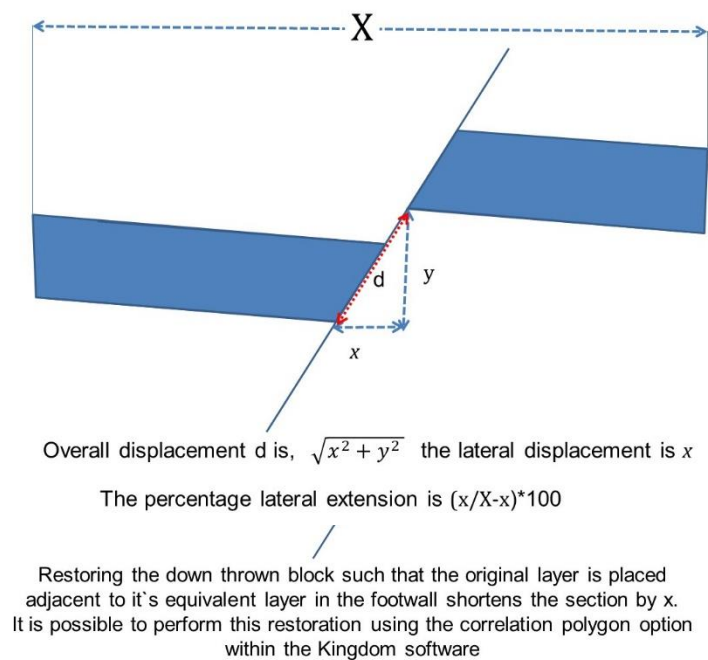


Figure 7-62: Illustration of fault displacement estimation

Figure 7-63: Method for calculating the lateral extension.

This technique has been used to restore a north-east to south-west line on either side of the major wrench fault zone. The amount of extension to the south-east of the wrench fault zone is in the region of 20% (Figure 7-66) which would, if applied to the entire fault zone, indicate for a total fault zone of 100km an extension amounting to 15km. In a 50km section, therefore the lateral extension would be 8km. The equivalent amount of extension in the western region is around 5% (Figure 7-65). The difference in lateral displacements (between 5% to the west and 20% to the east) is accommodated via the means of the trans-tensional set of faults seen within the strike-slip fault zone.

Over a 50km length of section on either side of the north-east to south-west lineament, which is the order of magnitude that is present within the 3D volume, the difference in southerly displacement of the end of the transect should be in the region of 15%, or an amount equal to 7.5km. This order of magnitude is in line with the estimates derived from two other means of estimating the lateral displacement, as well as that suggested by Leduc (2012).

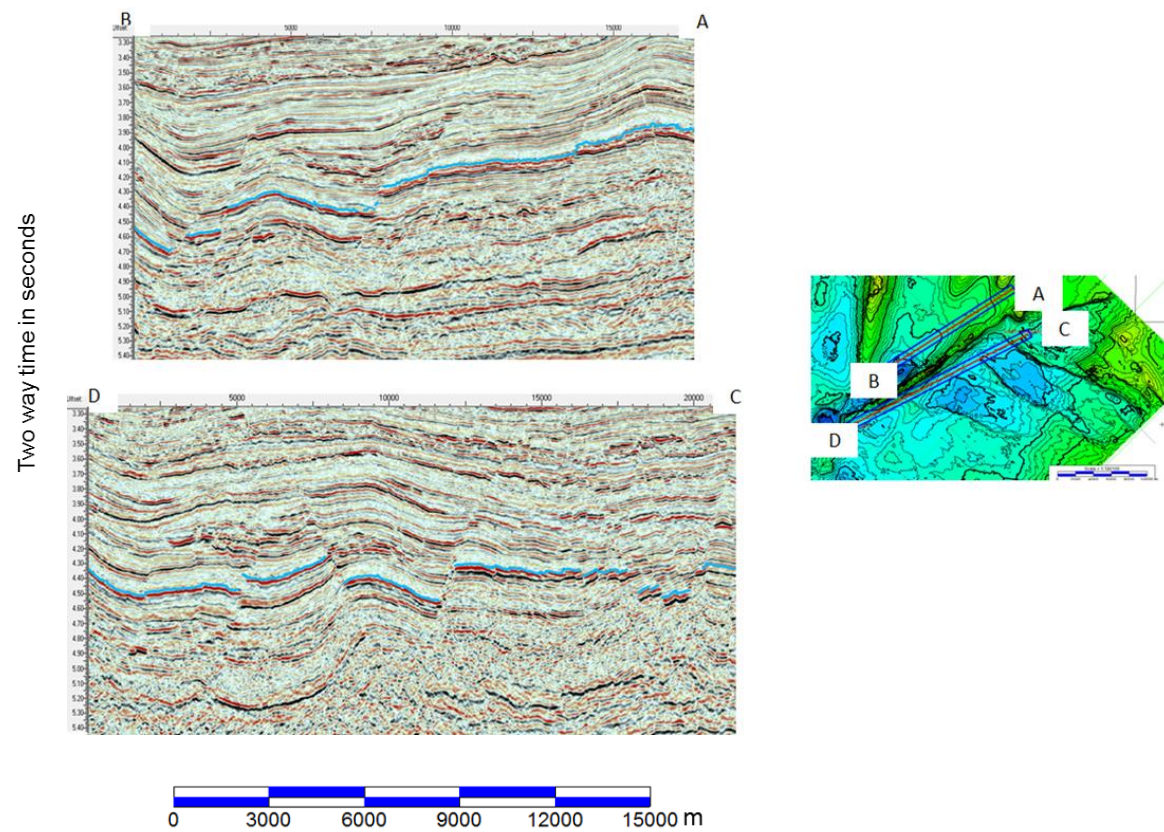


Figure 7-64: Portion of two seismic lines on either side of the Mahin fault zone; the two lines are used to illustrate the varying degree of extension on either side of the strike-slip fault zone in the following figures.

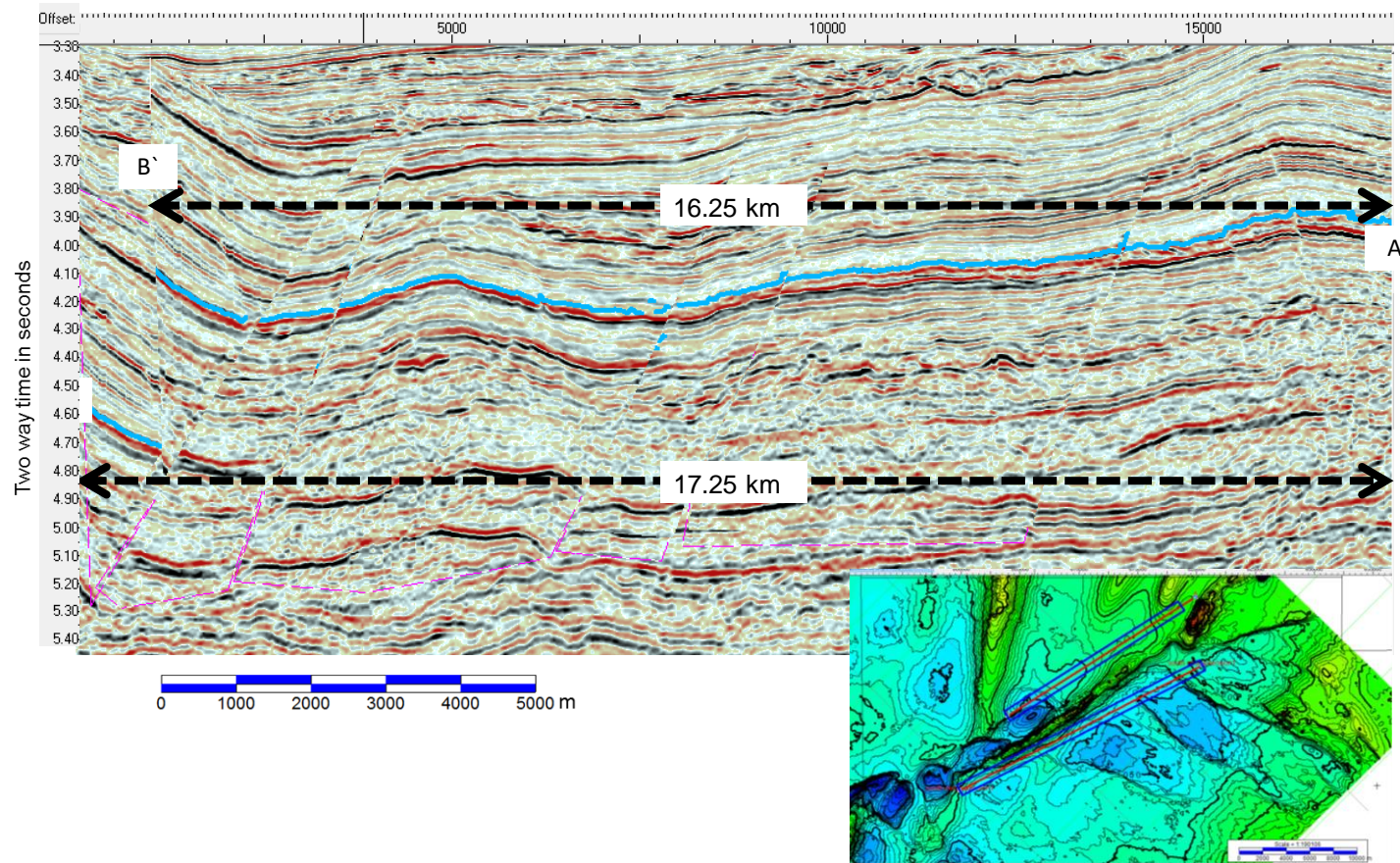
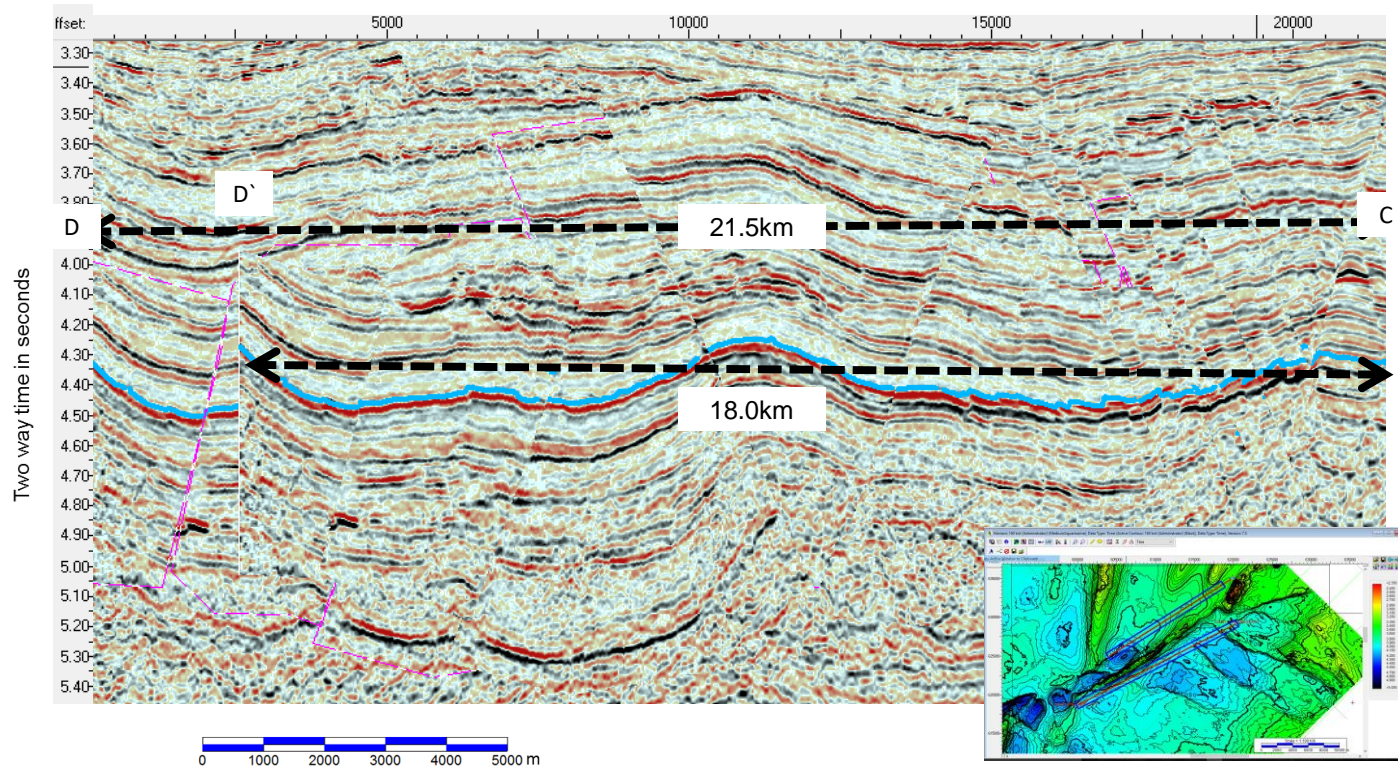


Figure 7-65: Portion of a random line that lies to the north of and runs parallel to the Mahin fault zone.



The overall length of the section is 21.5 km; after restoring horizon 200 (the blue marker), the equivalent length is 18.0 km. This implies that the original 18.0km has been extended to 21.5km as a percentage, this amounts to approximately 20%.

Figure 7-66: Portion of a random track through the volume, which runs to the south of and parallel to the Mahin fault zone.

In the preceding three figures (Figure 7-64, Figure 7-65, and Figure 7-66), the estimate of the degree of extension is outlined for two lines that lie on opposite sides of the Avon/Mahin fault zone.

An alternative way of estimating the degree of lateral displacement is by tracing the offset of piercing points. This approach has been used at four stratigraphic levels where slope channels have been mapped. In order for this method to work, the correct stratigraphic correlation is required to ensure that the same stratigraphic level is correlated across the fault zone. The use of seismostratigraphy (Mitchum Jr. et al., 1977) to match high and low stands on either side of the fault zones was required. In order to identify the channels in map view, root mean square amplitude extractions were calculated in windows, as follows. Three of these channel displacements are shown in Figure 7-68 to Figure 7-73.

These observations indicate that movement along the fault has been fairly continuous, with the deeper stratigraphic levels being offset to a larger degree than the later deposited, shallower channels. In Figure 7-67, this is outlined. In Figure A, there is no displacement of the channel – which is represented by the sinuous line – along the fault, which is indicated by the diagonal line that runs from the south-west to the north-east. In Figure B, the channel has been displaced in a right lateral sense. A younger channel (in green) is then deposited in Figure C. Later movement along the fault displaces both the green and the blue channels (D). This is repeated for a younger channel in red. The cumulative motion is recorded by the oldest channel displacement.

An additional support for the amount of displacement was gained by mapping the isochrone thickness of the interval between horizons 160 and 200. Although this is complicated by the late-stage transpressional motion along the fault zone, away from the immediate disturbed interval it is possible to trace the extension of two pre-existing grabens. This approach is used to estimate the amount of displacement at horizon 160. The 5km that is required to realign the grabens ties in with the channel restoration noted above.

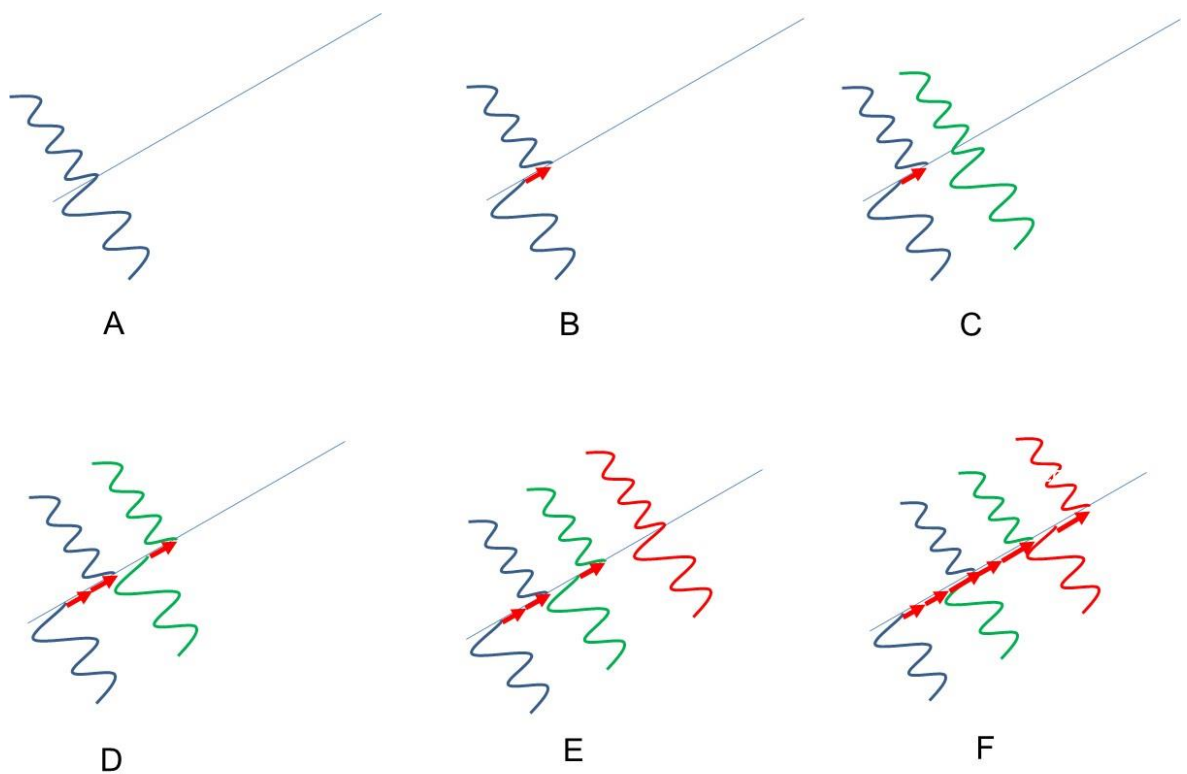


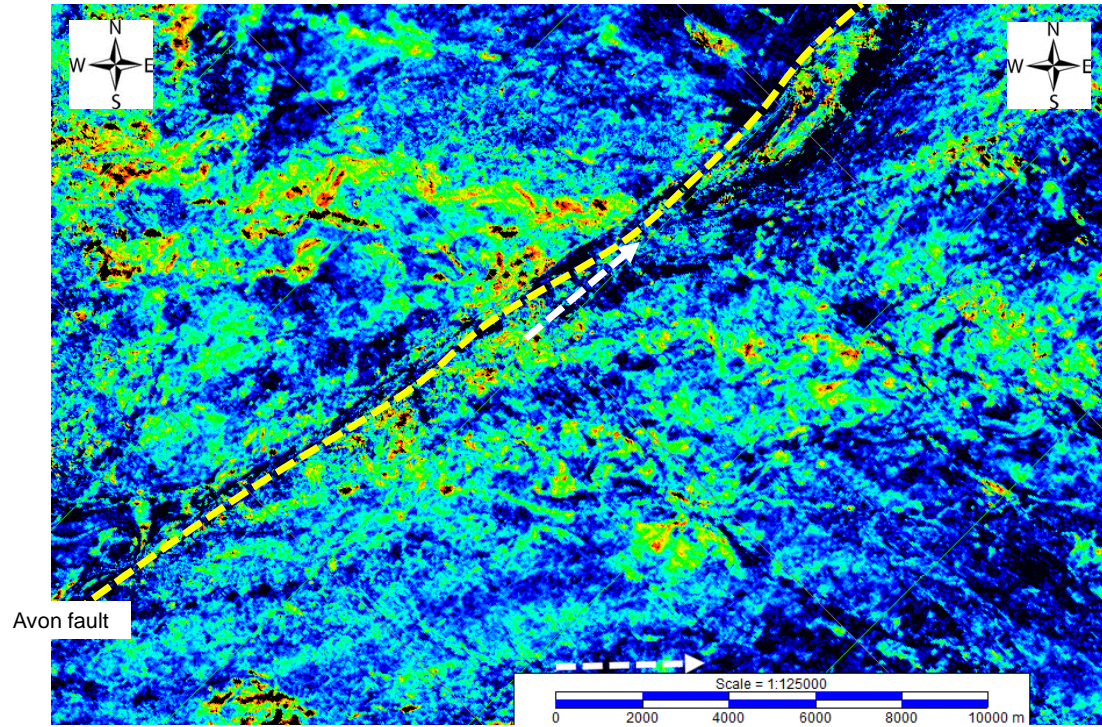
Figure 7-67: Displacement of channels by lateral movement.

In Figure 7-68, the green and yellow colours represent the channels within the interval. The white arrow indicates the direction that the south-eastern block needs to move to align with the channels to the north-west.

In Figure 7-70, the presence of a number of slope channels can be identified by the blue colours. The slope channels tend to contain mixed lithologies that generate a variety of acoustic boundaries not found in the background fine-grained sediments. It is evident that both the northern and southern channels systems are offset at the Mahin fault zone, as shown by the black dashed line. The white arrows indicate the sense of displacement along the fault of the channels due to right lateral strike-slip motion.

In Figure 7-71, the south-eastern half of the map shown in Figure 7-70 has been laterally shifted by approximately 5km. Following this shift, the two main slope channel complexes now lie adjacent to each other on the opposite side of the fault zone, supporting the conclusion that the fault in this region has moved some 5km since the deposition of the channels.

RMS amplitude extraction from a window within the Middle Miocene (between horizon 130 and a pseudo-horizon 75 milliseconds above horizon 130). The apparent offset at this level, indicated by the white arrow, of the channel system by the Avon fault (yellow dashed line) is estimated to be 3.5km.



The green and red amplitudes are seen to meander across the mapped interval. This is interpreted to indicate the presence of a channel system. The northern limit of the channel system is offset by the dextral movement along the Avon fault.

Figure 7-68: RMS extraction of the interval between horizon 130 and 100ms above the horizon.

Shifting the south-eastern portion of the map in Figure 7-68 by 3,5km aligns the norther margin of the mapped channel systems across the Avon/Mahin fault zone. The white arrow indicates the sense of relative displacement.

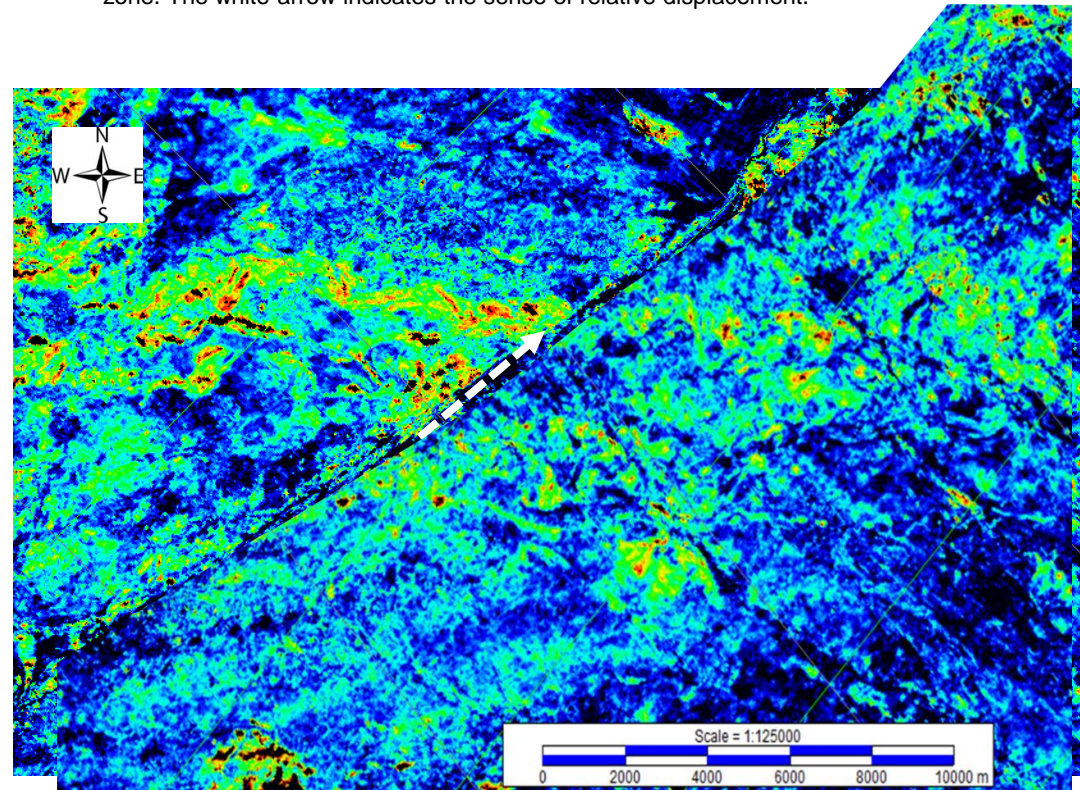
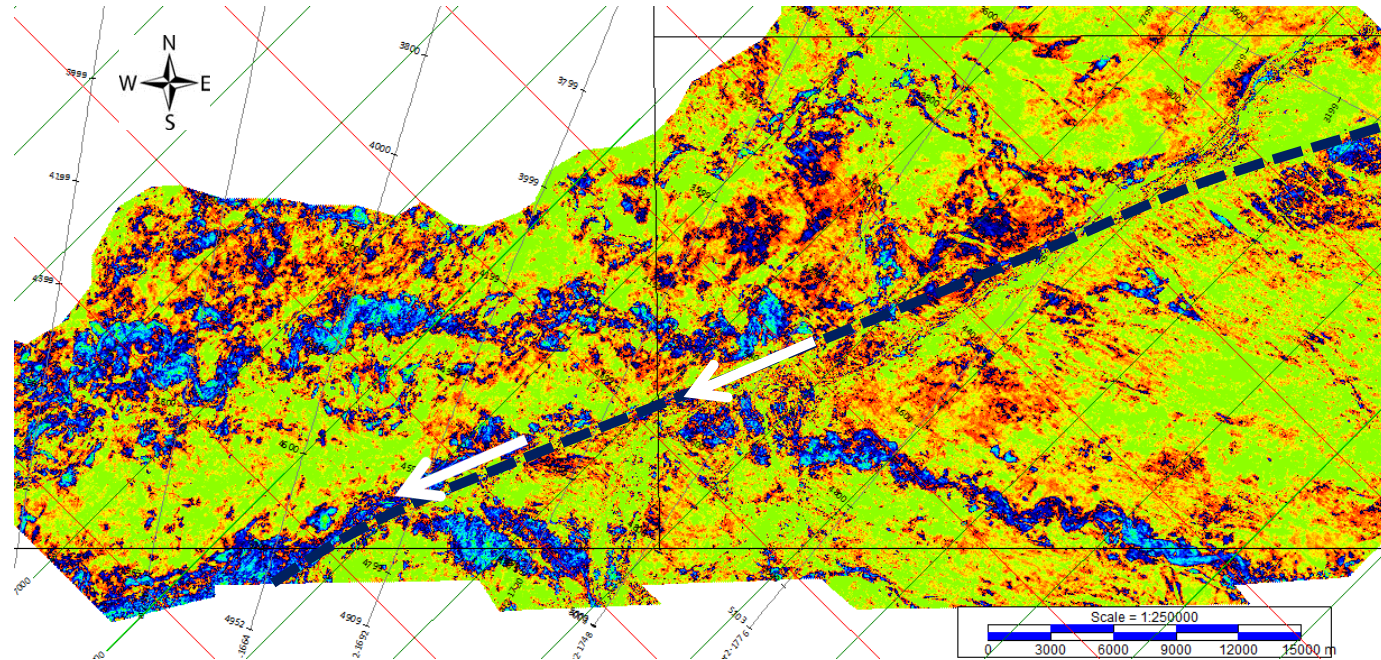


Figure 7-69: RMS extraction from horizon 130 to 100ms above the horizon, with the south-eastern block shifted 4km to the north-east.

The lateral shift of the south-eastern block by 3.5km aligns the channels across the Avon/Mahin fault zone

RMS amplitude extraction from a window in the Middle Miocene (between horizon 160 and a pseudo-event 100ms below horizon 160). The blue colours are interpreted to be slope channel deposits which have their provenance beyond the boundary of the 3D volume in the east. The dashed black line is the location of the Mahin transcurrent fault zone.



The white arrows indicate the inferred lateral displacement, measured at 6.2km, of the channels as a result of dextral movement along the Mahin fault (the dashed black line). The displacement measured for both of the channels is similar.

Figure 7-70: RMS extraction of a window 100ms below horizon 160. The blue colours represent a series of slope channels.

By moving the south-eastern part of the map in figure by 6.2km along the dashed black line (which represents the location of the Mahin fault zone), an alignment of the two significant channel complexes is achieved.

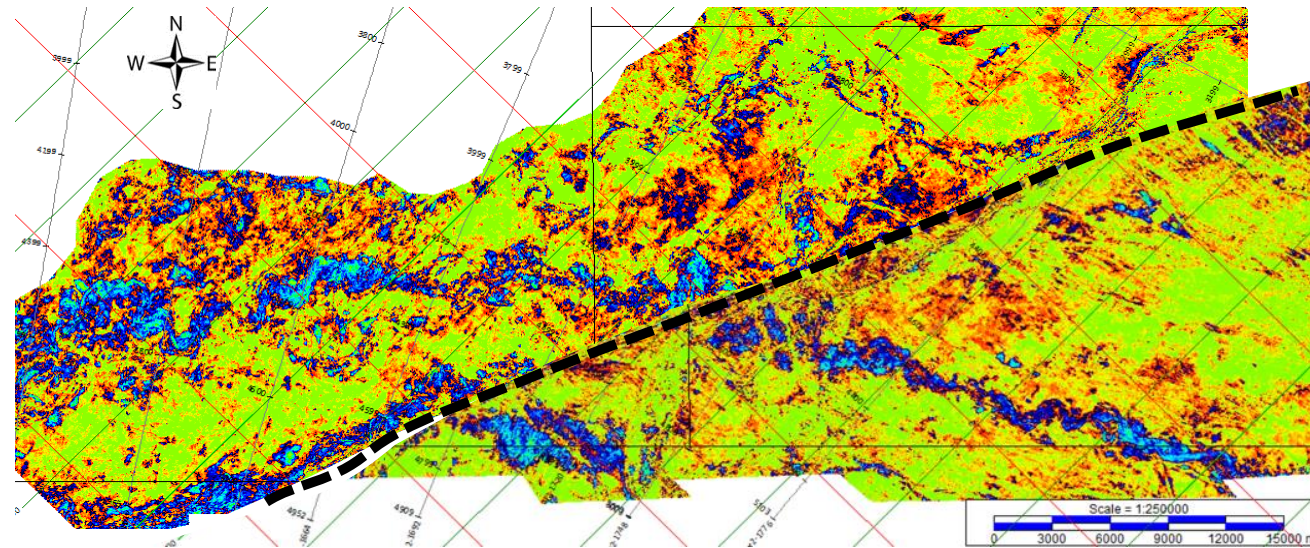
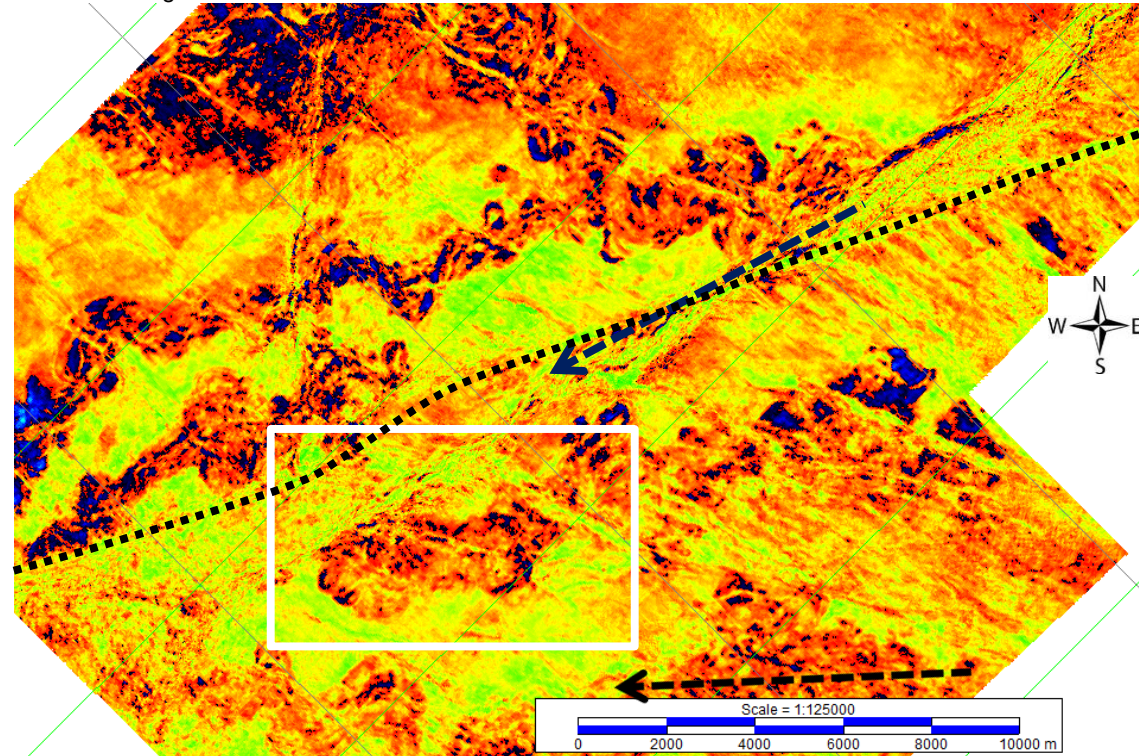


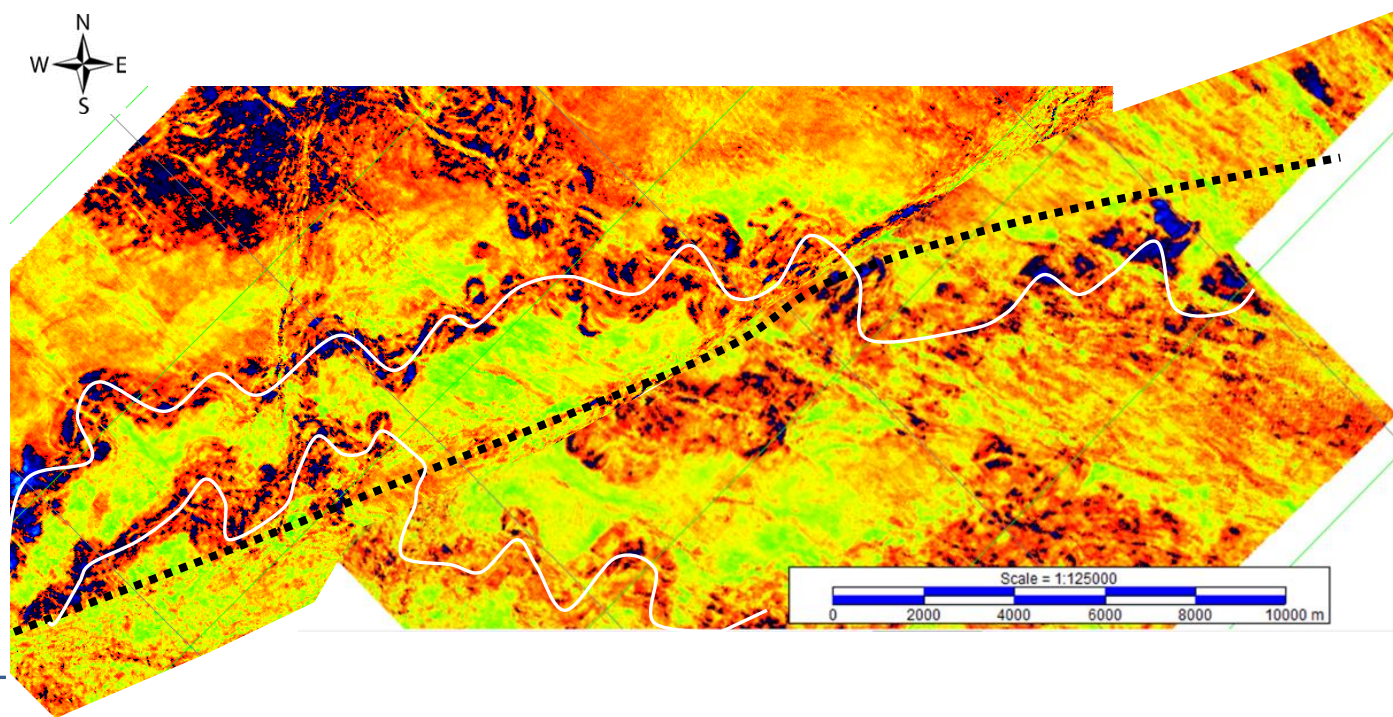
Figure 7-71: In this figure, the map has been split at the Avon/Mahin fault zone and moved approximately 5km.

RMS Amplitude extracted from an interval between 300 and 400ms below horizon 160. The red/blue amplitudes are interpreted to be slope channel belts. Also present is an interpreted terminal splay highlighted in the white rectangle. The amplitudes to the east of the transcurrent fault zone are less well-defined due to the large amount of post-depositional faulting.



The black arrow represents the inferred sense of relative lateral displacement of the south-eastern portion with respect to the north-western region - a distance of 7.8km.

Figure 7-72: RMS amplitude extracted from a window in the Lower Miocene, showing the location of two channel belts.



By moving the south-eastern region by 7.8km towards the north-east, a good fit of the two slope channels is observed across the transcurrent fault zone (black dashed line). The terminal splay identified in the previous figure is interpreted to have been located in a trans-tensional depression adjacent to the active fault zone. It is therefore not present to the north-west of the main fault zone.

Figure 7-73: A reconstruction of the channel belts after shifting them by 7.8km in a dextral sense.

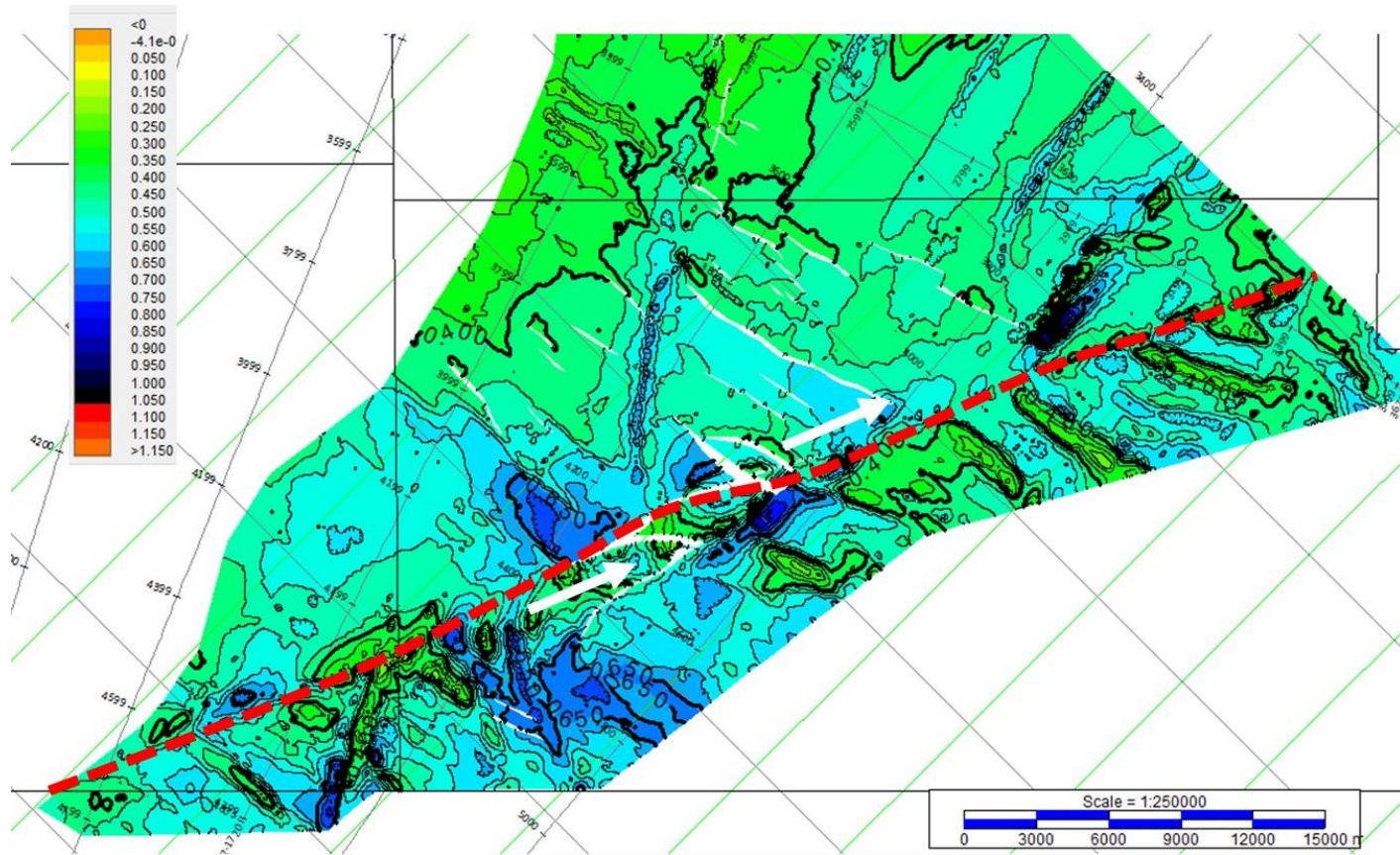


Figure 7-74: Isochrone map of the interval between horizons 160 and 200.

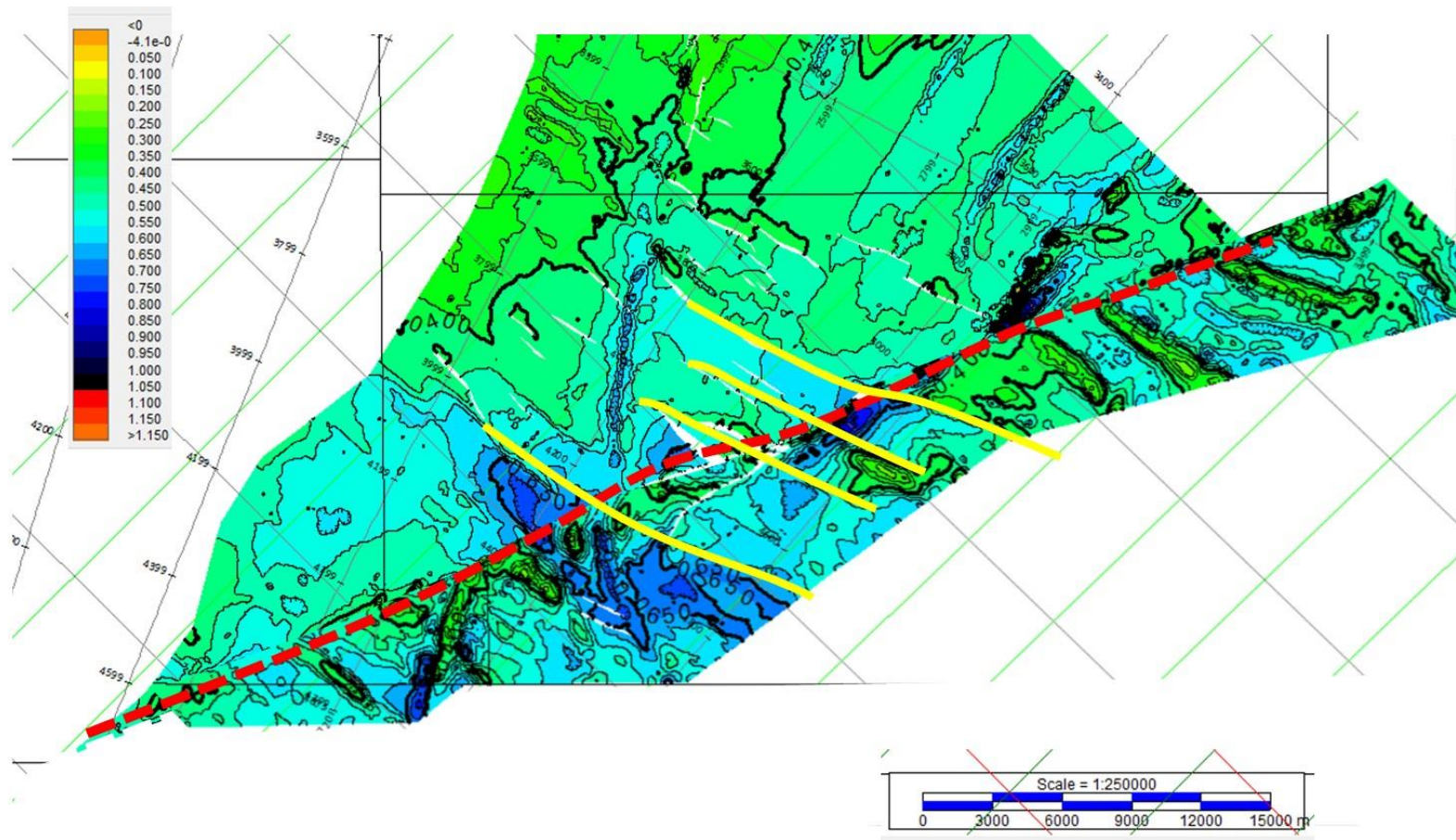


Figure 7-75: Isochrone of thickness between horizons 160 and 200, with the south-eastern domain shifted by 7km to the north-east.

In Figure 7-75, the alignment of the isochrone thicks across the fault zone line-up, once the south-eastern section is restored via a 5km shift to the north-east. The yellow lines are indicative of the original extensional faults that predated the onset of lateral displacement.

In Table 7-1 are listed the calculated offsets along the length of the Avon/Mahin fault zone. The increase of lateral displacement with depth suggests that the Mahin fault has been active from the Early Miocene up to the Pliocene. The Pliocene and younger movement is outlined in the following section. The estimated ages of the horizons mapped, if correct, suggest that the fault displacement has not been uniform. The rate at which the lateral movement occurred is interpreted to have been greatest during the Middle Miocene (between horizons 130 and 160).

This period coincides with the main influx of the slope channel complexes from the east.

Table 7-1: Calculated lateral displacement along the Avon/Mahin zone.

| Horizon | ID | Approx Age Ma | Method | Estimated Displacement km | Rate of Slip km/Ma |
|----------------------|-----|------------------|--------------------|------------------------------|-----------------------|
| Sea Bed | 0 | 0 | | 0 | |
| Top Miocene | 100 | 5 | Channel Offset | 2.5 | 0.50 |
| Base Upper Miocene | 130 | 9 | Channel Offset | 3.5 | 0.25 |
| Base Middle Miocene | 160 | 12 | Channel Offset | 6.2 | 0.90 |
| Lower Middle Miocene | 190 | 16 | Channel Offset | 7.8 | 0.40 |
| Top Lower Miocene | 200 | 18 | Fault displacement | 7.5 | |
| Base Miocene | 200 | 17 | Relative extension | 7.5 | |
| Base Miocene | | | Leduc (2012) | 7.0 | |

7.3.7.2.2 Avon fault zone

In contrast to the Mahin fault zone, this tectonic lineament is considered to represent transpressional motion. The presence of a number of high-relief anticlines can be observed in the maps of the shallow Base Pliocene (horizon 100). It was not possible to identify any convincing piercing points that could be used to establish the sense of displacement along this fault zone. However, the degree of displacement at the base of the Pliocene may indicate that 2.5km of dextral movement has taken place during the Pliocene until the recent period. The recent channels seen at and close to the sea bed are not seen to be offset. It is interpreted that regional stress altered such that the lateral strike slip motion in the region shifted to fault SSA. The isochrones of the thickness between the shallow horizons do not exhibit large variations across the fault zone.

7.3.7.3 Timing of movement

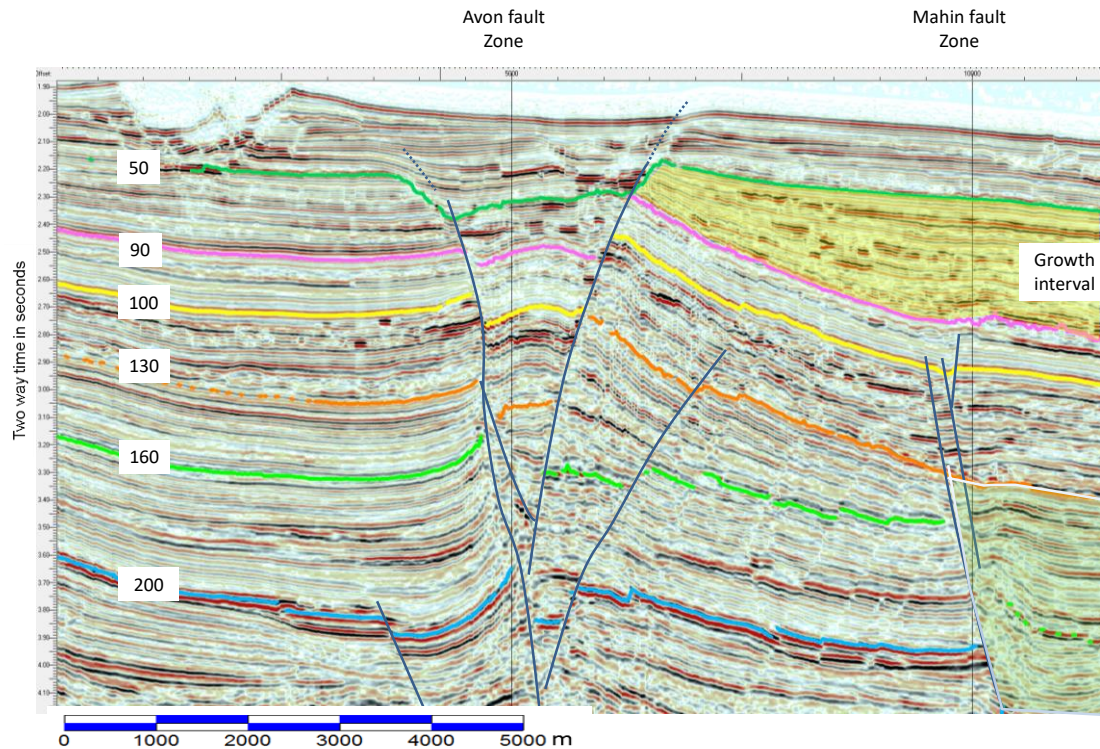


Figure 7-76: Seismic cross section through the northern portion of the survey, showing the "negative flower structure" associated with the Avon fault.

The image in Figure 7-76 shows a vertical transect through the Avon and Mahin faults. It is interpreted that the timing of movement on the Avon fault occurred in the Pliocene to Pleistocene era (the yellow shaded region). The Mahin fault shows the major growth to have taken place in the Middle Miocene (below horizon 130 – the green shaded area). The horizons that are highlighted indicate limited amounts of thickness variation across the Avon fault zone. The upper limits of the faulting have been eroded by the down-cutting of the Mahin canyon. The presence of a number of smaller fault zones that are found close to the southern termination of the Avon fault may indicate that they are conjugate strike-slip faults or tear faults formed as a result of compression from the south-east, which accompanies the Niger Delta gravitational push.

7.3.7.3.1 Recent movement

As noted above, the Avon/Mahin fault zone has been active from at least the Lower Miocene (horizon 200 times) and is still active today, as evidenced by the presence of anticlines at the present-day sea bed and the appearance of linear fault traces in the near sea-bed similarity extractions.

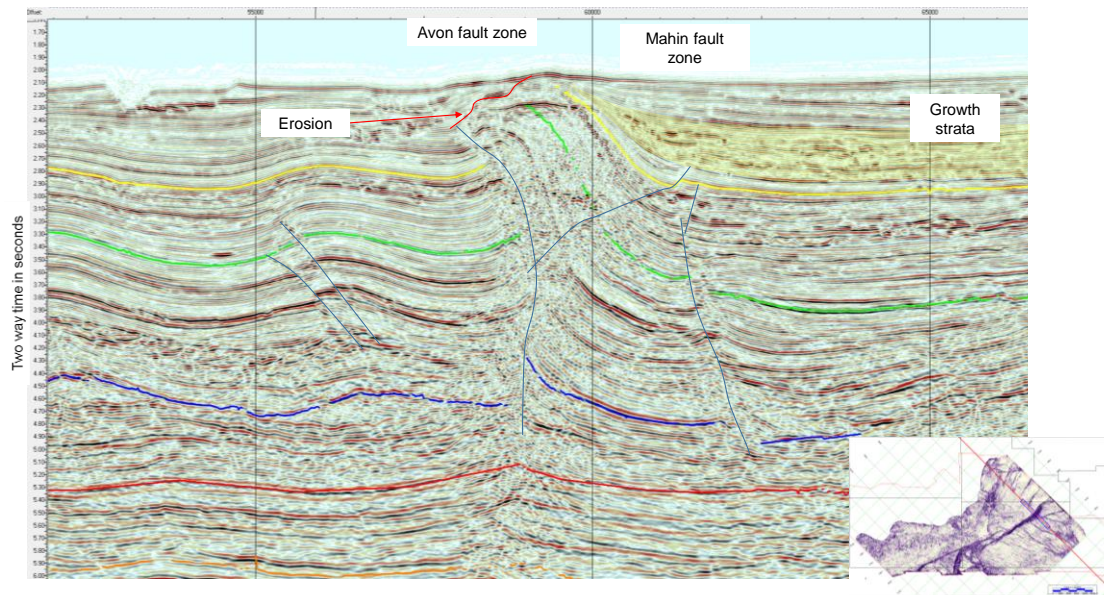


Figure 7-77: Seismic Cross section through the Transpressional portion of the Avon Fault zone, showing a characteristic "pop-up" structure.

In Figure 7-77, the yellow shaded region indicates the period of interpreted growth of the compressional anticline. The surface of the anticline shows evidence of syn-tectonic erosion, which supports the late-stage movement on this structure. The evidence in both Figure 7-76 and Figure 7-77 is interpreted to indicate that movement along the Avon fault took place in the Pliocene. The most recent Pleistocene episode of activity is the influx of Mahin canyon-sourced sediments that have been deposited post the major tectonic disturbance associated with the Avon fault.

Additional evidence to support the interpretation that the Avon fault is a relatively recent structural feature is indicated by the examining the isochrone of the interval between the present-day sea bed and the Base Pliocene (horizon 100). This map indicates that the interval is thinner over the crests of the anticlines. This thinning is attributed to the onlap of sediments onto emergent highs (Figure 7-78).

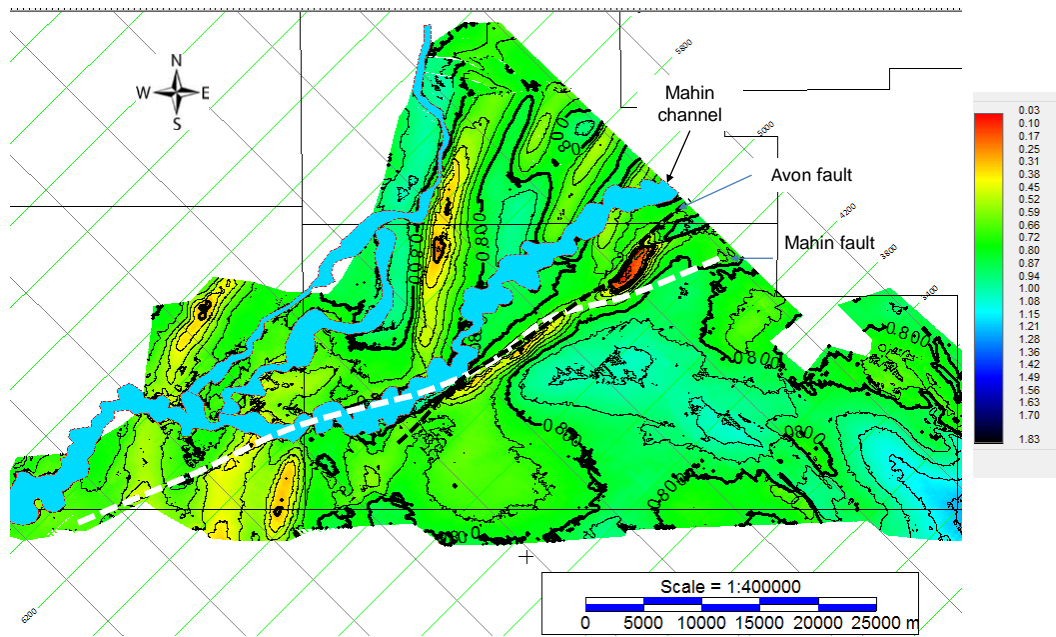


Figure 7-78: Isochrone of the Pliocene to recent interval.

In Figure 7-78, the presence of the thin regions corresponds to the location of the recently formed anticlines. The amount of displacement that has occurred in the Pliocene to recent has been estimated at 2.5km, by measuring the amount of displacement at the level of the Base Pliocene event (horizon 100).

The Mahin fault appears to have been active throughout the Miocene. A number of pieces of evidence support this observation. In the western portion of the region (the present day compressional zone), there are a number of normal faults that have been mapped. These faults are seen to terminate at or around the middle Miocene (horizon 160), as illustrated in section 7.3.2. They appear to have been syn-sedimentary in nature, having with the faulting largely ceased by the time that horizon 160 is deposited. As supporting evidence for this syn-sedimentary nature, an isochrone of the interval between horizons 160 and 200 (Figure 7-74) demonstrates that growth occurred during this interval, on both sides of the Mahin fault zone. The isochrone for the Upper Miocene interval (between horizons 130 and 160), on the other hand, indicates that the normal faulting to the north-west of the Avon/Mahin fault zone was no longer active.

7.3.7.3.2 Early movement

The early motion is interpreted to be primarily trans-tensional, as evidenced by the predominance of normal faulting in the interval that is capped by horizon 160 (see section 7.3.3.1). The isochrones for the various intervals, away from the Avon/Mahin disturbance, all indicate a thickening of section associated with the extension.

The Mahin fault zone, on the other hand, displays a change in character, notably below horizon 130, which would indicate that the majority of the lateral displacement took place along this trans-tensional fault. In Figure 7-74, the thickness of the interval between horizons 160 and 200 indicates that there were a number of horsts and grabens present on both sides of the Avon/Mahin fault zone during this period (the blue colours are the thicker intervals and indicate the presence of the grabens). As seen, it is striking that there is an absence of extensional faulting in the post-horizon 160 interval on the north-western side of the lineament. This would suggest that the lateral displacements along the fault commenced at or around horizon 160.

Figure 7-79 illustrates the growth in the hanging wall of the western boundary fault of the Mahin fault zone. The growth occurs in the interval below horizon 160, which also coincides with the calculated largest rate of lateral movement (Table 7-1) and the influx of slope channels from the east. This period is also the period of extensive growth of extensional faulting in the region to the south-east of the fault zone.

The whole of the Niger Delta is interpreted to be deformed in response to the gravitational imbalance between the thick shelfal/shoreline section and the thin deep-water interval (Wu et al., 2015). The delta has an arcuate geometry such that the orientation of the principle stress, which should remain orthogonal to the direction of thinning, alters from north-east to south-west in the centre of the delta to a more south-east to north-west in the region of this study (Figure 7-80). The centre of the delta thins onto the oceanic abyssal plain; however, in the north-west of the delta where this study is located, this is not the case. In the case of the delta's central sector, the lateral motion downslope terminates in the outer thrust belt (Cohen and McClay, 1996; Bilotti and Shaw, 2005; Corredor et al., 2005; Morley et al., 2011; Wu et al., 2015). In the north-west of the delta, lateral motion of sediment due to gravitational sliding is constrained; instead of the sediments moving downslope, they are blocked from moving in an orthogonal sense down slope they are blocked by a sediment pile that has been sourced from the north.

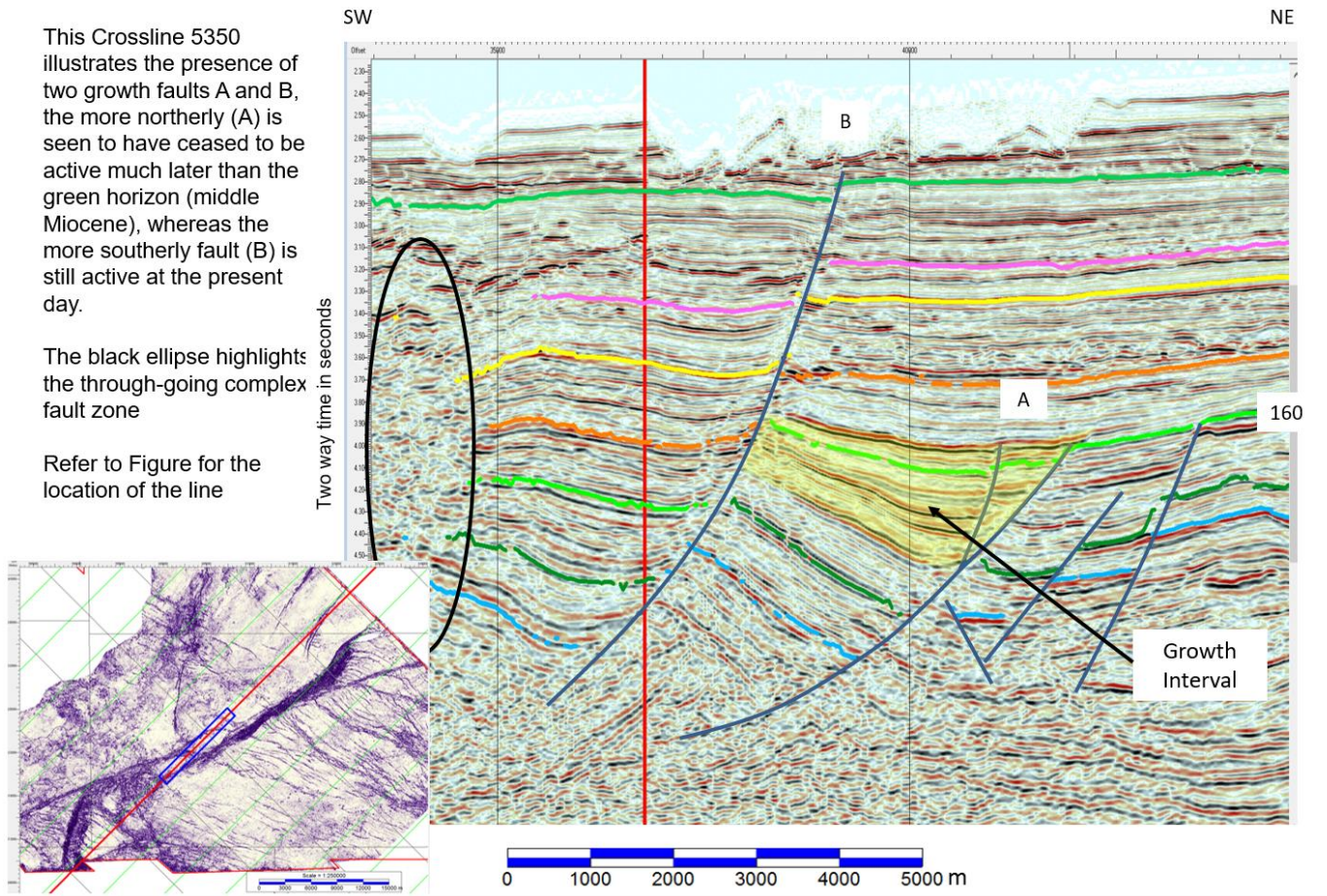


Figure 7-79: Seismic line running along the western side of the Mahin fault zone.

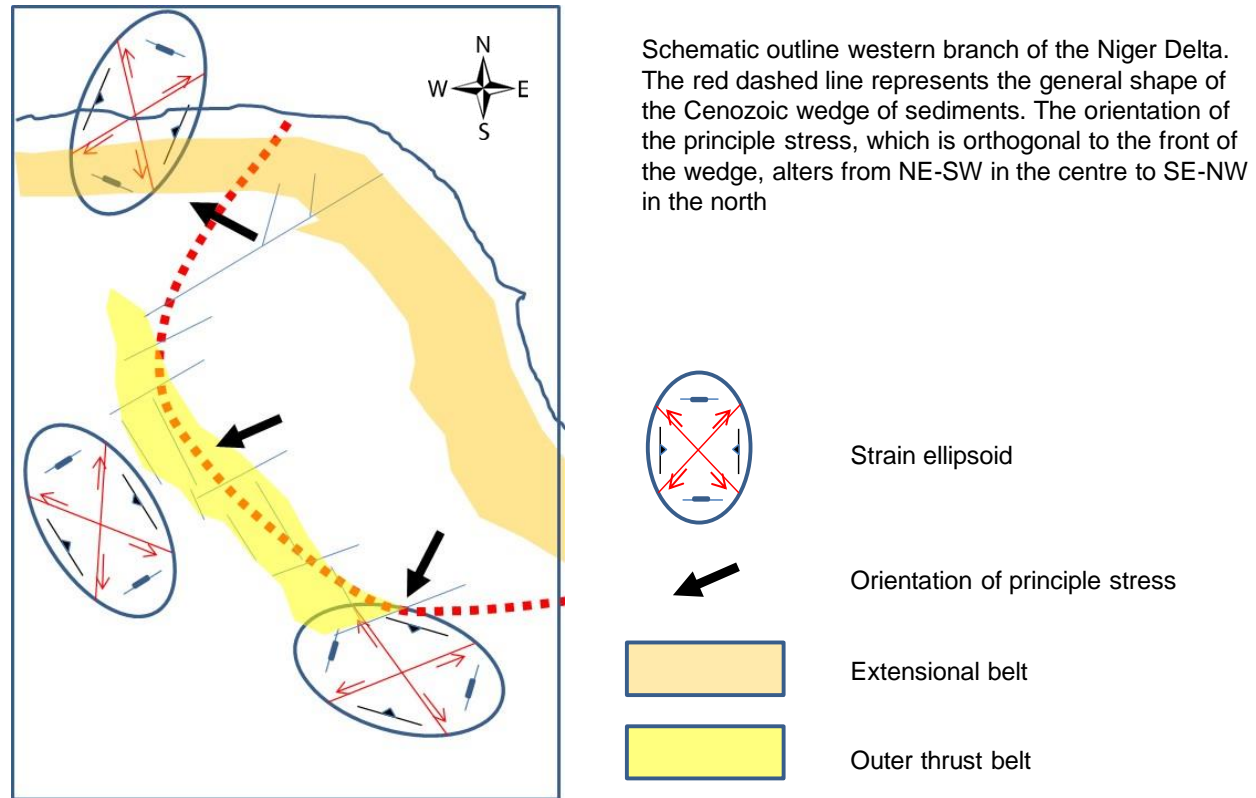


Figure 7-80: Illustration of how the principle stress direction alters across the Niger Delta.

Chapter 8

Contents

| | | |
|-------|---|-----|
| 8 | Discussion | 271 |
| 8.1 | Mass transport apron as the Cenozoic detachment interval..... | 272 |
| 8.1.1 | Origin of the mass transport deposits | 272 |
| 8.1.2 | Nature of mass transport deposits | 276 |
| 8.2 | Origin of the large-scale levees | 279 |
| 8.2.1 | Contourites | 279 |
| 8.2.2 | Turbidites..... | 280 |
| 8.2.3 | Nature of the levees | 282 |
| 8.3 | The origin of the Avon/Mahin fault zone..... | 287 |
| 8.3.1 | Is there a deep basement control?..... | 287 |
| 8.3.2 | Gravity imbalances in the Cenozoic..... | 292 |
| 8.3.3 | Evolution of the Avon/Mahin fault zone..... | 296 |

8 Discussion

The linkage between sediment distribution and the subsequent tectonic deformation, as outlined in the preceding chapters, points to the observation that the structural arrangement is a function of the prior sedimentation. In this chapter, the observations concerning the nature of both the sedimentary processes and the subsequent deformation are collected together.

The two sedimentary processes that have contributed most to the deformation are the deposition of a widespread apron of mass transport deposits (chapter 6.3.4) and the formation of the large-scale levees (chapter 6.3.3).

The origin and role of mass transport deposits and the role they play as a constituent part of the thin-skinned deformation is outlined, along with the nature of the subsequent deformation. The nature of the construction of the levees, being diachronous and accomplished in a multiphase manner, has led to localised tectonic stress variations and subsequent deformation that is limited to the margins of these features (chapter 7.3.5).

The observation that the upper surface of the mass transport deposit at the base of the Cenozoic is the lower boundary of the thin-skinned deformation raises the question as why this is the case. In the following sections, one explanation for this being the case is outlined.

The deformation within the levees appears unrelated to the deltaic tectonics associated with the growth of the Niger Delta cone. One possible explanation for this deformation is included in this set of observations.

The origin and nature of the transcurrent fault zone (chapter 7) that passes through the region that has been studied is discussed and an interpretation of the history of this disturbance is outlined, along with a possible explanation for its initial formation and subsequent motion.

8.1 Mass transport apron as the Cenozoic detachment interval

8.1.1 Origin of the mass transport deposits

The Albian to Turonian shallow marine deposits located along the Benin Embayment shelfal region that have been found in the exploration wells are comprised of lithified carbonates and sands (Kaki et al., 2012). Overlying the Turonian shallow marine sands are sediments that are comprised mainly of fine-grained shelf and deep-water deposits (Onuoha and Ofoegbu, 1988; Olabode, 2006; Kaki et al., 2012), which range in age up to the present day.

The section that underlies the Base Cenozoic mass transport deposit is assumed to be Upper Cretaceous in age, as discussed in chapter 5. During the Campanian and Maastrichtian, a rise in global sea levels is observed (Mitchum Jr. et al., 1977; Vail et al., 1977). Towards the end of this period, as a result of this forced regression, the deep water would have led to the limited deposition of hemipelagic sediments and an increase in percentage terms of pelagic organic material at the sea bed.

An interpretation of the evolution of the basin margin is illustrated in Figure 8-1 and Figure 8-2.

1. The Albian to Turonian shelf margin to slope break noted above is interpreted to have been a relatively sharp with the margin eroded and talus deposited in the adjacent deep water.
2. With the rise in relative sea level in the Upper Cretaceous, this shelf and steep slope were submerged and overlain by deep marine deposits. The Upper Cretaceous marine section comprised shales that are known to on-lap and overstep the palaeo shelf margin. Of note is the interval of organic rich shale noted by Kaki (2012), which is referred to as the lower Araromi shale.
3. The deep-water Upper Cretaceous section was gradually transgressed by the outbuilding of a shallow water shelfal sequence in the Palaeocene and Eocene. This shelfal sequence, as it built out over the underlying section, would have

undergone compaction. The fossil shelf would not have compacted as much as the adjacent marine shales. This could have led to an uneven surface at the location of the fossil shelf break.

4. Shales are known to compact under the influence of an increasing sediment load that is deposited above them. The remnant shelfal sediments, however, do not compact. This lateral difference in compaction leads to an increase in slope of the marine shales over the palaeo shelf edge. This increase in slope gradient, combined with a weak layer of low shear strength, are key factors in the destabilising of shelf margin strata (Cartwright and Jackson, 2008).
5. The shelfal region would have remained unstable with the deposition of shelfal material throughout the Oligocene to the Miocene. This is interpreted to have led to the further collapse of the section overlying the decollement layer.

The presence of an organic rich shale within the Upper Cretaceous section noted above is interpreted to be a layer of low shear strength; it is known that under increasing temperature and pressure, organic rich shale generates hydrocarbons (Demaison and Murriss, 1984; Osborne and Swarbrick, 1997). The expulsion of hydrocarbons can lead to the onset of overpressure – a contributing factor in the lowering of stress.

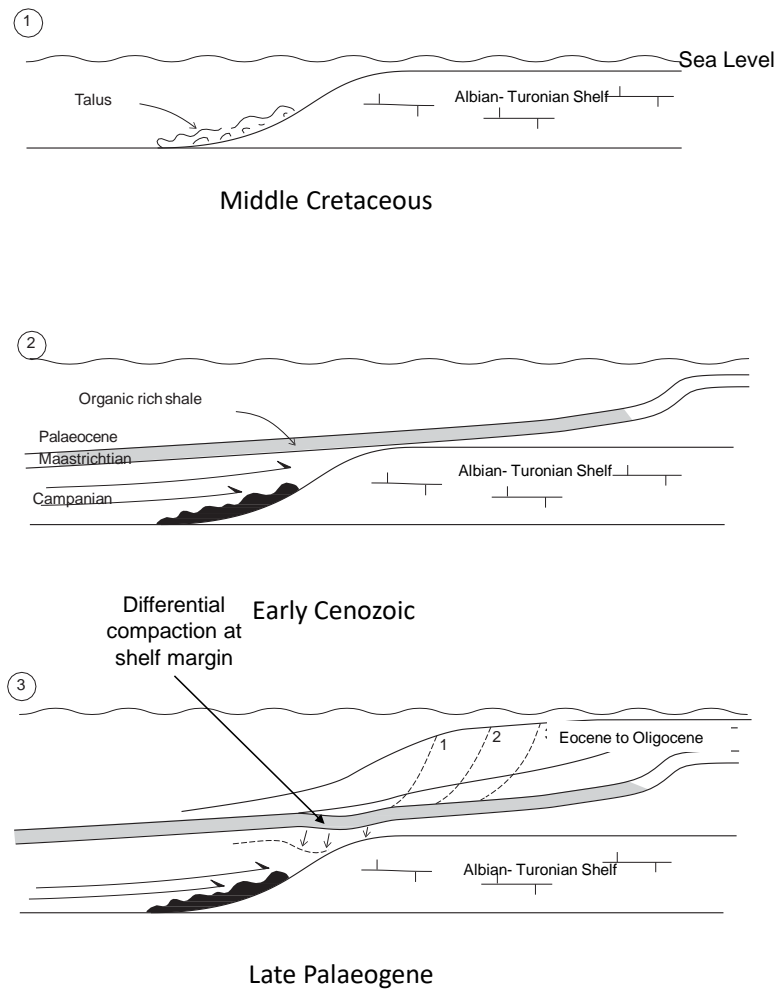


Figure 8-1: Early evolution of the mass transport complex: creation of the conditions that allowed the formation of the mass transport complexes.

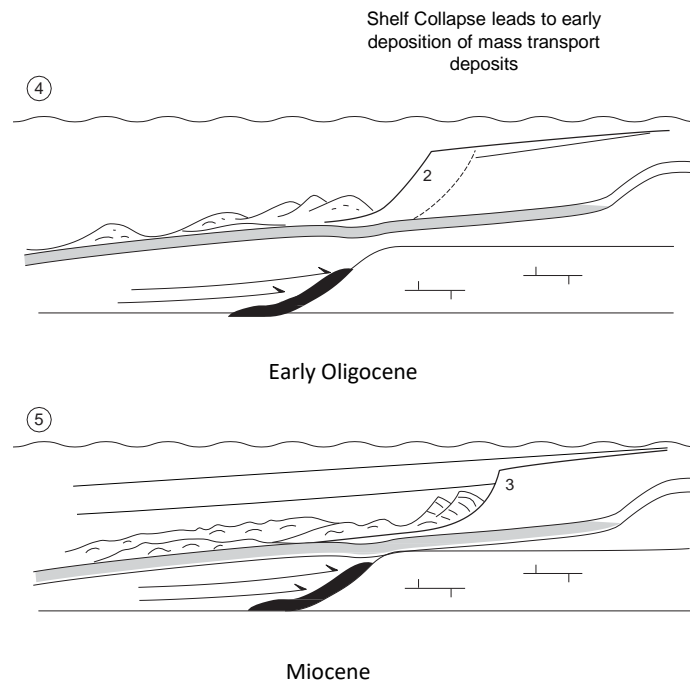


Figure 8-2: regressive nature of the mass transport complex formation.

The presence of pre-existing canyons along the shelf margin would have added to the complexity of the shelfal collapse deformation. The sides of the canyons, as well as the shelf margin, are interpreted to have been cannibalised by the headward advance of the collapse. The presence of a number of fan-shaped mass transport deposits that have been mapped is an indication of the likely presence of a canyon as the focal point of sediment outflow over the slope and into the basin.

The Avon canyon described by Olabode (Olabode and Adekoya, 2008) is one such canyon. Other canyons are present to the west of the Avon canyon, including the Lagos and Seme canyons. These additional canyons are known to play a role in the trapping mechanism of oil and gas accumulation on the present-day shelf margin (the Ogo Aje and Seme).

The location of the canyons may be linked to the syn rift or basement fabric. As noted in chapter 5, the syn-rift seismic character is noted to alter across a roughly north-south lineament, which – if projected northwards – would lie in the region of the Avon canyon.

The distribution of the mass transport deposits mapped immediately overlying the detachment layer indicate that there were two source areas for the fan-like bodies that were deposited. The more easterly can be interpreted to have originated from a source

located close to the mouth of the Avon canyon. The source of the western lobe cannot be defined due to a lack of data over the assumed source area, but is interpreted to be linked to the Lagos canyon (chapter 6).

8.1.2 Nature of mass transport deposits

8.1.2.1 Composition of mass transport deposits

The sediments that comprise the internal matrix of the mass transport complexes are unknown. However, if they are derived from the collapse of the shelf that lay to the north, it can be inferred that the material within the deposits are a mix of those found at the palaeo shelf margin. The shelf during the Palaeogene, as encountered in the wells to the north, was mainly comprised of shales, with minor interbeds of sands and limestones (Kaki et al., 2012). It is interpreted, therefore, that the composition of the mass transport deposits will be heterolithic, but with a large shale component because the portion of the shelf that has been affected by the collapse would have been more distal than that which remains in place. The presence of kilometre-scale blocks recognised in the melange indicates that the matrix also includes blocks of previously lithified sediments.

The similarities observed between the mass transport deposits mapped in this study with those identified elsewhere around the globe (Moscardelli and Wood, 2016) lends support to the interpretation of the these deposits as mass transport deposits. As an example, the image in Figure 8-3 bears a strong resemblance to the image in chapter 6 (Figure 6-46).

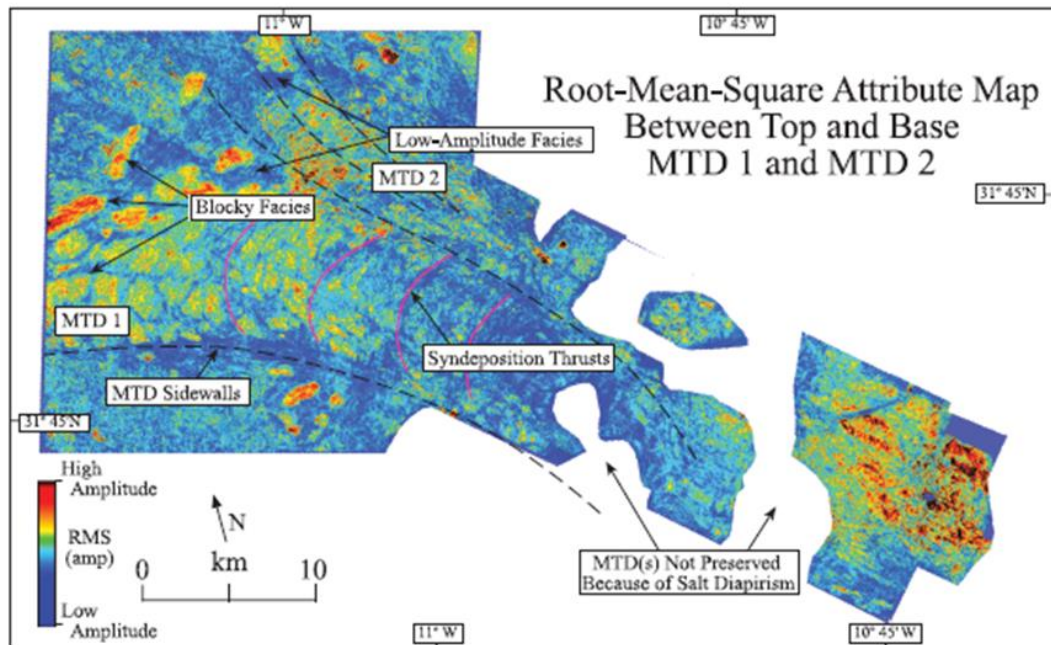


Figure 19. Root-mean-square attribute map of the interval between the merged tops and bases of mass-transport deposit (MTD) 1 and MTD 2. The map shows the distribution of high-amplitude MTD blocks within fluidlike, low-amplitude, chaotic facies. Syndepositional thrusts and distinct sidewalls are visible. Postdepositional salt diapirism has partly displaced the mass-transport complex in the east part of the study area.

Figure 8-3: Illustration of a mass transport complex offshore Morocco (Dunlap et al., 2010).

The assumption, therefore, that the interval at the base of the Cenozoic is indeed a mass transport complex raises the question as to why its upper surface is a detachment layer.

8.1.2.2 Permeability in mass transport deposits

Because the deposit is buried beneath further sediment, the overburden stress increases and the water is expelled. If, however, the internal permeability is low, the water cannot escape quickly enough and the water then supports some of the overburden stress; this leads to overpressure within the deposit. Low permeability is characteristic of fine-grained laminated sediments, notably shale (Mann and Mackenzie, 1990; Hege M. Nordgard Bolas et al., 2004; Twiss and Moores, 2007). Sediments with higher permeability include sandstones and limestones and mixed sand/shale compositions. Mass transport deposits may fall into this latter category.

The heterolithic nature of a mass transport complex, when combined with the random distribution of the constituent material, can lead to remobilisation of the sediments post-deposition. The presence of sediment dykes, which can occur under these conditions, can lead to localised regions of enhanced permeability (Cartwright et al., 2007; Hurst et al., 2007) within the deposit; evidence of this process is found in chapter 7. The permeability of the overlying interval is key to how the release of the entrained water that

was deposited along with the matrix material in the mass transport complex can escape. An overburden of sand, as in Figure 6-54, will allow the rapid escape of water. However, a blanket of low-permeability shale that may have lower permeability than the mass transport deposit will prevent the water from bleeding off in a rapid manner.

8.1.2.3 Overpressure generation

In section 7.3.4.1, the role of overpressure in the facilitation of lateral movements of strata was outlined. When the above observations are combined, it can be inferred that it is possible that the upper surface of the mass transport, overlain by a blanket of low permeability shales, can lead to the generation of overpressure within the shale. When combined with an uneven distribution of stress at the overpressured layer, lateral movement of the sediment pile can occur (Cohen and McClay, 1996; McClay et al., 2003).

The high-amplitude reflector that is present at the top of the mass transport interval would suggest that the horizon marks a large contrast in acoustic impedance. This may also be attributable to the presence of an overpressured layer. An increase in the degree of overpressure leads to a lowering of acoustic impedance (Brown, 1996; Yilmaz and Doherty, 2000), which in turn may generate a large acoustic boundary.

Bearing in mind the above evidence, it is interpreted that the upper surface of the mass transport deposit can be considered to be a detachment surface. In Figure 8-4, the yellow interval represents the mass transport complex; the faulting that is present in the overlying interval is seen to sole out at the upper surface of the complex. Similar examples of this arrangement are seen in Figures 6-47 to Figure 6-50.

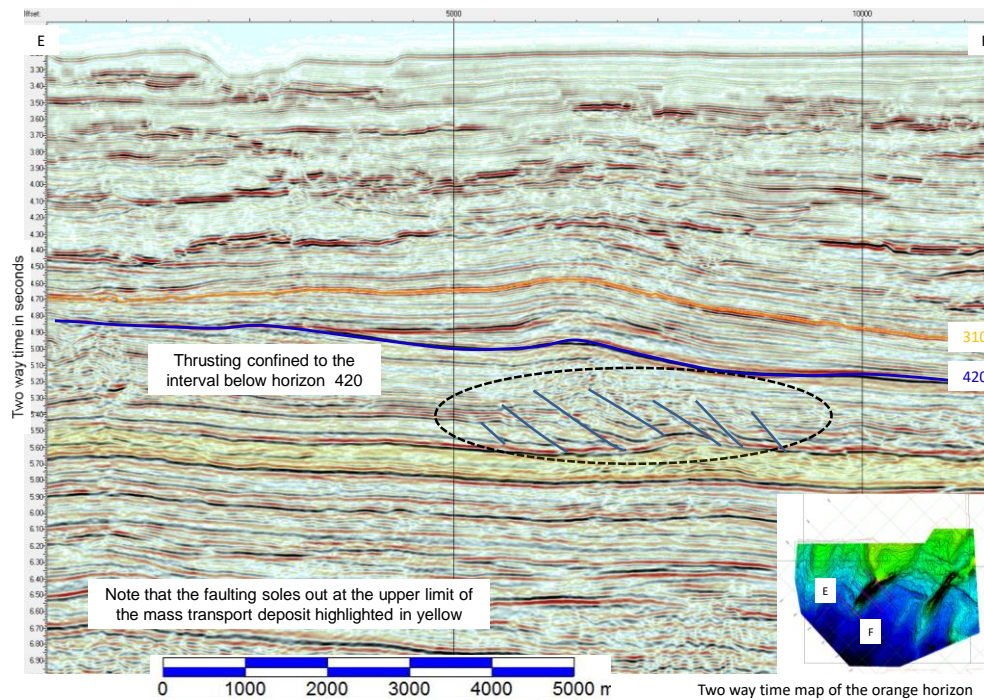


Figure 8-4: Seismic line illustrating the upper surface of the mass transport deposit acting as a detachment layer.

8.2 Origin of the large-scale levees

Following the widespread deposition of the mass transport apron, a period of low-energy sediment influx is observed. The seismic character of the section that overlies the upper surface of a mass transport deposit is that of low-reflection strength horizons that are seen to rise and fall due to the presence of a series of approximately coast orthogonal ridges and troughs. The Palaeogene section (which lies between horizons 510 and 410) is mapped as being thicker towards the western margin of the survey and to thin towards the east (chapter 4). The reflection geometries observed within the thickest portion of this interval are seen in cross section to be comprised of large wave-like features.

Two possibilities were considered for the origin of these sediment piles.

8.2.1 Contourites

The recognition of wave-like structures in deep water can be an indicator of the presence of ocean-bottom currents (Viana et al., 2003; Faugères and Stow, 2008; Zenk, 2008; Rebesco et al., 2014). The bottom-circulating currents move sediment along the sea bed in the same manner that wind moves loose grains of sand in a desert. The construction of contourite drifts as a result of this action can lead to the formation of large, low-relief sedimentary bodies that have been observed to be orthogonal to the shelf margin (Lucchi

and Rebesco, 2007). However, contourite drifts in general are asymmetric, in that the dips of the opposing slopes are steeper on one flank when compared to the other. Adjacent drifts display the same asymmetry. The build-ups seen in this study exhibit asymmetry; however, the asymmetry is reversed between adjacent mounds. The geometry within the ridges and their orientation bears some similarity to that recognised by other authors as being the result of bottom-circulating currents (Stow and Mayall, 2000; Rodriguez and Anderson, 2004). Because the cessation of the build-up of these mounds may coincide with the onset of “ice house” conditions, the end of ridge construction could, therefore, be related to the alteration of significant ocean-bottom current circulation as the onset of circum-Antarctic oceanic circulation (Bickert and Henrich, 2011).

This is interpreted to be related to the opening of the Beagle channel in the south Atlantic, which allowed circum-Antarctic flow of oceanic water (Faugères and Mulder, 2011). This rearrangement of oceanic currents led to the glaciation of Antarctica and a drop in global sea levels. The current flows in the central Atlantic (Duarte and Viana, 2007) are assumed to have been altered at this time and the action of bottom-circulating currents appears to have diminished as a result. As a result of this change, the depositional environment was altered and sediment transport downslope became the dominant process. However, the evidence within the data would indicate that the ridges continue to build after the onset of ice-house conditions.

With the geometry and timing of construction being at odds with the interpretation of them being contourites, the inference is that they most likely have turbiditic origin.

8.2.2 Turbidites

Turbidity currents carry sediments from the shelfal region into deep water down the steeper gradients found on the slope. The constituent parts of the turbidity flow can include material that ranges in particle size from coarse-grained to fine-grained (Reading and Richards, 1994). In those that carry coarse-grained material, these particles can drop out of suspension as the current slows down, whereas the fine-grained material can travel further and be spread over a larger lateral distance. The fine-grained material drops out when the current velocity slows down over the change in slope. The change in slope can be both down-dip and lateral. The lateral velocity reduction leads to the accumulation of sediments in levees along the flanks of the turbidity flume (Reading and Richards, 1994; Kneller, 1995). The asymmetry seen in contourite drifts is less prevalent in the turbidite levees that are seen to have steep slopes, adjacent to the central valley and lower dips on the slopes on the opposite side of the build-up.

The construction of these levees commenced immediately post the deposition of the mass transport apron (chapter 6). It persisted into the Miocene, when the influence of the Niger Delta progradation become the major influence in lateral sediment dispersal into the deep water.

These levees described in chapter six with their elongate axis running in a predominantly north-south orientation are interpreted to be formed as a result of turbidity current outflow from the shelfal region that lies to the north of the survey area. The absence of any channel-like character within the adjacent synclines indicates that there may be little or no coarse-grained material in these features (Figure 6-57). Any coarse-grained material would have dropped from the turbidity flow, preferentially in the axis of the thalwegs.

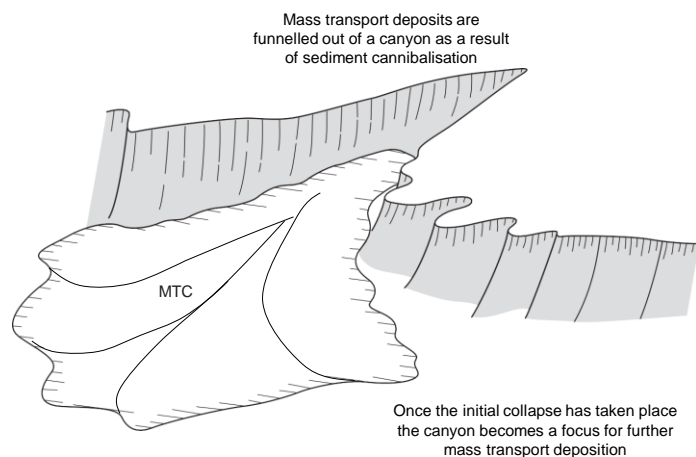


Figure 8-5: The process of mass transport emplacement can be related to the cannibalisation and focussing of outflow from a canyon system.

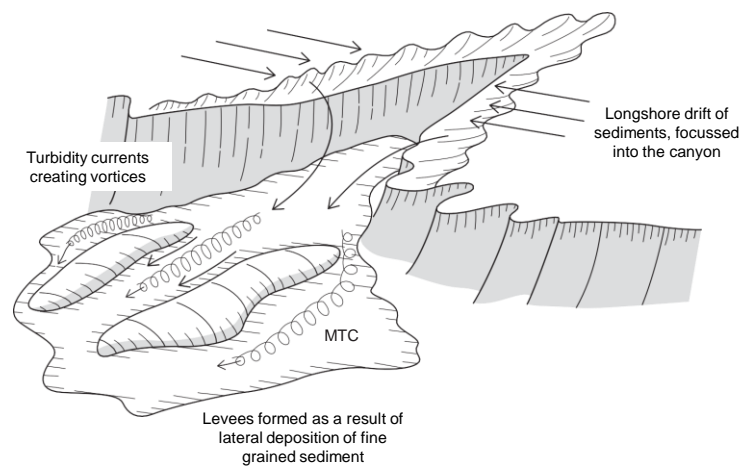


Figure 8-6: The evolution of the large-scale levees; low sediment input into the canyon leads to low-energy deposits being fed from the canyon.

The evidence obtained from the interpretation (chapter 6.3) and the comparison to other similar sedimentary features support the interpretation that these levees were formed by the accumulation of fine-grained sediment along the banks of a persistent set of linear turbidity thalwegs (Galloway, 1998; Kane et al., 2010). In Figure 8-6, the assumed origin of the levees is illustrated. The headward erosion of the shelf margin led to the creation of canyons, which initially fed the slope and basin floor with mass transport deposits. Following a rise in sea level, the head wall erosion became limited and the main erosion took place along the flanks of the canyon (Olabode and Adekoya, 2008). The material eroded from the flanks of the canyons is interpreted to be outer shelf, which is most likely to be fine-grained (Reading and Richards, 1994) because there is limited evidence of a major fluvial entry point that could supply coarse material.

The outflow of turbidity currents from the canyon mouth would have been turbulent in nature and the velocity of the flows variable between the centre of the thalwegs and the margins. This velocity variation (Kneller, 1995) led to the slower-moving flanks dropping their load and the faster-moving axis of the thalwegs carrying their loads further into the basin.

8.2.3 Nature of the levees

8.2.3.1 Internal geometry

The construction of the largest levee, located at the western margin of the survey, is interpreted to have occurred in several phases. Within the lower portion of the build-up, the wavelength between adjacent levee apexes is in the order of 4 to 5km; however, by

the time the construction of the levees ceased, the wavelength between the crest of the largest levee to the levee to the east was 14km (Figure 8-7).

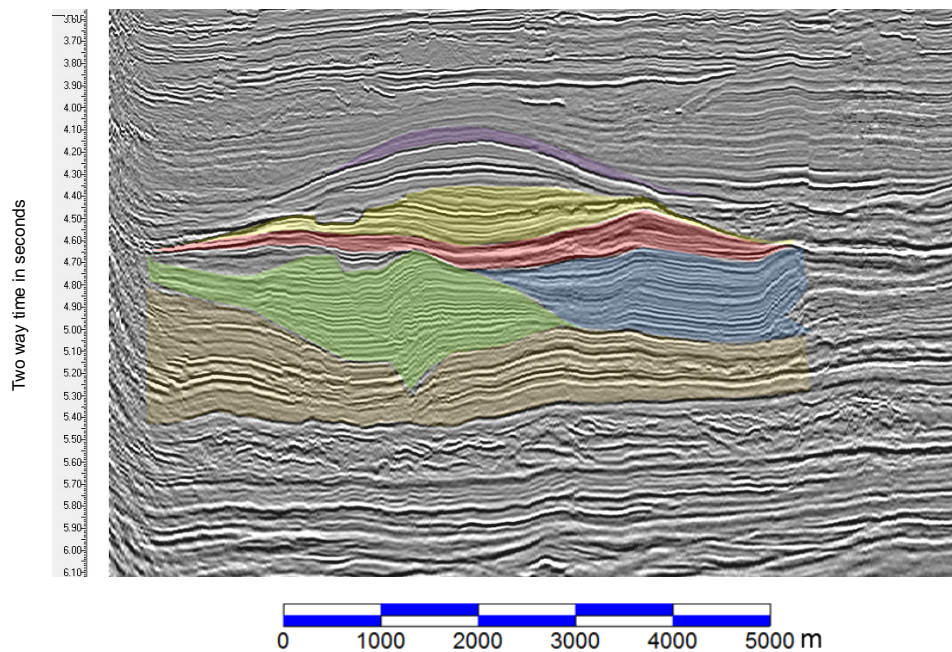


Figure 8-7: Illustration of multiphase levee construction; the various coloured intervals are indicative of several different phases of construction.

8.2.3.2 Intra-levee deformation

The accumulation of sediments within the body of the levees described above (Figure 8-7) led to the creation of lateral stress variations as the shift in deposition took place. The vertical stress that was present at the surface of the underlying mass transport deposit below the thickest part of the levee would have been greater than that present at the centre of the adjacent syncline. This variation in lateral stress in the presence of a weak basal layer is interpreted to have resulted in the lateral movement of the section over the basal surface.

The shift in the crest of the levees with time would have led to a shift in the stress variation. It could be expected, therefore, that the lateral motion would vary with time as well. The varied orientation of the reverse fault stacks (Figure 8-8) outlined in section 7.3.5 indicates that the deformation took place in a number of episodes. The set of faults identified at the western margin of the survey are limited both vertically and laterally to the internal portion of the deepest levee. In this image, there are at least six sets of faults

with similar strike orientations. They are interpreted to indicate six separate changes in stress orientation within the levee.

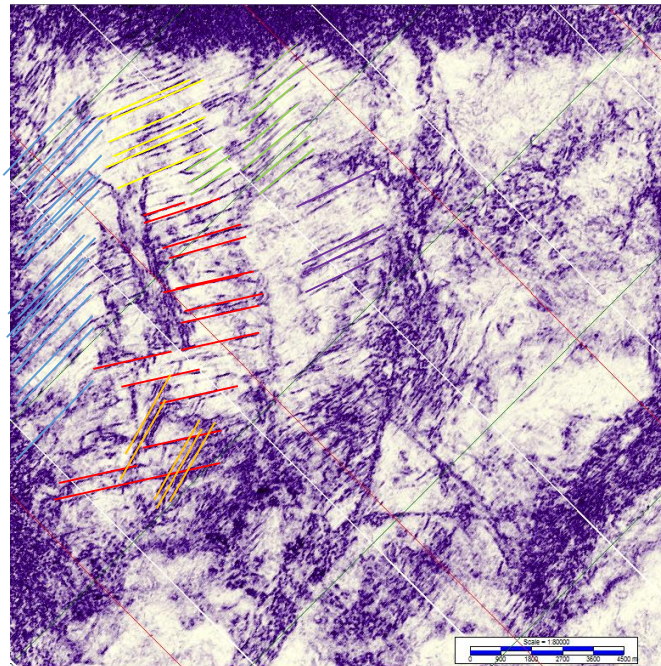


Figure 8-8: Similarity extraction of horizon 465 (see Figure 8-10), showing several groups of faults with varying strike directions highlighted by the coloured lines.

The combination of a weak substrate and an overburden stress imbalance is interpreted to have led to the downslope motion of the levees. The variation in the fault orientation is a reaction to the change in stress orientation because the location of the thickest part of the ridge shifted due to shifting sediment patterns.

In Figure 8-10, the suite of faults marked in blue in Figure 8-8 at the western margin of the survey are limited to the isochrone thick. The interpretation of this relationship is that the faulting was restricted to a levee that was thicker than the surrounding region.

In Figure 8-10, the faulting seen at the western limit of the data strikes in a north-east to south-west direction. It is limited in areal extent to the region of the thickest section (the blue region). This relationship is interpreted to indicate that the thickness is a controlling factor in the deformation.

The orientation of the faults would suggest that the principle stress direction was oriented in a generally north-west to south-east direction. This orientation would tie in with the motion of the deformed section moving outwards and downslope from the thick fan deposit inferred to be present at the opening of the Lagos canyon. The fault zones highlighted in yellow in Figure 8-11 are interpreted to be the result of dextral motion, associated with the downslope motion of the levee complex.

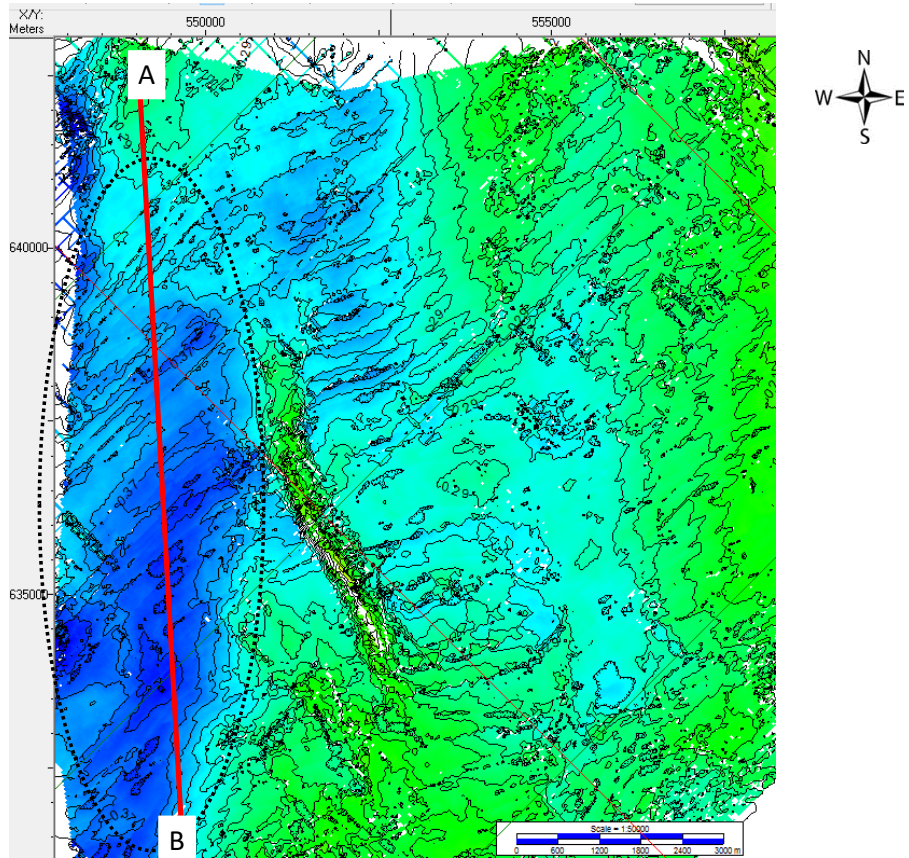


Figure 8-8: Isochrone of the interval between horizon 500 (green) and 465 (blue) as illustrated in Figure 8-10.

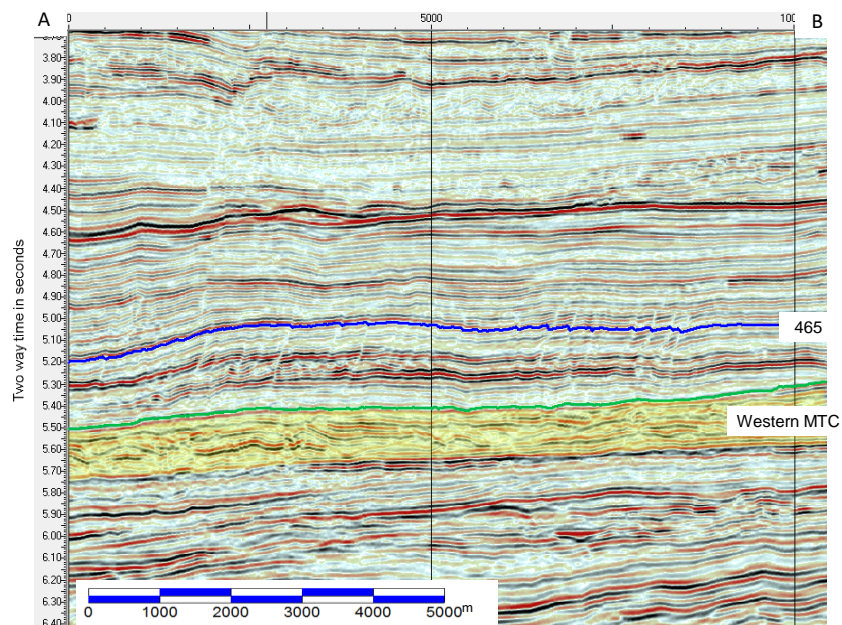


Figure 8-9: Seismic line highlighted in Figure 8 9 that shows the faulting present at horizon 465, but absent at the top of the mass transport complex.

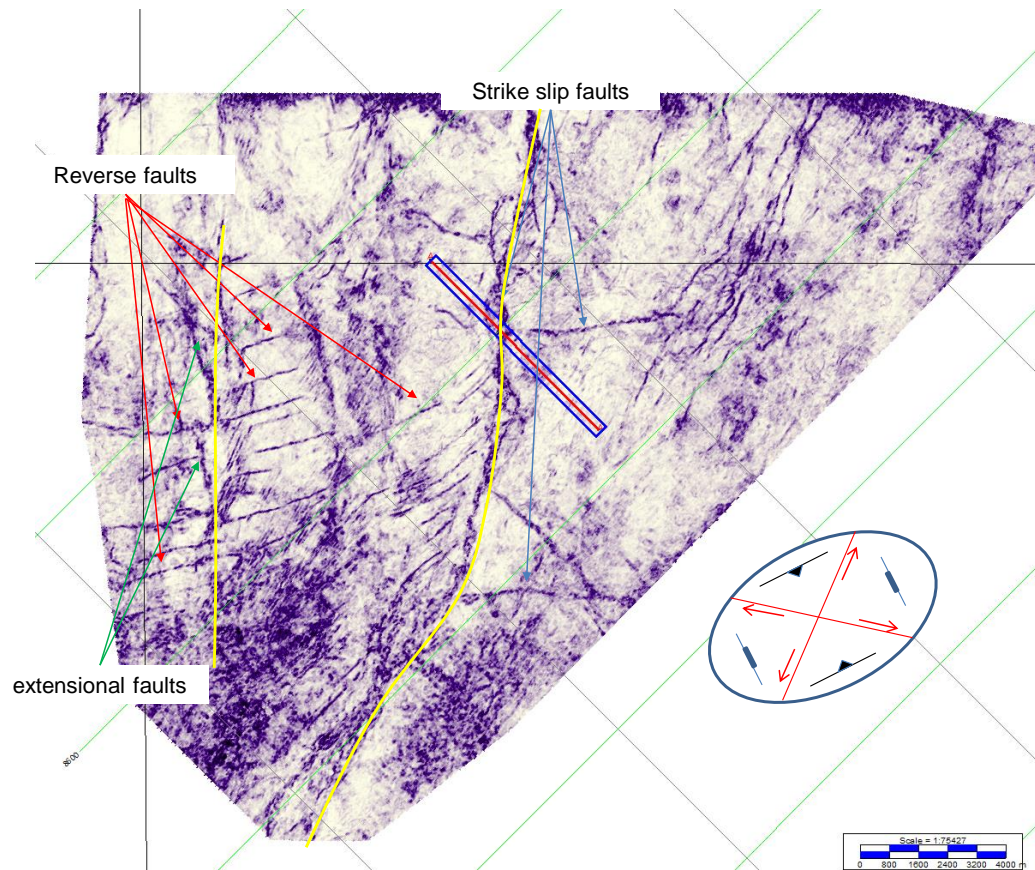


Figure 8-10: Similarity attribute for horizon 425, with inferred stress regime indicated.

8.3 The origin of the Avon/Mahin fault zone

8.3.1 Is there a deep basement control?

8.3.1.1 Syn rift

In order to establish what role the underlying terrain may have upon the thin-skinned tectonics, the nature of the Cretaceous interval was studied. The data in this interval varies in quality such that confidence in mapping events over any great distance was problematic. However, some broad trends could be recognised.

The presence of oceanic transform faults has been identified as one possible influence on the disturbances seen in the Cenozoic interval. (Davies et al. 2005; Briggs et al., 2009; Wu et al., 2015). The coincidence of the chain fracture zone with the separation of the Niger Delta into two lobes lends support to this idea further to the south.

The regional gravity data (Haack et al., 2000; Sandwell et al., 2014), indicates that there may be a minor oceanic transform fault present to the south-west of the 3D survey. The gravity data does not provide enough clarity to indicate whether or not it extends into area covered by the 3D data. The free air anomaly map (Figure 8-12) indicates that if present, the trace of the transform fault – as it terminates within the continental region – lies in the southern half of the 3D survey.

There is a clear angular unconformity (the break up unconformity) recognised at the top of the syn rift section (as outlined in Chapter 5.2). In the western region of the survey, the horizon picked as the surface which corresponds to this hiatus, horizon 800, is seen to be a relatively uniform surface that dips gently towards the south (Figure 8-13).

Further east, the surface has a more undulating morphology, with a series of east-to-west-trending ridges present. These ridges appear to be related to the differential erosion of the underlying sediments. The section underlying the unconformity is interpreted to be comprised of a number of tilted half grabens. The footwalls of the faults that bound the half grabens are the location of the ridges that are mapped at the break-up unconformity (see section 5.2). This is assumed to be due to the fact that the footwalls are, in general, less prone to erosion than the sediments in the hanging wall. This morphology is in marked contrast to the planar nature of the unconformity seen in the west.

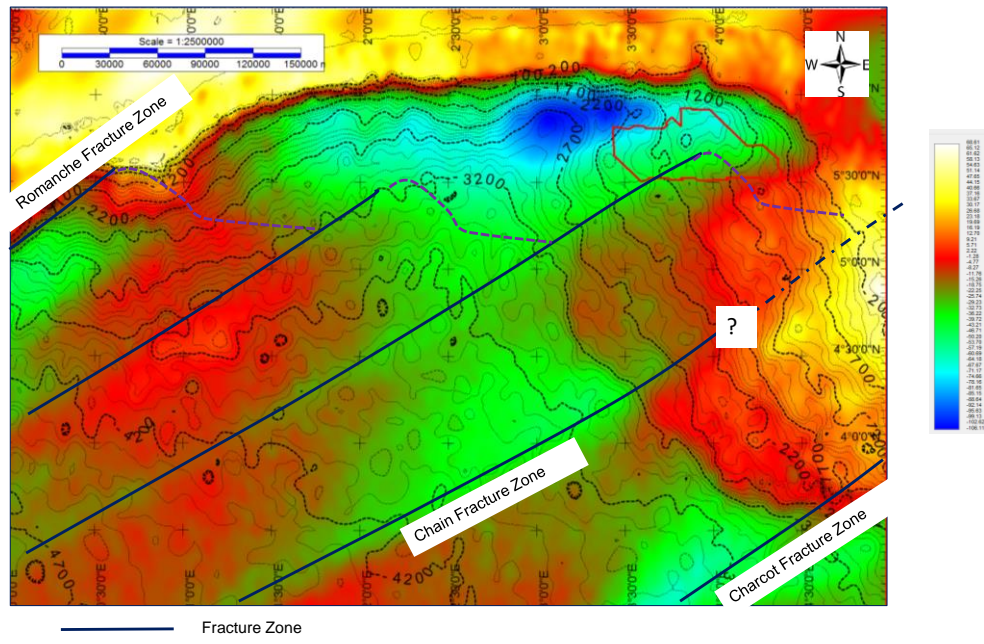


Figure 8-11: Gravity free air anomaly map showing the location of oceanic fracture zones; the survey area is highlighted by the red polygon.

In addition to the morphology of the unconformity surface, the syn rift interval is marked by a number of differing packages of varying seismic reflection character. The reflection pattern found in this eastern interval indicates that there has been a high degree of post-sedimentary tectonic deformation. The deformation is limited to the section that underlies the break up unconformity, indicating that this phase of structural modification took place prior to the deposition of the sediments that overlie the break-up unconformity.

In the eastern region of the survey, as noted above, there are a number of half grabens interpreted. They appear to be limited in their western extent by a north-south lineament. To the south, it is thought that the sediments are absent due to erosion or non-deposition.

It is unclear what the sub-unconformity substrate is comprised of; it could be pre-existing continental terrain, similar to that which underlies the syn-rift sediments, or it may be composed of transitional-to-oceanic crustal material. Isolated high-amplitude events are present within this generally transparent interval; the orientation of these high-amplitude events is that of a southerly dipping plane, in contrast to the sediments within the syn rift interval, which tend to dip in a northerly direction. These may represent seaward dipping reflectors, associated with many oceanic margins. If this is the case, then the section to the south of the half graben terrain may well be oceanic in nature.

The offset in this southern limit is interpreted to represent the presence of a large-scale structural lineament that runs in a north-south orientation. Tracing this lineament is challenging due to the poor quality of the data, notably in the region of the Avon/Mahin

fault zone. With the data that is of high enough quality, it was possible to identify the regions where there is clear evidence of reflection packages beneath the break-up unconformity, which are assumed to be sediments of Barremian to Aptian age. The distribution of these reflection packages indicates that the lineament does not correspond to the location of the Avon/Mahin fault zone because there are clear indications of the syn rift sediments well to the west of the Avon/Mahin fault zone.

It is not possible to rule out the presence of a thoroughgoing fault within this deep sedimentary package because it cannot be mapped with confidence.

8.3.1.2 Mid to Upper Cretaceous

The section that overlies the break-up unconformity is notably less tectonically deformed than both the underlying syn rift and the overlying Cenozoic intervals. The Senonian unconformity represents a major hiatus that took place during the period between the Aptian and the Cenozoic. A horizon has been interpreted, which is considered to represent this hiatus. This horizon can be traced on either side of the Avon/Mahin fault zone. There is a pronounced nose mapped at this horizon. This was recognised by generating an isochrone of the interval between the Senonian unconformity and the Base Cenozoic (Figure 8-13). The nose plunges from the north-west to the south-east, passing beneath the Avon/Mahin fault zone. It is, therefore, implied that there has been no lateral offset of this interval.

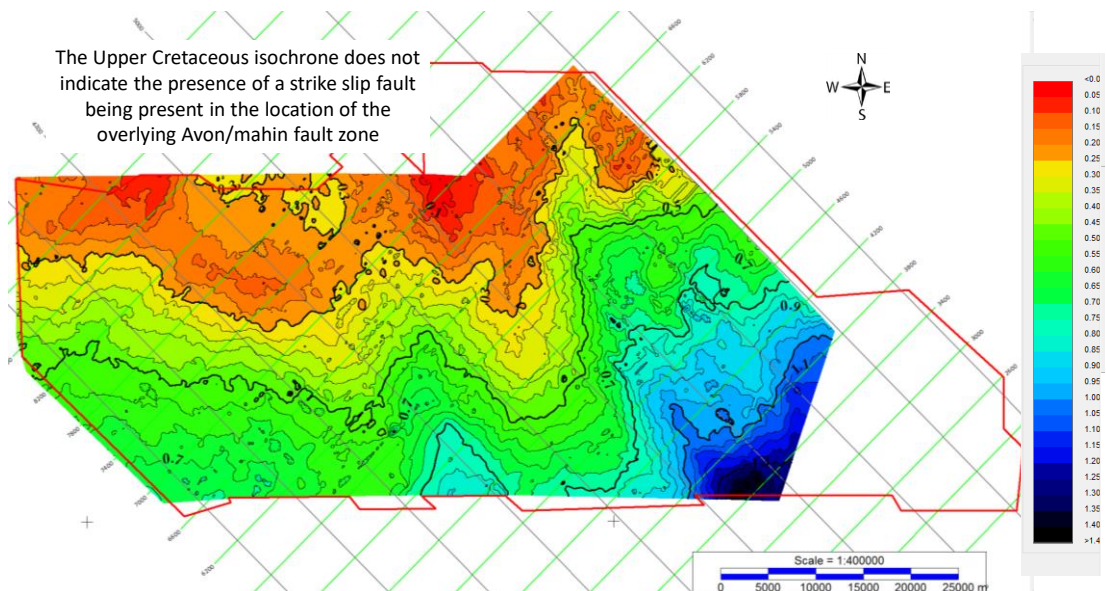


Figure 8-12: Upper Cretaceous isochrone, illustrating the presence of a structural nose running from the north-west to the south-east.

A horizon was mapped in the interval between the break-up unconformity and the base of the Senonian unconformity, attributed to the Mid-Albian unconformity. The extent of the horizon is limited to the north and east by the down-cutting erosion that is associated with the Senonian unconformity (Figure 8 13). The trace of this erosional limit is a linear one, which runs in a north-west to south-east direction. There is no apparent displacement of this horizon truncation identified in the map.

The two pieces of mapping described above do not lend any support to the presence of any transcurrent faulting being present within the Mid to Upper Cretaceous.

From the examination of the deeper stratigraphy presented above, it is inferred that the deformation within the Cenozoic section was not the result of basement influences or Upper Cretaceous phenomena. The presence of the thrusting noted in the Campanian (chapter 7) is located several tens of kilometres from the location of the Avon/Mahin fault zone and therefore are not considered to have played a direct role in the origin of the strike-slip motion.

The interval can be divided into two principle depositional systems: the Niger Delta, which is prograding from the east, and the Benin Basin, which is shedding sediments from the north. The Lower Cenozoic is thought to be primarily comprised of sediments which have their provenance in the north. This Palaeogene interval is thickest in the west of the survey area, as evidenced by the isochrone (Figure 8 17). The Neogene section is primarily sourced via deposition that emanates from the east, as can be seen in the isochrone of the interval between the sea bed and the Base Neogene (horizon 420).

The material that constitutes the Benin basin shelfal region is interpreted to have been derived from north-to-south flowing rivers and sediments carried from the Cretaceous Benue Delta and the Cenozoic Niger Delta via longshore drift. This process is known to be active today (Burke, 1972). The deposits that were transported in this manner are assumed to have become constituent parts of the shelfal portion of the Benin basin.

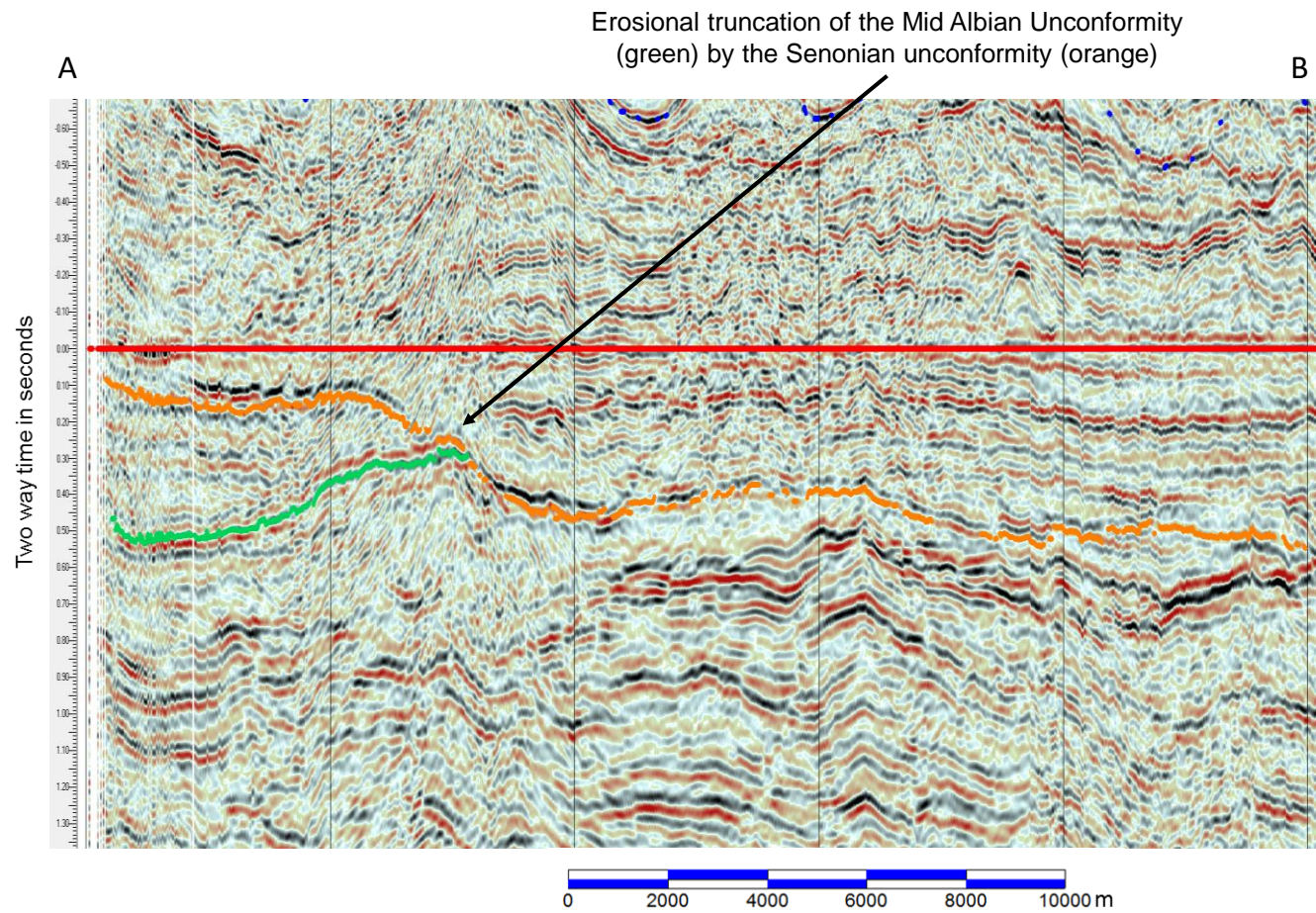


Figure 8-13: Seismic line illustrating the truncation of the Mid Albian (horizon 785) by the Senonian unconformity (horizon 680).

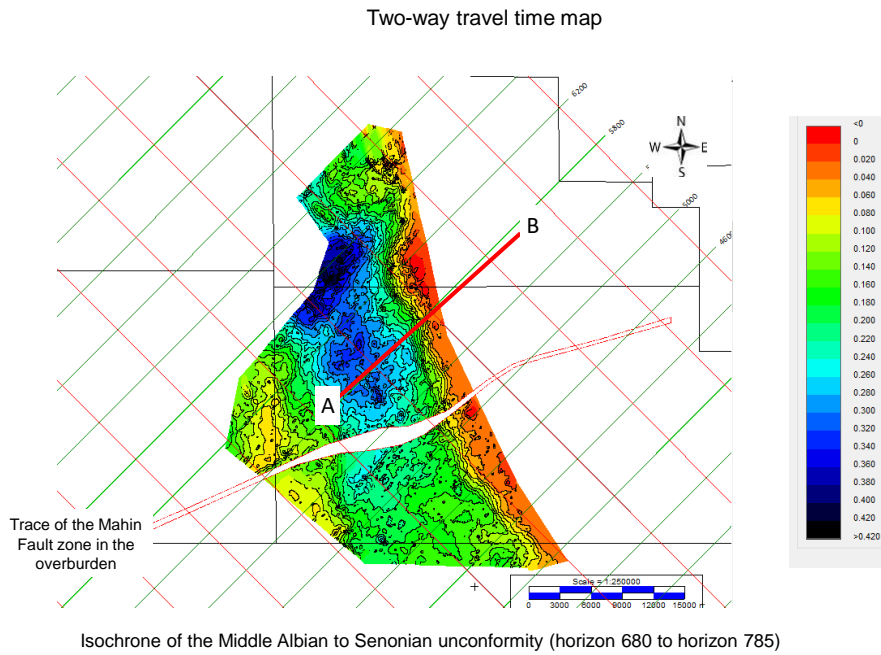


Figure 8-14: Thickness of the Albian to Turonian interval (between horizon 785 and 680) the location of Figure 8-13 is highlighted in red.

8.3.2 Gravity imbalances in the Cenozoic

The Cenozoic interval in the survey area is comprised of a wedge of sediments, which are thickest in the east and thin towards the west.

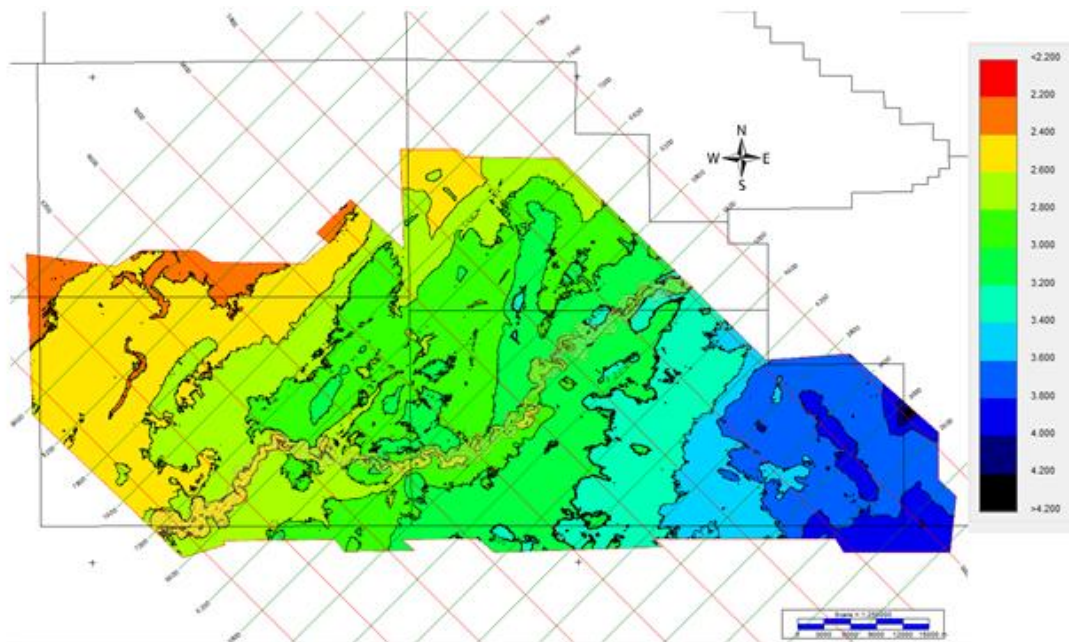


Figure 8-15: Cenozoic thickness in twt, note the thickening towards the south-east.

A marked difference in the thickness of the Palaeogene and Neogene interval exists. The isochrone of the interval between the assumed base of the Cenozoic and the interpreted base of the Oligo-Miocene (Figure 8 17) highlights the relatively thin section present in the east from the thicker western region. In the western region, the map highlights the presence of a number of approximately north-to-south trending ridges and accompanying synclines. These have been discussed in chapter 6.3.

In contrast, the isochrone of the interval between the sea bed and the base of the assumed Oligo-Miocene (horizon 420) indicates that this section is thicker in the east than in the west; the thick section in the eastern region is assumed to be a result of the deltaic progradation of the Niger Delta.

The structural deformation seen in the Palaeogene interval in the western drifts (section 6.3.3) appears limited to the strata found within this interval. The lateral displacement of the strata within this interval over an underlying detachment outlined in section 7.3.5 appears to have ceased by the middle of the Cenozoic.

The lateral movement of strata over an underlying detachment layer was noted in section 7.3. Of the key elements of the classical three components of deltaic deformation – extension, translation, and compression – the compressional portion requires a barrier to the unhindered motion. This may be due to the basal layer no longer being relatively low in shear strength, or a change of dip at the toe of the slope, for example (the critical taper criteria).

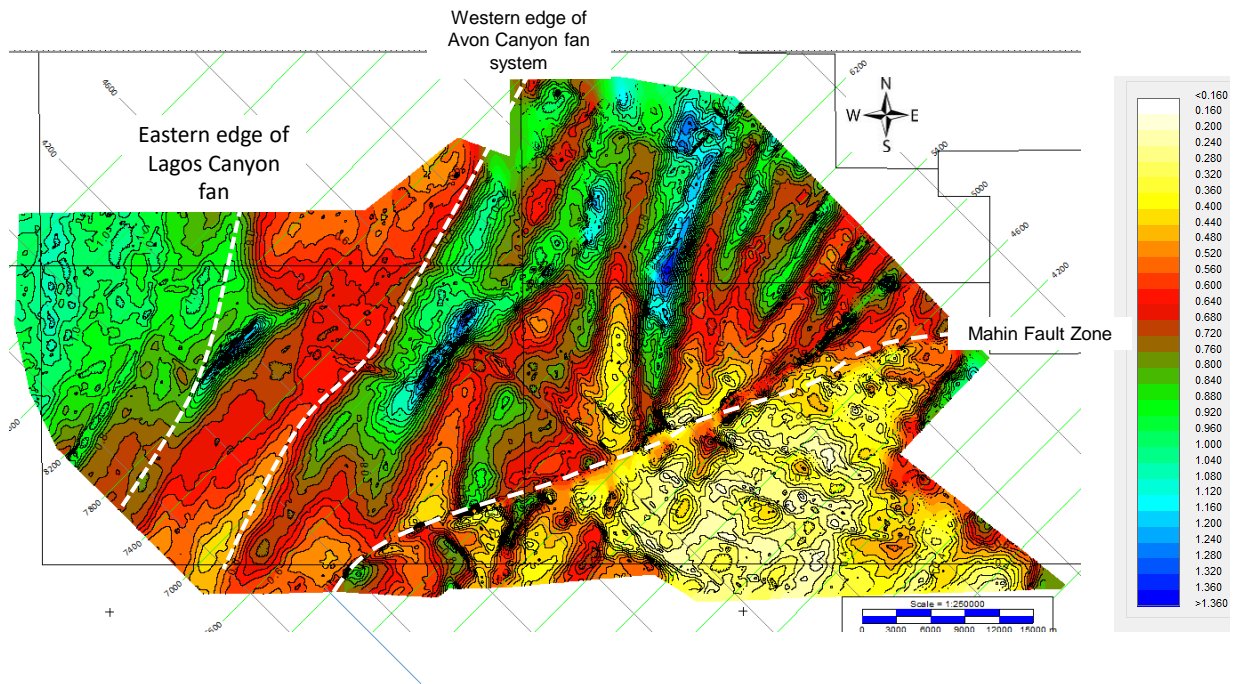


Figure 8-16: Thickness of the Palaeogene in twt.

The thickness of the Neogene is seen to thicken towards the south east, this is interpreted to be as a result of the outbuilding of the Niger Delta

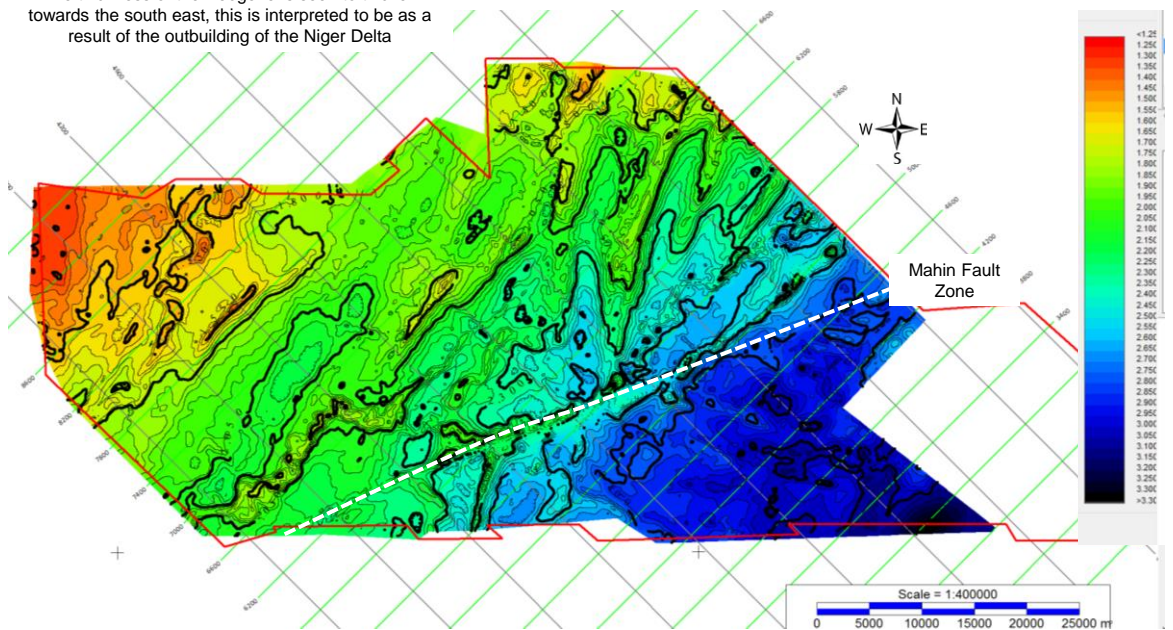


Figure 8-17: Thickness of the Neogene in twt.

The mapping of several channel levee complexes on either side of the fault zone that was outlined in chapter supports the premise that dextral strike-slip movement has occurred.

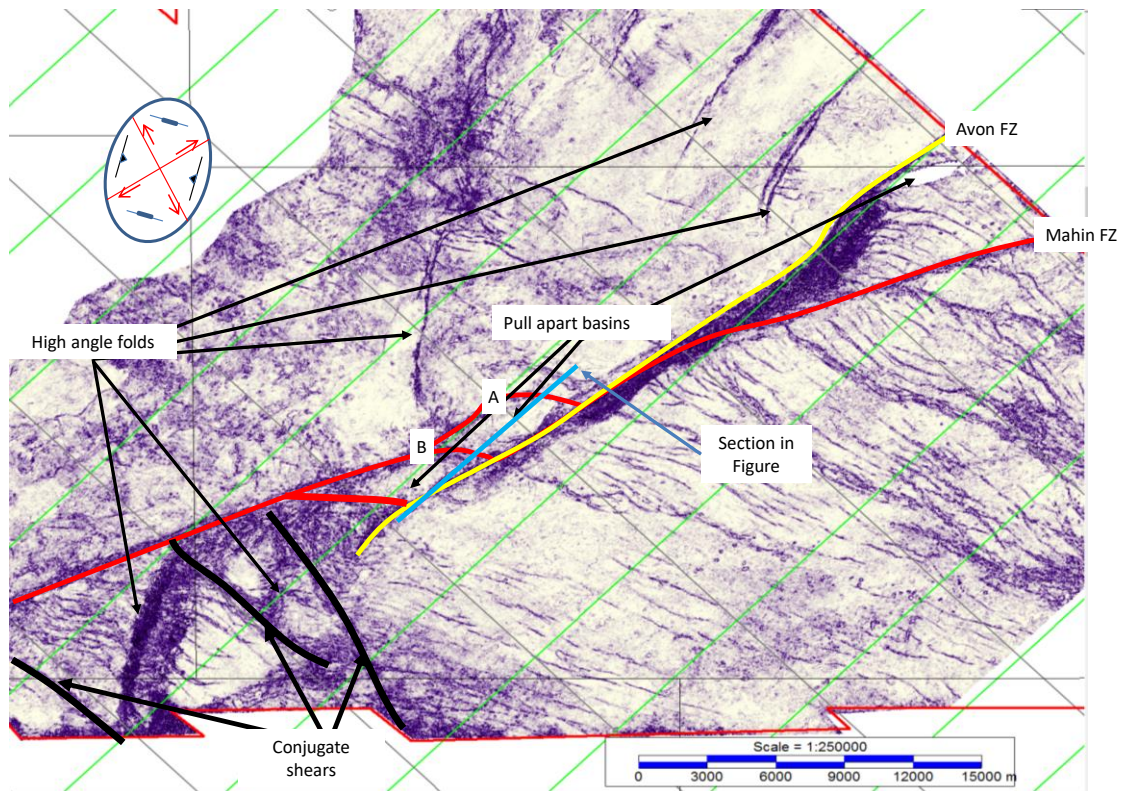


Figure 8-18: Similarity attribute for Middle Miocene (horizon 160), showing the main strike-slip and compressional trends.

The gravity-driven downslope motion of the thick Neogene interval is limited by two major factors: the competence of the basal detachment layer, and the dip of the basal layer. The centre of the northern lobe of the Niger Delta has built out over an abyssal plain that forms the continental rise. The northern flank of the deltaic cone, however, is laid down upon the slope that rises to the Benin Embayment shelf. This lateral barrier alters the basal slope of the detachment and the gravity-driven motion alters as a consequence. The inability of the sediment pile to slide under the influence of gravity up this northern flank either stops the movement or deflects it. The deflection in this case is taken up by the alteration of the direction of lateral motion. This lateral change results in the formation of a lateral strike-slip boundary.

In Figure 8-19, the key faults that have been recognised are illustrated. The red and yellow lines trace strike-slip faults that strike in a north-east to south-west direction. The black lines represent strike-slip faults that are oriented in a north-west to south-east direction. These are interpreted to be conjugate shears that are developed in response to the application of a compressive stress, which is shown in the strain ellipsoid.

8.3.3 Evolution of the Avon/Mahin fault zone

A series of isochrone maps have been used to establish the development of the present-day structural configuration. The shallow isochrones, between the sea bed and the Base Pliocene (horizon 100) for example (Figure 8-20), highlight the difference in the thickness of the section on either side of the Avon/Mahin fault zone. The eastern region, which is thicker within this interval, implies the creation of more accommodation space in the east than in the west. The thick interval at the eastern edge of the survey is the location of a large synthetic/antithetic pair of faults that has created a local graben. Within this depression, there are a number of slope-channel complexes that are seen to be focused through this excess accommodation space created by these faults.

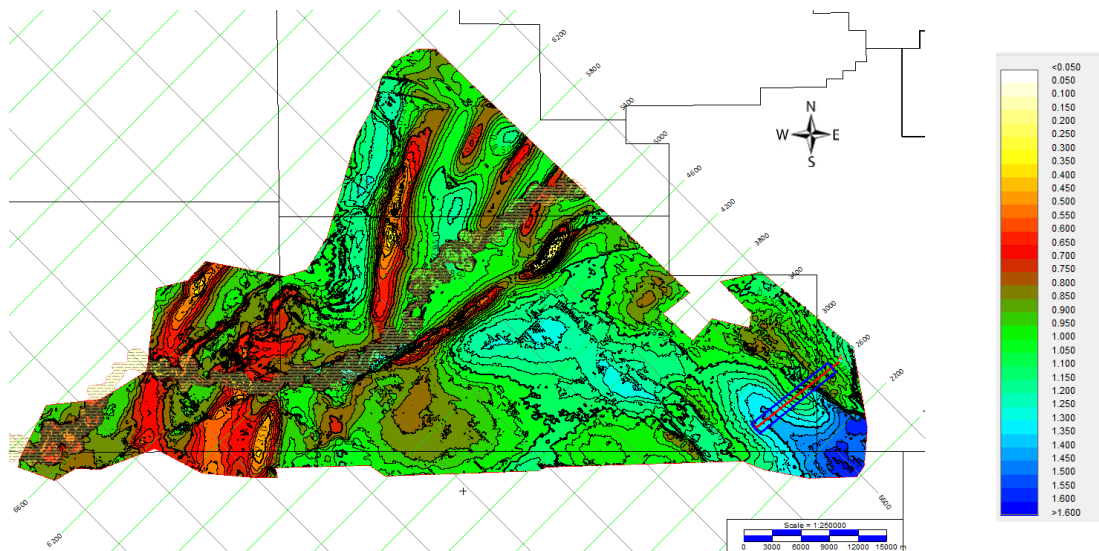


Figure 8-19: Thickness of the Pliocene to recent interval (between sea bed and horizon 100).

The map also highlights the location of the folds and thrust anticlines that are present to the east of the Avon/Mahin fault zone.

The Upper Miocene isochrone (Figure 8-21) points to further evidence that the eastern region is thicker than the west. To the east of the Avon/Mahin fault zone, a number of horst and grabens were recognised. The thicker intervals that represent the grabens are oriented in a north-west to south-east strike direction. They are seen to be limited towards the north-west by the Avon/Mahin fault zone. This map provides evidence that there was a greater degree of extension to the south-east of the lineament than to the region to the north-west during the Upper Miocene. Another aspect of this isochrone is the diminished amount of vertical thickness in the region of the folds and thrust

anticlines. This suggests that there was limited tectonic deformation taking place to the north-west of the Avon/Mahin fault zone during the Upper Miocene.

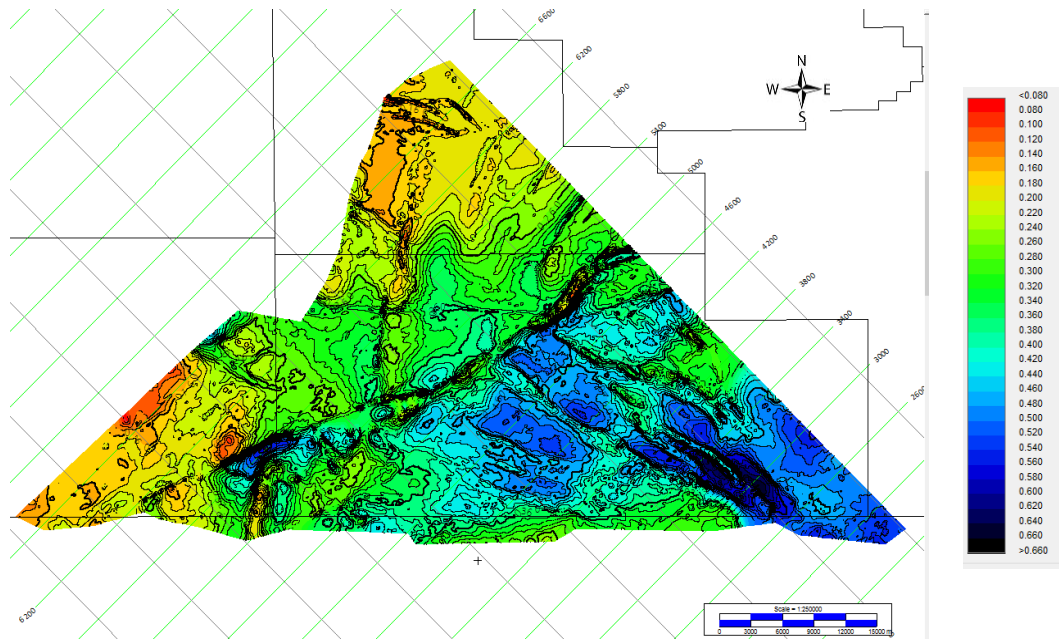


Figure 8-20: Isochrone of the Upper Miocene thickness (between horizons 100 and 130).

The anticlines are the location of thicker intervals; however, this is partly explained by the apparent thickness that is present as a result of the increase dip of the sediments along the flank and over the crest of the folds. The difference between the isochrone in Figure 8 20 and in Figure 8 21 is an indication that the majority of the folding that is present took place in the Pliocene to recent times. This late-stage movement is interpreted to be the result of movement along the Avon fault zone, as discussed in chapter 7. This is in contrast to the primarily extensional faulting that took place to the south-east of the fault zone during the Miocene.

The isochrone that represents the Middle Miocene (Figure 8 22) confirms the evidence of more pervasive extension to the south of the fault, compared to the north-west. In this figure, there is evidence of four grabens to the south-east of the fault zone and some indication of thicker intervals in the region of the folds; however, as noted above, this is most likely due to the tectonic, as opposed to depositional thickening associated with the geometry of the recently folded structures. In addition, there are a number of isochrone thick intervals within the fault zone, which are interpreted as pull-apart basins. The isochrone also picks out the presence of thicker isolated pull-apart basins in the immediate vicinity of the fault zone (chapter 7). The relatively uniform thickness of this interval to the north-west is evidence of no significant fault activity in this region during the period that is spanned by the two horizons.

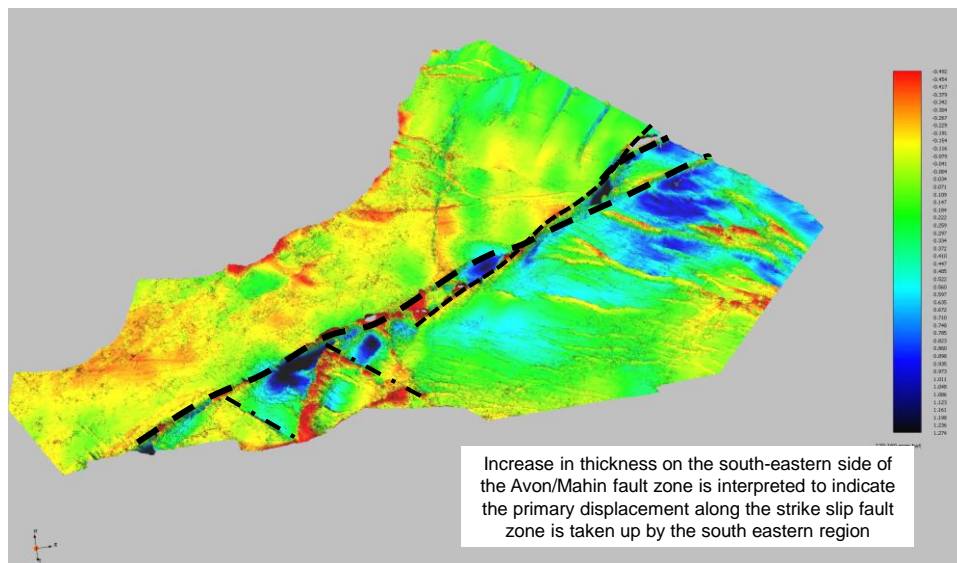


Figure 8-21: Perspective view of the isochrone of the thickness of the Middle Miocene interval (between horizons 130 and 160).

The Lower Miocene isochrone (between horizon 190 and horizon 160) is the shallowest interval in which there is evidence of significant extension present to the north-west of the fault zone. To the north-west, there is evidence of a number of grabens being present, as evidenced by the thicker intervals that are present.

In addition, the presence of the fault labelled NW1 has its maximum throw immediately adjacent to the Avon/Mahin fault zone. The distribution of the strain measured along the northern boundary fault plane (chapter 7.3.3) also indicates that the throw is increasing as it approaches the Avon/Mahin fault zone.

One other observation that lends support to the strike-slip interpretation is that the faults in the south-eastern region strike in a manner that resembles a fan. This fan-like spreading of the faults is interpreted to signify that the southern region adjacent to the Avon/Mahin fault zone has expanded to a greater extent than the region at the eastern edge of the survey.

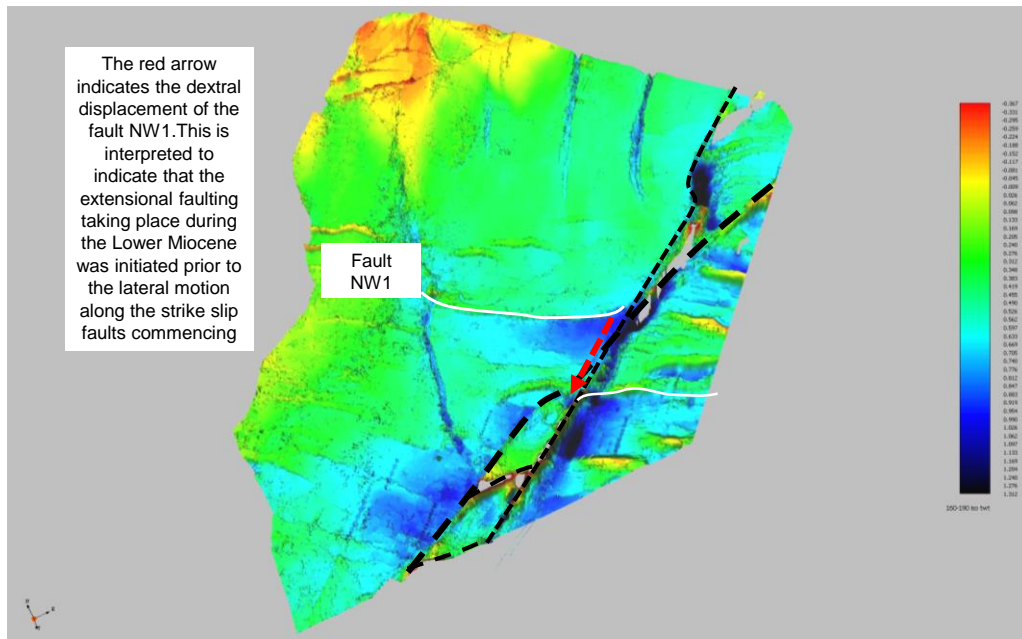


Figure 8-22: Perspective view of the Lower Miocene isochrone.

The south-eastern side of the fault is inferred to have moved south-westwards and resulted in the formation of the outer thrust belt; this lateral motion commenced during the Lower to Middle Miocene, but is interpreted to have diminished by the Pliocene. The locking-up of the outer thrust belt would have prevented further south-westwards motion; this in turn would have prevented any extension. Subsequent lateral movement was therefore accommodated by shortening in the region of study and the creation of transpressional motion. Also in turn, this may have led to the movement being accommodated on the conjugate strike-slip faults and the commencement of the thrusting and reverse faulting during the Pliocene to recent period.

Chapter 9

Contents

| | | |
|-------|---|-----|
| 9 | Conclusions..... | 300 |
| 9.1 | Twin sources of sedimentation | 300 |
| 9.1.1 | Benin Basin | 301 |
| 9.1.2 | The Niger Delta | 302 |
| 9.2 | Structural styles | 302 |
| 9.2.1 | Deltaic styles | 302 |
| 9.2.2 | Fan/levee style | 304 |
| 9.3 | Mass transport complex as the detachment..... | 305 |

9 Conclusions

The results of the work carried out during this study have led to a number of conclusions.

They are broken down into three main themes;

- The region is influenced by sediments which have been derived from two inter-fingering provenance areas
- The Cenozoic tectonic deformation is controlled by the presence of the two regions of sediment influx, as opposed to a single sedimentary system
- The thin skinned tectonic deformation is linked to the presence of an apron of mass transport deposits

9.1 Twin sources of sedimentation

The location of this study lies at the intersection of the north-western lobe of the Niger Delta with the east west trending Benin Basin. As a result of this juxtaposition the influence of both basins and their depositional settings has created a tectonic environment which displays some unusual structural deformation.

Most observations concerning deltaic tectonics have been made on the assumption that there is unlimited accommodation space which can be occupied by the outgrowth of the deltaic sediments (Doust and Omatsola 1990; Morley and Guerin 1996). When this accommodation space is limited by the presence of a barrier the unconfined models no longer hold up.

The north western region of the Niger delta is one such region where the sediments of the Benin Basin, which lies to the north and which is coeval with the Niger delta formation, prevent the unrestricted spread of pro delta deposits. The interplay between the sediment inputs from the two basins has led to a tectonic regime that is a hybrid of both deltaic and deep marine processes.

9.1.1 Benin Basin

The Benin Basin (Kaki et al. 2012) has been an active source of sediment deposition since the mid Cretaceous, whereas the growth of the Niger Delta is primarily an Eocene to recent event (Evamy et al. 1978). The older Cretaceous sediments of the Benin Basin underlie the 3D survey area, where they have been buried beneath the younger Niger Delta and younger Cenozoic Benin sourced deposits (Morgan 2003) as outlined in chapters 3 and 5. These Cretaceous sediments remain poorly understood due to a lack of well data. In addition the presence of deposits derived from a delta which pre dates the Niger Delta, the Benue Delta, have been interpreted to be present within the Upper Cretaceous interval. The evidence for the presence of Cretaceous deposits being present in the 3D survey area is provided by the surrounding regional data which pins the age of the detachment layer to the base of the Cenozoic (Doust and Omatsola 1990; Bilotti and Shaw 2005; Briggs et al. 2009; Maloney et al. 2012).

The Benin Basin is an east to west striking basin which is comprised of a shelfal area, which has existed since the mid Cretaceous, where sediments of a shallow marine nature have been found during oil and gas exploration drilling (MacGregor et al. 2003). To the south of the shelf lies a region of deep water sedimentation. The transition between the shelf and the deep water is dominated by unstable shelf collapse (Maloney et al. 2012) and the spread of mass transport deposits over a wide area. The nature of the shelf to deep water transition prior to the onset of the shelfal collapse, which is interpreted to have occurred around the Cretaceous to Cenozoic boundary, is unknown as it has been cannibalised by the later shelfal collapse.

The apron of mass transport deposits derived from the Benin Basin shelf margin collapse separate a deep relatively undeformed interval, from a complexly faulted overburden. The overburden faulting is interpreted to be unrelated to the arrangement of the strata which lie beneath the apron of mass transport deposits. This phenomenon was illustrated in both chapter 6 and 7. A further example is include in Figure 9-1.

Overlying the mass transport deposit apron are deposits which are interpreted to have been derived from canyons which were eroded into the Benin shelf in the north, which pre dated the outbuilding of the Niger Delta. Turbidity currents (Posamentier and Kolla

2003) are considered to be the primary transport mechanism for the transport of fine grained material from the canyons into the deep water. The down slope transport of the suspended material is interpreted to result in the emplacement of large scale levees and associated synclines which were deposited with the apexes orientated orthogonally to the shelf edge. The location of the levees was plotted in relation to the known canyon systems (Olabode and Adekoya 2008) and the strike of the levees when projected beyond the limits of the 3D survey point towards the location of the mouth of the canyons (chapter 6).

9.1.2 The Niger Delta

The onset of deposition from the Niger Delta in the Eocene gave rise to the input of sediments from the east. The outbuilding of the Niger Delta cone was deposited over a largely flat abyssal plain. However in the north-western margin of the delta the presence of the thick Palaeogene section would have acted as a barrier to the distribution of the sediments. The delta prograded towards the west such that large quantities of sediment reached the study area during the Oligo/Miocene (Corredor et al. 2005). This aggradation of sediment led to the gravitational tectonics which are observed throughout the Niger Delta. The presence of a series of slope channel deposits seen within the Miocene interval indicates that the 3D survey is located in a region which has been located on the continental slope from the Oligo/Miocene until the present day (Deptuck et al. 2003).

9.2 Structural styles

9.2.1 Deltaic styles

Conventional tectonic models for deltaic deformation over a mobile substrate focus on the three principle deformation styles seen in deltas across the globe. In the classic deltaic tectonic model (Allen 1965; Cohen and McClay 1996; McClay et al. 2003; Corredor et al. 2005; Aikulola et al. 2010), the three major structural styles recognised are extensional listric, normal and counter regional faulting, a transition zone of limited deformation and a toe thrust region. In addition to these three main structural provinces there are recognised within the Niger Delta a number of strike slip, or tear, faults.

9.2.1.1 Extension

The listric normal faults are assumed to sole out at depth at a horizon which is considered to be a detachment plane with low effective stress with the dip of the fault plane diminishing with depth. Within the region covered in this study no examples of listric faulting have been observed. There is an assumption that, since the area covered by

this work is in a relatively distal location relative to the extensional zone that the strata which should be found updip from the 3D volume have been deformed in this manner,(Maloney et al. 2012).

There is a great deal of extensional faulting recognised in the 3D volume. However as noted above the faulting does not fit the conventional listric style within the area covered by the 3D. The extensional faults, in general, within the Cenozoic section tip out at depth within the Cenozoic, above a pronounced detachment zone with no apparent flattening of the fault planes with depth, this characteristic of the faulting was outlined in Chapter 7. The faults are observed to maintain a steep dip from the upper tip to the base tip out. None of the faulting within the Cenozoic appears to be deep rooted, (i.e. none appear to cut through the basal mass transport deposit).

9.2.1.2 Transition

The transition zone is in general assumed to be relatively undeformed, this would appear to be the case for the Niger Delta. (Bilotti and Shaw 2005; Corredor et al. 2005); in this study there is limited evidence of a region of little or no structural modification. The study lies to the north of the documented translation zone of the Niger Delta

9.2.1.3 Toe Thrust Region

The third structural domain is the thrust belt. In this study there is ample evidence of compressional deformation, however the orientation of the apparent stress regime does not fit into a simple toe thrust model (Corredor et al. 2005). The compressional deformation observed in this study does not mirror the styles observed in the toe thrust regions and an alternative explanation is required. The uneven morphology of the section which underlies the Niger Delta is interpreted to have played a significant role in the subsequent thin skinned tectonic deformation.

9.2.1.4 Transcurrent/Tear faulting

The major tectonic element recognised within the 3D data volume is a linear structural feature, which is interpreted to be a dextral strike slip fault zone (Leduc et al. 2012) the fault zone is referred to herein as the Avon/Mahin fault zone. The sense of lateral displacement has been estimated using a number of approaches. The three approaches used; were mapping the lateral dislocation of palaeo channel levee complexes, which provides the most convincing evidence; measuring the degree of extension observed on either side of the fault zone and laterally shifting two major fault planes on either side of the fault zone to fit with their pre displacement throws.

Mapping of three stratigraphically separate channel systems across the fault zone has allowed their displacement to be estimated and indicates that the motion along the fault has been diachronous. The estimate of maximum measured lateral displacement has been calculated to be in the region of 7.9km for the deepest mapped channel system. The shallowest mapped channel system is interpreted to have been offset by 3.2km.

Unlike most significant strike slip fault zones found globally, the Avon/Mahin fault zone appears to be unrelated to any basement involvement.

This Avon/Mahin strike slip fault zone is interpreted to have arisen as a result of lateral stress being generated within the deposits due to the lack of accommodation space for the distal deposition of Niger Delta sourced sediments along the north-western margin of the deltaic cone.

The Avon/Mahin fault zone is interpreted to have evolved through three stages of deformation

- An early extensional phase with the formation of a series of east to west striking horst and grabens.
- Trans tensional displacement along the Mahin fault, with the establishment of a series of pull apart mini basins
- Transpressional motion along the Avon fault, leading to the formation of a number of high relief thrust anticlines.
-

9.2.2 Fan/levee style

An early Cenozoic phase of tectonic modification is interpreted to have occurred, during which the internal modification of the north to south striking ridges noted above took place. This deformation is interpreted to have been linked to the presence of a slope and basin floor fan system comprised of sediments derived from canyons within the Benin Basin shelfal region (Olabode and Adekoya 2008).

Within the levee and thalweg complex that is present at the western margin of the survey area the internal faulting is considered unusual for a deltaic setting. It would appear that there have been several episodes of faulting within this ridge. Suites of closely spaced reverse faults with common strike directions, are recognised. The vergence of the faults, which is generally updip, is nearly uniform within each of the fault suites. The nature of these faults is such that they do not fit neatly into the conventional deltaic compression model.

The observation that the faulting is limited to the lower Cenozoic indicates that the deformation took place towards the end of this depositional cycle, but prior to the onset of the Neogene Niger delta sedimentation.

One explanation as to the reason for the unusual fault pattern could be linked to the critical taper theory (Dahlen 1990) which was posited for accretionary prisms and identified as a contributing factor to some of the deep water thrusting in the Niger Delta outer thrust belt (Bilotti and Shaw 2005).

9.3 Mass transport complex as the detachment

The ubiquitous presence of mass transport deposits at the base of the faulted overburden suggests that the mass transport deposits play a significant role in the basal detachment mechanism. The movement of strata over a basal glide plane is recognised as being linked to the presence of a weak layer of low shear strength. This weak layer is interpreted to be due to an elevated pore pressure.

Mass transport deposits are comprised of previously fluidised sediments. The motion of the chaotically sorted blocks of rocks and interstitial clay is enabled by the presence of a high fluid content. When there is limited overburden deposited over a mass transport deposit the interstitial water remains in situ (Strachan 2002). With the increase in overburden by subsequent deposition the normal stress increases and the water is then liberated at the upper surface of the mass transport deposit. This water, trapped by the overburden then becomes overpressured. This overpressured layer then acts as the detachment.

The observation that the Cenozoic deformation does not extend below the upper surface of the base Tertiary mass transport complex provides strong evidence that the upper surface is the mechanically weak layer upon which the overburden has migrated laterally.

The seismic data where it is well imaged provides the evidence that the base of the overburden tectonic deformation is limited in a vertical sense by the upper surface of the mass transport complexes. This is illustrated in the image below.

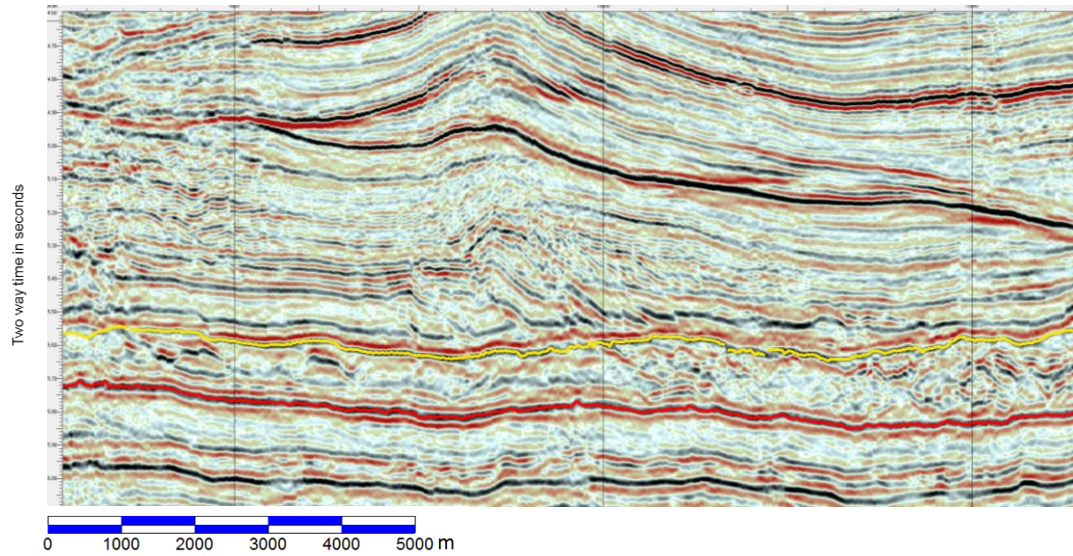


Figure 9-1 Seismic line illustrating the relationship between the upper surface of the mass transport complex (yellow horizon) and the tectonic deformation in the overburden

In the above figure the mass transport complex is interpreted to be present between the red and yellow horizons. The section which overlies the yellow horizon has been subject to compressional deformation along a basal detachment which is coincident with the upper surface of the mass transport deposit.

References

Abers, G. and McCaffrey, R. 1988. Active deformation in the New Guinea fold-and-thrust belt : seismological evidence for strike slip faulting and basement involved thrusting. *Journal of Geophysical Research: Solid Earth* 93(B11), pp. 13332-13354.

Adeleye, D. R. 1975. Nigerian Late Cretaceous Stratigraphy and Palaeogeography. *AAPG Bulletin* 59(12), pp. 2303-2313.

Adeogba, A. A. et al. 2005. Transient fan architecture and depositional controls from near-surface 3-D seismic data, Niger Delta continental slope. *AAPG Bulletin* 89, pp. 627-643.

Aikulola, U. et al. 2010. Investigating fault shadows in the Niger Delta. *The Leading Edge* 29(1), pp. 16-22.

Ali, J. R. and Hall, R. 1995. Evolution of the boundary between the Philippine Sea Plate and Australia: palaeomagnetic evidence from eastern Indonesia. *Tectonophysics* 251(1–4), pp. 251-275.

Allen, J. R. L. 1965. late Quaternary Niger Delta, and adjacent areas; sedimentary environments and lithofacies. *AAPG Bulletin* 49, pp. 547-600.

Alves, T. M. 2010. 3D Seismic examples of differential compaction in mass-transport deposits and their effect on post-failure strata. *Marine Geology* 271(3–4), pp. 212-224.

Alves, T. M. 2015. Submarine slide blocks and associated soft-sediment deformation in deep-water basins: A review. *Marine and Petroleum Geology* 67, pp. 262-285.

Austin, J. A. and Uchupi, E. 1982. Continental-Oceanic Crustal Transition Off Southwest Africa. *AAPG Bulletin* 66(9), pp. 1328-1347.

Avbovbo, A. A. 1978. Tertiary lithostratigraphy of the Niger Delta. *AAPG Bulletin* 62(2), pp. 295-206.

Avbovbo, A. A. et al. 1986. Depositional and structural styles in Chad Basin of northeast Nigeria. . *AAPG Bulletin* 70(12), pp. 1787-1798.

Barker, C. 1972. Aquathermal Pressuring—Role of Temperature in Development of Abnormal-Pressure Zones. *AAPG Bulletin* 56(10), pp. 2068-2071.

Basile, C. et al. 2005. Phanerozoic geological evolution of the Equatorial Atlantic domain. *Journal of African Earth Sciences* 43(1–3), pp. 275-282.

Basile, C. et al. 1993. The Ivory Coast-Ghana transform margin: A marginal ridge structure deduced from seismic data. *Tectonophysics* 222(1), pp. 1-19.

Baudon, C. and Cartwright, J. A. 2008. 3D seismic characterisation of an array of blind normal faults in the Levant Basin, Eastern Mediterranean. *Journal of Structural Geology* 30(6), pp. 746-760.

Benkhelil, J. et al. 1998. Sedimentary and structural characteristics of the Cretaceous along the Cote D'Ivoire-Ghana transform margin and in the Benue trough: A comparison. *Proceedings of the Ocean Drilling Program, Scientific Results* 159, pp. 93-99.

Bickert, T. and Henrich, R. 2011. Chapter 12 - Climate Records of Deep-Sea Sediments: Towards the Cenozoic Ice House. In: Heiko, H. and Thierry, M. eds. *Developments in Sedimentology*. Vol. Volume 63. Elsevier, pp. 793-823.

Bilotti, F. and Shaw, J. H. 2005. Deep-water Niger Delta fold and thrust belt modeled as a critical-taper wedge: The influence of elevated basal fluid pressure on structural styles. *AAPG Bulletin* 89(11), pp. 1475-1491.

Bonne, K. P. M. 2014. Reconstruction of the evolution of the Niger River and implications for sediment supply to the Equatorial Atlantic margin of Africa during the Cretaceous and the Cenozoic. *Geological Society, London, Special Publications* 386(1), pp. 327-349.

Boult, P. and Kaldi, J. 2005. *Evaluating fault and cap rock seals*. Tulsa, Okla.: American Association of Petroleum Geologists.

Briggs, S. E. et al. 2009a. Crustal structure of the deepwater west Niger Delta passive margin from the interpretation of seismic reflection data. *Marine and Petroleum Geology* 26(6), pp. 936-950.

Briggs, S. E. et al. 2009b. Thrusting in oceanic crust during continental drift offshore Niger Delta, equatorial Africa. *Tectonics* 28(1), pp. n/a-n/a.

Briggs, S. E. et al. 2006. Multiple detachment levels and their control on fold styles in the compressional domain of the deepwater west Niger Delta. *Basin Research* 18, pp. 435-450.

Brown, A. R. 1996. *Interpretation of three-dimensional seismic data*. 4th ed. AAPG.

Brown Jr, L. F. and Fisher, W. L. 1977. *Seismic-Stratigraphic Interpretation of Depositional Systems: Examples from Brazilian Rift and Pull-Apart Basins: Section 2. Application of Seismic Reflection Configuration to Stratigraphic Interpretation*. Tulsa: AAPG.

Brownfield, M. E. and Charpentier, R. C. 2006. Geology and Total Petroleum Systems of the Gulf of Guinea Province of West Africa. *US geological Survey Bulletin* 2207C, pp. 1-32.

Bruce, C. L. 1973. Pressured Shale and Related Sediment Deformation: Mechanism for Development of Regional Contemporaneous Faults'. *AAPG Bulletin* 57(5), pp. 878-886.

- Bryn, P. et al. 2005a. Explaining the Storegga Slide. *Marine and Petroleum Geology* 22(1–2), pp. 11-19.
- Bryn, P. et al. 2005b. Contourites and their relevance for mass wasting along the Mid-Norwegian Margin. *Marine and Petroleum Geology* 22(1–2), pp. 85-96.
- Bull, S. et al. 2009. A review of kinematic indicators from mass-transport complexes using 3D seismic data. *Marine and Petroleum Geology* 26(7), pp. 1132-1151.
- Burke, K. 1972. Longshore Drift, Submarine Canyons, and Submarine Fans in Development of Niger Delta'. *AAPG Bulletin* 56(10), pp. 1975-1983.
- Burke, K. et al. 2003. *Africa's petroleum systems: four tectonic 'Aces' in the past 600 million years* Geological Society of London.
- Butler, R. and Iacopini, D. 2009. Strain and Displacement Analysis Using the Displacement/Distance Method: Application to 3D Seismic Data from a Deep Water Thrust Belt In: *AAPG Hedberg Conference, Deepwater Fold and Thrust Belts*. Tirrenia, Italy, October 4-9, 2009.
- Canals, M. et al. 2004. Slope failure dynamics and impacts from seafloor and shallow sub-seafloor geophysical data: case studies from the COSTA project. *Marine Geology* 213(1–4), pp. 9-72.
- Cardona, S. et al. 2016. Fabric Development and Pore-Throat Reduction in a Mass-Transport Deposit in the Jubilee Gas Field, Eastern Gulf of Mexico: Consequences for the Sealing Capacity of MTDs. In: Lamarche, G. et al. eds. *Submarine Mass Movements and their Consequences: 7th International Symposium*. Cham: Springer International Publishing, pp. 27-37.
- Carter, R. M. 1975. A discussion and classification of subaqueous mass-transport with particular application to grain-flow, slurry-flow, and fluxoturbidites. *Earth-Science Reviews* 11(2), pp. 145-177.
- Cartwright, J. et al. 2007. Seal Bypass systems. *AAPG Bulletin* 91(8), pp. 1141-1166.
- Cartwright, J. A. and Jackson, M. P. A. 2008. Initiation of gravitational collapse of an evaporite basin margin: The Messinian saline giant, Levant Basin, eastern Mediterranean. *Geological Society of America Bulletin* 120(3-4), pp. 399-413.
- Cartwright, J. A. et al. 1995. Fault growth by segment linkage: an explanation for scatter in maximum displacement and trace length data from the Canyonlands Grabens of SE Utah. *Journal of Structural Geology* 17(9), pp. 1319-1326.
- Chapin, M. et al. 2002. Integrated seismic and subsurface characterization of Bonga Field, offshore Nigeria. *The Leading Edge* 21(11), pp. 1125-1131.

- Chapple, W. M. 1978. Mechanics of thin-skinned fold-and-thrust belts. *Geological Society of America Bulletin* 89(8), pp. 1189-1198.
- Clark, J. D. and Pickering, K. T. 1996. Architectural Elements and Growth Patterns of Submarine Channels: Application to Hydrocarbon Exploration. *AAPG Bulletin* 80(2), pp. 194-221.
- Cobbold, P. R. et al. 2009. Structural consequences of fluid overpressure and seepage forces in the outer thrust belt of the Niger Delta. *Petroleum Geoscience* 15, pp. 3-15.
- Cobbold, P. R. et al. 2004. Mechanism of thin-skinned detachment in the Amazon Fan: assessing the importance of fluid overpressure and hydrocarbon generation. *Marine and Petroleum Geology* 21(8), pp. 1013-1025.
- Cohen, H. A. and McClay, K. 1996. Sedimentation and shale tectonics of the northwestern Niger Delta front. *Marine and Petroleum Geology* 13(3), pp. 313-328.
- Corredor, F. et al. 2005. Structural styles in the deep-water fold and thrust belts of the Niger Delta. *AAPG Bulletin* 89(6), pp. 753-780.
- Crans, W. and Mandl, G. 1980. ON THE THEORY OF GROWTH FAULTING*: GENESIS OF THE "UNIT". *Journal of Petroleum Geology* 3(2), pp. 209-236.
- Crans, W. and Mandl, G. 1981. ON THE THEORY OF GROWTH FAULTING PART II(b):GENESIS OF THE "UNIT"* . *Journal of Petroleum Geology* 3(3), pp. 333-355.
- Crans, W. et al. 1980. ON THE THEORY OF GROWTH FAULTING*: A GEOMECHANICAL DELTA MODEL BASED ON GRAVITY SLIDING. *Journal of Petroleum Geology* 2(3), pp. 265-307.
- Cross, N. E. et al. 2009. Three-dimensional seismic geomorphology of a deep-water slope-channel system: The Sequoia field, offshore west Nile Delta, Egypt. *AAPG Bulletin* 95(8), pp. 1063-1086.
- Dahlen, F. A. 1990. Critical Taper Models of Fold-and-Thrust Belts and Accretionary Wedges. *Annual Review of Earth and Planetary Science* 18, pp. 55-99.
- Damuth, J. E. 1994. Neogene gravity tectonics and depositional processes on the deep Niger Delta continental margin. *Marine and Petroleum Geology* 11(3), pp. 320-346.
- Davies, R. J. et al. 2005. Termination of a fossil continent-ocean fracture zone imaged with three-dimensional seismic data: The Chain Fracture Zone, eastern equatorial Atlantic. *Geology* 33(8), pp. 641-644.
- de Matos, R. M. D. 1992. The Northeast Brazilian Rift System. *Tectonics* 11(4), pp. 766-791.

de Matos, R. M. D. 1999. History of the north east Brazilian rift system: kinematic implications for the break up between Brazil and West Africa. *Geological Society, London, Special Publications* 153, pp. 55-73.

Demaison, G. and Murriss, R. J. 1984. *Petroleum Geochemistry and Basin Evaluation*. Tulsa: AAPG.

Deptuck, M. E. et al. 2003. Architecture and evolution of upper fan channel-belts on the Niger Delta slope and in the Arabian Sea. *Marine and Petroleum Geology* 20(6–8), pp. 649-676.

Deptuck, M. E. et al. 2007. Migration–aggradation history and 3-D seismic geomorphology of submarine channels in the Pleistocene Benin-major Canyon, western Niger Delta slope. *Marine and Petroleum Geology* 24(6–9), pp. 406-433.

Dooley, T. et al. 2013. Coeval extension and shortening above and below salt canopies on an uplifted, continental margin, Application to the northern Gulf of Mexico. *AAPG Bulletin* 97(10), pp. 1737-1764.

Dooley, T. P. and Schreurs, G. 2012. Analogue modelling of intraplate strike-slip tectonics: A review and new experimental results. *Tectonophysics* 574–575, pp. 1-71.

Doust, H. and Omatsola, E. 1990. Niger Delta: Divergent Passive Margin Basins. *AAPG Memoir* 48, pp. 201-238.

Duarte, C. S. L. and Viana, A. 2007. *Santos Drift System: stratigraphic organization and implications for late Cenozoic palaeocirculation in the Santos Basin, SW Atlantic Ocean*. London: The Geological Society of London.

Dunlap, D. B. et al. 2010. Seismic geomorphology of offshore Morocco's east margin, Safi Haute Mer area. *AAPG Bulletin* 94(5), pp. 615-642.

Elsley, G. R. and Tieman, H. 2011. *A comparison of Prestack Depth and Prestack Time Imaging for the Paktoa Complex, Canadian Beaufort MacKenzie Basin*. Tulsa: AAPG.

Emery, K. O. et al. 1975. Continental Margin Off Western Africa: Angola to Sierra Leone. *AAPG Bulletin* 59(12), pp. 2209-22265.

Emmons, R. C. 1969. Strike-slip rupture patterns in sand models. *Tectonophysics* 7(1), pp. 71-87.

Evamy, B. D. et al. 1978. Hydrocarbon Habitat of Tertiary Niger Delta. *AAPG Bulletin* 62(1), pp. 1-39.

Faereth, R. B. and Saetersmoen, B. H. 2008. Geometry of a major slump structure in the Storegga slide region offshore western Norway. *Norwegian journal of Geology* 88, pp. 1-11.

Fairhead, J. D. 1988. Mesozoic plate tectonic reconstructions of the central South Atlantic Ocean: The role of the West and Central African rift system. *Tectonophysics* 155(1–4), pp. 181-191.

Fairhead, J. D. and Binks, R. M. 1991. Differential opening of the Central and South Atlantic Oceans and the opening of the West African rift system. *Tectonophysics* 187(1–3), pp. 191-203.

Fairhead, J. D. and Okereke, C. S. 1987. A regional gravity study of the West African rift system in Nigeria and Cameroon and its tectonic interpretation. *Tectonophysics* 143(1–3), pp. 141-159.

Faugères, J.-C. and Mulder, T. 2011. Chapter 3 - Contour Currents and Contourite Drifts. In: Heiko, H. and Thierry, M. eds. *Developments in Sedimentology*. Vol. Volume 63. Elsevier, pp. 149-214.

Faugères, J. C. and Stow, D. A. V. 2008. Chapter 14 Contourite Drifts: Nature, Evolution and Controls. In: Rebesco, M. and Camerlenghi, A. eds. *Developments in Sedimentology*. Vol. Volume 60. Elsevier, pp. 257-288.

Freund, R. 1974. Kinematics of transform and transcurrent faults. *Tectonophysics* 21, pp. 93-134.

Frey-Martínez, J. et al. 2006. Frontally confined versus frontally emergent submarine landslides: A 3D seismic characterisation. *Marine and Petroleum Geology* 23(5), pp. 585-604.

Galloway, W. E. 1975. *Process framework for describing the morphologic and stratigraphic evolution of deltaic depositional systems*. Houston Geological society.

Galloway, W. E. 1998. Siliciclastic Slope and Base-of-Slope Depositional Systems: Component Facies, Stratigraphic Architecture, and Classification. *AAPG Bulletin* 82(4), pp. 569-595.

Gamboa, D. et al. 2010. MTD distribution on a 'passive' continental margin: The Espírito Santo Basin (SE Brazil) during the Palaeogene. *Marine and Petroleum Geology* 27(7), pp. 1311-1324.

Gee, M. J. R. et al. 2007. The Brunei slide: A giant submarine landslide on the North West Borneo Margin revealed by 3D seismic data. *Marine Geology* 246(1), pp. 9-23.

Genik, G. J. 1993. Petroleum Geology of Cretaceous-Tertiary Rift Basins in Niger, Chad, and Central African Republic. *AAPG Bulletin* 77(8), pp. 1405-1434.

Graue, K. 2000. Mud volcanoes in deepwater Nigeria. *Marine and Petroleum Geology* 17(8), pp. 959-974.

- Guiraud, R. et al. 1992. Chronology and geodynamic setting of Cretaceous-Cenozoic rifting in West and Central Africa. *Tectonophysics* 213(1–2), pp. 227-234.
- Guiraud, R. and Bosworth, W. 1997. Senonian basin inversion and rejuvenation of rifting in Africa and Arabia: synthesis and implications to plate-scale tectonics. *Tectonophysics* 282(1–4), pp. 39-82.
- Guiraud, R. et al. 2005. Phanerozoic geological evolution of Northern and Central Africa: An overview. *Journal of African Earth Sciences* 43(1–3), pp. 83-143.
- Haack, R. C. et al. 2000. *Niger Delta Petroleum Systems, Nigeria*. AAPG.
- Haq, B. U. et al. 1987. Chronology of fluctuating sea levels since the triassic. *Science (New York, N.Y.)* 235(4793), pp. 1156-1167.
- Harding, T. P. 1974. Petroleum Traps Associated with Wrench Faults. *AAPG Bulletin* 58(7), pp. 1290-1304.
- Harding, T. P. 1985. Seismic characteristics and identification of negative flower structures, positive structures and positive structural inversion. *AAPG Bulletin* 69, pp. 582-700.
- Hedberg, H. D. 1970. Continental Margins from Viewpoint of the Petroleum Geologist. *AAPG Bulletin* 54(1), pp. 3-43.
- Hege M. Nordgard Bolas et al. 2004. Origin of overpressures in shales: Constraints from basin modeling
AAPG Bulletin 88(2), pp. 193-211.
- Heine, C. et al. 2013. Kinematics of the South Atlantic rift. *Solid Earth* 4(2), pp. 215-253.
- Heinio, P. and Davies, R. J. 2006. Degradation of compressional fold belts: Deep-water Niger Delta. *AAPG Bulletin* 90(5), pp. 753-770.
- Heiniö, P. and Davies, R. J. 2007. Knickpoint migration in submarine channels in response to fold growth, western Niger Delta. *Marine and Petroleum Geology* 24(6–9), pp. 434-449.
- Henrich, R. and Hüneke, H. 2011. Chapter 5 - Hemipelagic Advection and Periplatform Sedimentation. In: Heiko, H. and Thierry, M. eds. *Developments in Sedimentology*. Vol. Volume 63. Elsevier, pp. 353-396.
- Hodgson, D. M. et al. 2011. Submarine slope degradation and aggradation and the stratigraphic evolution of channel–levee systems. *Journal of the Geological Society of London* 168, pp. 625-628.

- Hubral, P. 1980. Wavefront curvatures in three-dimensional laterally inhomogeneous media with curved interfaces. *GEOPHYSICS* 45(5), pp. 905-913.
- Hüneke, H. and Henrich, R. 2011. Chapter 4 - Pelagic Sedimentation in Modern and Ancient Oceans. In: Heiko, H. and Thierry, M. eds. *Developments in Sedimentology*. Vol. Volume 63. Elsevier, pp. 215-351.
- Hunter, S. E. et al. 2007. *The Eirik Drift: a long term barometer of North Atlantic deep water flux of Cape Farewell Greenland*. London: The Geological Society of London.
- Hurst, A. et al. 2007. *Sand injectites : implications for hydrocarbon exploration and production*. Tulsa, Okla.: American Association of Petroleum Geologists.
- Imber, J. et al. 2003. Hanging wall fault kinematics and footwall collapse in listric growth fault systems. *Journal of Structural Geology* 25, pp. 197-208.
- Japsen, P. 1993. Influence of lithology and Neogene uplift on seismic velocities in Denmark; Implications for depth conversion of maps. *AAPG Bulletin* 77(2), pp. 194-211.
- Kaki, C. et al. 2012. Geology and Petroleum Systems of the Offshore Benin Basin (Benin). *Oil & Gas Science and Technology – Rev. IFP Energies nouvelles*, 68(2), pp. 363-381.
- Kane, I. A. et al. 2010. Submarine channel levee shape and sediment waves from physical experiments. *Sedimentary Geology* 223(1–2), pp. 75-85.
- King, S. J. and Cartwright, J. A. 2010. Mass Transport Deposits and Their Role in Thin Skinned Tectonics - An Example from the NW Niger Delta In: *AAPG Annular Conference*. New Orleans.
- Kneller, B. 1995. Beyond the turbidite paradigm: physical models for deposition of turbidites and their implications for reservoir prediction. *Geological Society, London, Special Publications* 94(1), pp. 31-49.
- Kolla, V. et al. 2007. Deep-water and fluvial sinuous channels—Characteristics, similarities and dissimilarities, and modes of formation. *Marine and Petroleum Geology* 24(6–9), pp. 388-405.
- Kostenko, O. V. et al. 2008. Structural evaluation of column-height controls at a toe-thrust discovery, deep-water Niger Delta. *AAPG Bulletin* 92(12), pp. 1615-1638.
- Kvalstad, T. J. et al. 2005. The Storegga slide: evaluation of triggering sources and slide mechanics. *Marine and Petroleum Geology* 22(1–2), pp. 245-256.
- Leduc, A. M. et al. 2009. Relationship between Structural Deformation and Sediment Dispersal in the Western Niger Delta In: *AAPG Hedberg Conference, deep Water Fold and Thrust Belts*. Tirrenia, Italy, 4-9 October 2009.

Leduc, A. M. et al. 2012. The lateral strike-slip domain in gravitational detachment delta systems: A case study of the northwestern margin of the Niger Delta. *AAPG Bulletin* 96(4), pp. 709-728.

Lehner, P. and De Ruiter, P. A. C. 1977. Structural History of Atlantic margin of Africa. *AAPG Bulletin* 61(7), pp. 961-981.

Li, M. and Zhao, Y. 2014. Chapter 3 - Seismic Coherence Technique. In: Zhao, M.L. ed. *Geophysical Exploration Technology*. Oxford: Elsevier, pp. 63-74.

Little, T. A. and Jones, A. 1998. Seven million years of strike-slip and related off-fault deformation, northeastern Marlborough fault system, South Island, New Zealand. *Tectonics* 17(2), pp. 285-302.

Lucchi, R. G. and Rebesco, M. 2007. *Glacial contourites on the Antarcctic Peninsula margin: insight for palaeoenvironment and palaeoclimate conditions*. London: The Geological Society of London.

Macauley, R. V. and Hubbard, S. M. 2013. Slope channel sedimentary processes and stratigraphic stacking, Cretaceous Tres Pasos Formation slope system, Chilean Patagonia. *Marine and Petroleum Geology* 41, pp. 146-162.

MacGregor, D. S. et al. 2003. *Play fairways of the Gulf of Guinea transform margin*. Special Publications: Geological Society of London.

Magbagbeola, O. A. and Willis, B. J. 2007. Sequence stratigraphy and syndepositional deformation of the Agbada Formation, Robertkiri field, Niger Delta, Nigeria. *AAPG Bulletin* 91(7), pp. 945-958.

Malod, J. A. and Kemal, B. M. 1996. The Sumatra margin: oblique subduction and lateral displacement of the accretionary prism. *Geological Society, London, Special Publications* 106(1), pp. 19-28.

Maloney, D. et al. 2012. Structure of the footwall of a listric fault system revealed by 3D seismic data from the Niger Delta. *Basin Research* 24(1), pp. 107-123.

Maloney, D. et al. 2009. The Implications of Detachment Unit Deformation on Fold and Thrust Belt Evolution: Examples from the Deepwater Niger Delta In: *AAPG Hedberg Conference, Deep Water Fold and Thrust Belts*. Tirrenia, Italy, October 4-9, 2009.

Maloney, D. et al. 2010. New insights into deformation mechanisms in the gravitationally driven Niger Delta deep-water fold and thrust belt. *AAPG Bulletin* 94(9), pp. 1401-1424.

Mann, D. M. and Mackenzie, A. S. 1990. Prediction of pore fluid pressures in sedimentary basins. *Marine and Petroleum Geology* 7(1), pp. 55-65.

Masclé, J. 1973. Diapiric Structures off Niger Delta. *AAPG Bulletin* 57(9), pp. 1672-1678.

- McClay, K. et al. 2003. Analogue models of delta systems above ductile substrates. *Geological Society, London, Special Publications* 216(1), pp. 411-428.
- McHargue, T. et al. 2011. Architecture of turbidite channel systems on the continental slope: Patterns and predictions. *Marine and Petroleum Geology* 28(3), pp. 728-743.
- Middleton, G. V. 1993. Sediment Deposition from Turbidity Currents. *Annual Review of Earth and Planetary Sciences* 21, pp. 89-114.
- Mitchum Jr., R. M. et al. 1977. *Seismic stratigraphy and global changes of sea level, part 6: stratigraphic interpretation of seismic reflection patterns in depositional sequences*. AAPG.
- Mitra, S. 2002. Structural models of faulted detachment folds. *AAPG Bulletin* 86(9), pp. 1673-1694.
- Molnar, P. and Tapponnier, P. 1975. Cenozoic Tectonics of Asia: Effects of a Continental Collision: Features of recent continental tectonics in Asia can be interpreted as results of the India-Eurasia collision. *Science* 189(4201), pp. 419-426.
- Morgan, R. 2003. Prospectivity in ultradeep water: the case for petroleum generation and migration within the outer parts of the Niger Delta apron. *Geological Society, London, Special Publications* 207, p. 14.
- Morgan, R. 2004. Structural controls on the positioning of submarine channels on the lower slopes of the Niger Delta. In: Cartwright, J. et al. eds. *Geological Society, London, Memoirs*. Vol. 29. London: The Geological Society of London.
- Morley, C. K. 2003. Mobile shale related deformation in large deltas developed on passive and active margins. *Geological Society, London, Special Publications* 216(1), pp. 335-357.
- Morley, C. K. and Guerin, G. 1996. Comparison of gravity-driven deformation styles and behavior associated with mobile shales and salt. *Tectonics* 15(6), pp. 1154-1170.
- Morley, C. K. et al. 2011. Deepwater fold and thrust belt classification, tectonics, structure and hydrocarbon prospectivity: A review. *Earth-Science Reviews* 104(1-3), pp. 41-91.
- Moscardelli, L. and Wood, L. 2016. Morphometry of mass-transport deposits as a predictive tool. *Geological Society of America Bulletin* 128(1-2), pp. 47-80.
- Moscardelli, L. et al. 2006. Mass-transport complexes and associated processes in the offshore area of Trinidad and Venezuela. *AAPG Bulletin* 90(7), pp. 1059-1088.
- Mourgues, R. et al. 2009. An experimental investigation of gravity-driven shale tectonics in progradational delta. *Tectonophysics* 474(3-4), pp. 643-656.

Mulder, T. 2011. Chapter 2 - Gravity Processes and Deposits on Continental Slope, Rise and Abyssal Plains. In: Heiko, H. and Thierry, M. eds. *Developments in Sedimentology*. Vol. Volume 63. Elsevier, pp. 25-148.

Naylor, M. A. et al. 1986. Fault geometries in basement-induced wrench faulting under different initial stress states. *Journal of Structural Geology* 8(7), pp. 737-752.

Nemec, W., Steel, R.J., Gjelberg, J, Colinson, J.D., Prestholm, E., Oxnevad, I.E. 1988. Anatomy of Collapsed and Re-established Delta Front in Lower Cretaceous of Eastern Spitsbergen: Gravitational Sliding and Sedimentation Processes. *AAPG Bulletin* 72(4), pp. 454-476.

Nielsen, T. et al. 2008. Chapter 16 Seismic Expression of Contourite Depositional Systems. In: Rebesco, M. and Camerlenghi, A. eds. *Developments in Sedimentology*. Vol. Volume 60. Elsevier, pp. 301-321.

Normark, W. R. et al. 1993. Turbidite systems: State of the art and future directions. *Reviews of Geophysics* 31(2), pp. 91-116.

Nürnberg, D. and Müller, R. D. 1991. The tectonic evolution of the South Atlantic from Late Jurassic to present. *Tectonophysics* 191(1-2), pp. 27-53.

Olabode, S. O. 2006. Siliciclastic slope deposits from the Cretaceous Abeokuta Group, Dahomey (Benin) Basin, southwestern Nigeria. *Journal of African Earth Sciences* 46(3), pp. 187-200.

Olabode, S. O. and Adekoya, J. A. 2008. Seismic stratigraphy and development of Avon canyon in Benin (Dahomey) basin, southwestern Nigeria. *Journal of African Earth Sciences* 50(5), pp. 286-304.

Onuoha, K. and Ofoegbu, C. O. 1988. Subsidence and evolution of Nigeria's continental margin: implications of data from Afowo-1 well. *Marine and Petroleum Geology* 5(2), pp. 175-181.

Onuoha, K. M. 1999. Structural features of Nigeria's coastal margin: an assessment based on age data from wells. *Journal of African Earth Sciences* 29(3), pp. 485-499.

Osborne, M. J. and Swarbrick, R. E. 1997. Mechanisms for Generating Overpressure in Sedimentary Basins: A Reevaluation. *AAPG Bulletin* 81(6), pp. 1023-1041.

Petters, S. W. 1984. An ancient submarine canyon in the Oligocene-Miocene of the western Niger Delta. *Sedimentology* 31(6), pp. 805-810.

Poblet, J. and McClay, K. R. 1996. Geometry and Kinematics of Single-Layer Detachment Folds. *AAPG Bulletin* 80(7), pp. 1085-1109.

Posamentier, A. S. et al. 1992. Forced Regressions in a Sequence Stratigraphic Framework: Concepts, Examples and Exploration Significance. *AAPG Bulletin* 76(11), pp. 1679-1709.

Posamentier, H. W. 2003. Depositional elements associated with a basin floor channel-levee system: case study from the Gulf of Mexico. *Marine and Petroleum Geology* 20(6-8), pp. 677-690.

Posamentier, H. W. and Kolla, V. 2003. Seismic Geomorphology and Stratigraphy of Depositional Elements in Deep-Water Settings. *Journal of Sedimentary Research* 73(3), pp. 367-388.

Pubellier, M. and Ego, F. 2002. Anatomy of an escape tectonic zone: Western Irian Jaya (Indonesia). *Tectonics* 21(4), pp. 1-1-1-16.

Rabelo, I. R. et al. 2007. Parameterization of meander-belt elements in high-resolution three-dimensional seismic data using the GeoTime cube and modern analogues. *Geological Society, London, Special Publications* 277(1), pp. 121-137.

Reading, H. G. and Richards, M. 1994. Turbidite Systems in Deep-Water Basin Margins Classified by Grain Size and Feeder System¹. *AAPG Bulletin* 78(5), pp. 792-822.

Rebesco, M. et al. 2014. Contourites and associated sediments controlled by deep-water circulation processes: State-of-the-art and future considerations. *Marine Geology* 352, pp. 111-154.

Reijers, T. 2011. Stratigraphy and sedimentology of the Niger Delta. *Geologos*.

Richardson, S. E. J. et al. 2011. Structure and evolution of mass transport deposits in the South Caspian Basin, Azerbaijan. *Basin Research* 23(6), pp. 702-719.

Rodriguez, A. B. and Anderson, J. B. 2004. Contourite origin for shelf and upper slope sand sheet, offshore Antarctica. *Sedimentology* 51(4), pp. 699-711.

Rowan, M. G. et al. 2004. Gravity-driven Fold Belts on Passive Margins. In: McClay, K.R. ed. *Thrust tectonics and hydrocarbon systems*. AAPG.

Sandwell, D. T. et al. 2014. New global marine gravity model from CryoSat-2 and Jason-1 reveals buried tectonic structure. *Science* 346(6205), pp. 65-67.

Sapin, F. et al. 2012. Counter-regional normal faults in shale-dominated deltas: Origin, mechanism and evolution. *Marine and Petroleum Geology* 37(1), pp. 121-128.

Schultz-Ela, D. D. 2001. Excursus on gravity gliding and gravity spreading. *Journal of Structural Geology* 23(5), pp. 725-731.

Schultz, M. R. and Hubbard, S. M. 2005. Sedimentology, stratigraphic architecture and ichnology of gravity flow deposits partially ponded in a growth fault controlled slope

minbasin, Tres Pasos formation, Southern Chile. *Journal of Sedimentary Research* 75, pp. 440-453.

Shaw, J. H. et al. 2004. Structural Controls on Growth Stratigraphy in Contractional Fault-related Folds. In: McClay, K.R. ed. *Thrust tectonics and hydrocarbon systems*. Vol. 82. AAPG.

Shipp, R. C. et al. 2011. *Mass-transport deposits in deepwater settings*. Tulsa , Okla.: SEPM (Society for Sedimentary Geology).

Short, K. C. and Stauble, A. J. 1967. Outline Geology of Niger Delta. *AAPG Bulletin* 51(5), pp. 761-779.

Shultz, M. R. et al. 2005. Deposition and stratigraphic architecture of an outcropping ancient slope system: Tres Pasos Formation, Magallanes Basin, southern Chile. *Geological Society, London, Special Publications* 244(1), pp. 27-50.

Solheim, A. et al. 2005. The Storegga Slide complex: repetitive large scale sliding with similar cause and development. *Marine and Petroleum Geology* 22(1–2), pp. 97-107.

Stewart, S. 1999. Geometry of thin-skinned tectonic systems in relation to detachment layer thickness in sedimentary basins. *Tectonics* 18(4), pp. 719-732.

Stow, D. A. V. and Mayall, M. 2000. Deep-water sedimentary systems: New models for the 21st century. *Marine and Petroleum Geology* 17(2), pp. 125-135.

Strachan, L. J. 2002. Slump-initiated and controlled syndepositional sandstone remobilization: an example from the Namurian of County Clare, Ireland. *Sedimentology* 49, pp. 25-41.

Surlyk, F. and Lykke-Andersen, H. 2007. Contourite drifts, moats and channels in the Upper Cretaceous chalk of the Danish Basin. *Sedimentology* 54(2), pp. 405-422.

Talling, P. J. 2014. On the triggers, resulting flow types and frequencies of subaqueous sediment density flows in different settings. *Marine Geology* 352, pp. 155-182.

Talling, P. J. et al. 2012. Subaqueous sediment density flows: Depositional processes and deposit types. *Sedimentology* 59(7), pp. 1937-2003.

Tsvankin, I. and Thomsen, L. 1992. Nonhyperbolic reflection moveout and the inverse problem for transversely isotropic media. *SEG Technical Program Expanded Abstracts 1992*. Society of Exploration Geophysicists, pp. 1348-1351.

Tucker, P. 1982. 1. Pitfalls Revisited. *Pitfalls Revisited*. Society of Exploration Geophysicists, pp. 1-19.

Tucker, P. and Yorston, H. 1973. 1. Pitfalls in Seismic Interpretation. *Pitfalls in Seismic Interpretation*. Society of Exploration Geophysicists, pp. i-57.

Tuitt, A. et al. 2012. Modelling of sediment wedge movement along low-angle detachments using ABAQUS™. *Geological Society, London, Special Publications* 367(1), pp. 171-183.

Twiss, R. J. and Moores, E. M. 2007. *Structural Geology*. New York: Freeman.

Vail, P. R. et al. 1977. *Seismic stratigraphy and global changes of sea level, part 4: global cycles of relative changes of sea level*. AAPG.

van Borren, L. F. A. et al. 1996. *Geology and Hydrocarbon Resources of Negara Brunei Darussalam*. Brunei: Syabus.

Van Rensbergen, P. et al. 1999. Re-evaluation of mobile shale occurrences on seismic sections of the Champion and Baram deltas, offshore Brunei. *Journal of the Geological Society of London* 156, pp. 633-650.

Van Wagoner, J. C. et al. 1990. *Siliciclastic Sequence Stratigraphy in Well Logs, Cores and Outcrops*. . American Association of Petroleum Geologists.

Vendeville, B. C. and Jackson, M. P. A. 1992. The rise of diapirs during thin-skinned extension. *Marine and Petroleum Geology* 9(4), pp. 331-354.

Viana, A. et al. 2003. The Sao Tome´ deep-sea turbidite system (southern Brazil Basin): Cenozoic seismic stratigraphy and sedimentary processes. *AAPG Bulletin* 87(5), pp. 873-894.

Wiener, R. W. et al. 2009. Contractional Domains of the Niger Delta: Structural Styles, Influence of Mobile Shale, and Structural-Stratigraphic Evolution In: *AAPG Hedberg Conference, Deepwater Fold and Thrust Belts*. Tirrenia, Italy, October 4-9, 2009.

Wijono, J. et al. 2015. The Application of seismic attributes to determining geomorphology of submarine canyons: new insights from Giant Foresets Formation, Taranaki Basi, New Zealand. In: *39th Annual Conference*. Jakarta. Jakarta: Indonesian Petroleum Association.

Wilcox, R. E. et al. 1973. Basic Wrench Tectonics. *AAPG Bulletin* 57(1), pp. 74-96.

Wilson, J. T. 1965. A new class of faults and their bearing on continental drift. *Nature* 207, pp. 343-347.

Wood, L. J. 2011. *Shale tectonics*. Tulsa, OK: American Association of Petroleum Geologists.

Wright, L. D. and Coleman, J. M. 1973. Variations in Morphology of Major River Deltas as Functions of Ocean Wave and River Discharge Regimes. *AAPG Bulletin* 57(2), pp. 370-398.

Wu, J. E. et al. 2015. Niger Delta gravity-driven deformation above the relict Chain and Charcot oceanic fracture zones, Gulf of Guinea: Insights from analogue models. *Marine and Petroleum Geology* 65, pp. 43-62.

Wu, J. E. et al. 2009. 4D analogue modelling of transtensional pull-apart basins. *Marine and Petroleum Geology* 26(8), pp. 1608-1623.

Yardley, G. S. and Swarbrick, R. E. 2000. Lateral transfer: a source of additional overpressure? *Marine and Petroleum Geology* 17(4), pp. 523-537.

Yilmaz, O. and Doherty, S. M. 2000. *Seismic data analysis: processing, inversion and interpretation*. Tulsa: Society of Exploration Geophysicists.

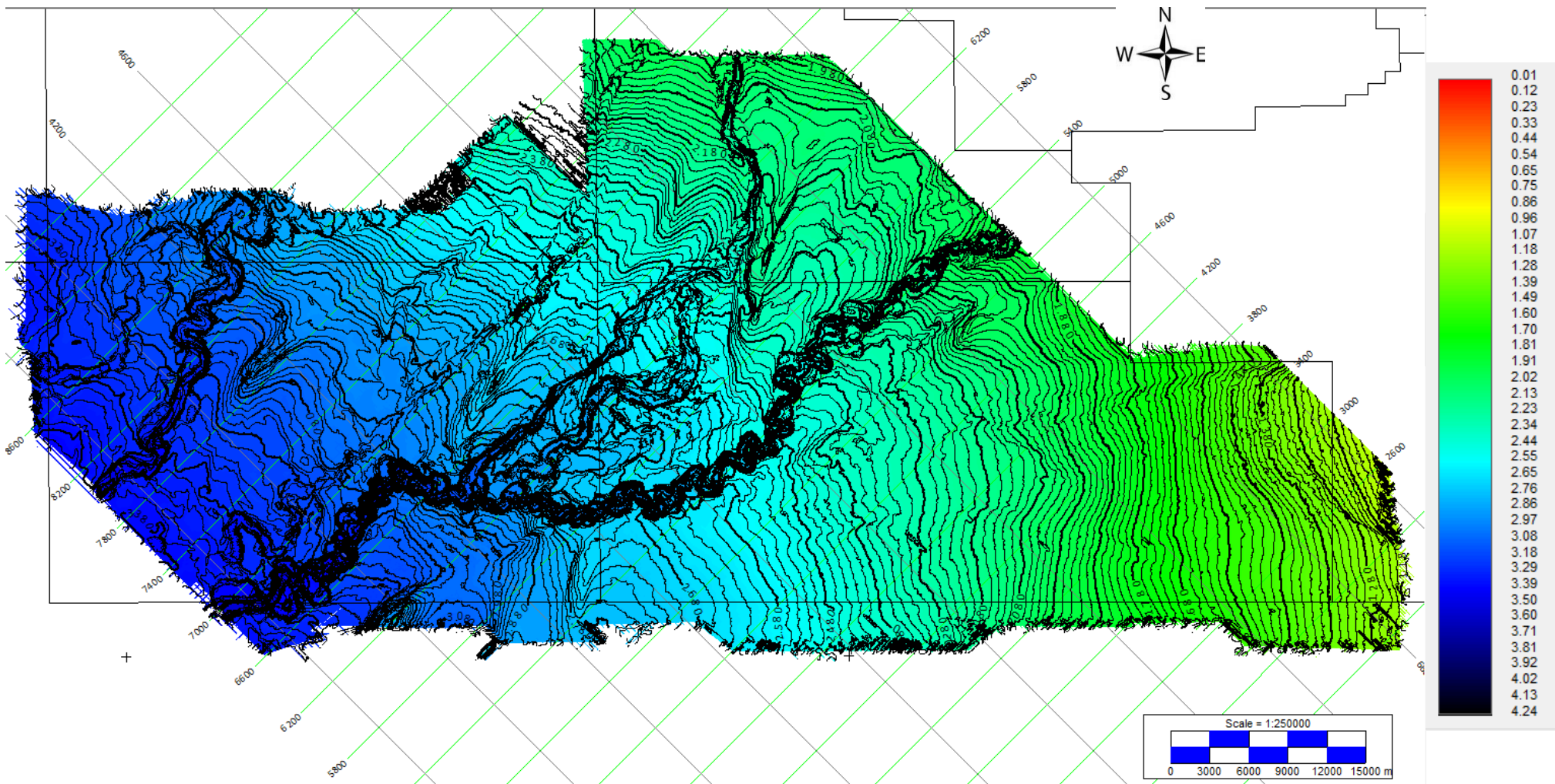
Zenk, W. 2008. Chapter 4 Abyssal and Contour Currents. In: Rebesco, M. and Camerlenghi, A. eds. *Developments in Sedimentology*. Vol. Volume 60. Elsevier, pp. 35-57.

Zhang, J. 2013. Effective stress, porosity, velocity and abnormal pore pressure prediction accounting for disequilibrium and unloading. *Marine and Petroleum Geology* 45, pp. 2-11.

Appendix A

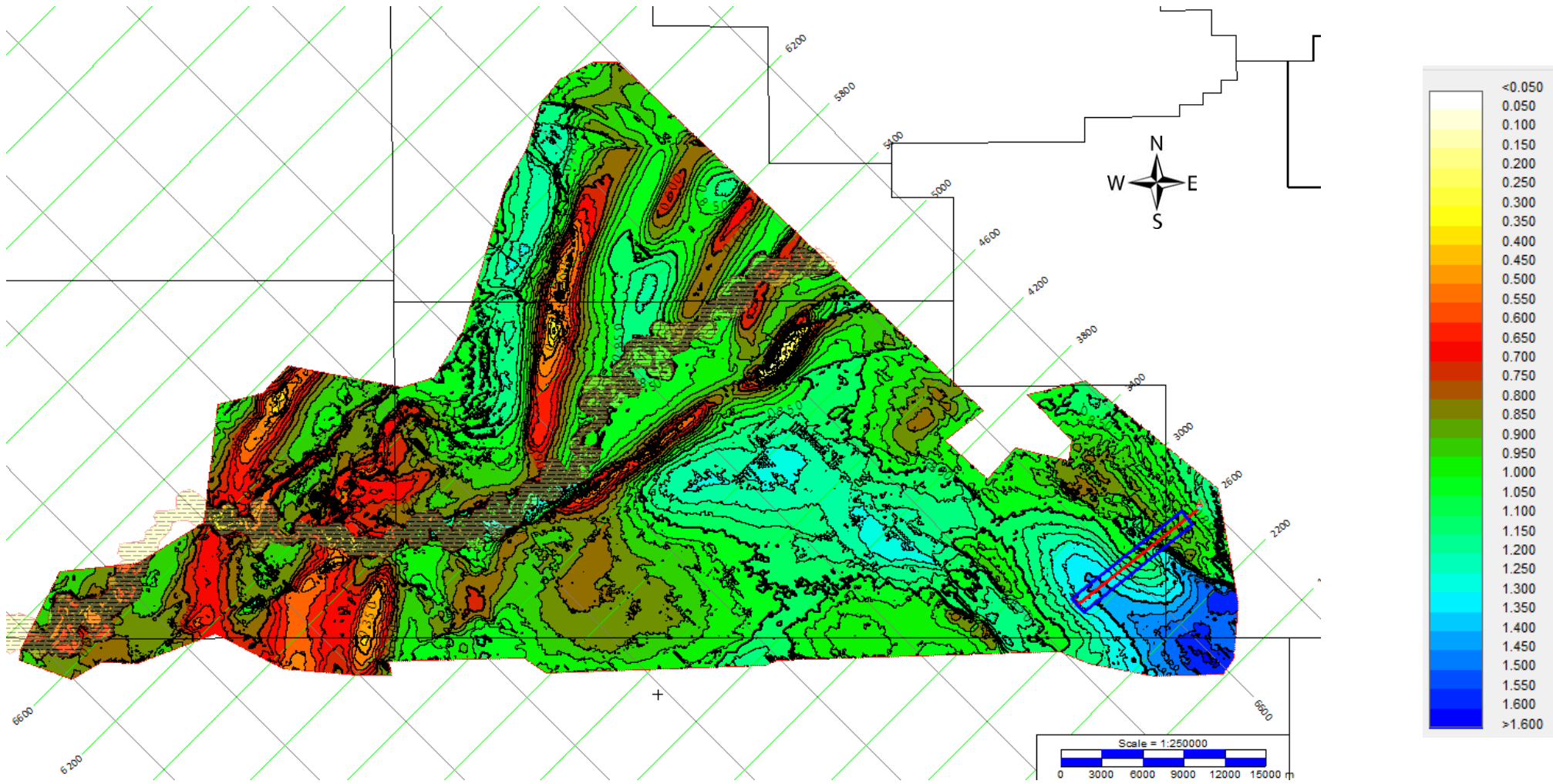
Two-way time maps

Two-way travel time map



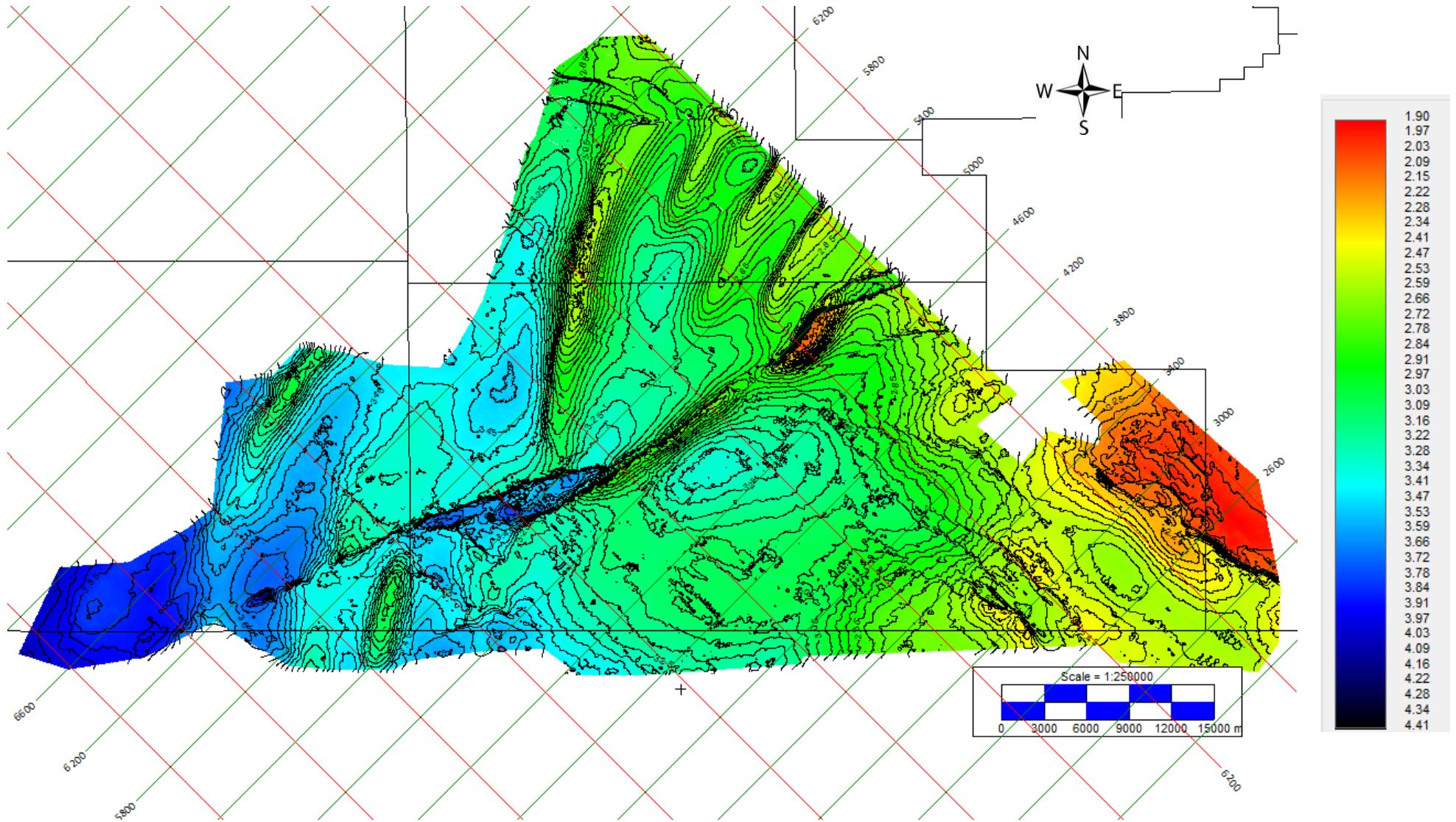
Sea Bed

Two-way travel time map



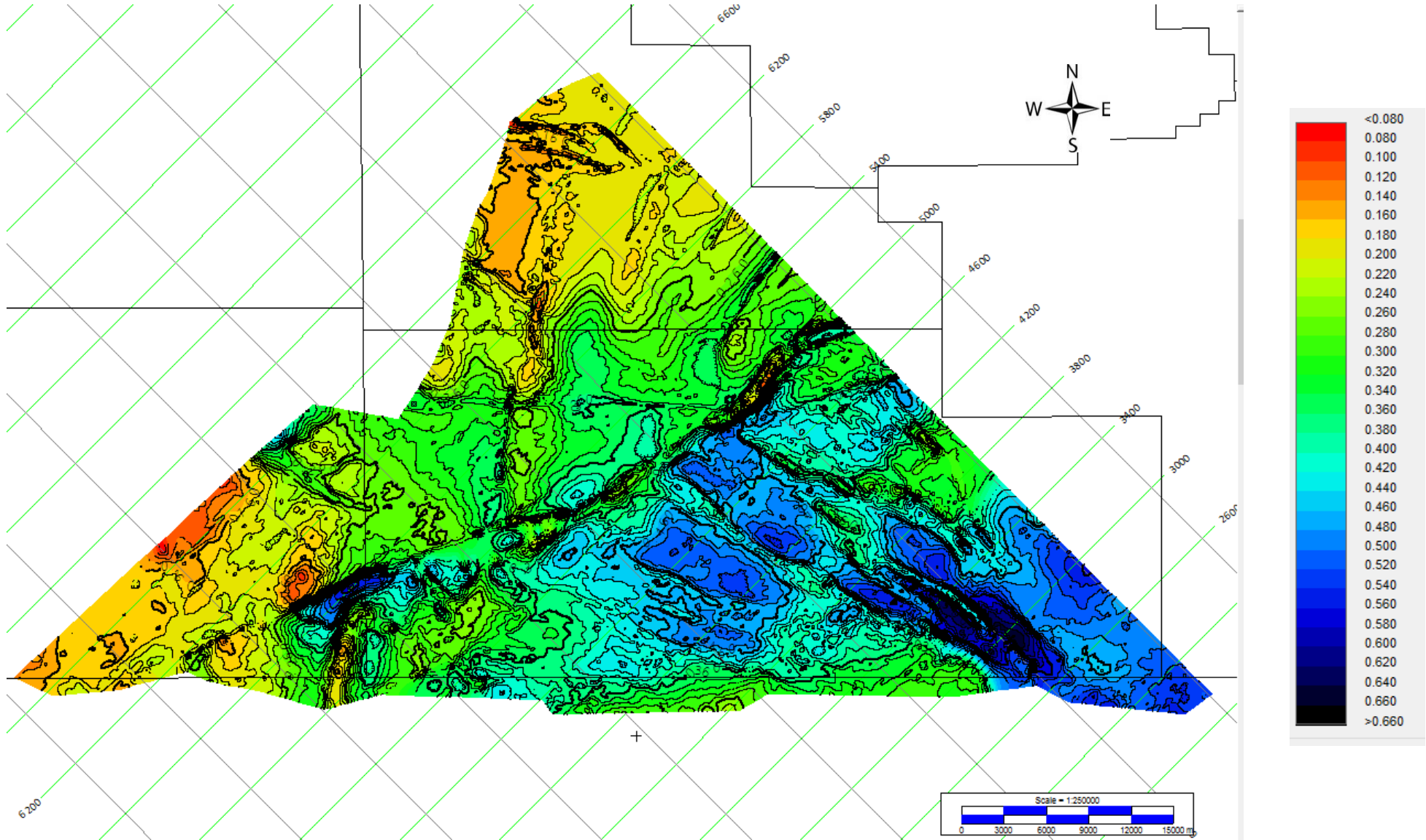
Isochrone of the Plio/Pleistocene (Sea Bed to Horizon 100)

Two-way travel time map



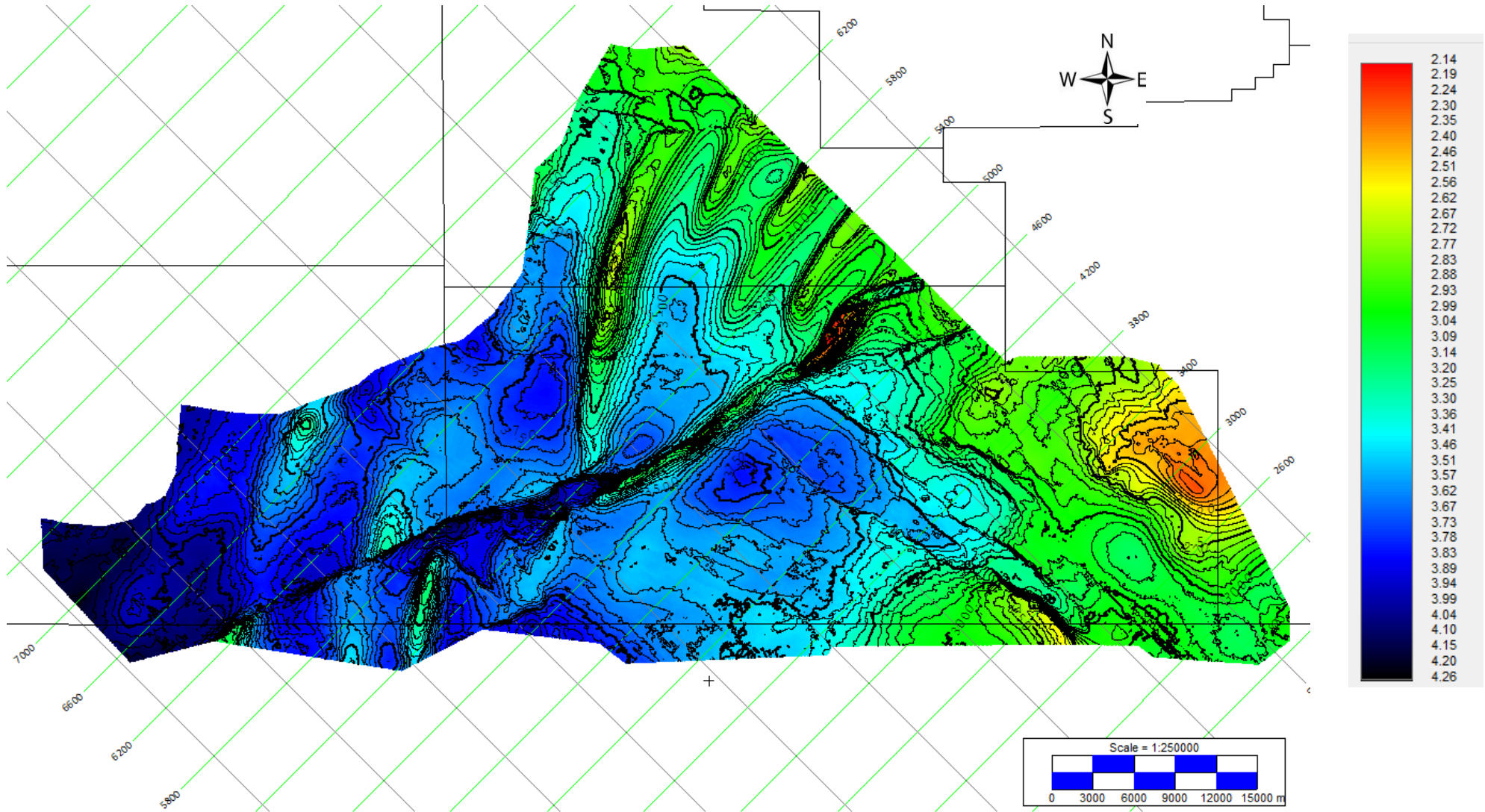
Top Miocene (Horizon 100)

Two-way travel time map



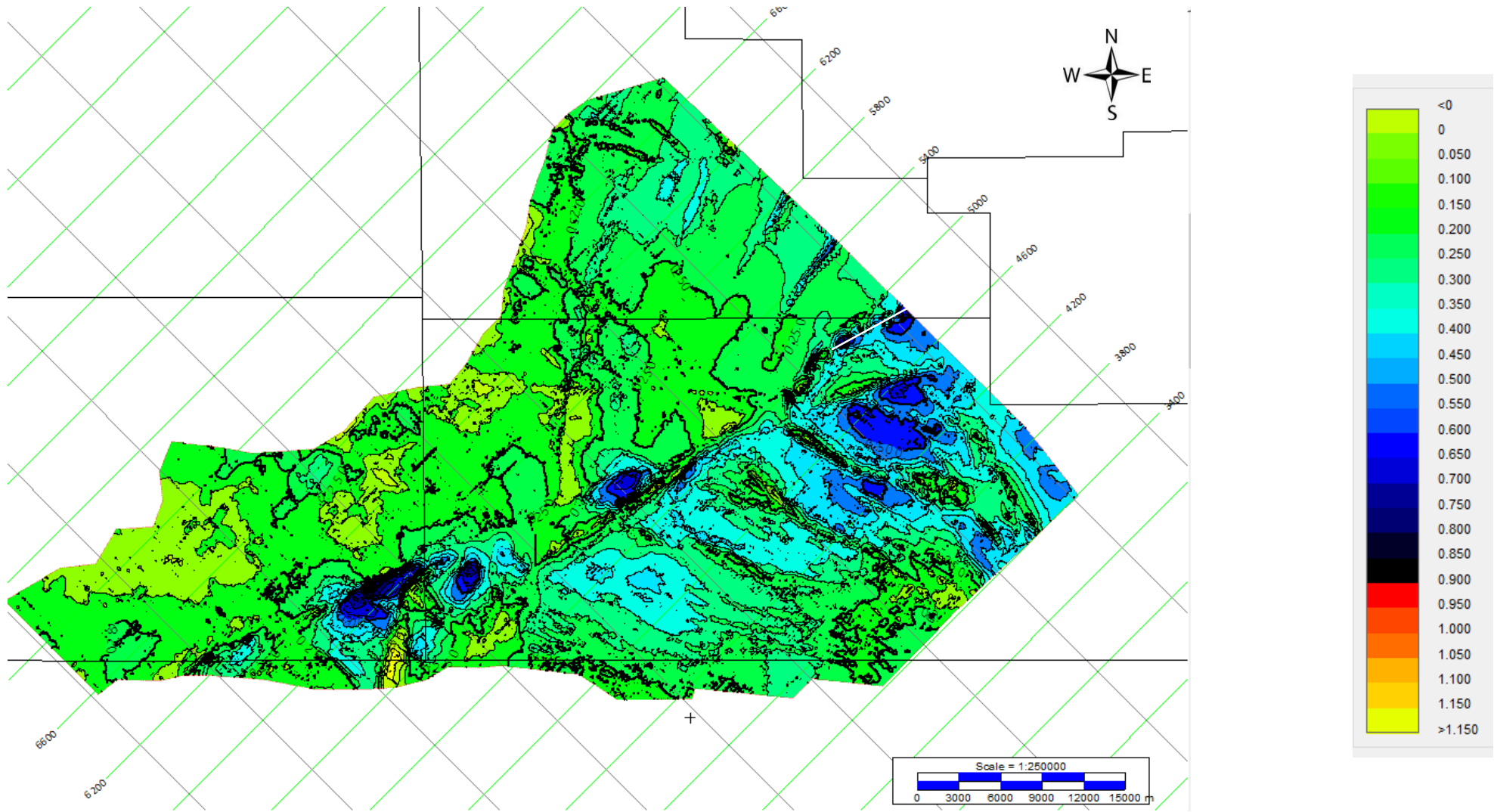
Isochrone of the Upper Miocene (horizon 100 to horizon 130)

Two-way travel time map



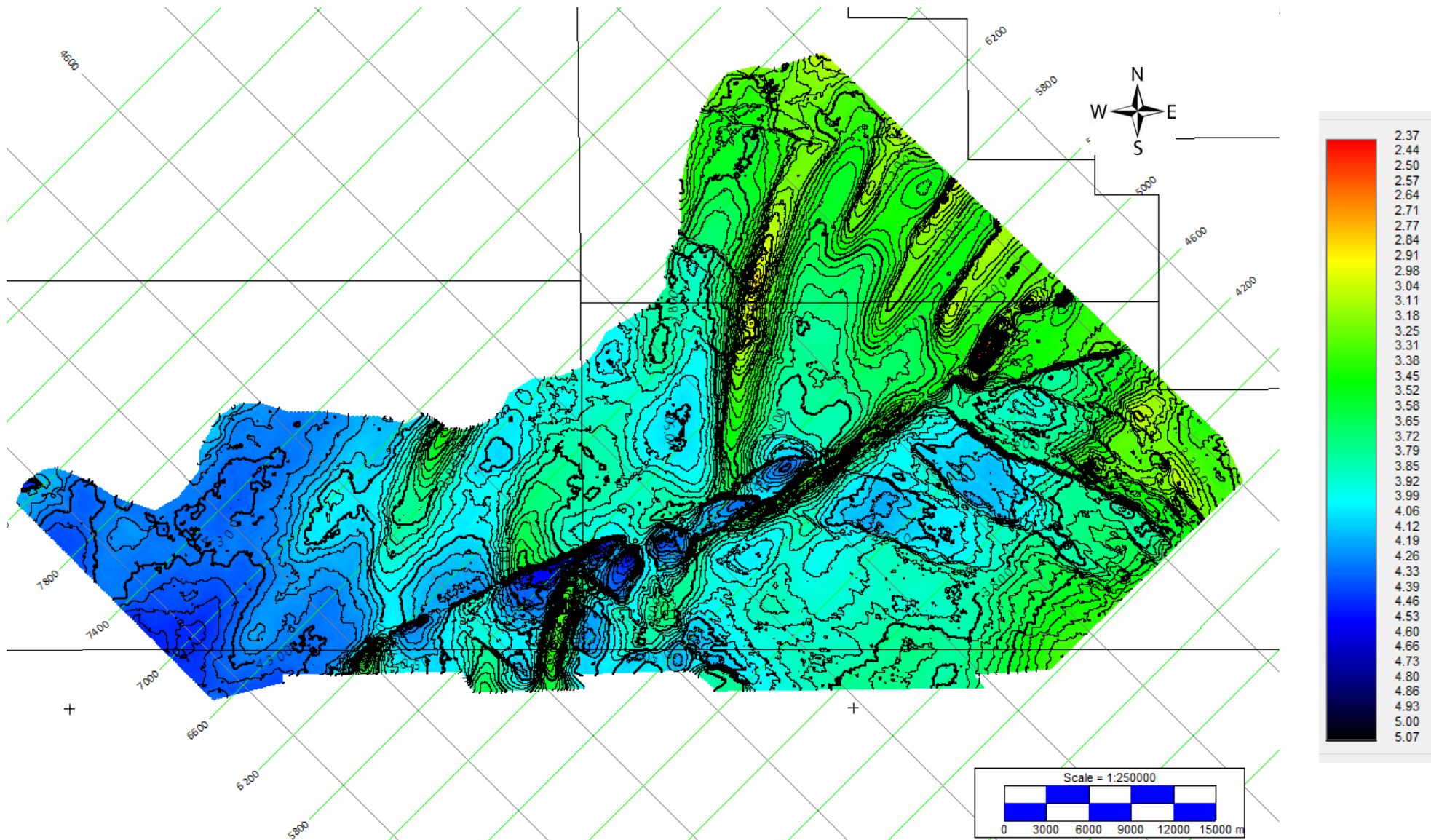
Near Base of the Upper Miocene (Horizon 130)

Two-way travel time map



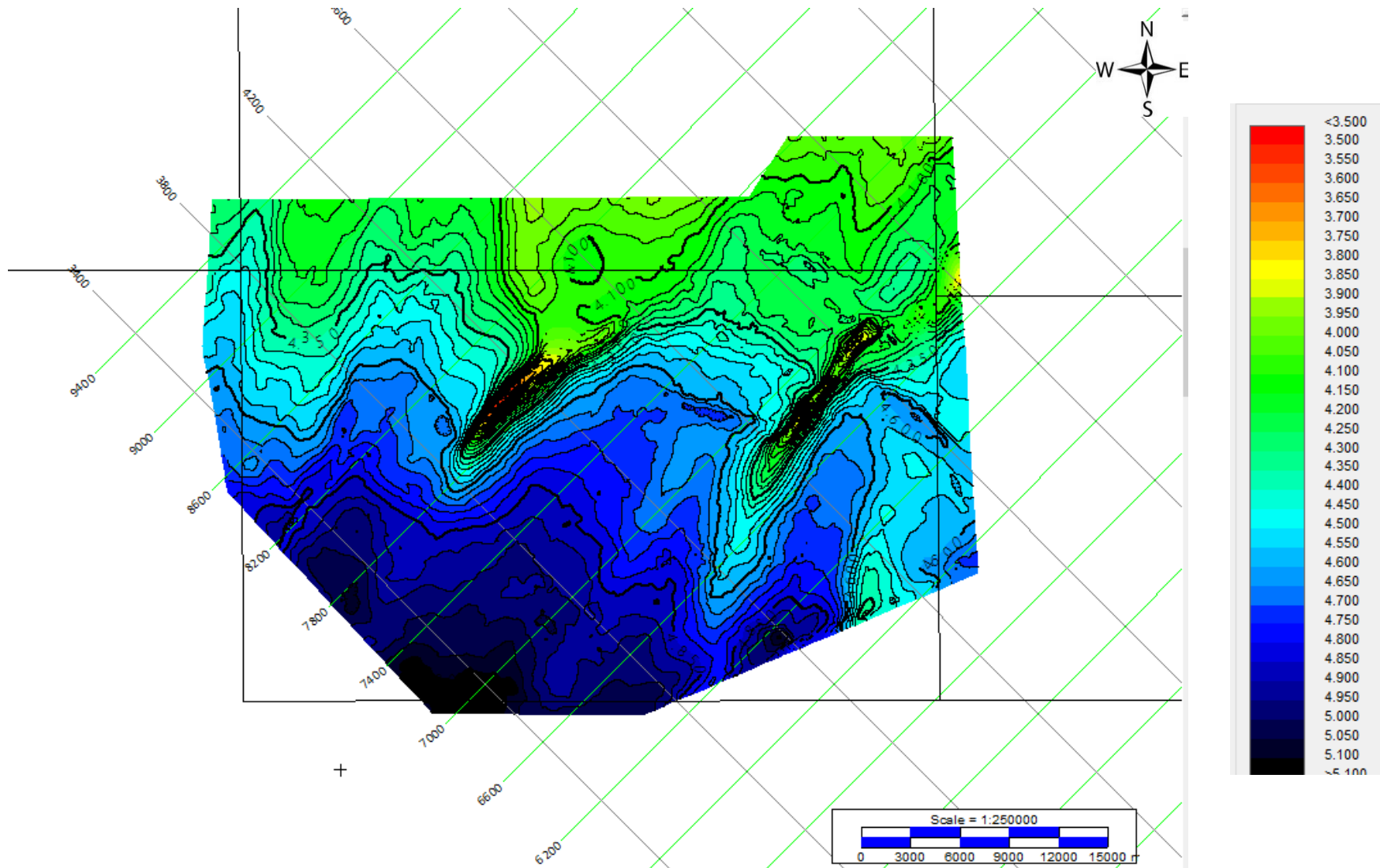
Isochrone of the Middle Miocene (horizon 130 to horizon 160)

Two-way travel time map



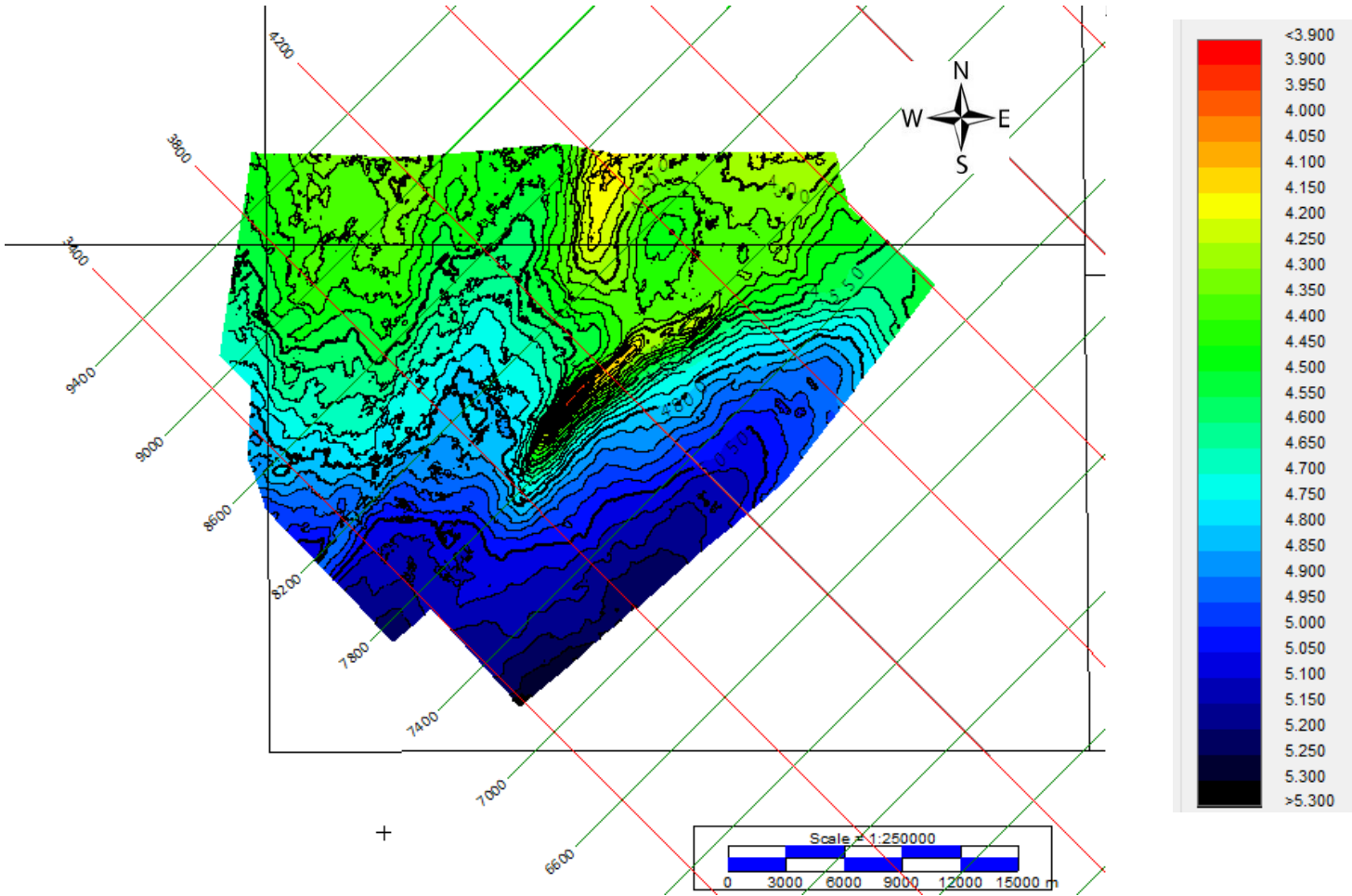
Near Top Middle Miocene (horizon 160)

Two-way travel time map



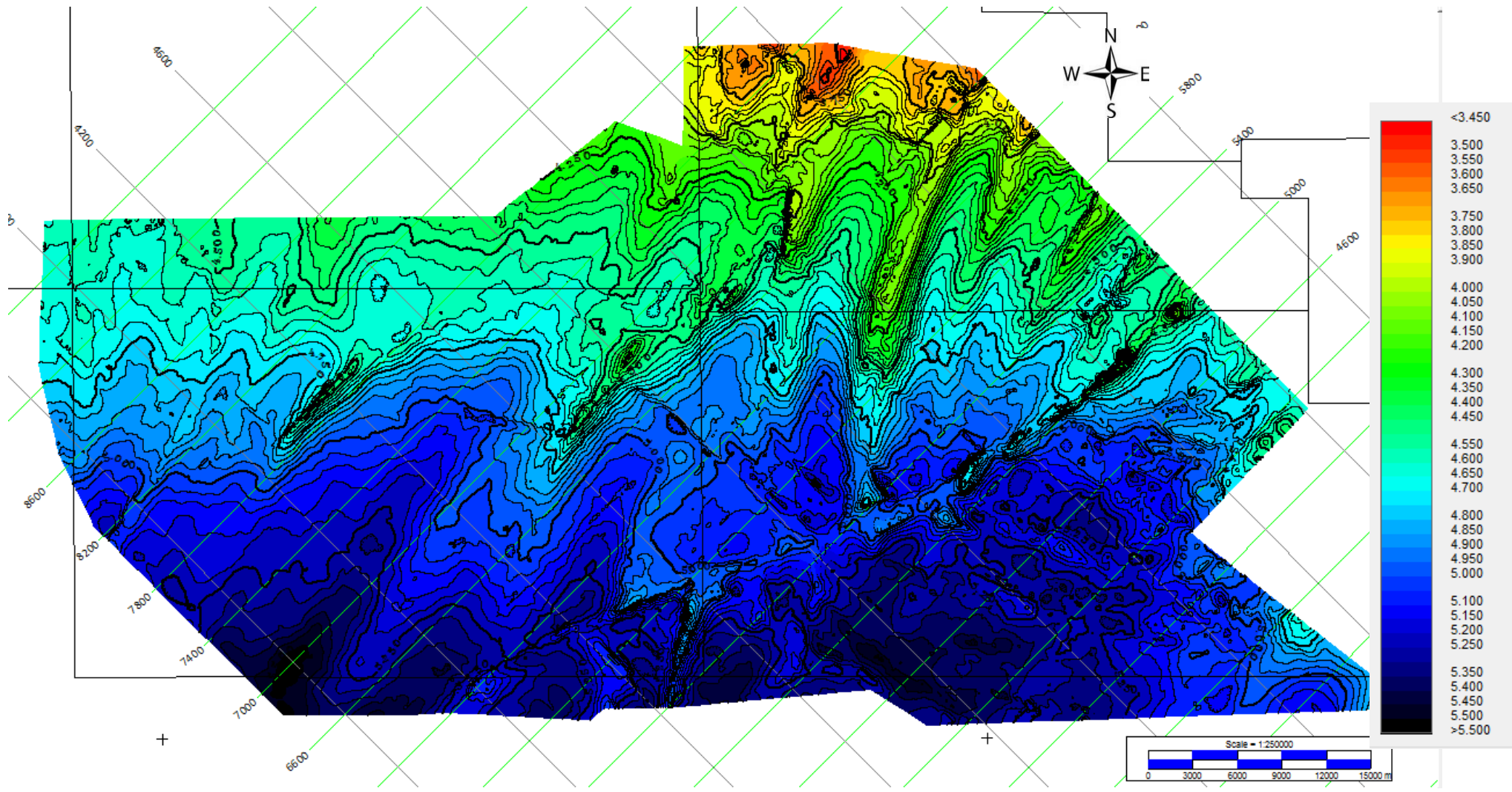
Upper Oligocene (horizon 310)

Two-way travel time map



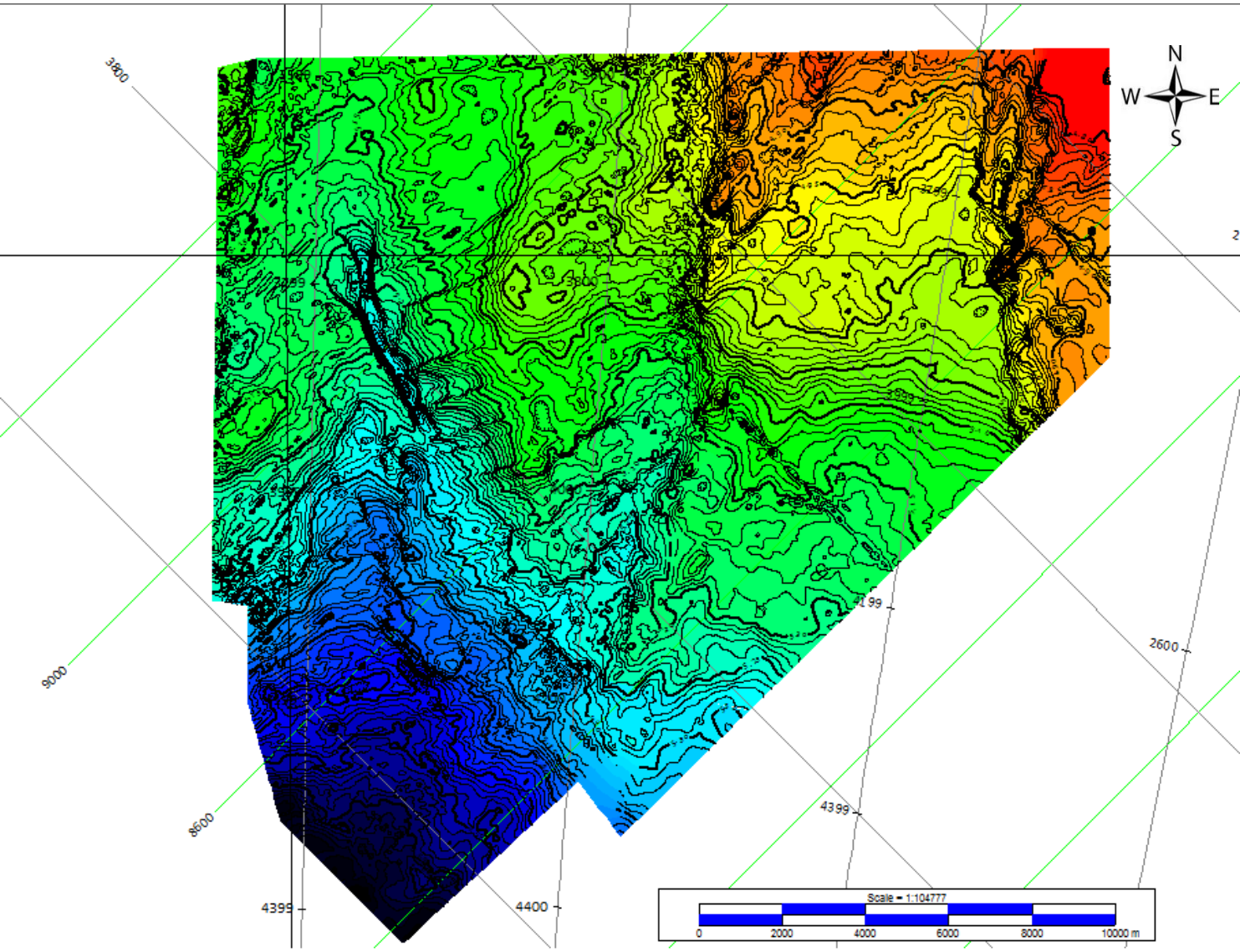
Near top Oligocene (horizon 300)

Two-way travel time map



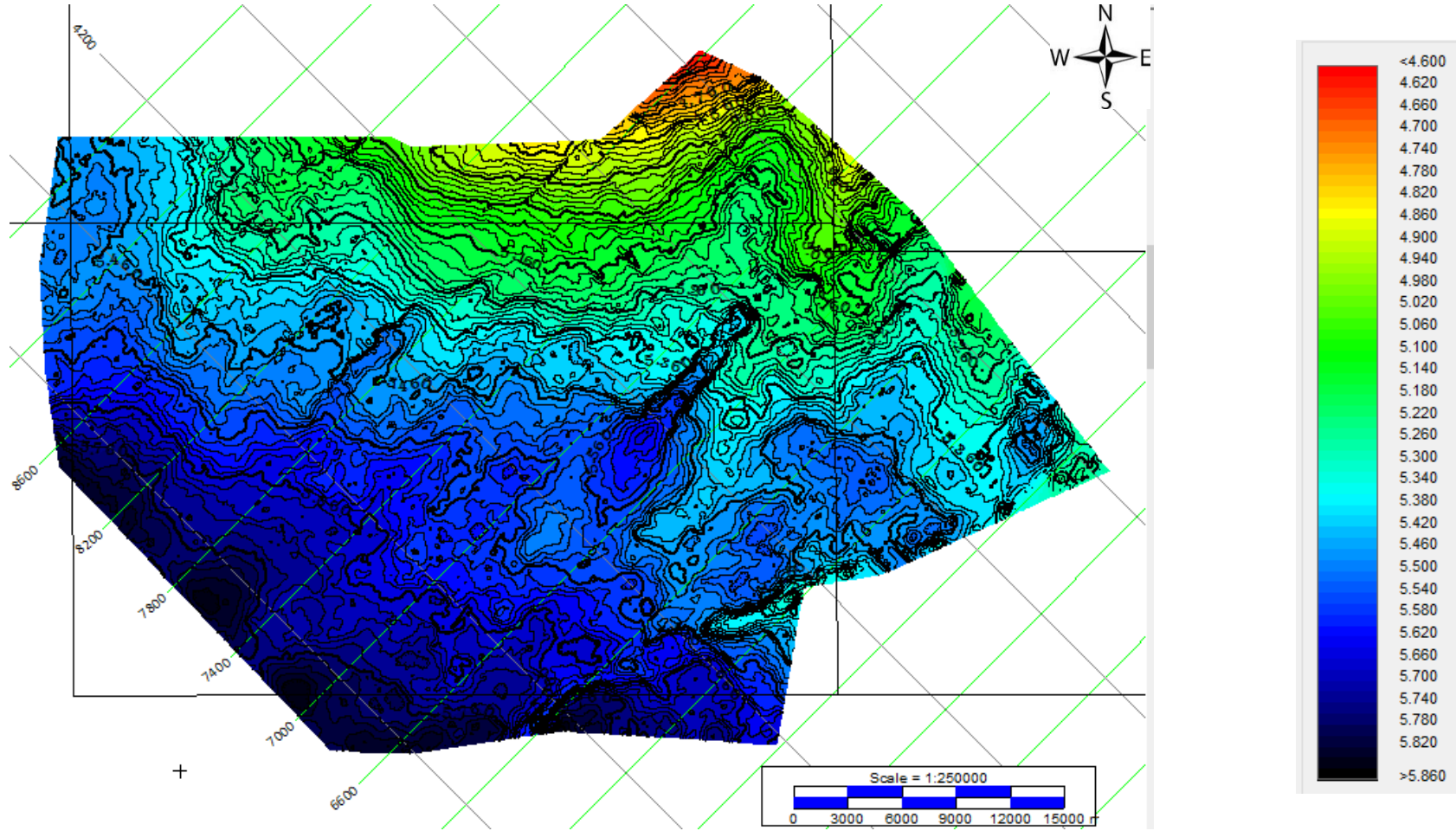
Base Neogene (horizon 420)

Two-way travel time map



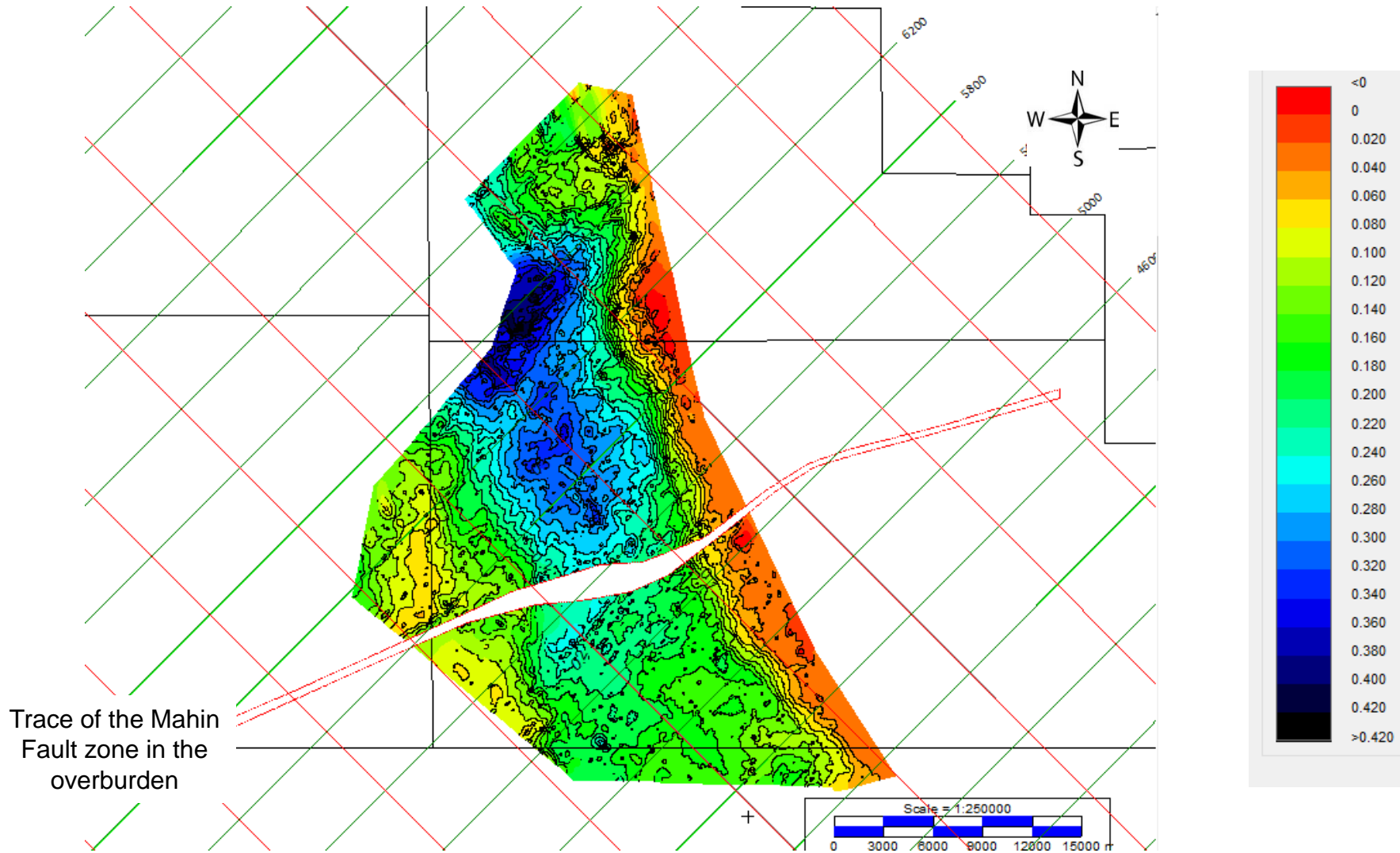
Intra Eocene (?) (horizon 470)

Two-way travel time map



Upper surface of mass transport complex (horizon 510)

Two-way travel time map



Isochrone of the Middle Albian to Senonian unconformity (horizon 680 to horizon 785)

